On the embryonic and post-embryonic development of
Pseudopallene sp. (Arthropoda, Pycnogonida)
with special focus on neurogenesis and nervous system differentiation

Dissertation

zur Erlangung des akademischen Grades

doctor rerum naturalium

(Dr. rer. nat.)

im Fach Biologie

eingereicht an der

Mathematisch-Naturwissenschaftlichen Fakultät I

der Humboldt-Universität zu Berlin

von

Dipl. Biol. Georg Brenneis

Präsident der Humboldt-Universität zu Berlin

Prof. Dr. Jan-Hendrik Olbertz

Dekan der Mathematisch-Naturwissenschaftlichen Fakultät I

Prof. Stefan Hecht, Ph.D.

Gutachter/innen:

1. Prof. Dr. Gerhard Scholtz
2. PD Dr. Angelika Stollewerk
3. Prof. Dr. Steffen Harzsch

Tag der mündlichen Prüfung: 12. Februar 2013

„Das Beschriebene macht etwas deutlich, das zwar dem *Wahrheitswillen* des Beschreibenden, aber nicht der Wahrheit entspricht. Wir beschreiben einen Gegenstand und glauben, wir haben ihn wahrheits*gemäß* und wahrheits*getreu* beschrieben, und müssen feststellen, es ist nicht die Wahrheit. Wir machen einen Sachverhalt deutlich, und es ist nicht und niemals der Sachverhalt, den wir deutlich gemacht haben wollen, es ist immer ein anderer.

[…]

Was hier beschrieben ist, ist die Wahrheit und ist doch nicht die Wahrheit, weil es nicht die Wahrheit sein kann.“

Thomas Bernhard – *Der Keller*

VOLUME 1

INDEX

1. Introduction

Encompassing almost 85% of all described living animal species, the Euarthropoda and their closest relatives Onychophora (velvet worms) and more arguably Tardigrada (water bears) are the most speciose metazoan taxon by far (Giribet and Edgecombe 2012; see e.g. Meusemann et al. 2010; Campbell et al. 2011; Rota-Stabelli et al. 2010, 2011 for recent studies on onychophoran and tardigrade affinities). Euarthropods are generally recognized to comprise the four major extant lineages Chelicerata (spiders, scorpions and their kin, plus potentially sea spiders), Myriapoda (centipedes, millipedes and their allies), Crustacea (lobsters, crayfish, crabs and many more) and the overwhelmingly diverse Hexapoda (insects and close relatives, such as springtails and proturans) (e.g. Ax 1999; Brusca and Brusca 2003; Westheide and Rieger 2006). The unparalleled species richness of euarthropods goes hand in hand with an enormous diversity of morphological forms and body plans, making the unraveling of its evolution a challenging and fascinating task. In order to reconstruct the evolutionary transformations that eventually led to the present-day diversity over the long geological history of euarthropods (dating back to the Cambrian at least, e.g. Budd and Telford 2009), solid hypotheses on their phylogenetic relationships are indispensible (see Edgecombe 2010; Giribet and Edgecombe 2012 for recent overviews on the topic).

The euarthropod nervous system provides 'a wealth of valuable characters that can be used for phylogenetic inferences' (Harzsch 2007) at the adult anatomical level as well as during its development. In fact, it has been considered 'a particularly suitable organ in which to search for characters to reconstruct evolutionary relationships between the major arthropod groups' (Whitington and Bacon 1997), due to notable structural diversity but at the same time retention of a very similar architectural principle in the different lineages. This paves the way for homologization of neural elements and their respective sub-parts (Whitington 1995). The corresponding architectural principle of the euarthropod central nervous system (CNS) is especially evident during embryonic development. The CNS is formed via segmental units of differentiating neural tissue, the neuromeres, which are at least transiently arranged in rope-ladder-like fashion, comprising ganglion anlagen with intra-segmental transverse commissural pathways and inter-segmental connectives (e.g. Whitington 1995; Whitington et al. 1996; Harzsch et al. 1997, 1998; Mittmann and Scholtz 2003; Vilpoux et al. 2006; Kirsch and Richter 2007; Boyan et al. 2008; Brenneis and Richter 2010 (adults); Fritsch and Richter 2010, 2012; Linne and Stollewerk 2011; Ungerer et al. 2011b). Comparison of various features of adult neuroarchitecture and more recently also development have led to the formulation of scenarios on arthropod nervous system evolution and suggestions or at least preferences of different hypotheses on euarthropod phylogeny (e.g. Holmgren 1916; Hanström 1928; Harzsch et al. 2005a; Harzsch 2006, 2007). Beyond that, first 'neural cladistics' have been conducted, being

hitherto, however, based on adult neuroanatomical characters alone (e.g. Strausfeld et al. 2006a; Strausfeld and Andrew 2011).

One of the most intriguing aspects of nervous system development in euarthropods is the occurrence of distinctly different modes of early neurogenesis. In hexapods and at least some crustaceans (malacostracans and branchiopods), neurogenesis is coupled to a specialized neuronal precursor type, the neuroblast (NB) (e.g. Wheeler 1891; McMurrich 1895; Bate 1976; Thomas et al. 1984; Hartenstein and Campos-Ortega 1984; Doe and Goodman 1985a; Dohle 1976; Scholtz 1992; Truman and Ball 1998; Ungerer and Scholtz 2008; Ungerer et al. 2011a, 2012). NBs are stem cell-like dividing neuronal precursors (SCNPs) that are comparably big and divide repeatedly in asymmetric fashion, thereby 'self-renewing' and 'budding off' a smaller daughter cell into the interior of the embryo (e.g. Stent 1998; Richter et al. 2010). The smaller daughter cell is termed ganglion mother cell and represents in turn a neuronal precursor type that (typically) undergoes one terminal division, giving rise to immature post-mitotic neurons and/or glial cells (e.g. Fürstenberg et al. 1998). Recent work revealed detailed correspondences between some NB cell lineages of a crustacean (Ungerer 2006; Ungerer and Scholtz 2008: *Orchestia cavimana*) compared to hexapods (e.g. Bossing et al. 1996: *Drosophila melanogaster*). In addition to this, striking similarities in (1) soma position, axon morphology and molecular marker expression of several pioneer neurons of the ventral nerve cord (Thomas et al. 1984; Whitington et al. 1993, 1996; Duman-Scheel and Patel 1999; Ungerer and Scholtz 2008), (2) ommatidium structure of the lateral eyes (e.g. Paulus 2000; see also discussions in Dohle 2001; Richter 2002; Müller et al. 2003) and (3) several additional features of adult neuroanatomy (e.g. Harzsch et al. 2005a; Harzsch 2006; Strausfeld and Andrew 2011) indicate that hexapods and crustaceans form a monophyletic group. This group has been termed Tetraconata (Dohle 2001) and is in good agreement with virtually all molecular analyses (e.g. Regier et al. 2008, 2010; von Reumont et al. 2009, 2012; Andrew 2011; Campbell et al. 2011). Hence, it represents by now one of the uncontested nodes in the arthropod tree, although internal tetraconate relationships remain contentious (e.g. Jenner 2010).

NBs as defined above are considered one of the apomorphies of tetraconates, since no evidence for this specialized neuronal precursor type has been uncovered in recent studies on early neurogenesis in chelicerates and myriapods (Whitington et al. 1991; Stollewerk et al. 2001; Mittmann 2002, 2003; Dove and Stollewerk 2003; Kadner and Stollewerk 2004; Chipman and Stollewerk 2006; Döffinger and Stollewerk 2010; Linne and Stollewerk 2011). In these two taxa, mostly post-mitotic immature neurons/glial cells immigrate actively into the embryo in a number of cell internalization sites (CISs) per hemi-segment, thereby clustering transiently in groups of flask-shaped cells. Cell proliferation occurs scattered in the apical neuroectoderm between the CISs. At least in myriapods, some indications of a more ordered process of

neuroectodermal cell proliferation have been noted and discussed (Whitington et al. 1991; Dove and Stollewerk 2003; Eriksson and Stollewerk 2010b; Whitington and Mayer 2011). Yet, with regard to the existence of any specialized neuronal precursor cell types, the available myriapod data remain still inconclusive. Analogous to this, also the phylogenetic placement of the myriapod lineage within euarthropods remains still insufficiently clarified. During the last two decades, a chelicerate-myriapod sister group relationship as so-called Paradoxopoda or Myriochelata has repeatedly received support in molecular analyses (e.g. Friedrich and Tautz 1995; Cook et al. 2001; Mallatt et al. 2004, 2006; Pisani et al. 2004; Dunn et al. 2008; Roeding et al. 2009). However, this stands opposed to the morphologically well-supported Mandibulata concept (e.g. Edgecombe 2010 for details), which advocates myriapods as sister group to tetraconates. Interestingly enough, the similarities in the neurogenesis mode have been discussed as potential apomorphy of Myriochelata (Dove and Stollewerk 2003; Kadner and Stollewerk 2004; Mayer and Whitington 2009a). Yet, in light of resurfacing Mandibulata support in a number of recent molecular studies (e.g. Rota-Stabelli and Telford 2008; Regier et al. 2008, 2010; Rota-Stabelli et al. 2010, 2011; Campbell et al. 2011; Rehm et al. 2012), the symplesiomorphic character of the chelicerate-myriapod-like neurogenesis mode appears more plausible. In accordance with this view, it has been repeatedly argued for as part of the euarthropod stem species pattern (e.g. Harzsch 2003, 2006, 2007; Harzsch et al. 2005a; Eriksson and Stollewerk 2010b; Ungerer et al. 2011a).

However, this assessment still lacks new data on Pycnogonida, or sea spiders. They represent an exclusively marine euarthropod lineage with more than 1300 described extant species (Arango and Wheeler 2007), which has resisted confident phylogenetic placement since its first description (see Dunlop and Arango 2005 for review). The majority of recent molecular analyses tend to recover pycnogonids within Chelicerata, as sister group to all other chelicerate taxa (Fig. 1A; e.g. Bourlat et al. 2008; von Reumont et al. 2009, 2012; Koenemann et al. 2010; Meusemann et al. 2010; Regier et al. 2010; Rota-Stabelli et al. 2010; Campbell et al. 2011; Rehm et al. 2012). Yet, this traditional textbook view (e.g. Ax 1999; Brusca and Brusca 2003; Westheide and Rieger 2006) receives often only relatively low support values in the analyses. In addition, it is also at the morphological level faced with persisting paucity of convincing apomorphies, the chelate first limb pair being the most promising one (Dunlop and Arango 2005). Due to this, an alternative hypothesis proposing pycnogonids as sister group to all remaining euarthropods – the so-called Cormogonida (Fig. 1B; e.g. Zrzavý et al. 1997; Edgecombe et al. 2000 (morphological analysis only); Giribet et al. 2001; Scholtz and Edgecombe 2006) – is sometimes still considered as being feasible (e.g. Bamber 2007; but see discussion in Edgecombe 2010).

Remarkably, the few histological studies covering pycnogonid nervous system development report the presence of conspicuously big cells within so-called ‘ventral organs’ (Morgan 1891;

Dogiel 1913; Sanchez 1959; Winter 1980). The latter represent no proper organs but segmentally arranged and bilaterally paired cell thickenings of the neuroectoderm that are confluent with the basally underlying ganglion anlagen. The big cells are said to show high proliferation activity and have been interpreted by almost all authors as teloblast-like cells/'neuroblasts' that produce ganglion cell material (Morgan 1891; Dogiel 1913; Winter 1980; but see Sanchez 1959). In one instance (Winter 1980), they are even explicitly claimed to differentiate early during neurogenesis and generate radial columns of ganglion cells by repeated radial divisions (Fig. 2). Given our current knowledge on the distribution of the different neurogenesis modes in the four major euarthropod lineages, the description of SCNPs in sea spiders is highly intriguing in light of their putative affinities with chelicerates. If the presence of SCNPs were to be confirmed in present-day investigations, tetraconates would no longer represent the only euarthropod lineage that is characterized by the presence of such specialized neuronal precursor cells. Against a phylogenetic background, such a finding would accordingly call for a critical reassessment of the validity of SCNPs in general and NBs in particular as apomorphy of the tetraconate lineage.

This unresolved situation represents the primary motivation and starting point for the present study on pycnogonid nervous system development. Notably, however, not only nervous system development but pycnogonid development in general remains poorly understood compared to other arthropod lineages with their well-established model organisms. This is not only reflected in its complete omission in one of the classic overviews on arthropod development (Anderson 1973), it is also evident in the limitations of the developmental studies undertaken since then. The majority of the latter investigate exclusively post-embryonic development in varying detail, with a massive focus on external morphology (e.g. Bain 2003a; Vilpoux and Waloszek 2003; Bogomolova and Malakhov 2004; Lovely 2005; Maxmen 2006; Bogomolova 2007, 2010; Cano and López-González 2009; Cano Sánchez and López-González 2010; Burris 2011; Lehmann et al. 2011). By contrast, a mere handful of recent works address aspects of embryonic development (e.g. Winter 1980; Brenneis 2007; Brenneis et al. 2008; Ungerer and Scholtz 2009; Machner and Scholtz 2010). For this reason, an additional objective of the present study is to contribute data for a better understanding of pycnogonid morphogenesis in general.

With *Pseudopallene* sp., a pycnogonid representative of the Callipallenidae was chosen for the investigations. In contrast to many other pycnogonid taxa, Callipallenidae do not possess the 'typical' free-living protonymphon larva (Arnaud and Bamber 1987) with a proboscis and just three pairs of limbs, the chelifores plus palpal and ovigeral larval limbs (e.g. Bogomolova 2007; Burris 2011; Lehmann et al 2011). Instead, they exhibit a more pronounced embryonization of development (e.g. Nakamura 1981; Bain 2003a; Bogomolova and Malakhov 2003, 2004). This facilitates investigation of development up to more advanced stages, because embryos and early

larvae are carried on the father's ovigers throughout embryonic as well as early post-embryonic development and thus remain comparatively easily accessible. To address the different aspects of development in *Pseudopallene* sp., a combination of scanning electron microscopy, histology, fluorescent nuclear staining and immunolabeling in conjunction with confocal laser-scanning microscopy and computer-aided 3D analysis was used.

In a first step, embryonic and post-embryonic morphogenesis of *Pseudopallene* sp. will be described (3.1. and 3.2., respectively). Staging systems that are introduced in these chapters will be subsequently used as reference for the studies on embryonic and post-embryonic neurogenesis in the ventral nerve cord (3.3. and 3.4., respectively), neurogenesis and formation of the brain anlage (3.5.) and an overview of the establishment of the major axonal pathways of the CNS (3.6.). As an outlook for future studies, first (fragmentary) expression data of genes involved in neurogenesis will be presented (3.7.). According to the primary objective of this study, the obtained data on pycnogonid nervous system development will be discussed in light of the currently best-supported hypothesis on arthropod phylogeny with a critical reevaluation of different aspects of arthropod neurogenesis and its evolution.

2. Materials and Methods

2.1. List of abbreviations used in text and figures

α – anti
acb – anterior commissural bundles
ad – adult
AF – autofluorescence
ald – antero-lateral depression
amc – antero-medial cell cluster
an – anus
a-p – antero-posterior
apc – apical cell cluster
ASH – achaete-scute homologue
br – brain (anlage)
brc – brain cell cluster
cd – central depression
cec – circum-esophageal connective
CIS – cell internalization site
cg – chela gland
ch – chelifore
chn – cheliforal neuropil
chs – cheliforal somata
CLSM – confocal laser-scanning microscopy
CNS – central nervous system
con – connective
cut – cuticle (exuvia)
cx – coxa
dc – deutocerebrum
dovc – dorsal ovigeral commissure
dpac – dorsal palpal commissure
ea – eye anlage
EC – ectodermal cell
EPC – epidermal cell
ES – embryonic stage
eso – esophagus
fe – femur
ff – fixed chela finger
GC – ganglion cell
GMC – ganglion mother cell
GN – glomerulus-like neuropil
hb – hind body region
HO – hypocerebral organ
IHC – immunohistochemistry
INP – intermediate neuronal precursor
ls – lateral sensory organ
mab – monoclonal antibody
MBN – mushroom body-like neuropil
mc – median proliferation cluster
mf – movable chela finger
mg – midgut
mgd – midgut diverticulum
mo – mouth
NB – neuroblast
NP – neuronal precursor
ns – nervous system
'on' – 'optic nerve'
ot – ocular tubercle
ov – oviger
pa – palp
pc – protocerebral region
pcb – posterior commissural bundles
pccb – protocerebral commissural bundle
pcn – protocerebral neuropil
p-d – proximo-distal
pg – posterior ganglion (anlage)
pha – pharynx
PNC – proneural cluster
PND – proneural domain
poc – pre-oral commissure
pp – pedipalp
ppoc – posterior pre-oral commissure
ppp – pre-proboscideal pit
pr – proboscis
pro – propodus
proc – proctodeum
PS – post-embryonic stage
pvc – postero-ventral commissure
rn – rostral nerve (dorsal pr-nerve)
sc – scape
SCNP – stem cell-like neuronal precursor
seg – sub-esophageal ganglion
SEM – scanning electron microscopy
sg – spinning gland
sgp – spinning gland process
sto – stomodeum
sub-ad – sub-adult
ta – tarsus
tb – tibia
tc – terminal claw
VMR – ventral midline region
VNC – ventral nerve cord
VNE – ventral neuroectoderm
vo – 'ventral organ'
vovc – ventral ovigeral commissure
vpac – ventral palpal commissure
vpn – ventral proboscis nerve
WISH – whole-mount *in-situ* hybridization
wl – walking leg (anlage)
wlg – walking leg ganglion (anlage)

2.2. CHEMICAL SOLUTIONS

A list of all used solutions is provided in Appendix A (volume 2).

2.3. TERMINOLOGY

The term Eucheliceratа is herein used for all chelicerates excluding Pycnogonida (e.g. Ax 1999; Dunlop 2010). Within Pycnogonida, the traditional taxonomic classification proposed by Hedgpeth (1947) is applied throughout the study. It is still widely used in the pycnogonid literature (e.g. Child 1979, 1998; Stock 1994) and has been tested in recent phylogenetic analyses (Arango and Wheeler 2007; Nakamura et al. 2007). At species level, names were updated to the current suggestions by Bamber and El Nagar (2012) and Arango and Brenneis (submitted).
Different stages during embryonic and post-embryonic development are abbreviated as ES (= embryonic stage) and PS (= post-embryonic stage), being numbered consecutively for each of the two developmental phases. The term sub-adult is herein applied to specimens with the overall external morphology of an adult, except for the lack of gonopores and the presence of an apophysis on the oviger (only in males of some pycnogonid taxa, including Callipallenidae). However, these sub-adult specimens may still undergo more than one molt before reaching maturity.

For descriptions of nervous system development and neuroanatomy, the terminology recently suggested by Richter and colleagues (2010) has been followed whenever applicable. In accordance with Whitington (2007), the term ‘neurogenesis’ is herein applied to cover all processes that lead to the generation of post-mitotic but still immature neurons and glial cells. Accordingly, all subsequent cell differentiation processes, such as axonogenesis, are clearly discriminated and excluded from neurogenesis. The neutral expression ‘nervous system development’ represents an inclusive term for the entirety of cell generation and differentiation processes.
In recent literature (see e.g. Whitington 2007, but Stollewerk 2008), the term ‘neuronal precursor’ (NP) has been used to designate different cell types during nervous system development. Here, it is applied in line with Whitington (2007) and Richter and colleagues (2010), being restricted to neurogenesis and designating a progenitor cell that has already entered the neural pathway but is not yet post-mitotic. Hence, a NP divides at least once more, giving rise either to further NPs or to post-mitotic immature neurons and/or glial cells. The neutral term ‘ganglion cell’ (GC) has been chosen to accommodate post-mitotic neurons and glial cells in all differentiation stages, since unequivocal distinction especially between immature cells of both types was not possible.

Recent descriptions of neurogenesis in euchelicerates and myriapods introduced the terms 'invagination sites' (Stollewerk et al. 2001) or 'immigration sites' (Mittmann 2003) to designate evenly spaced spots of cell internalization in the neuroectoderm of one hemi-segment. Yet, the term 'invagination' is confusing with respect to late processes of neurogenesis, during which the whole central area of a hemi-neuromere may invaginate to from a conspicuous depression (e.g. Mittmann 2003; Whitington 2007). Some authors also claim that 'immigration' fails to describe the early processes correctly, suggesting instead 'ingression' (Mayer and Whitington 2009a; Whitington and Mayer 2011). However, since both terms describe an interiorly directed movement of a cell without direct involvement of a division, they are here considered as representing synonyms. For the sake of terminological consistency, 'immigration' is applied in the present text with respect to the interior movement of single cells. Nonetheless, it has to be noted that in some euchelicerate and myriapod representatives tiny local pits ('invaginations') are indeed observable in the sites where several adjacent apical cells are in the process of immigration (e.g. in spiders). To acknowledge this mixture of phenomena and avoid terminological conflicts, the neutral term 'cell internalization site' (CIS) is herein given preference and suggested for future studies.

All positional information provided for nervous system sub-structures follows the neuraxis. Due to a gradual dorsal flexure of the protocerebral region and the cheliforal neuromere, the anterior pole of the neuraxis deviates from the body axis from late embryonic development onwards. To minimize dorsal-ventral ambiguities resulting from these discrepancies between body axis and neuraxis, cell positions are whenever possible described as 'apical' (i.e., close to the surface) and 'basal' (i.e., further interior) instead of 'ventral' and 'dorsal'.

2.4. Main object of investigation: *Pseudopallene* sp. (Pycnogonida, Callipallenidae)

2.4.1. Specimen collection

The great majority of investigations were carried out on *Pseudopallene* sp. Sub-adult and adult specimens were collected in coastal waters near Eaglehawk Neck, Tasmania, in autumn 2008 and 2009. During SCUBA diving, individuals were taken by hand from their favorite prey, the arborescent soft bryozoan *Orthoscuticella* sp. (Cheilostomata, Catenicellidae), put into small plastic jars and transferred into buckets of fresh sea water upon return to the surface (Fig. 3A). Adult males bearing batches of embryos and/or PS 1 and PS 2 were singled out in a field laboratory, the batches being thereupon carefully removed from the ovigers with tweezers, roughly sorted according to developmental stage using a stereo microscope and subsequently fixed (see 2.4.3.). Since PS 3 has already left the male, this and all older stages had to be collected directly from the bryozoan colonies. For this purpose, pieces of the latter were brought to the

field laboratory and checked under the stereo microscope, all collected post-embryonic stages being then fixed according to planned investigations. Additionally, some bryozoans as well as sub-adult and adult specimens of *Pseudopallene* sp. were transported to the laboratory in Berlin, kept in a sea water aquarium and freshly fixed prior to nervous system studies.

2.4.2. Species identification

At the time of specimen collection, the *Pseudopallene* forms found in the coastal waters near Eaglehawk Neck were identified as *Pseudopallene ambigua* STOCK, 1956, which is traditionally considered as being a widely distributed, predominantly canary yellow species in South Australian waters (Staples 1997). Although the Tasmanian specimens show the same canary yellow coloration like *P. ambigua* (Fig. 3A,B), they were noticed to exhibit variations in the specific measures and proportions of single morphological sub-structures in comparison to the latter. By now, a detailed investigation of adult morphology in combination with genetic markers (mitochondrial cytochrome oxidase I and nuclear ribosomal internal transcribed spacers) could demonstrate that the Tasmanian *Pseudopallene* do not represent *P. ambigua* (Arango and Brenneis, submitted). Unexpectedly, however, not only one but at least three closely related yellow species could be discriminated in the collected Tasmanian material, none of them having been previously described. For morphological diagnosis of these three species, a combination of different characters, such as overall body size, proboscis shape (Fig. 3C-E), propodus shape, propodal heel spines (Fig. 3F-H) and serration of the ovigeral claw have to be taken into account. In the current work, the use of new names for the identified *Pseudopallene* species is not intended to make these names available with respect to the International Code of Zoological Nomenclature (disclaimer according to Art. 8.3). The names will be formally published in Arango and Brenneis (submitted).

These recent findings have some important implications for the present study.

(1) The embryonic material used herein represents a mixture of different species. However, no striking and consistent morphological differences could be assessed between investigated embryonic specimens. This indicates that the high similarity characterizing the adults is also found during embryonic development of the closely related species. In contrast to this, performed gene expression studies certainly suffered from the previously unrecognized mixture of species (see 3.7.).

(2) Also the post-embryonic material collected in the field potentially represents an assemblage of different species. To address this issue, the two genetic markers were also applied to some of the post-embryonic specimens, which thereby could be assigned to one of the three species, namely *Pseudopallene constricta* n. sp. (Fig. 3E,G; Arango and Brenneis, submitted). This

molecular identification finds morphological support in the correspondences of the taxonomically important propodus shape and heel spination in the investigated post-embryonic stages and the adults of *P. constricta*. Nonetheless, to account for the remaining uncertainty, the description of post-embryonic morphogenesis (see 3.2.) has been neutrally kept under the undetermined name *Pseudopallene* sp. (with the exception of the sub-adult stage that is unequivocally identifiable as *P. constricta* on morphological grounds alone). The focus is set on the major morphogenetic events and transformation processes, not on the exact measures and proportions of sub-structures or taxonomically important spination patterns.

2.4.3. Fixation procedures

Different fixation procedures were required for the range of conducted investigations. An overview of these procedures is given in Table 1. If not stated otherwise, fixation was carried out at ambient temperature. Long-term storage in absolute methanol was observed to result in shrinkage of the cytoplasmic compartment of the embryonic cells, especially in early morphogenesis stages. Hence, methanol-stored material was found to be sub-optimal for analyses of cell shapes in the embryonic ectoderm.

Tab. 1: Overview of fixation procedures conducted on *Pseudopallene* sp.

Fixative	Fixation time, post-treatments & long-term storage	Developmental stage	Applied methods
PFA/SW	several months at 4°C, transfer into PBS + 0,1%NaN_3 & storage at 4°C	ES, PS	IHC, SEM (ES, PS 1&2)
PFA/SW	30-40 min, gradual transfer into absolute methanol & storage at 4°C	ES, PS1&2	IHC
PFA/SW	8 h – overnight, gradual transfer into absolute methanol & storage at -20°C	ES, PS 1&2	WISH
PFA/SW	overnight, direct processing	sub-ad, ad	IHC
Bouin's	30-40 min, several washes + storage in 70% ethanol at 4°C	ES, PS, sub-ad, ad	SEM (ES), histology
70% ethanol	several months at 4°C	PS, sub-ad, ad	SEM
RNAlater	several months at -20°C	ES, PS 1	total RNA extraction

2.4.4. Removal of egg membrane and specimen dissection

Prior to all subsequent procedures, fixed embryonic samples had to be freed from the surrounding layers of elastic matrix (used by the males to glue the eggs into batches) and from the egg membrane. Different chemical approaches (enzymatic digestion of matrix with proteinase K; membrane removal using differing concentrations of bleach; rupturing of membrane via rigorous shaking in heptane-methanol-mixture) proved unsuccessful or did not bear reproducible results. Consequently, egg membrane removal was accomplished manually, using ground dissection needles or electrochemically etched tungsten tips in combination with sharpened watchmaker forceps (Dumont 5). With the same tools some embryos and early PS 1 were freed of the attaching yolk, thus allowing flat preparations for later analyses. In order to investigate neuroarchitecture as well as neurogenic events in post-embryonic stages, sub-adults and adults, specimens were carefully dissected, the nervous system being completely removed for further processing.

2.5. Investigation of additional species

2.5.1. Pycnogonid representatives other than *Pseudopallene* sp.

Selected developmental stages of other pycnogonid species were investigated for comparison to *Pseudopallene*.

(1) A limited number of ethanol-preserved embryos and hatched larvae of *Callipallene* sp. (Callipallenidae) were collected from a single egg-bearing male in Eaglehawk Neck, Tasmania.

(2) Ethanol-preserved hatched larvae of *Stylopallene cheilorhynchus* Clark, 1963 (Callipallenidae) were kindly provided by David Staples (Museum Victoria, Melbourne, Australia).

(3) A culture of *Pycnogonum litorale* (Ström, 1762) (Pycnogonidae) is being constantly kept in the laboratory in Berlin. Embryos can be directly collected from the males after successful copulation and fertilization (see Brenneis 2007 for details on husbandry). Fixation was carried out in PFA/PBS for 30 min (embryos) or 3 h (adult CNS), fixed material being directly processed after fixation.

(4) Early larvae of *Nymphon gracile* Leach, 1814 (Nymphonidae) already used by Brenneis (2007) were briefly reinvestigated in the course of the present work (see Brenneis 2007 for fixation procedure).

(5) A handful of sub-adult and adult individuals of *Cilunculus japonicus* (Turpaeva, 1990) were kindly provided by Prof. Dr. Günther Pass (University of Vienna, Austria), who in turn obtained

them from Dr. Katsumi Miyazaki (Kyoto University, Japan). Only general observations on the gross anatomy of the CNS were made.

2.5.2. Spider species for comparison

Selected embryonic stages of the two laboratory model spiders *Cupiennius salei* (Keyserling, 1877) and *Parasteatoda tepidariorum* (C.L. Koch, 1841) were studied with regard to some features of embryonic neurogenesis. Fixed embryos were provided by Dr. Carsten Wolff from the laboratory in Berlin (see Wolff and Hilbrant 2011; Mittmann and Wolff 2012 for fixation procedures).

2.6. Scanning electron microscopy (SEM)

Samples were dehydrated in a graded ethanol series (15%, 30%, 50%, 60%, 70%, 80%, 90%, 96%, 2x100%, each step at least 1 h). In a first test run, they were afterwards either air-dried in hexamethyldisilazane (HMDS) with an intermediate pre-incubation step in a 1:1 mixture of ethanol and HMDS, or processed in a critical point dryer (Bal-Tec CPD 030). Critical point drying proved to yield better results and was subsequently used as standard procedure. All material was sputtered with gold, using a Bal-Tec SCD 005 sputter coater. No consistent qualitative differences could be assessed between PFA/SW- and Bouin-fixed embryonic specimens. SEM micrographs were taken with a Zeiss LEO 1430.

2.7. Fluorescence stainings

2.7.1. Nuclear stains and F-actin labeling

An overview of all tested fluorescent markers tested in the course of this study is given in Table 2. For the description of the overall appearance of the different embryonic and the first post-embryonic stage, some samples were washed in TBS, cooked therein for 10 min, cooled down and stained with the nucleic acid marker Sytox® Green overnight at 4°C.

Nuclear counterstaining with Hoechst (H33342) was conducted after or during the final washing steps of immunohistochemical stainings (see 2.7.2.) or phalloidin labeling. Incubation lasted at least 1 h, being occasionally extended overnight at 4°C.

Labeling of F-actin was repeatedly attempted with different phallotoxins, but yielded positive results only once for a handful of embryos that had been freshly fixed in the laboratory in Berlin. Fresh fixation and avoidance of extended storage periods (irrespective of storage medium) appear hence pivotal for phallotoxin stainings of *Pseudopallene* embryos. In the single occasion of positive staining, samples were incubated in TRITC-coupled phalloidin solution for 90 min at room temperature.

Tab. 2: Fluorescent markers tested on *Pseudopallene* sp. in the course of the study.

Fluorescent marker	Concentration	Result
Nuclear marker		
Hoechst H33342 (INVITROGEN MOLECULAR PROBES®, #H1399)	1 µg/ml in PBS	positive
Hoechst H33258 (SIGMA, #861405)	1 µg/ml in PBS	positive, not as distinct as H33342
Sytox® Green Nucleic Acid Stain (INVITROGEN MOLECULAR PROBES®, #S7020)	5 µM in TBS	positive
Phallotoxin (labeling of F-actin to visualize i.a. cortical cytoskeleton)		
TRITC phalloidin (SIGMA, #P1951)	50 µg/ml in PBS	positive, only in freshly fixed material, bleaching fast
Alexa® phalloidin (INVITROGEN MOLECULAR PROBES®, #A12379)	5 U/ml ≈ 0,165 µM in PBS	negative, only stored material available for tests
BODIPY® FL phallacidin (INVITROGEN MOLECULAR PROBES®, #B607)	5 U/ml ≈ 0,165 µM in PBS	negative, only stored material available for tests
Lipophilic marker (labeling of phospholipid bilayers to visualize plasma membrane)		
FM 1-43FX (INVITROGEN MOLECULAR PROBES®, #F35355)	5 µg/ml in ddH_2O	positive but weak, only in freshly fixed material, bleaching fast

2.7.2. Immunohistochemistry

2.7.2.1. Pre-treatments

The nervous system of post-embryonic stages, sub-adults and adults of pycnogonids is equipped with a well-developed neural sheath (increasingly pronounced with ongoing development) and additionally surrounded by fibrous connective tissue. To facilitate antibody penetration through these barriers, dissected nervous systems were in a first step treated with 3-5 short pulses in a bath ultrasonicator (ELMA® Transsonic 310; 35 kHz). Hereafter, exposure to a collagenase-hyaluronidase mixture (1 h at 37°C), repeated short rinsing in PBS and an additional incubation in proteinase K solution (up to 1h at 37°C) were performed. Enzymatic digestion was followed by a post-fixation step in 4% PFA/PBS (15-20 min at RT) and thorough washing in several changes of PBTx (at least 2 h at RT) on a horizontal shaker (NEOLAB® DOS-20S, 55-70 rpm).

2.7.2.2. Applied antibodies and antisera

An overview of all primary antibodies/-sera and secondary antibodies tested in the course of this study is given in Tables 3 and 4, respectively. For several of the primary antibodies/-sera no positive results could be obtained in pycnogonids. In some cases, a likely reason for this may be insufficient epitope similarity between the proteins of the original target organism and pycnogonids (e.g. *α Dm ELAV* as marker for differentiated neurons in *Drosophila* or *α 8B7* as marker for axonal projections and NBs in *Schistocerca*). In other instances, the chosen fixation procedures and especially the non-availability of living specimens for fresh fixation may account for the failure (e.g. *α HRP* as general neuronal marker or *α cleaved caspase-3* as general apoptosis marker). In numerous studies (e.g. Pileri et al. 1997, Shi et al. 2001, Kiernan 2008), different antigen retrieval protocols for reduction of (potential) antigen masking due to formaldehyde fixation have been tested and evaluated. Cooking of samples for several minutes in 1mM EDTA-NaOH solution (ph 8,0) has been considered the most reliable method for a wide range of antigens in the exhaustive study of Pileri and colleagues (1997), Yet, tests of this procedure yielded no positive results for the fixed stages of *Pseudopallene* sp.
Monoclonal antibodies against acetylated alpha-tubulin as well as tyrosinated tubulin (Table 2) were applied to visualize cytoskeleton. Heterodimers of alpha-tubulin and beta-tubulin are the basic components of microtubules, which represent an important part of the cellular cytoskeleton. They are subject to post-translational modifications, two of them being acetylation/deacetylation and detyrosination/tyrosination (Janke and Kneussel 2010).

(1) Acetylation is common and found in many cell types, being often encountered in stable microtubule assemblies (Hammond et al. 2008). Microtubule acetylation is non-uniformly distributed in neurons (Janke and Kneussel 2010) and recent evidence suggests a critical role of acetylation of alpha-tubulin in neuronal migration, dendrite projections and arborizations at least in mice (Creppe et al. 2009). Several studies have already taken advantage of acetylated alpha-tubulin labeling to follow the establishment of the major axonal pathways during the development of different arthropods (e.g. Harzsch et al. 1997; Mittmann and Scholtz 2003; Mayer and Whitington 2009b; Fischer and Scholtz 2010; Fritsch and Richter 2010, 2012; Ungerer et al. 2011b), including pycnogonids (Maxmen et al. 2005; Brenneis et al. 2008). Prior work has shown (Brenneis 2007) that the cytoskeleton of all embryonic cells of pycnogonids is rich in acetylated alpha-tubulin, which allows assessment of cell shapes in the ectoderm during development.

(2) The gene-encoded protein of alpha-tubulin is characterized by a C-terminal tyrosine (= tyrosinated alpha-tubulin), which can be reversibly removed via detyrosination (Hammond et al. 2008). In interphase cells, microtubules enriched in tyrosinated alpha-tubulin have been indicated to be more dynamic than microtubules rich in detyrosinated tubulin (Kreis 1987). The

tyrosinated sub-class is therefore expected in regions of dynamic change of the cytoplasm, for instance in the growth cones of neurons (Janke and Kneussel 2010). Comparable to acetylated alpha-tubulin, labeling against tyrosinated alpha-tubulin was herein also used to assess the shapes of ectodermal cells, which are subject to dynamic changes due to cell movements relating amongst others to neurogenesis. During mitosis, tyrosinated tubulin shows a similar distribution to total tubulin (Gundersen and Bulinski 1986) and allows visualization of the spindle apparatus, which holds as well for acetylated alpha-tubulin (personal observation).

An IgG fraction of a rabbit antiserum against phosporylated histone H3 [pSer^{10}] (PH3; Table 2) was used to reveal the location of cells undergoing mitosis in fixed specimens. In eukaryotic cells, histones represent a major component of the chromatin. Phosphorylation of histone H3 is positively correlated with mitotic chromosome condensation (e.g. Goto et al. 1999) and is at least in one site of the amino-terminal tail (serine 10) conserved throughout eukaryotes (e.g. Wei et al. 1998). In *Pseudopallene* sp., the antiserum against the Ser^{10} phosphorylation site could be used to reliably visualize dividing cells in pro-, meta- and early anaphase. Mitoses in advanced anaphase or telophase were frequently still labeled, albeit weakly. Due to this, PH3 labeling was always performed in combination with a nuclear counterstain, which allowed confirmation of co-localization of PH3 and DNA as well as reliable identification of advanced mitosis stages amongst the surrounding ectodermal cells.

2.7.2.3. Antibody incubations

Prior to antibody exposure, samples were blocked for at least 1h in PBTx+N. Primary and secondary antibodies were diluted in PBTx+N, incubation times lasted at minimum overnight and were sometimes extended up to 72 h, especially for the dissected nervous systems of post-embryonic stages. Antibody incubation was followed by thorough washing in PBTx (at least 4 h at RT with several changes of the buffer) on a horizontal shaker. Omission of the primary antibodies resulted in complete loss of signal.

2.7.3. Mounting of samples

Cooked and Sytox®Green-stained samples were transferred into DABCO-Glycerol, whereas immunohistochemically processed material was put into Vectashield® Mounting Medium (VECTOR LABORATORIES, Inc.). Clearing of samples was performed in both cases overnight at 4°C. For mounting, tiny pieces of plasticine were fixed to the corners of cover slips, acting as spacers and thus preventing squeezing of the objects. Preferably, cover slips of small size (10x10 mm or 12x12 mm) were used, since they allowed more controlled fine adjustment of the distance between slide and cover slip. Mounted objects were stored in darkness at 4°C until further processing.

Tab. 3: Primary antibodies/-sera tested on *Pseudopallene* sp. and their respective dilutions.

Primary antibody/-serum	**Dilution**	**Result in *Pseudopallene* sp.**
α acetylated alpha-tubulin, mouse mab 6-11 B-1 (SIGMA, #T6793)	1:100	positive
α tyrosinated tubulin, mouse mab TUB-1A2 (SIGMA, #T9028)	1:500	positive
α phospho-Histone H3 [pSer^{10}], IgG fraction of rabbit serum (SIGMA, #H0412)	1:200	positive
α serotonin, rabbit serum (IMMUNOSTAR, #20080)	1:1000	positive
α 8B7, mouse mab (provided by G. Boyan, LMU München)	1:200	negative
α HRP, rabbit mab (JACKSON IMMUNORESEARCH/DIANOVA, #323-005-021)	1:10 – 1:30	negative
α Dm ELAV, mouse mab 9F8A9, supernatant (DEVELOPMENTAL STUDIES HYBRIDOMA BANK)	1:10	negative
α synorf1, mouse mab 3C11, supernatant (DEVELOPMENTAL STUDIES HYBRIDOMA BANK)	1:10	negative
α Cs prospero, rat polyclonal antiserum (provided by M. Weller)	1:200	negative
α cleaved Caspase-3 (Asp175), rabbit serum (CELL SIGNALING, #9661)	1:20	negative
α Dm invected/engrailed, mouse serum, supernatant (provided by H. Saumweber, HU-Berlin)	1:1	negative

2.8. ANALYSIS AND DOCUMENTATION OF FLUORESCENCE STAININGS

2.8.1. Stereo microscope images

Fluorescence images of Sytox®Green-stained embryos were taken with a ZEISS Lumar V12, z-stacks being created with ZEISS AxioVision software (Version 4.7.10) and subsequently merged to a single image with extended depth of field using HELICONSOFT Helicon Focus software (Version 4.50).

Tab. 4: Applied secondary antibodies and their respective dilutions.

Secondary antibody	Dilution
α mouse IgG (H+L) affini pure Cy™3, goat mab (JACKSON IMMUNORESEARCH/DIANOVA, #115-165-003)	1:200
α rabbit IgG (H+L) Alexa Fluor® 488, goat mab (INVITROGEN MOLECULAR PROBES®, #A11038)	1:400 – 1: 500
α rat IgG (H+L) FITC, donkey mab (JACKSON IMMUNORESEARCH/DIANOVA, #712-095-153)	1:500
α rat IgG (H+L) Cy™3, donkey mab (JACKSON IMMUNORESEARCH/DIANOVA, #712-165-153)	1:500

2.8.2. Confocal laser-scanning microscopy (CLSM)

Image stacks of selected objects were taken with a LEICA DM IRE2 confocal laser-scanning microscope equipped with a LEICA TCS SP2 AOBS laser-scan unit. Depending on the structure of interest and intended z-resolution, step sizes ranging from 0,3 µm to 2,00 µm were chosen between successive scanning planes. Based on the emission characteristics of the applied fluorochromes in a given object, a combination of UV laser (405 nm wavelength → Hoechst, autofluorescence of cuticle), Argon laser (488 nm wavelength → Sytox®Green, Alexa Fluor® 488) and Helium-neon laser (543 nm → Cy™3, TRITC) was selected for the recordings.

2.8.3. Analysis of CLSM data

Analyses of the CLSM data were performed with the 3D reconstruction program 'Imaris' (BITPLANE AG, Switzerland, Version 7.0.0).

Within the 'Surpass mode' of this program, three-dimensional volumes are generated from the recorded image stacks. A volume can be turned and rotated in every spatial dimension, zoomed in and out and be modified by a number of additional tools (see below).

The 'Extended section mode' of Imaris allows simultaneous visualization of virtual transverse, horizontal and sagittal sections with individually definable thickness (via inclusion of a variable number of images). This tool was used for analysis and visualization of the cellular organization of the developing neuroectoderm, involved cell movements and the orientation of mitoses in regions of cell proliferation.

The 'Blend' option of Imaris renders scanned structures non-transparent and thus facilitates evaluation of surface and external shape of an object.

2.8.3.1. Cell counts

Counts of the overall cell number within hemi-neuromeres and apical cell clusters were conducted on tubulin-labeled specimens with nuclear counterstain. They were performed with the 'Spots' tool in conjunction with an 'Ortho-slicer' in the 'Surpass mode'. The combination of both tools allows manual marking of structures (in this case nuclei) coupled to an automatic recording of the number of applied spots. Recognition of single nuclei for manual marking requires a minimum resolution throughout the scanned object. Since the apico-basal dimensions of the hemi-ganglion anlagen increase significantly during development, only insufficient resolution is achieved in the deepest layers of a whole-mount scan. To overcome this problem, counts of later post-embryonic stages (PS 2 and PS 6) were based on a combination of scans from the ventral and the dorsal side of the ganglia. In the overlapping region of the two scans, cells had to be individually identified in both scans, in order to prevent double marking.

2.8.3.2. Nucleus measurements

Throughout development of *Pseudopallene* sp., measurements of nuclei in the neuromere of walking leg segment 1 were performed, using the 'Measurement Points' tool in the 'Surpass mode'. In histological sections as well as in fluorescent nuclear stains with tubulin labeling, the nucleus was observed to take up the major part of the overall volume of ectodermal cells. Therefore, measurement of nucleus size was considered sufficient to assess differences in overall cell size. Measurements were conducted independently in at least two embryos or post-embryonic specimens of the same developmental stage. Ten nuclei were measured in each hemi-neuromere, i.e., twenty nuclei per specimen. They were measured along their elongated axis, which in the great majority of cases was oriented in an approximately apico-basal direction, at least in the embryonic stages. This analysis was performed to gain a general idea of ectodermal cell sizes during the course of development. It was not designed as basis for statistical analysis and assessment of *statistically* significant differences. This is also reflected in the relatively low sample size of studied specimens per developmental stage.

2.8.3.3. Selective removal of obstructing 'non-target' structures

Frequently, labeled 'non-target' cell layers obstructed an unhindered view of interior structures of interest in embryos and post-embryonic stages. To overcome these limitations, two different tools were applied (separately or in combination) in the 'Surpass mode' of Imaris. 'Clipping planes' represent a fast and reliable way to virtually remove 'non-target' layers surrounding the structures of interest. In this study, this tool was mainly used for the presentation of the axonogenesis data. Additionally, application of 'Contour surfaces' was used to selectively mask

three-dimensionally more complex 'non-target' regions, which were found to be closely interlacing with the structures of interest.

2.8.3.4. Two-dimensional projections of 'curved' optical sections

During development, the neuroectodermal regions do not maintain a planar structure. They are characterized by a locally heterogeneous stratification along the apico-basal axis, the formation of depressions and local compressions due to overlying limb anlagen. In order to depict arrangements of cells and cell groups within apical or basal ectodermal cell layers in curved regions more precisely, a combination of several 'Oblique Slicers' were applied in the 'Surpass Mode'. They were orientated to follow the curvature of the targeted cell layer. As a result, a virtual 3D-curved section plane is created. An image taken from such a slightly curved plane represents a 2D projection of the cell layers instead of a true planar section. As a result of this, spatial arrangements of sub-structures towards the periphery of the image appear slightly closer spaced than in reality (as in any other image taken from a 3D object). For the purposes of the analyses performed in the present work, the advantages of this approach clearly outweighed these slight distortions.

2.9. HISTOLOGY

Bouin-fixed embryonic and post-embryonic stages, sub-adults and adults were embedded in the plastic resin Technovit 7100 (KULZER Histo-Technik) following the manufacturer's standard protocols. Precise orientation of embryonic specimens during the embedding procedure proved difficult especially in earlier stages (ES 3 to ES 6), due to minimal contrast of the dehydrated whitish embryo and yolk against the white embedding form. To increase the contrast of embryonic tissues, samples were therefore rehydrated prior to embedding in a graded ethanol series and briefly stained in deionized water containing some drops of Delafield's solution (MERCK, hematoxylin solution). Although the staining solution failed to penetrate the egg membrane, it led to an inhomogeneous and asymmetric blue staining pattern of the externally attaching egg matrix. 'Stained' embryonic samples were positioned in ventral, anterior, or lateral view under a stereo microscope against a black background and a sketch of the matrix staining pattern in the respective orientation was drawn. This sketch was subsequently used during the embedding procedure to orientate the samples. As a result of this, at least some of the embryonic samples turned out to be reasonably well orientated with regard to the intended section plane. Semithin sections (1,5 µm) were cut with a MICROM HM 355 microtome, stretched at 60°C on a heating plate and stained in a first step with methylene blue-azure II solution, followed by a counterstain in basic fuchsin solution. Sections were embedded in Roti®-Histokitt (ROTH) under cover slips. Photographs of selected sections were taken with a ZEISS Axioskop 2

plus microscope equipped with a digital camera (ZEISS AxioCam HRc) and used to complement the CLSM data. An overview of all section series produced in the course of this study is provided in Appendix B (volume 2).

2.10. INVESTIGATION OF GENE EXPRESSION PATTERNS

2.10.1. Target genes

Five candidate genes/gene families were selected for expression pattern analyses during neurogenesis.

2.10.1.1. Achaete-scute homologues (ASH)

The achaete-scute gene family encodes transcription factors with a conserved basic Helix-Loop-Helix domain, which are expressed early during neurogenesis in all studied euarthropods and in onychophorans (e.g. Cabrera et al. 1987; Skeath and Carroll 1992: *Drosophila melanogaster*; Stollewerk et al. 2001; Döffinger et al. 2010: *Cupiennius salei*; Dove and Stollewerk 2003: *Glomeris marginata*; Wheeler et al. 2003: *Tribolium castaneum*; Kadner and Stollewerk 2004: *Lithobius forficatus*; Wheeler and Skeath 2005: *Triops longicaudatus*; Eriksson and Stollewerk 2010a,b: *Euperipatoides kanangrensis*; Ungerer et al. 2011a: *Daphnia magna*). Mutant analyses on the fruitfly *D. melanogaster* (e.g. Cabrera et al. 1987; Jiménez and Campos-Ortega 1990) and RNAi experiments on the beetle *T. castaneum* (Wheeler et al. 2003) and the spider *C. salei* (Stollewerk et al. 2001) have demonstrated that members of the achaete-scute gene family have a proneural function, i.e., their expression promotes neurogenesis and is required to confer ectodermal cells the potential to adopt neural fate. The same role of ASH has been deduced in non-functional studies on other arthropods, based on the early temporal onset of expression coupled to a spatial correlation of subsequent neurogenic events in ASH-positive cell regions (but see Ungerer et al. 2011a, 2012).

2.10.1.2. Delta and Notch

The Notch-signaling pathway is employed in numerous processes of development involving cell fate decisions. During early neurogenesis of the fruitfly *D. melanogaster* and the spider *C. salei*, genes of the Notch-signaling pathway have a so-called 'neurogenic' function, i.e., they antagonize proneural gene function and lead within ASH-positive proneural clusters/domains to a restriction of the number of cells that eventually enter the neural pathway (e.g. Lehmann et al. 1981, 1983; Skeath and Carroll 1992; Stollewerk 2002). Apart from hexapods and spiders, expression of the two neurogenic genes Delta and Notch has been demonstrated in the neuroectoderm of several other arthropod taxa (e.g. Dove and Stollewerk 2003: *G. marginata*; Kadner and Stollewerk 2004: *L. forficatus*; Chipman and Stollewerk 2006: *S. maritima*; Eriksson

and Stollewerk 2010a,b: *E. kanangrensis*; Ungerer et al. 2012: *D. magna*). Delta represents one of the ligands of the trans-membrane receptor protein Notch. Upon binding of Delta, the intracellular domain of Notch splits off, migrates into the nucleus and activates different processes, one of them (Enhancer of split) repressing ASH transcription, which in turn decreases transcription of the extracellular ligand Delta (see also Skeath and Thor 2003; Stollewerk 2008). Via this 'canonical' pathway, Notch-signaling between directly adjacent ASH-positive cells leads to a process termed 'lateral inhibition' (e.g. Simpson 1990; Heitzler and Simpson 1991; Cau and Blader 2009), during which proneural expression is locally restricted to single cells (prospective NBs of hexapods). However, there is by now additional evidence of a cis-inhibitory pathway of the Notch receptor, which may help to explain adoption of neural fate of directly adjoining cells, as observed in the neuroectoderm of euchelicerates, myriapods and branchiopods (see Ungerer et al. 2012 for more details and discussion).

2.10.1.3. Snail and Prospero

Members of the Snail family as well as Prospero have been shown to be expressed during nervous system development of a spider (Stollewerk et al. 2003; Weller and Tautz 2003: *C. salei*), a crustacean (Ungerer et al. 2011a, 2012: *D. magna*) and some hexapods (e.g. Broadus and Doe 1995: *Schistocerca* sp.; Vaessin et al. 1991; Ip et al. 1994; Broadus and Doe 1995: *D. melanogaster*). In *C. salei*, both genes are thought to be involved in neuronal differentiation. *Cs*-Prospero is consistently expressed in differentiating neurons in pan-neural fashion (Weller and Tautz 2003; Döffinger and Stollewerk 2010), whereas *Cs*-Snail expression is more transient, predates *Cs*-Prospero expression and is found only in sub-sets of immigrating prospective neurons (Stollewerk et al. 2003; Weller and Tautz 2003). In *D. magna* and *D. melanogaster*, Snail is expressed in the asymmetrically dividing NBs (e.g. Ashraf and Ip 2001; Ungerer et al. 2011a, 2012). In *D. melanogaster*, it is involved in the asymmetric distribution of Prospero protein into the generated ganglion mother cells (e.g. Knoblich et al. 1995; Spana and Doe 1995). Within the latter cell type, Prospero migrates into the nucleus to inhibit NB transcription factors and activate neuronal differentiation genes (Doe 2008; Southall and Brand 2009).

2.10.2. Laboratory procedures

So far, the genome of *Pseudopallene* sp. is not sequenced. In order to obtain gene specific DIG-labeled RNA probes for *in-situ* hybridization, a series of laboratory procedures had to be performed, including RNA extraction from embryonic material, cDNA synthesis, construction of degenerate primers with subsequent PCRs, cloning of gene fragments, picking of clones, sequence analysis, synthesis of DIG-labeled RNA probe and RACE PCRs. A comprehensive description of these procedures is provided in Appendix C (volume 2).

2.10.3. Whole-mount *in-situ* hybridization (WISH)

Only methanol-stored, PFA/SW-fixed embryonic specimens were used for *in-situ* hybridizations. The following protocol was established in the group of Dr. Angelika Stollewerk (Queen Mary University, London), being adapted and modified from standard protocols used in this laboratory.

Day 1:	Rehydration	→ 70%, 50%, 30% MetOH/PBTw (each step at least 5 min)
		→ washing in PBTw (3x 5 min)
	Pre-treatments	→ exposure to Proteinase K solution (10 µg/ml in PBTw, 10 min, RT)
		→ washing in PBTw (2-3 quick changes)
		→ post-fixation in FA/PBTw (20-25 min, RT)
		→ washing in PBTw (3x 5 min)
	Pre-hybridization	→ transfer samples into small baskets inserted in 5-well plates containing PBTw
		→ replacement of PBTw with 500 µl Hyb buffer per well
		→ placement of 5-well plates in waterbath (overnight, 65°C)
Day 2:	Hybridization	→ addition of 1,5-2 µl of DIG labeled RNA probe to 500 µl Hyb buffer in 1,5 ml Eppendorf tube
		→ RNA denaturation by heating of mixture in heat block (10 min, 85°C)
		→ placement of tubes on ice, then pre-warming to 65°C in waterbath
		→ exchange of buffer in 5-well plates against pre-warmed probe/Hyb buffer mixture
		→ incubation of 5-well plates in waterbath (overnight, 65°C)
Day 3:	Washing	→ washing in Hyb wash buffer (1x 15 min, 1x 60 min, 65°C)
		→ washing in 2x SSC/0,1% Tween-20 (1x 15 min, 65°C)
		→ washing in 0,2x SSC/0,1% Tween-20 (3x 15 min, 65°C)
		→ washing in PBTw (at least 3x 5 min, RT, gentle shaking)
		→ transfer samples from baskets into embryo dishes
	Antibody application	→ blocking with Perkin Elmer blocking buffer (2x 60 min, RT, gentle shaking)
		→ 1:2000 dilution of AP-coupled anti-DIG antibody (mouse Fab fragments, ROCHE, #11093274910) in blocking buffer
		→ apply antibody solution to samples
		→ incubation (overnight, 4°C)
Day 4:	Washing	→ washing in PBTw (at least 5x 20 min, RT, gentle shaking)
		→ washing in AP buffer (at least 5x 5 min, RT, gentle shaking)

AP detection

→ exchange of AP buffer against freshly prepared NBT/BCIP staining buffer

→ incubation in the dark (RT, gentle shaking)

→ checking of staining in regular intervals (has to be tested for every probe individually, perhaps staining over 1 or 2 nights at 4°C necessary)

→ stopping of reaction by washing in PBTw (3x 5 min, RT, shaking)

→ gradual transfer of samples into absolute methanol

- 70%, 50%, 30% MetOH/PBTw (each step at least 5 min)
- 100% MetOH

→ storage at 4°C or -20°C until further use

2.10.4. Documentation of gene expression data

Specimens were counterstained with Sytox®Green and flat-prepped on microscopic slides. Z-stacks of images were taken manually with a ZEISS Axioskop 2 plus fluorescence microscope equipped with a ZEISS AxioCam HRc digital camera. For non-fluorescent images microscopic slides were underlain with a white background and two separate light sources were obliquely directed on the object from the sides. Z-stacks were merged to a single image using HELICONSOFT Helicon Focus software.

2.11. PRESENTATION OF DATA

Global contrast and brightness values of some of the images were adjusted using ADOBE Photoshop CS3. All figures were compiled in ADOBE Illustrator CS3. If not explicitly stated otherwise, anterior is (1) to the top in all ventral or dorsal aspects and in horizontal sections and (2) to the left in lateral aspects and sagittal sections. In anterior or posterior aspects and transversal sections, dorsal is to the top.

Apart from snapshots, short movies (avi-format) were generated in Imaris, using the 'Animation' mode. They were down-sized to compressed avi-files with the freeware FormatFactory (Version 2.96).

The figures as well as explanations of all movies are found in volume 2 of this thesis. The movie files and a digital version of all figures (pdf-file) can be found on the CD attached to volume 2.

3. RESULTS

3.1. EMBRYONIC MORPHOGENESIS OF *PSEUDOPALLENE* SP.

Embryonic morphogenesis of *Pseudopallene* sp. was investigated on fixed material to obtain a general overview of the major developmental events taking place from germ band stage up to the hatching of the larva. All descriptions are based on fixed material taken from egg-bearing males collected in their natural habitat. Hence, the established staging system relies exclusively on the morphological appearance of the embryos. Ten embryonic stages have been distinguished during embryonic morphogenesis of *Pseudopallene* sp. The descriptions in the next paragraphs have been designed to follow the developmental processes of specific embryonic sub-structures or sub-regions across the different stages, as opposed to a strictly stage-wise description of the complete embryo. However, the onset of characteristic developmental features and events and their further course are set in relation to all embryonic stages in Figure 4.

3.1.1. General aspects

The exact duration of embryonic development in *Pseudopallene* sp. remains to date unknown. Only fragmentary data for two egg batches cultured at 15°C over several days in the laboratory in Berlin are available. In one egg batch, development from zygote to 4-8-cell stage took 4 days. First signs of a loosely arranged germ disc were detectable after 9 days and a more compact germ disc/early germ band was visible after approximately 12 days. Subsequent to this, the embryos showed signs of misdevelopment. In the second egg batch, development from embryonic stage 7-8 up to the hatching larva lasted about 12 days, upon which the larvae misdeveloped as well. Based on this, embryonic development of *Pseudopallene* sp. can be assumed to take more than a month, its complete duration lying probably closer to two months.
During early embryonic development of *Pseudopallene* – up to the first stages described herein – the eggs show local deformations (e.g. Fig. 5D). These deformations are a consequence of the dense packing of eggs into batches by the male. The egg membrane is tightly fitted around the embryo and the narrow space left in between is filled with peri-embryonic liquid. After manual removal of the egg membrane from fixed specimens, traces of this liquid remain locally attached to the embryonic tissues and often cover details in SEM preparations, especially at cellular level (e.g. Fig. 6E). With the onset of embryonic cuticle secretion (ES 7 and later, Figs. 7; 8), the embryonic liquid is less problematic, but from this point on the developing cuticle conceals some of the morphogenetic changes. In ES 7, the cuticle is still delicate and resembles a locally wrinkled layer on the surface of SEM preparations (Fig. 7J,L). Soon afterwards, the entire embryo is completely covered by the embryonic cuticle, which is most strongly developed on the anterior head region (including the chelifore anlagen) and on the dorsal side of the egg (ES

8, Fig. 8B-D). Due to this thick coverage, even simple nuclear stains are often not successful in these regions of the embryo. During late embryonic development (ES 9 and 10) a second cuticle is secreted underneath the first one (Fig. 8M-O). This second cuticle represents that of post-embryonic stage 1 (Fig. 10), while the covering embryonic cuticle is molted simultaneously with the shedding of the egg membrane.

3.1.2. Shape and extension of the developing embryo

Embryonic development of *Pseudopallene* is characterized by the formation of a germ band that covers part of the ventral hemisphere of the egg and comprises small, densely packed cells. ES 1 represents a late germ band, which shows a characteristic '8'-like shape (Fig. 5A). Its margins are surrounded by a number of loosely arranged flattened extra-embryonic cells. The dorsal hemisphere is made up of large yolk-containing cells, the macromeres (Fig. 5E). One of the wide ends of the germ band will give rise to the future anterior head region (protocerebral region and cheliforal/deutocerebral segment). The narrow waist of the '8' represents the area from which the palpal and ovigeral segments originate. The cells of the opposite wide end of the '8' give rise to walking leg segments 1 and 2 and the hind body region. Hence, primordia of all future segments present in the hatching stage seem to be prefigured already on the late germ band. At this stage, nuclear stains provide no indications of a posterior growth zone in form of regionally concentrated cell divisions close to one end of the germ band. The lack of clear landmarks makes it difficult to decide in ES 1 which side of the germ band represents the anterior and which the posterior end. This becomes first unambiguously possible in the next stage (ES 2, Fig. 5B,C), when the primordia of the stomodeum and the chelifores are formed at the anterior end. Subsequently, the germ band expands just slightly and its 8-shaped outline remains recognizable (ES 3, Fig. 5G,H; ES 4, Fig. 6A,B). By contrast, the loose single-layered sheath of extra-embryonic cells that surrounds the germ band is spreading continuously from the ventral towards the dorsal hemisphere. It covers the entire ventral hemisphere around the germ band and begins to overgrow the dorsal side anteriorly in ES 3 (Fig. 5G,H), continuing to expand during ES 4 (Fig. 6D,F) and enclosing the dorsal hemisphere completely later on (ES 5). The exact fate of the yolk-containing macromeres has not been followed in detail in the present study. From ES 5 onwards, the 8-shaped outline of the embryo is lost, due to an ongoing lateral extension of the prospective palpal and ovigeral segments at the waist (Fig. 6K). With ongoing development, the embryo extends across the entire ventral hemisphere (ES 6, Fig. 7A,B,D) and continues to reach further dorsally (ES 7-10) – a process similar to the dorsal closure described for other arthropods. As a consequence, the area of loose extra-embryonic cells steadily diminishes. Only a dorso-median single-layered stripe of loosely arranged cells is still discernible after the hatching of post-embryonic stage 1 (PS 1, Fig. 10J). However, with the

applied techniques it remains ambiguous whether these cells are remnants of the extra-embryonic cell layer or rather have their origin in the dorsally growing embryonic tissue during dorsal closure.

3.1.3. Development of the stomodeum and the proboscis

The stomodeum is forming at the anterior end of the germ band. At the beginning of its formation, anti-tubulin labeling coupled to nuclear stains show a tubulin-positive, nuclei-free area surrounded by cells with apical nuclei (early ES 2, Fig. 5C). The tubulin signal relates to apically extending cell processes of flask-shaped immigrating cells with basally displaced nuclei (Movie 1). When first discernible, the stomodeum lumen appears as an antero-posteriorly elongated slit-like opening (ES 2, Fig. 5B,D,F). Soon after, this lumen takes the shape of an equilateral triangle with one of its corners pointing posteriorly (ES 3, Fig. 5H,J). Tubulin labeling conveys the impression of a sub-division of the directly surrounding ectodermal tissue into three regions, corresponding to the three sides of the triangular stomodeum (Fig. 5J). Thus, already before the actual outgrowing of the proboscis, a first indication of the later tripartite composition is observable. The proboscis anlage begins to grow out in ES 4. The stomodeum lumen is distinctly Y-shaped (Fig. 6A-C,E-G), being formed at the center of three surrounding cell populations (Fig. 6E,F). The positions of these cell populations correspond to the three future proboscis antimeres (i.e., an unpaired antero-dorsal one and a pair of bilaterally symmetric ventro-lateral ones). The elevation of the proboscis anlage is more pronounced in the two ventro-lateral parts, suggesting higher cell proliferation and growth rates in these regions. Also, the separation of the cell populations is more distinct between the two ventro-lateral cell populations. Slightly further advanced stages of proboscis differentiation show a more continuous and faintly demarcated ridge of cells that surrounds the three sub-units and starts to overgrow them (Fig. 6G; Movie 2; see also Movies 22-27). Consequently, the major part of the three early cell populations is displaced internally and forms the primordia of the prospective pharynx (ES 5, Fig. 6M). During ongoing development, the overgrowing ectodermal tissue retains weak signs of the underlying tripartition, in form of shallow distal indentations at the positions of the future antimere borders. As seen in the three earlier cell populations, the indentation at the posterior side is slightly more pronounced, forming a distinct notch (ES 5 and 6, Figs. 6M; 7F,G). During later embryonic development (ES 7) this notch becomes very conspicuous (Fig. 7M,N; Movie 3) and as a result of this, a transverse section through the distal-most portion the proboscis anlage of later stages is vaguely reminiscent of a horseshoe that surrounds the triangular mouth opening.

From ES 4 to 6, the proboscis anlage shifts from its anterior position in a postero-ventral direction. In the course of this process, cellular material positioned lateral to the proboscis

anlage is shifted further antero-laterally. Thus, a distinctly lobed anterior region, the pre-cheliforal lobe, is formed, reminiscent of the head lobe region of other arthropod groups. At first, the contra-lateral pre-cheliforal lobes are medially separated by a narrow stripe containing just few cells (ES 5, Fig. 6K), but later on both sides are medially fused (ES 6, Fig. 7E). As a second consequence of the proboscis shift, the proximal bases of the chelifore anlagen come to lie in a lateral position to the proboscis (see below).

3.1.4. Development of the chelifore

In ES 2, the primordium of the prospective chelifore is discernible in nuclear and tubulin stainings (Fig. 5B,C). It arises clearly postero-lateral to the stomodeum. Initially, it is not elevated from the germ band. Instead, the area of the chelifore primordium becomes separated from more medial cells by a semi-circular furrow, where cellular material starts to sink inwards. Soon after (late ES 2), the semi-circular chelifore anlage is more distinctly demarcated, its future distal pole facing medially (Fig. 5D,F). A thin ectodermal cell stripe separates it medially from its contra-lateral counterpart. The chelifore anlage continues to grow in a medial direction, thereby starting to cover the formerly separating ectodermal cell stripe and pressing it further into the embryo (ES 3, Fig. 5G,H,J). Eventually, the contra-lateral chelifore anlagen touch medially, whereupon their distal portions begin to flatten (ES 4, Fig. 6A-C,E-G). A constriction arises along the proximo-distal axis (p-d axis) of the developing appendage, marking the border between the chelifore's proximal podomere, the future scape, and its second one, the prospective palm (Fig. 6B,F). This constriction becomes more evident in the following stages, coupled with a further expansion of the distal limb bud portions (ES 5, Fig. 6K). A first tiny indentation at the distal tip indicates the onset of the differentiation of the prospective fixed chela finger (= outgrowth of the palm) and the third podomere, the movable chela finger (Fig. 6L). The anlage of the movable finger develops into a bulging round cell mass, which in ES 6 is about twice as massive as the one of the fixed finger (Fig. 7A,C,E). Subsequently, the chelifore attains its distinct external articulation (ES 7, Fig. 7J,K). The movable and fixed fingers of the chela start to taper distally, differentiating into the sharp tips of the hatching stage (ES 7 and later, Figs. 7J,K; 8B,J,M). At the inner margin of the fixed finger, a sub-terminal tiny outgrowth is developed (Figs. 7K; 8K). Beginning with ES 8, the chelifores are covered by the strongly developed embryonic cuticle. Manual removal of this cuticle in the pre-hatching ES 10 reveals the sclerotized tips of the larval chela (Fig. 8M,N). The movable finger bears a single terminal sickle-shaped tip, whereas the fixed finger possesses in addition to its terminal tip a smaller sub-terminal spine that corresponds to the earlier sub-terminal outgrowth (Fig. 8N).

Due to the postero-ventral shift of the proboscis from ES 4 to 6 (see above), the orientation of the p-d axis of the chelifore is changed. The proximal region of the appendage anlage is shifted

anteriorly and the future scape comes to lie lateral to the proboscis (Figs. 6L; 7E,F). As a consequence of this movement, the more distal portion of the chelifore is pointing postero-medially. This distal portion extends over the ventral side of the limbless palpal and ovigeral segment anlagen.

3.1.5. Development of the cheliforal glands

In ES 3, a small group of ectodermal cells immigrates interiorly at the lateral (i.e., future proximal) margin of the chelifore anlage, each of the cells turning flask-shaped during the process (Fig. 5I). These are the first cells contributing to the formation of the spinning gland in the scape of the chelifore. In ES 4, the number of immigrating cells has increased to more than a dozen (Fig. 6I). In the region of their immigration, a shallow depression has formed externally and nuclear stains show distinct 'holes' in these areas, indicating the lack of apical nuclei (Fig. 6B,C). This region is often surrounded by dividing cells (Fig. 6H). In tubulin-labeled specimens, a narrow central channel is visible between the apical processes of the flask-shaped cells (Fig. 6H). The cells move deeper into the scape and remain connected to the apical surface via a tubulin-positive narrow tube (ES 6, Fig. 7G). This tube continues distally into an external short process at the distal margin of the scape (first elevation in ES 5, more distinct in ES 6, Fig. 7D,G,H), the position of which is indicated in nuclear stains again by a conspicuous nuclei-free 'hole' (Fig. 7B). Soon after (ES 7), this spinning gland process bears a distal pore (Fig.7K) and from ES 9 on, the spinning gland is already functional. Thread-like secretions are frequently found to project from the pore of the process (Fig. 8G,K,N) and attaching to the interior of the egg membrane.
In ES 6, at the distal tip of the roundish movable finger anlage, massive immigration of cells is observed (Fig. 7H). These are the first cells of the prospective chela gland. Later on, the chela gland cells form a compact and conspicuous cluster that is connected via a central tube-like projection to the tip of the movable finger (ES 7, Fig. 7I,O). This immigration of cellular material from the distal tip of the movable finger might be one of the reasons for its external change from bulging-roundish to distally tapering, as described above. The chela gland is expanding further and it reaches well into the scape, as can be observed in nuclear stains (ES 8 and later stages, Fig. 8A,E,I). Up to the hatching of post-embryonic stage 1, an external pore relating to this gland was not detected.

3.1.6. Development of post-cheliforal appendages and the hind body region

In the first four embryonic stages described herein, no external signs of post-cheliforal appendage primordia are observable. Directly posterior to the cheliforal segment, the developing palpal and ovigeral segments do not exhibit any anlagen of limb buds during the entire embryonic development. Due to the morphogenetic shifts of proboscis and chelifores (see

above), the palpal and ovigeral regions are covered by the distal parts of the chelifore anlage from ES 5 onwards and the primordium of walking leg 1 seems to arise directly posterior to the chelifore. Initially, the anlagen of walking legs 1 and 2 are shallow but wide-stretching elevations (ES 6, Fig. 7B-D), but soon after they start bulging out more distinctly (ES 7, Fig. 7I,J,L). In lateral view of ES 7, the proximal base of walking leg 1 reaches already halfway towards the dorsal side (Fig. 7L). Beginning with ES 8, embryonic cuticle is covering the post-cheliforal regions of the embryo more strongly (Fig. 8). Nevertheless, it remains possible to distinguish the walking leg anlagen from the surrounding regions. Comparable to the early chelifore development, furrows begin to form at the median, anterior and posterior margins of the elevated limb bud areas (late ES 7, Fig. 7L; more distinct in ES 8, Fig. 8B,D), most likely as a result of cell proliferation and an inwards directed cell movement. These furrows continue to deepen and finally converge underneath the appendage anlagen, the walking legs being thus 'carved out' of the surrounding tissue. As in the chelifore, the appendages' future distal tips point medially and the proximal portion is positioned at the dorso-lateral side of the embryo. As a consequence of the deepening furrows, the yolk-filled entodermal regions that were lying directly below the former two-dimensional walking leg elevations are now enclosed in the proximal portion of the three-dimensional limb anlagen and form the primordia of the future midgut diverticula. Because of their yolk-content, the diverticula regions are less intensely labeled in nuclear stains when compared to the distal tips and outer margins of the leg anlagen (ES 8 and later stages, Fig. 8A,E,I). Nuclear stains of these stages show sometimes concentric rings at the walking leg tips (e.g. Fig. 8A). These relate to the further distal elongation of the legs, which leads to a compression and telescope-like infolding of the tissue due to space constraints in the tightly fitting egg membrane. With further development, the walking legs start to cover the ventro-medial ectodermal region until they finally touch the respective contra-lateral counterpart (ES 9, Fig. 8E,F). In the pre-hatching ES 10, the embryonic cuticle is not firmly attached to the embryo anymore (Fig. 8J-L) and the second cuticle (= cuticle of post-embryonic stage 1) is already formed underneath (Fig. 8M-O). The embryonic cuticle lies as a loose undivided sheath on top of the complete post-cheliforal region, having at no time enveloped the developing walking leg anlagen of earlier stages from all sides (in contrast to the chelifores). Underneath the embryonic cuticle, the distal ends of the walking legs are extremely compressed. They do not cross the midline of the embryo and are still folded in telescope-like fashion (Fig. 8M,O). Only after hatching, these appendage anlagen unfold completely (Fig. 10C,E).

The hind body region begins to bulge out in ES 6, in a postero-medial position to the anlagen of walking leg 2 (Fig. 7D). It remains still confluent with the more anterior ventral ectoderm for some time (see ES 8, Fig. 8A,B), but is distinctly demarcated from the surrounding tissue from

ES 9 onwards (Fig. 8E,F,I,M). At this stage, it has assumed a wedge-like shape. Its antero-ventrally directed pole resembles the posterior tip of developing trunk.

3.1.7. Paired segmental depressions related to nervous system development

Bilaterally symmetric pairs of depressions are formed along the ventro-medial ectoderm of the embryo. They are part of the neuroectoderm and relate to internalization processes of cells in the course of nervous system development, which will be described in detail in section 3.3.
The depressions start out very shallow, but deepen with ongoing development and in part remain even visible through the initially delicate embryonic cuticle. In the brain region of ES 5, a small pair of invaginations is found close to the midline region, anterior to the proboscis (Fig. 6J,M). This pre-proboscideal pair deepens into conspicuous pits (ES 6, Fig. 7E,F) and subsequently disappears without leaving any external traces (ES 7, Fig. 7M). In contrast to this, a pair of longer persisting, bilaterally symmetric depressions develops in (1) the pre-cheliforal lobes, (2) antero-medially to the chelifore (wedged between proboscis anlage and base of the chelifore), (3) in the palpal and (4) in the ovigeral segments (both covered by the distal chelifore portion) and medially to (5) the first and (6) the second pair of walking legs, respectively (Figs. 7A,B,E,I,J,M; 8B). Initial signs of these segmentally arranged depressions are occasionally discernible as early on as ES 4, but in the majority they are only clearly visible in nuclear stains and SEM preparations of ES 5 and the following stages. With the advancing differentiation of the embryonic cuticle in the anterior head region (ES 8) and the extension of the walking leg anlagen over the ventral side of the embryo (ES 9), an unhindered external view of these structures is made impossible.

3.2. Post-embryonic development of *Pseudopallene* sp.

Six post-embryonic stages plus a sub-adult stage could be distinguished in the collected post-embryonic material of *Pseudopallene* sp. The morphological differences of consecutive stages point to intermittent molts. The actual molting, however, was observed only between PS 1 and PS 2. A summary of post-embryonic morphogenesis, including an overview of all identified stages and their respective degree of differentiation of various external structures and body regions is presented in Figure 9.

3.2.1. Habitat and coloration of the post-embryonic stages

Hatching of PS 1 takes place simultaneously with molting of the embryonic cuticle. This stage is lecithotrophic, contains a copious amount of yellowish yolk and stays attached to the father's ovigers (Fig. 10A,B). At first, also PS 2 remains attached to the father's ovigers (Fig. 12A), but in contrast to PS 1, the majority of the yellow yolk has already been used up. Thus, PS 2 is more

transparent. This allows discerning some internal structures through the cuticle (Fig. 12B,C), the most conspicuous being the whitish mass of the CNS, comprising already the anlagen of all four walking leg ganglia. PS 2 is the oldest stage found on the ovigers and represents the stage leaving the father. All following stages, from PS 3 up to the sub-adults, are completely free-living and found clinging to the bryozoan colonies on which the adults prey. Most likely, these stages also feed on the bryozoans. The free-living post-embryonic specimens are less clear (Figs. 14A,D; 15A) and have a yellowish (sub-)cuticular pigmentation similar to the sub-adults and adults (Fig. 17A). This coloration hampers observation of internal structures *in vivo* and in fixed material under the stereo microscope. However, in living specimens, the slightly deeper colored orange midgut diverticula are frequently visible through the cuticle and seen to extend into the articulated walking legs (data not shown).

3.2.2. External body segmentation

The body of a newly hatched PS 1 is egg-shaped and lacks external segmentation lines (Fig. 10D,E). Inter-segmental constrictions are formed one at a time during each of the subsequent three molts. Accordingly, PS 2 shows only a single distinct constriction between the walking leg segments 1 and 2, which leads to the external delimitation of the anterior cephalosoma (Fig. 12E). In PS 4, the adult condition has been reached, being characterized by a distinct cephalosoma, the separate walking leg segments 2 and 3 and the posterior walking leg segment 4 from which the finger-like anal tubercle is projecting (Fig. 15C,D).

3.2.3. Ocular tubercle

PS 1 lacks eyes and shows no indication of the ocular tubercle at the antero-dorsal body pole (Fig. 10D,E). The ocular tubercle is first visible as a slight elevation in PS 2 (Fig. 12E). Laterally, elevations of the lateral sensory organs start to protrude, but pigmented eye cups are still missing, at least in specimens still attaching to the father (Fig. 12C). In PS 3 – the first completely free-living stage – the four pigmented eye cups are fully developed on a still rather shallow ocular tubercle with distinctly protruding lateral sensory organs (Fig. 14C,D). The ocular tubercle attains its more elevated shape in PS 4, being then positioned antero-dorsally on the cephalosoma (Fig. 15C,D). From this stage on, no further significant structural changes occur (see Figs. 16F).

3.2.4. Proboscis

Orientation: The orientation of the p-d axis of the proboscis is shifting during post-embryonic development. In PS 1, the proboscis is ventrally directed (Fig. 10C,E) and in PS 2 it bends slightly more postero-ventrally (Fig. 12D). From PS 3 to PS 6, the long proboscis points almost directly

posteriorly, running along the ventral side of the trunk (Figs. 14B; 15B; 16A,E,F). When the sub-adult stage is reached, it has shifted again slightly further anteriorly, resulting in its final postero-ventrally directed p-d axis.

Shape: In PS 1, the proboscis is cylindrical and bears distally a triangular mouth opening with a pronounced notch on the posterior margin (Fig. 10F). Thus, the distal-most portion of the proboscis retains the vaguely horseshoe-like shape of late embryonic stages (see 3.1.3.). After the molt to PS 2, the mouth opening is distinctly Y-shaped, it is surrounded by an elevated cuticular ridge with a very deep posterior constriction and two shallow antero-lateral ones, lying in line with the extending arms of the Y-shaped mouth (Fig. 12F). In the following stages, the proboscis base grows increasingly wider in comparison to its distal tip. In PS 3, the beginning tapering along the p-d axis remains almost imperceptible (Fig. 14E). In PS 4, however, the proboscis base has already reached twice the diameter of the tip (Fig. 15B,F) and in the following PS 5 and PS 6, it expands even further to almost threefold the tip's diameter (Fig. 16F). The actual tapering does not extend along the entire p-d axis, but is restricted to the proximal two thirds of the proboscis. The distal third of the proboscis resembles a slender cylindrical tube (Figs. 15B,F; 16F). The cuticular ridge surrounding the Y-shaped mouth is retained throughout these changes, but the previously pronounced indentations at the borders of the proboscis antimeres become increasingly less distinct from PS 3 onwards (Figs. 14E; 15F; 16G). In PS 6, a row of three inconspicuous pores on each of the three sides of the Y-shaped mouth is observable (Fig. 16G).

3.2.5. Chelifore and its associated glands

In all post-embryonic stages, the three-articled chelifore flanks the proboscis laterally. In PS 1, it is the only functional appendage. The latero-distal margin of the scape bears the short spinning gland process with a distal pore (Fig. 10H). The associated gland's thread-like secretions serve to attach the individual specimens to the egg matrix surrounding the father's ovigers. The fixed chela finger bears a strongly sclerotized terminal tip and a second, outwards positioned sub-terminal tip. The movable finger narrows into just one sclerotized tip that grips in between the latter two when the chela is closed (Fig. 10G). In PS 2, the scape is elongated in relation to the palm and reaches twice the length of the latter (Fig. 12D). The spinning gland process is still retained (Fig. 12F). From PS 3 on, the scape has almost three times the length of the palm and the spinning gland process is reduced (Fig. 14B,E). The palm has attained a characteristic trapezoid shape, widening from proximal to distal, and the movable finger is articulating at the palm's distal side. On the palm, setae with presumable sensory function become increasingly numerous with the number of post-embryonic molts (Figs. 14B,E; 15B,E; 16B,F; Movie 4).

From PS 2 to PS 6, the movable finger terminates in a peculiar corkscrew-like tip (Figs. 12D,G; 14E; 15E; 16F). At the end of a tube-like extension projecting from this curved tip, an external pore of the massive chela gland (see 3.1.5.) is located (Fig. 12G). In PS 2, the chela gland extends beyond the proximal border of the scape, its most proximal portion running laterally to the entodermal midgut diverticulum that reaches into the proximal portion of the chelifore (Fig.12H; Movie 4). The gland's extensions were not followed in later stages. Notably, a corresponding external pore is found at the tip of the fixed chela finger from PS 2 to PS 6 (Fig. 12G). However, neither a distinct connection of this pore to the copious chela gland, nor the presence of a second chela gland could be unambiguously ascertained.

3.2.6. Palp and oviger

In *Pseudopallene*, both sexes lack the palp and not even a primordial anlage of it is discernible during development. There is no indication of an oviger anlage during embryonic development (see 3.1.6.), first external signs of oviger development being detectable in PS 3. The primordium is a minute cuticular bulge at the ventral side of the trunk, just posterior to the insertion of the proboscis (Fig. 14F). In PS 4, this bulge has elongated into an unarticulated finger-like projection (Fig. 15A,F). After the next molt (PS 5), the oviger comprises six externally distinguishable podomeres and a poorly defined terminal claw (Fig. 16B,C). The uneven appearance of the distal-most sixth podomere is indicative of the ongoing internal development. This region was observed to bear distally one or few leaf-shaped cuticular outgrowths as first signs of the future strigilis. The terminal claw is distally equipped with a similar leaf-shaped cuticular outgrowth (Fig. 16C). In PS 6, the oviger is finally fully developed, comprising ten podomeres plus the terminal claw (Fig. 16H). The podomeres 6 to 10 arise most likely by sub-division of the sixth podomere of PS 5. The distal-most four podomeres form now the strigilis, each podomere being equipped with a row of spines resembling denticulate leafs. The margins of the terminal claw are distinctly denticulate, i.e., bearing a row of tiny cuticular pointed teeth (Fig. 16H).

3.2.7. Walking legs

In PS 1, the elongate anlagen of walking legs 1 and 2 show no external articulation (Fig. 10C,E). The cuticle fits the developing appendages just loosely, with locally more stretched and bumpy regions where underlying tissue of the developing walking legs presses against it. Distally, the limb anlagen grow more slender, but lack a sharp terminal claw. In SEM preparations of PS 1, the primordium of walking leg 3 is barely discernible as a slight elevation that is covered by wrinkled cuticle (Fig. 10I). However, in nuclear stains, it is recognizable as a small bud flanking the ventrally directed anal tubercle (Fig. 10J). Shortly before the molt from PS 1 to PS 2, the entire cuticle is more tautened, due to the pressure from the growing tissues underneath (Fig.

11A). In nuclear stains of such stages, an internal folding of the walking leg tissue due to spatial constraints is visible (Fig. 11F,G). After manual removal of the cuticle, the extreme compression is also visible in SEM preparations and it is evident that the differentiating proximal parts of the future walking legs (i.e., regions of coxae 1-3, femur and tibia 1) are interiorly curled into a compressed s-shape prior to the molt (Fig. 11H,I). Due to this, a direct correlation of regions along the externally visible p-d axis walking leg anlagen to future definite podomeres proves difficult in PS 1. Based on a combination of the SEM data and nuclear stains, only the distal-most portion of pre-molting PS 1 walking leg anlagen, being demarcated by a distinct external cuticular fold (Fig. 11A-D,F,H), can be securely identified as giving rise to the tarsus, propodus and terminal claw. The already sclerotized spines of the prospective propodus heel and terminal claw are pressed into the interior by the cuticle of PS 1 (Fig. 11H). During the molt from PS 1 to PS 2 the cuticle rips horizontally in anterior to posterior direction, usually starting at the base of the proboscis and the chelifore scapes (Fig. 11B-E). PS 2 emerges antero-dorsally from the exuvia, which remains in one piece, except for the old chelifore cuticle that (at first) stays attached to the chelifores (Fig. 11E). During and after the molt, walking legs 1 and 2 stretch dramatically and are now truly articulated. In contrast to PS 1, the cuticle of PS 2 is covered with bifurcating sensory setae (Fig. 11H; also briefly discernible in Movie 4). Walking leg 1 has already attained the adult number of nine podomeres (from proximal to distal: coxa1, coxa2, coxa3, femur, tibia1, tibia2, tarsus, propodus and terminal claw lacking auxiliary claws) (Figs. 12I; 13A). Walking leg 2 has only seven podomeres (Figs. 12J; 13B). These podomeres can be set into relation to the future adult ones, based on their shape and position along the p-d axis of the leg as well as some faint external lines that seem to correspond to internal sub-divisions. They represent (1) the three equally long coxae, (2) a transient podomere that will sub-divide into the future femur and tibia1, (3) tibia 2, (4) a podomere with close resemblance to the future propodus, which will proximally most likely give rise to the tarsus and (5) the terminal claw. The anlage of walking leg 3 of PS 2 is just an unarticulated limb bud that extends posteriorly and flanks the anal tubercle (Figs. 12D,E,J; 13B). From PS 3 to PS 5, this leg differentiation pattern is shifted posteriorly, in a stepwise fashion of one body segment per molt (Figs. 14G,H; 15G,H; 16D). Accordingly, PS 3 has a nine-articled walking leg 2, a seven-articled walking leg 3 and an unarticulated limb bud of walking leg 4. PS 5 is the first stage with four articulated walking legs possessing adult composition.

3.2.8. Anal tubercle (‘Abdomen’)

Orientation: From PS 1 to PS 3, the anal tubercle is directed ventrally and positioned in between the posterior-most walking leg anlagen of the respective stage (Figs. 10I,J; 12D,J; 14B,H). From PS 4 on, it projects horizontally, in line with the body axis (Figs. 15B,C; 16B).

Proctodeum and anal opening: PS 1 possesses still no anal opening and histological sections show that the proctodeum is formed during this stage (Fig. 10K). At the distal-most point of the hind body region, cells immigrate and establish contact with the still yolk-filled larval midgut. Nuclear stains distinctly show the basal displacement of nuclei at the point of the proctodeum formation (Fig. 10J). Externally, this region is only characterized by a shallow indentation of the cuticle (Fig. 10I). After the molt to PS 2, the slit-like cuticular fold at the position of the future anus is visible (Figs. 12J; 13B). However, in none of the investigated PS 2 specimens, the anal opening was observed to be distinctly open. Therefore, it cannot be excluded that it opens only after the next molt to PS 3, which has definitely started active feeding.

3.2.9. The sub-adult of *Pseudopallene constricta* n. sp.

The ocular tubercle of the sub-adult of *Pseudopallene constricta* n. sp. does not show any significant changes in comparison to PS 6 (Fig. 17E). The proximal two thirds of the massive proboscis are cylindrical, being set off from the more distal portion by a conspicuous constriction. The distal third of the proboscis shows a pronounced tapering, which leads to its cone-shape without the slender tube-like appearance of the preceding stages (Fig. 17A,B). The Y-shaped mouth at the tip of the proboscis lacks the surrounding unornamented cuticular ridge of the previous stages. Instead, each of its sides is flanked by three roundish papillae with a central pore (Fig. 17C,D). These papillae correspond in their position to the three minute pores observed on each side of the mouth in PS 6. They are placed within a field of small tube-like projections, some of which also bearing an opening at their distal pole (Fig. 17D). Apparently, these papillae and small tubes possess glandular function. The chelifore has undergone significant modifications. Its scape is sub-equal in length to the bulky palm and its distally projecting fixed finger (Fig. 17A,B). The movable finger has lost its slender corkscrew-like protrusion and is now more massive with a simple tapering distal tip (Fig. 17G), making the chela more suitable for gripping and crushing compared to the preceding stages. The chela tips are directed medially and positioned directly in front of the mouth opening (Fig. 17A,B,G). No pores of chela glands could be found at the tips. The oviger's structure has not changed significantly. It is folded underneath the ventral side of the trunk (Fig. 17G). Each of the strigilis podomeres still bears a single row of leaf-like spines (Fig. 17H). The three coxae of the walking legs have further differentiated, coxa 2 being now distinctly longer than coxa 1 and coxa 3 (Fig. 17G). Indicative of the sub-adult stage, the coxae 2 of all walking legs still lack gonopores on their ventral side (Fig. 17F).

3.3. Embryonic neurogenesis of the VNC of *Pseudopallene* sp.

3.3.1. General aspects

Tubulin immunolabeling was used to assess changes in cell shapes and cell arrangements and the general cellular composition in the ventral ectoderm and the pre-cheliforal lobe (see 3.5.) (Fig. 18 for overview). In the post-cheliforal ventral ectoderm, the neuromeres of the palpal and ovigeral segments and the ones of the walking leg segments 1 and 2 develop during embryogenesis and form ganglion anlagen. Only a weak antero-posterior developmental gradient is observable between these ventral neuromeres, their segment primordia having been early on prefigured in the germ band of ES 2 (see 3.1.). In late embryonic stages (ES 8 and later), first neurogenic processes posterior to the anlage of walking leg ganglion 2 are detectable, relating to the neuromere of walking leg segment 3. It is wedged between the posterior portions of the limb buds of walking leg pair 2 and the developing hind body region and is at hatching still significantly less differentiated than the more anterior ones. The general processes of early neurogenesis were found to be the same in all ventral neuromeres. However, morphogenetic movements within the germ band impede detailed investigation on some neuromeres at least for part of embryonic development. This holds in particular for the ones of the palpal and ovigeral segments, which are increasingly covered by the distal portions of the elongating and anteriorly shifting chelifore anlagen from ES 4 onwards (see 3.1.). Due to this, observations on these neuromeres in flat-preparations of germ bands required prior removal of the tightly fitting chelifore anlagen, which proved difficult without damage to the directly underlying palpal and ovigeral ectoderm. The medial ectodermal region of walking leg segments 1 and 2 is freely visible for the major part of embryogenesis, being only in the latest stages (ES 9 and ES 10) covered by the walking leg anlagen. However, with the outgrowth of the latter (ES 5 and later), the neurogenic area starts to become considerably compacted along the medio-lateral axis. This event is accompanied by the beginning formation of paired central depressions in the corresponding neuromeres, which is generally more pronounced in walking leg segment 2. For these reasons, the neuromere of walking leg 1 was considered the most promising candidate for the analysis of spatial patterns in terms of easy accessibility and extent of morphogenetic rearrangements. Giving rise to the first unfused separate ganglion of the prospective VNC, it was furthermore chosen for nucleus measurements (see 3.3.7.) and cell counts (see 3.3.8.).

3.3.2. Early neurogenesis in the ventral neuroectoderm (ES 2 – ES 4)

3.3.2.1. Basally directed nucleus migration and stratification of the ventral neuroectoderm

In early ES 2, the post-cheliforal ectoderm of the germ band is single-layered, consisting predominantly of columnar cells with apical nuclei that are elongated in apico-basal direction. It

is underlain by a single layer of flattened and loosely distributed entodermal cells (Fig. 19C,C'; Movies 5; 6). At this stage, unequivocal recognition of the ectodermal region from which the nervous system is going to originate – the ventral neuroectoderm (VNE) – is still difficult.

In slightly older embryos (ES 2-3), the apico-basal structure of the medial ectodermal region has started to change. The nuclei of some columnar cells have been displaced in a basal direction, representing the first step of a cell's immigration from the apical epithelium into the interior of the embryo. The apical portion of these cells narrows slightly during and after the nucleus migration and tubulin labeling shows their cortex more intensely stained than in the surrounding cells (Fig. 19A-C'; Movies 5; 6). Some of the cells are found singly within the ectoderm, others are encountered in small clusters or in row-like arrangements (Fig. 19A'-C'). However, neither a bilaterally symmetric pattern, nor a repeated spatial arrangement along the antero-posterior axis (a-p axis) was detected at this stage. This early cell immigration initiates the apico-basal thickening of the medial ectoderm region and represents the onset of neurogenic cell internalization.

During ES 3, basal displacement of nuclei is encountered in an increasing number of cells in the VNE, due to which the latter assumes a distinctly stratified structure. This allows more reliable demarcation of the VNE from the more lateral ectodermal regions. The nuclei in the VNE are at first arranged in two and later in three apico-basal levels (late ES 3, Fig. 19F,F'). From late ES 3 onwards, it becomes possible to delimit segmental neuromeres along the a-p axis, based on the arrangement of cell nuclei, especially in more basal sections of the ectoderm (Fig. 19E). Yet, none of the immigrating cells has so far detached from the apical ectoderm. Analyses of complete series of optical sections indicate them to either possess an only slightly narrowed apical cell cortex or to be of flask-like shape, the apical cell cortex having constricted to a slender, intensely tubulin-stained process (Fig. 19D-F'). Typically, the basally displaced nuclei of the immigrating neurogenic cells remain slightly elongated in apico-basal direction.

3.3.2.2. Formation of localized cell internalization sites in the VNE

In late ES 3, flask-shaped cells start to be more clearly arranged in small groups, often directly adjacent to other cells with basally displaced nucleus (Figs. 19D-F'). With ongoing development towards ES 4, the groups of flask-shaped immigrating cells become distinctly defined with their apically bundled cell processes (Figs. 18; 19I,I'). In histological sections, however, such localized cell internalization areas (CISs) can be detected only with difficulties and hence unreliably (Fig. 20). In the VNE of tubulin-labeled embryos, the bundled cell processes show typically strong signal, allowing identification of CISs in horizontal sections based on more intensely labeled apical spots among the less intensely stained cortical cytoskeleton of surrounding cells (Figs. 19G,G'; 21; 22; Movies 7; 8). Notably, the degree of convergence of the apical cell processes

within a CIS varies between different embryos and also within the same specimen. Due to this, the tubulin-positive spots are in some cases small and distinct, in others bigger and more diffuse (Figs. 21; 22; Movies 9-11). In the latter instance, investigation of transverse optical sections was used to confirm the existence of a CIS. Typically for *Pseudopallene*, CISs are positioned in close proximity to each other, being often separated only by a single cell with apical nucleus (Figs. 20A; 21A,C; 22). Where clearly assessable, CISs in ES 4 were observed to include four to six, rarely also more flask-shaped cells. CISs are often surrounded by cells whose nuclei are basally displaced and appear to be still in the initial processes of cell immigration (Fig. 19F,F',I). With further development, these cells will most likely be included in the CIS they adjoin. Therefore, it seems unlikely that CISs are characterized by fixed and constant cell numbers. Rather, the latter appear to be changing over time due to continuing recruitment of surrounding cellular material.

3.3.2.3. CIS pattern in walking leg neuromere 1 of ES 4

It was not possible to recognize a specific temporal sequence in the formation of CISs, which includes a lack of distinguishable temporal 'waves' or 'pulses' in the emergence of CIS sub-sets. In ES 4, when the CISs are most clearly delimitable, a largely bilaterally symmetric arrangement in stereotypic positions is observable in the VNE of walking leg segment 1 (Fig. 22; Movies 9-11; see also Fig. 21A for largely bilaterally symmetric arrangement in ovigeral neuromere): Four CISs can be identified in the antero-lateral region of each hemi-neuromere in an arrangement resembling the corners of a trapezoid (anterior-most solid arrowheads in Fig. 22). Posterior to them, two very closely adjoining CISs are found (posterior-most solid arrowheads in Fig. 22). They are positioned at the lateral margin of a primordial apical depression that starts to develop in the VNE during ES 4 due to ongoing formation of flask-shaped cells. This primordial depression encompasses at first the postero-medial regions of the hemi-neuromere and will grow to encompass its entire central region up to ES 5 (see 3.3.2.4.). Within it, four to five additional CISs in characteristic positions are frequently but not consistently delimitable (open arrowheads in Fig. 22). It remains unclear whether the occasional failure to detect some of these CISs relates to a lack of resolution or whether some of the CISs are only forming during ES 4 within regions of previously less concentrated cell immigration. In total, the number of detectable CISs per walking leg hemi-neuromere 1 in ES 4 ranges accordingly between six and eleven, in dependence of the observed embryo. Due to this comparatively low number it was refrained from assigning the identified CISs into a row and column pattern.

3.3.2.4. Cell divisions in the VNE during early neurogenesis (ES 2 – ES 4)

Throughout embryonic morphogenesis, cell proliferation of neuronal precursors (NPs) is encountered in the post-cheliforal VNE. In general, no strictly bilaterally symmetric division pattern of identifiable cells is observable at any time. From ES 2 to ES 4, cell divisions are almost

exclusively positioned apically in the VNE and do not show any traces of morphological asymmetry (Fig. 23; see also Figs. 19D,G; 20; 21A,B). Early on, they lie within the single-layered neuroepithelium. Following the beginning stratification of the VNE, dividing NPs are positioned in the apical-most nucleus level. As shown by the orientation of the spindle apparatus (visualized via tubulin labeling) and the arrangement either of chromosomes during metaphase and anaphase or of the newly forming nuclei during telophase, the great majority of divisions have tangential orientation, i.e., occur in parallel to the surface of the VNE (Fig. 23; Movie 6; see also Figs. 19D,G; 20; 21A,B). As a consequence, the two resulting daughter cells will at least initially lie side by side within the apical layer. No indications of a predominant antero-posterior or medio-lateral orientation of the divisions are assessable (Fig. 21A; 23). Occasionally, deviations from a perfect tangential orientation of meta- and anaphase profiles occur, especially in ES 4, when the regular arrangement of cells with apical nucleus is increasingly disintegrating due to continuing cell immigration around the formed CISs. However, the oblique inclination of such divisions is almost always closer to a tangential rather than a radial orientation (just two mitoses in all investigated embryos showed a radial orientation). Therefore, it is likely to represent a phenomenon related to the adjacent cell movements instead of an intrinsic change of the division mode. NPs divide regularly but not exclusively in direct vicinity of cell internalization areas (Figs. 21A; 22A,A',C,C',D; 23E,F). Based on the transient expansion of a dividing NP and an accompanying shift of the surrounding tissue, slight spatial distortions of the CIS pattern in the closely packed hemi-neuromeres are occasionally observable (e.g. Fig. 22D). Very few divisions take place in a more basal position within the VNE. Only in two instances, a dividing NP was found within a CIS (Fig. 23F), whereas in all other cases, the CISs lacked mitotic activity completely. Hence, the great majority of immigrating neurogenic cells in the VNE of *Pseudopallene* do not appear to be NPs but rather post-mitotic immature ganglion cells (GCs).

3.3.3. Neurogenesis of the VNC of advanced embryonic stages (ES 5 – ES 10)

3.3.3.1. Formation of segmental depressions and first detachment of cells from the VNE

As a consequence of the ongoing basal displacement of nuclei in the remaining apical cells of the VNE, the surface in the center of each hemi-neuromere becomes gradually nucleus-free. Only cell processes remain in apical position, while the basally displaced nuclei lie in a compact multi-layered mass, representing the hemi-ganglion anlage (Fig. 24A-C). The nucleus-free apical region forms a shallow depression that gradually deepens into a conspicuous invagination towards the end of embryonic development. In the walking leg neuromeres, this development begins already in late ES 4 (Figs. 22; 23E) and is more pronounced from ES 5 onwards (Fig. 24). In the palpal and ovigeral neuromeres, it takes place slightly later, during ES 6 (see Movies 25-

27). Each central depression of a walking leg segment is laterally flanked by the increasingly protruding limb bud (Figs. 24F; 26B,C,E,F; see 3.1.6). Within the nuclei-free depressions, distinct local CISs are in general not traceable anymore amongst the ubiquitous apical cell processes (Figs. 18; 24; 25; 29A,B). Occasionally, more closely attaching bundles of apical cell processes are still encountered in ES 5 and ES 6, yet unambiguous assignment of these processes to distinct groups of basally displaced nuclei was only in exceptions possible (Fig. 24F). The great majority of future GCs are still attached to the apical surface, but first detached cells with apico-basally flattened nuclei are found at the basal side of the hemi-ganglion anlagen of ES 5 (Fig. 24C). Up to ES 6, a loose basal-most layer of detached GCs has formed, especially at the anterior side of the growing hemi-ganglion anlagen (Figs. 24F; 25B). Amongst the apical-most cells, NPs with slightly enlarged nuclei can be detected in comparison to the more basally located cells (Fig. 24F; 28A-C; see also 3.3.4.).

3.3.3.2. Scattered NPs in basal regions of the ganglion anlagen

In the walking leg neuromeres of ES 5 and ES 6, proliferating NPs are still found apically, close to the margins of the nuclei-free depressions as well as in its center (Figs. 24A,A',D,D'; 25). Optically, the PH3-labeled condensing/condensed chromosomes of dividing NPs and their surrounding cytoplasm stand out conspicuously against the nuclei-free cell processes that form the apical surface of the depression (Movie 12). From ES 6 on, not only the apical cells, but also one or two basally detached cells are encountered in division in PH3-labeled specimens (Figs. 24E; 25B). Accordingly, not all of the cells in hemi-ganglion anlagen have already become post-mitotic prior to or during immigration. Instead, some still represent NPs that divide at least once more before terminal differentiation into neurons or glial cells. Although the exact ratio of post-mitotic GCs and NPs amongst the immigrating cells remains unclear, the comparably low number of observed mitoses in the basal-most cell layers may be taken as evidence for a predominance of the GCs. Also in later embryonic stages (ES 8 – ES 10), single divisions are occasionally found far basally in the ganglion anlagen (Fig. 26H).

3.3.3.3. Emergence of big apical cells – a stem cell-like dividing NP type

From ES 7 to ES 10, transversal sections through ventral hemi-ganglion anlagen reveal three rough apico-basal cell regions, which become increasingly distinct with ongoing development.
Within the apical-most region that lines the central depression, big cells of spindle- or flask-shape with an ellipsoid nucleus are encountered, being intermingled with some smaller cells (Figs. 26, 27; Movies 14; 15). In nuclear counterstains, the ellipsoid nucleus of the big cells is generally less intensely labeled than the more lateral ectodermal cells and the more basal nuclei within the hemi-ganglion anlage (Fig. 26, 28). Similarly, they are slightly less stained by methylene blue-azur II in histological sections (Fig. 27). These cells slowly increase in size

towards the end of embryonic development (see 3.3.4.). Furthermore, they are frequently found in division (Figs. 26A,B,C,D,E,G,H,I; 27B-D; Movies 12; 14; 15), more than half of the labeled mitoses in the ganglion anlagen being encountered in the apical-most cell region. The marked proliferation activity at the apical side of the hemi-ganglion anlagen strongly indicates the big cells to represent morphologically distinct NPs that provide additional GC material. Notably, these big NPs divide asymmetrically. The intensely PH3-labeled early phases of mitosis (pro-, meta- and early anaphase) do not show any easily detectable deviations of a symmetric cell division (Figs. 27D; 28). However, morphological asymmetry becomes apparent in the weakly PH3-labeled late stages of mitosis, which are accompanied by the onset of cytokinesis (Figs. 28; 29; Movies 12-15). One of the forming daughter cells is bigger, with a more voluminous cytoplasmatic compartment, in which center the chromatin of the newly forming nucleus has often a curved shape (e.g. Fig. 29C,C'). The other daughter cell is smaller, the chromatin of its newly forming nucleus appears in late stages frequently rectangular and is positioned closely attached to the cell side the spindle pole has occupied during early mitosis (e.g. Fig. 29C,C'). The chromatin of the forming nucleus in the smaller daughter cell is often more intensely labeled than the chromatin of the bigger daughter cell. Apical asymmetric divisions can be observed throughout the remainder of embryonic development (Fig. 28). Especially in ES 6 and ES 7, when the central invaginations are not yet as deep, the orientation of the divisions was found to be tangential or slightly oblique (Fig. 28A-F; Movies 12-14). In case of an oblique orientation, the bigger daughter cell in general occupies the more apical position. With increasing medio-lateral compression and deepening of the central invaginations, determination of division orientations becomes more difficult since all cells and their arrangement become distorted by compaction. Especially at the margins of the depressions, strongly oblique and apparently radial orientations are detectable in late stages (e.g. Fig. 28G, but see discussion 4.2.2.3.). The asymmetric division mode of the big NPs can account for the mixed composition of the apical-most cell region in the hemi-ganglion anlagen, smaller cells lying interspersed between the big NPs (see 3.3.3.4.).

Cell counts of the big NPs in walking leg segment 1 provide no evidence for dramatic fluctuations in their numbers across the late embryonic stages. A range of typically 30 to 40 big NPs per hemi-ganglion anlage was counted from late ES 6 to ES 10. This range may be slightly biased since the gradual size differences between big NPs as well as interspersed smaller apical cells impede in some instances unambiguous morphological identification of cells with intermediate size. However, this does not affect the phenomenon of a similar range as such. In conjunction with the asymmetric division mode, the comparatively constant range of big NPs over time suggests that this cell type divide at least temporarily in a stem cell-like manner, i.e., a division would lead to their self-renewal and a smaller daughter cell. For that reason they are henceforth termed stem cell-like dividing neuronal precursors (SCNPs).

In late embryonic stages (ES 8 – ES 10), the apical cell region with the SCNPs shows first signs of a partial separation from the underlying hemi-ganglion anlage (e.g. Fig. 26D'; Movie 15).

3.3.3.4. Sub-apical intermediate NPs

A sub-apical layer of smaller cells with more intensely labeled nuclei is located basal to the rough apical SCNP layer (Figs. 26; 27; 28). Frequently, some of these cells appear to be in the process of immigration, being flask-shaped with apically attaching cell processes that extend between the apical SCNPs (Fig. 26B,C,E,F,H,I). From ES 7 onwards, mitoses are encountered in this sub-apical cell region, i.e., directly below or close to the apical SCNPs (Figs. 26A',B,C,D',E,F,G',H,I; 27A,C), but still apical to the main mass of differentiating GCs. Compared to the mitosis profiles of the SCNPs, the ones encountered in sub-apical position are smaller and no signs of morphological asymmetry could be detected. Accordingly, the sub-apical cell layer comprises an additional type of intermediate neuronal precursor (INP). The sub-apical INP divisions are in particular located in the anterior and posterior portions of the hemi-neuromeres (Fig. 26A',D',G'), prefiguring regions that will later on establish the main connections between the apical neuromere portions with the proliferating SCNPs and the underlying differentiating hemi-ganglion anlagen proper (see 3.4.). Given the observed cell arrangements, it seems plausible that the sub-apical INPs represent smaller daughter cells of the SCNPs, having immigrated prior to their own proliferation activity. However, with the available data this relationship cannot be proven directly.

3.3.3.5. Basal hemi-ganglion anlage with post-mitotic differentiating GCs

The basal-most layer in a hemi-ganglion anlage comprises detached immature GCs and already differentiating neurons (e.g. Fig. 26A'',D'',G''). This layer is continuously gaining in size during ongoing development and constitutes in late embryonic stages the main portion of the hemi-ganglion anlagen in terms of volume and cell number (Fig. 26 B,C,E,F,H,I, see also Fig. 31). At its apical side, especially in the anterior and posterior regions of the hemi-ganglion anlage, it is confluent with the sub-apical INP cell layer. From late ES 6 onwards, axonogenesis is detectable in the ventral hemi-ganglion anlagen (Figs. 26A'',D'',G''; 27B; see 3.6.).

3.3.4. Nucleus measurements in hemi-neuromeres of walking leg segment 1

In order to assess whether (1) the immigrating GCs in early stages differ in size from the apical ones and whether (2) the observed size differences between the big SCNPs and the other cell types go back to an actual size increase of the former or a size decrease of the latter, nuclei in the neuromere of walking leg segment 1 were measured throughout development. In the early stages (ES 2-3 to ES 4-5), a distinction was made between cells with apical nucleus and flask-

shaped cells with basally displaced nucleus (see yellow and dark red squares in Fig. 30). With the formation of the central depression from ES 5 onwards, only the apical-most nuclei of the enlarging NPs were measured (red circles in Fig. 30).

In early stages of neurogenesis (ES 2-3 to ES 4-5), no marked differences in nucleus size are observable between the apical cells and the immigrating ones. The mean nucleus extension ranges between eleven and twelve micrometers in both cell categories (Fig. 30). Accordingly, cell size does not distinguish the early immigrating GCs (being later on organized in CISs) from the neuroectodermal cells that retain an apical nucleus. If any size change occurs over this developmental period, it is a slight decrease in nucleus extension in both cell categories from ES 3-4 to ES 4-5. As soon as the central depression has formed (dashed line A in Fig. 30), the measurements indicate a slight increase in the nucleus extensions of the neuroectodermal cells (= enlarging SCNPs) that line it. From ES 6 onwards, a mean value exceeding twelve micrometer is observed for the first time, which continues to increase until the end of embryonic development (Fig. 30). In ES 9-10, the elongated nucleus axis of the apical SCNPs has reached a mean of almost 16 micrometers. However, in this late stage, the apical nuclei were found to be compressed and distorted along their medio-lateral axis, due to the lateral pressure exerted by the massively developed walking leg anlagen. For this reason, it has to be assumed that the measured mean overestimates the actual mean of uncompressed nuclei (which have been measured in the other stages). A value between 14 and 15 micrometers – as encountered in the directly preceding and following stages – would appear therefore a more reliable estimate. Irrespective of this issue, the nucleus measurements clearly corroborate the previously noted enlargement of the SCNPs (see 3.3.3.3.). As the absolute values of the standard deviations demonstrate, individual nucleus sizes of the apical big cells vary to a certain extent (Fig. 30). Due to this, cases occur, in which it is not unequivocally possible to decide whether a given cell represents a small SCNP or rather a big representative of the interspersed immigrating cells. Accordingly, nucleus size alone is not always sufficient for reliable cell type identification across the entire development.

3.3.5. Ventral midline region and origin of the ventral epidermis

3.3.5.1. Stratification and compaction of the ventral midline region during early neurogenesis

In ES 2 and early ES 3, the ventral midline region (VMR) is two to three cells wide, being enclosed on both sides by the VNE. The VMR of these early stages is generally characterized by the apical position of almost all its nuclei, even after immigration of cells has started in the more lateral VNE regions (Fig. 19A-C'; Movies 5; 6). With ongoing development towards ES 4, the medio-lateral extensions of the VMR are gradually diminishing, its cells being wedged between the more distinctly delimitable anlagen of the hemi-neuromeres (Fig. 19D-I'). During this period,

nuclei have become basally displaced in the VMR, leading to its stratified structure. Occasionally, VMR stratification remains slightly less pronounced than in the laterally adjoining hemi-neuromeres (Figs. 19F,F',I,I'; 21B,D,F; Movies 9-11). Within the VMR, no unpaired median CISs are recognizable. Yet, it is closely flanked by bilaterally paired, medial CISs from the adjacent hemi-neuromeres in some regions (Fig. 21A,C). Mitoses are encountered apically and where observed to exhibit tangential orientations (Figs. 21A,C,G; 22B'; Movie 10).

3.3.5.2. Cell death and further VMR compaction during formation of hemi-ganglion anlagen

From late ES 3 to late ES 4, nuclear counterstains show numerous small condensed bodies of inhomogeneously stained chromatin amongst the cells of the medio-laterally compressed VMR. Similar structures are found at the margins of the developing hemi-neuromeres, occasionally also basally within the latter (Figs. 19E,F,H,I; 22A',C',D; Movies 9-11). Such chromatin-rich bodies are neither labeled by the PH3 antibody, nor do they exhibit the typical tubulin-positive labeling of the surrounding cytoskeleton. Due to this, they are inferred to represent pycnotic bodies related to cell death. So far, it remains unresolved whether the cell death is spontaneous or developmentally programmed, since the tested apoptosis marker (α cleaved caspase 3) failed to give positive results in any of the fixed material at any stage. However, a similar distribution pattern of pycnotic bodies was repeatedly observed between ES 3 and ES 4, which speaks in favor of non-random, programmed cell death. From ES 5 onwards, the two hemi-neuromeres of a segment are virtually touching at the midline (Figs. 24C,F; 25A), resembling more clearly the compact anlagen of the prospective hemi-ganglia. The nuclei of the remaining VMR cells are found either directly apically (see 3.3.5.3.) or basally between the hemi-ganglia (Fig. 24C,F; Movies 12; 14; 15), their number having been apparently further reduced slightly prior to and during the median approach of the latter. From ES 6 to ES 10, some of the midline cells are encountered wedged between the growing hemi-ganglion anlagen, being medio-laterally compressed and often unpaired (Figs. 24F; 26A',D',H,F;I; e.g. Movie 15). Judging from their position and flattened appearance, they have differentiated into glial cells. Furthermore, some of the basal-most cells show distinct cytoskeletal tubulin labeling and are in close contact with the first transversally extending axonal growth cones of the segmental commissures during ES 7 (Fig. 26A''; see also 3.6.3.2.). Also in later stages, several intensely tubulin-stained medial cells directly adjoin the embryonic commissures (e.g. Figs. 26D'',G''; 36D), presumably going back to the few basal-most displaced cells of the early embryonic VMR.

3.3.5.3. Origin of the ventral epidermal cells

The few remaining apical cells of the VMR differentiate into epidermis cells. From ES 5 onwards, they start to become increasingly distinct from the enlarging SCNPs and interspersed flask-shaped cells within the central depressions (Fig. 24A',C,D'; Movies 14; 15) The VMR-

derived median epidermal cells are arranged in an irregular longitudinal 'row' that is one to two cells wide (Fig. 26A,B,C,D,E,F,G,I; see also Fig. 22E). The ectodermal cells lying directly anterior, lateral and posterior to each apical depression adopt epidermal fate as well. As soon as the central depression has formed in the hemi-segments, these cell regions start to become morphologically recognizable based on a generally intense staining of their oval, comparatively small nuclei (Fig. 24A',D'). At the depression's peripheral rim, unequivocal distinction of prospective neural and epidermal cells is occasionally still difficult on morphological grounds alone, since some of the neural cells at this border (NPs or immature GCs) show initially a less flask-shaped appearance. With the ongoing enlargement of the SCNPs and the depression's deepening into a prominent invagination, delineation of the flanking epidermis regions becomes easier (Figs. 26A,D,G; 28A-G,I). The smaller epidermis cells come to lie on top of the peripheral-most SCNPs of the hemi-ganglion anlagen. Thus, the entire rim of the deepened invagination is apically covered by the prospective epidermis in late embryonic stages. The apical closure of the epidermis takes place during post-embryonic development only (see 3.4.3.4.)

3.3.6. Cell counts in hemi-neuromeres of walking leg segment 1

Complete cell counts in hemi-neuromeres of the walking leg segment 1 were conducted in all relevant stages of embryonic development (see Movie 20 for general principle of cell count). The obtained cell numbers were used to elucidate (1) for how long new cellular material is added to the nervous system and (2) whether a significant increase of cell numbers can be assessed during any of the developmental phases. Up to ES 7, hemi-neuromere counts were conducted on at least two specimens of each developmental stage, with the exception of ES 4-5 and ES 5, each being represented by a single specimen only. In early embryonic stages (ES 2-3 to ES 4-5), cells with apical nucleus and cells with basally displaced nucleus were distinguished (see yellow versus dark red coloration in Fig. 31A-C), in order to obtain an estimator for the number of immigrating cells during this developmental period. Due to ambiguities regarding the exact extensions of the VNE in ES 2-3 and in part still in ES 3, cell counts in these early stages were performed to represent *maximal* estimators, i.e., cells at a hemi-neuromere's borders (including the VMR) were included rather than excluded from the count. With the formation of the central depression, only small apical cells positioned at the latter's rim were distinguished from SCNPs, flask-shaped immigrating cells and basally detached GCs and INPs (see green versus dark red coloration in Fig. 31A,D,E). This was done to account for immature and thus morphologically difficult to distinguish epidermis cells. Therefore, the cell portion depicted in green potentially (but not necessarily) resembles a mixture of epidermal and neural cell types. The cell number in the dark red category represents accordingly a minimal estimator of neural cell types (SCNPs,

INPs, GCs) in the different stages. The exact numbers of the cell counts are listed in Appendix D (volume 2).

In late ES 2 (ES 2-3), slightly less than 140 cells were counted in the hemi-neuromere of walking leg segment 1. From ES 3 onwards, the overall cell number in this hemi-neuromere has increased to approximately 200 and was found to stay in a remarkably similar range up to ES 6, where the overall number barely passes 200. This is surprising, in light of the ongoing cell divisions in the apical VNE throughout these developmental stages. The comparably high number of cells in ES 3 compared to the following stages can be the result of ambiguity of cell identity at the margins of the hemi-neuromere, the performed maximal cell counts being likely to include also several non-VNE cells. However, also from ES 4 onwards no marked trend towards an overall increase of cell numbers is detectable. A possible explanation for this finding can be the occurrence of cell death within or at the margins of the hemi-neuromere, especially close to and within the VMR. Comparison of the ratio and absolute numbers of apical cells on the one hand and immigrating GCs on the other shows a gradual but continuous increase of the latter from ES 2-3 up to ES 6 (Fig. 31A) coupled to a decrease of the apical cells. Starting with approximately 60 cells with basal nucleus in ES 2-3, the number of the immigrating cells increases slowly to about 170 in ES 6. In line with the morphological processes on early neurogenesis, this speaks in support of a gradual sequential immigration of ectodermal cells in slowly and transiently formed CISs rather than any partially synchronized immigration in distinct temporal ‘waves’ or ‘pulses’.

Beginning with late ES 6 and continuing throughout the rest of embryonic development, a marked increase of cell numbers is observable in the analyzed hemi-ganglion anlagen (Fig. 31A,D,E). In ES 8, the overall cell number has already more than doubled in comparison to ES 6 (~450 versus ~200 cells, respectively) and eventually approaches 550 cells in a pre-hatching late embryo. The small amount of apical rim cells that could not be assigned with absolute certainty to epidermal or neural fate decreases during later stages, because the apical hemi-neuromere portion comprising the SCNPs becomes more distinctly set off from the surrounding smaller epidermis cells. Notably, the marked increase of cell numbers from late ES 6 onwards shows a temporal correlation to the emergence of the SCNPs. Given the high number of mitoses observed in the SCNPs and sub-apical INPs during this developmental phase, the cell count analyses further underline the important role both cell types play in the generation of GCs.

3.4. Post-embryonic neurogenesis of the VNC of *Pseudopallene* sp.

3.4.1. Antero-posterior developmental gradient in the VNC

During post-embryonic development, new segmental ganglia are added posteriorly to the still incomplete VNC of the hatching larva (Fig. 32). In line with the pronounced anamorphic development of the posterior walking leg segments (see 3.2.) a distinct developmental gradient along the a-p axis is encountered between the early differentiated 'embryonic' ganglion anlagen of walking legs 1 and 2 and the 'post-embryonic' ganglion anlagen of walking legs 3 and 4 (Fig. 32). Neurogenesis of these 'post-embryonic' segmental ganglion anlagen starts prior to the protrusion of the corresponding limb buds and they represent morphologically delimitable units already before external demarcation of the corresponding segment borders has set in. Accordingly, the onset of early neurogenesis relating to walking leg neuromere 3 is already detectable during late embryogenesis, whereas the first limb bud primordium of walking leg 3 is only apparent in PS 1 (see 3.2.). While the ganglion anlage of walking leg segment 3 becomes morphologically recognizable during PS 1 and represents a well-defined entity already after the molt to PS 2 (Fig. 32), the external segment border between walking leg segments 2 and 3 is only differentiated in the following PS 3. A similar sequence of development is characteristic for the components of walking leg segment 4.

3.4.2. Cell counts during post-embryonic development

All segmental ganglia of the VNC – including the 'embryonic' ones – exhibit a constant increase in overall size throughout post-embryonic development. In theory, different processes can lead to ganglion size increase, including (1) differentiation and growth of the ganglionic neuropil, (2) size increase of all or some neuronal somata, (3) addition of new cell material into the ganglia, or (4) a combination of these three factors. To test whether new cells are added to the early developed 'embryonic' ganglia and thereby whether neurogenesis is persisting into the post-embryonic phase, nuclei counts were performed. In continuation of the embryonic analyses, nuclei in hemi-ganglia of walking leg segment 1 were counted in early and late PS1 as well as in PS 2 and PS 6 (Fig. 31; Movie 20). The results unequivocally demonstrate a considerable increase in GC numbers during post-embryonic development, their number per hemi-ganglion having more than tripled from less than 600 in a pre-hatching ES 9-10 to approximately 1900 in PS 6. Accordingly, ongoing neurogenesis is confirmed as one factor contributing to post-embryonic ganglion growth.

3.4.3. Neurogenesis in post-embryonic stage 1

3.4.3.1. Formation of ventral ectodermal pits

In early PS 1, the ventrally protruding chelifores and the unarticulated limb buds of walking leg 1 and 2 impede an unhindered view at the ventral ectoderm (see 3.2.). Following manual dissection of these limbs, a cuticular cover of the ventral ectoderm is visible, which is only loosely attached to the underlying tissue (at least in SEM preparations, Fig. 33A). Underneath the cuticle, the pronounced apical depression characteristic for each 'embryonic' hemi-ganglion anlage of the VNC (pa-2wl) in late embryonic stages (see 3.3.5.) has further invaginated to form a deep pit with a clearly defined, sharp apical rim (Figs. 33C-E; 34A,D-F; Movie 16). Due to the a-p developmental gradient, the hemi-ganglion anlagen of walking leg segment 3 still shows only slight apical depressions (Figs. 34G; 35H). The cuticle regions covering the ventral pits frequently exhibit a corresponding inwards directed depression (Fig. 33B).

3.4.3.2. Ganglion anlagen proper and nascent apical cell clusters

In early PS 1, the ganglion anlagen of the VNC represent compact cell agglomerations that are positioned directly ventral to the still yolk-filled midgut (Fig. 34A). Up to walking leg ganglion 2, the differentiating neuropil core of each hemi-ganglion anlage is clearly recognizable in its dorsal half (Figs. 34A,C-F; 37). The somata of the neurons contributing to the neuropil form a cortex around the latter. The minimal thickness of this cortex is found at the dorsal side, where the neuropil is only partially covered by one or maximally two soma layers. Positioned apically, i.e., at the ventral side of each hemi-ganglion anlage, the big SCNPs first encountered during the second phase of embryonic neurogenesis are persisting and line the interior of the deeply invaginated pits (Fig. 34A,C-F; 37; Movie 16) that are apically encircled by distinctly smaller future epidermis cells. During PS 1, the apical portion of the hemi-ganglion anlage encompassing the deep pit starts to resemble a morphologically distinct entity (Figs. 34D-F; 36B,D). Initially, this 'nascent' apical cell cluster remains still attached to the apical surface and stays anteriorly and posteriorly confluent with the basal portion of the hemi-ganglion anlage. The latter contains the differentiating neurons and represents the prospective hemi-ganglion proper. With ongoing development, a distinct separation line (presumably formed by the original basal lamina of the neuroectoderm) between the nascent apical cluster and the underlying future hemi-ganglion proper is easily recognizable in transverse histological sections (Fig. 34D-F; see also Movie 16 for IHC data), both sub-structures being sometimes even slightly set off from each other (Fig. 34D). Along this separation line, some scattered pycnotic bodies are observable (Fig. 34A,F), which might point to an involvement of apoptosis in the separation process.

3.4.3.3. Cell proliferation in nascent apical cell clusters and connecting cell streams

Nuclei measurements of the SCNPs lining the deep invaginations in the nascent apical cell clusters of early PS 1 show them to be of a size comparable to late embryonic stages (Fig. 30). In walking leg segment 1, their number per nascent cluster lies in the same range of 30 to 40 cells typical for late embryonic development. In further agreement, considerable mitotic activity is found in the apical portions of the hemi-ganglion anlagen (Fig. 35A; Movie 16), which is to a large part attributable to divisions of the SCNPs within the nascent clusters (Figs. 35D-G; 36; 37), but also to sub-apical divisions of smaller INPs. The latter divisions are mostly encountered in the anterior and posterior regions where the cells of nascent apical cluster and the prospective hemi-ganglion proper are still confluent (Figs. 35F,G; 36B,D; 37A,D; Movie 16). Since cell numbers within the hemi-ganglion proper increase during this developmental phase, the persisting anterior and posterior connecting regions represent most likely cell streams along which apically generated cell material moves basally. In advanced cell division stages of the apical SCNPs signs of asymmetry are still recognizable, whereas such asymmetries were not encountered in the sub-apical divisions (Fig. 37A,C,D). Up to this point, the start of post-embryonic development is not accompanied by any significant changes of the neurogenic processes within the ventral ganglion anlagen.

3.4.3.4. Detachment of apical cell clusters and formation of defined cell streams

In late PS 1, the ventral ectoderm of walking leg segment 3 exhibits still merely a pair of shallow apical depressions (Fig. 35H). Contrasting to this, the ventral ectoderm extending from the palpal to the walking leg 2 segments shows either only paired tiny ‘holes’ (e.g. palpal segment, Fig. 35B,D) or no signs of the previous deep invaginations any longer (ovigeral – walking leg 2 segment, Fig. 35B,E-G). This is due to the proceeding internalization and detachment of the apical cell clusters from the prospective epidermal cell layer. The cells that have been lining the invagination of each nascent apical cell cluster in early PS 1 approach each other centrally during the detachment process, leading at first to a narrowing of the apical opening and eventually to its complete closure. As a consequence of these cell movements, a small cavity is formed in the center of each cluster, the originally apical poles of the cells being oriented internally, i.e., towards the central cavity (Figs. 35E-G; 36E,G; Movie 17). Initially, the small epidermal cells that have been encircling the invagination’s apical rim follow the centrally directed movement but are not incorporated into the internally detaching cluster. Instead, they remain in apical position and form a continuous thin epidermal layer as soon as the apical opening has been closed (Figs. 35D-G; 36F,H; Movie 17). Accordingly, the detachment of the apical clusters results in the final and complete spatial separation of cells with neural and epidermal fate. Notably, the internalization of the ganglion anlagen does not seem to be

characterized by a 'proper' active overgrowing by the future ventral epidermis. Rather, it appears to be more passive, being driven by the steady approach of the apical poles of the cells in the apical clusters of the hemi-ganglion anlagen.
Compared to early PS 1, the anterior and posterior confluent cell regions connecting apical cluster and corresponding hemi-ganglion anlage proper gradually begin to represent more defined streams (Fig. 36E',G'; Movie 17). Each stream is characterized by intense tubulin labeling and comprises several cells within its diameter.

3.4.3.5. Decreasing cell size and reduced mitotic activity in apical cluster-stream-system

In late PS 1, the apical cell clusters still comprise bigger SCNPs with weakly labeled nuclei, interspersed with smaller cells with more brightly stained nuclei (Fig. 36E,G; Movie 17). The majority of cells are of spindle- to flask-shaped appearance, extending cell processes towards the central cavity of a cluster. Notably, nuclei measurements in the apical clusters of walking leg ganglion 1 indicate a slight decrease in the size of the apical SCNPs compared to the preceding stage (Fig. 30). This decrease appears to be accompanied by reduced mitotic activity in very late PS 1 (Fig. 35B). Mitoses are found in the cluster-stream-systems, going back either to the bigger SCNPs within the clusters, or alternatively to smaller, more sub-apical cells that lie often in the clusters' periphery, close to the origin of the anterior and posterior cell streams or within the cell streams themselves (Figs. 35D-G; 36; Movie 17).

3.4.4. Neurogenesis in post-embryonic stage 2

3.4.4.1. The VNC of post-embryonic stage 2

During the post-embryonic development of *Pseudopallene*, PS 2 shows most clearly the considerable a-p developmental gradient between the anterior 'embryonic' ganglia (seg – 2wlg) and the more posterior 'post-embryonic' ganglia (3&4wlg). Three different developmental states of the segmental ganglion anlagen can be observed within a single specimen of PS 2 (Fig. 38A).
The 'embryonic' ganglia have gained in overall size and are less compressed than in the preceding stages. Their respective ganglionic neuropils have increased markedly, occupying by now a major part of the dorsal half of each ganglion (Fig. 38A-D,G; Movie 18). From PS 2 onwards, the limbs innervated by walking leg ganglia 1 and 2 are articulated and functional (see 3.2.). In correlation to this, the paired apical clusters of all 'embryonic' ganglia have completely detached from the epidermis (Figs. 38A-D; 39C; Movie 18), representing compact roundish to ellipsoid cell agglomerations at the ventral side of the latter (Fig. 39D). In part, they are distinctly separated from the epidermis by longitudinal muscles (Figs. 38A,C; 39C; Movie 18). In contrast to this, the anlagen of the 'post-embryonic' walking leg ganglia 3 and 4 are significantly less differentiated, a developmental gradient being apparent even between the two.

The anlage of walking leg ganglion 3 is already characterized by nascent apical cell clusters that have as yet not separated from the epidermis (Figs. 38A,E; 39D; 40G). The one of walking leg ganglion 4 represents only a spatially restricted ventral accumulation of cells, the nuclei of which being arranged in one to two apico-basal levels (Figs. 38F; 40H). Typical for early stages of neurogenesis, the neurogenic cells are in part flask-shaped, mitoses are found apically and no morphologically distinct NP types can be identified as yet (Fig. 40H). In terms of size, the observable a-p gradient of the apical cell clusters is directly opposite to the underlying ganglia/ganglion anlagen proper, anterior clusters being slightly smaller and more compact than more posterior ones (Fig. 39D; see also 3.4.6.).

3.4.4.2. Sensory and glandular structures of the ventral epidermis and their (non-)relation to the apical cluster-stream-system

In contrast to the preceding PS 1, the cuticle of the actively moving PS 2 is equipped with numerous bifurcating setae (see 3.2.) and tiny slit-like glands (see e.g. Movie 4). Some of these structures are also covering the ventral side of the trunk, in the regions overlying the ganglia/ganglion anlagen of the VNC (Fig. 39A,B). Neither in histological sections, nor in analyses of complete stacks of optical sections with Imaris a connection between the detached apical clusters of the 'embryonic' ganglia and the epidermal sensory or glandular structures could be detected (Fig. 39C). Rather, innervation of the sensory setae is accomplished via delicate peripheral nerve branches running within or directly underneath the loose cellular network of the epidermis (data not shown). Hence, no indications for a direct involvement of the apical cluster-stream-system in the processing of sensory setae's input could be found and any role of the clusters in external secretion of the slit-like glands is here excluded.

3.4.4.3. Disappearance of big SCNPs in apical cell clusters

The only mitoses in the anterior VNC of PS 2 are encountered in the apical cluster-stream-system. (Fig. 40A,C-F; Movies 18; 21). Based on the developmental snapshots obtained by PH3 labeling, mitotic activity seems to have further decreased. Some clusters do not exhibit any mitotic profiles, in others one to two mitoses are detectable, but only very rarely more than that were detected (Fig. 40A,C-F). Although some differences in cell sizes and nuclear staining intensity are still observable within a cluster, these are by far not as significant as in the preceding stages (Fig. 40C-F; Movies 18; 21). Nuclei measurements demonstrate that the cells in the clusters have further decreased in size and fall with a mean of 10 to 11 micrometers even below the value measured for the immigrating neurogenic cells during early embryonic neurogenesis (Fig. 30). Hence, based morphology alone, SCNPs are not distinguishable anymore in the anterior cell clusters of the VNC, whereas they are still easily identifiable in the nascent apical cluster of the more posterior anlage of walking leg ganglion 3 (Figs. 38E; 40G). It could

not be unequivocally resolved whether the SCNP type has completely ceased to exist in the anterior clusters (i.e., has either undergone apoptosis or terminal division) or is only not traceable any longer due to its size decrease and the limitations of the applied methods. The observed mitoses prove that at least some of the cluster cells are not (yet) post-mitotic, but unambiguous indications of asymmetric divisions were not detected. Compared to PS 1, the anterior and posterior streams of each cluster have further diminished in diameter, this process following again an a-p developmental gradient, being more pronounced in the more anterior segmental ganglia (Figs. 38B-D,G; 40C-F; Movies 18; 21).

3.4.5. Neurogenesis in post-embryonic stages 3 to 6, the sub-adult and the adult

3.4.5.1. The VNC from PS 3 to adult

In the two post-embryonic stages following PS 2, the 'post-embryonic' segmental ganglia gain on the more anterior ones in terms of overall size, cell number and neuronal differentiation. In PS 4, all four walking leg ganglia eventually exhibit a corresponding level of development (Fig. 32). Posterior to walking leg ganglion 4, a pair of transient, small posterior ganglion anlagen is encountered in PS 3 and PS 4 (Fig. 32, see also 3.4.7. and Fig. 59).

From PS 3 to PS 6, the walking leg ganglia of adjoining segments are touching each other (Fig. 32), but stay anatomically completely separated by their well-developed neural sheaths. In the following sub-adult (Fig. 32) and adult stages (not shown), such a close spatial proximity is only retained between the sub-esophageal ganglion and walking leg ganglion 1. The more posterior ganglia are distinctly separated and inter-connected by paired longitudinal connectives that lack a cortex of neuronal somata but contain elongated, flattened nuclei of glial cells that ensheath separate axon bundles within the connectives (not shown).

Up to the adult, the ganglia of the VNC show a considerable increase of the volume of the ganglionic neuropil (Fig. 42A,F,K). At the same time, also the number of GCs is significantly growing (at least up to PS 6), as evidenced by the cell counts performed for the hemi-ganglia of walking leg segment 1 (see 3.4.2. and Fig. 31).

3.4.5.2. Persisting low mitotic activity in apical cluster-stream-systems

The apical cell clusters persist as roundish to ellipsoid structures on the ventral side of the ganglia from PS 3 to PS 6 (Figs. 41; 42A-E; Movie 19), but often assume a more antero-posteriorly elongated shape in the sub-adult and adult stages (Fig. 42F,H-J,K,M-O). They are separated from the ganglia by the well-developed ganglionic neural sheath (Fig. 42). The only connections of a cluster into the interior of the respective ganglion are the anterior and posterior streams, which penetrate the neural sheath (Figs. 41; 42C-E,H-J,M-O; Movie 19) and have continued to decrease in diameter. Already in PS 3 they represent in all ventral ganglia –

except for the slightly less developed walking leg ganglion 4 – just tubulin-positive fibrous strands (Fig. 41A,B; Movie 19). Cluster cells situated close to one of the cell streams are typically characterized by elongated nuclei (Fig. 41D-H,I,J) that are sometimes found to extend into the respective narrow stream (Fig. 41I). This is suggestive of continuing GC/NP migration into the underlying ganglion. Along the apico-basal extension of the cell streams, only few cells with elongated, often intensely stained nucleus are found (Fig. 41D,F,J; Movie 19). Compared to the early post-embryonic stages 1 and 2, even fewer mitoses occur in the VNC. These are exclusively restricted to the apical cluster-stream-systems (Figs. 41; 42C,J; Movie 19). Frequently, cluster-stream-systems do not show any mitotic profiles. Judging from the nucleus measurements, the cell size within the clusters has further decreased, mean nucleus size never exceeding 10 micrometers (Fig. 30).

3.4.6. Cell numbers in the apical clusters during post-embryonic development

From PS 2 to the adult stage, the number of cells per apical cluster was determined for each ventral ganglion/ganglion anlage (see Movie 20). Since PS 5 specimens were extremely scarce in the collected material, this post-embryonic stage had to be excluded from the analysis. Due to the compact shape and well-defined borders of the apical clusters, cell numbers could be reliably counted in almost all ventral ganglia/ganglion anlagen of the included stages. This excludes only the anlagen of walking leg ganglion 3 and 4 in PS 2, which are not yet showing detached and clearly demarcated apical clusters. Two main trends can be extracted from the obtained results (Fig. 43, more descriptive statistics listed in Appendix E, volume 2).

(1) In specimens of earlier post-embryonic stages (PS 2 – PS 4), the clusters of more posterior ganglia/ganglion anlagen generally comprise more cells than the anterior ones. Accordingly, the apical clusters are bigger in the more posterior ganglia/ganglion anlagen, which are less developed. This intra-individual antero-posterior trend is more pronounced in the earlier stages (PS 2 and PS 3) and gradually subsides with the diminishing developmental differences between the ‘embryonic’ and ‘post-embryonic’ ventral ganglia.

(2) With ongoing development, a gradual intra-segmental decrease in cell numbers per cluster is detectable. Starting out with more than 50 cells (minimum) per cluster, this number constantly diminishes towards 40 or less in the adult.

This demonstrates that the cell divisions in the apical cluster-stream-systems do not result in a lasting increase of cell numbers within the clusters themselves. Since no systematic occurrence of pycnotic bodies (as indicators for cell death) was observed within the clusters, it can be concluded that some cells leave the latter during the post-embryonic phase. In light of the simultaneous cell number increase in the completely ensheathed ventral ganglia (Fig. 31), these

findings lend additional support to the inferred direction of cell movement from apical clusters into the underlying ganglia. Based on all available evidence, the apical cluster-stream-systems are here therefore identified as the source of GC material during the post-embryonic phase. Although identification of different cell types within the clusters could not be accomplished, the observed cell divisions indicate the presence of at least one type of NP. Based on the persistence of the cluster-stream-system throughout post-embryonic development into adulthood, it remains at least feasible that this presently unidentified NP type possesses self-renewing properties.

3.4.7. Glomerulus-like neuropils in the VNC ganglia of *Pseudopallene* sp.

In histological sections of *Pseudopallene* adults and less distinctly also in PS 6, a scattered clustered arrangement of glomerulus-like neuropils (GNs) was identified ventro-laterally in each walking leg ganglion (Figs. 42C,D,M-O; 44B-F,I-L). At least some of the GNs appear to be of ellipsoid shape or even distinctly medio-laterally elongated (Fig. 44D-F). Similar but less voluminous neuropilar structures were encountered in the sub-esophageal ganglion (Fig. 44G,H), being herein preliminarily interpreted as GNs as well. However, given the current data amount and quality, this latter interpretation awaits confirmation by additional studies. A detailed description of the exact arrangement, number, shape and architecture of the GNs lies beyond the scope of the present work and should be focus of separate investigations. The detection of segmentally arranged GNs as characteristic primary centers in the olfactory pathway indicates separate olfactory input into the VNC ganglia. Notably, the apical cluster-stream-systems and the GNs show close spatial vicinity in the in the walking leg ganglia (Figs. 42C,D,M-O; 44B,C,E,F) and presumably also in the palpal and ovigeral neuromeres.

3.5. Neurogenesis of the pre-cheliforal lobe of *Pseudopallene* sp. and formation of the brain anlage

3.5.1. Morphogenetic movements of the pre-cheliforal lobe

In early germ band stages (ES 2 to ES 4), the pre-cheliforal lobe of each body half is positioned lateral to the stomodeum/outgrowing proboscis anlage and anterior to the gradually forming post-stomodeal limb bud of the chelifore. With the onset of the posteriorly directed shift of the proboscis anlage during late ES 4, the entire pre-cheliforal lobe starts to assume a more anterior position in the germ band, being accompanied by the proximal portion of the chelifore anlage at its posterior margin. In ES 6, the major morphogenetic rearrangements at the anterior pole of the germ band have been concluded, the anterior portion of the pre-cheliforal lobe has medially fused with its contra-lateral counterpart anterior to the proboscis and the chelifore base is located lateral to the latter (see 3.1.4. and Fig. 78)

3.5.2. Early neurogenesis in the pre-cheliforal lobe of *Pseudopallene* sp.

The developmental processes of early neurogenesis in the pre-cheliforal lobe are very similar to the ones observed during neurogenesis of the VNC. The ectoderm starts out single-layered, consisting of columnar cells with apical nuclei (Fig. 45A-B'). It is underlain by a loose network of embryonic entodermal cells that enclose the yolk (Fig. 45B,B',D,D'). In early ES 2, simultaneously to the first cell immigration that initiates stomodeum formation, some of the columnar ectodermal cells of the pre-cheliforal lobe show basally displaced nuclei (Fig. 45A''-B'). With ongoing development towards ES 3 (Fig. 45C-D'), the number of basally displaced nuclei has increased (Fig. 45C''), due to which the ectoderm has locally assumed a stratified structure with two apico-basal nuclei levels (Fig. 45D'). Single flask-shaped cells are encountered within the ectoderm (Fig. 45D,D'), but morphologically distinct CISs are still lacking (see Figs. 18; 45C for lack of intensely tubulin-labeled spots). In late ES 3, first indications of nascent CISs become apparent in the distinctly stratified ectoderm with two apico-basal nuclei levels. However, based on tubulin labeling, unequivocal identification of the primordial CISs within the tightly packed cells remains difficult at this stage (Fig. 45E-F'). In ES 4, CISs have become more distinct, being readily identifiable in tubulin-labeled embryos due to the strong staining of the apically converging cell processes (Fig. 46A,A'; Movie 22). From this point onwards, they remain clearly distinguishable for a longer developmental time span than in the VNC, some of them being still identifiable in ES 6 (Movies 23-26).

During the early processes of neurogenesis, cell proliferation is to the great majority encountered apically (Fig. 45A,A',C,C',E,E'), the divisions being oriented tangentially (Fig. 45 A',C',D,D',E') but without predominant direction within the plane of the ectoderm and without signs of asymmetry. Only exceptionally mitoses occur in sub-apical position (Fig. 45E'',F').

3.5.3. Spatial arrangement of CISs in the pre-cheliforal lobe (ES 4 – ES 6)

In ES 4, the CISs of the pre-cheliforal lobe comprise few cells (~4-6, see Fig. 47A'-B') and could be partially mapped during the following stages (Fig. 46). Notably, in ES 4, the CISs exhibit still different degrees of distinctness, some being still in a nascent state. This indicates a temporal sequence of their formation. However, with the available amount of successfully processed specimens a reliable reconstruction of a temporal order could not be achieved. The schematic drawings in Figure 46 show CIS patterns based on the correspondences observed in embryos of the same stage and in closely following stages, each spot representing a single CIS. In addition to those CISs depicted therein, some smaller and less consistently observed ones were occasionally detected within single specimens. Due to their inconsistent presence, they were omitted in the generalized schemes. Identified CISs are color-coded, whereby certain sub-groups have been labeled identically. This coloration has been applied (1) to facilitate description of

identified CIS patterns and (2) to indicate the inclusion of CISs in the same invaginating sub-regions during subsequent brain formation (see 3.5.4.). It does not imply any direct genealogical relationships between CISs. A black spot stands for a CIS that could not be unequivocally assigned to any of the other sub-groups in the stage in question.

The maximal number of CISs within the pre-cheliforal lobe of *Pseudopallene* sp. was observed from late ES 4 to late ES 5, more than twenty being identifiable during this developmental period (Fig. 46C-H). Amongst these CISs, five regional sub-groups and a single unpaired CIS were distinguished in the overall pattern.

3.5.4. Formation of the brain anlage

From late ES 4 onwards, the anlage of each brain hemisphere is formed via basal GC detachment from the CISs and by invagination and internal detachment of bigger sub-areas of the pre-cheliforal lobe. The latter are here termed the pre-proboscideal pit, the antero-lateral depression and the central depression, their development being separately treated in the following sections.

3.5.4.1. Antero-medial CISs and pre-proboscideal pit – the antero-dorsal part of the brain primordium

In ES 4, an antero-medial sub-group of five to six CISs (red spots in Fig. 46) is located antero-lateral to the proboscis anlage in the pre-cheliforal lobe. Within this sub-group, the three medial-most CISs are well-defined and readily identifiable up to late ES 5 based on their characteristic arrangement in the corners of a triangle (red arrowheads in Fig. 46), with one of the corners pointing anteriorly. Lateral to these, three additional but generally smaller CISs are encountered, being initially roughly arranged in a longitudinal line, which is subsequently distorted due to morphogenetic movements and the local invagination process setting in during late ES 4. In ES 5, a small invagination has formed in the center of the ectodermal area demarcated by the antero-medial CISs, growing deeper and more pronounced in ES 6 (Figs. 46E';F,G',H,I',J; 47E,F,G,H,I,J'; Movies 23-26). This invagination resembles the pre-proboscideal pit (see also 3.1.7.). It includes more and more cellular material from its margins, as evidenced by the step-wise incorporation of the antero-medial CISs, which remain recognizable while still apical (Fig. 46E',F,G',H) and in part even after inclusion into the invagination (Fig. 47G'). During the invagination process of the pre-proboscideal pit, the basally displaced regions largely retain their apico-basal structure, being two to three nuclei layers thick (Fig. 47D,F,H,J'). In late ES 6, the lumen of the deep pit has already significantly diminished. Its walls are closely approached and leave only a small central canal (Fig. 48A',B; Movie 27), which is surrounded by a cluster of internalized cells (Fig. 48B). Surrounding the tiny apical opening of the canal, smaller prospective epidermal cells are arranged (Fig. 48A',B). In ES 7, complete detachment of the cell

cluster from the apical surface has taken place. The internalized cells are positioned anterior to the pharynx and close to the midline region (Fig. 48A'',C'') and extend far basally into the embryo. Due to a dorsal flexure of the anterior neuraxis in relation to the body axis during late embryology, this position will in the hatching stage translate into the posterior to postero-dorsal side of the brain in relation to the body axis. The early invagination of ectodermal cell material in the pre-proboscideal pit may represent one of the driving factors for the morphogenetic shifts in the pre-cheliforal lobe. The continuous displacement of cellular material into the interior results in a diminishing apical area in the antero-medial region of the lobe and thus presumably further amplifies the effect of the posteriorly shifting proboscis anlage by 'dragging' lateral tissue regions in a medial direction.

During the invagination process, divisions are encountered at the pit's margins (Fig. 47C,E,I) and also in the invaginated regions (Fig. 47E',F), predominantly in apical position (in relation to the apico-basal stratification of the ectoderm). From late ES 5 onwards, some scattered NP mitoses are observable in far basal position, at the posterior or medial side of the invaginating cell cluster (Figs. 47G', 48A''). In this region, first cells have dissociated from the cluster. In ES 6, they have become more numerous (Fig. 47I') and axonogenesis has been initiated, leading to the formation of a primordial pre-oral commissure posterior to the pre-proboscideal cell cluster (see 3.6.2.). An increasing number of neurons differentiate in this part of the brain anlage in the following embryonic and early post-embryonic stages (ES 7 to PS 2) and a basally extending lobed brain hemisphere is formed. Notably, an antero-medial agglomeration of cells with typically stronger cytoskeletal tubulin labeling remains distinguishable far basally, at the antero-dorsal side of the growing brain hemisphere (posterior related to the body axis, Figs. 48E',E''G; 49; 50B',B''; 51; Movie 29). These cells show indications of being organized in smaller sub-clusters (Fig. 51B-B''). Similar to the SCNPs of the VNC, some of these antero-medial basal cells are bigger than the surrounding ones, being often characterized by a less intense nuclear counterstain (Figs. 48E'-G; 50B',B''; Movie 29) and a lighter methylene blue-azure II staining in histological sections (Figs. 34A; 49A-B'). Cell proliferation takes place in this region during late embryogenesis and early post-embryonic development (Figs. 48E',E''; 49A-C; 50B';B''; 51; Movie 29) and some asymmetric divisions could be observed up to PS 1 (e.g. Fig. 49B') as well as smaller and not directly apical ones (Fig. 49A,A',C).

Based on the developmental sequence and the observed cell division characteristics, it is concluded that some of the cells that are internalized in the pre-proboscideal pit differentiate into morphologically distinct SCNPs after dissociation from the apical ectoderm. Occupying a position anterior and slightly dorsal to the forming brain neuropil, these cells generate further cellular material during early post-embryonic development. However, in contrast to the VNC, no cell proliferation was detected in more advanced post-embryonic stages (PS 3 and later).

With ongoing brain differentiation during post-embryonic development, the neuronal somata of the brain form a contiguous cortex around the considerably increasing protocerebral neuropil (Figs. 34A; 38A; 42A,F,K; 52; 53). In later stages (including adults), this cortex surrounds the growing brain neuropil from all sides except postero-dorsally (ventro-posteriorly in body axis perspective, Fig. 42A,F,K; Movie 30). Judging from the development, the somata of the neurons deriving from the pre-proboscideal pit and its related NPs are mainly located anteriorly and dorsally within in the brain cortex (dorsally and posteriorly in body axis perspective). Unfortunately, neither histological sections, nor general tubulin labeling (Figs. 52; 53) or more specific immunolabeling of serotonin-like and histamine-like immunoreactive sub-structures (data not shown) enabled unambiguous identification of structured neuropils that are established and/or targeted by these neurons (as e.g. the arcuate body).

3.5.4.2. Lateral CISs and antero-lateral depression – the anlagen of lateral sensory organ, eyes, 'optic nerve' and optic neuropils

During ES 4, the five lateral CISs (green spots in Fig. 46) occupy a lateral position in the pre-cheliforal lobe. The originally anterior-most and posterior-most of the CISs are discernible up to late ES 5 (green arrowheads in Fig. 46), whereas the remaining three were generally found to be less pronounced in the tubulin-labeled specimens. At the lateral margins, the morphogenetic movements within the pre-cheliforal lobe result in the most significant positional changes of the cellular material. Hence, the originally lateral ectodermal region demarcated by the lateral CISs shifts into an increasingly antero-lateral position, being in late ES 5 already at the same antero-posterior level with the pre-proboscideal pit (Figs. 46G',H; 47G,G'; Movie 25). During this time, the region exhibits a stratification into one to two apico-basal nuclei levels, the single lateral CISs being interspersed therein (Fig. 47D,F,H). With ongoing basal displacement of the apical cells surrounding the lateral CISs, an apically nuclei-free area of a transversally oblong and slightly curved shape has formed in ES 6 (Figs. 46I',J; 47I; Movie 26). It represents the antero-lateral depression of the pre-cheliforal lobe (see also 3.1.7.), which is involved in the formation of the eyes, the lateral sensory organ and (at least) the two optic neuropils. The depression's transversally oblong extensions transform into a more circular shape up to late ES 6 (Fig. 48A,A'; Movie 27), which appearance is retained up to early PS 1 (Fig. 48C,C',E; also Fig. 7M).

In basal horizontal sections from late ES 4 to ES 6, the basally displaced and later on already partially detached cellular material of the antero-lateral depression is situated lateral to the antero-medial cells of the pre-proboscideal pit (Figs. 47C',E',G',I'). In contrast to the latter, clustered flask-shaped cells remain attached to the apical ectodermal surface layer in further advanced embryonic stages (ES 7 and later). This apical cell region does not significantly increase in thickness and stays connected to the lateral side of the already compacted lobed anlage of the brain hemisphere via a cell stream that emanates from its basal side (Fig. 48

A'',C'',E',F,G) and extends underneath the apical epidermis (Fig. 48C'',D). A slender antero-lateral neurite bundle spans between the lateral region of the developing protocerebral neuropil and the apically attaching cells of the depression, being embedded within the cell stream (e.g. Figs. 48F,G; 50B,B'; see also 3.6.2.). This neurite bundle establishes the pathway of the so-called 'optic nerve', which in adults resembles a loose assemblage of neurite bundles that also connect to the lateral sensory organ and the dorsal integument (see e.g. Hoek 1881, Hanström 1928). After hatching, the larval brain of PS 1 has almost completely detached from the apical epidermis, which it still underlies closely (Fig. 49B-C'). The cell stream of the antero-lateral depression represents one of the two persisting direct connections of the larval brain to the apical ectoderm. Underneath the cuticle of late PS 1, the area of the antero-lateral depression is sub-divided in a lateral, medial and anterior sub-region (Fig. 50A; Movie 29). The cells of the lateral sub-region are directly connected to the underlying brain via the cell stream (Fig. 50B,B'; Movie 29). Apically, a semi-circular furrow has formed, delineating this lateral sub-region from the more medial and anterior ones (Fig. 50A,B). In the tiny area enclosed by this furrow, cellular material is slightly protruding from the surrounding epidermis (Fig. 50A). Position and slight elevation characterize these lateral cells as the anlage of the prospective lateral sensory organ, which is externally first detectable in PS 2. The sub-regions medial and anterior to the anlage of the lateral sensory organ each represent a smaller cluster of mostly flask-shaped cells (Fig. 50A-B'). Each cell cluster is connected to the cell stream via a separate slender neurite bundle (Fig. 50B'; Movie 29). Based on their position, the relation to the anlage of the lateral sensory organ and their connection to the 'optic nerve'/antero-lateral cell stream, these cell clusters can be identified as primordia of the two eyes of each body half, which will be fully pigmented and functional only in PS 3 (or presumably late PS 2). With the available data, it remains ambiguous whether the two eye anlagen have formed through a sub-division of the antero-lateral depression or via new cell immigration in adjacent ectodermal areas. In PS 2, the gap between eye anlagen and the lateral sensory organ on the one hand and brain on the other is bridged by the 'optic nerve', which still resembles a cell stream with embedded neurite bundles (Figs. 38A; 51A-A'').

Throughout embryonic and early post-embryonic development, mitoses are encountered in the cells of the antero-lateral depression, most of them being positioned apically (Figs. 47H',I,J; 48A,A',C',G; 50B; Movie 29). In more advanced stages, cell divisions are also found within the cells stream (Fisg. 48E'; 50B'; 51A-A'',E,E''; Movie 29). Some slightly bigger cells are observable in advanced embryonic and early post-embryonic stages (e.g. Fig. 48E,E'). However, they do not form a distinct apical layer comparable to the big SCNPs in the VNC. In the studied material, no clear indications of asymmetric divisions could be detected. The cell proliferation amongst the apical cells and within the cell stream of the prospective 'optic nerve' indicates a continuing

contribution of new cellular material into antero-lateral portion of the brain up to early post-embryonic stages.

The predominant cell stream structure of this pathway in PS 1 and early PS 2 (Figs. 38A; 51A-A'',E-E''; 52A-B) transforms into the more typical architecture of a nerve from PS 3 onwards, due to incorporation of more axons (Fig. 52C-E'). However, distal to the contiguous cortex of the brain, irregularly distributed agglomerations of somata are still encountered in between separate neurite bundles of this 'optic nerve' (e.g. Fig. 52D,D). These agglomerations persist into the adult (Fig. 53A,A'; Movie 30) and are here termed antero-lateral thickenings (adapting the nomenclature of a recent study (Lehmann et al. 2012), in which they are coined dorso-lateral thickening with reference to the body axis). Directly proximal to the neural sheath of the brain, the 'optic nerve' splits within the soma cortex, somata being found intermingled with its sub-bundles (Fig. 52C,D,E). During post-embryonic development, an apical and a basal optic neuropil differentiate in the anterior portion of the brain (Fig. 52), representing the primary targets of separate sub-bundles of the 'optic nerve' (Fig. 52C-F'). The apical optic neuropil is embedded in the antero-lateral brain cortex and distinctly set off from the central protocerebral neuropil core (Figs. 42A,F,K; 52C',D',E',F'; 53B). It is of a roundish to oval shape. A curved tract running at the antero-dorsal side of the central protocerebral neuropil and receiving neurites from the neurons of the antero-dorsal soma cortex spans between the two contra-lateral apical optic neuropils (Fig. 53B). The basal optic neuropil is located within the anterior portion of the central protocerebral neuropil core, directly basal to the cortex (Fig. 52B,C,D,E,F). A sub-bundle of the 'optic nerve' encircles it posteriorly and continues medially, where it finally crosses with its contra-lateral counterpart at the antero-dorsal side of the protocerebrum (Fig. 52C-F'). In the adult brain, the interneuron somata surrounding the optic neuropils are comparably cytoplasm-poor, reminiscent of globuli cells (Movie 30). The positional correspondence of the antero-lateral depression and the related antero-lateral cell stream with the two developing optic neuropils speaks strongly for an involvement of the immigrating cells of the former in the formation of these adult brain sub-structures.

3.5.4.3. Medial, central and posterior CISs, central depression and cheliforal groove - the ventral part of the brain primordium and the apical brain cell cluster

In ES 4, a shallow central depression is detectable in the pre-cheliforal lobe within the area encircled by the antero-medial and lateral CISs, the antero-lateral proboscis wall and the developing chelifore (Fig. 47B'). This central depression becomes more pronounced and medio-laterally compressed during development towards ES 6 (Fig. 47D',H'; Movies 23-26), but never forms a deep invagination comparable to the pre-proboscideal pit.

Four conspicuous medial CISs are reliably found in the region that forms the medial margin of the central depression and the proximal portion of antero-lateral proboscis wall (blue spots and

arrowheads in Fig. 46). They are first discernible in ES 4, but become more distinct during development towards ES 5, resembling the corners of a trapezoid. Even in ES 6, all four medial CISs remain identifiable in tubulin-labeled specimens, their apically converging cell processes having by then approached at the medial margin of the central depression. In this stage, the basally displaced portions of the constituting flask-shaped cells radiate obliquely into the proximal portion of the proboscis wall.

From late ES 4 onwards, identifiable CISs are found in the middle of the central depression, including three conspicuous ones that lie initially directly medial to the lateral CISs (yellow spots and arrowhead in Fig. 46). These three central CISs shift antero-medially with ongoing development. In ES 6, only two of the central CISs were still traceable, either due to fusion of two of them or because of the complete detachment of one CIS.

At the posterior margin of the central depression, three posterior CISs are located close to the anteriorly shifting chelifore bases and the lateral side of the proboscis anlage (gray spots and arrowheads in Fig. 46). Similar to the central CISs, the posterior ones were first unambiguously identified in late ES 4 and could be traced in part up to ES 6. Due to their close proximity to the chelifore base and the neuroectodermal cells wedged between the latter and the proboscis anlage, it could not be unequivocally ascertained whether the posterior CISs are of protocerebral or rather of deutocerebral nature.

Up to late ES 4, the medial, central and posterior CISs comprise approximately five cells each, cell divisions being found in the usual apical positions and only in rare exceptions slightly basally displaced (e.g. Fig. 47D'). During the medio-lateral compression of the central depression, the ectoderm grows thicker along the apico-basal axis, exhibiting already four to five nuclei levels in late ES 5 (Fig. 47H'). Within this multi-layered ectodermal region, the CISs have become more closely spaced but remain morphologically distinct. They reach far basally (e.g. Movie 25) and include by then more cells, the nuclei of which being arranged around the centrally bundled cell processes (Fig. 47F',H'). This indicates additional recruitment of apical cells into the CISs during development. In late ES 5, first cells have dissociated basally from the CISs and from ES 6 onwards, axonogenesis and neuropil formation takes place in this basal region (Fig. 48A'',C''-D'). The apical remainder of the central depression has become nuclei-free in ES 6 (Fig. 48A,A',C,C'; Movies 26; 27), reliable recognition of CISs being no longer possible from late ES 6 onwards (but see Fig. 48A'). The depression's posterior portion is medio-laterally compressed by the proboscis anlage and the anteriorly shifted chelifore base. Posteriorly, it is confluent with a nuclei-free groove wedged between proboscis and chelifore, which is underlain by the flask-shaped cells of the deutocerebral neuromere. As stated above, the protocerebral vs. deutocerebral nature of the posterior CISs in the pre-cheliforal lobe could not be clarified beyond doubt. Yet, in basal horizontal sections of some specimens in different stages, a weak

demarcation line that presumably represents the border between immigrating cells of the protocerebral region (including the posterior CISs) and the ones of the deutocerebral neuromere could be tentatively identified (Figs. 47E',G'; 48A-A''). This demarcation line is positioned anterior to the region in which the two branches of the cheliforal segmental nerve will develop. During subsequent development, the cells of the deutocerebral neuromere shift further anteriorly and no trace of a border line between protocerebral and deutocerebral somata remains recognizable. Instead of the confluent shallow central depression and cheliforal groove, a conspicuous apical invagination develops (ES 8 and later; Fig. 48E-E'') and during PS 1 (Figs. 34B; 35C, 50B). As in the hemi-ganglion anlagen of the VNC, this invagination is lined by spindle-shaped big SCNPs interspersed with smaller cells (e.g. Figs. 34B; 35C; 48E-E''), which form together a nascent apical brain cell cluster. Basally, this nascent cell cluster is confluent with the ventral side of the brain anlage (Figs. 35C; 48E-E''; 50B,B'; Movies 28; 29). Apical and sub-apical mitoses are observed during late embryology (e.g. 48E',E'') and early PS 1 (Fig. 35C; 49B; 50B; Movies 28; 29), some of the apical ones with indications of asymmetry (Fig. 49B). During post-embryonic development, the nascent brain cell cluster undergoes exactly the same development as its counterparts in the VNC. It has completely detached from the apical ectoderm in PS 2 (Figs. 38A; 39D), is by then characterized by a tiny central cavity and diminishing cell streams into the brain cortex (Fig. 40B; Movie 21), low mitotic activity in cluster and streams is detectable during ongoing post-embryonic development (Figs. 40A,B; 41D; Movie 21) and both structures persist into adulthood (Figs. 42A,F,G,K,L; 53A), the cluster with slightly reduced cell numbers compared to PS 2 (Fig. 43). Deviating from the VNC pattern, the cell streams emerge antero-medially and postero-laterally from the brain cell cluster rather than anterior and posterior to it (Movie 21). In PS 1, the cluster is positioned directly anterior to the segmental nerve branches of the cheliforal neuromere (Movie 28). In later post-embryonic stages, it is located at a level exactly between the growing central protocerebal neuropil and the smaller cheliforal neuropil (Figs. 38B; 42A,F,K). Due to this and the uncertainties regarding the exact brain neuromere borders in the preceding embryonic development, unequivocal assignment of the anterior brain cell cluster to any of the two brain components is (currently) not possible.

In adults, regions of more densely packed cytoplasm-poor neuronal somata fitting the definition of globuli cells are located close to region where the brain cluster's streams enter the soma cortex (Fig. 53A,A'; Movie 30). The degree of demarcation of these globuli cell regions from the surrounding somata in the cortex was observed to differ between investigated specimens. One of the regions occupies the ventral side of the brain, the other is positioned at its lateral side (Fig. 53A'; Movie 30). Both regions border the central protocerebral neuropil rather than the more posterior cheliforal neuropil. From the ventral globuli cell region, a conspicuous bundle of

parallel axons (‘pedunculus’) extends dorsally (shown in transversal section in Fig. 52) where some of the neurites from both hemispheres establish a transverse midline-spanning tract (Fig. 53C). This leads to a U-shape of the overall structure (see Movie 21 for this characteristic arrangement in PS 2). At the lateral side of the midline-spanning tract, an intermingling with neurite projections from more anterior interneurons located in the vicinity of the apical optic neuropils as well as ascending axons from the cheliforal neuromere and circum-esophageal connectives is detectable (Fig. 53C). Based on these general observations, it is here tentatively suggested that the U-shaped sub-structures represent part of mushroom body-like neuropils (MBNs) that have been previously described by Strausfeld and colleagues (1998, 2006a) (Fig. 44A). The lateral globuli cell cluster borders a slightly lobed lateral region of the central protocerebral neuropil. This neuropilar lobe is inter-connected to its contra-lateral counterpart by a very prominent tract, traversing antero-ventrally to the aforementioned midline-spanning tract of the putative MBNs (Fig. 52).

3.5.4.4. Unpaired antero-median CIS and unpaired antero-median cell proliferation region of the brain anlage

In late ES 4, a single, unpaired antero-median CIS (light blue spots and arrowheads in Fig. 46) is positioned directly anterior to the proximal portion of the slowly outgrowing proboscis wall. The ectoderm of this median fusion region of the pre-cheliforal lobes is not as thick as in the surrounding regions and is easily damaged during embryo dissection. For this reason, the antero-median CIS could not be consistently detected in all investigated samples. However, having been clearly identified in specimens of late ES 4 and late ES 5 specimens (Figs. 46G’; 47G), its presence within this developmental time span appears reasonably well supported.

Beginning in late embryonic stages (ES 8 and later), an unpaired median cell agglomeration is discernible at the anterior side of the developing brain, lying between the still distinctly lobed anlagen of the brain hemispheres (Figs. 48E’’-G; 49A,C’; 50B’,B’’; 51A-D’’). Some of the cells in this median cell cluster are bigger than the surrounding ones and cell proliferation was observed up to PS 2 (Figs. 48E’’-G; 49C’; 51D’). The developmental origin of this unpaired antero-median proliferation region could not be followed in detail. However, based on positional correspondences, its derivation from the antero-median CIS appears very likely. A brain structure deriving from this cell proliferation region was not identified.

3.6. Axonogenesis in the CNS of *Pseudopallene* sp.

3.6.1. General remarks

In *Pseudopallene* sp., the neurites of differentiating neurons are labeled by antibodies against acetylated as well as tyrosinated alpha-tubulin. This enables to follow establishment of the major axonal pathways in the developing nervous system. The cytoskeleton of neuronal somata is tubulin-positive as well, but due to the general cytoskeletal staining in all embryonic cells, individual identification of the former was often not possible. The general cytoskeletal labeling also impeded secure tracing of the first delicate neurites amongst the tightly packed somata in the initial stages of axonogenesis. Hence, the presented results give a overview of the temporal sequence of the establishment of the major axonal pathways with only few remarks on the exact position identified pioneer neurons. The focus is set on axonogenesis in the CNS during embryonic development and the first two post-embryonic stages. Where possible, some comments on the later development are being made. Additionally, description of the development of two transient posterior ganglion anlagen has been included in this section.

3.6.2. Axonogenesis in the brain region (protocerebral region and cheliforal neuromere)

3.6.2.1. The protocerebral region

In ES 6, the first axonal pathways are pioneered in the brain region (Fig. 54A). These include the primary pre-oral commissure, the already mentioned antero-lateral neurite bundle, which prefigures the pathway of the future 'optic nerve' (see 3.5.4.2.), and the anlage of the circum-esophageal connective. The primary pre-oral commissure is established posterior to the invaginating cell cluster of the pre-proboscideal pit and spans between the more lateral cell regions underlying the central depressions. Short neurites extending medially from the latter cell region into the commissure anlage indicate its involvement in early commissure formation (Fig. 54A). The thin antero-lateral neurite bundle extends between the cells underlying the antero-lateral depression and the lateral-most part of pre-oral commissure. The location of its pioneering neurons remains unclear. The first anlage of the circum-esophageal connective is represented by a slender neurite bundle. Already in late ES 6 and early ES 7, the pre-oral commissure and circum-esophageal connective each encompass at least along some portions more than one neurite bundle (Fig. 54B,C). From mid ES 7 to ES 8, more and more differentiating protocerebral neurons surround the convergence point of the pre-oral commissure, antero-lateral neurite bundle and circum-esophageal connective. In this region, the prospective central protocerebral neuropil starts to differentiate (Figs. 48C'',D; 54D; 55A,B). An

increasing number of projecting neurites runs in parallel and in close vicinity to the still slender antero-lateral neurite bundle (Figs. 54D; 55A,B). Most of the neurites stem from differentiating interneurons located in the cell clusters of the pre-proboscideal pit and the central depression, being sent centrally into the prospective protocerebral neuropil. In the lateral portion of the pre-oral commissure of ES 7, the course of the transversally oriented neurite bundles indicates different regions of their origin. More anterior transversal bundles start to be distinguishable from posterior ones, the latter being confluent with the circum-esophageal connective (Figs. 54D; 55A). In ES 8, weak signs of a beginning sub-division into two separate transversal components are encountered within the median region of the pre-oral commissure (Fig. 55B). They represent an anterior protocerebral commissure bundle and a more posterior pre-oral commissure bundle. The latter appears to comprise transversally directed neurites of protocerebral as well as of deutocerebral origin. During late embryonic development (ES 9 and later) and early post-embryonic development (PS 1), the central neuropil of the protocerebral region becomes more pronounced and sub-structured (Fig. 55C,D). In ES 9, the pre-oral commissure has lost its compact architecture, being by then distinctly sub-divided into an anterior protocerebral bundle and a posterior pre-oral bundle (Fig. 55C). Lateral to the commissural bundles, the protocerebral neuropil represents a dense network of neurites projections, receiving input from anteriorly and laterally positioned somata (Fig. 55C). In hatching PS 1, the increased central protocerebral neuropil has assumed a rectangular shape (Figs. 49B',B''; 55D; Movie 28). At its posterior side, the posterior pre-oral commissure traverses, whereas further anteriorly more than one commissure bundle spans between the neuropil cores. The antero-lateral neurite bundle, which is embedded within the cell stream between antero-lateral depression and detached larval brain, is still slender (Figs. 49B',B''; 55C,D). In this stage, it is again clearly separated from the centrally directed neurite projections of surrounding protocerebral interneurons.

3.6.2.2. The cheliforal neuromere

The cells of the cheliforal neuromere are located postero-lateral to the protocerebral neuropil region and lateral to the anlage of the circum-esophageal connective. Notably, in late ES 6 and early ES 7, the portion of the circum-esophageal connective directly adjacent to the cheliforal neuromere remains more delicate than its more posterior regions (Fig. 54B,C). This may be indicative of a slight temporal delay in cheliforal axonogenesis compared to the more posterior palpal and ovigeral neuromeres. Apparently, contribution of cheliforal neurons to the pioneered connective begins only after fasciculation and anteriorly directed growth of neurites of the palpal and ovigeral neuromeres has already set in (note two parallel neurites/neurite bundles in the circum-esophageal connective of Fig. 54B). In line with this interpretation, the first clear

neurite extensions of cheliforal neurons close to the circum-esophageal connective were encountered only in early ES 7 (Fig. 55C). In mid ES 7, axonogenesis of the cheliforal neuromere has gained momentum (Fig. 54D). The neuropil of this neuromere becomes continuously more distinct and up to ES 8, it already resembles a well-defined region (Fig. 55A,B). First delicate anlagen of the two main branches of the cheliforal segmental nerve are discernible in mid ES 7 (Fig. 54D), becoming more massive in late ES 7 and ES 8 (Fig. 55A,B). Judging from the course of the neurites, the cheliforal neurons contribute at least to the posterior pre-oral commissure bundle (Fig. 55A). During late embryonic (ES 9 and later) and early post-embryonic development (PS 1 and PS 2), the cheliforal neuropil gains slowly in volume, but does not undergo any significant positional shifts or architectural changes (Figs. 52A-B'; 55C,D). From PS 3 onwards, the pre-oral transversal connection of the contra-lateral cheliforal neuropils has become more pronounced, spanning posterior to the central protocerebral neuropil (Fig. 52C). With the applied general labeling of neurites, a possible contribution of cheliforal axons to the post-oral commissure (see below) could not be unequivocally resolved.

3.6.3. Axonogenesis in the neuromeres of the VNC

3.6.3.1. Establishment of the main longitudinal pathway

The main longitudinal axonal pathway of the VNC is pioneered from anterior to posterior. In mid ES 6, the posterior continuation of the primary longitudinal neurite bundle that has pioneered the circum-esophageal connective runs along the basal (i.e., dorsal) side of the palpal and ovigeral neuromeres and begins to extend into walking leg neuromere 1 (Fig. 56A). It represents the first post-oral axonal structure, no transverse commissure bundles being as yet differentiated. In late ES 6 and more distinctly in early ES 7, a delicate longitudinal bundle crosses into walking leg neuromere 2 (Fig. 56B,C) and from ES 8 onwards, a slender bundle extends beyond the latter, into the hind body region where the neuromere of walking leg segment 3 is beginning to form (Fig. 57A-C). Possibly, this entire longitudinal pathway is established by the same neurite bundle that has first pioneered the circum-esophageal connective and thereafter continued to grow posteriorly. However, consistent damage of the delicate bundle during dissection as well as fasciculation of additional neurites to the primary longitudinal bundle in the palpal and ovigeral neuromeres (Figs. 54B,C; 56A,B) rendered unambiguous back-tracing towards a putative circum-esophageal pioneer impossible. Therefore, contribution of palpal and/or ovigeral neurons in the pioneering of the post-ovigeral portion of the primary longitudinal pathway cannot be ruled out. By contrast, involvement of far posterior pioneer neurons with anteriorly extending growth cones can be excluded, due to the successive posterior elongation of the primary longitudinal bundle. In ES 7, a secondary longitudinal neurite bundle runs in parallel and slightly lateral to the primary one, extending along the

circum-esophageal connective, through the palpal and ovigeral neuromeres (Figs. 54D; 55A) and into the anterior portion of walking leg 1 neuromere (Fig. 56C). Differences in the posterior extension of this secondary bundle in the two body halves of single specimens indicate that it grows from anterior to posterior (Fig. 56C). However, the exact position of all contributing neuronal somata remains again unresolved. In ES 8, the segmental commissures up to walking leg neuromere 1 are already well-developed (see below), the longitudinal bundles that span between them representing by now compact connective anlagen, due to inclusion of additional neurites (Fig. 57A). Between the neuromeres of walking legs 1 and 2, the prospective connective retains the bipartite composition of primary and secondary neurite bundle. The more lateral secondary neurite bundle extends still not as far posteriorly as the primary one (Fig. 57A). In the latest embryonic stages (ES 9 & ES 10), also this connective anlage has compacted and slightly increased in diameter (Fig. 57B,C). Only the longitudinal bundle extending into the hind body region retains its bipartite structure, which eventually becomes indistinguishable in PS 1 (Fig. 58A,B)

No unpaired longitudinal median neurite bundle extends between the bilaterally paired connectives at any time of development (including the adult).

3.6.3.2. Establishment of the commissural pathways in the ventral neuromeres

During late ES 6 and early ES 7 (Fig. 54B,C), the segmental commissure of the ovigeral neuromere is pioneered, prior to the palpal commissure. The latter is only detectable from mid ES 7 onwards (Figs. 54D; 55A; 56C), its emergence completing the circum-oral nerve ring, which represents a typical feature of arthropod axonogenesis. Up to late ES 7, the palpal commissure remains slightly less pronounced than its ovigeral counterpart (Figs. 54D; 55A; 56C), but from ES 8 onwards, this difference is not recognizable anymore (Figs. 55B,C; 57A-C). Neither of the two commissures is divided into distinct sub-bundles during embryonic development. Yet, at their intersection with the neurites of the longitudinal pathway, the course of the bundles indicates a contribution of anteriorly as well as posteriorly located somata in the respective neuromere (Figs. 56B,C; 57A).

Posterior to the ovigeral neuromere, the establishment and differentiation of segmental commissures follows a strict a-p gradient (Figs. 56B,C; 57A-C; 58A-C). During ES 7, first transversally oriented neurites pioneer the segmental commissure in walking leg neuromere 1 (Figs. 26A''; 56B; Movie 14). The pioneer neurons of this first transversal connection are positioned at the basal side of the antero-lateral portion of the neuromere (Fig. 26A''), in which region first cells have detached during neurogenesis (see 3.3.3.1.). Prior to the crossing of the ventral midline region, the transversal projections are found in close contact to intensely tubulin-labeled basal cells of this region (Figs. 26A''; 56B), which potentially serve as landmarks

for the transversally oriented growth cones. However, based on tubulin markers alone, their exact nature (glial vs. neuronal) could not be clarified. Up to the early post-embryonic stages, several of such conspicuous medial somata can still be found in close association with the commissures (Figs. 26G''; 34C,E; 36D; Movies 16-18). Upon crossing of the midline region, axonogenesis along the commissural pathway proceeds rapidly in the walking leg neuromeres. Already in ES 8, the commissure anlage of walking leg neuromere 1 comprises numerous parallel neurite bundles (Fig. 57A; Movie 15). These have their origin in neuronal somata positioned anteriorly as well as posteriorly in the neuromere (Fig. 26D'',G''). Yet, the commissure anlage itself shows no distinct division into anterior and posterior sub-commissures during the entire embryonic development (Fig. 57A-C). In walking leg neuromere 2, the segmental commissure is pioneered between ES 7 and ES 8. In the latter stage, a transient bipartite sub-structure could be identified in the differentiating commissure anlage (Fig. 57A). But in ES 9 and ES 10, no clear indications of this sub-division are retained (Fig. 57B,C). The commissure of walking leg neuromere 3 is established only in PS 1 (Figs. 35H; 58A,B) and has already developed into a compact bundle in the corresponding ganglion anlage of PS 2 (Fig. 58C). Early stages of commissural pioneering in walking leg neuromere 4 were not found in the investigated material. However, as demonstrated by its absence in early PS 2 (Fig. 58C) but already prominet presence in PS 3 (Fig. 59A), this commissure's pioneering and elaboration has to take place between these two stages.

3.6.3.3. Formation of sub-esophageal ganglion and sub-division of embryonic commissures

In late embryonic development (ES 8 and later), the palpal and ovigeral neuromeres begin to fuse, during which process the segmental commissures gradually approach each other (Figs. 55B,C; 57A-C). This leads to the formation of the sub-esophageal ganglion, which is already clearly delimitable in the hatching PS 1 (Figs. 32A; 34A; 55D; 58A,B) and has separated from the apical ectoderm as one compact unit in PS 2 (Figs. 38A; 39D; 58C; Movie 21). Within the growing ganglionic neuropil of the early post-embryonic stages, the two embryonic commissures remain at least in part distinguishable. From PS 1 onwards, the commissures of both neuromeres are sub-divided into a ventral and a dorsal bundle (Fig. 58A-C). The ventral bundles lie further apart from each other and remain sharply defined in PS 2 (Fig. 58C; Movie 21), whereas the dorsal bundles become completely embedded in neuropil and develop into a considerably more complex system of transversal tracts (Movies 19; 21).

Similar to palpal and ovigeral neuromeres, a sub-division of the commissures is detectable in the two anterior walking leg neuromeres during early post-embryonic development. Beginning in walking leg neuromere 1 and slightly later followed in walking leg neuromere 2, a separate postero-ventral commissure bundle is set off from the remaining transversally spanning

elements (Fig. 58A-C; Movies 16-18). This postero-ventral bundle remains distinct up to the adult stage (Fig. 44C,F). In between the more anterior transversal bundles, the volume of neuropil extending between the two contra-lateral ganglionic neuropil cores is increasing during post-embryonic development. In PS 1 and PS 2, an anterior and a posterior sub-area of commissural tracts starts to differentiate within this region (Fig. 58A-C), each comprising several apico-basally stacked bundles (Movies 16-18). In later post-embryonic stages (PS 3 – adults), the commissural architecture of the ventral ganglia has not been followed in detail.

3.6.3.4. Segmental and inter-segmental nerves

Beginning with mid ES 7, the segmental nerves of palpal and ovigeral neuromeres are distinctly recognizable (Figs. 54D; 55A; 56C). First signs of these segmental nerve anlagen were occasionally detectable as early as mid ES 6 (Fig. 56A), but this temporal pattern was not consistently recovered (compare to Fig. 56B). In ES 8, the two segmental nerves are extending laterally at the same level as the corresponding commissure (Figs. 55B; 57A). With ongoing fusion, the palpal nerve is transiently shifted anteriorly in relation to the palpal commissure (Figs. 55C; 57B,C). Weak signs of this are still recognizable in PS 1 (Figs. 55D; 58A,B), but not apparent anymore in PS 2 (Fig. 58C). From ES 9 onwards, the palpal segmental nerve is more delicate than the ovigeral counterpart. In contrast to the latter, the palpal segmental nerve does not innervate a limb at any time, because *Pseudopallene* neither develops a palp as adult, nor does it show any palpal limb anlage during the entire development (see 3.1.6. and 3.2.6.). Therefore, the adult 'palpal' segmental nerve lacks any afferents and efferents relating to leg musculature and leg sensory structures. Instead, it branches upon leaving the sub-esophageal ganglion, innervating the integument as well as musculature at the base of the proboscis (not shown). Up to PS 2, the ovigeral segmental nerve extends ventro-laterally to a sub-cuticular cell agglomeration, which most likely includes the precursor cells involved in prospective oviger development that is externally first detectable in PS 3. In the adult, the fully developed oviger is innervated by this nerve (not shown).

The segmental nerve anlagen of the two first walking legs are clearly discernible in ES 8 (Fig. 57A; Movie 15), the one of walking leg neuromere 2 being still delicate. Both segmental nerves grow more compact due to incorporation of further neurites. The developing root of a walking leg nerve is typically undivided (Figs. 57A-C; 58A-C, note Fig. 57A for variation of this pattern) and the nerve's bifurcation into the future *ramus dorsalis* and *ramus ventralis* is located close to the apical surface of the ganglionic soma cortex or distal to it (Fig. 58A-C). The segmental nerve of a functional walking leg ganglion bifurcates always distal to the soma cortex (not shown).

The first inter-segmental nerve anlage is detectable in late PS 1. It branches from the connective between the ganglion anlagen of walking legs 1 and 2, its root lying close to the ganglionic

neuropil of the former (Fig. 58B). It remains the only inter-segmental nerve in PS 2 (Fig. 58C; see Movie 20 for this nerve in PS 6). An additional inter-segmental nerve between the walking leg ganglia 2 and 3 is first detectable in PS 3 (Fig. 32B). In PS 4, the last inter-segmental nerve is developed between the walking ganglia 3 and 4 (Fig. 32B). Hence, establishment of the inter-segmental nerves follows a strict a-p gradient, in good temporal correlation with the external segmentation process. Only when an external inter-segmental border between adjacent walking leg segments is developed, an inter-segmental nerve is differentiated between the corresponding walking leg ganglia (targeting amongst others the inter-segmental longitudinal musculature). At no time, an inter-segmental nerve is developed between the palpal and ovigeral neuromeres that form the composite sub-esophageal ganglion or between the latter and walking leg ganglion 1.

3.6.3.5. The posterior ganglion anlagen (‘abdominal ganglia’)

Between early PS 2 and PS 3, two small posterior ganglion anlagen develop posterior to walking leg ganglion 4 (Figs. 32B; 59A,D). In PS 3, they are each characterized by a compact commissure similar to the walking leg ganglion anlagen and are inter-connected by longitudinally spanning connectives (Fig. 59A). The second of the posterior ganglion anlagen is apically still attached to the ventral cuticle via flask-shaped cells, which include several big SCNPs (Fig. 59D). In contrast to this, the first posterior ganglion anlage is fully detached from the apical surface, with a small cell cluster on its ventral side (Fig. 59D). These findings suggest the developmental mode in the small posterior ganglia to be similar to the one encountered in the segmental walking leg ganglia. A paired longitudinal neurite bundle, the proctodeal nerve, extends posteriorly from the second posterior ganglion anlage (Fig. 59A) and enters the anal tubercle. Neither segmental, nor inter-segmental nerves are developed. Already in PS 4, both ganglion anlagen have decreased in size (Figs. 32A; 59B). They have approached walking leg ganglion 4 more closely, the connectives between the latter and the first posterior ganglion anlage being more compact and significantly shortened (Fig. 59B). As a consequence, the commissure and small neuropil of the first posterior ganglion anlage has moved closer to the neuropil of walking leg ganglion 4. Furthermore, the paired connectives spanning between both posterior ganglion anlagen as well as the posteriorly emanating proctodeal nerves have approached medially (Fig. 59B). This anterior shift of the posterior ganglion anlagen continues and a partial fusion with walking leg ganglion 4 sets in. In PS 6, both posterior ganglion anlagen are still recognizable as separate units (Figs. 44D; 59E), whereas they are eventually fused with the postero-dorsal side of walking leg ganglion 4 in sub-adults and adults (Fig. 59C,F,G). Dorsal to the neuropil of the resulting composite ganglion, a prominent neural sheath still separates the somata of the two ontogenetically distinct structures (Fig. 59F), but ventral to it, unequivocal delimitation has become impossible. Two closely approached, short commissures traverse the midline far

dorsally and directly posterior to the prominent neural sheath. (Fig. 59C,G). Presumably, they represent the originally well-separated commissures of the posterior ganglion anlagen, which have been displaced anteriorly during the fusion process. This is supported by the complete lack of any further posterior commissure, the paired proctodeal nerve being the only further caudally extending neurite bundle (Fig. 59C,F,G).

3.7. Gene expression patterns during embryonic neurogenesis

3.7.1. Success of degenerate PCRs and *in-situ* hybridizations

As already explained (see 2.4.2.), the embryonic material used for RNA extraction and cDNA synthesis very likely represents a mixture of three closely related *Pseudopallene* species. As a consequence, it remains currently unknown to which exact species obtained sequences of the five genes/gene families belong. Therefore, it will be neutrally spoken of *Pseudopallene* genes.

Only for four of the five chosen genes/gene families DIG-labeled RNA probes for *in-situ* hybridization could be obtained, out of which only two gave positive results with the used adapted protocol (Table 5). RACE PCR on the short *Pseudopallene*-ASH fragment that had been obtained with degenerate primers from the cDNA (77bp) consistently failed. The reason for the failure remains unknown, an overall degradation of the used cDNA being unlikely, since gene fragments of up to ~700 bp (*Pseudopallene*-Notch) were amplified from the same material. Hence, no data are as yet available on the expression of the presumptive proneural gene(s) of the acheate-scute family. Similarly, performed RACE PCRs on the comparatively short fragments obtained for *Pseudopallene*-Snail and *Pseudopallene*-Prospero (313 bp and 428 bp, respectively) failed to give positive results. WISH attempts with RNA probes synthesized from the available short fragments remained unsuccessful for both genes. Due to this, positive WISH was so far only achieved for *Pseudopallene*-Delta and *Pseudopallene*-Notch, the RNA probes of both genes exceeding 500 bp in length (Table 5). The latter value may therefore represent a minimal length for successful WISH in *Pseudopallene*. The amino acid sequence of the *Pseudopallene*-Delta fragment shows highest similarities to the published sequences of *Parasteatoda tepidariorum* Delta and of *Cupiennius salei* Delta1 (61% in both cases). The *Pseudopallene*-Notch fragment is most similar to the published Notch amino acid sequence of *Cupiennius salei* (75%) and *Lithobius forficatus* (71%).

The methanol-stored embryos fixed for WISH were more fragile than PFA- or PBS-stored material. Dissection of the attaching egg membrane resulted in a considerable loss of material prior to the WISH procedures. Furthermore, only in a sub-set of identically treated embryos showed specific signal. This could be related to different species identities of the used embryos and insufficient sequence similarities of the probes (which are each specific for one species). For

these reasons, no complete series of stained embryonic stages could be obtained before the available embryonic material was used up completely. Accordingly, the observations of Delta and Notch expression patterns rely on few specimens and remain fragmentary, collection of new embryonic material being necessary to fill remaining gaps.

3.7.2. Expression patterns of *Pseudopallene*-Delta

In ES 4, Delta shows low levels of expression throughout the germ band (Fig. 60). Within the neuroectoderm, expression levels are higher than in the surrounding regions. This holds especially for the brain region (including cheliforal neuromere) and the palpal and ovigeral neuromeres of the prospective VNC (Fig. 60A'). In the brain region, but in part also in the VNE, the CISs are distinctly Delta-positive, the apically bundled processes of their cells showing intense staining (Fig. 60A',B,B'). The VMR exhibits only low Delta expression (Fig. 60A'). Apart from the neuroectoderm, higher levels of expression are also found in the immigrating cell cluster of the prospective spinning gland (Fig. 60A,A').

Tab. 5: Obtained fragment lengths and corresponding conserved protein domains for the five target genes/gene families in *Pseudopallene* sp. General success of WISH (in case probes were synthesized) and RACE-PCRs are given in the right columns.

Gene / Gene family	Length of obtained fragment [bp]	Conserved protein domains (source)	WISH	RACE-PCR
Notch	686	Calcium-binding EGF repeats (according to CDD at NCBI)	positive	-
Delta	549	Delta serrate ligand (DSL) domain (according to CDD at NCBI)	positive	-
Prospero	428	part of Prospero homeodomain + carboxyterminal Prospero domain (according to Weller and Tautz 2003)	negative	without success
Snail	313	zinc-finger DNA-binding domains (according to Kerner et al. 2009)	negative	without success
ASH	77	part of basic Helix-Loop-Helix (bHLH) motif (according to Ayyar et al. 2010)	-	without success

In ES 6, the neuroectoderm is still characterized by distinct Delta expression, which appears to be most pronounced in the clearly demarcated anlagen of walking leg ganglia 1 and 2 (Fig. 60C-D'). Within the latter, slightly heterogeneous transcript levels are detectable, the cytoplasm of several of the apical cells being more intensely stained (Fig. 60D,D'). Some of these strongly Delta-positive cells represent big SCNPs in division (Fig. 60D,D'). Also the apical ectodermal cells of the VMR show Delta expression at this stage (Fig. 60D). In the remaining ectoderm, the transcript is found only in significantly lower concentrations, with the exception of the strongly stained immigrating cells of the prospective chela gland (Fig. 60C,C'). In contrast to ES 4, Delta expression in the cells of the almost fully differentiated spinning gland appears to be down-regulated, no strong staining being found in this region any longer (Fig. 60C,C').
In late ES 7, the expression pattern has changed only insignificantly (Fig. 60E-F'): The cells of the brain primordium and developing VNC exhibit distinctly stronger expression than the remaining ectoderm. The anlagen of walking leg ganglia 1 and 2 retain the highest expression levels (Fig. 60E,E'), including the apical cell layer that comprises the SCNPs in the deepening depressions (Fig. 60F). Apparently, transcript concentration within the cells of the growing chela glands has decreased, but is still slightly higher than in the surrounding ectoderm (Fig. 60E,E'). In comparison to ES 6, the ventro-median ectoderm posterior to the anlage of walking leg ganglion 2 shows slightly stronger Delta expression (Fig. 60E'). Within this region, the walking leg neuromere 3 becomes recognizable during ES 8.
The results demonstrate an involvement of *Pseudopallene*-Delta during a considerable period of embryonic neurogenesis as well as in gland development.

3.7.3. Expression patterns of *Pseudopallene*-Notch

Pseudopallene-Notch is expressed ubiquitously within the ectoderm but with varying transcript concentrations in different regions and over time (Fig. 61).
In ES 4, Notch is found at comparatively high levels in the neuroectoderm. In contrast to *Pseudopallene*-Delta, no CISs with markedly higher transcript concentrations can be distinguished (Fig. 61A,A'). Similarly, the immigrating cells of the future spinning gland are not characterized by distinctly elevated expression levels.
In ES 6, strong signal is detectable in the neuroectoderm (Fig. 61B,B'). The ganglion anlagen of the two walking leg segments are distinctly set off from the surrounding ectodermal tissue. Similar to *Pseudopallene*-Delta, Notch transcript concentrations appear to be slightly heterogeneous among the cells of the ganglion anlagen (Fig.61B,B'). Apart from the brain region and VNE, some ectodermal cells/cell clusters in the outgrowing walking leg anlagen show slightly elevated expression levels, being probably related to peripheral nervous system development (Fig. 61B'). Furthermore, the complete proboscis and chelifore anlagen exhibit

notable Notch expression, the anlagen of spinning as well as chela glands being inconspicuous within the latter.

In late ES 8, the already strongly developed embryonic cuticle prevents in general penetration of the RNA probes in WISHs, leading instead to a dark surface staining in the NBT/BCIP-staining reaction (Fig. 61C,C'). Occasionally, however, rupture of the superficial cuticle without accompanying damage of the underlying ectodermal tissue allows observation of some embryonic body regions. In such a case, Notch expression was still discernible in the anlagen of walking leg ganglia 1 and 2, but at lower levels compared to the previous stages (Fig. 61C,C').

4. Discussion

4.1. Embryonic and post-embryonic development of *Pseudopallene* sp.

4.1.1. General aspects

Within pycnogonids, different modes of early embryonic development have been distinguished, in dependence of the amount of yolk present in the eggs (e.g. Dogiel 1913). Yolk-rich eggs of callipallenids (Morgan 1891: *Callipallene brevirostris*; Sanchez 1959: *Callipallene emaciata*; Sekiguchi et al. 1971*: Propallene longiceps*; Hooper 1980: *Parapallene avida*) and a nymphonid (Dogiel 1913: *Nymphon spinosum*) have been reported to undergo total unequal first cleavages, which results in the formation of distinct macromeres and micromeres. In the framework of this work, the early cleavages of the developing embryo of *Pseudopallene* sp. were not studied and hence no further insights into division patterns and resulting cell arrangements in pre-gastrulation stages can be provided. However, in the earliest stages described herein (ES 1 and ES 2), comparatively very large macromeres make up the dorsal hemisphere of the egg, whereas an elongated 8-shaped germ band comprising already hundreds of small cells is extending along the ventral hemisphere. This situation is clearly indicative of previous unequal cleavage(s) and significant differences in division rates between dorsal and ventral hemisphere during the preceding development. These general phenomena are in line with previous descriptions of callipallenids and those nymphonids with yolk-rich eggs, while they were not detected in pycnogonids with smaller eggs (e.g. Morgan 1891; Meisenheimer 1902; Dogiel 1913; Sanchez 1959; Ungerer and Scholtz 2009). In further difference, the latter group does not develop a germ band that is clearly set off from the extra-embryonic regions of the egg. As already suggested by Ungerer and Scholtz (2009), the early development witnessed in callipallenids resolves as a derived feature within pycnogonids when evaluated against the background of recent phylogenetic analyses (Arango and Wheeler 2007; Nakamura et al. 2007; Arabi et al. 2010).

4.1.2. The stomodeum and the development of the proboscis

One of the characteristic and autapomorphic features of pycnogonid morphology is their anterior sucking apparatus, the proboscis (Dunlop and Arango 2005). In adults, the proboscis with the mouth opening at its tip is part of the cephalosoma and shows a tripartite architecture, being composed of an unpaired dorsal part, or antimere, and two bilaterally symmetric ventro-lateral antimeres. The ectodermally derived pharynx passes centrally through the proboscis and exhibits a characteristic triangular shape (e.g. Miyazaki 2002; Fahrenbach and Arango 2007).

The investigation of embryonic morphogenesis in *Pseudopallene*, as representative of the callipallenids, corroborates in major aspects the recently obtained results on the pycnogonid

Pycnogonum litorale (Brenneis 2007; Machner and Scholtz 2010). In addition, our understanding of the ongoing developmental events during proboscis formation can be refined.

(1) The triangular/Y-shaped lumen of the stomodeum/foregut is not evident ab origine*, but is attained prior to proboscis outgrowth.* In *Pseudopallene*, the first visible invagination of the stomodeal opening has a slit-like appearance, the slit extending along the embryonic a-p axis (ES 2). Its characteristic triangular shape is only attained afterwards, but still prior to the elevation of cell masses around this opening (ES 3). A comparable secondary reshaping towards a triangular stomodeal lumen has been reported only for *Achelia echinata* (Meisenheimer 1902) and a callipallenid representative, *Callipallene emaciata* (Winter 1980). However, while Meisenheimer's description of the timing of events is in full accordance with the present study, Winter observed that the stomodeal lumen retains an oval shape even after proboscis outgrowth has begun. Accordingly, he interprets the tripartite proboscis architecture as a result of a secondary restructuring. This description stands not only in contrast to Meisenheimer's and our results, but also to all other embryonic studies focusing on this aspect (Morgan 1891: *Tanystylum orbiculare*, *Phoxichilidium femoratum*, *Callipallene brevirostris*; Dogiel 1913: *Pycnogonum litorale, Phoxichilidium femoratum*; Machner and Scholtz 2010: *Pycnogonum litorale*). All of these studies report the triangular stomodeal lumen to be present at the latest when the outgrowth of the proboscis is initiated. Based on this wide consensus and the present reinvestigation of a callipallenid representative, Winter's (1980) description seems to be highly unlikely. Instead, the characteristic symmetry of the foregut is already laid down early and prior to external proboscis outgrowth. Whether the earlier non-triangular shape of the stomodeal lumen is a general feature of pycnogonid development requires still further investigations.

(2) The protruding tripartite primordium of the pharynx is overgrown by surrounding ectodermal tissue that forms the proboscis' outer wall. In *Pseudopallene*, proboscis outgrowth starts with the elevation of three more or less distinct cell populations which correspond in their positions to the proboscis antimeres (ES 4). Hence, the characteristic tripartite architecture of the future proboscis is already visible in its initial stages of development, which is in full accordance with Dogiel (1913), who reports the proboscis' tripartition *ab origine* (p. 589). In the course of the ongoing development, the three cell masses are first enclosed and subsequently distally covered by surrounding ectodermal tissue, being thus displaced into the interior of the developing proboscis (ES 5 and later). Consequently, the major part of the initial cell elevations has to be considered as the primordia of the future pharynx. Contrasting to this, proboscis formation in *Pycnogonum litorale* is not characterized by protruding separated cell masses at any stage, but rather shows an outgrowing of a more or less continuous ring (Machner and Scholtz 2010). However, similar to *Pseudopallene*, the distinctly triangular stomodeal lumen appears to be covered by surrounding ectodermal tissue, being thereby displaced interiorly (see their figs. 3A-

D; 4B). More intriguingly, it appears as if the stomodeal opening of their early stage 1 is ventro-laterally flanked by very shallow elevations (their fig. 3A), which might correspond to the ventro-lateral cell populations described here. Coverage of more taxa is needed to elucidate how the deviating types of proboscis development (distinctly elevated cell masses versus more continuous ring-like outgrowth) are distributed among extant sea spiders and which state represents the putatively plesiomorphic condition.

(3) There is no evidence for a pycnogonid labrum and its involvement in proboscis formation. The idea that a pre-oral element comparable to the labrum of other euarthropod taxa (nomenclature following Scholtz and Edgecombe 2006) takes part in the development of the proboscis has been considered as a possible scenario in the past (e.g. Hoek 1881; Adlerz 1888; Helfer and Schlottke 1935; Henry 1953) and found some favor in more recent accounts (Jager et al. 2006; Scholtz and Edgecombe 2006; Bitsch and Bitsch 2007). In particular, two structures have been discussed as a putative labrum homologue: the anlage of the dorsal antimere and the horseshoe-shaped stage of the outgrowing proboscis. However, neither of these hypotheses seems very likely for the following reasons:

Using SEM as well as immunohistochemical staining in conjunction with CLSM, no evidence for a distinct pre-oral labral outgrowth during embryonic morphogenesis of *Pseudopallene* could be found. This is in line with the recent SEM data on *Pycnogonum litorale* (Machner and Scholtz 2010) and corroborates older histological studies (e.g. Dohrn 1881; Meisenheimer 1902; Dogiel 1913). As already discussed above, the three initial cell masses surrounding the stomodeal lumen of *Pseudopallene* do not represent future external parts of the proboscis, but rather the primordia of the characteristic triangular/Y-shaped pharynx. Accordingly, a direct correspondence of the shallow unpaired dorsal cell population with the arthropod labrum is not given. Since no additional pre-oral structure is participating in proboscis formation, the proposed homologization of the dorsal proboscis antimere of adult pycnogonids with the arthropod labrum (Helfer and Schlottke 1935; Jager et al. 2006; Bitsch and Bitsch 2007) receives no support from embryology.

The distal-most portion of the developing proboscis shows weak signs of its underlying tripartite organization (ES 5 and 6), but with ongoing development the caudal notch becomes more pronounced and thus the appearance of a posteriorly interrupted ring surrounding the triangular mouth opening is achieved (ES 7 and later). This prominent notch at the posterior margin is even retained into the early post-embryonic period (PS 1 and PS 2). A horseshoe-like shape of the developing proboscis has been also depicted by Sanchez (1959) and Winter (1980) for embryos of *Callipallene emaciata*. However, Winter (1980) claims already the first external elevation of the proboscis to be horseshoe-shaped. Contrary to this, the present study reveals that in *Pseudopallene* this shape is only a secondary development. Other embryonic studies do

not agree with Winter's description either (Meisenheimer 1902; Dogiel 1913; Machner and Scholtz 2010). Hence, it seems feasible that Winter might have missed the initial events of proboscis outgrowth in *Callipallene emaciata*. In the light of all available developmental data and the current knowledge on pycnogonid phylogeny, the pronounced 'horseshoe stage' during callipallenid proboscis development seems to represent a derived feature. Therefore, it is questionable to assume this feature as representing the plesiomorphic condition of pycnogonid proboscis development and compare it with the labrum anlage of other euarthropod taxa (Scholtz and Edgecombe 2006).

In summary, development of *Pseudopallene* corroborates recent findings on *Pycnogonum litorale* (Brenneis 2007; Machner and Scholtz 2010), there being no morphologically identifiable structure resembling the arthropod labrum in Pycnogonida.

(4) No post-cheliforal structures are involved in the formation of the proboscis. The participation of post-cheliforal elements in proboscis formation has been repeatedly suggested. With the exception of a single embryonic investigation (Sanchez 1959), this view has been derived from the study of adult anatomy, in particular from the architecture of the proboscideal nervous system. However, theories that trace the ventro-lateral proboscis antimeres back to anterior extensions of a post-cheliforal segment (Wirén 1918; Sanchez 1959) stand in obvious conflict with the early outgrowing of the proboscis at the anterior pole of the embryo – well separated from the palpal and ovigeral regions (e.g. Meisenheimer 1902; Machner and Scholtz 2010; present study). Similarly, the involvement of a post-oral limb pair (e.g. Adlerz 1888) or more specifically palpal gnathobases (e.g. Helfer and Schlottke 1935; Westheide and Rieger 2006) in the formation of the ventro-lateral antimeres can be definitely rejected: None of the differentiating larval appendages of a developing protonymphon shows a median outgrowth comparable to a palpal gnathobase (Meisenheimer 1902; Dogiel 1913; Machner and Scholtz 2010). Even more compelling evidence is provided by callipallenid development: *Pseudopallene* and other callipallenids completely lack any trace of palpal or ovigeral appendage anlagen during embryonic development (Morgan 1891; Sanchez 1959; Winter 1980; present study). This renders further speculations about their possible participation in proboscis formation superfluous. Hence, embryonic development unambiguously demonstrates that the pycnogonid proboscis develops independently from any post-cheliforal elements.

4.1.3. Is there an 'egg-protonymphon' in Callipallenidae?

The most common hatching stage of pycnogonids is the protonymphon larva (e.g. Bain 2003b for summary). This larva bears a proboscis and three pairs of functional appendages, the chelifores and two three-articled larval limbs, the latter two corresponding in position to the adult palps and ovigers (if developed). Studies on Hox gene expression and neuroanatomy have

revealed that these three appendages are affiliated with the deutocerebral, tritocerebral and the following fourth segment (Jager et al. 2006; Manuel et al. 2006; Brenneis et al. 2008). The post-ovigeral region of a protonymphon is still fairly undifferentiated and comprises only the primordia of the first and sometimes also of the second walking leg ganglion (e.g. Bogomolova and Malakhov 2003: *Achelia borealis*; Bogomolova 2007: *Nymphon brevirostre*, *N. micronyx*) and in some cases already a shallow elevation of the future walking leg 1 (e.g. Bogomolova and Malakhov 2006; Bogomolova 2007: *Nymphon grossipes*; Cano Sánchez and López-González 2010: *Nymphon unguiculatum*). Regardless of the mode of post-embryonic development that follows the protonymphon stage in the various pycnogonid taxa (e.g. Bain 2003b; Bogomolova 2007 for summaries), the palpal and ovigeral larval limbs are always developed without any known exception. In contrast to this, the hatching stage of callipallenids is not a protonymphon but a further developed stage, which has been coined 'attaching larva' (Nakamura 1981, see 4.1.5. for critical discussion). This larva is lecithotrophic and already shows anlagen of at least two pairs of walking legs (see 4.1.4. for more details). Interestingly enough, it has been suggested by Nakamura (1981) that the late pre-hatching embryos of callipallenids with the already secreted embryonic cuticle should be considered as a protonymphon stage. Yet, as demonstrated herein and reported in older investigations (e.g. Dohrn 1881; Morgan 1891; Meinert 1899; Sanchez 1959; Winter 1980), the late embryos in callipallenid development already exhibit a considerably advanced level of differentiation in the post-ovigeral segments and hence should not be considered as being homologous to a protonymphon stage.

Nevertheless, this raises the question whether there is any earlier embryonic stage that exhibits sufficient resemblance to a protonymphon to qualify as an 'egg-protonymphon'. The phenomenon of an embryonized larval stage is well known from many crustaceans, in particular malacostracans (Scholtz 2000). Similar (but not synapomorphic) to the protonymphon larva of pycnogonids, the ancestral free-living nauplius larva of crustaceans is characterized by its anterior three pairs of appendages (Walossek and Müller 1990; Dahms 2000). These are the first and second antennae and the mandibles. In crustaceans that possess yolk-rich eggs and hatch at more advanced stages up to direct development, a free-living nauplius larva is absent. Nevertheless, often an embryonized nauplius larva, the so-called egg-nauplius can be recognized (Scholtz 2000). This egg-nauplius is characterized by an advanced development of the naupliar region and its structures compared to the post-naupliar segments of the embryo (Scholtz 2000).

If the crustacean egg-nauplius is taken as a model, a pycnogonid 'egg-protonymphon' should be characterized by the anlagen of the three larval appendages and a significant developmental gradient between the 'protonymphon region' and 'post-protonymphon region'. Yet, both these criteria are not fulfilled in any callipallenid species studied so far. In *Pseudopallene*, no distinct limb anlagen are encountered in the palpal and ovigeral segments during embryonic

development, which is in line with all other detailed embryonic studies on callipallenids (Morgan 1891: *Callipallene brevirostris*; Sanchez 1959; Winter 1980: *Callipallene emaciata*). Presumable anlagen of palpal and ovigeral appendages during embryonic development of callipallenids have been reported only twice. Meinert (1899) depicts two tiny buds in the position expected for palpal and ovigeral limbs in a late embryonic stage of *Pseudopallene spinipes* (his plate 1, fig. 8). However, he also describes an earlier stage of the same species, where he could find no trace of the corresponding anlagen although the primordium of the more posterior walking leg 1 is already quite prominent (his plate 1, fig. 7). Accordingly, the putative palpal and ovigeral limb buds would have to develop later than the more posterior appendages, only to be again atrophied completely in the hatching stage (Meinert 1899, plate 1, fig. 9; Bogomolova and Malakhov 2004). This timing of limb outgrowth seems very unlikely and since Meinert himself discussed his results with some caution (Meinert 1899, 20f), it might well be that it represents a misinterpretation. The second instance of putative embryonic anlagen of palpal and ovigeral limbs has been reported for *Propallene kempi* (Gnanamuthu 1950). But when comparing the provided drawings of late embryonic stages in *P. kempi* with the hatching stage of the closely related *Propallene longiceps* (Nakamura 1981) as well as data presented here for *Pseudopallene*, it becomes clear that Gnanamuthu confused the anterior with the posterior body pole. Hence, the structures labeled as proboscis, chelifore, palpal and ovigeral larval limbs relate in reality to the future hind body region and the anlagen of two (or even three?) walking legs. Hence, no convincing evidence for embryonic limb anlagen in the palpal and ovigeral segments of any studied callipallenid representative is available.

In addition to this, the a-p developmental gradient along the segment anlagen that are already developed during embryonic development is only weakly pronounced in callipallenids. The primordium of the 'post-protonymphon' region of the future hatching larva of *Pseudopallene* is already detectable very early during embryonic development. Cellular material that will give rise to walking leg segments 1 and 2 is represented in one widened end of the 8-shaped germ band stage. Although the initial anlagen of walking legs 1 and 2 arise delayed in comparison to the chelifore primordium, they do so almost simultaneously. In another callipallenid, *Callipallene emaciata*, the primordia of chelifore and the walking legs even arise around the same time (Sanchez 1959; Winter 1980). Also nervous system development of callipallenids is not characterized by a pronounced a-p gradient between the neuromeres of the 'protonymphon region' and those of the embryonic walking leg segments (Dohrn 1881; Morgan 1891; Sanchez 1959; Winter 1980; present study). As shown for *Pseudopallene*, first immigration of neurogenic cells is found almost simultaneously in the entire VNE and the segmental apical depressions develop even slightly earlier in the two embryonic walking leg segments than in the more anterior palpal and ovigeral segments (ES 5 vs. ES 6, respectively). While pioneering of the

major longitudinal axonal pathway proceeds from anterior to posterior, the segmental establishment of the commissural pathways follows no monotonous antero-posterior sequence. Instead of the palpal commissure, the one of the ovigeral neuromere is pioneered first, being soon after followed by the more posterior commissure anlage of walking leg neuromere 1 and the temporally delayed palpal one. Hence, no significant difference in the temporal onset of segmental axonogenesis can be assessed between the ventral 'protonymphon neuromeres' and the more posterior ones.

Taken together, the lack of embryonic palpal and ovigeral limb anlagen in combination with the rapid differentiation of the anterior walking leg segments leads to an absence of any embryonic stage in which the 'protonymphon-region' exhibits a significantly advanced degree of differentiation in comparison to the more posterior regions. Accordingly, callipallenid embryology does not show any stage that resembles an embryonized 'egg-protonymphon', a result that is in accordance with Bouvier, who made a comparable claim as early as 1923.

4.1.4. The hatching larvae within Callipallenidae – a comparison

Nakamura (1981) was the first to describe the complete post-embryonic development of a callipallenid, *Propallene longiceps*. Similar to *Pseudopallene*, this species develops an embryonic cuticle, which is simultaneously molted with the shedding of the egg membrane. As mentioned in the previous section, Nakamura proposes a correspondence of the late pre-hatching embryo to the protonymphon larva of other pycnogonid taxa and considers it as the '1st instar larva'. As a consequence, he designates the actual hatching stage as '2nd instar larva', a staging scheme that was adopted in a later work on callipallenid development (Bain 2003a: *Austropallene cornigera*). However, in light of the absence of any embryonized callipallenid stage comparable to a hatched protonymphon larva and the counterintuitive approach of including a developmental period prior to hatching into post-embryonic development, it is here suggested to consider the shedding of the egg membrane as the unmistakable beginning of the post-embryonic period in callipallenids. All stages prior to this sharply defined event are part of embryonic morphogenesis.

To date, data on post-embryonic development are not yet available for all taxa included in the Callipallenidae. Yet, comparison of the hatching larvae in the studied taxa shows already some notable differences (Fig. 62).

Pseudopallene: A fragmentary description of the late embryonic development as well as the two first post-embryonic stages of *Pseudopallene spinipes* (Meinert 1899; Bogomolova and Malakhov 2003, 2004) indicate a course of development very similar to *Pseudopallene* sp. investigated here, which includes the characteristics of the hatching larva.

Propallene: Compared to *Pseudopallene*, the hatching larva of *Propallene longiceps* ('2nd instar larva' sensu Nakamura 1981) bears less prominent anlagen of walking leg pairs 1 and 2, which assume an elongated (but still unarticulated) shape only after the next molt (Nakamura 1981). Apparently, *P. longiceps* hatches with a slightly less developed trunk and undergoes an additional molt before reaching a stage comparable to the hatching PS 1 of *Pseudopallene*.

Stylopallene: Similar to *Pseudopallene*, newly hatched larvae of *Stylopallene cheilorhynchus* as well as *S. longicauda* possess two elongate unarticulated anlagen of walking leg pairs 1 and 2 and an internally but barely externally detectable primordium of walking leg 3 (Fig. 63A-C).

Austropallene: In *Austropallene cornigera*, the earliest described post-embryonic stage closely resembles the PS 1 of *Pseudopallene* (Bain 2003a). The author, however, follows the staging scheme proposed by Nakamura (1981) and considers this stage as '3rd instar' (Bain 2003a). Unfortunately, embryonic development of *A. cornigera* was not investigated and the actual hatching never described. Hence, it remains somewhat ambiguous whether the first described stage does indeed represent the hatching larva.

Parapallene: A casual observation of the development of *Parapallene avida* (Hooper 1980) proves vague in its description of the hatching larva. The earliest depicted post-embryonic stage possesses two elongated but apparently unarticulated walking leg anlagen (with terminal claw?) plus a prominent limb bud of walking leg 3 that appears further developed than the corresponding primordium in *Pseudopallene*, *Austropallene* and *Stylopallene*.

Callipallene: In the genus *Callipallene*, detailed embryonic studies (Morgan 1891: *C. brevirostris*; Dohrn 1881; Sanchez 1959; Winter 1980: *C. emaciata*) have demonstrated that walking leg pairs 1-3 and the primordium of walking leg pair 4 are already developed prior to hatching. In the hatching larva, walking legs 1-3 are already relatively long and folded on the ventral side, their distal tips being directed anteriorly. Externally, they are still unarticulated and covered by a loosely fitting cuticle, although especially in the distal portions demarcations of future podomeres begin to show through the latter (Fig. 63D-F).

Neopallene: Dohrn (1881) reports for *Neopallene campanellae* a development comparable to *C. emaciata*, including the morphology of the hatching larva.

These examples illustrate that the degree of differentiation of the post-ovigeral trunk and hence the degree of embryonization of development varies significantly between different callipallenid taxa (Fig. 62). On one end, *Propallene* hatches from the egg at a comparatively early stage with only primordial anlagen of walking legs 1 and 2, whereas hatching larvae of *Callipallene* species and *Neopallene* almost resemble adult morphology. However, even the relatively 'early' hatching larva of *Propallene* still differs from the widespread protonymphon larva of many other

pycnogonid groups by a more significantly advanced level of trunk development in combination with the absence of palpal and ovigeral larval limbs. Judging from available data, the trend towards an embryonized development represents a general callipallenid feature. Accordingly, the observed differences between the callipallenid hatching larvae might even be indicative of a gradual embryonization of development during the evolution of this pycnogonid lineage. Unfortunately, however, reliable hypotheses on the interrelationships of callipallenid taxa are still lacking.

4.1.5. The callipallenid hatching stage: 'attaching larva' vs. 'walking leg-bearing larva'

Since the complete description of development of *Propallene longiceps* (Sekiguchi et al. 1971; Nakamura 1981), the advanced hatching larva of callipallenids with the anlagen of at least two walking legs is known as 'attaching larva'. This name relates to the behavior of the newly hatched offspring, remaining attached to the father's oviger for one or more molts and abandoning it only after the first articulated and functional walking legs have developed. However, already older investigations (e.g. Dogiel 1913) and more recent studies (Bogomolova and Malakhov 2006; Bogomolova 2007, 2010; Cano and López-González 2009; Cano Sánchez and López González 2010) have highlighted the existence of pycnogonid species in which big lecithotrophic protonymphon larvae hatch from the egg membrane and subsequently remain attached to the father's oviger for the major part of their post-embryonic development. This illustrates that attachment of offspring is not exclusive for hatching callipallenid larvae with an advanced level of differentiation of the post-ovigeral trunk (see also discussions in Bogomolova and Malakhov 2006; Bogomolova 2007; Burris 2011). Accordingly, Nakamura's behavior-based term 'attaching larva' proves not precise enough. Therefore, it is here proposed to substitute this term into the more morphology-based name 'walking leg-bearing larva'. The possession of anlagen of at least two walking legs is a distinctive morphological feature of hatching stages of callipallenids and probably also some nymphonids (see 4.1.6.). This stands in clear contrast to all types of hatching protonymphon larvae (free-living and actively feeding as well as attaching and lecithotrophic) with their fairly undifferentiated post-ovigeral region. Therefore, 'walking leg-bearing larva' represents a less confusing and more precise designation. Importantly, and contrary to earlier accounts on the post-embryonic development of pycnogonids (e.g. Bain 2003b; Burris 2011), it has to be emphasized that the callipallenid 'walking leg-bearing larvae' do not represent a morphologically uniform and definable stage as the protonymphon larva. Instead, this term unifies hatching larvae that share an advanced but often differing degree of post-ovigeral trunk development and the lack of palpal and ovigeral larval limbs (Figs. 62; 63).

4.1.6. Callipallenid-nymphonid relationships and their bearing on the evolution of pycnogonid hatching stages

The free-living protonymphon larva is generally considered as being the ancestral hatching stage of Pycnogonida. However, against the background of recent phylogenetic analyses (Arango and Wheeler 2007; Arabi et al. 2010), it cannot be conclusively answered whether this widespread larval stage does indeed represent a plesiomorphic feature of sea spider development (Fig. 64). This is due to the complete lack of developmental data in the potential early offshoots Austrodecidae and Colossendeidae. But even if not necessarily the ancestral larval stage, there can be no doubt that the free-living protonymphon must have arisen close to the base of the tree of crown-group pycnogonids. Callipallenidae are recovered well nested within the tree and their mode of embryonic development which terminates in an advanced walking leg-bearing larva is clearly resolved as a derived state (Fig. 64). All recent investigations indicate a close relationship of Callipallenidae and Nymphonidae (Arango and Wheeler 2007; Nakamura et al. 2007; Arabi et al. 2010), both groups forming together a monophylum. Within the Nymphonidae, different modes of post-embryonic development with different types of hatching stages occur, including not only the free-living protonymphon larva (Bogomolova 2007: *Nymphon micronyx*, *N. brevirostre*) but also the significantly bigger lecithotrophic protonymphon larva (e.g. Bogomolova and Malakhov 2006; Bogomolova 2007, 2010: *Nymphon grossipes, N. macronyx*; Cano Sánchez and López-González 2010: *Nymphon unguiculatum*). Interestingly enough, there is also a single fragmentary description of a nymphonid with prolonged embryonic development similar to callipallenids, in the species *Nymphon brevicaudatum* (Hoek 1881, 137ff, plate 19).

The recovery of a callipallenid-nymphonid monophylum has led to the proposition that the prolonged development of offspring on the male's ovigers might have evolved just once within pycnogonids (Nakamura et al. 2007). Yet, contrary to this suggestion, a recent study on the post-embryonic development of the Antarctic ammotheid species *Ammothea glacialis* clearly demonstrates the occurrence of advanced post-embryonic stages with prolonged attachment at the male's ovigers (Cano and López-González 2009). Interestingly, the extended attachment of lecithotrophic post-embryonic stages is predominantly found in polar species within nymphonids. This might be indicative of an ecological influence on the mode of development within different pycnogonid taxa (Bain 2003b; Bamber 2007) and of the independent evolution of this trait.

For callipallenids, on the other hand, no deviation from the attaching mode of development is known to date, irrespective of the geographic range or depth the different species are found. Apparently, post-embryonic development of callipallenids is less environmentally influenced and could thus contain phylogenetically valuable information. How then might this

developmental pathway have evolved within the recently supported callipallenid-nymphonid clade? While one phylogenetic study (Nakamura et al. 2007) lacks resolution to resolve internal relationships, the other two studies recover Callipallenidae as paraphyletic grouping, which either contains polyphyletic (Arango and Wheeler 2007) or monophyletic nymphonids (Arabi et al. 2010). From an evolutionary-developmental perspective, these results paint a rather unexpected picture. The more direct development of callipallenids is suggested as the ancestral condition within the putative callipallenid-nymphonid clade. Along the evolutionary branch(es) leading to nymphonids, this embryonized developmental mode then changed again into pathways with a protonymphon larva as hatching stage. This implies that after a considerable embryonization of development within callipallenids – including the loss of any stage with distinct similarity to a protonymphon – a reemergence of the putatively ancestral hatching stage of Pycnogonida must have occurred in the lineage to Nymphonidae. The reemergence of the protonymphon stage obviously also encompasses the reoccurrence of the two functional, three-articled larval appendages of the palpal and ovigeral segments. During callipallenid development, no traces of these limbs are seen, whereas most – if not all – nymphonids develop and retain them in several following post-embryonic stages (e.g. Dogiel 1913; Bogomolova and Malakhov 2006; Bogomolova 2010; Cano Sánchez and López-González 2010).

Recent phylogenetic studies have predominantly highlighted multiple independent reduction events of chelifores, palps and ovigers in adults of different pycnogonid taxa (Arango 2002, 2003; Arango and Wheeler 2007; Nakamura et al. 2007). Thereby, they challenged the long-standing perception of pycnogonid evolution as being characterized by a gradual reduction of these appendages (e.g. Hedgpeth 1947; Stock 1994; Munilla 1999). So far, the evolutionary changes of the anterior limbs have been exclusively discussed at the adult level. However, the case of callipallenids and nymphonids illustrates two aspects, which have not been given explicit attention before: Firstly, it might indicate the exact opposite phenomenon of reduction, i.e., the reemergence of the palps in adults, following an apparent previous loss during evolution. While many callipallenids are palpless, all nymphonids do bear prominent five-articled palps. Secondly, a similar reemergence of the palpal and ovigeral larval limbs is observed during embryonic and post-embryonic development. This latter process seems partly independent of the evolutionary alterations at the adult level, i.e., despite the evolutionarily secondary absence of palpal and ovigeral limbs during embryonic and early larval development in callipallenids, the adults possess ovigers and in some cases short palps. In contrast to this, nymphonids develop their adult palps and their ovigers from embryonic limb anlagen which might represent reemerged structures themselves. Taken together, this could indicate that the developmental program underlying the development of the first three pycnogonid appendages allows even more plasticity than recognized before. Hence, the one-way-road of reduction alone

– be it in a single gradual process or rather in multiple independent events – might prove insufficient to describe head appendage diversity of extant sea spiders.

The phenomenon of loss and reacquisition of complex morphological structures is by no means a new idea to evolutionary biology and has been already discussed in other studies on arthropod evolution (e.g. Scholtz 2000; Whiting et al. 2003). Of particular interest for the highlighted aspects of callipallenid and nymphonid development is a comparable pattern observed in the evolution of crustacean nauplius larvae. As mentioned above, the loss of a free-living nauplius resulted in an embryonized egg-nauplius in various crustacean lineages. However, there is good evidence that within malacostracan Crustacea a free-living nauplius larva reappeared in Euphausiacea and decapod Dendrobranchiata (see Scholtz 2000). This secondarily free-living nauplius must have derived from a former egg-nauplius. This scenario seems likely since some features of nauplius larvae are maintained in the embryonized egg-nauplii, such as early differentiation of naupliar appendages and a certain degree of differentiation (Scholtz 2000). This stands in contrast to the discussed scenario in the callipallenid-nymphonid clade within pycnogonids. Here, the entire loss of embryonic anlagen of palpal and ovigeral limbs and often also adult palps in callipallenids renders it more difficult to understand the reappearance of embryonic palp and oviger anlagen and adult palps in nymphonids.

Starting out from the results of Arango and Wheeler (2007) and Arabi and co-workers (2010), it would be highly desirable to include more terminal taxa of callipallenids and nymphonids in future studies in order to resolve their interrelationships in more detail and gain a better understanding of evolutionary transformations in the development of these two groups. Beyond this 'mapping approach', developmental characters as such should be included in the analyses, having been so far largely or even completely neglected in the adult morphology-based classifications (e.g. Munilla 1999) and recent phylogenetic analyses (Arango 2002, 2003; Arango and Wheeler 2007; Nakamura et al. 2007; Arabi et al. 2010). Ultimately, only future investigations combining developmental characters with adult morphology and sequence data will enable to assess to what extent and at what taxonomic levels development contains valuable phylogenetic information.

4.1.7. Walking leg development in Pycnogonida

The composition of the adult walking legs is one of the most conserved features of extant pycnogonids (Arnaud and Bamber 1987). With the exception of the first pair in *Nymphonella* (see Ohshima 1933), a walking leg always consists of nine podomeres (from proximal to distal: coxa 1, coxa 2 and coxa 3, femur, tibia 1, tibia 2, tarsus, propodus and terminal claw). Frequently, the differentiation of a walking leg encompasses three distinct stages that are separated by two intermittent molts. First, an unarticulated limb bud is transformed via one molt into a long and

articulated leg that still comprises an incomplete number of podomeres. Only after the next molt, the adult composition is attained.

5.1.7.1. From limb bud to articulated walking leg

The internal articulation processes underlying the dramatic metamorphosis of a small and externally unarticulated limb bud into a significantly longer and many-articled leg remain poorly understood. Sanchez (1959) describes four distinguishable folded tissue regions underneath the cuticle of a limb bud in *Nymphon gracile*, which are referred to as proto-podomeres. The author even included details on the further sub-division of these putative proto-podomeres but documentation of this developmental process remains unsatisfactory. As shown for *Pseudopallene* sp., spatial constraints within the limb bud cuticle force the underlying walking leg tissue into numerous folds that cannot be unambiguously related to future leg podomeres, especially in more proximal regions. Hence, tissue folds alone do not permit infallible identification of future podomere regions. The constraints of the surrounding cuticle even lead to a compressed s-shape of the p-d axis of the developing walking legs 1 and 2 in externally linear-looking limb anlagen. A similar observation has already been made in *Pycnogonum litorale* (Dogiel 1913, p. 651, fig. 72) and in *Propallene longiceps* (Nakamura 1981). Due to this, also direct correlation of external cuticle folds along a limb bud's p-d axis with future podomere borders has to be carried out with caution, especially when only external morphology has been investigated. For instance, descriptions of intermediate two- or three-articled legs in early post-embryonic stages of callipallenids (e.g. Meinert 1899: *Pseudopallene circularis, 'Pallene brevirostris', Callipallene hastata*; Bogomolova and Malakhov 2003, 2004: *Pseudopallene spinipes*) certainly correspond to cuticle folds of externally unarticulated limb buds with underlying compressed tissue as in PS 1 of *Pseudopallene* in this study. Reports of three-articled walking leg stages in some Nymphonidae (Bogomolova and Malakhov 2006: *Nymphon grossipes*; Bogomolova 2010: *Nymphon macronyx*), have been recently questioned in a study of the post-embryonic development of *Nymphon unguiculatum* (Cano Sánchez and López-Gonzáles 2010). It is here agreed with the latter authors that the true articulation of these early leg stages is insufficiently proven. And even if the two constrictions along the elongate limb buds in nymphonids should indeed demarcate an early internal regionalization into three parts, the relationships between these early regions and the future leg podomeres remain to be established yet.

To gain a better understanding of initial regionalization events and podomere specification, investigation of pycnogonid species with a more accessible and (externally) less drastic walking leg development seems crucial. Promising candidates for such studies may be found again within Callipallenidae. During embryonic and post-embryonic development of *Pseudopallene* sp.,

the anlagen of walking leg pairs 1 and 2 are too compressed to reveal more insights in this regard. But within the genera *Callipallene* and *Neopallene*, embryonic development terminates in a well-advanced hatching larva with long and anteriorly extended walking legs that appear to be internally far – perhaps even completely – differentiated (Fig. 63D-F; Dohrn 1881; Morgan 1891; Winter 1980). Therefore, investigation of embryonic morphogenesis in this group would enable to follow walking leg development into late stages without the intermittent molts occurring in most other pycnogonid groups. Coupled with studies on the expression patterns of genes known to be involved in arthropod leg segmentation (e.g. Prpic and Damen 2009) this would not only contribute to a better understanding of the developmental processes within pycnogonids, but eventually also enable comparisons to other arthropod taxa.

4.1.7.2. *Femur-tibia 1* and *tarsus-propodus* precursor podomeres as plesiomorphic feature of pycnogonid development?

The first truly articulated stage during pycnogonid walking leg differentiation shows in the majority of cases still an incomplete number of podomeres. In *Pseudopallene*, the anlagen of walking legs 1 and 2 are already developed during embryonic development, while the remaining two walking leg pairs arise sequentially during post-embryonic development. Apart from walking leg pair 1, the external differentiation of the walking legs follows a three-stage-sequence with two intermittent molts. The intermediate articulated leg is already functional and comprises only seven podomeres, two of them representing transient precursor podomeres. In line with this study, a precursor podomere giving rise to the adult femur and tibia1 has been explicitly reported in several instances (e.g. Dohrn 1881: *Neopallene campanellae*; Morgan 1891: *Tanystylum orbiculare*; Sanchez 1959: *Nymphon gracile*; Nakamura 1981: *Propallene longiceps*; Bain 2003a: *Austropallene cornigera*; Bogomolova 2007: *Nymphon grossipes*; Bogomolova 2010: *Nymphon macronyx*) and the term *femur-tibia 1* has recently been introduced for this transient structure (Cano Sánchez and López-Gonzáles 2010: *Nymphon unguiculatum*). More distally, incompletely articulated walking leg stages often lack a podomere resembling the adult tarsus. This study does not provide evidence for the origin of this podomere in *Pseudopallene*. However, in other species, the split of the future tarsus from the proximal region of a propodus-like precursor podomere has been repeatedly described (Dohrn 1881: *Neopallene campanellae*; Sanchez 1959: *Nymphon gracile*; Bogomolova 2007: *Nymphon grossipes*; Bogomolova 2010: *Nymphon macronyx*) and the term *tarsus-propodus* has been proposed for the corresponding transient structure (Cano Sánchez and López-Gonzáles 2010: *Nymphon unguiculatum*). Apparently, *femur-tibia 1* and *tarsus-propodus* are widespread precursor podomeres (or at least specific developmental sub-regions) occurring in the differentiating walking legs of different pycnogonid taxa. Hence, they are here tentatively suggested as characteristic and plesiomorphic feature of pycnogonid walking leg development. However, as there is still a lack of

developmental data on potentially basally branching taxa such as Austrodecidae and Colossendeidae (e.g. Arango and Wheeler 2007; Arabi et al. 2010) this evaluation has to remain preliminary.

4.1.7.3. Variations in the pattern of pycnogonid walking leg development

Comparison across different taxa shows that a three-stage-sequence of walking leg differentiation as described for walking leg pairs 2-4 of *Pseudopallene* sp. (unarticulated limb bud – incompletely articulated leg – nine-articled leg) represents a recurrent motif of pycnogonid development. However, there are also several deviations from this pattern. For instance, in line with our results on *Pseudopallene* sp., the unarticulated limb bud of walking leg pair 1 in all other investigated callipallenids attains adult articulation through one molt only, thus skipping the incompletely articulated leg stage (Nakamura 1981: *Propallene longiceps*; Bain 2003a: *Austropallene cornigera*; Bogomolova and Malakhov 2003, 2004: *Pseudopallene spinipes*; personal observation: *Stylopallene* sp.). Alternatively, sometimes a distinct elevation of the cuticle precedes the unarticulated limb bud of all or only some walking legs, leading in this case to four externally discernible stages of walking leg development (e.g. Okuda 1940: *Achelia alaskensis*; Dearborn 2003: *Achelia gracilipes*; Bogomolova 2007: *Nymphon grossipes*; Bogomolova 2010: *Nymphon macronyx*; Cano Sánchez and López-González 2010: *Nymphon unguiculatum*).

In addition, the composition of the still incompletely articulated legs can vary. The seven-articled stage described for *Pseudopallene* is a widespread feature. But in some other callipallenids (Nakamura 1981: *Propallene longiceps*; personal observation: *Stylopallene* sp.) and also other pycnogonid groups (Dearborn 2003: *Achelia gracilipes*), the first articulated leg stages comprise already eight podomeres. In these cases, the tarsus and propodus are already fully separated, but never femur and tibia 1. An interesting differentiation pattern is found in *Pycnogonum litorale*, the post-embryonic development of which having been documented no less than three times (Dogiel 1913; Behrens 1984; Vilpoux and Waloszek 2003). Surprisingly, the descriptions of walking leg differentiation differ between these studies, but due to the thorough documentation with SEM micrographs, Vilpoux and Waloszek (2003) are clearly the most reliable source. Walking leg pair 1 of *P. litorale* passes not only through a seven-articled but also an additional eight-articled stage (with separated tarsus and propodus) before attaining the adult composition. On the other hand, walking leg pairs 3 and 4 do not possess any incompletely articulated stage and transform via a single molt from limb bud to adult composition (similar to walking leg pair 1 in callipallenids). Hence, walking leg development in *P. litorale* shows a decrease of intermediate stages along the antero-posterior body axis. Finally, studies on Phoxichilidiidae with their endoparasitic post-embryonic development (e.g. Dogiel 1913; Lebour 1916, 1945) and on species with ectoparasitic development characterized by

synchronized differentiation of all four walking legs (e.g. Ohshima 1933: *Nymphonella tapetis*; Ohshima 1937: *Ammothea* sp.; Salazar-Vallejo and Stock 1987: *Ammothella spinifera*) have described a more gradual elongation of the walking leg anlagen, with no clear mention of podomere numbers in the different stages. However, in the first SEM study on the post-embryonic development of a phoxichilidiid (Lovely 2005: *Phoxichilidium tubulariae*), walking leg differentiation is reported as adhering to the widespread three-stage-sequence, the incompletely articulated leg stages being already formed during the endoparasitic phase and at that point not yet functional. Similarly, Maxmen (2006) briefly mentions an intermediate seven-articled walking leg stage preceding the completely articulated adult leg in the phoxichilidiid *Anoplodactylus eroticus*. Hence, more recent evidence suggests that even in the clearly derived endoparasitic developmental pathway of Phoxichilidiidae, a similar pattern of leg differentiation is found.

4.1.7.4. Comparison of walking leg differentiation across pycnogonids

Cross-species comparisons of structural and temporal patterns of walking leg differentiation have been conducted previously for restricted numbers of pycnogonid species, often in form of space-consuming tables (e.g. Bain 2003a,b; Gillespie and Bain 2006; Cano Sánchez and López-González 2010). In an attempt to depict the documented patterns in a concise form that facilitates comparison across more species, an abbreviated notation in matrix fashion is here introduced, as exemplified for *Pseudopallene* sp. in Figure 65. The rows of the matrix represent the four walking legs, whereas the columns depict the sequence of post-embryonic stages. Each matrix entry represents the number of externally differentiated podomeres ('+' standing for a first externally visible primordium, '0' for the unarticulated limb bud) of a given walking leg in a specific post-embryonic stage. This short form of notation visualizes (1) the sequence of the anlage of the walking legs during post-embryonic development based on the shift of the entries in the different rows, (2) the different stages of the external articulation process of each walking leg in its respective row and finally (3) the number of developed walking legs and their structural composition in specific post-embryonic stages within single columns. For cross-species comparisons, the matrices of different representatives can be easily aligned one below the other. Due to the differing degree of trunk and walking leg differentiation in hatching protonymphon larvae (with no walking leg anlagen at all) and walking leg-bearing larvae, the alignment of the columns (= post-embryonic stages) has to be based on a corresponding degree of development in the post-ovigeral region (= number of walking leg anlagen), as opposed to the species-specific numbers of developmental stages. An overview of aligned matrices as extracted from the literature is given in Figure 66. Here, similarities and differences in the developmental patterns are easily detectable. Within Callipallenidae, for instance, identical patterns are found

in *Pseudopallene* sp. and *Austropallene cornigera*. *Propallene longiceps*, on the other hand, differs in the structure of the incompletely articulated legs (tarsus already differentiated) and the fragmentary data on *Stylopallene* sp. indicate a pattern corresponding to this. With a better coverage of pycnogonid taxa and filling of gaps in so far fragmentary descriptions (gaps in matrices indicate missing stages), the inclusion of such developmental patterns into future cladistic studies may indeed contribute to the resolution of pycnogonid interrelationships.

4.1.8. Late post-embryonic and sub-adult stages of *Pseudopallene* sp.

From PS 6, it was not possible to ascertain the exact number of molts before the sub-adult stage is reached in *Pseudopallene* sp. Size differences between PS 6 specimens could be indicative of the existence of several, externally hard to distinguish stages. Accordingly, PS 6 as described herein potentially represents a grouping of different late molting stages. Notably, no stage representing an intermediate condition between PS 6 morphology and the sub-adult appearance was found, although the latter differs significantly from the former in the shape of the proboscis and the chelifores. This suggests that the observed changes do indeed occur during a single molt. In order to resolve the remaining uncertainties, a more rigorous sampling over an extended time period and especially the establishment of a successful laboratory culture would prove invaluable. In addition, further investigations of internal organogenesis promise to be useful since, for instance, the degree of differentiation in the gonad anlagen has been already shown to exhibit significant differences in externally similar looking late post-embryonic stages of *Propallene longiceps* (Nakamura 1981). Nonetheless, apart from the laboratory culture-based study on the latter species (Nakamura 1981), the present work represents the currently most complete description of post-embryonic development in a callipallenid.

4.2. Nervous system development of Pycnogonida

Neurogenesis of *Pseudopallene* sp. is here roughly divided into three phases (Fig. 67).

(1) Initially, cells immigrate from the neuroectoderm, being predominantly post-mitotic and forming transiently recognizable local CISs. Additional cell material is generated by unordered tangential divisions in the apical layer of the neuroectoderm.

(2) In a second phase, an invagination begins to form in each hemi-neuromere and big conspicuous SCNPs differentiate apically. These are characterized by high mitotic activity and an asymmetric mode of division, the divisions being mostly tangential or with a slightly oblique inclination. Between the SCNPs, the generated smaller cells appear to immigrate basally, at least some of them representing INPs that divide morphologically symmetric.

(3) Finally, after formation of prominent ganglion anlagen, the apically invaginating cell portions completely detach from the ectoderm and a pair of cell clusters persists at the apical side of each segmental ganglion (anlage). The clusters stay connected to the latter by fibrous strands, which penetrate through the neural sheath into the ganglion's soma cortex. No big SCNPs are distinguishable within the clusters anymore, but low mitotic activity remains detectable within them and the connecting strands.

To evaluate the representativeness of these three neurogenic phases for Pycnogonida on the whole, the findings on *Pseudopallene* will be compared to available data on other representatives.

4.2.1. The initial phase of neurogenesis in other pycnogonid species

Some additional but more fragmentary observations were made on other pycnogonid species in the course of this study.

4.2.1.1. Cell patterns in the neuroectoderm of *Callipallene* sp.

A limited supply of embryos from a single egg-bearing male of another Tasmanian callipallenid representative, *Callipallene* sp., was available for comparative studies. In early stages of embryonic morphogenesis, distinct tubulin-labeled spots are visible in the neuroectoderm, most clearly in the pre-cheliforal lobe and medial to the chelifore anlage (Fig. 68A,B). As in *Pseudopallene*, these relate to bundled apical cell processes in CISs that comprise only few cells (~5, Fig. 68C). Mitoses as revealed with the nuclear counterstain are positioned apically (Fig. 68 B). In further accordance with *Pseudopallene*, the CIS pattern in the neuroectoderm of walking leg segment 1 of such early stages encompasses just few, clearly separated CISs in the anterior region of the hemi-neuromere (5-6), whereas first signs of an apically nuclei-free depression are

detectable posteriorly (Fig. 68G,H). The anterior CISs show a similar spatial arrangement in both species. However, in *Callipallene*, they are not as closely spaced as in *Pseudopallene*, being separated by two to three apical cells with smaller nuclei (Fig. 68G,H). During later stages of embryonic development, paired apical depressions have formed in all four walking leg neuromeres (Fig. 68D,E) and a depression is encountered in the pre-cheliforal lobe that most likely corresponds to the antero-lateral depression in *Pseudopallene* (Fig. 68E). In the walking leg neuromeres, several tubulin-labeled spots indicate at least partially persisting CISs during early stages of the paired depressions (Fig. 68F).

In summary, the observed ectodermal cell arrangements during early neurogenesis of *Callipallene* sp. indicate similar processes to the ones described for *Pseudopallene*. One difference lies in the slightly higher number and smaller size of the cells in the neuroectoderm of *Callipallene*.

4.2.1.2. Cell patterns in the neuroectoderm of *Pycnogonum litorale*

Embryonic development of *Pycnogonum litorale* terminates in the hatching of a protonymphon larva that bears only three pairs of limbs, the chelifores and the palpal and ovigeral larval limbs. Previous attempts to follow early neurogenesis in this species at cell level (Brenneis 2007) were largely unsuccessful, due to the minute size of the embryos and the disadvantageous complete covering of the embryonic VNE by the limb anlagen (see Machner and Scholtz 2010). Due to recent improvements of the dissection techniques, first analyzable stainings of the embryonic neuroectoderm could be achieved. Tubulin labeling reveals intensely labeled apical spots in the pre-cheliforal brain region (Fig. 69A), wedged between chelifore and proboscis anlagen and medial to the palpal and ovigeral larval limb buds (Fig. 69B). The spots are arranged in a partially bilaterally symmetric pattern and relate to apically attaching cell processes. In contrast to the callipallenid representatives, the embryonic VNE of *P. litorale* comprises remarkably few cells (Fig. 69C), which contain small yolk/lipid droplets (unspecifically labeled in Fig. 69C; see also Meisenheimer 1902 for *Achelia echinata*). Due to this, assessment of cell shapes in the more intricate pattern of cytoskeletal tubulin labeling proves difficult and also F-actin staining by phallotoxins consistently fails in these embryonic stages, even on freshly fixed material (Brenneis 2007). Therefore, it remains currently unresolved whether single cells or small groups of cells immigrate at the spots indicated by high tubulin signal. During post-embryonic development of *P. litorale*, the characteristic nuclei-free depressions are encountered apically in the developing ganglion anlagen of the VNC (Brenneis 2007).

Although still fragmentary, these data indicate that the general neurogenic processes in the indirectly developing *P. litorale* are comparable to callipallenids with their embryonized development.

4.2.1.3. The initial phase of pycnogonid neurogenesis in previous embryological studies

In support of an initial phase of pycnogonid neurogenesis prior to the differentiation of big SCNPs, most previous studies described a 'thickening' of the ectoderm as the first indications of the developing neuromeres (Morgan 1891; Meisenheimer 1902; Dogiel 1913; Sanchez 1959). However, the exact processes leading to this initial thickening remain unresolved. Only Winter (1980) in his study on *Callipallene emaciata* explicitly describes conspicuous big neuronal precursor cells ('neuroblasts') during the very beginning of neurogenesis and claims them to produce GC material by repeated divisions. Clearly, the latter description cannot be substantiated by the here presented data on *Pseudopallene* sp. and *Callipallene* sp. Instead, it could be demonstrated that immigration of mostly post-mitotic cells causes the early thickening of the pycnogonid neuroectoderm, with new cellular material being produced by tangential cell divisions in the apical layer. To all appearances, Winter's description seems to be based on an extrapolation of his observations on advanced neurogenesis stages into the initial neurogenic phase. This becomes even more plausible when examining the micrographs of his sections, since also his earliest depicted stage shows already smaller GCs basal to the big SCNPs (his fig. 4.1, p. 33). Accordingly, the initial neurogenic processes were missed by Winter (1980). Considering the difficulties encountered in the present investigation during analysis of histological sections alone, it is not overly surprising that no CISs were identified in previous studies. Recognition of CISs in sections is complicated by their often slightly oblique extension of the flask-shaped cells into the embryo as well as the embryo's strong curvature around the yolk. Therefore, CISs are only identifiable in few 'perfectly' oriented sections of a series.

4.2.2. The second phase of neurogenesis in other pycnogonid species

In two other pycnogonid species, occurrence of big SCNPs was checked in early post-embryonic stages.

4.2.2.1. NPs in the hatching larva of *Stylopallene cheilorhynchus*

The walking leg-bearing larva of *Stylopallene cheilorhynchus* (Fig. 63A-C) shows a similar degree of trunk and nervous system differentiation like the hatching stage of *Pseudopallene* sp. In the available specimens, nuclear stains coupled to labeling with the 'membrane' marker FM 1-43FX revealed conspicuous cells at the apical side of the developing ventral ganglia (Fig. 70A-C). Compared to the apical epidermis cells and the interspersed and more basal GCs, these cells are distinctly bigger, their nuclei are less intensely labeled and several of them were in mitosis during fixation (Fig. 70A-C). Furthermore, slight morphological asymmetry of the forming daughter cells is observable in late mitotic stages of these cells, when cytokinesis has already set in (Fig. 70B). The orientation of these asymmetric divisions was found to be tangential to

slightly oblique. Basal to the uneven layer of the big cells, few symmetric divisions of smaller cells could be detected (Fig. 70C).

These results are in good agreement with the data on *Pseudopallene* and speak for the occurrence of corresponding apical SCNPs and smaller sub-apical INPs during advanced neurogenesis of *Stylopallene cheilorhynchus*.

4.2.2.2. NPs in post-embryonic stage 2 of *Nymphon gracile*

Similar findings were made in a single available specimen of post-embryonic stage 2 of *Nymphon gracile*. This species hatches as a protonymphon larva without any external anlagen of walking legs, but its PS 2 already shows minute limb buds of walking leg 1. At the apical side of the corresponding ganglion anlage, big and mitotically active SCNPs are located (Fig. 70D-F), which have not been as significantly enlarged in the preceding protonymphon stage (Brenneis 2007). Although the big SCNPs and their mitotic activity of PS 2 were already described by the present author (Brenneis 2007), he failed at that time to recognize the asymmetry that is detectable in late stages of their mitosis (Fig. 70E,F). In the investigated specimen, the asymmetric divisions were oriented again tangentially to slightly obliquely.

Based on these findings, a correlation between the differentiation of SCNPs and the embryonized development of callipallenids can be excluded. Instead, SCNPs are indicated to represent a more general feature of pycnogonid neurogenesis, regardless of the developmental modes of the different taxa.

4.2.2.3. The second phase of pycnogonid neurogenesis in previous developmental studies

The proposal of big SCNPs as a characteristic feature of a second phase during pycnogonid neurogenesis receives strong support from previous studies. With the exception of a single investigation (Meisenheimer 1902), all previous works covering pycnogonid neurogenesis report big cells that line paired segmental depressions at the apical side of the advanced ganglion anlagen of different species in so-called ‘ventral organs’ (Morgan 1891; Dogiel 1911, 1913; Sanchez 1958, 1959; Winter 1980; Figs. 2; 71B,E). In further accordance, high mitotic activity of these cells was noted, which led to their interpretation as NPs. Only Sanchez (1958, 1959) does not consider the big cells to be involved in neurogenesis, assigning to them instead a neurosecretory function. This interpretation is primarily based on the histological staining characteristics of the central cavity in the advanced apical cell clusters of *Nymphon gracile*. However, the plausibility of this claim is here questioned. As shown in detail for *Pseudopallene*, the continuity of the apical region of SCNPs with the developing ganglion anlagen, the notable increase of GCs within the latter and the simultaneous concentration of most mitoses in the layer of the SCNPs provide strong evidence for their production of new GC material. While Morgan (1891) could detect no predominant direction of the SCNP divisions, Winter (1980)

reports mostly radial spindle orientations. According to him, this leads to the formation of radial rows of GCs at the basal side of the SCNPs (Fig. 2). In contrast to this, the present study shows that divisions of the apical SCNPs are mostly oriented tangentially or with a slightly oblique inclination. Notably, however, with ongoing invagination of the apical depressions, unequivocal assessment of division orientations becomes problematic within the increasingly three-dimensional cell arrangements and the accompanying disintegration of the 2D layer-like structure of the neuroectoderm. Due to the progressing invagination process, the apical and basal poles of the cells in the peripheral portions of the invagination cease to be aligned with the apico-basal axis of the ventral embryonic hemisphere. Dividing cells close to the rim of a invagination can thus be seen as exhibiting radial-like spindle orientation in relation to the complete embryo – which might have been done by Winter (1980). However, when taking the inwards-outwards directed apical and basal poles of the cells in these regions as reference, this might be more correctly be designated a tangential division. The latter interpretation is herein preferred, since the polarity of a cell in its local environment appears a more appropriate reference system for descriptions in specific tissues.

Previously, more details on their exact division mode of the big SCNPs have not been provided (Morgan 1891; Dogiel 1911, 1913; Sanchez 1958, 1959; Winter 1980; Brenneis 2007). Hence, this study pioneers in the detection of morphologically asymmetric divisions of the SCNPs and their distinction from an additional INP type that is mostly located basal to the latter. This asymmetry represents one of the important arguments in support of a stem cell-like division mode, which means that the SCNPs self-renew during each division at least in a certain developmental time span. Further support for this view is provided by the relative constancy in their numbers during late embryonic and early post-embryonic development (ES 7 – PS 1), despite their high proliferation activity and the constantly increasing number of GCs. In these stages of development, the only feasible external source for 'new' big apical cells would be the ectodermal regions surrounding the apical depressions. However, ongoing cell recruitment from these regions appears highly unlikely, since epidermal differentiation has already set in.

Meisenheimer's failure to detect any big SCNPs (Meisenheimer 1902) is understandable in light of the different phases of pycnogonid neurogenesis. He investigated the embryonic development of *Achelia echinata*, a species that hatches as a protonymphon larva. Previous studies (Dogiel 1913; Sanchez 1959) as well as recent work (Brenneis 2007; Machner and Scholtz 2010) have shown that neither apical neuroectodermal invaginations, nor big SCNPs are formed during embryonic development of species hatching as a protonymphon larva (with the possible exception of some nymphonids). Rather, their differentiation falls completely into the post-embryonic phase of development (Dogiel 1913; Sanchez 1959; Brenneis 2007; see above). Hence, embryonic neurogenesis of species hatching as protonymphon larva appears to encompass

solely the initial neurogenic phase, which is characterized by immigration of predominantly post-mitotic GCs. This is in part also corroborated by the first results on *P. litorale* described above (Fig. 69A,B).

4.2.3. The third phase of neurogenesis in other pycnogonid species

In agreement with the development of *Pseudopallene*, detachment of the invaginating apical cell regions comprising the SCNPs (= 'ventral organs') is reported in all previous investigations (Morgan 1891; Dogiel 1911, 1913; Sanchez 1959; Winter 1980). Similarly, the formation of a tiny cavity in the center of the detaching SCNPs, the latter's initially high proliferation activity and a subsequent decrease in their size and division activity is documented. However, the detached apical cells do not form persisting apical clusters *external* to the ganglion anlagen in all pycnogonid taxa. In fact, during late post-embryonic development, this feature has been so far solely described for nymphonid representatives (Dogiel 1911, 1913: *Nymphon spinosum*, *N. grossipes*; Sanchez 1958, 1959: *N. gracile*; Bogomolova and Malakhov 2003: *N. grossipes*) (Fig. 71A-D). In all other studied representatives, the big SCNPs are upon apical detachment incorporated into the underlying ganglia (Fig. 71E). With progressing development, they become gradually indistinguishable from the surrounding GCs due to size decrease and the disappearance of the central cavity (Morgan 1891: *Callipallene brevirostris*, *Tanystylum orbiculare*; Dogiel 1913: *Anoplodactylus pygmaeus*, *A. petiolatus*; Sanchez 1959: *Achelia echinata*, *Anoplodactylus angulatus*, *Endeis spinosa*, *Callipallene emaciata*; Winter 1980: *C. emaciata*; personal observation: *Pycnogonum litorale*). Hence, peristence of apical cell clusters as structures that are anatomically separated from the ganglia (in the sense of being located external to the neural sheath) cannot be postulated as a general feature of pycnogonid nervous system development and adult anatomy. Apparently, this feature is not even consistently recovered within Callipallenidae, as the development of *Callipallene* species illustrates (Morgan 1891; Sanchez 1959; Winter 1980).

Interestingly enough, however, for *N. spinosum* as representative of nymphonids that do possess externally located clusters, Dogiel (1911, 1913) describes very similar fibrous connecting strands into the underlying ganglia (Fig. 71C). But in contrast to his cautious interpretations for this species, any direct connection of the clusters with the slit-like glands of the ventral integument and the bifurcating sensory setae could be clearly rejected for *Pseudopallene*. Based on the structural similarities of cluster and connecting streams, it seems very likely that identical cellular dynamics as in *Pseudopallene* can be recovered during nymphonid nervous system development. Importantly, the lack of an external cluster-stream-system in other pycnogonid representatives does not *per se* exclude the existence of a corresponding but as yet unrecognized proliferating system *within* the ganglia. To shed more light on this issue, further studies using

mitosis labeling preferably in combination with S-phase specific cell proliferation markers would be highly desirable. A possible functional role of the cluster-stream-system will be discussed in the section focusing on comparable structures in other arthropod taxa (see 4.3.5.).

4.2.4. Posterior ganglion anlagen during pycnogonid nervous system development

During post-embryonic development of *Pseudopallene* sp., two posterior ganglion anlagen are transiently recognizable. These are most pronounced in PS 3, have already decreased in size in PS 4 and are finally fused with the ganglion of walking leg segment 4 in sub-adults and adults. To date, it is unclear whether cell migration, cell death or a mixture of both mechanisms leads to the size decrease of these ganglion anlagen. In several previous studies, one or two transiently separate 'abdominal ganglia' at the postero-dorsal margin of walking leg ganglion 4 have been noted (Dohrn 1881: *Callipallene emaciata*, *Endeis spinosa*; Hoek 1881: *Colossendeis proboscidea*; Morgan 1891: *Callipallene brevirostris*; Dogiel 1911, 1913: *Achelia laevis*, *E. spinosa*, *Nymphon spinosum*; Winter 1980: *C. emaciata*). Dohrn (1881) even mentions the persistence of these two ganglia as separate units in adults of *E. spinosa*, but this claim finds no confirmation by Dogiel (1913), who reports their complete fusion with the last walking leg ganglion. Hence, it is possible that Dohrn's description is based on an immature specimen, which he misidentified as adult. In confirmation of the present study, the same apical central depressions and later on small apical cell clusters have been reported during development of the posterior ganglion anlagen in *N. spinosum* (Dogiel 1911, 1913) and *C. emaciata* (Winter 1980). Furthermore, Hoek (1881) was able to delimit two small dorsal neuropilar cores at the posterior side of the extensive neuropil of walking leg ganglion 4 in adults of *Nymphon strömi* and *Boreonymphon robustum*, which he assigns to fused posterior ganglion anlagen. These overall correspondences across five pycnogonid taxa characterize transient posterior ganglion anlagen as a widespread and probably plesiomorphic developmental feature in crown-group pycnogonids.

In phylogenetic and evolutionary studies, interpretation of the anal tubercle of crown-group pycnogonids as vestige of a formerly segmented posterior trunk region is widely entertained. Especially in the framework of the Chelicerata concept, it has been considered as representing a reduced opisthosoma (e.g. Weygoldt and Paulus 1979; Wheeler and Hayashi 1998; Ax 1999; Westheide and Rieger 2006; Dunlop 2010). In support of this scenario, the posterior-most limbless trunk region of several fossils that have been placed within the pycnogonid lineage exhibit external segmentation or at least traces thereof (Bergström et al. 1980: *Palaeoisopus problematicus*, *Palaeopantopus maucheri*; Siveter et al. 2004: *Haliestes dasos*; Poschmann and Dunlop 2006: *Flagellopantopus blocki*). The occurrence of posterior ganglion anlagen during development of extant pycnogonids may be seen as additional evidence corroborating this view. Indications for their serial homology to the walking leg ganglia are (1) their posterior position

in line with the segmental ganglia of the rope-ladder-like VNC, (2) their inter-connection to the latter via paired longitudinal connectives (prior to fusion), (3) their similar formation process with paired apical depressions and briefly persisting apical cell clusters (in nymphonids and callipallenids) and (4) the establishment of a commissure per posterior ganglion anlage. Based on this, the posterior ganglion anlagen of extant pycnogonids can be interpreted as vestiges of formerly fully formed ganglia, the segments of which having been reduced in the pycnogonid stem-lineage. Remarkably, inclusion of the fossils in phylogenetic analyses has placed some of these specimens not in the stem-lineage but rather within the crown-group of pycnogonids (Siveter et al. 2004; Arango and Wheeler 2007). If true, this would indicate independent reduction events of posterior trunk segmentation within crown-group pycnogonids. However, due to low support values, these findings should be considered with care.

It has been shown herein that the onset of segmental neurogenesis during the anamorphic post-embryonic development of *Pseudopallene* predates the emergence of limb buds or any other morphologically distinct signs of segment formation. An identical temporal sequence has been described in earlier studies (e.g. Morgan 1891; Okuda 1940; Nakamura 1981; Bogomolova and Malakhov 2003). Accordingly, the persisting formation of posterior ganglion anlagen in extant sea spiders without differentiation of corresponding trunk segments may be speculated to be related to a pycnogonid-specific temporal sequence in the formation of segmental sub-structures. In this scenario, only those segment differentiation processes subsequent to neurogenesis initiation would have been completely 'silenced' in the posterior-most trunk region during pycnogonid evolution. One of the next steps towards a better understanding of this developmental aspect would be the investigation of segment polarity genes. This could help to assess how many – or if any – segment primordia are prefigured in the differentiating hind body region during pycnogonid development. A similar approach has led to the identification of putative vestigial segment anlagen in the embryonic pleon of the decapod *Cherax destructor* (Scholtz 1995) and in the abdomen of the cirripede *Sacculina carcini* (Gibert et al. 2000).

Against this background, nervous system development and adult neuroarchitecture of ten- and twelve-legged pycnogonid species represents an intriguing field of investigation. Such extra-legged species are known in three different pycnogonid taxa (Pycnogonidae, Colossendeidae, Nymphonidae), most of them having a morphologically similar eight-legged 'sister-species' (see Hedgpeth 1947). This indicates that additional leg-bearing segments have independently evolved within crown-group Pycnogonida. At nervous system level, it would be interesting to investigate how many 'super-numerous' posterior ganglion anlagen are developed in extra-legged representatives. A negative correlation between the number of additional segmental ganglia and the one of the posterior ganglion anlagen could hint on a reactivation of segment differentiation processes in posterior segment primordia of formerly eight-legged forms.

4.3. Pycnogonid neurogenesis compared to other arthropod taxa

As basis for a comparison of pycnogonid neurogenesis in the broader framework of arthropod phylogeny and evolution, an overview of several key aspects of early neurogenesis in hexapods, crustaceans, euchelicerates and myriapods will be given in the next section (4.3.1.), being followed by a summary of the current knowledge on neurogenesis in putative euarthropod outgroups (4.3.2.). The actual comparison with pycnogonid neurogenesis follows separately (4.3.3. – 4.3.5.).

4.3.1. Neurogenesis in the four major euarthropod lineages – a review

4.3.1.1. NBs versus CISs

Early neurogenesis in the hexapod VNE has been studied in greatest detail (e.g. Wheeler 1891; Bate 1976; Hartenstein and Campos-Ortega 1984; Thomas et al. 1984; Doe and Goodman 1985a; Hartenstein et al. 1987; Doe 1992; Truman and Ball 1998; Wheeler et al. 2003) (Fig. 72E). Here, a special type of SCNP is encountered, the neuroblast (NB) (Wheeler 1891). A NB is a comparably big cell that divides repeatedly and asymmetrically in stem cell-like fashion (Stent 1998; Richter et al. 2010). During each asymmetric division, the NB 'self-renews' and a smaller cell is 'budded off' basally, i.e., NB divisions occur (roughly) in radial direction. The smaller cell is termed ganglion mother cell (GMC) and represents an INP, which undergoes typically just one terminal division into two immature post-mitotic GCs that differentiate into neurons and/or glial cells (Fürstenberg et al. 1998). Hexapod NBs are specified from ASH-positive proneural cell clusters in the single-layered VNE via cell-cell interaction processes involving Notch-signaling (Taghert et al. 1984; Doe and Goodman 1985b; Cabrera et al. 1987; Heitzler and Simpson 1991; Campos-Ortega 1994; Martín-Bermudo et al. 1995; Cau and Blader 2009) and subsequently immigrate into a sub-apical position before starting proliferation (e.g. Hartenstein and Campos-Ortega 1984; Doe and Goodman 1985a; Wheeler et al. 2003).

In crustaceans (Fig. 72D), the cellular processes of early neurogenesis have been thoroughly investigated only in some taxa. In malacostracans, the existence of SCNPs is well-documented, these cells having been also coined NBs (e.g. McMurrich 1895; Dohle 1976; Dohle and Scholtz 1988; Scholtz 1990, 1992; Harzsch et al. 1998; Harzsch 2001). However, their homology to hexapod NBs has been matter of some debate (see Ungerer 2006 for comprehensive discussion) not least due to the completely different formation process of malacostracan NBs via an invariant cell division pattern as well as their maintenance within the apical VNE during proliferation activity. A recent study of the cell lineages of some NBs in the amphipod *Orchestia cavimana* (Ungerer 2006; Ungerer and Scholtz 2008) revealed detailed similarities to identified *Drosophila* NB lineages (e.g. Bossing et al. 1996). This finding represents first compelling

evidence for homology of hexapod and malacostracan NBs. The genetic network underlying early neurogenic processes of malacostracans remains currently unknown. Apart from malacostracans, indications for branchiopod NBs have been presented in several studies (Gerberding 1997: *Leptodora kindtii*; Duman-Scheel and Patel 1999: *Triops longicaudatus, Artemia franciscana*; Harzsch 2001: *Triops cancriformis*, *Artemia salina*; Wheeler and Skeath 2005: *Triops longicaudatus*; Müller 2006: *Triops cancriformis*). More recent morphological investigations on the cladoceran *Daphnia magna* coupled to gene expression studies (including ASH, Asense, Snail, Prospero, Notch and Delta) were able to further substantiate this claim (Ungerer et al. 2011a, 2012). The genetic mechanisms leading to the specification of branchiopod NBs amongst the neuroectodermal cells remain only partly resolved. Interesingly, ASH does not seem to serve a proneural function, since Snail is the first (known) gene expressed in the forming NBs (Ungerer et al. 2011a). Furthermore, also Notch-signaling does not lead to canonical lateral inhibition, NBs differentiating instead directly adjacent to each other (Ungerer et al. 2012). The lack of a spatio-temporally fixed NB formation sequence (Ungerer et al. 2012) speaks furthermore against the involvement of an invariant cell division pattern in the post-naupliar germ band. Beyond branchiopods and malacostracans, neurogenesis has never been studied at any level in several potentially crucial taxa, such as, for instance, Cephalocarida or Remipedia.

In several euchelicerate taxa, histological studies early on demonstrated the formation of numerous small apical 'pits' in the early VNE, relating to groups of cells with basally displaced nuclei (e.g. Xiphosura: Kingsley 1893; Scorpiones: Brauer 1894; McClendon 1904; Araneae: Pross 1966; Amblypygi: Weygoldt 1975; Uropygi: Kästner 1951). Since then, recent studies on *Limulus polyphemus* (Mittmann 2002, 2003) and especially on the two spiders *Cupiennius salei* and *Parasteatoda tepidariorum* (Stollewerk et al. 2001, 2003; Stollewerk 2002, 2004; Weller and Tautz 2003; Döffinger and Stollewerk 2010; Linne and Stollewerk 2011) have significantly increased our understanding of the early neurogenic processes in these representatives (Fig. 72B). The previously identified groups of ectodermal cells were demonstrated to relate to localized CISs. The regions of their formation in the VNE are prefigured by domains of ASH expression (Stollewerk et al. 2001), within which the number of actually immigrating cells is restricted by Notch-signaling (Stollewerk 2002). The CISs persist in the VNE for several days, comprising mostly post-mitotic immature GCs that subsequently detach and differentiate basally. Mitoses are predominantly encountered in the apical layer of the VNE and no exclusive spatial association of apical mitoses with CISs is assessable (Stollewerk et al. 2001; Mittmann 2002, 2003; Weller and Tautz 2003). Yet, at least in *L. polyphemus*, they are regularly recovered in direct CIS vicinity and also in some flask-shaped cells within CISs (Mittmann 2003). In addition, also several basally detached cells of the xiphosuran and spiders have been found in division, which demonstrates that a least some of the immigrating cells still represent NPs as defined

herein. However, no divisions in the euchelicerate VNE are morphologically asymmetric. Also at the molecular level, only symmetric distribution of *Cs*-prospero protein is observable during cell divisions in the VNE of *C. salei* (as opposed to asymmetric distribution during NB divisions in *Drosophila melanogaster*) (Weller and Tautz 2003).

Histological studies on myriapods report the initial thickening of the VNE as being based on considerable cell proliferation coupled to cell immigration (e.g. Heymons 1901: *Scolopendra* sp.; Tiegs 1940*: Hanseniella agilis,* Tiegs 1947: *Pauropus silvaticus*; Dohle 1964: *Glomeris marginata*). Heymons (1901) explicitly mentions apical tangential divisions that compensate for the 'loss' of apical ectodermal cells due to immigration. Only Knoll (1974) in his study on *Scutigera coleoptrata* claims the existence of slightly bigger proliferating cells ('neuroblasts') that give rise to rows of GCs. However, recent studies on early neurogenesis have demonstrated the formation of localized CISs similar to euchelicerates in almost all major myriapod taxa (Whitington et al. 1991: *Ethmostigmus rubripes*; Dove and Stollewerk 2003: *Glomeris marginata*; Kadner and Stollewerk 2004: *Lithobius forficatus*; Chipman and Stollewerk 2006: *Strigamia maritima*; Mayer and Whitington 2009a; Whitington and Mayer 2011: *Hanseniella agilis*; pauropodans not yet reinvestigated) (Fig. 72C). Where studied, high levels of local ASH expression predated CIS formation in the VNE and Notch and especially Delta expression is elevated within immigrating cells (Dove and Stollewerk 2003; Kadner and Stollewerk 2004; Chipman and Stollewerk 2006). In this early neurogenic phase, mitoses have been predominantly detected in the apical cell layer of the VNE, at least in a millipede (Dove and Stollewerk 2003). However, apart from Heymons (1901), a special orientation of these divisions is not reported. It appears therefore somewhat surprising that Whitington (2007) depicts *radial* division orientations in his scheme on VNE development. Notably, cell proliferation is encountered either directly abutting or even within CISs (Whitington et al. 1991; Dove and Stollewerk 2003). In later stages of neurogenesis, segmentally paired depressions invaginate in the myriapod VNE, being lined by spindle-shaped cells with basally displaced nuclei. These apical cell regions have been named 'ventral organs' or 'ganglionic pits'. All available studies agree in the considerable cell proliferation within the apical cell layer of them and/or sub-apical to it (Heymons 1901; Tiegs 1940, 1947; Dohle 1964; Knoll 1974; Whitington et al. 1991), indicating these regions as sources for additional GCs. At least initially, the organization in separate CISs is retained, the cell groups in the CISs radiating from the invaginations (Dohle 1964; Whitington et al. 1991; Chipman and Stollewerk 2006; Pioro and Stollewerk 2006). Eventually, the cells lining the paired invaginations detach from the apical surface and form transitory ganglionic cavities within the ventral soma cortex of the ganglion anlagen. These are initially still areas of mitotic activity but then gradually degenerate (Heymons 1901; Tiegs 1947; Dohle 1964; exception: Tiegs 1940: Symphyla, eversible sacs as derivatives of 'ventral organs').

4.3.1.2. Numbers and spatio-temporal patterns of CISs and NBs

In contrast to the fundamental differences regarding the generation and internalization of GCs, several similarities in the morphological processes have been pointed out as being characteristic for all four major euarthropod lineages.

(1) A similar number of about 30 CISs/NBs is encountered in a characteristic grid-like arrangement per 'typical' euarthropod ventral hemi-neuromere. The CISs/NBs of a ventral hemi-neuromere are at least transiently arranged in a characteristic grid-like pattern comprising seven rough transverse rows. This has been suggested to be a conserved character of euarthropod neurogenesis (e.g. Stollewerk and Simpson 2005; Stollewerk and Chipman 2006; Stollewerk 2008; Döffinger and Stollewerk 2010), being controlled by early embryonic axis patterning genes, as shown for the positioning of proneural clusters of *Drosophila melanogaster* (e.g. Skeath et al. 1992, 1994; Skeath 1998) A recent comparative study has evaluated correspondences of the CIS arrangements of the two spider models and a myriapod and additionally discussed several similarities to the NB pattern of hexapods (Döffinger and Stollewerk 2010). Apart from an overall arrangement in seven rough transverse rows, correspondences of CIS/NB numbers in the posterior rows have been highlighted, the two posterior-most ones being correspondingly placed in the engrailed expression domain (e.g. Doe 1992; Condron et al. 1994; Broadus et al. 1995; Duman-Scheel and Patel 1999; Stollewerk and Chipman 2006). Nonetheless, deviations in the grid-like arrangement of typical '30' GICs/NBs are apparent and for some important taxa exact numbers remain still unknown.

Hexapods and myriapods are reasonable close to 30, with 30-31 NBs per thoracic hemi-neuromere of hexapods (excluding median NB; Bate 1976: *Locusta migratoria*; Doe and Goodman 1985a: *Schistocerca americana*; Doe 1992, Broadus et al. 1995: *Drosophila melanogaster*; Truman and Ball 1998: *Ctenolepisma longicaudata*; but Tamarelle et al. 1985: *Carausius morosus* with 28 NBs) and 30-33 reported CISs per ventral hemi-neuromere of myriapods (Whitington et al. 1991: *Ethmostigmus rubripes*; Dove and Stollewerk 2003, Döffinger and Stollewerk: *Glomeris marginata*; Kadner and Stollewerk 2004: *Lithobius forficatus*; Chipman and Stollewerk 2006: *Strigamia maritima*; Pioro and Stollewerk 2006: *Archispirostreptus* sp.).

In crustaceans, however, complete NB maps are to this day not available. NB sub-sets have been identified during certain developmental phases of different malacostracan representatives (excluding median NBs; e.g. Dohle 1976: 13 NBs in *Diastylis rathkei*; Scholtz 1992: estimation of 25-30 NBs during early embryonic development of *Cherax destructor*; Harzsch and Dawirs 1994, Harzsch et al. 1998: 7-10 NBs during mid- and late-embryonic and post-embryonic development of *Hyas araneus*; Harzsch et al. 1998: 5 NBs in mid-embryonic stages of *Homarus americanus*; Harzsch 2001: 14-18 NBs at 35% of embryonic development of *Palaeomonetes argentinus*; Sullivan and Macmillan 2001: 7 NBs in late embryonic stages of *Cherax destructor*; Ungerer 2006,

Ungerer and Scholtz 2008: 13-16 NBs in *Orchestia cavimana*, extrapolation to 26-32 NBs per hemi-neuromere; Fabritius-Vilpoux et al. 2008: 11 putative engrailed-positive NBs in the parthenogenetic form of *Procambarus fallax*). Also in branchiopods, complete NB maps are so far still missing (Gerberding 1997: 23 NBs depicted for one embryonic stage of *Leptodora kindtii*; Ungerer et al. 2012: maximally 25 NBs observed in *Daphnia magna*). Accordingly, only numbers lower than 30 are actually confirmed for crustaceans. As a consequence, also the degree of similarity of the crustacean NB arrangement compared to hexapods is still not fully assessable. During early neurogenesis of the decapods *Cherax destructor* and *Palaeomonetes argentinus* (Scholtz 1992; Harzsch 2001, respectively) NBs have been said to be roughly arrayed in a grid-like pattern. Yet, exact number and width of rows is not completely resolved (6-7 rows à 4-5 NBs based on extrapolation of Scholtz 1992; only 5 rows à 3-4 NBs in Harzsch 2001). In branchiopods, the NB arrangement even deviates from a regular grid-like pattern, each ventral hemi-neuromere of *Daphnia magna* (Ungerer et al. 2012) and most likely also of *Triops longicaudatus* (Wheeler and Skeath 2005) being characterized by a NB-free central region. Since crustaceans constitute to all appearances a paraphyletic grouping from which the hexapod lineage arose (see 4.3.6.1.), further clarification of their early neurogenesis patterns is crucial for detailed comparisons and evolutionary considerations.

On a similar note, assessment of 'typical' CIS numbers in euchelicerates suffers from poor sampling. Here, explicit CIS numbers are available only for the two spider models (Döffinger and Stollewerk 2010: 38 CISs in *Cupiennius salei*, 37 CISs in *Parasteatoda tepidariorum*) and a xiphosuran (Mittmann 2003: ~30 CISs in *Limulus polyphemus*). In the latter, a pattern of only 5-6 transiently recognizable transverse rows à 4-5 CISs is described for the prosomal hemi-neuromeres (Mittmann 2003). Developmental SEM studies on scorpions with yolk-rich eggs have revealed distinct small pits in the VNE that certainly correspond to CISs (e.g. Farley 2001; Simonnet et al. 2004). At least in the latter study, their arrangement appears to be similar to the one described for spiders (Simonnet et al. 2004, their figs. 1; 4a), but an explicit description is not provided. With this current paucity of data, it appears more appropriate to speak of a range of 30 to 40 CISs per euchelicerate hemi-neuromere. In order to assess the extent of variation in CIS number and arrangement within the euchelicerate lineage more securely, additional investigations of neurogenesis in non-model taxa are needed.

In summary, the patterning mechanism in the euarthropod VNE that leads to evenly spaced and spatially stereotypic ASH expression in proneural clusters/domains from which CISs and NBs are specified (exception: branchiopods and potentially other crustaceans) is plastic enough to have allowed modifications of numbers as well as spatial rearrangements of CISs/NBs within different lineages (see also Döffinger and Stollewerk 2010). This has one important implication. A common origin of CISs and NBs as 'local entities' of neuronal cell internalization (and in part

generation) may be argued for based on the overall similarity of the pattern 'type' as well as of the underlying genetic network (e.g. Stollewerk and Simpson 2005; Stollewerk and Chipman 2006; Döffinger and Stollewerk 2010). Yet, more specific homologization attempts, for instance, of single CISs and NBs cannot be based on positional (and temporal) clues alone. Rather, they need to be founded on more exhaustive investigation of specific neuronal identity genes (see e.g. Döffinger and Stollewerk 2010) as well as ideally on cell lineage studies, which are to date completely lacking in myriapods, eucheliceratesand also in pycnogonids.

(2) CISs and NBs form sequentially within hemi-neuromeres. A formation of CIS/NB sub-sets in temporally distinct 'pulses' has been described for different representatives (e.g. Hartenstein and Campos-Ortega 1984; Hartenstein et al. 1987; Doe 1992: *D. melanogaster*; Stollewerk et al. 2001; Stollewerk 2002: *C. salei*; Dove and Stollewerk 2003: *G. marginata*) and discussed as as a similar feature in the dynamics of early neurogenesis across euarthropod taxa (Stollewerk and Simpson 2005; Stollewerk and Chipman 2006). Contrary to the latter notion, detailed descriptions of the dynamics in the grasshopper *S. americana* (Doe and Goodman 1985a) have demonstrated a temporally stereotypic but sequential formation of the NBs (see their fig. 5). A similar sequence was observed in the primarily apterygote *C. longicaudata* (Truman and Ball 1998). On this basis, sequential NB formation within single hemi-neuromeres is here considered to represent the more plausible plesiomorphic hexapod condition (in agreement with Ungerer 2006). The synchronized pulse-like formation of NB sub-sets in *D. melanogaster* may be correlated to the very fast development in this species. Furthermore, especially the late 'pulses' in *D. melanogaster* might to a certain extent represent a discretization artifact. In line with this notion, it is mentioned in their first description Doe (1992, p. 857) that 'it is important to note that these stages are 'snapshots' of the developing NB pattern and intermediate patterns can be observed' and also later studies documented variations (e.g. Bossing et al. 1996; Schmidt et al. 1997). Within crustaceans, there is no evidence for pulse-like formation of NB sub-sets at all. In fact, malacostracan NB differentiation is strictly sequential, being coupled to the invariant cell division pattern in the post-naupliar germ band (e.g. Dohle 1976; Scholtz 1990, 1992; Ungerer 2006). In contrast to this, no stereotypic sequence of NB formation could be observed in the branchiopod *Daphnia magna* (Ungerer et al. 2012). The only euchelicerate and myriapod representatives for which distinct temporal pulses of CIS formation have been described are *C. salei* (Stollewerk et al. 2001) and *G. marginata* (Dove and Stollewerk 2003), respectively. But in other myriapods, comparable occurrence of 'pulses' could not be assessed (Kadner and Stollewerk 2004: *L. forficatus*) or even clearly refuted (Chipman and Stollewerk 2006: *S. maritima*). In addition to this, Dove and Stollewerk (2003) provide no conclusive evidence for truly pulse-like dynamics of CIS formation. Their results rely on a series of fixed stages, based on which an underlying sequential formation of single CISs cannot be excluded with certainty.

Along these lines, different ASH transcript levels in the proneural domains of the VNE (fig. 7 in Dove and Stollewerk 2003) may not necessarily represent stochastic variations of one expression 'pulse'. Rather, it may indicate unresolved temporal dynamics of sequential proneural gene expression. The same argumentation holds for the studies on the spider *C. salei* (Stollewerk et al. 2001; Stollewerk 2002). Hence, the available evidence for a pulse-like formation of CISs/NBs as a widespread feature of euarthropod neurogenesis is herein not considered as being convincing. However, the sequential character of the formation process lies beyond doubt (Fig. 72B-E).

4.3.2. Neurogenesis in the putative euarthropod outgroups

4.3.2.1. Neurogenesis in Tardigrada

Data on neurogenesis in tardigrades are scarce and incomplete. In fact, apart from a brief mention of singly immigrating cells that are each said to give rise to entire future ganglia (Hejnol and Schnabel 2005) virtually nothing is known. As a consequence, only superficial comparisons can be drawn, which currently just serve to introduce noise in the playground of evolutionary scenarios. Without any doubt, general tardigrade development and neurogenesis in particular need to be studied in more detail.

4.3.2.2. Neurogenesis in Onychophora

Older histological studies of onychophoran neurogenesis have only described a general thickening of the VNE (e.g. Kennel 1886; Sedgwick 1888; Pflugfelder 1948) but mentioned already a distinction of apical columnar cells and underlying smaller roundish cells. Only Pflugfelder (1948) claims the occurrence of asymmetric divisions in the VNE, but does neither specify the orientation of the divisions, nor depict any in his drawings. An investigation by Eriksson and colleagues (2003) refined the previous findings by reporting three different apico-basal cell layers during neurogenesis in the head region, the sub-apical cell layer being formed by segregation of single NPs, the basal-most representing the differentiating neuronal cells. However, more recent studies resulted in contradictory interpretations regarding the nature of the segregating NPs. A morphological investigation claimed them to represent SCNPs similar to hexapod NBs (Mayer and Whitington 2009a). Two additional studies on onychophoran neurogenesis contradicted this view based on morphology and gene expression patterns (Eriksson and Stollewerk 2010a,b). They not only refuted the existence of SCNPs but furthermore interpreted several neurogenesis features as derived within the onychophoran lineage. Remarkably, at the observational level, the three recent studies agree in almost all aspects (see also Whitington and Mayer 2011) (Fig. 72A). Contrary to euarthropod CISs/NBs, the segregating NPs of onychophorans are not formed in spatio-temporally stereotypic sites, which

finds further support in a corresponding lack of locally restricted and stereotypically arranged ASH and Delta expression domains in the neuroectoderm (Eriksson and Stollewerk 2010a,b). The exact mechanism of the 'unordered' NP specification in onychophorans remains so far unresolved. Upon segregation, the NPs show a morphologically symmetric mode of division. Due to this, characterization of this cell type as SCNPs receives no evident support from morphology. But to date not a single molecular marker known to be asymmetrically distributed to the sister cells during hexapod and branchiopod NB divisions has been investigated. Therefore, rejection of the SCNP nature of the onychophoran NPs still lacks corroboration from this side. Furthermore, it is still unclear whether each singly immigrating cell represents a NP or whether some are already post-mitotic immature neurons. Additional investigations of exact division patterns and cell lineage studies are needed to provide further insights regarding the genealogical relationships within the three-layered ectoderm. Importantly, the apical-most VNE layer containing the big columnar cells should be characterized in more detail. For this region Pflugfelder (1948) claims the occurrence of asymmetric divisions leading to the thickening of the VNE and it is here that the segregating NPs (independent of their exact nature) are born over a considerable developmental time span. The NPs are smaller than the columnar cells. Yet, it remains currently insufficiently resolved whether this size difference is already apparent from the moment of their birth in the apical-most layer or rather is a consequence of post-natal differentiation prior to or during immigration. Somewhat astonishingly, only one of the recent investigations (Eriksson and Stollewerk 2010a) mentions predominantly tangential divisions in the apical-most VNE layer (in the brain region) and depicts late mitotic phases. However, the provided images do not clearly bear out the symmetry vs. asymmetry of the divisions.

Apart from the protocerebral region, the onychophoran VNE is said to be characterized by binary fate decisions, i.e., cells with prospective neural and epidermal fate are specified in the same ectodermal cell area. This was discussed as another similarity between tetraconates and onychophorans (Mayer and Whitington 2009a). However, the correctness of this description appears again not satisfactorily established. During advanced onychophoran development, the so-called 'ventral organs' (VOs) differentiate in the region of the neuroectodermal thickening, representing segmentally arranged, multi-layered cell accumulations apical to the more basal nerve cords. The VO of the protocerebral region invaginates and detaches from the apical ectoderm, forming an apical cluster, the hypocerebral organ, at the ventral side of the brain (e.g. Eriksson et al. 2003; 2005, see 4.3.5.3. for further discussion). Hence, this anterior-most region of the neuroectoderm does not assume epidermal fate. However, the VOs in the trunk do not invaginate. Instead they atrophy dramatically during further development (Mayer and Whitington 2009b; Whitington and Mayer 2011). In adults, the only remaining signs of them are spatially restricted 'ventral pits' (e.g. Mayer 2007). Remarkably, due to this extreme

degeneration of the VOS (as transformations of the earlier VNE) it remains unclear where exactly the cells of the adult ventral epidermis have their origin. They might be the last survivors of the degenerating and spatially diminishing ventral organs. Alternatively, they could as well originate from more peripheral regions and move centrally in the wake of the retreating VOs. For this reason, the advocated binary fate decisions of the onychophoran VNE are here still considered as an ambiguous issue.

This critical view receives further impetus from the fact that exact function and fate of the VO cells remains insufficiently resolved. Recent studies have demonstrated the occurrence of almost ubiquitous DNA synthesis with only scattered mitoses within the VO cells (Mayer et al. 2010a) and apoptosis during later VO degeneration (Mayer and Whitington 2009b). Yet, apoptosis in late stages does not automatically account for the fate of all cells that have been previously formed. Earlier reports of their involvement in neurogenesis (e.g. Pflugfelder 1948) have been recently contradicted (Mayer and Whitington 2009b; Mayer and Whitington 2011). This rejection is mainly based on (1) the spatial segregation of the VOs from the nerve cords and on (2) the already well-established axonal scaffold of the latter at the time of VO differentiation. Obviously, the latter argument in itself does not exclude continuing neurogenesis, as shown in the present study. Similarly, also the former argument does not necessarily speak against a neurogenic function. Apart from Pflugfelder (1948) (Fig. 73A), at least two additional studies (Kennel 1886; Sedgwick 1888) discuss and unmistakably depict persisting cell strands between the apically degenerating VOs and the spatially separated nerve cords (Fig. 73C-E). Kennel (1886) even explicitly considers the possibility that migration of cells along these strands into the nerve cords has major part in VO decrease, although deeming it unlikely (p. 21). But as indicated by the results presented here, anatomically separate cell regions can represent a source for cellular material to the CNS (see 4.3.5. for further examples from decapod crustaceans). Since the published new data on onychophoran neurogenesis do not allow refutation of the documented cell strands, it remains feasible that these were missed by the recent investigators (Mayer and Whitington 2009b; Whitington and Mayer 2011). In fact, indications of locally concentrated connections as shown by Pflugfelder (1948) have been recovered in early developmental stages of the VOs in the head region (Fig. 73B, unpublished data kindly provided by J. Eriksson). Accordingly, a role of VOs as sources for neuronal cell material during advanced stages of onychophoran development is herein still considered as being plausible.

4.3.3. The initial phase of pycnogonid neurogenesis compared to other arthropods

The lack of SCNPs during the initial phase of embryonic neurogenesis in *Pseudopallene* and other pycnogonids represents a major difference to all studied hexapods as well as malacostracan and branchiopod crustaceans. In contrast to this, formation of transiently recognizable CISs in the pycnogonid neuroectoderm shows similarities to euchelicerates and myriapods.

4.3.3.1. The slow 'crystallization' process of CISs in *Pseudopallene* sp.

In *Pseudopallene*, the earliest phase of neurogenesis from the slow stratification of the VNE via scattered basal displacement of nuclei up to the 'crystallization' of recognizable CISs extends over several of the embryonic stages established herein (Fig. 67). Contrary to this, no such slow and gradual development of CISs as such has been reported in any euchelicerate or myriapod representative. Two possible explanations for this circumstance are feasible.

(*1) Embryonic development of pycnogonids is slow compared to development of the studied euchelicerates and myriapods.* In *Pseudopallene* sp., the embryonic development up to hatching of the walking leg-bearing larva was herein roughly estimated to take between 1 and 2 months at 15°C, a water temperature that is also encountered in the natural habitat during the reproductive season (13- 15°C, personal observation). By comparison, in *Pycnogonum litorale*, a representative that hatches as small protonymphon larva without any post-ovigeral trunk segments, embryonic development alone lasts about three weeks at 15°C and high percentages of misdeveloping embryos are encountered at 20°C or higher water temperatures (personal observation). The post-embryonic anamorphic development of this species takes additionally several months (Behrens 1984; personal observation). As a consequence of the slow development of pycnogonids, a finer resolution of the successive basal displacement of cells belonging to prospective CISs may be achievable than in fixed material of the faster developing spiders or myriapods (e.g. Kadner and Stollewerk 2004: ~ 14 days embryonic development of *Lithobius forficatus* at 25°C; Brena and Akam 2012: ~48 days of embryonic development of *Strigamia maritima* at 13°C (almost half of the time in early cleavages, germ band development far more rapid); Mittmann and Wolff 2012: ~7-8 days embryonic development of *Parasteatoda tepidariorum* at 25°C, approximately twice as long in *Cupiennius salei*).

(2) No focus on CIS formation process in previous investigations. Studies on euchelicerates and myriapods have predominantly focused on the number and arrangement of CISs and their composition and structure as soon as they have become recognizable in the VNE (Stollewerk et al. 2001; Dove and Stollewerk 2003; Mittmann 2003; Kadner and Stollewerk 2004). However, the exact formation process of single CISs as such was never documented in detail. Accordingly, it

is feasible that a faster but nonetheless gradual basal displacement of cells (as opposed to a concerted simultaneous immigration) in the regions of the prospective CISs does occur but has not been resolved.

4.3.3.2. CIS number and array in *Pseudopallene* compared to euchelicerates and myriapods

In *Pseudopallene*, between six to eleven very closely spaced CISs could be identified within a hemi-neuromere of walking leg segment 1 prior to the formation of the central apical depression, from which point on recognition of CISs was no longer possible. A comparably low number of CISs was encountered in a corresponding hemi-neuromere of *Callipallene*, although this represents only one 'snapshot' of development due to limited availability of developmental stages. Notably, in the ventral hemi-neuromeres of myriapods (e.g. Heymons 1901; Tiegs 1940, 1947; Dohle 1964; Whitington et al. 1991; Pioro and Stollewerk 2006) and apparently also in some – but not all – euchelicerates (Weygoldt 1965: *Neobisium muscorum*; Mayer and Whitington 2009a, 2011: *Steatoda grossa*), a central apical invagination similar to pycnogonids is formed in advanced neurogenesis stages. Yet, in all recently studied species, the 30 or more CISs are already recognizable and arranged in the typical grid-like pattern prior to this invagination process. The investigated pycnogonids fall distinctly below that value.

In contrast to the present study, the majority of recent investigations on euchelicerates and myriapods relied on F-action labeling of the cortical cytoskeleton for cell shape assessment and CIS identification (e.g. Stollewerk et al. 2001; Dove and Stollewerk 2003; Mayer and Whitington 2009a; Döffinger and Stollewerk 2010). In light of this, it could be feasible that the low number of recognized CISs in the pycnogonid VNE is due to insufficient resolution of the cell arrangements with the applied tubulin labeling. Yet, tubulin labeling has been also shown to reliably reveal the CISs in the VNE of *Limulus polyphemus* (Mittmann 2003), *Cupiennius salei* (Döffinger and Stollewerk 2010) and *Parasteatoda tepidariorum* (Linne and Stollewerk 2011). This result has been additionally confirmed in the course of this study by staining experiments in the latter two species (see Figs. 74; 76). Hence, a general problem with tubulin labeling as such cannot be assessed. In addition to this, the comparably low cell number in the hemi-neuromeres as well as the close vicinity of the identified CISs in *Pseudopallene* make it unlikely that huge numbers of additional CISs were missed. Based on this, the lower number of CISs during early neurogenesis of *Pseudopallene* seems to represent a real difference to the studied euchelicerates and myriapods.

The identified CISs in the *Pseudopallene* were found to arise in spatially stereotypic positions, which is especially evident in the anterior portion of the hemi-neuromere. However, owing to their low number, no obvious row-column-like arrangement was apparent. This finding stands

again in contrast to the studied euchelicerates and myriapods, but is clearly no independent character from the CIS number.

4.3.3.4. Temporal sequence of CIS formation in *Pseudopallene* sp.

In *Pseudopallene*, neither temporally distinct 'pulses' of CIS formation could be observed, nor was a clearly sequential emergence of the few CISs assessable. However, due to the partially difficult identification of CISs in the tightly packed VNE and the exclusive reliance on morphologically staged specimens, it is also feasible that slight temporal differences in CIS formation remained unresolved between ES 3 and ES 4.

4.3.3.5. Genetic network underlying CIS formation in *Pseudopallene* sp.

The current lack of expression data on *Pseudopallene*-ASH represents an obvious shortcoming of the present study. Expression of at least one ASH has been observed in neuroectodermal domains that prefigure the locations of subsequent CIS formation in spiders and myriapods (Stollewerk et al. 2001; Dove and Stollewerk 2003; Kadner and Stollewerk 2004) and a proneural function has been demonstrated for *C. salei* (Stollewerk et al. 2001). Therefore, it would be highly interesting to elucidate whether corresponding ASH expression domains are identifiable in the pycnogonid VNE in spatial correlation with subsequently forming CISs. This is here considered very likely, but remains unproven. Furthermore, the temporal appearance of ASH expression could help to confirm or potentially readjust the exact onset of neural commitment within the VNE. Based on morphology alone, the scattered basal displacement of nuclei in columnar cells has been interpreted as the beginning of neurogenesis. However, it cannot be excluded with absolute certainty that these earliest stratification events represent a restructuring of the ectoderm without already involving the commitment of cells to the neural pathway. Within arthropods, such an early VNE with multi-layered structure and tightly packed cells has been described, for instance, in the millipede *Glomeris marginata* (Dove and Stollewerk 2003). Hence, expression patterns of proneural genes within the early VNE of *Pseudopallene* would prove invaluable for exact temporal calibration of the onset of cell movements in the VNE specifically related to neurogenesis.

In accordance with spiders and myriapods (Stollewerk 2002; Dove and Stollewerk 2003; Kadner and Stollewerk 2004; Chipman and Stollewerk 2006), the available data on *Pseudopallene* allow to conclude that Delta expression exhibits elevated levels in the formed CISs. Based on the few successfully labeled embryos in the appropriate stages, resolution of a CIS formation sequence was again not possible with this molecular marker. Nonetheless, in future studies, Delta expression might represent a useful tool complementing the challenging morphological analyses in this regard. Reliable description of the dynamics of CIS formation in pycnogonids is still pending such additional investigations.

4.3.3.6. CISs – static entities or dynamic sites of cell recruitment and dissociation?

In some previous works, different numbers of flask-shaped cells per CIS in euchelicerates and myriapods have been mentioned as difference between these two euarthropod taxa (Dove and Stollewerk 2003; Stollewerk 2008). This notion was based on the observation of only 5-9 cells per CIS in *Cupiennius salei*, (Stollewerk et al. 2001) versus 11-13 and 12 cells per CIS of *Glomeris marginata* and *Strigamia maritima*, respectively (Dove and Stollewerk 2003; Stollewerk and Chipman 2006). However, it is unlikely that these numbers reflect lineage-specific characteristics of euchelicerate and myriapod neurogenesis. Firstly, the CISs of the centipede *Lithobius forficatus* have been reported to comprise 5-9 cells – identical to the spider *C. salei* (Kadner and Stollewerk 2004). Secondly, the CISs of the xiphosuran *Limulus polyphemus* were described as being composed of 8-12 cells each (Mittmann 2003). Hence, no consistent numerical differences are assessable between the two lineages. The pioneering studies on euchelicerate and myriapod neurogenesis of the last decade describe sequential formation of CISs per hemi-neuromere, their persistence for a several days of development and final disappearance due to detachment of the constituting flask-shaped cells from the apical surface (Stollewerk et al. 2001; Stollewerk 2002; Dove and Stollewerk 2003). In some cases, the number of GCs being internalized by this CIS detachment process was even estimated (e.g. Mittmann 2003, Stollewerk 2004). This implies a rather 'static' nature of CISs as discreet entities with constant cell numbers. However, such a 'static' description represents almost certainly a discretization artifact based on the investigation of selected fixed stages. In agreement with the results of this work, several studies present evidence for a more dynamic nature of CISs.

(1) Immigrating flask-shaped cells detach sequentially from each CIS. While CISs are visible at the ectodermal surface, successive dissociation of single cells from the CISs has been described for euchelicerates (Mittmann 2003; Weller and Tautz 2003; Döffinger et al. 2010; Linne and Stollewerk 2011) and discussed for myriapods (Chipman and Stollewerk 2006) (Fig. 72B,C). This is evident in the onset of segmental axonogenesis and neuropil formation basal to the persisting CISs and could be confirmed during the present study for the two spiders *C. salei* and *Parasteatoda tepidariorium* (data not shown). Consequently, cell detachment is no fully synchronized process in CISs (as shown e.g. in Stollewerk 2008, fig. 19.1). In accordance with this view, first detached basal GCs appear gradually in the pre-cheliforal lobe and the VNE of *Pseudopallene* sp. during ES 5 and ES 6 – directly prior to the onset of axonogenesis – when most cells in the corresponding neuromeres are still flask-shaped and apically attaching.

(*2) At least some CISs recruit additional cells over an extended time span of neurogenesis.* In addition to the slow formation process of CISs described here for *Pseudopallene*, a compositional change of already recognizable CISs is most clearly observable in the pre-cheliforal lobe (but to

a lesser extent also in the VNE). Some of the identified central CISs change their morphology over time, comprising in later stages significantly more cells than in the beginning. Accordingly, these CISs are dynamic in terms of cell numbers and might be more fittingly characterized as stereotypically positioned areas of continuous apical cell recruitment and successive basal cell detachment. Similar phenomena are also encountered during spider neurogenesis (Fig. 72B). In *C. salei*, so-called 'primary' and 'secondary' CISs have been described (Stollewerk 2004; Linne and Stollewerk 2011). The 'secondary' CISs are less numerous (~25 per ventral hemi-neuromere) but comprise up to 40 cells each, as opposed to the 5-9 cells of 'primary' CISs. Whereas the original description of 'secondary' CISs implied their *de novo* formation in temporal overlap with the complete detachment of the 'primary' GICs (Stollewerk 2004), the more recent study clearly advocates transformation of some 'primary' GICs into the cell-rich 'secondary' ones (Linne and Stollewerk 2011). This aspect of spider neurogenesis was briefly reinvestigated in the course of the present study. Using the detailed CIS map of Döffinger and Stollewerk (2010), the 'primary' CISs in ventral hemi-neuromeres of *C. salei* were identified in comparable (and even slightly later) developmental stages (Fig. 74A-C). The obtained results are in good accordance with the published map, all 38 'primary' CISs having been recovered (compare Fig. 74C to Döffinger and Stollewerk 2010, their fig. 1B,C). Investigation of the cellular composition of the single CISs revealed significant differences, some being small with low cell numbers, others comprising already far more than the 9 cells reported as maximum of 'primary' CISs (Fig. 74D-G). This finding clearly supports a dynamic nature of the spider CISs as areas that recruit apical cell material over an extended time span. The reduced number of the persisting cell-rich CISs also indicates not only sequential CIS formation but also sequential CIS dissociation.

One interesting aspect of this 'differential' CIS development is its general correspondence to NB lineages in hexapods (and presumably also in crustaceans). Here, NBs within one hemi-neuromere differentiate not only sequentially but exhibit furthermore differences in their proliferation rates and in the overall duration of their proliferation activity (e.g. Bate 1976: *Locusta migratoria*; Shepherd and Bate 1990: *Schistocerca gregaria*). Accordingly, considerable differences in the cell numbers of different NB lineages are encountered (e.g. Bossing et al. 1996; Schmidt et al. 1997; Schmid et al. 1999 for comprehensive studies on *Drosophila melanogaster*). This corresponds to differences in cell numbers and varying persistence times of CISs in the neuroectoderm of *C. salei* and at least in the pre-cheliforal lobe of *Pseudopallene*. Furthermore, the successive basal dissociation and subsequent differentiation of immature GCs from CISs is reminiscent of the first differentiation of the basal-most (i.e., oldest) immature GCs in hexapod and malacostracan NB lineages, which here go back to division of the GMCs (e.g. Goodman and Spitzer 1979; Doe and Goodman 1985a; Hartenstein et al. 1987; Ungerer and Scholtz 2008).

4.3.4. The second phase of pycnogonid neurogenesis compared to other arthropods

4.3.4.1. Advanced neurogenesis in pycnogonids vs. myriapods

The descriptions of advanced neurogenesis in myriapods exhibit some remarkable similarities to pycnogonids (see also 4.3.1.1; compare Figs. 67, 72C). Notably, slightly bigger proliferating cells ('neuroblasts') have been once reported during neurogenesis of the scutigeromorph *Scutigera coleoptrata* (Knoll 1974), but recent investigations did not find evidence for distinct cell size differences in the VNE of other centipedes (Whitington et al. 1991; Kadner and Stollewerk 2004; Chipman and Stollewerk 2006; Stollewerk and Chipman 2006). However, Knoll's drawings show the bigger proliferating cells in advanced stages of neurogenesis with multi-layered hemi-ganglion anlagen and the beginning formation of the paired apical invaginations (Knoll 1974, his figs. 48, 49). Unfortunately, in none of the recent centipede studies, cell types, cellular arrangements or cell division patterns were investigated in correspondingly late stages. In millipedes, Dohle (1964) describes for *G. marginata* extensive cell proliferation within the paired segmental invaginations of advanced neurogenesis, but cellular characterization and proliferation in late stages have again not been satisfactorily addressed in recent investigations on this species (Dove and Stollewerk 2003; Pioro and Stollewerk 2006; Döffinger and Stollewerk 2010). Most intriguingly, the location of cell divisions within the 'ventral organs' of symphylans and especially pauropodans (Tiegs 1940, 1947) largely corresponds to the ones of SCNPs and INPs of *Pseudopallene*. Cell proliferation is observed within morphologically distinct, apical spindle-shaped cells as well as sub-apical to them (and to a lesser extent also scattered in the basal ganglion anlage). However, no mention of morphologically asymmetric divisions is made by Tiegs (1940, 1947) and more recent investigations (Mayer and Whitington 2009a) do not extend into these advanced developmental stages. Hence, advanced myriapod neurogenesis still awaits detailed reinvestigation and has the potential to be highly interesting from a comparative perspective.

4.3.4.2. Advanced neurogenesis in pycnogonids vs. onychophoran VOs

At the current state, a meaningful evaluation of the similarities between advanced neurogenesis in pycnogonids (and myriapods) and the onychophoran VOs is challenging. Not only remains it unresolved whether the VOs of the onychophoran trunk are actually involved in neurogenesis (see 4.3.2.2.). Also detailed descriptions of their cellular arrangements, the possible existence of different cell types and the exact location of cell divisions are lacking. Ubiquitous DNA synthesis has been demonstrated in the conspicuously big columnar cells of the trunk VOs, having been speculated to be related to endocycling, i.e., DNA replication without cell division (Mayer et al. 2010a). But symmetry and orientation of those divisions that do occur as well as cell fate remain unresolved. In contrast to this, the VO of the protocerebrum is known to show

during its invagination still the three-layered structure characteristic of the earlier neuroectoderm (Eriksson et al. 2003, Eriksson and Stollewerk 2010a). Here, the bigger columnar cells of the apical cell layer generate cellular material by tangential divisions (Eriksson and Stollewerk 2010a), NPs segregate from this apical layer into sub-apical position and give rise to immature GCs by divisions on their own. In the adult hypocerebral organ, these distinct cell types and their layering are lost (Eriksson et al. 2005). Should the cellular characteristics and arrangements of the invaginating protocerebral VO prove representative for the trunk VOs (apart from the invagination and persistence), a general correspondence to the apico-basal cell type arrangement during advanced neurogenesis of pycnogonids (and potentially myriapods) might be feasible. But as in myriapods, this necessitates further studies on advanced neurogenesis in the onychophoran trunk.

4.3.4.3. Pycnogonid SCNPs vs. tetraconate NBs

The asymmetrically dividing SCNPs that enlarge during the second phase of pycnogonid neurogenesis are obviously reminiscent of crustacean and hexapod NBs (e.g. crustaceans: Dohle 1976; Scholtz 1992; Harzsch 2001; Ungerer and Scholtz 2008; Ungerer et al. 2011a; hexapods: Wheeler 1891; Bate 1976; Doe and Goodman 1985a; Hartenstein et al. 1987; Doe 1992). This raises the question, how many detailed similarities beyond size and division mode provide arguments for a common origin of both NP types.

(1) The two NP types do not share a corresponding time of differentiation. Tetraconate NBs emerge at the beginning of neurogenesis, their proliferation activity generating the vast majority of future GCs. The pycnogonid SCNPs enlarge only after the initial phase of neurogenesis has already led to a considerable thickening of the neuroectoderm.

(2) The two NP types do not share a similar cell type environment during their formation. Pycnogonid SCNPs arise in an apical depression in the center of each hemi-neuromere, representing an ectodermal region that will eventually adopt neural fate in its entirety. The mechanism underlying pycnogonid SCNP specification within this central neuroectodermal depression remains to date unknown. Ventral epidermal cells have their origin in the more peripheral regions of the hemi-segment. In crustaceans and hexapods, NBs differentiate in the apical ectodermal layer in direct vicinity and intermingled with prospective epidermal cells. Hence, tetraconate NBs differentiate in an ectodermal region with binary fate, although the NB specification processes differs between crustaceans and hexapods.

(3) The two NP types do not share a corresponding orientation of their asymmetric divisions. Pycnogonid SCNPs were here observed to divide tangentially or with a slightly oblique inclination. Due to this, the generated smaller daughter cells of pycnogonid SCNPs are not

automatically internalized during division but rather seem to immigrate independently. By contrast, tetraconate NBs divide (predominantly) in radial direction. In malacostracans and branchiopods, intermittent deviations from radial NB divisions are documented (e.g. Dohle 1976; Ungerer 2006; Ungerer et al. 2012). However, the resulting daughter cells appear to assume epidermal fate, whereas all cells generated in the central invagination of pycnogonids adopt neural fate.

(4) Pycnogonid SCNPs share with crustacean NBs the apical position in the VNE. This similarity holds only if the inner surface of the central invaginations in pycnogonids is still considered as being apical, which view is herein preferred (see 4.2.2.3.). The apical position contrasts to hexapod NBs, which immigrate and detach from the apical VNE before their proliferation activity in a sub-apical layer. Recent works have favored the hexapod mode of NB immigration as representing the plesiomorphic condition of tetraconates (e.g. Ungerer and Scholtz 2008; Ungerer et al. 2011a, 2012; Whitington and Mayer 2011). If true, apically maintained crustacean NBs would represent a derived feature that is useless in comparisons with non-tetraconate arthropods. This view will be more closely scrutinized later on (see 4.3.6.)

(5) Pycnogonids and tetraconates share sub-apical INPs. The smaller sub-apical INPs of pycnogonids show a morphologically symmetric mode of division. Their correspondence to tetraconate GMCs may be suggested. However, compelling evidence for this suggestion remains currently scarce. Neither the genealogical relationship of the sub-apical pycnogonid INPs to the apical SCNPs, nor the number of divisions undergone by each INP could be established in this study.

In summary, apart from relative cell size and asymmetric division mode, hardly any striking similarities are currently assessable between pycnogonid SCNPs and tetraconate NBs. Based on the complete set of known characteristics of these two NP types, their homologization appears only poorly substantiated. Nonetheless, this is not to say that common origin from an ancestral SCNP type can be definitely refuted (see 4.3.6.2.). More studies are needed to better understand the characteristics and relationships of the two pycnogonid NP types (SCNPs and INPs) and allow more detailed comparisons to tetraconate NBs and GMCs. For instance, continuation of the started expression studies of *Pseudopallene*-Snail and *Pseudopallene*-Prospero as well as investigation of additional genes, such as, e.g. Asense, should be future next steps for their characterization at the molecular level. By comparison, NBs and/or GMCs of hexapods (Doe et al. 1991; Vaessin et al. 1991; Brand et al. 1993; Spana and Doe 1995; Ashraf and Ip 2001; Wheeler et al. 2003; Southall and Brand 2009) as well as of the cladoceran *Daphnia magna* (Ungerer et al. 2011a, 2012) are characterized by specific Snail-, Prospero- and Asense-expression patterns. In addition, application of *in-vivo* cell proliferation markers (e.g. BrdU, EdU) or attempts of direct

single cell labeling might help to shed more light on the genealogical relationships and division patterns of the SCNPs and sub-apical INPs. Yet, both of these techniques rely on the ready availability of live material in the appropriate developmental stages. For this reason, a successful laboratory culture of a pycnogonid with embryonized development represents a pivotal prerequisite for future studies seeking to resolve these aspects. Some of the important questions that still need to be answered are:

(1) What mechanism underlies specification of SCNPs in the pycnogonid neuroectoderm?

(2) Do all SCNPs divide exclusively asymmetrically or do they switch intermittently to symmetric divisions?

(3) Do all of the interspersed smaller apical cells and the sub-apical cells represent INPs or do they include already immature post-mitotic GCs?

(4) Does each sub-apical INP directly undergo terminal division or does it divide repeatedly?

4.3.5. The third phase of pycnogonid neurogenesis compared to other arthropods

4.3.5.1. Cluster-stream-system – a putative life-long neurogenic niche in Pycnogonida

The results of this study indicate the systems of apical cell clusters and connecting cell streams of brain and ventral ganglia in *Pseudopallene* to represent sources for additional GC material during post-embryonic development and up to adult life.

During the last twenty years, a notable number of studies have addressed adult neurogenesis in another euarthropod taxon, the decapod crustaceans. Already in older studies (Bazin and Demeuzy 1968; Bazin 1969, 1970, 1971), an enigmatic 'deutocerebral organ' had been identified at the ventral side of the brain of various decapods, but its function remained obscure. Using a combination of newer techniques, this deutocerebral organ has by now been characterized as a system of life-long neurogenesis (e.g. Harzsch and Dawirs 1996; Harzsch et al. 1999; Schmidt 1997, 2001, 2002, 2007a; Schmidt and Harzsch 1999; Schmidt and Derby 2011; Chaves da Silva et al. 2012; see Beltz and Sandeman 2003; Schmidt 2007b; Sandeman et al. 2011 for reviews), with some recent contributions focusing on its development in crayfish (Song et al. 2009; Sintoni et al. 2012). In all investigated decapods, the neurogenic niche is affiliated with the deutocerebrum and could exemplarily be shown to give rise to cells that subsequently differentiate into olfactory interneurons associated with the primary olfactory centers, the glomeruli in the olfactory lobe. This life-long neurogenic system almost always consists of a small cluster of glial-like cells with a central cavity, the 'niche', that is connected to the two deutocerebral soma clusters 9 and 10 (nomenclature following Sandeman et al. 1992) via elongated 'migratory streams' (exception: separate niches in clusters 9 and 10 in spiny lobsters, e.g. Bazin 1971; Schmidt 2001, 2007a). Along the latter, cells migrate from the niche into the clusters 9 and 10.

Immunolabeling of PH3 and *in-vivo* proliferation markers have demonstrated cell divisions in the niche itself and along the migratory streams as well as considerable proliferation in the region where the migratory streams enter into clusters 9 and 10, the 'proliferation zones'. Here, the immature cells subsequently differentiate into olfactory interneurons. To date, it is still matter of some debate what kind of NPs are found in the niche (local SCNPs (adult NBs) vs. non-self-renewing NPs recruited from outside the niche; see e.g. Song et al. 2009; Schmidt and Derby 2011 vs. Sandeman et al. 2011, respectively).

Interestingly, the gross architecture of the cell clusters with central cavity and two connecting cell streams of *Pseudopallene* and the occurrence of cell divisions in both sub-structures correspond to the neurogenic niche of most decapods. Yet, the niche of decapod taxa has been shown to be closely associated with the vascular system or even directly connected to it (e.g. Schmidt and Derby 2011; Chaves da Silva et al. 2012; Sintoni et al. 2012). This feature seems to be lacking in pycnogonids, which are devoid of a complex vascular system. The circulation of the hemolymph is driven by a simple tube-like heart that is located dorsally to a horizontal septum ('Dohrn's septum'), which merely divides the body cavity in a dorsal and a ventral sub-compartment (e.g. Dohrn 1881; Bogomolova and Malakhov 2011). Notwithstanding this difference, the other gross architectural similarities to the system of life-long neurogenesis in decapods may be taken as further indirect support of the deduced neurogenic function of the pycnogonid cluster-stream-system advocated herein.

4.3.5.2. Spatial 'fit' of cluster-stream-systems and primary and secondary olfactory centers

As sources for olfactory interneurons, the decapod neurogenic niches are encountered exclusively in the deutocerebrum, which houses the glomeruli as primary olfactory centers. In addition to this, two studies could demonstrate localized cell proliferation in the adult lateral protocerebrum of true crabs and hermit crabs (Schmidt 1997; Schmidt and Harzsch 1999), although the structural organization of the proliferating regions remains unresolved. This cell proliferation is found spatially related to the neuronal somata of the hemi-ellipsoid bodies, which process input from ascending olfactory projection neurons of the deutocerebrum, i.e., they represent secondary olfactory centers. Similarly, studies on hexapods have revealed addition of globuli cells ('Kenyon cells') to the mushroom bodies in the adult protocerebrum in some (but not all) investigated species (e.g. Cayre et al. 1994, 1996; Dufour and Gadenne 2006; Zhao et al. 2008). Mushroom bodies represent multi-functional association centers that receive amongst others also input from ascending olfactory projection neurons located in the deutocerebral antennal lobe (e.g. Strausfeld et al. 1998, Wolff et al. 2012). Thus, they represent as well secondary olfactory centers in the hexapod olfactory pathway. Hence, there is a specific

correlation of adult neurogenesis and the olfactory pathway in decapod crustaceans and some hexapods.

To date, the olfactory pathway of pycnogonids is still insufficiently understood. In previous studies, GNs have neither been described in the pycnogonid brain, nor in the VNC (Wirén 1918; Hanström 1919, 1928; Helfer and Schlottke 1935; Sanchez 1959; Winter 1980). Furthermore, the exact position and structure of pycnogonid chemoreceptors remains vague. Stock (1978) conducted experiments on the chemical sense of different species and could unambiguously demonstrate directed movement towards different cnidarian prey that was not visible for the tested animals. Such positive attraction was also observable in *Endeis spinosa* – a species in which both sexes lack chelifores and palps, females even the ovigers – and also in *Nymphon gracile* after selective experimental removal of chelifores, palps or ovigers. Based on this, Stock (1978) concludes that chemoreceptors are most likely distributed on different parts of the pycnogonid body, including the walking legs, which is as well suggested by King (1973) and Arnaud and Bamber (1987). The most precise available description of the pycnogonid olfactory pathway was provided by Strausfeld and colleagues (1998, 2006a). They report existence of few GNs in all walking leg ganglia of *Ammothea hilgendorfi*. These GNs are said to receive sensory input from setae on each walking leg and to be associated to olfactory interneurons that ascend into small MBNs in the brain. However, merely a rough schematic overview is depicted (Fig. 44A). The GNs identified in this work within the walking leg ganglia of *Pseudopallene* corroborate the findings of Strausfeld and colleagues (1998, 2006a). Furthermore, indications for the existence of small GNs in the sub-esophageal neuromeres of *Pseudopallene* provide incentive for future investigations. Irrespective of the more specific structure of the pycnogonid GNs, their location within the walking leg ganglia speaks for the existence of olfactory interneurons in the latter. In light of this, the array of cluster-stream-systems of *Pseudopallene* at the ventral side of each ventral ganglion and the entering of the streams into the ventral soma cortex close to the ventral GNs represents a notable correlation. In correspondence to the decapod neurogenic niche, it might indicate an involvement of the pycnogonid cluster-stream-system in the replenishment of interneurons associated with the primary olfactory centers.

In *Pseudopallene*, also each brain hemisphere bears a cluster-stream-system at its ventral side (anterior side in terms of body axis). Its cell streams were found to enter the brain soma cortex in the vicinity of more densely packed, small cytoplasm-poor somata of globuli cells, from which bundles of parallel axons project. Due to these characteristics and the spatial correspondence to neuropils mentioned by Strausfeld and colleagues (1998, 2006a), these brain regions have been herein interpreted as MBNs (see also 4.4.2.1.). If proven correct, the cluster-stream-system of the brain would be found in direct vicinity of putative second order neuropils of the olfactory pathway. This could be an additional noteworthy correlation with regard to

observed adult cell proliferation in some hexapod mushroom bodies and decapod hemi-ellipsoid bodies.

Doubtlessly, more detailed investigations on the adult pycnogonid cluster-stream-system – including *in-vivo* proliferation markers and TEM – are still needed to (1) unequivocally establish whether it is involved in the generation of future globuli cells and olfactory interneurons, (2) obtain a better understanding of its proliferation dynamics in general and (3) better characterize its constituting cell types, for instance, a potential glial nature of the cluster cells.

4.3.5.3. Existence of olfactory neurogenic niches in other arthropod taxa?

Recent studies and reviews on life-long neurogenesis in decapods have highlighted structural similarities of the decapod neurogenic niche to vertebrate stem cell niches, which also occur in association with the olfactory pathway of the nervous system (e.g. Sullivan et al. 2007; Sandeman et al. 2011; Schmidt and Derby 2011, see references therein). Hence, the presence of olfactory neurogenic niches has been concluded to represent a relatively common phenomenon especially in long-lived animals, being potentially based on similar (but not necessarily homologous) underlying mechanisms (e.g. Sandeman et al. 2011). In line with this notion, pycnogonids do not only develop slowly but are also long-lived under laboratory conditions, surviving several years (e.g. *Pycnogonum litorale*: personal observation; *Colossendeis* sp.: personal communication Arno Otten, Aquarium Wilhelmshaven). Furthermore, the cluster-stream-system in *Pseudopallene* with its partially confirmed vicinity to olfactory centers may speak for a more common occurrence of (segmentally differently affiliated) neurogenic niches within arthropods. A logical next step is a targeted search for corresponding phenomena in the remaining arthropod lineages.

So far, data on euchelicerates and myriapods are scarce. Nonetheless, some classical French studies provide evidence for the existence of niche-like cell clusters with central cavity (‘organes neuraux intracérébraux’) in the developing and adult protocerebrum of some diplopod species (Juberthie-Jupeau 1967) and opilionids (Juberthie 1964; Juberthie and Muñoz-Cuevas 1970). Remarkably, these cell clusters are found in association with the globuli cells of the mushroom bodies. In one study, they have even been explicitly reported to generate additional globuli cells (Juberthie and Muñoz-Cuevas 1970). The diplopod and opilionid niche-like clusters represent no separate units lying external to the soma cortex of the brain but are embedded apically within the globuli cells of the mushroom bodies. This location is similar to the regions of adult neurogenesis in hexapod mushroom bodies, where morphologically delimitable cells clusters are found apically within globuli the cells (e.g. Dufour and Gadenne 2006; Cayre et al. 2007; Zhao et al. 2008), each cluster containing a NB persisting into adulthood. It is also reminiscent of the adult neurogenic system of spiny lobsters (e.g. Bazin 1971; Schmidt 2001, 2007a; Schmidt and

Derby 2011) and true crabs (Bazin 1968), in which the niches themselves are also located ventrally embedded in the brain soma clusters. Finally, it corresponds as well to the putatively 'atrophying' cell clusters of the ventral ganglion anlagen in some pycnogonids, which are incorporated into the soma cortex but were so far not traceable into adults (e.g. Morgan 1891; Sanchez 1959; Fig. 71E). Interestingly, in some opilionid species, a single big cluster is also persisting at the posterior side of the composite sub-esophageal ganglion with an anteriorly directed cell stream of supposedly newly generated neuronal material (Juberthie and Muñoz-Cuevas 1970). However, its association to GNs is not mentioned.

Another potentially comparable phenomenon within euchelicerates represents the persistence of 'epithelial vesicles' in the VNC of the spider *Cupiennius salei* in post-hatching stages (Stollewerk 2004) (Fig. 72B). These vesicles derive from the advanced 'secondary' CISs and encompass undifferentiated neuroepithelial cells. Some of the vesicles are known to persist at least into the early larval stages and were recently also encountered in the larval brain (Döffinger et al. 2010). It is assumed that complete dissociation of the vesicle cells takes place during subsequent post-embryonic development. Based on the observations during embryonic development, this event is thought to be not connected to notable mitotic activity (Stollewerk 2004). However, so far neither the post-embryonic dissociation, nor the related cell division dynamics have been subject of further investigation. Therefore, the exact fate of all vesicles remains to date unresolved.

The most intriguing instance of a niche-like cell cluster is encountered in onychophorans as putative euarthropod outgroup. In the protocerebral region, the VO invaginates and detaches from the apical ectoderm to form the hypocerebral organ (HO) that is ventrally attached to the adult brain (e.g. Pflugfelder 1948, Eriksson et al. 2003). To this day, the function of the HO has remained elusive. In the most recent contributions on this structure (Eriksson et al. 2003, 2005), it is speculated whether it serves a glandular function, potentially similar to the corpora allata in hexapods. However, hexapod corpora allata and onychophoran HOs do neither share corresponding segmental affiliation, position in relation to the CNS and type of connection to the latter, nor do they have a similar development (Bullock and Horridge 1965; Cassier 1979). Contrary to this, several HO characteristics are similar to the decapod neurogenic niches and (where known) to the pycnogonid cluster-stream-system.

(1) Position with respect to the CNS. The HO is located ventral and externally attached to the protocerebral region of the brain (Eriksson et al. 2003, 2005).

(2) Gross architecture. In the HO, cells with inwards directed apical poles and peripherally displaced nuclei surround a central cavity. The HO is not innervated by the brain but connected to it via strands of cells (Eriksson et al. 2005).

(3) Persisting cell proliferation in adults. Numerous mitoses have been observed among the HO cells in adult onychophorans (Eriksson et al. 2005).

(4) Ultrastructure of cells. The cells constituting the HO are characterized amongst others by numerous mitochondria, a well-developed Golgi apparatus, conspicuous cytoplasmic vesicles and the existence of tight cell junctions towards the central cavity (Eriksson et al. 2005). The same characteristics are found in the predominant type I cells of the crayfish neurogenic niche (Chaves da Silva et al. 2012), indicating possible secretory functions.

(5) Concentric layers of material within the central cavity. The substance within the HO central cavity is organized in concentric layers and shows positive PAS (Periodic acid-Schiff) reaction, which might indicate its cuticular nature (Eriksson et al. 2005). A similar onion-shaped appearance of the niche's central cavity coupled to positive PAS reaction has been described in some crayfish and very pronounced in the peculiar neurogenic system of clawed lobsters (Bazin 1969, 1970).

(6) Direct derivative of elements of embryonic CNS neurogenesis. The adult HO is a direct derivative of the invaginating protocerebral VO, which in turn represents a transformation of the protocerebral neuroectoderm (Pflugfelder 1948; Eriksson et al. 2003; Eriksson and Stollewerk 2010a). The same relationships hold for the segmental cluster-stream-systems of *Pseudopallene*. Furthermore, elements of the crayfish neurogenic niche were recently shown to originate in a 'deutocerebral proliferative system' which initially still encompasses some of the deutocerebral NBs and their GMCs as well as potentially other NP types (Sintoni et al. 2012).

(7) Affiliation with brain region housing the olfactory centers. Although VOs develop along the entire length of the onychophoran trunk, only the protocerebral region is characterized by the persistence of paired HOs. In contrast to all extant euarthropods, onychophorans possess a fully developed limb pair affiliated with the protocerebral region, the 'primary antennae' (e.g. Eriksson and Budd 2000, nomenclature following Scholtz and Edgecombe 2006). Receiving input from this sensory appendage, onychophoran olfactory glomeruli are found exclusively in the protocerebral neuropil together with the mushroom bodies (e.g. Schürmann 1987; Strausfeld et al. 2006b). Hence, HO and primary and secondary olfactory centers show a fitting segmental affiliation.

Based on this list of features, the onychophoran HOs are here considered a promising candidate for a neurogenic niche. As in pycnogonids, experiments applying proliferation markers with focus on the adult nervous system would help to test this notion.

4.3.6. On the evolutionary course of euarthropod neurogenesis

4.3.6.1. Contentious phylogenetic relationships of the major arthropod lineages

Currently, scenarios on the evolution of arthropod neurogenesis are faced with the fundamental problem of unsatisfactorily resolved phylogenetic relationships of the four major euarthropod lineages. Unification of hexapods and crustaceans in a clade Tetraconata (Dohle 2001) or Pancrustacea (Zrzavý and Štys 1997) is in an overwhelming number of current studies uncontested (e.g. Regier et al. 2008, 2010; von Reumont et al. 2009, 2012; Andrew 2011; Campbell et al. 2011; Strausfeld and Andrew 2011, but see Bäcker et al. 2008). Furthermore, also the paraphyly of crustaceans receives considerable support from the great majority of comprehensive studies, although the exact interrelationships to hexapods remain debated (e.g. Roeding et al. 2009; Jenner 2010; Regier et al. 2010; von Reumont et al. 2010, 2012; Andrew 2011; Strausfeld and Andrew 2011). With tetraconates being firmly established, two key issues of importance are left in the discussion on the basal nodes in the euarthropod tree.

Firstly, the position of Pycnogonida either as sister group to Euchelicerata or as earliest extant offshoot within euarthropods, i.e., as sister group to 'Cormogonida' (e.g. Zrzavý et al. 1997; Egdecombe et al. 2000 (morphological analysis only); Giribet et al. 2001). Notably, the results of almost all recent phylogenetic analyses, do not find evidence for the latter hypothesis anymore. Pycnogonids as sister group to euchelicerates are on the other hand regularly recovered, albeit frequently with relatively low support values (e.g. Bourlat et al. 2008; Roeding et al. 2009; Regier et al. 2010; Rota-Stabelli et al. 2010; Campbell et al. 2011; Rehm et al. 2012). Nonetheless, given the virtually non-existent corroboration of the Cormogonida hypothesis, it is here deemed unjustified to artificially perpetuate the debate on this issue. In light of this, the Chelicerata hypothesis and its inherent homologization of the pycnogonid chelifore and euchelicerate chelicera is herein given clear preference over the Cormogonida hypothesis.

Secondly, the monophyly of Myriapoda and their position either as sister group to Tetraconata (Mandibulata hypothesis) or as closest relatives of Chelicerata (Paradoxopoda or Myriochelata hypothesis). Monophyly of Myriapoda has been indicated in recent molecular studies (e.g. Regier et al. 2010; Rota-Stabelli et al. 2011), a neurocladistic analysis (Strausfeld and Andrew 2011) and strongly advocated in recent reviews (Edgecombe 2010; Shear and Edgecombe 2010; Giribet and Edgecombe 2012). It can be supported by several potential morphological apomorphies (see Edgecombe 2010), due to which this view has been adopted herein. More problematic is the phylogenetic position of monophyletic myriapods. Anatomical characters, such as the antenniform deutocerebral appendage, the mandible as first post-tritocerebral appendage with particular structural characteristics (Edgecombe et al. 2003), several features of neuroarchitecture (e.g. Harzsch et al. 2005a; Harzsch 2006; Sombke et al. 2012; neurocladistic analysis: Strausfeld and Andrew 2011) and aspects of midline development (Linne et al. 2012)

speak in favor of a sister group relationship of myriapods and tetraconates. In contrast to this, numerous molecular studies of the last two decades have indicated sister group affinities between chelicerates and myriapods (e.g. Friedrich and Tautz 1995; Cook et al. 2001; Mallatt et al. 2004; Pisani et al. 2004; Roeding et al. 2009). However, in more recent molecular analyses, better support for mandibulates has resurfaced (Bourlat et al. 2008; Rota-Stabelli and Telford 2008; Regier et al. 2008, 2010; Rota-Stabelli et al. 2010, 2011; Campbell et al. 2011; Rehm et al. 2012). The interpretation of the revealed similarities of early neurogenesis in euchelicerates and myriapods as synapomorphy of both lineages or alternatively as plesiomorphic feature of euarthropod neurogenesis depends critically on the position of myriapods (Kadner and Stollewerk 2004; Stollewerk and Chipman 2006; Mayer and Whitington 2009a). Given the better morphological evidences and the reawakened support in molecular studies, the Mandibulata hypothesis is here considered the more reliable backbone for evolutionary scenarios. Nonetheless, to date, the alternative hypothesis cannot be disregarded with comparable confidence as in the Chelicerata versus Cormogonida case.

4.3.6.2. Two scenarios on the evolution of euarthropod neurogenesis

Most recent contributions on the evolution of euarthropod neurogenesis have primarily focused on two distinct modes involving either spatially stereotypic CISs (euchelicerates and myriapods) *or* specialized SCNPs (crustaceans and hexapods) (e.g. Harzsch 2003, 2006; Harzsch et al. 2005a; Simpson and Stollewerk 2005; Stollewerk and Chipman 2006; Stollewerk 2008; Eriksson and Stollewerk 2010b; Whitington and Mayer 2011). In some recent discussions, however, the occurrence of different modes of neurogenesis in spatially separate regions of the CNS of one organism have been highlighted (Eriksson and Stollewerk 2010b; Ungerer et al. 2011a). This includes, for instance, the formation of the pars intercerebralis and pars lateralis in the brain of *Drosophila melanogaster* via groups of immigrating cells rather than NBs (de Velasco et al. 2007) as well as the direct immigration of immature neurons pioneering the protocerebral commissure in the brain of *Schistocerca gregaria* (Boyan and Williams 2008). Similarly, development of the (peripheral) stomatogastric nervous system of insects is characterized by segregation of groups of cells from a placode in the dorsal stomodeum wall (Hartenstein 1997). These phenomena have been used to argue for CISs as the plesiomorphic condition within euarthropods. Compared to the other lineages, one of the most intriguing features of pycnogonid neurogenesis is the sequential formation of CISs *and* specialized NPs in exactly the same neuroectodermal region. This illustrates that neurogenesis in a given region does not necessarily have to follow the same mode throughout the entire development of an organism. Superficially, a similar developmental sequence is also encountered during optic lobe development of *Drosophila* (Green et al. 1993; Hartenstein et al. 1996). Here, an optic placode invaginates to form an internalized transitory

epithelial vesicle, from which only subsequently NBs differentiate. However, the ~80 cells of the invaginated optic placode retain at first their epithelial character and it remains unclear, whether some of them differentiate directly into neurons prior to NB formation.

Two possible scenarios of the evolution of euarthropod neurogenesis are considered in the following, being set against the Chelicerata and Mandibulata hypotheses (Fig. 75). The first scenario presents a simple and conflict-free explanation of the pycnogonid features of neurogenesis that advocates convergent evolution of specialized SCNPs. The second takes the lack of detailed data at cell level during advanced neurogenesis into account (especially in myriapods), resulting in an intriguing but more speculative view. Due to the current gaps in the available data on adult neurogenesis in most arthropod groups apart from decapod crustaceans, it was refrained from including this aspect in the following evolutionary considerations.

***Scenario 1: Spatially stereotypic CISs are part of the euarthropod stem species pattern and pycnogonid SCNPs and tetraconate NBs evolved convergently* (Fig. 75A).**

Sequential formation of CISs in a grid-like pattern represents the ancestral condition within euarthropods. Formation of each CIS is predated by elevated levels of ASH-expression in spatially stereotypic VNE domains (data for pycnogonids still missing). Cellular material for recruitment in CISs is generated by apical tangential divisions in the VNE. In the euarthropod stem species pattern, all cells in the central VNE region in each hemi-segment eventually adopt exclusively neural fate. Presumably, paired segmental invaginations have formed during advanced neurogenesis as part of the internalization and detachment process of the central neural VNE region (occurrence in pycnogonids and myriapods and some euchelicerates as well as in the protocerebral region of onychophorans).

The lower number of CISs in pycnogonids compared to euchelicerates and myriapods resembles an apomorphic feature (see remarks below). Pycnogonid SCNPs and tetraconate NBs do not share a common origin but evolved independently in both lineages. In several (but not all) extant euchelicerate taxa, no central invaginations of the hemi-neuromeres are encountered any longer (e.g. Mittmann 2003: *Limulus polyphemus*; Stollewerk 2004, Wolff and Hilbrant 2011: *Cupiennius salei*; Mittmann and Wolff 2012: *Parasteatoda tepidariorum*). However, due to insufficient coverage of extant euchelicerate taxa it remains unclear to what extent this feature bears any phylogenetically useful information within the euchelicerate lineage.

Also within the tetraconate lineage, paired segmental invaginations are no longer formed (apomorphic) and the cells of the central VNE region are subject to epidermal versus neural fate decisions (apomorphic). In light of the currently strongly supported paraphyly of crustaceans and the available data on malacostracans and branchiopods, the maintenance of NBs in apical position within the VNE appears plausible (and parsimonious) as ancestral feature of tetraconates. Segregation of NBs and formation of a sub-apical cell layer would accordingly

represent a derived character state of hexapods (possibly also in putatively closely related crustacean taxa that have not been studied in detail, e.g. Remipedia or Cephalocarida).
Any superficial similarities between onychophoran and tetraconate/hexapod neurogenesis represent convergent phenomena (singly segregating NPs, binary fate decisions in central VNE region; see evaluation of these features in 4.3.2.2.).

Remarks on scenario 1: Since in the investigated euchelicerates and myriapods the complete set of CISs is formed sequentially within each hemi-neuromere, it can be speculated whether this sequential process has been truncated during pycnogonid evolution and substituted by the second phase of neurogenesis involving apomorphic SCNPs. This would explain the low number of CISs and the related 'loss' of the supposedly ancestral grid-like CIS arrangement in pycnogonids. Interestingly, Stollewerk and Simpson (2005) briefly consider for the tetraconate lineage a relationship between the differentiation of specialized NBs and a low number of cells in the VNE (although the *causal* interrelationship of these two factors during evolution remains unclear). In comparison to several euchelicerates and myriapods, the pycnogonid VNE has a small area coupled to a low overall number of cells (Fig. 76 for comparison to spiders). At least for extant pycnogonids this alone seems to account for the lack of additional CISs, which would need to recruit additional – but non-existent – cellular material from the apical cell layer. On evolutionary scale, the differentiation of pycnogonid SCNPs might thus be speculated to represent a similar but convergent phenomenon to the evolution of tetraconate NBs, allowing generation of sufficient GC material in a small area of few cells.
So far, possible correlations between overall cell numbers, cell size, VNE area and CIS numbers during neurogenesis have been given only little attention within euchelicerates. Clearly, reinvestigation of representatives with small embryos and low overall cell numbers would be desirable in order to test the constancy of the CIS pattern within this lineage. Pseudoscorpions, for instance, develop from an initially very small yolk-poor egg (Anderson 1973). They possess not only comparably few cells in the differentiating VNE, but also develop paired central invaginations during neurogenesis, similar to pycnogonids (Weygoldt 1965: *Neobisium muscorum*; his fig. 36). Similarly, the initially minute embryos of viviparous scorpions seem to be characterized by low cell numbers when neurogenesis sets in. Interestingly, Mathew (1956) describes for *Heterometrus scaber*, a representative of this group, the formation of big conspicuous 'neuroblasts' that divide and give rise to GCs. Although clearly in need of confirmation, this correlation of embryo size, cell numbers and potential occurrence of specialized NPs is at least noteworthy. In light of their disjunct distribution in the euchelicerate tree (e.g. Weygoldt and Paulus 1979; Shultz 1990; Dunlop 2010; Regier et al. 2010), the specialized development of pseudoscorpions (see Weygoldt 1965) and scorpion vivipary have to be considered as independently derived states of arachnid development (Anderson 1973).

Reinvestigations in these taxa would be highly interesting in order to evaluate to what extent low embryonic cell numbers are accompanied by changes in the mode of neurogenesis in comparison to cell- and yolk-rich euchelicerate embryos. This would also help to further illuminate the plasticity of euarthropod neurogenesis, especially with respect to the putative convergent evolution of specialized NP types.

Contrary to any notions of 'primitiveness' or 'ancestrality' (in the sense of retention of plesiomorphic character states) based on the early offshoot of the pycnogonid lineage within chelicerates, this scenario suggests some of the neurogenic processes in crown-group Pycnogonida to have been derived within the pycnogonid stem-lineage. This renders them useless for the reconstruction of the ancestral euarthropod pattern.

***Scenario 2: Spatially stereotypic CISs as well as SCNPs are part of the euarthropod stem species pattern* (Fig. 75B).**

The formation of CISs in stereotypic positions remains an ancestral character of euarthropods. In addition, an ancestral NP type similar to the pycnogonid SCNP is postulated in the stem species of crown-group euarthropods, although the exact timing of its differentiation during neurogenesis remains ambiguous. Either it is spatially associated with the CISs (see remarks below) or alternatively differentiates only during advanced neurogenesis, as in pycnogonids. Similar to scenario 1, the cells in the central VNE region in each hemi-segment of the euarthropod ancestor adopt exclusively neural fate and paired segmental invaginations may have been formed during advanced neurogenesis.

The low number of CISs is an apomorphic feature of the pycnogonid lineage, since xiphosurans and spiders exhibit 30 or more GICs in a pattern roughly similar to myriapods. The existence of SCNPs as such is plesiomorphic for pycnogonids.

Within euchelicerates, a reduction of the SCNP type is assumed, since recent studies did not uncover any indications of such specialized cells (Stollewerk et al. 2001, 2003; Stollewerk 2002, 2004; Mittmann 2002, 2003; Weller and Tautz 2003). Instead neurogenesis via CISs has become more pronounced and elaborated in euchelicerates. The sequentially specified CISs differ in their persistence time and the numbers of recruited cells. If taking (some) spiders as model, the cells of some late CISs persist as separate epithelial vesicles after detachment from the apical VNE and differentiate only during post-embryonic development (Stollewerk 2004; Linne and Stollewerk 2011).

Crucially, the occurrence of SCNPs in the apical VNE of myriapods is assumed. These divide potentially in tangential direction as in pycnogonids (see remarks below).

The tetraconate NBs derive from the ancestral SCNP, their change of division orientation from tangential to radial being apomorphic. The occasional intermittent switch to tangential divisions of malacostracan and branchiopod NBs may represent a last reminiscence of the plesiomorphic

condition. As in the first scenario, the apical position of NBs in paraphyletic crustaceans represents the plesiomorphic state that has been retained from the ancestral euarthropod SCNP. Segregation of hexapod NBs is apomorphic.

Remarks on scenario 2: Obviously, this scenario hinges on the existence of specialized SCNPs in myriapods. Although the latter assumption remains to date unsatisfactorily proven, such a hypothesis can be argued for based on the findings of different studies of myriapod neurogenesis. Whitington and colleagues (1991) frequently detected single labeled cells within the CISs of the scolopendromorph *Ethmostigmus rubripes* in BrdU experiments. Furthermore, they reported dye-coupling of all cells of one CIS, which is also found in hexapod NBs and their early progeny (e.g. Boyan and Williams 2008: *Schistocerca gregaria*). They concluded that each group of immigrating cells might represent a 'proliferative unit'. Similarly, Dove and Stollewerk (2003) describe in the VNE of the millipede *Glomeris marginata* apically dividing cells, which are slightly bigger than the surrounding ones and are found in association with or even within the CISs. These findings were interpreted in favor of SCNPs in the myriapod VNE and of an intermediate mode of neurogenesis between eucheliceratesand tetraconates (Dove and Stollewerk 2003). Lastly, in the geophilomorph chilopod *Strigamia maritima*, each of the CISs comprises a single apical cell to which all other flask-shaped cells attach (Chipman and Stollewerk 2006; Stollewerk and Chipman 2006). Again, this has been recently speculated to represent a first specialization of VNE cells on the way to tetraconate NBs (Eriksson and Stollewerk 2010b; Whitington and Mayer 2011), but data on cell division patterns are so far completely lacking. However, in this particular case of *S. maritima*, the strongly supported emergence of the geophilomorph lineage well nested within chilopods has to be taken into account (e.g. Giribet and Edgecombe 2006; Edgecombe 2007; Murienne et al. 2010). The lack of a comparable conspicuous apical cell in the CISs of the most likely more basally branching *Lithobius forficatus* (Kadner and Stollewerk 2004) as well as in the millipede *G. marginata* as outgroup (Dove and Stollewerk 2003; Döffinger and Stollewerk 2010) make it unlikely that a cell as in *S. maritima* represents an ancestral myriapod feature. Nonetheless, that does not exclude its evolution from a less 'exposed' specialized SCNP in the apical VNE. Taken together, it is remarkable that indications of more ordered cell proliferation and potentially even specialized NPs have been independently presented in several recent investigations, especially during the early phase of neurogenesis. In addition to this, advanced neurogenesis as described in classical myriapod studies and encountered in pycnogonids shows some notable correspondences (see 4.3.4.1.). This renders targeted reinvestigation of the cellular processes during the complete time span of myriapod neurogenesis highly desirable.

4.3.6.3. Concluding remarks

The proposed evolutionary scenarios result from mapping of different features of arthropod neurogenesis on a phylogram and a subsequent attempt to explain the observed distribution patterns in conflict-free and (mostly) parsimonious ways. It is almost needless say that this approach suffers from severe limitations. Most prominent are (1) the partially unsatisfactorily settled phylogenetic relationships of some of the involved lineages, (2) data availability for only a limited number of representatives, being considered as 'typical' for vast and diverse lineages and (3) the significant differences in the data quality and detail between model and non-model organisms.

Clearly, the evolution of neurogenic mechanisms did neither stop within the major euarthropod lineages, nor is it familiar with the rational concept of parsimony – let alone bound to it. Hence, convergent evolution at cell type level represents an immanent risk of parsimony-based scenarios as presented here. To a certain extent homoplasy might even be expected exactly because of the observable diversity of adult nervous system architecture, which necessitates evolutionary modifications of the developmental processes giving rise to these adult structures. By definition, neurogenesis focuses predominantly at the cellular level, dealing 'only' with NP types that eventually give rise to immature GCs, but do not offer much in terms of morphological complexity. Therefore, if aiming at far-reaching homology assessments for arthropods as a whole, it is of paramount importance to obtain detailed, comparable and densely sampled data for a broad range of taxa. This represents the only feasible way to minimize the risk of misinterpretation and maximize the chance of uncovering homoplastic vs. homologous similarities. To create a truly solid foundation for evolutionary scenarios on arthropod neurogenesis, the involved cell types, their genealogical interrelationships (lineage studies) and additionally the differentiating adult structures (neuron and glial types, neuropils etc.) still need to be clarified in more non-model organisms in combination with molecular cell type characteristics and ideally also functional analyses. In this regard, the shortcomings of the obtained data on pycnogonid neurogenesis are still considerable and call for future investigations. The poor recent sampling within the euchelicerate lineage apart from the spider models has been highlighted. The need for descriptions of myriapod neurogenesis throughout the entire development has been repeatedly given notice. Lastly, the likely paraphyly of crustaceans makes additional studies in more non-malacostracan representatives absolutely pivotal in order to unravel NB evolution with the tetraconate lineage.

Only with denser taxon coverage, the different features of neurogenesis and their combination in extant representatives eventually might contribute genuinely to the resolution of the relationships of *all* arthropod lineages in phylogenetic analyses.

4.4. On the pycnogonid brain

4.4.1. Bipartite versus tripartite composition of the pycnogonid brain

A widely accepted consensus regarding the composition of the euarthropod head region has emerged in the last decade, being founded on Hox- and segment polarity gene expression data as well as reevaluation and reinvestigation of neuroanatomical evidences from various arthropod lineages (e.g. Damen et al. 1998; Telford and Thomas 1998; Mittmann and Scholtz 2003; Simonnet et al. 2004; Eriksson et al. 2010), including pycnogonids (Jager et al. 2006; Manuel et al. 2006; Brenneis et al. 2008; but see Maxmen et al. 2005). According to this recent view, the anterior head region of euarthropods is tripartite. It comprises (1) the anterior-most protocerebral unit without proper limb, (2) the deutocerebral segment bearing the chelifore/chelicera in pycnogonids/euchelicerates and (first) antenna in mandibulates and (3) the following segment, which is affiliated with palp/pedipalp in pycnogonids/euchelicerates, second antenna in crustaceans and no limb in myriapods and hexapods (e.g. Scholtz and Edgecombe 2006 for comprehensive review). Also the neuromeres corresponding to three anterior head parts have been homologized as proto-, deuto- and tritocerebrum, forming together the tripartite euarthropod compound brain, or syncerebrum (e.g. Harzsch 2004; Scholtz and Edgecombe 2005, 2006). However, while the segmental identity and homology of these three neuromeres is convincingly established, the status of all three of them as constituting parts of the ancestral euarthropod brain is more debatable, depending on the exact definition of 'brain'.
Pycnogonids can serve as an excellent example for this. In *Pseudopallene*, the supra-esophageal compound ganglion of the CNS (herein termed 'brain') encompasses the protocerebrum and the deutocerebral neuromere affiliated with the chelifore. The following neuromere of the palpal segment is fused with the ovigeral neuromere in the ventral sub-esophageal ganglion and remains connected to the supra-esophageal neuromeres via circum-esophageal connectives. This situation is typical for pycnogonids (e.g. Dohrn 1881; Hoek 1881; Wirén 1918; Henry 1953; Winter 1980; Fig. 77; see also Movie 21 for PS 2 of *Pseudopallene*) and has been recognized early on in embryological studies of the early 20th century (Meisenheimer 1902; Dogiel 1913). Recently, Richter and colleagues (2010) suggested a strictly morphological definition of 'brain' as representing 'the most prominent anterior condensation of neurons' and of the arthropod 'syncerebrum' in particular as being 'formed by fusion or close association of several neuromeres'. According to these definitions, pycnogonids are best characterized as possessing a bipartite compound brain that lacks a tritocerebrum, since the sub-esophageal palpal neuromere remains anatomically separated from the supra-esophageal protocerebral and deutocerebral neuromeres.

However, as Richter and colleagues (2010) do not miss to point out, 'tritocerebral' neuromeres of many euchelicerates are located in sub-esophageal position. Similarly, in some adult crustaceans they extend along the 'circum-esophageal connectives' (see e.g. Holmgren 1916; Hanström 1923; Chaigneau 1994 for examples) or are in some extreme cases even distinctly sub-esophageal (e.g. Kirsch and Richter 2007: *Leptodora kindtii*). In an attempt to rescue the concept of a tripartite euarthropod compound brain, a more comprehensive criterion for the definition of its posterior border is discussed. It suggests morphological fusion of neuromeres and/or their affiliation with a 'cephalized' limb pair as diagnostic criteria for a brain neuromere. It follows that the neuromeres connected to the euchelicerate pedipalps or the crustacean second antennae would be considered as tritocerebrum, irrespective of their exact position in relation to the esophagus and their degree of fusion to the deutocerebrum. Yet again, application of this definition on pycnogonids leads to questionable results. In Nymphonidae, Colossendeidae and several Ammotheidae, the well-developed 'cephalized' sensory palp would result in the recognition of a tripartite brain. But in those pycnogonid lineages, which completely lack palps, like Pycnogonidae, Endeidae, Phoxichilidiidae and representatives of Callipallenidae (e.g. *Pseudopallene*, *Stylopallene*, *Callipallene*), identification of a bipartite brain would be the consequence. The gross neuroanatomy of both groups, however, does not show major differences. In the opinion of the author, this is problematic – to say the least. It illustrates the difficulties of establishing clear-cut and meaningful but at the same time inclusive and applicable taxon-spanning morphological definitions for complex anatomical structures, which are naturally subject to evolutionary transformation processes in the separate lineages (in this particular case the complicated process of cephalization, see e.g. Scholtz and Edgecombe 2006).

Based on these complications, an exclusively neuroanatomy-based definition of the pycnogonid brain is here given preference. Adhering to this, the pycnogonid compound brain is bipartite rather than tripartite. The sub-esophageal palpal neuromere that is linked to the brain by circum-esophageal connectives (Fig. 77; note considerable length of connectives in *Pycnogonum litorale*) does not qualify as third brain part, or tritocerebrum, irrespective of the presence or absence of palps.

In euchelicerates, not only a sub-esophageal origin of the pedipalpal neuromere (e.g. Mittmann and Scholtz 2003; Harzsch et al. 2005b: *Limulus polyphemus*; Linne and Stollewerk 2011: *Parasteatoda tepidariorum*, *Cupiennius salei*) but also a predominantly sub-esophageal position in adults is apparent. However, due to condensation and fusion of at least all prosomal neuromeres during embryonic development, soma-free circum-esophageal connectives do not persist between adult deutocerebrum and pedipalpal neuromere (e.g. Holmgren 1916; Hanström 1928; Babu 1965; Bullock and Horridge 1965 for overviews). This impedes unequivocal morphology-based delimitation of 'brain' and VNC or rather leads to the recognition of a

massive compound brain in which only the anterior-most affiliated limbs are 'cephalized'. Nonetheless, the retained sub-esophageal position of the pedipalpal neuromere is similar to the palpal neuromere of pycnogonids and differs from the more anterior localization of the corresponding tritocerebral neuromere in adults of myriapods, most crustaceans and hexapods. This adult position of the palpal/pedipalpal neuromere represents thus a characteristic feature of all extant chelicerates, in contrast to the segmentally homologous but more anteriorly positioned mandibulate tritocerebrum.

A recent investigation on onychophoran brain composition demonstrated via backfills that the neuronal somata associated with the slime papilla nerve are sub-esophageally located within the anterior-most portions of the medullary cords (Mayer et al. 2010b). This led to the conclusion that only the neuromeres corresponding to the euarthropod proto- and deutocerebrum constitute the onychophoran supra-esophageal brain, innervating the 'primary' antennae and jaws, respectively. Similar interpretations had been reached in earlier works (e.g. Scholtz and Edgecombe 2005, 2006, but note here conceptualization as 'tripartite brain' due to 'cephalized' slime papillae), with the exception of another recent study that erroneously claimed a tripartite composition (Strausfeld et al. 2006b). As a consequence of the situation in onychophorans, a bipartite composition of a morphologically separate supra-esophageal compound brain can be plausibly argued for as plesiomorphic character of euarthropods.

(1) Pycnogonids with their only partially fused segmental ganglia represent the only clear-cut extant example of this plesiomorphic condition (Fig. 77).

(2) An evolutionary trend of CNS condensation in the euchelicerate lineage impedes unequivocal morphological distinction (and definition) of a posterior brain boundary in extant representatives, but the plesiomorphic supra- versus sub-esophageal arrangement of neuromeres is nonetheless retained.

(3) Within the mandibulate lineage, further cephalization led to an apomorphic anterior migration of the post-esophageally originating tritocerebral neuromere during development and thus in some taxa to the formation of an anatomically delimitable, tripartite and supra-esophageal compound brain in adults (e.g. in hexapods). However, as for instance illustrated within different crustacean taxa, the degree of the anterior displacement of the tritocerebral neuromere and its fusion to the proto-deutocerebrum shows lineage-specific variations. Some of these, such as the distinctly post-esophageal tritocerebral neuromere of *Leptodora kindtii* (Kirsch and Richter 2007), represent clearly derived conditions.

This scenario deviates from the conclusions drawn by Mayer and colleagues (2010b), in suggesting a more recent emergence of a tripartite and morphologically delimitable brain, only within the mandibulate lineage of crown-group euarthropods.

4.4.2. Remarks on the neuroarchitecture of the pycnogonid brain

A detailed and reliable description of pycnogonid brain architecture at the level of neuropilar sub-regions is to date not available. Classical histological studies addressing this subject either remain superficial and incomplete (Hanström 1919, 1928) or appear questionable (Winter 1980) in light of the fragmentary data of more recent investigations (Strausfeld et al. 1998; Lehmann et al. 2012). Also the here obtained results on *Pseudopallene* allow unfortunately only limited resolution of pycnogonid brain architecture. In spite of this, some key aspects will be discussed in the following paragraphs, in order to illuminate some pathways for future investigations.

4.4.2.1. Mushroom body-like neuropils (MBNs)

Out of the classical studies, only Winter (1980) identifies putative MBNs. But judging from their position, his 'mushroom bodies' rather seem to represent the recently identified second visual neuropils (Lehmann et al. 2012), which have been herein termed basal optic neuropils. Strausfeld and colleagues (1998, 2006a) characterize the pycnogonid MBNs as lacking a calyx and possessing heterolaterally extending lobes. In agreement with this, no structure representing a calyx was found basally to the ventral globuli cell region of *Pseudopallene*, the parallel axons ('pedunculus') of these neurons extending directly into the protocerebral neuropil. The here described midline-spanning tract with its laterally surrounding neuropil regions most likely represents part of the heterolateral 'lobe-region' of Strausfeld and colleagues (2006a). However, a second lateral region of globuli cell agglomerations with an underlying slightly lobed neuropil was identified, being transversally inter-connected by a prominent transverse tract to its bilaterally symmetric counterpart. The position of this complex along the a-p axis is in good accordance with the so-called 'second optic neuropil' ('Sehmasse 2') identified by Winter (1980) in *Endeis spinosa*. Yet, the results on the optic neuropils of *Pseudopallene* and the recent study on the optic pathway of pycnogonids (Lehmann et al. 2012) again contradict Winter's interpretation of this neuropil system. As a consequence, it remains currently unclear, to which brain structure in other euarthropods the lateral globuli cell-system might corresponds (if to any at all). Its relation to the putative MBNs cannot be excluded, although the apparent lack of a prominent connection makes this interpretation questionable. This illustrates that the localization and exact architecture of MBNs in the pycnogonid brain is in need of further confirmation.

4.4.2.2. 'Optic nerve', antero-lateral thickening and optic neuropils

Already early on, it was recognized that the 'optic nerve' of pycnogonids represents only a loose assemblage of neurite bundles (Hoek 1881; see Lehmann et al. 2012 for recent reconstruction). The bundles constituting this 'nerve' do not only span between the protocerebrum and retinula

cells of the eyes, but also contain neurites to/from the lateral sensory organs (e.g. Hanström 1928) and the dorsal integument. Based on this, the appropriateness of the term 'optic nerve' has been already critically discussed by Hoek (1881).

The antero-lateral thickening, which represents an external protrusion of the brain soma cortex, was already observed by Hanström (1919, 1928), who describes it as 'gangliösen Lobus opticus' (Hanström 1928). In line with Lehmann and colleagues (2012), this thickening is here not considered as 'ganglion', since it represents only a loose assemblage of neuronal somata and neurite bundles. Within this thickening, bundling of the axons constituting the 'optic nerve' takes place but apparently no dendritic arborizations are encountered (Lehmann et al. 2012), which is the defining character of neuropils. To all appearances, Winter (1980) missed this structure.

Two optic neuropils are present in *Pseudopallene*. This finding concurs with the description of Lehmann and colleagues (2012) for different pycnogonid species. The identification of a second basal optic neuropil extends the fragmentary descriptions of Hanström (1919, 1928), in which only a single optic neuropil was recognized, corresponding to the apical one of this study. Winter's erroneously identified 'Sehmasse 2' as well as his misinterpretation of the true basal optic neuropil as mushroom body (Winter 1980) has already been given notice above. Notably, the course of the different neurite bundles of the 'optic nerve' as revealed here by tubulin labeling indicate a parallel rather than a serial set-up of the two optic neuropils. This means that some bundles enter the apical optic neuropil, whereas others by-pass the latter and extend into the basal optic neuropil. A similar result was obtained by Cobalt backfills of Lehmann and colleagues (2012) (see also their fig. 4c). Due to this parallel set-up, it was here refrained from naming the optic neuropils 'first' and 'second', since this terminology implies a serial arrangement along the optic pathway. Considering the ordered parallel arrangement of the single neurite bundles along the 'optic nerve' up to the antero-lateral thickening (see reconstruction in Lehmann et al. 2012), it would be of interest to follow their course individually also beyond the latter structure. To date, it is not clearly resolved whether the parallel array is upheld further 'downstream'. If so, this could indicate parallel processing of the anterior and posterior eyes' sensory input in the two separate optic neuropils. Any specific target regions of the respective optic neuropil interneurons remain currently unknown.

4.4.2.3. The elusive pycnogonid arcuate body

In onychophorans and euchelicerates, the arcuate body is an unpaired midline-spanning neuropil of the protocerebrum that has a characteristic crescent shape and a stratified structure (Strausfeld 1998; Loesel et al. 2002; 2011; Loesel 2004; Harzsch et al. 2005b; Strausfeld et al. 2006a,b; Döffinger et al. 2010; Richter et al. 2010). In contrast, the most prominent midline

neuropil in the mandibulate protocerebrum (potentially excluding millipedes; see Loesel et al. 2002) is termed central body. To this day, the evolutionary transformation series of unpaired midline neuropils within arthropods remains unsatisfactorily settled (see Richter et al. 2010). However, a common origin of arcuate body and central body from an ancestral midline-spanning neuropil of the arthropod stem species has repeatedly been considered as being likely (e.g. Loesel et al. 2002, 2011; Strausfeld et al. 2006a; Homberg 2008).

The position, structure and connectivity of the pycnogonid arcuate body are still ambiguous and in part completely unknown. Old studies (Hanström 1919, 1928; Winter 1980) identified within the pycnogonid brain a small unpaired midline-spanning neuropil ('central body') in postero-ventral position (body axis relation, i.e., dorso-posterior with regard to neuraxis). This neuropil is reported to be of oval shape without signs of stratification or columnar architecture. In the same position, Strausfeld and colleagues (2006a) report an unpaired but crescent-shaped midline neuropil, which they homologize to the onychophoran and euchelicerate arcuate body. However, neither architectural features are discussed (or known), nor are any images depicted. In contrast, Lehmann and colleagues (2012) identified a small midline-spanning neuropil directly basal to the basal optic neuropils and tentatively suggest it to represent the pycnogonid arcuate body instead of the more posterior one described in earlier investigations. None of the studies provides any details on the connectivity of the putative arcuate body.

Herein, no distinctly set off unpaired midline neuropil was recognized with the applied techniques in the brain of *Pseudopallene*. If following Hanström's original description (Hanström 1919), this neuropil would have to be located directly posterior to the curved transverse tract spanning between the apical optic neuropils. However, neither tubulin labeling, nor the distribution of serotonin-like and histamine-like immunoreactive neuropilar regions (not shown) led to the identification of a delimitable midline-spanning neuropil within this location, let alone indications of stratification or columnar architecture. Hence, the present study fails to contribute to the resolution of the arcuate body issue in pycnogonids.

4.4.3. Comparison of early brain development to previous embryological studies

This study reveals the formation of distinct CISs in the pre-cheliforal lobe of pycnogonids (Fig. 78), similar to euchelicerates (e.g. Farley 2001; Döffinger et al. 2010; Wolff and Hilbrant 2011; Mittmann and Wolff 2012) and myriapods (Dove and Stollewerk 2003; Kadner and Stollewerk 2004). It could be shown that the CISs arise in a stereotypic pattern, the development and transformation of this pattern being traceable over a certain developmental time span. Furthermore, a correlation of identified CISs with bigger invaginating areas during subsequent development is indicated (Fig. 78). This correlation of stereotypically arranged CISs with specific

areas of cell internalization speaks for a spatially and temporally well-ordered formation process of the brain anlage of *Pseudopallene*.

Comparable to the VNC, earlier studies on pycnogonid development only described a general thickening of the brain ectoderm (Morgan 1891; Meisenheimer 1902; Dogiel 1913; Sanchez 1959) or claimed early differentiation of 'neuroblasts' (Winter 1980). As in the ventral neuromeres, development of the pre-cheliforal lobe of *Pseudopallene* indicates the latter description as being erroneous. Some of the older works mention weak invaginations in the pre-cheliforal lobe during neurogenesis of callipallenids (Morgan 1891, Winter 1980). Winter (1980) distinguishes two main areas in the pre-cheliforal lobe of *Callipallene emaciata*, one lying anterior to the proboscis and the other more antero-laterally. The latter region is said to slightly invaginate during embryonic development and give rise amongst others to the eye anlagen. Based on his descriptions, a correspondence of these two regions to the pre-proboscideal pit and antero-lateral depression of *Pseudopallene*, respectively, appears very likely. However, in contrast to callipallenids, the embryonic pre-cheliforal lobe of pycnogonids hatching as protonymphon larva is devoid of invaginating regions (Meisenheimer 1902; Dogiel 1913; Brenneis 2007; Machner and Scholtz 2010). So far, it has not been investigated whether any invaginations arise during brain differentiation in the post-embryonic development of these representatives. But even if they do occur in later stages, the timing of their formation would be significantly different from the one in callipallenids, where they arise slightly prior to axonogenesis in direct relation with the early GC immigration and detachment. In contrast to this, the nervous system of the protonymphon larvae is already well-developed and functional at hatching (e.g. Maxmen et al. 2005; Brenneis et al. 2008). Since recent phylogenetic studies indicate the emergence of callipallenids well nested within crown-group pycnogonids (Arango and Wheeler 2007; Nakamura et al. 2007; Arabi et al. 2010) (Fig. 64), postulation of antero-lateral depression, pre-proboscideal pit and central depression as pycnogonid ground pattern features is currently not tenable. However, the lack of externally recognizable sub-regions during protonymphon development does almost certainly not indicate a fundamentally different mode of brain development. Preliminary evidence for a pattern of evenly spaced immigrating cells/CISs in the pre-cheliforal lobe has been presented for *Pycnogonum litorale* as representative with protonymphon larva (see Fig. 69). Comparative analyses of this pattern in *P. litorale* to the one in *Pseudopallene* are the next step to assess similarities at this level. In addition, more comprehensive gene expression studies could help to uncover a regionalization of the pre-cheliforal lobe in protonymphon-developers that eludes morphological description but might nonetheless correspond to the invaginating cell areas of callipallenids (e.g. Dachshund expression for characterization of putative MBN anlagen, see Döffinger et al. 2010: *Cupiennius salei*; Noveen et al. 2000: *Drosophila melanogaster*).

Out of all previous studies, only Winter (1980) mentions placodes of big SCNPs at the basal side of the brain primordium of *Callipallene emaciata*, which are in positional correspondence to the unpaired antero-median and the paired antero-lateral clusters of *Pseudopallene*. A stereotypic arrangement of the brain SCNPs at single cell level was not recognized, but this aspect has also not been in the focus of this study. As in the VNC, it remains currently unclear in which genealogical relation the internalized SCNPs and preceding CISs of the pre-cheliforal lobe stand to each other.

Previous authors express no doubt regarding the exclusively cheliforal, i.e., deutocerebral affiliation of the apical brain cell cluster/'ventral organ' (Dogiel 1913; Sanchez 1959; Winter 1980). Here, it was refrained from assigning the area from which this cluster originates either to protocerebral region or the cheliforal neuromere. This is based on the lack of clear landmarks in the morphologically rearranging transition region between central depression and cheliforal groove, a circumstance that also Morgan (1891) remarked on for *Callipallene brevirostris*. Interestingly, the apical brain cell cluster's antero-medial stream enters the soma cortex in close vicinity to the ventral globuli cell region of the putative MBNs. This is indicative of a protocerebral affiliation of the adult cluster-stream-system. Yet, this does not necessarily exclude its deutocerebral origin or at least partial contribution to it. Accordingly, additional investigations are needed to shed more light on this issue, one being the study of segment polarity gene expression.

5. SUMMARIES

5.1. English summary

This study addresses different aspects of the development of the sea spider *Pseudopallene* sp. (Pycnogonida, Callipallenidae), which exhibits a prolonged embryonic development. A combination of (1) SEM, (2) histology, (3) fluorescent markers and immunolabeling coupled to CLSM and 3D analysis and (4) gene expression studies is used to investigate embryonic and post-embryonic morphogenesis and in particular focus on processes of early neurogenesis and subsequent events of nervous system differentiation. The latter include the formation of the brain, ventral ganglia and the sequence in the establishment of the axonal scaffold of the CNS. Staging systems of the embryonic and post-embryonic phases are established and subsequently used as reference.

The embryonic development of the proboscis is characterized by initial protrusion of three cell populations that are later on involved in pharynx formation. In advanced stages, the distal proboscis portion transiently assumes a horseshoe-like shape, but no morphological structure corresponding to the euarthropod labrum is detectable at any time of development. Based on the complete lack of palpal and ovigeral limbs and the early differentiation of walking leg segments 1 and 2 during embryonic morphogenesis, the presence of an embryonized protonymphon stage during callipallenid development is rejected. A comparison of the advanced hatching larvae of callipallenids to other pycnogonid larval types leads to the suggestion of the morphology-based term ‘walking leg-bearing larva’, as opposed to ‘attaching larva’. Evolution of pycnogonid hatching stages is reevaluated in light of recent phylogenetic analyses. Specifically, the reemergence of the ancestral protonymphon larva and reappearance of palpal and ovigeral larval limbs as well as adult palps in the nymphonid lineage are discussed. This challenges the perception of a reduction-based head appendage evolution within the pycnogonid lineage. Starting out from the three-stage-sequence of walking leg differentiation in *Pseudopallene*, temporal and structural patterns in other pycnogonid taxa are discussed and a podomere number notation in matrix fashion is proposed to facilitate multiple-species comparisons.

Early neurogenesis of the future VNC shares notable similarities with euchelicerate and myriapod representatives. These include (1) the lack of morphologically different cell types in the early VNE, (2) formation of transiently recognizable and stereotypically arranged CISs, (3) immigration of mostly post-mitotic immature GCs, (4) elevated levels of Delta gene expression in the immigrating cells and (5) almost exclusive restriction of tangentially oriented cell proliferation to the apical neuroectoderm. However, based on the comparably low number of the CISs per hemi-neuromere, no grid-like pattern has been recognized. These findings are in good accordance with a placement of pycnogonids either as sister group to euchelicerates or to all extant euarthropods, but do not contribute to this issue’s further resolution. In a following

neurogenesis phase, the formation of an invagination in each hemi-neuromere is accompanied by significant enlargement of the apical cells. High mitotic activity of the bigger cells and their asymmetric division mode are documented, coupled to a marked ganglion cell number increase in the underlying hemi-ganglion anlagen. The big cells are therefore suggested to represent stem cell-like dividing neuronal precursors (SCNPs). After a review of several aspects of arthropod neurogenesis, the validity of specialized neuroblasts as synapomorphy of Tetraconata (crustaceans + hexapods) is reevaluated. With the available data, cellular homology of pycnogonid SCNPs and crustacean-hexapod neuroblasts with their specific division pattern remains currently unclear. To acknowledge this, two possible scenarios on the evolution of arthropod neurogenesis are discussed and the need for further studies on pycnogonids and other euarthropod lineages – especially myriapods and more crustacean taxa – is emphasized.

During post-embryonic development of *Pseudopallene*, the apically invaginating cell regions with size-decreasing SCNPs detach internally and form persisting cell clusters at the apical side of the hemi-ganglia. The clusters retain a connection to the underlying soma cortex via fibrous strands. Although big SCNPs are no longer distinguishable in these stages, mitoses exclusively within clusters and cell streams as well as continuing increase of ganglion cell numbers characterize the cluster-stream-systems as the sources of the additional cell material. Their close spatial vicinity to glomeruli-like neuropils in the ventral ganglia suggest the cluster-stream systems to represent segmentally arranged neurogenic niches associated with the central olfactory pathway. Similarities to the well-characterized adult neurogenic niche in the decapod deutocerebrum are evaluated. Potential candidates for other olfaction-related adult neurogenic systems in arthropods are discussed, including the hypocerebral organ of Onychophora.

The general neurogenic processes in the pre-cheliforal lobe closely correspond to the ventral neuroectoderm. Due to more distinct definition of the early CISs, their arrangement and development over time could be partially mapped. In favor of a spatio-temporally well-ordered brain formation process, CISs sub-groups could be assigned to three bigger invaginating areas, i.e. the pre-proboscideal pit and the antero-lateral and central depressions. However, with the exception of the antero-lateral depression (being involved in the formation of the eyes and the two optic neuropils) insufficient resolution of adult brain architecture renders correlation of invaginating areas with future brain sub-structures still speculative. Pycnogonids are pointed out as euarthropod taxon showing a gross anatomical separation of a supra-esophageal proto-deutocerebral compound ‘brain’ and the sub-esophageal tritocerebral (palpal) neuromere. In contrast to a recent suggestion, this bipartite structure of the supra-esophageal ‘brain’ is resolved as plesiomorphic euarthropod condition. The anteriorly directed shift of the tritocerebral neuromere and its supra-esophageal fusion with the proto-deutocerebrum during ontogeny represents an apomorphy derived within the mandibulate lineage.

5.2. Deutsche Zusammenfassung

Die vorliegende Arbeit befasst sich mit verschiedenen Aspekten der Entwicklung der Asselspinne *Pseudopallene* sp. (Pycnogonida, Callipallenidae), welche sich durch eine verlängerte Embryonalentwicklung auszeichnet. Die embryonale und post-embryonale Morphogenese wird untersucht und die Entwicklungsprozesse der frühen Neurogenese und nachfolgende Ereignisse der Nervensystemdifferenzierung (Bildung des Gehirns und der ventralen Ganglien, sowie Etablierungssequenz der axonalen Hauptbahnen) in größerem Detail beleuchtet. Hierzu wird eine Kombination von (1) Rasterelektronenmikroskopie, (2) Histologie, (3) Fluoreszenzfarbstoffen und Immunohistochemie im Zusammenspiel mit konfokaler Laser-scanning Mikroskopie und anschließender 3D Analyse, sowie (4) Genexpressionsstudien genutzt. Sowohl die embryonale als auch für die post-embryonale Entwicklungsphase werden in definierte Stadien eingeteilt, welche anschließend als Referenzsystem dienen.

Die Entwicklung der Proboscis zeichnet sich durch das Hervorwachsen von drei Zellmassen aus, welche später Teile des Pharynx formen. In fortgeschrittenen Stadien nimmt der distale Proboscisabschnitt vorübergehend eine hufeisenförmige Gestalt an, jedoch lässt sich zu keinem Zeitpunkt eine morphologische Struktur identifizieren, die dem Labrum der übrigen Euarthropoden ähnelt.

Aufgrund des Fehlens von Palpen- und Ovigeranlagen sowie der frühen Differenzierung der Laufbeinsegmente 1 und 2 wird die Existenz eines embryonisierten Protonymphon-Stadiums während der Embryonalentwicklung von Callipalleniden widerlegt. Basierend auf einem Vergleich der Larvenformen anderer Pycnogonidentaxa zu den Schlupfstadien der Callipalleniden wird für letztere die Bezeichnung ‚walking leg-bearing larva' im Gegensatz zur etablierten ‚attaching larva' vorgeschlagen. Die mögliche Evolution verschiedener Larvenformen wird vor dem Hintergrund jüngerer phylogenetischer Studien bewertet. Hierbei werden insbesondere das potentielle Wiederauftreten der ursprünglichen Protonymphonlarve und die Wiederausbildung von larvalen und adulten Palpen- und Ovigerextremitäten innerhalb der Nymphonidae diskutiert. Dies stellt die verbreitete Auffassung eines rein reduktionsbasierten Evolutionsverlaufs der Kopfextremitäten innerhalb der Pycnogonida in Frage.

Zur Erleichterung eines Vergleichs der abweichenden strukturellen und zeitlichen Muster während der Laufbeindifferenzierung verschiedener Pycnogonidentaxa wird eine übersichtliche Matrixschreibweise vorgeschlagen.

Die Entwicklungsprozesse der frühen Neurogenese des ventralen Nervensystems zeigen Übereinstimmungen zu untersuchten Eucheliceraten und Myriapoden. Diese betreffen (1) das Fehlen rein morphologisch differenzierbarer Zelltypen, (2) die zwischenzeitliche Bildung

stereotypisch angeordneter Zellinternalisierungszentren, (3) die Immigration von vorwiegend post-mitotischen Ganglionzellen, (4) eine erhöhten Delta-Expression in den immigrierenden Zellen und (5) das fast ausschließliche Auftreten tangential orientierter Zellproliferation im apikalen Neuroektoderm. Jedoch wird aufgrund der vergleichsweise geringen Anzahl von Zellinternalisierungszentren pro Hemineuromer keine gitterartige Anordnung erkannt. Die generellen Ähnlichkeiten lassen sich konfliktfrei mit der Auffassung von Pycnogoniden entweder als Schwestergruppe zu den Euchelicerаten oder auch zu allen übrigen Euarthropoden vereinbaren, ohne diesbezüglich jedoch eine Klärung herbeizuführen. Den frühen Neurogeneseprozessen folgt in jedem Hemineuromer ein Invaginatieren des zentralen Neuroektoderms, welches bemerkenswerterweise durch eine Vergrößerung der apikalen neuroektodermalen Zellen begleitet wird. Hohe mitotische Aktivität und asymmetrischer Teilungsmodus der vergrößerten Zellen sowie ein konstanter Zuwachs der basalen Ganglionzellen in den Hemiganglionanlagen werden dokumentiert. Aufgrund dessen werden die großen Zellen hier als neuronale Vorläuferzellen mit stammzellartigem Teilungsmodus interpretiert. Das Vorhandsein eines solchen Zelltyps innerhalb der Pycnogonida erfordert eine erneute kritische Prüfung der Validität von spezialisierten neuronalen Vorläuferzellen mit stammzellartigem Teilungsmodus als Synapomorphie der Tetraconata (Krebse und Insekten) (hier Neuroblasten genannt). Anhand der vorliegenden Daten bleibt es zurzeit noch fraglich, ob die spezialisierten neuronalen Vorläuferzellen der Pycnogonida und Tetraconata einen gemeinsamen Ursprung haben, d.h. homolog zueinander sind. Dem Rechnung tragend werden zwei mögliche Szenarien zur Evolution der Neurogenese innerhalb der Arthropoda diskutiert. Die Notwendigkeit von weitergehenden Studien an Pycnogoniden, jedoch insbesondere auch an Myriapoden und zusätzlichen Taxa der Crustaceen wird hervorgehoben.

Während der post-embryonalen Entwicklung von *Pseudopallene* lösen sich die invaginierten Zellregionen (inklusive der spezialisierten neuronalen Vorläufer) vom oberflächlichen Ektoderm ab. Auf der apikalen Seite der Hemiganglien bilden sie distinkte Zellcluster, die mit dem darunterliegenden Somacortex über fibrilläre ‚streams' verbunden bleiben. Große neuronale Vorläuferzellen sind von diesem Zeitpunkt an nicht mehr unterscheidbar, aber weiterer Zuwachs an Ganglionzellen sowie exklusive Zellproliferation in den cluster-stream-Systemen weisen letztere als anhaltende Quellen für Ganglionzellen aus. Die räumliche Dichte zu glomeruli-artigen Neuropilen deutet darauf hin, dass die cluster-stream-Systeme möglicherweise segmentale neurogene Nischen in Assoziation mit dem olfaktorischen System darstellen. Ähnlichkeiten mit der neurogenen Nische im Deutocerebrum adulter Decapoda (Crustacea) werden aufgezeigt, sowie weitere ‚Kandidaten' für olfaktion-assozierte neurogene Nischen in Arthropoden diskutiert, inklusive des Hypocerebralorgans der Onychophoren.

Die Neurogeneseprozesse im pre-cheliforalen Lobus zeigen weitgehende Übereinstimmungen zum ventralen Neuroektoderm. Die Anordnung und Entwicklung der verhätnismäßig klar definierten Zellinteralisierungszentren wird dokumentiert. Hierbei ist es möglich, Untergruppen von identifizierten Zentren drei größeren invaginierenden Regionen (prä-proboscideale Grube und antero-laterale sowie zentrale Mulde) zuzuweisen, was auf einen auf zellulärer Ebene räumlich-zeitlich wohlgeordneten Gehirnbildungsprozess hindeutet. Jedoch erschwert die mangelnde Auflösung der Gehirnanatomie adulter Pycnogoniden eine eindeutige Korrelation der drei Entwicklungsregionen mit differenzierten Gehirnstrukturen. Lediglich die antero-laterale Mulde ist mit Sicherheit an der Bildung der Augen, des lateralen Sinnesorgans, des ‚optischen Nervs' und der beiden optischen Neuropile beteiligt.

Pycnogoniden zeigen eine Trennung vom supra-ösophageal gelegenen proto-deutocerebralen Gehirn und dem sub-ösophagealen tritocerebralen Palpenneuromer. Im Gegensatz zu einem jüngsten Vorschlag, wird in der vorliegenden Arbeit die zweiteilige Zusammensetzung des supra-ösophagealen Gehirns als plesiomorpher Zustand der Euarthropoden aufgelöst. Die während der Ontogenese auftretende anterior gerichtete Verschiebung des tritocerebralen Neuromers und dessen Fusion mit dem proto-deutocerebrum stellt eine Apomorphie dar, die erst innerhalb der Mandibulatenlinie evolviert ist.

6. References

Adlerz G (1888) Bidrag till pantopodernas morfologi och utvecklingshistoria. Bihang till Kungliga Svenska Vetenskaps-Akademiens Handlingar 13:1-25

Anderson DT (1973) Embryology and Phylogeny in Annelids and Arthropods. Pergamon Press, Oxford, pp. 1-495

Andrew DR (2011) A new view on insect-crustacean relationships II. Inferences from expressed sequence tags and comparisons to neural cladistics. Arthropod Structure and Development 40:289-302

Arabi J, Cruaud C, Couloux A, Hassanin A (2010) Studying sources of incongruence in arthropod molecular phylogenies: sea spiders (Pycnogonida) as a case study. Comptes Rendus Biologies 333:438-453

Arango CP (2002) Morphological phylogenetics of the sea spiders (Arthropoda: Pycnogonida). Organisms, Diversity and Evolution 2:107-125

Arango CP (2003) Molecular approach to the phylogenetics of sea spiders (Arthropoda: Pycnogonida) using partial sequences of nuclear ribosomal DNA. Molecular Phylogenetics and Evolution 28:588-600

Arango CP, Brenneis G (submitted) New species of Australian *Pseudopallene* based on colour, morphology and DNA (Pycnogonida: Callipallenidae).

Arango CP, Wheeler WC (2007) Phylogeny of the sea spiders (Arthropoda, Pycnogonida) based on direct optimization of six loci and morphology. Cladistics 23:1-39

Arnaud F, Bamber RN (1987) The biology of Pycnogonida. Advances in Marine Biology 24:1-96

Ashraf SI, Ip YT (2001) The *snail* protein family regulates neuroblast expression of *inscuteable* and *string*, genes involved in asymmetry and cell division in *Drosophila*. Development 128:4757-4767

Ax P (1999) Das System der Metazoa II. Ein Lehrbuch der phylogenetischen Systematik. Gustav Fischer Verlag, Stuttgart, pp. 1-384

Ayyar S, Negre B, Simpson P, Stollewerk A (2010) An arthropod *cis*-regulatory element functioning in sensory organ precursor development dates back to the Cambrian. BMC Biology 8:127

Babu KS (1965) Anatomy of the central nervous system of arachnids. Zoologische Jahrbücher der Anatomie 82:1-154

Bäcker H, Fanenbruck M, Wägele JW (2008) A forgotten homology supporting the monophyly of Tracheata: the subcoxa of insects and myriapods re-visited. Zoologischer Anzeiger 247:185-207

Bain BA (2003a) Postembryonic development in the pycnogonid *Austropallene cornigera* (Family Callipallenidae). Invertebrate Reproduction and Development 43:181-192

Bain BA (2003b) Larval types and a summary of postembryonic development within the pycnogonids. Invertebrate Reproduction and Development 43:193-222

Bamber RN (2007) A holistic re-interpretation of the phylogeny of the Pycnogonida Latreille, 1810 (Arthropoda). Zootaxa 1668:295-312

Bamber RN, El Nagar A (2012) Pycnobase: World Pycnogonida Database. Available online at http://www.marinespecies.org/pycnobase.

Bate CM (1976) Embryogenesis of an insect nervous system I. A map of the thoracic and abdominal neuroblasts in *Locusta migratoria*. Journal of Embryology and Experimental Morphology 35:107-123

Bazin F (1969) Étude comparée d'un organe deutocérébral chez les Crustacés Décapodes Reptantia. Comptes Rendus Hebdomadaires des Séances de l'Académie des Sciences 269:958-961

Bazin F (1970) Étude comparée de l'organe deutocérébral des Macroures Reptantia et des Anomoures (Crustacés Décapodes). Archives de Zoologie Expérimentale et Générale 111:245-264

Bazin F (1971) Les organes deutocérébraux chez deux Crustacés Décapodes Macroures Reptantia: *Panulirus regius* de Brito Capello, *Scyllarus arctus* (L.). Bulletin de la Société Zoologique de France 96:87-92

Bazin F, Demeuzy N (1968) Existence d'organes intracérébraux énigmatiques chez le Crustacé Décapode *Carcinus maenas* (L.). Comptes Rendus Hebdomadaires des Séances de l'Académie des Sciences 267:356-358

Behrens W (1984) Larvenentwicklung und Metamorphose von *Pycnogonum litorale* (Chelicerata, Pantopoda). Zoomorphology 104:266-279

Beltz BS, Sandeman DC (2003) Regulation of life-long neurogenesis in the decapod crustacean brain. Arthropod Structure and Development 32:39-60

Bergström J, Stürmer W, Winter G (1980) *Palaeoisopus*, *Palaeopantopus* and *Palaeothea*, pycnogonid arthropods from the Lower Devonian Hunsrück Slate, West Germany. Paläontologische Zeitschrift 54:7-54

Bitsch J, Bitsch C (2007) The segmental organization of the head region in Chelicerata: a critical review of recent studies and hypotheses. Acta Zoologica 88:317-335

Bogomolova EV (2007) Larvae of three sea spider species of the genus *Nymphon* (Arthropoda: Pycnogonida) from the White Sea. Russian Journal of Marine Biology 33:145-160

Bogomolova EV (2010) *Nymphon macronyx* (Arthropoda, Pycnogonida), another pycnogonid species with "lecytotrophic protonymphon" development. Zoologiceskij Zhurnal 89:528-544

Bogomolova EV, Malakhov VV (2003) Larvae of sea spiders (Arthropoda, Pycnogonida) from the White Sea. Entomological Review 83:222-236

Bogomolova EV, Malakhov VV (2004) Fine morphology of larvae of sea spiders (Arthropoda: Pycnogonida) from the White Sea. Zoologiya Bespozvonochnykh 1:3-28

Bogomolova EV, Malakhov VV (2006) Lecithotrophic protonymphon is a special type of postembryonic development of sea spiders (Arthropoda, Pycnogonida). Doklady Biological Sciences 409:328-331

Bogomolova EV, Malakhov VV (2011) Structure of the body cavity of the sea spider *Nymphon brevirostre* Hodge, 1863 (Arthropoda: Pycnogonida). Russian Journal of Marine Biology 37:348-365

Bossing T, Udolph G, Doe CQ, Technau GM (1996) The embryonic central nervous system lineages of *Drosophila melanogaster*. I. Neuroblast lineages derived from the ventral half of the neuroectoderm. Developmental Biology 179:41-64

Bourlat SJ, Nielsen C, Economou AD, Telford MJ (2008) Testing the new animal phylogeny: a phylum level molecular analysis of the animal kingdom. Molecular Phylogenetics and Evolution 49:23-31

Bouvier E-L (1923) Pycnogonides. Faune de France 7:1-70

Boyan G, Williams JLD (2008) Evidence that the primary brain commissure is pioneered by neurons with a peripheral-like ontogeny in the grasshopper *Schistocerca gregaria*. Arthropod Structure and Development 37:186-198

Boyan G, Williams JLD, Herbert Z (2008) Fascicle switching generates the chiasmal neuroarchitecture in the embryonic central body of the grasshopper *Schistocerca gregaria*. Arthropod Structure and Development 37:539-544

Brand M, Jarman AP, Jan LY, Jan YN (1993) *Asense* is a *Drosophila* neural precursor gene and is capable of initiating sense organ formation. Development 119:1-17

Brauer A (1894) Beiträge zur Kenntnis der Entwicklungsgeschichte des Skorpions II. Zeitschrift für wissenschaftliche Zoologie 59:351-435

Brena C, Akam M (2012) The embryonic development of the centipede *Strigamia maritima*. Developmental Biology 363:290-307

Brenneis G (2007) Aspects of the development of sea spiders (Arthropoda, Pycnogonida). Humboldt-Universität zu Berlin. Diploma thesis, pp. 1-132

Brenneis G, Richter S (2010) Architecture of the nervous system in Mystacocarida (Arthropoda, Crustacea) - an immunohistochemical study and 3D reconstruction. Journal of Morphology 271:169-189

Brenneis G, Ungerer P, Scholtz G (2008) The chelifores of sea spiders (Arthropoda, Pycnogonida) are the appendages of the deutocerebral segment. Evolution and Development 10:717-724

Broadus J, Doe CQ (1995) Evolution of neuroblast identity: *seven-up* and *prospero* expression reveal homologous and divergent neuroblast fates in *Drosophila* and *Schistocerca*. Development 121:3989-3996

Broadus J, Skeath JB, Spana EP, Bossing T, Technau G, Doe CQ (1995) New neuroblast markers and the origin of the aCC/pCC neurons in the *Drosophila* central nervous system. Mechanisms of Development 53:393-402

Brusca RC, Brusca GJ (2003) Invertebrates. 2 edn. Sinauer Associates, Sunderland, pp. 1-936

Budd GE, Telford MJ (2009) The origin and evolution of arthropods. Nature 457:812-817

Bullock TH, Horridge GA (1965) Structure and Function in the Nervous Systems of Invertebrates. W.H. Freeman and Company, San Francisco, pp. 1-1610

Burris ZP (2011) Larval morphologies and potential developmental modes of eight sea spider species (Arthropoda: Pycnogonida) from the southern Oregon coast. Journal of the Marine Biological Association of the United Kingdom 91:845-855

Cabrera CV, Martinez-Arias A, Bate M (1987) The expression of three members of the *achaete-scute* gene complex correlates with neuroblast segregation in *Drosophila*. Cell 50:425-433

Campbell LI, Rota-Stabelli O, Edgecombe GD, Marchioro T, Longhorn SJ, Telford MJ, Philippe H, Rebecchi L, Peterson KJ, Pisani D (2011) MicroRNAs and phylogenomics resolve the relationships of Tardigrada and suggest that velvet worms are the sister group to Arthropoda. Proceedings of the National Academy of Sciences 108:15920-15924

Campos-Ortega JA (1994) Genetic mechanisms of early neurogenesis in *Drosophila melanogaster*. Journal of Physiology 88:111-122

Cano E, López-González PJ (2009) Novel mode of postembryonic development in *Ammothea* genus (Pycnogonida: Ammotheidae) from Antarctic waters. Scientia Marina 73:541-550

Cano Sánchez E, López-González PJ (2010) Postembryonic development of *Nymphon unguiculatum* Hodgson 1915 (Pycnogonida, Nymphonidae) from the South Shetland Islands (Antarctica). Polar Biology 33:1205-1214

Cassier P (1979) The corpora allata of insects. International Review of Cytology 57:1-73

Cau E, Blader P (2009) Notch activity in the nervous system: To switch or not to switch? Neural Development 4:36

Cayre M, Scotto-Lomassese S, Malaterre J, Strambi C, Strambi A (2007) Understanding the regulation and function of adult neurogenesis: contribution from an insect model, the house cricket. Chemical Senses 32:385-395

Cayre M, Strambi C, Charpin P, Augier R, Meyer MR, Edwards JS, Strambi A (1996) Neurogenesis in adult insect mushroom bodies. The Journal of Comparative Neurology 371:300-310

Cayre M, Strambi C, Strambi A (1994) Neurogenesis in an adult insect brain and its hormonal control. Nature 368:57-59

Chaigneau J (1994) Systéme nerveux. I. Cytologie, histologie et anatomie. In: Grassé P-P (ed) Traité de Zoologie. Anatomie, Systématique, Biologie. 7 Crustacés. Masson, Paris, pp. 235-300

Chaves da Silva PG, Benton JL, Beltz BS, Allodi S (2012) Adult neurogenesis: ultrastructure of a neurogenic niche and neurovascular relationships. PloS ONE 7:e39267. doi:39210.31371/journal.pone.0039267

Child CA (1979) Shallow water Pycnogonida of the Isthmus of Panama and the coasts of Middle America. Smithsonian Contributions to Zoology 23:1-86

Child CA (1998) The marine fauna of New Zealand: Pycnogonida (sea spiders). NIWA Biodiversity Memoirs 109:1-71

Chipman AD, Stollewerk A (2006) Specification of neural precursor identity in the geophilomorph centipede *Strigamia maritima*. Developmental Biology 290:337-350

Condron BG, Patel NH, Zinn K (1994) *engrailed* controls glial/neuronal cell fate decisions at the midline of the central nervous system. Neuron 13:541-554

Cook CE, Smith ML, Telford MJ, Bastianello A, Akam M (2001) *Hox* genes and the phylogeny of the arthropods. Current Biology 11:759-763

Creppe C, Malinouskaya L, Volvert M-L, Gillard M, Close P, Malaise O, Laguesse S, Cornez I, Rahmouni S, Ormenese S, Belachew S, Malgrange B, Chapelle J-P, Siebenlist U, Moonen G, Chariot A, Nguyen L (2009) Elongator controls the migration and differentiation of cortical neurons through acetylation of α-tubulin. Cell 136:551-564

Dahms HU (2000) Phylogenetic implications of the crustacean nauplius. Hydrobiologia 417:91-99

Damen WGM, Hausdorf M, Seyfarth EA, Tautz D (1998) A conserved mode of head segmentation in arthropods revealed by the expression of *Hox* genes in a spider. Proceedings of the National Academy of Sciences 95:10665-10670

de Velasco B, Erclik T, Shy D, Sclafani J, Lipshitz H, McInnes R, Hartenstein V (2007) Specification and development of the pars intercerebralis and pars lateralis, neuroendocrine command centers in the *Drosophila* brain. Developmental Biology 302:309-323

Dearborn GK (2003) Post-embryonic development of the sea spider *Achelia gracilipes* (Chelicerata: Pycnogonida). University of Alberta. Master thesis. pp. 1-86

Doe CQ (1992) Molecular markers for identified neuroblasts and ganglion mother cells in the *Drosophila* central nervous system. Development 116:855-863

Doe CQ (2008) Neural stem cells: balancing self-renewal with differentiation. Development 135:1575-1587

Doe CQ, Chu-LaGraff Q, Wright DM, Scott MP (1991) The *prospero* gene specifies cell fates in the *Drosophila* central nervous system. Cell 65:451-464

Doe CQ, Goodman CS (1985a) Early events in insect neurogenesis. I. Development and segmental differences in the pattern of neuronal precursor cells. Developmental Biology 111:193-205

Doe CQ, Goodman CS (1985b) Early events in insect neurogenesis. II. Role of cell interactions and cell lineage in the determination of neuronal precursor cells. Developmental Biology 111:206-219

Döffinger C, Hartenstein V, Stollewerk A (2010) Compartmentalisation of the precheliceral neuroectoderm in the spider *Cupiennius salei*: Development of the arcuate body, the optic ganglia and the mushroom body. The Journal of Comparative Neurology 518:2612-2632

Döffinger C, Stollewerk A (2010) How can conserved gene expression allow for variation? Lessons from the dorso-ventral patterning gene *muscle segment homeobox*. Developmental Biology 345:105-116

Dogiel V (1911) Studien über die Entwicklungsgeschichte der Pantopoden. Nervensystem und Drüsen der Pantopodenlarven. Zeitschrift für wissenschaftliche Zoologie 99:109-146

Dogiel V (1913) Embryologische Studien an Pantopoden. Zeitschrift für wissenschaftliche Zoologie 107:575-741

Dohle W (1964) Die Embryonalentwicklung von *Glomeris marginata* (Villers) im Vergleich zur Entwicklung anderer Diplopoden. Zoologische Jahrbücher der Anatomie 81:241-310

Dohle W (1976) Die Bildung und Differenzierung des postnauplialen Keimstreifs von *Diastylis rathkei* (Crustacea, Cumacea). II. Die Differenzierung und Musterbildung des Ektoderms. Zoomorphologie 84:235-277

Dohle W (2001) Are the insects terrestrial crustaceans? A discussion of some new facts and arguments and the proposal of the proper name 'Tetraconata' for the monophyletic unit Crustacea + Hexapoda. Annales de la Société Entomologique de France (NS) 37:85-103

Dohle W, Scholtz G (1988) Clonal analysis of the crustacean segment: the discordance between genealogical and segmental borders. Development 104 Supplement:147-160

Dohrn A (1881) Die Pantopoden des Golfes von Neapel und der angrenzenden Meeres-Abschnitte. Fauna und Flora des Golfes von Neapel und der angrenzenden Meeres-Abschnitte. Verlag von Wilhelm Engelmann, Leipzig, pp. 1-252

Dove H, Stollewerk A (2003) Comparative analysis of neurogenesis in the myriapod *Glomeris marginata* (Diplopoda) suggests more similarities to chelicerates than to insects. Development 130:2161-2171

Dufour M-C, Gadenne C (2006) Adult neurogenesis in a moth brain. The Journal of Comparative Neurology 495:635-643

Duman-Scheel M, Patel NH (1999) Analysis of molecular marker expression reveals neuronal homology in distantly related arthropods. Development 126:2327-2334

Dunlop JA (2010) Geological history and phylogeny of Chelicerata. Arthropod Structure and Development 39:124-142

Dunlop JA, Arango CP (2005) Pycnogonid affinities: a review. Journal of Zoology, Systematics and Evolutionary Research 43:8-21

Dunn CW, Hejnol A, Matus DQ, Pang K, Browne WE, Smith SA, Seaver E, Rouse GW, Obst M, Edgecombe GD, Sørensen MV, Haddock SHD, Schmidt-Rhaesa A, Okusu A, Møbjerg Kristensen R, Wheeler WC, Martindale MQ, Giribet G (2008) Broad phylogenomic sampling improves resolution of the animal tree of life. Nature 452:745-749

Edgecombe GD (2007) Centipede systematics: progress and problems. Zootaxa 1668:327-341

Edgecombe GD (2010) Arthropod phylogeny: An overview from the perspectives of morphology, molecular data and the fossil record. Arthropod Structure and Development 39:74-87

Edgecombe GD, Richter S, Wilson GDF (2003) The mandibular gnathal edges: Homologous structures throughout Mandibulata? African Invertebrates 44:115-135

Edgecombe GD, Wilson GDF, Colgan DJ, Gray MR, Cassis G (2000) Arthropod cladistics: combined analysis of histone H3 and U2 snRNA sequences and morphology. Cladistics 16:155-203

Eriksson BJ, Budd GE (2000) Onychophoran cephalic nerves and their bearing on our understanding of head segmentation and stem-group evolution of Arthropoda. Arthropod Structure and Development 29:197-209

Eriksson BJ, Stollewerk A (2010a) The morphological and molecular processes of onychophoran brain development show unique features that are neither comparable to insects, nor to chelicerates. Arthropod Structure and Development 39:478-490

Eriksson BJ, Stollewerk A (2010b) Expression patterns of neural genes in *Euperipatoides kanangrensis* suggest divergent evolution of onychophoran and euarthropod neurogenesis. Proceedings of the National Academy of Sciences 107:22576-22581

Eriksson BJ, Tait NN, Budd GE (2003) Head development in the onychophoran *Euperipatoides kanangrensis* with particular reference to the central nervous system. Journal of Morphology 255:1-23

Eriksson BJ, Tait NN, Budd GE, Janssen R, Akam M (2010) Head patterning and *Hox* gene expression in an onychophoran and its implications for the arthropod head problem. Development, Genes and Evolution 220:117-122

Eriksson BJ, Tait NN, Norman JM, Budd GE (2005) An ultrastructural investigation of the hypocerebral organ of the adult *Euperipatoides kanangrensis* (Onychophora, Peripatopsidae). Arthropod Structure and Development 34:407-418

Fabritius-Vilpoux K, Bisch-Knaden S, Harzsch S (2008) *Engrailed*-like immunoreactivity in the embryonic ventral nerve cord of the Marbled Crayfish (Marmorkrebs). Invertebrate Neuroscience 8:177-197

Fahrenbach WH, Arango CP (2007) Microscopic anatomy of Pycnogonida: II. Digestive system. III. Excretory system. Journal of Morphology 268:917-935

Farley RD (2001) Development of segments and appendages in embryos of the desert scorpion *Paruroctonus mesaensis* (Scorpiones: Vaejovidae). Journal of Morphology 250:70-88

Fischer AHL, Scholtz G (2010) Axogenesis in the stomatopod crustacean *Gonodactylaceus falcatus* (Malacostraca). Invertebrate Biology 129:59-76

Friedrich M, Tautz D (1995) Ribosomal DNA phylogeny of the major extant arthropod classes and the evolution of myriapods. Nature 376:165-167

Fritsch M, Richter S (2010) The formation of the nervous system during larval development in *Triops cancriformis* (Bosc) (Crustacea, Branchiopoda): an immunohistochemical survey. Journal of Morphology 271:1457-1481

Fritsch M, Richter S (2012) Nervous system development in Spinicaudata and Cyclestherida (Crustacea, Branchiopoda) - comparing two different modes of indirect development by using an event pairing approach. Journal of Morphology 273:672-695

Fürstenberg S, Broadus J, Doe CQ (1998) Asymmetry and cell fate in the *Drosophila* embryonic CNS. International Journal of Developmental Biology 42:379-383

Gerberding M (1997) Germ band formation and early neurogenesis of *Leptodora kindti* (Cladocera): first evidence for neuroblasts in the entomostracan crustaceans. Invertebrate Reproduction and Development 32:63-73

Gibert JM, Mouchel-Vielh E, Quéinnec E, Deutsch JS (2000) Barnacle duplicate *engrailed* genes: divergent expression patterns and evidence for a vestigial abdomen. Evolution and Development 2:194-202

Gillespie JM, Bain BA (2006) Postembryonic development of *Tanystylum bealensis* (Pycnogonida, Ammotheidae) from Barkley Sound, British Columbia, Canada. Journal of Morphology 267:308-317

Giribet G, Edgecombe GD (2006) Conflict between datasets and phylogeny of centipedes: an analysis based on seven genes and morphology. Proceedings of the Royal Society B 273:531-538

Giribet G, Edgecombe GD (2012) Reevaluating the arthropod tree of life. Annual Reviews of Entomology 57:167-186

Giribet G, Edgecombe GD, Wheeler WC (2001) Arthropod phylogeny based on eight molecular loci and morphology. Nature 413:157-161

Gnanamuthu CP (1950) Notes on the morphology and development of a pycnogonid, *Propallene kempi* (Calman), from Madras plankton. Proceedings of the Zoological Society of Bengal 3:39-47

Goodman CS, Spitzer NC (1979) Embryonic development of identified neurones: differentiation from neuroblast to neurone. Nature 280:208-214

Goto H, Tomono Y, Ajiro K, Kosako H, Fujita M, Sakurai M, Okawa K, Iwamatsu A, Okigaki T, Takahashi T, Inagaki M (1999) Identification of a novel phosphorylation site on histone H3 coupled with mitotic chromosome condensation. The Journal of Biological Chemistry 274:25543-25549

Green P, Hartenstein AY, Hartenstein V (1993) The embryonic development of the *Drosophila* visual system. Cell and Tissue Research 273:583-598

Gundersen GG, Bulinski JC (1986) Distribution of tyrosinated and nontyrosinated α-tubulin during mitosis. The Journal of Cell Biology 102:1118-1126

Hall TA (1999) BioEdit: a user-friendly biological sequence alignment editor and analysis program for Windows 95/98/NT. Nucleic Acids Symposium Series 41:95-98

Hammond JW, Cai D, Verhey KJ (2008) Tubulin modifications and their cellular functions. Current Opinion in Cell Biology 20:71-76

Hanström B (1919) Zur Kenntnis des centralen Nervensystems der Arachnoiden und Pantopoden. Stockholms Universitet. Doctoral thesis, pp. 1-191

Hanström B (1923) Untersuchungen über das Gehirn, insbesondere der Sehganglien der Crustaceen. Arkiv för Zoologi 16:1-119

Hanström B (1928) Vergleichende Anatomie des Nervensystems der wirbellosen Tiere unter Berücksichtigung seiner Funktion. Springer Verlag, Berlin, pp. 1-628

Hartenstein AY, Nassif C, Green P, Hartenstein V (1996) Early neurogenesis in the *Drosophila* brain. The Journal of Comparative Neurology 370:313-329

Hartenstein V (1997) Development of the insect stomatogastric nervous system. Trends in Neurosciences 20:421-427

Hartenstein V, Campos-Ortega JA (1984) Early neurogenesis in wild-type *Drosophila melanogaster*. Roux's Archives of Developmental Biology 193:308-325

Hartenstein V, Rudloff E, Campos-Ortega JA (1987) The pattern of proliferation of the neuroblasts in the wild-type embryo of *Drosophila melanogaster*. Roux's Archives of Developmental Biology 196:473-485

Harzsch S (2001) Neurogenesis in the crustacean ventral nerve cord: homology of neuronal stem cells in Malacostraca and Branchiopoda? Evolution and Development 3:154-169

Harzsch S (2003) Ontogeny of the ventral nerve cord in malacostracan crustaceans: a common plan for neuronal development in Crustacea, Hexapoda and other Arthropoda? Arthropod Structure and Development 32:17-37

Harzsch S (2004) The tritocerebrum of Euarthropoda: a "non-*drosophilo*centric" perspective. Evolution and Development 6:303-309

Harzsch S (2006) Neurophylogeny: Architecture of the nervous system and a fresh view on arthropod phylogeny. Integrative and Comparative Biology 46:162-194

Harzsch S (2007) The architecture of the nervous system provides important characters for phylogenetic reconstructions: examples from the Arthropoda. Species, Phylogeny and Evolution 1:33-57

Harzsch S, Anger K, Dawirs RR (1997) Immunocytochemical detection of acetylated α-tubulin and *Drosophila* synapsin in the embryonic crustacean nervous system. International Journal of Developmental Biology 41:477-484

Harzsch S, Dawirs RR (1994) Neurogenesis in larval stages of the spider crab *Hyas araneus* (Decapoda, Brachyura): proliferation of neuroblasts in the ventral nerve cord. Roux's Archives of Developmental Biology 204:93-100

Harzsch S, Dawirs RR (1996) Neurogenesis in the developing crab brain: postembryonic generation of neurons persists beyond metamorphosis. Journal of Neurobiology 29:384-398

Harzsch S, Miller J, Benton J, Beltz B (1999) From embryo to adult: persistent neurogenesis and apoptotic cell death shape the lobster deutocerebrum. The Journal of Neuroscience 19:3472-3485

Harzsch S, Miller J, Benton J, Dawirs RR, Beltz B (1998) Neurogenesis in the thoracic neuromeres of two crustaceans with different types of metamorphic development. The Journal of Experimental Biology 201:2465-2479

Harzsch S, Müller CHG, Wolf H (2005a) From variable to constant cell numbers: cellular characteristics of the arthropod nervous system argue against a sister-group relationship of Chelicerata and "Myriapoda" but favour the Mandibulata concept. Development, Genes and Evolution 215:53-68

Harzsch S, Wildt M, Battelle B, Waloszek D (2005b) Immunohistochemical localization of neurotransmitters in the nervous system of larval *Limulus polyphemus* (Chelicerata, Xiphosura): evidence for a conserved protocerebral architecture in Euarthropoda. Arthropod Structure and Development 24:327-342

Hedgpeth JW (1947) On the evolutionary significance of the Pycnogonida. Smithsonian Miscellaneous Collections 106:1-53

Heitzler P, Simpson P (1991) The choice of cell fate in the epidermis of *Drosophila*. Cell 64:1083-1092

Hejnol A, Schnabel R (2005) The eutardigrade *Thulinia stephaniae* has an indeterminate development and the potential to regulate early blastomere ablations. Development 132:1349-1361

Helfer H, Schlottke E (1935) Pantopoda. Dr. H. G. Bronns Klassen und Ordnungen des Tierreichs, Akademische Verlagsgesellschaft m.b.H., Leipzig, pp. 1-314

Henry LM (1953) The nervous system of the Pycnogonida. Microentomology 18:16-36

Heymons R (1901) Die Entwicklungsgeschichte der Scolopender. Zoologica 33:1-244

Hoek PPC (1881) Report on the Pycnogonida, dredged by H.M.S. Challenger during the years 1873-76. Challenger Report, Zoology 3:1-167

Holmgren N (1916) Zur Vergleichenden Anatomie des Gehirns von Polychaeten, Onychophoren, Xiphosuren, Arachniden, Crustaceen, Myriapoden und Insekten. Vorstudien zu einer Phylogenie der Arthropoden. Kungliga Svenska Vetenskapsakademiens Handlingar 56:1-303

Homberg U (2008) Evolution of the central complex in the arthropod brain with respect to the visual system. Arthropod Structure and Development 37:347-362

Hooper J (1980) Some aspects of the reproductive biology of *Parapallene avida* Stock (Pycnogonida: Callipallenidae) from Northern New South Wales. The Australian Zoologist 30:473-483

Ip YT, Levine M, Bier E (1994) Neurogenic expression of *snail* is controlled by separable CNS and PNS promoter elements. Development 120:199-207

Jager M, Murienne J, Clabaut C, Deutsch J, Le Guyader H, Manuel M (2006) Homology of arthropod anterior appendages revealed by *Hox* gene expression in a sea spider. Nature 441:506-508

Janke C, Kneussel M (2010) Tubulin post-translational modifications: encoding functions on the neuronal microtubule cytoskeleton. Trends in Neurosciences 33:362-372

Jenner RA (2010) Higher-level crustacean phylogeny: consensus and conflicting hypotheses. Arthropod Structure and Development 39:143-153

Jiménez F, Campos-Ortega JA (1990) Defective neuroblast commitment in mutants of the *achaete-scute* complex and adjacent genes of *D. melanogaster*. Neuron 5:81-89

Juberthie C (1964) Recherches sur la biologie des Opilions. Annales de Spéléologie 19:1-238

Juberthie C, Muñoz-Cuevas A (1970) Rôle des organes neuraux d'un Opilion Gonyleptidae, *Pachylus quinamavidensis*, dans la formation des globuli des corpora pedunculata. Comptes Rendus Hebdomadaires des Séances de l'Académie des Sciences 270:1028-1031

Juberthie-Jupeau L (1967) Existence d'organes neuraux intracérébraux chez les Glomeridia (Diplopodes) épigés et cavernicoles. Comptes Rendus Hebdomadaires des Séances de l'Académie des Sciences 264:89-92

Kadner D, Stollewerk A (2004) Neurogenesis in the chilopod *Lithobius forficatus* suggests more similarities to chelicerates than to insects. Development, Genes and Evolution 214:367-379

Kästner A (1951) Zur Entwicklungsgeschichte von *Telyphonus caudatus* L. (Pedipalpi). Zoologische Jahrbücher Abteilung für Anatomie und Ontogenie der Tiere 71:1-55

Kennel J (1886) Entwicklungsgeschichte von *Peripatus edwardsii* Blanch. und *Peripatus torquatus* n. sp. Arbeiten aus dem zoologisch-zootomischen Institut Würzburg 8:1-93

Kerner P, Hung J, Béhague J, Le Gouar M, Balavoine G, Vervoort M (2009) Insights into the evolution of the *snail* superfamily from metazoan wide molecular phylogenies and expression data in annelids. BMC Evolutionary Biology 9:94

Kiernan JA (2008) Histological and Histochemical Methods. Theory and Practice. 4 edn. Scion Publishing Limited, Bloxham, pp. 1-606

King PE (1973) Pycnogonids. Hutchinson & Co, London, pp. 1-144

Kingsley JS (1893) The embryology of *Limulus*. Part II. Journal of Morphology 8:195-268

Kirsch R, Richter S (2007) The nervous system of *Leptodora kindtii* (Branchiopoda, Cladocera) surveyed with confocal scanning microscopy (CLSM), including general remarks on the branchiopod neuromorphological ground pattern. Arthropod Structure and Development 36:143-156

Knoblich JA, Jan LY, Jan YN (1995) Asymmetric segregation of *Numb* and *Prospero* during cell division. Nature 377:624-627

Knoll HJ (1974) Untersuchungen zur Entwicklungsgeschichte von *Scutigera coleoptrata* L. (Chilopoda). Zoologische Jahrbücher der Anatomie 92:47-132

Koenemann S, Jenner RA, Hoenemann M, Stemme T, von Reumont BM (2010) Arthropod phylogeny revisited, with a focus on crustacean relationships. Arthropod Structure and Development 39:88-110

Kreis TE (1987) Microtubules containing detyrosinated tubulin are less dynamic. The EMBO Journal 6:2597-2606

Lebour MV (1916) Notes on the life history of *Anaphia petiolata* (Kröyer). Journal of the Marine Biological Association of the United Kingdom 11:51-56

Lebour MV (1945) Notes on the Pycnogonida of Plymouth. Journal of the Marine Biological Association of the United Kingdom 26:139-165

Lehmann R, Dietrich U, Jiménez F, Campos-Ortega JA (1981) Mutations of early neurogenesis in *Drosophila*. Roux's Archives of Developmental Biology 190:226-229

Lehmann R, Jiménez F, Dietrich U, Campos-Ortega JA (1983) On the phenotype and development of mutants of early neurogenesis in *Drosophila melanogaster*. Roux's Archives of Developmental Biology 1983:62-74

Lehmann T, Heß M, Melzer RR (2012) Wiring a periscope - ocelli, retinula axons, visual neuropils and the ancestrality of sea spiders. PLoS ONE 7:e30474. doi:30410.31371/journal.pone.0030474

Lehmann T, Weinzierl C, Melzer RR (2011) SEM description of the first larval instar of *Achelia assimilis* (Pycnogonida: Ammotheidae). Journal of the Marine Biological Association of the United Kingdom 91:1081-1087

Linne V, Eriksson BJ, Stollewerk A (2012) *Single-minded* and the evolution of the ventral midline in arthropods. Developmental Biology 364:66-76

Linne V, Stollewerk A (2011) Conserved and novel functions for *Netrin* in the formation of the axonal scaffold and glial sheath cells in spiders. Developmental Biology 353:134-146

Loesel R (2004) Comparative morphology of central neuropils in the brain of arthropods and its evolutionary and functional implications. Acta Biologica Hungarica 55:39-51

Loesel R, Nässel DR, Strausfeld NJ (2002) Common design in a unique midline neuropil in the brains of arthropods. Arthropod Structure and Development 31:77-91

Loesel R, Seyfarth EA, Bräunig P, Agricola HJ (2011) Neuroarchitecture of the arcuate body in the brain of the spider *Cupiennius salei* (Araneae, Chelicerata) revealed by allatostatin-, proctolin-, and CCAP-immunocytochemistry and its evolutionary implications. Arthropod Structure and Development 40:210-220

Lovely EC (2005) The life history of *Phoxichilidium tubulariae* (Pycnogonida: Phoxichilidiidae). Northeastern Naturalist 12 (1):77-92

Machner J, Scholtz G (2010) A scanning electron microscopy study of the embryonic development of *Pycnogonum litorale* (Arthropoda, Pycnogonida). Journal of Morphology 271:1306-1318

Mallatt JM, Garey JR, Shultz JW (2004) Ecdysozoan phylogeny and Bayesian inference: first use of nearly complete 28S and 18S rRNA gene sequences to classify the arthropods and their kin. Molecular Phylogenetics and Evolution 31:178-191

Mallatt J, Giribet G (2006) Further use of nearly complete 28S and 18S rRNA genes to classify Ecdysozoa: 37 more arthropods and a kinorhynch. Molecular Phylogenetics and Evolution 40:772-794

Manuel M, Jager M, Murienne J, Clabaut C, Le Guyader H (2006) *Hox* genes in sea spiders (Pycnogonida) and the homology of arthropod head segments. Development, Genes and Evolution 216:481-491

Martín-Bermudo MD, Carmena A, Jiménez F (1995) Neurogenic genes control gene expression at the transcriptional level in early neurogenesis and in mesectoderm specification. Development 121:219-224

Mathew AP (1956) Embryology of *Heterometrus scaber*. Zoological Memoirs of the University of Travancore Research Institute 1:1-96

Maxmen A (2006) Pycnogonid development and the evolution of the arthropod body plan. Harvard University, Cambridge (Massachusetts). PhD thesis, pp. 1-177

Maxmen A, Browne WE, Martindale MQ, Giribet G (2005) Neuroanatomy of sea spiders implies an appendicular origin of the protocerebral segment. Nature 437:1144-1148

Mayer G (2007) *Metaperipatus inae* sp. nov. (Onychophora: Peripatopsidae) from Chile with a novel ovarian type and dermal insemination. Zootaxa 1440:21-37

Mayer G, Kato C, Quast B, Chisholm RH, Landman KA, Quinn L (2010a) Growth patterns in Onychophora (velvet worms): lack of a localised posterior proliferation zone. BMC Evolutionary Biology 10:339

Mayer G, Whitington PM (2009a) Velvet worm development links myriapods with chelicerates. Proceedings of the Royal Society B 276 (1673):3571-3579

Mayer G, Whitington PM (2009b) Neural development in Onychophora (velvet worms) suggests a step-wise evolution of segmentation in the nervous system of Panarthropoda. Developmental Biology 335:263-275

Mayer G, Whitington PM, Sunnucks P, Pflüger H-J (2010b) A revision of brain composition in Onychophora (velvet worms) suggests that the tritocerebrum evolved in arthropods. BMC Evolutionary Biology 10:255

McClendon JF (1904) On the anatomy and embryology of the nervous system of the scorpion. Biological Bulletin 8:38-55

McMurrich JP (1895) Embryology of the isopod Crustacea. Journal of Morphology11:63-154

Meinert F (1899) Pycnogonida. The Danish Ingolf-Expedition 3:1-71

Meisenheimer J (1902) Beiträge zur Entwicklungsgeschichte der Pantopoden. I. Die Entwicklung von *Ammothea echinata* Hodge bis zur Ausbildung der Larvenform. Zeitschrift für wissenschaftliche Zoologie 72:191-248

Meusemann K, von Reumont BM, Simon S, Roeding F, Strauss S, Kück P, Ebersberger I, Walzl M, Pass G, Breuers S, Achter V, von Haeseler A, Burmester T, Hadrys H, Wägele JW, Misof B (2010) A phylogenomic approach to resolve the arthropod tree of life. Molecular Biology and Evolution 27:2451-2464

Mittmann B (2002) Early neurogenesis in the horseshoe crab *Limulus polyphemus* and its implication for arthropod relationships. Biological Bulletin 203:221-222

Mittmann B (2003) Die Embryologie des Pfeilschwanzkrebses *Limulus polyphemus* (Xiphosura, Chelicerata) und anderer Arthropoden unter besonderer Berücksichtigung der Neurogenese. Humboldt-Universität zu Berlin. Doctoral thesis, pp. 1-126

Mittmann B, Scholtz G (2003) Development of the nervous system in the "head" of *Limulus polyphemus* (Chelicerata: Xiphosura): morphological evidence for a correspondence between the segments of the chelicerae and of the (first) antennae of Mandibulata. Development, Genes and Evolution 213:9-17

Mittmann B, Wolff C (2012) Embryonic development and staging of the cobweb spider *Parasteatoda tepidariorum* C.L. Koch, 1841 (syn.: *Achaearanea tepidariorum*; Araneomorphae; Theridiidae). Development, Genes and Evolution 222:189-216

Miyazaki K (2002) On the shape of foregut lumen on sea spiders (Arthropoda: Pycnogonida). Journal of the Marine Biological Association of the United Kingdom 82:1037-1038

Morgan TH (1891) A contribution to the embryology and phylogeny of the pycnogonids. Studies from the Biological Laboratory of the Johns Hopkins University Baltimore 5:1-76

Müller CHG, Rosenberg J, Richter S, Meyer-Rochow VB (2003) The compound eye of *Scutigera coleoptrata* (Linnaeus, 1758) (Chilopoda: Notostigmophora): an ultrastructural reinvestigation that adds support to the Mandibulata concept. Zoomorphology 122:191-209

Müller F (2006) Neuroblasten bei *Triops cancriformis*? Eine Untersuchung zur Neurogenese eines "Niederen Krebses" (Notostraca, Branchiopoda). Humboldt-Universität zu Berlin. Diploma thesis, pp. 1-56

Munilla T (1999) Evoluciøn y filogenia de los picnogønidos. In: Melic A, de Haro JJ, Mendez M, Ribera I (eds) Evoluciøn y filogenia de Arthropoda. Zaragoza, pp 273-279

Murienne J, Edgecombe GD, Giribet G (2010) Including secondary structure, fossils and molecular dating in the centipede tree of life. Molecular Phylogenetics and Evolution 57:301-313

Nakamura K (1981) Post-embryonic development of a pycnogonid, *Propallene longiceps*. Journal of Natural History 15:49-62

Nakamura K, Kano Y, Suzuki N, Namatame T, Kosaku A (2007) 18S rRNA phylogeny of sea spiders with emphasis on the position of Rhynchothoracidae. Marine Biology 153:213-223

Noveen A, Daniel A, Hartenstein V (2000) Early development of the *Drosophila* mushroom body: the roles of *eyeless* and *dachshund*. Development 127:3475-3488

Ohshima H (1933) Young pycnogonids found parasitic on nudibranchs. Annotationes Zoologicae Japonenses 14:61-66

Ohshima H (1937) The life-history of "*Nymphonella tapetis*" Ohshima ("Pantopoda, Eurycydidae"). Extrait des Comptes Rendus du XII Congress International de Zoologie - Lisbonne 1935:1616-1627

Okuda S (1940) Metamorphosis of a pycnogonid parasitic in a hydromedusa. Journal of the Faculty of Science, Hokkaido Imperial University, Series 6 7:73-86

Paulus HF (2000) Phylogeny of the Myriapoda - Crustacea - Insecta: a new attempt using photoreceptor structure. Journal of Zoological Systematics and Evolutionary Research 38:189-208

Pflugfelder O (1948) Entwicklung von *Paraperipatus amboinensis* n. spec. Zoologische Jahrbücher Abteilung für Anatomie und Ontogenie der Tiere 69:443-492

Pileri SA, Roncador G, Ceccarelli C, Piccioli M, Briskomatis A, Sabattini E, Ascani S, Santini D, Piccaluga PP, Leone O, Damiani S, Ercolessi C, Sandri F, Pieri F, Leoncini L, Falini B (1997) Antigen retrieval techniques in immunohistochemistry: Comparison of different methods. Journal of Pathology 183:116-123

Pioro HL, Stollewerk A (2006) The expression pattern of genes involved in early neurogenesis suggests distinct and conserved functions in the diplopod *Glomeris marginata*. Development, Genes and Evolution 216:417-430

Pisani D, Poling LL, Lyons-Weiler M, Hedges SB (2004) The colonization of land by animals: molecular phylogeny and divergence times among arthropods. BMC Biology 2:1

Poschmann M, Dunlop J (2006) A new sea spider (Arthropoda: Pycnogonida) with a flagelliform telson from the Lower Devonian Hunsrück Slate, Germany. Palaeontology 49:983-989

Pross A (1966) Untersuchungen zur Entwicklungsgeschichte der Araneae [*Pardosa hortensis* (Thorell)] unter besonderer Berücksichtigung des vorderen Prosomaabschnittes. Zeitschrift für Morphologie und Ökologie der Tiere 58:38-108

Prpic NM, Damen WGM (2009) *Notch*-mediated segmentation of the appendages is a molecular phylotypic trait of the arthropods. Developmental Biology 326:262-271

Regier JC, Shultz JW, Ganley ARD, Hussey A, Shi D, Ball B, Zwick A, Stajich JE, Cummings MP, Martin JW, Cunningham CW (2008) Resolving arthropod phylogeny: Exploring phylogenetic signal with 41 kb of protein-coding nuclear gene sequence. Systematic Biology 57:920-938

Regier JC, Shultz JW, Zwick A, Hussey A, Ball B, Wetzer R, Martin JW, Cunningham CW (2010) Arthropod relationships revealed by phylogenomic analysis of nuclear protein-coding sequences. Nature 463:1079-1083

Rehm P, Pick C, Borner J, Markl J, Burmester T (2012) The diversity and evolution of chelicerate hemocyanins. BMC Evolutionary Biology 12:19

Richter S (2002) The Tetraconata concept: Hexapod-crustacean relationships and the phylogeny of Crustacea. Organisms, Diversity and Evolution 2:217-237

Richter S, Loesel R, Purschke G, Schmidt-Rhaesa A, Scholtz G, Stach T, Vogt L, Wanninger A, Brenneis G, Döring C, Faller S, Fritsch M, Grobe P, Heuer CM, Kaul S, Moeller OS, Müller CHG, Rieger V, Rothe BH, Stegner MEJ, Harzsch S (2010) Invertebrate neurophylogeny: suggested terms and definitions for a neuroanatomical glossary. Frontiers in Zoology 7:29

Roeding F, Borner J, Kube M, Klages S, Reinhardt R, Burmester T (2009) A 454 sequencing approach for large scale phylogenomic analysis of the common emperor scorpion (*Pandinus imperator*). Molecular Phylogenetics and Evolution 53:826-834

Rota-Stabelli O, Campbell L, Brinkmann H, Edgecombe GD, Longhorn SJ, Peterson KJ, Pisani D, Philippe H, Telford MJ (2011) A congruent solution to arthropod phylogeny: phylogenomics, microRNAs and morphology support monophyletic Mandibulata. Proceedings of the Royal Society B 278:298-306

Rota-Stabelli O, Kayal E, Gleeson D, Daub J, Boore JL, Telford MJ, Pisani D, Blaxter M, Lavrov DV (2010) Ecdysozoan mitogenomics: evidence for a common origin of the legged invertebrates, the Panarthropoda. Genome Biology and Evolution 2:425-440

Rota-Stabelli O, Telford MJ (2008) A multi-criterion approach to the selection of optimal outgroups in phylogeny: recovering some support for Mandibulata over Myriochelata using mitogenomics. Molecular Phylogenetics and Evolution 48:103-111

Salazar-Vallejo S, Stock JH (1987) Apparent parasitism of *Sabella melanostigma* (Polychaeta) by *Ammothella spinifera* (Pycnogonida) from the Gulf of California. Revista de Biologia Tropical 35:269-275

Sanchez S (1958) Cellules neurosécrétrices et organes infracérébraux de *Peripatopsis moseleyi* Wood (Onychophores) et neurosécrétion chez *Nymphon gracile* Leach (Pycnogonides). Archives de Zoologie Expérimentale et Générale Notes et Revue 96:57-62

Sanchez S (1959) Le développement des Pycnogonides et leurs affinités avec les Arachnides. Archives de Zoologie Expérimentale et Générale 98:1-102

Sandeman DC, Bazin F, Beltz BS (2011) Adult neurogenesis: examples from the decapod crustaceans and comparisons with mammals. Arthropod Structure and Development 40:258-275

Sandeman DC, Sandeman R, Derby C, Schmidt M (1992) Morphology of the brain of crayfish, crabs, and spiny lobsters: a common nomenclature for homologous structures. Biological Bulletin 183:304-326

Schmid A, Chiba A, Doe CQ (1999) Clonal analysis of *Drosophila* embryonic neuroblasts: neural cell types, axon projections and muscle targets. Development 126:4653-4689

Schmidt H, Rickert C, Bossing T, Vef O, Urban J, Technau GM (1997) The embryonic central nervous system lineages of *Drosophila melanogaster*. Developmental Biology 189:186-204

Schmidt M (1997) Continuous neurogenesis in the olfactory brain of adult shore crabs, *Carcinus maenas*. Brain Research 762:131-143

Schmidt M (2001) Neuronal differentiation and long-term survival of newly generated cells in the olfactory midbrain of the adult spiny lobster, *Panulirus argus*. Journal of Neurobiology 48:181-203

Schmidt M (2002) Adult neurogenesis in the central olfactory pathway of decapod crustaceans. In: Wiese K (ed) The Crustacean Nervous System. Springer-Verlag, Berlin, pp 433-453

Schmidt M (2007a) Identification of putative neuroblasts at the base of adult neurogenesis in the olfactory midbrain of the spiny lobster, *Panulirus argus*. The Journal of Comparative Neurology 503:64-84

Schmidt M (2007b) The olfactory pathway of decapod crustaceans - an invertebrate model for life-long neurogenesis. Chemical Senses 32:365-384

Schmidt M, Derby CD (2011) Cytoarchitecture and ultrastructure of neural stem cell niches and neurogenic complexes maintaining adult neurogenesis in the olfactory midbrain of spiny lobsters, *Panulirus argus*. The Journal of Comparative Neurology 519:2283-2319

Schmidt M, Harzsch S (1999) Comparative analysis of neurogenesis in the central olfactory pathway of adult decapod crustaceans by *in vivo* BrdU labeling. Biological Bulletin 196:127-136

Scholtz G (1990) The formation, differentiation and segmentation of the post-naupliar germ band of the amphipod *Gammarus pulex* L. (Crustacea, Malacostraca, Peracarida). Proceedings of the Royal Society of London B 239:163-211

Scholtz G (1992) Cell lineage studies in the crayfish *Cherax destructor* (Crustacea, Decapoda): germ band formation, segmentation, and early neurogenesis. Roux's Archives of Developmental Biology 202:36-48

Scholtz G (1995) Expression of the *engrailed* gene reveals nine putative segment-anlagen in the embryonic pleon of the freshwater crayfish *Cherax destructor* (Crustacea, Malacostraca, Decapoda). Biological Bulletin 188:157-165

Scholtz G (2000) Evolution of the nauplius stage in malacostracan crustaceans. Journal of Zoological Systematics and Evolutionary Research 38:175-187

Scholtz G, Edgecombe GD (2005) Heads, Hox and the phylogenetic position of trilobites. In: Koenemann S, Jenner R (eds): Crustacea and Arthropod Relationships. Crustacean Issues 16: 139-165

Scholtz G, Edgecombe GD (2006) The evolution of arthropod heads: reconciling morphological, developmental and palaeontological evidence. Development, Genes and Evolution 216:395-415

Schürmann FW (1987) Histology and ultrastructure of the onychophoran brain. In: Gupta AP (ed) Arthropod Brain. Its Evolution, Development, Structure, and Functions. John Wiley & Sons, New York, pp 159-180

Sedgwick A (1888) A monograph of the development of *Peripatus capensis*. Studies from the Morphological Laboratory in the University of Cambridge. Cambridge University Press Warehouse, London, pp. 1-146

Sekiguchi K, Nakamura K, Onuma S (1971) Egg-carrying habit and embryonic development in a pycnogonid, *Propallene longiceps*. Zoological Magazine 80:137-139

Shear WA, Edgecombe GD (2010) The geological record and phylogeny of Myriapoda. Arthropod Structure and Development 39:174-190

Shepherd D, Bate CM (1990) Spatial and temporal patterns of neurogenesis in the embryo of the locust (*Schistocerca gregaria*). Development 108:83-96

Shi S-R, Cote RJ, Taylor CR (2001) Antigen retrieval techniques: Current perspectives. The Journal of Histochemistry and Cytochemistry 49:931-937

Shultz JW (1990) Evolutionary morphology and phylogeny of Arachnida. Cladistics 6:1-38

Simonnet F, Deutsch J, Quéinnec E (2004) *Hedgehog* is a segment polarity gene in a crustacean and a chelicerate. Development, Genes and Evolution 214:537-545

Simpson P (1990) Lateral inhibition and the development of the sensory bristles of the adult peripheral nervous system of *Drosophila*. Development 109:509-519

Sintoni S, Benton JL, Beltz BS, Hansson BS, Harzsch S (2012) Neurogenesis in the central olfactory pathway of adult decapod crustaceans: development of the neurogenic niche in the brains of procambarid crayfish. Neural Development 7:1

Siveter DJ, Sutton MD, Briggs DEG, Siveter DJ (2004) A silurian sea spider. Nature 431:978-980

Skeath JB (1998) The *Drosophila* EGF receptor controls the formation and specification of neuroblasts along the dorsal-ventral axis of the *Drosophila* embryo. Development 125:3301-3312

Skeath JB, Carroll SB (1992) Regulation of proneural gene expression and cell fate during neuroblast segregation in the *Drosophila* embryo. Development 114:939-946

Skeath JB, Panganiban G, Selegue J, Carroll SB (1992) Gene regulation in two dimensions: the proneural *achaete* and *scute* genes are controlled by combinations of axis-patterning genes through a common intergenic control region. Genes and Development 6:2606-2619

Skeath JB, Panganiban GF, Carroll SB (1994) The *ventral nervous system defective* gene controls proneural gene expression at two distinct steps during neuroblast formation in *Drosophila*. Development 120:1517-1524

Skeath JB, Thor S (2003) Genetic control of *Drosophila* nerve cord development. Current Opinion in Neurobiology 13:8-15

Sombke A, Lipke E, Kenning M, Müller CHG, Hansson BS, Harzsch S (2012) Comparative analysis of deutocerebral neuropils in Chilopoda (Myriapoda): implications for the evolution of the arthropod olfactory system and support for the Mandibulata concept. BMC Neuroscience 13:1

Song C-K, Johnstone LM, Edwards DH, Derby CD, Schmidt M (2009) Cellular basis of neurogenesis in the brain of crayfish, *Procambarus clarkii*: neurogenic complex in the olfactory midbrain from hatchlings to adults. Arthropod Structure and Development 38:339-360

Southall TD, Brand AH (2009) Neural stem cell transcriptional networks highlight genes essential for nervous system development. The EMBO Journal 28:3799-3807

Spana EP, Doe CQ (1995) The *prospero* transcription factor is asymmetrically localized to the cell cortex during neuroblast mitosis in *Drosophila*. Development 121:3187-3195

Staples DA (1997) Sea spiders or pycnogonids (Phylum Arthropoda). In: Shepherd SA, Davies M (eds) Marine Invertebrates of Southern Australia Part III. Handbook of the Flora and Fauna of South Australia. South Australian Research and Development Institute, pp 1040-1072

Stent GS (1998) Developmental cell lineage. International Journal of Developmental Biology 42:237-241

Stock JH (1978) Experiments on food preference and chemical sense in Pycnogonida. Zoological Journal of the Linnean Society 63:59-74

Stock JH (1994) Indo-west pacific Pycnogonida collected by some major oceanographic expeditions. Beaufortia 44 (3):17-77

Stollewerk A (2002) Recruitment of cell groups through *Delta/Notch* signalling during spider neurogenesis. Development 129:5339-5348

Stollewerk A (2004) Secondary neurons are arrested in an immature state by formation of epithelial vesicles during neurogenesis of the spider *Cupiennius salei*. Frontiers in Zoology 1:3

Stollewerk A (2008) Evolution of neurogenesis in arthropods. In: Minelli A, Fusco G (eds) Evolving Pathways: Key Themes in Evolutionary Developmental Biology. Cambridge University Press, Cambridge, pp 356-377

Stollewerk A, Chipman AD (2006) Neurogenesis in myriapods and chelicerates and its importance for understanding arthropod relationships. Integrative and Comparative Biology 46:195-206

Stollewerk A, Simpson P (2005) Evolution of early development of the nervous system: a comparison between arthropods. BioEssays 27:874-883

Stollewerk A, Tautz D, Weller M (2003) Neurogenesis in the spider: new insights from comparative analysis of morphological processes and gene expression patterns. Arthropod Structure and Development 32:5-16

Stollewerk A, Weller M, Tautz D (2001) Neurogenesis in the spider *Cupiennius salei*. Development 128:2673-2688

Strausfeld NJ, Andrew DR (2011) A new view of insect-crustacean relationships I. Inferences from neural cladistics and comparative neuroanatomy. Arthropod Structure and Development 40:276-288

Strausfeld NJ, Hansen L, Li Y, Gomez RS, Ito K (1998) Evolution, discovery, and interpretations of arthropod mushroom bodies. Learning and Memory 5:11-37

Strausfeld NJ, Strausfeld CM, Loesel R, Rowell D, Stowe S (2006a) Arthropod phylogeny: onychophoran brain organization suggests an archaic relationship with a chelicerate stem lineage. Proceedings of the Royal Society B 273:1857-1866

Strausfeld NJ, Strausfeld CM, Stowe S, Rowell D, Loesel R (2006b) The organization and evolutionary implications of neuropils and their neurons in the brain of the onychophoran *Euperipatoides rowelli*. Arthropod Structure and Development 35:169-196

Sullivan JM, Benton JL, Sandeman DC, Beltz BS (2007) Adult neurogenesis: a common strategy across diverse species. The Journal of Comparative Neurology 500:574-584

Sullivan JM, Macmillan DL (2001) Embryonic and postembryonic neurogenesis in the ventral nerve cord of the freshwater crayfish *Cherax destructor*. Journal of Experimental Zoology 290:49-60

Taghert PH, Doe CQ, Goodman CS (1984) Cell determination and regulation during development of neuroblasts and neurones in grasshopper embryo. Nature 307:163-165

Tamarelle M, Haget A, Ressouches A (1985) Segregation, division, and early patterning of lateral thoracic neuroblasts in the embryos of *Carausius morosus* Br. (Phasmida: Lonchodidae). International Journal of Insect Morphology and Embryology 14:307-317

Telford MJ, Thomas RH (1998) Expression of homeobox genes shows chelicerate arthropods retain their deutocerebral segment. Proceedings of the National Academy of Sciences 95:10671-10675

Thomas JB, Bastiani MJ, Bate CM, Goodman CS (1984) From grasshopper to *Drosophila*: a common plan for neuronal development. Nature 310:203-207

Tiegs OW (1940) The embryology and affinities of the Symphyla, based on a study of *Hanseniella agilis*. Quarterly Journal of Microscopical Science 82:1-225

Tiegs OW (1947) The development and affinities of the Pauropoda, based on a study of *Pauropus silvaticus.* Part I. Quarterly Journal of Microscopical Science 88:165-267

Truman JW, Ball EE (1998) Patterns of embryonic neurogenesis in a primitive wingless insect, the silverfish, *Ctenolepisma longicaudata*: comparison with those seen in flying insects. Development, Genes and Evolution 208:357-368

Ungerer P (2006) Aspekte der Neurogenese von *Orchestia cavimana* (Amphipoda, Malacostraca, Crustacea). Humboldt-Universität zu Berlin. Doctoral thesis, pp 1-133

Ungerer P, Eriksson BJ, Stollewerk A (2011a) Neurogenesis in the water flea *Daphnia magna* (Crustacea, Branchiopoda) suggests different mechanisms of neuroblast formation in insects and crustaceans. Developmental Biology 357:42-52

Ungerer P, Eriksson BJ, Stollewerk A (2012) Unravelling the evolution of neural stem cells in arthropods: *Notch* signalling in neural stem cell development in the crustacean *Daphnia magna*. Developmental Biology online first: http://dx.doi.org/10.1012/j.ydbio.2012.08.025

Ungerer P, Geppert M, Wolff C (2011b) Axogenesis in the central and peripheral nervous system of the amphipod crustacean *Orchestia cavimana*. Integrative Zoology 6:28-44

Ungerer P, Scholtz G (2008) Filling the gap between identified neuroblasts and neurons in crustaceans adds new support for Tetraconata. Proceedings of the Royal Society B 275:369-376

Ungerer P, Scholtz G (2009) Cleavage and gastrulation in *Pycnogonum litorale* (Arthropoda, Pycnogonida): morphological support for the Ecdysozoa? Zoomorphology 128:263-274

Vaessin H, Grell E, Wolff E, Bier E, Jan LY, Jan YN (1991) *Prospero* is expressed in neuronal precursors and encodes a nuclear protein that is involved in the control of axonal outgrowth in *Drosophila*. Cell 57:941-953

Vilpoux K, Sandeman RE, Harzsch S (2006) Early embryonic development of the central nervous system in the Australian crayfish and the Marbled crayfish (Marmorkrebs). Development, Genes and Evolution 216:209-223

Vilpoux K, Waloszek D (2003) Larval development and morphogenesis of the sea spider *Pycnogonum litorale* (Ström, 1762) and the tagmosis of the body of Pantopoda. Arthropod Structure and Development 32:349-383

von Reumont BM, Jenner RA, Wills MA, Dell'Ampio E, Pass G, Ebersberger I, Meyer B, Koenemann S, Iliffe TM, Stamatakis A, Niehuis O, Meusemann K, Misof B (2012) Pancrustacean phylogeny in the light of new phylogenomic data: support for Remipedia as the possible sister group of Hexapoda. Molecular Biology and Evolution 29:1031-1045

von Reumont BM, Meusemann K, Szucsich NU, Dell'Ampio E, Gowri-Shankar V, Bartel D, Simon S, Letsch HO, Stocsits RR, Luan Y, Wägele JW, Pass G, Hadrys H, Misof B (2009) Can comprehensive background knowledge be incorporated into substitution models to improve phylogenetic analyses? A case study on major arthropod relationships. BMC Evolutionary Biology 9:119

Walossek D, Müller KJ (1990) Upper Cambrian stem-lineage crustaceans and their bearing upon the monophyletic origin of Crustacea and the position of *Agnostus*. Lethaia 23:409-427

Wei Y, Mizzen CA, Cook RG, Gorovsky MA, Allis CD (1998) Phosphorylation of histone H3 at serine 10 is correlated with chromosome condensation during mitosis and meiosis in *Tetrahymena*. Proceedings of the National Academy of Sciences 95:7480-7484

Weller M, Tautz D (2003) *Prospero* and *snail* expression during spider neurogenesis. Development, Genes and Evolution 213:554-566

Westheide W, Rieger R (2006) Spezielle Zoologie. Teil 1: Einzeller und Wirbellose Tiere. Spektrum Akademischer Verlag, Heidelberg, pp. 1-976

Weygoldt P (1965) Vergleichend-embryologische Untersuchungen an Pseudoscorpionen. III. Die Entwicklung von *Neobisium muscorum* Leach (Neobisiinea, Neobisiidae). Mit dem Versuch einer Deutung der Evolution des embryonalen Pumporgans. Zeitschrift für Morphologie und Ökologie der Tiere 55:321-382

Weygoldt P (1975) Untersuchungen zur Embryologie und Morphologie der Geißelspinne *Tarantula marginemaculata* C.L. Koch (Arachnida, Amblypygi, Tarantulidae). Zoomorphologie 82:137-199

Weygoldt P, Paulus HF (1979) Untersuchungen zur Morphologie, Taxonomie und Phylogenie der Chelicerata. II. Cladogramme und die Entfaltung der Chelicerata. Zeitschrift für zoologische Systematik und Evolutionsforschung 17:177-200

Wheeler SR, Carrico ML, Wilson BA, Brown SJ, Skeath JB (2003) The expression and function of the *achaete-scute* genes in *Tribolium castaneum* reveals conservation and variation in neural pattern formation and cell fate specification. Development 130:4373-4381

Wheeler SR, Skeath JB (2005) The identification and expression of *achaete-scute* genes in the branchiopod crustacean *Triops longicaudatus*. Gene Expression Patterns 5:695-700

Wheeler WC, Hayashi CY (1998) The phylogeny of the extant chelicerate orders. Cladistics 14:173-192

Wheeler WM (1891) Neuroblasts in the arthropod embryo. Journal of Morphology 4:337-343

Whiting MF, Bradler S, Maxwell T (2003) Loss and recovery of wings in stick insects. Nature 421:264-267

Whitington PM (1995) Conversation versus change in early axonogenesis in arthropod embryos: a comparison between myriapods, crustaceans and insects. In: Breidbach O, Kutsch W (eds) The Nervous System of Invertebrates: An Evolutionary and Comparative Approach. Birkhäuser Verlag, Basel, pp 181-219

Whitington PM (2007) The evolution of arthropod nervous systems: insights from neural development in the Onychophora and Myriapoda. In: Striedter GF, Rubenstein JLR (eds) Theories, Development, Invertebrates. Academic Press, Oxford, pp 317-336

Whitington PM, Bacon JP (1997) The organization and development of the arthropod ventral nerve cord: insights into arthropod relationships. In: Fortey RA, Thomas RH (eds) Arthropod Relationships. Chapman & Hall, London, pp 349-367

Whitington PM, Harris KL, Leach D (1996) Early axonogenesis in the embryo of a primitive insect, the silverfish *Ctenolepisma longicaudata*. Roux's Archives of Developmental Biology 205:272-281

Whitington PM, Leach D, Sandeman R (1993) Evolutionary change in neural development within the arthropods: axonogenesis in the embryos of two crustaceans. Development 118:449-461

Whitington PM, Mayer G (2011) The origins of the arthropod nervous system: Insights from the Onychophora. Arthropod Structure and Development 40 (193-209)

Whitington PM, Meier T, King P (1991) Segmentation, neurogenesis and formation of early axonal pathways in the centipede, *Ethmostigmus rubripes* (Brandt). Roux's Archives of Developmental Biology 199:349-363

Winter G (1980) Beiträge zur Morphologie und Embryologie des vorderen Körperabschnitts (Cephalosoma) der Pantopoda Gerstaecker, 1863. I. Entstehung und Struktur des Zentralnervensystems. Zeitschrift für zoologische Systematik und Evolutionsforschung 18:27-61

Wirén E (1918) Zur Morphologie und Phylogenie der Pantopoden. Zoologiska Bidrag från Uppsala 6:41-181

Wolff C, Hilbrant M (2011) The embryonic development of the central American wandering spider *Cupiennius salei*. Frontiers in Zoology 8:15

Wolff G, Harzsch S, Hansson BS, Brown S, Strausfeld N (2012) Neuronal organization of the hemiellipsoid body of the land hermit crab, *Coenobita clypeatus*: correspondence with the mushroom body ground pattern. The Journal of Comparative Neurology 520:2824-2846

Zhao X, Coptis V, Farris SM (2008) Metamorphosis and adult development of the mushroom bodies of the red flour beetle, *Tribolium castaneum*. Developmental Neurobiology 68:1487-1502

Zrzavý J, Hypsa V, Vlásková M (1997) Arthropod phylogeny: taxonomic congruence, total evidence and conditional combination approaches to morphological and molecular data sets. In: Fortey RA, Thomas RH (eds) Arthropod Relationships. Chapman & Hall, London, pp 97-107

Zrzavý J, Štys P (1997) The basic body plan of arthropods: insights from evolutionary morphology and developmental biology. Journal of Evolutionary Biology 10:353-367

ACKNOWLEDGMENTS

Gerhard Scholtz is thanked for the opportunity to study as charismatic animals as sea spiders in his lab, his support and constructive discussions over the years as well as his openness to occasionally differing opinions.

I am very grateful to Angelika Stollewerk for her instant consent to my inquiry regarding gene expression studies and the time and fruitful discussions I had during my stay in her group in London. This widened my personal horizon – even if *Pseudopallene* still refused full cooperation.

Claudia Arango and her devotion to pycnogonids significantly contributed to this project's realization by pointing out the Tasmanian dive sites, helping in animal collection and immersing herself in the resolution of the complex *Pseudopallene*-complex.

Many thanks to all lab members in Berlin and London! Thanks specifically to Edina Balczo for the practical introduction to molecular lab procedures and trying additional RACE PCRs, Renate Mbacke for histological work, Ekaterina Ponomarenko for translation of Russian literature, Petra Ungerer for critically reading some manuscript parts and Carsten Wolff for providing embryos of *C. salei* and *P. tepidariorum* (a.k.a. The Amazing Arschie-Aranea or AAA+).

The assistence of Karen Gowlett-Holmes and Mick Baron in animal collection is greatly appreciated. Paul Whitington, Roy Swain, Glenn Johnstone and Johnny Stark helped with the logistics of organizing chemicals for processing of collected specimens. David Staples provided egg-bearing males of *Stylopallene cheilorhynchus* and *S. longicauda*. Collection of animals and their offspring was made possible by permits of the Tasmanian Department of Primary Industries, Parks, Water and Environment (permit nos. 6039 and 9255). Export of collected material was permitted by the Australian Department of the Environment, Water, Heritage and the Arts (permit nos. WT2008-4394 and WT2009-4260).

I am grateful to Wilfried Bleiss, Maik Lehmann and Gabriele Drescher and to the group Pflanzenphysiologie (HU Berlin) for assistance with as well as maintenance of the SEM and CLSM, respectively. Jason Dunlop and the collection at the Naturkundemuseum Berlin facilitated literature hunting more than once.

The project was funded by the Deutsche Forschungsgemeinschaft (Scho 442/13-1). A scholarship of the Studienstiftung des deutschen Volkes covered the first sixth months and a short-term stipend of the Deutscher Akademischer Austauschdienst made the visit to London possible.

I am indebted to Nina Seifert, Philip Riel and their little girl Merle for a tranquil and very productive one-month period away from the normal day routine – this time was special!

Zero 7, Beth Gibbons, Marshall Mathers, Jack Black and Kyle Gass – strange as this mixture may seem, it kept me going during endless library sessions. Long live the D says the G!

Last but not least: 13155 in 56 seconds. – The fruits of considerable efforts from my side. Never again did I soar as high.

VERÖFFENTLICHUNGEN VON GEORG BRENNEIS

Publikationen

Brenneis G, Krapp F: The post-embryonic development of sea spiders (Arthropoda, Pycnogonida). Book chapter in Handbuch der Zoologie. *in preparation*

Arango CP, Brenneis G: New species of Australian *Pseudopallene* (Pycnogonida: Callipallenidae) based on colour, morphology and DNA. *submitted to* Zootaxa

Brenneis G, Arango CP, Scholtz G (2011b): Morphogenesis of *Pseudopallene* sp. (Pycnogonida, Callipallenidae) II: postembryonic development. Development, Genes and Evolution 221:329-350.

Brenneis G, Arango CP, Scholtz G (2011a): Morphogenesis of *Pseudopallene* sp. (Pycnogonida, Callipallenidae) I: embryonic development. Development, Genes and Evolution 221:309-328.

Richter S, Loesel R; Purschke G, Schmidt-Rhaesa A, Scholtz G, Stach T, Vogt L, Wanninger A, Brenneis G, Döring C, Faller S, Fritsch M, Grobe P, Hausen H, Heuer CM, Kaul S, Møller OS, Müller CHG, Rieger V, Rothe BH, Stegner MEJ, Harzsch S (2010): Invertebrate neurophylogeny: suggested terms and definitions for a neuroanatomical glossary. Frontiers in Zoology 7:29.

Brenneis G, Richter S (2010): Architecture of the nervous system in Mystacocarida (Arthropoda, Crustacea) – an immunohistochemical study and 3D reconstruction. Journal of Morphology 271:169-189.

Brenneis G (2010): Implikationen der Nervensystem-Entwicklung bei Asselspinnen (Arthropoda, Pycnogonida) für die segmentale Zusammensetzung der Kopfregion. Sitzungsberichte Gesellschaft Naturforschender Freunde zu Berlin (N.F.) 47:135-150.

Brenneis G, Ungerer P, Scholtz G (2008): The chelifores of sea spiders (Arthropoda, Pycnogonida) are the appendages of the deutocerebral segment. Evolution and Development 10:717-724.

Vorträge

Brenneis G: Fitting pieces and further puzzles – What 'nobody' can tell about the evolution of arthropod neurogenesis. Evolution and Development Seminar Series. 2012. University of Cambridge, UK

Brenneis G, Scholtz G: Neurogenesis in sea spiders – a further step towards the euarthropod ground pattern? 2nd International Congress on Invertebrate Morphology 2011. Cambridge, Massachusetts

Brenneis G: A nobody's contribution to nervous system evolution: Investigating neurogenesis in Pycnogonida. Symposium on the Evolution of the Arthropod Nervous System. 2009. Jena

Brenneis G, Richter S: 3D reconstruction of the nervous system in Mystacocarida (Arthropoda, Crustacea). Celebrating Darwin: From The Origin of Species to Deep Metazoan Phylogeny. 2009. Berlin

Scholtz G, Brenneis G: In search for enigmatic creatures of Tasmanian waters. Rotary Club of the Tasman Peninsula. 2008. Tasmania

Brenneis G, Scholtz G: Brain development in sea spiders and the segmental affiliation of their head appendages. 1st International Congress on Invertebrate Morphology 2008. Copenhagen

Brenneis G: Aspekte der Neurogenese von Asselspinnen (Arthropoda, Pycnogonida). Sitzung der Gesellschaft Naturforschender Freunde zu Berlin 2008. Berlin

Poster

Stegner, MEJ, Brenneis G, Richter S: Immunohistochemical survey on the central nervous system in Hutchinsoniella macracantha (Cephalocarida). Celebrating Darwin: From The Origin of Species to Deep Metazoan Phylogeny. 2009. Berlin

Brenneis G, Richter S: Immunohistochemical study and 3D reconstruction of the central nervous system of Mystacocarida. Advances in Crustacean Phylogenetics. 2008. Rostock, Germany & First International Conference on Invertebrate Morphology 2008. Copenhagen, Denmark

Brenneis G: Phylogenetic and evolutionary implications of arthropod neurogenesis and neuroarchitecture. EMBO Practical Course: Molecular Approaches to Evolution and Development 2008. Kristineberg, Sweden

Ungerer P, Brenneis G, Scholtz G: Phylogenetic and evolutionary implications of sea spider development (Arthropoda, Pycnogonida). The Evolution of the Animals: a Linnean tercentenary Celebration 2007. London. The Royal Society

Selbstständigkeitserklärung

Hiermit versichere ich, dass ich die vorliegende Dissertation selbstständig und nur unter Verwendung der angegebenen Quellen und Hilfsmittel erarbeitet und verfasst habe. Diese Arbeit wurde keiner anderen Prüfungsbehörde vorgelegt.

Berlin, den

Georg Brenneis

VOLUME 2

INDEX

Figures & Legends

Fig. 1: Two hypotheses on the phylogenetic position of Pycnogonida within Euarthropoda.
Left phylogram: Traditional placement of pycnogonids as sister group to Euchelicerata, both taxa forming together the Chelicerata (e.g. Ax 1999).
Right phylogram: Alternative placement of pycnogonids as sister group to all remaining euarthropod lineages, the latter representing the Cormogonida (Zrzavý et al. 1997).
Note the unresolved position of Myriapoda.

Fig. 2: Neurogenesis in *Callipallene emaciata* (Pycnogonida, Callipallenidae), modified from Winter (1980).
Three transversal sections through a trunk segment of embryos in different developmental stages. Shallow paired depressions form in the neuroectoderm (left) and continue to invaginate to form conspicuous pits, the so-called 'ventral organs' (middle). The big spindle-shaped cells lining the deep invaginations are 'neuroblasts' that give rise to radial rows of ganglion cells by repeated radial divisions and detach from the apical ectoderm to form sub-apical vesicles (right). Abbreviations: do – yolk; dod – yolk-filled midgut diverticulum; ent – entoderm; ekt – ectoderm; exa – limb bud; mes – mesoderm; n – neuron; vo – 'ventral organ'.

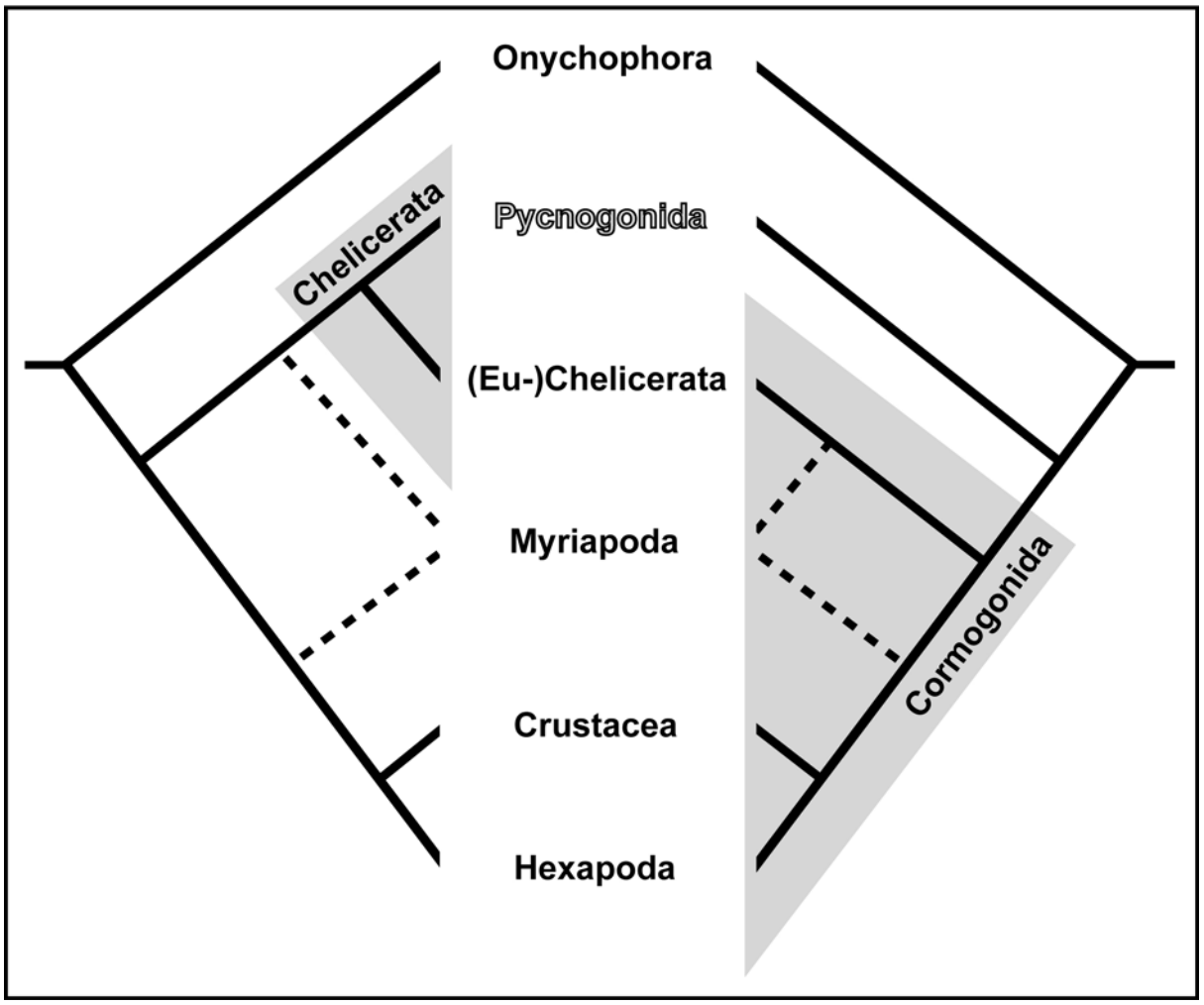
Onychophora
Pycnogonida
Chelicerata
(Eu-)Chelicerata
Myriapoda
Cormogonida
Crustacea
Hexapoda

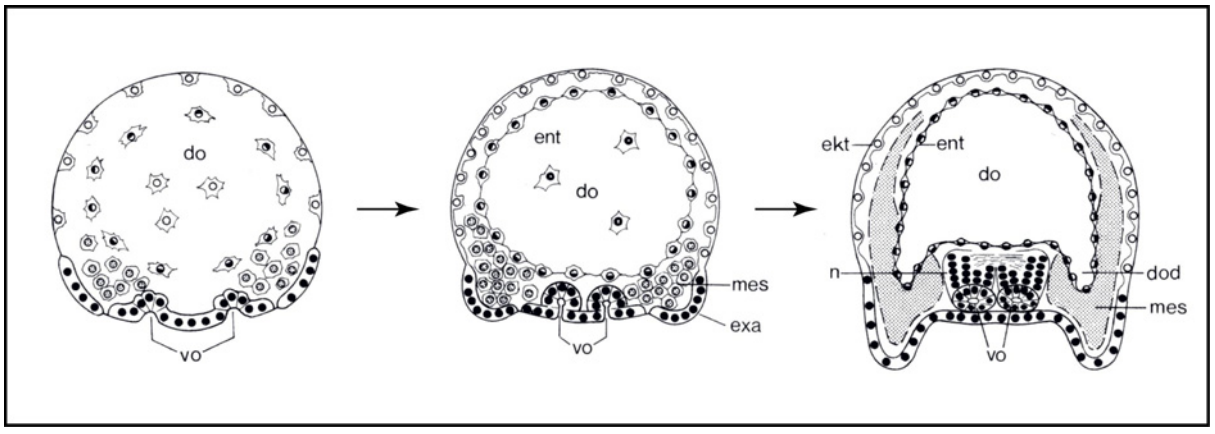
do
vo
ent
do
mes
exa
vo
ekt
ent
do
n
dod
mes
vo

Fig. 3: Three different plain yellow *Pseudopallene* species in coastal waters of Tasmania.
A Overview of collected pycnogonids on orange-brown arborescent soft bryozoans in a sea water-filled bucket, Eaglehawk Neck, 2009. **B** Close up live image of *Pseudopallene crocus* n. sp. on the arborescent soft bryozoan *Orthoscuticella* sp. **C-E** Frontal view of the cephalosoma of the plain yellow *Pseudopallene* forms, ethanol-stored material, stereo microscope images. **C** *P. crocus* n. sp. Note the constriction-less, distally tapering proboscis. **D** *P. constricta* n. sp. A distinct constriction about halfway along the proboscis (arrowheads) is one of the diagnostic features of this species. **E** *P. variabilis* complex. The Tasmanian specimens of this still unresolved species complex are smaller than *P. crocus* and *P. constricta*. They bear brownish-black markings on proboscis and chela tips (big arrowheads) and are frequently characterized by a distinct pre-ocular mound on the antero-dorsal cephalosoma (small arrowheads). **F-H** Tarsus, propodus and terminal claw of walking leg 3 of the plain yellow *Pseudopallene* forms, SEM micrographs, distal is up. **F** *P. crocus*. The propodus is only slightly curved. The barely elevated propodal heel bears a row of three to four robust long spines that increase in length distally, followed by two smaller spines (stippled oval). **G** *P. constricta*. The curvature of the propodus is more pronounced. The propodal heel is prominent, bearing stout, short spines (stippled oval). In relation to the propodus, the terminal claw is longer and more massive than in the other forms. **H** *P. variabilis* complex. Propodus and terminal claw are slender. The propodus is only slightly curved, its heel inconspicuous with a spine arrangement similar to *P. crocus*. Note the lower number and regular arrangement of the more distal minute sole spines compared to the other two forms.

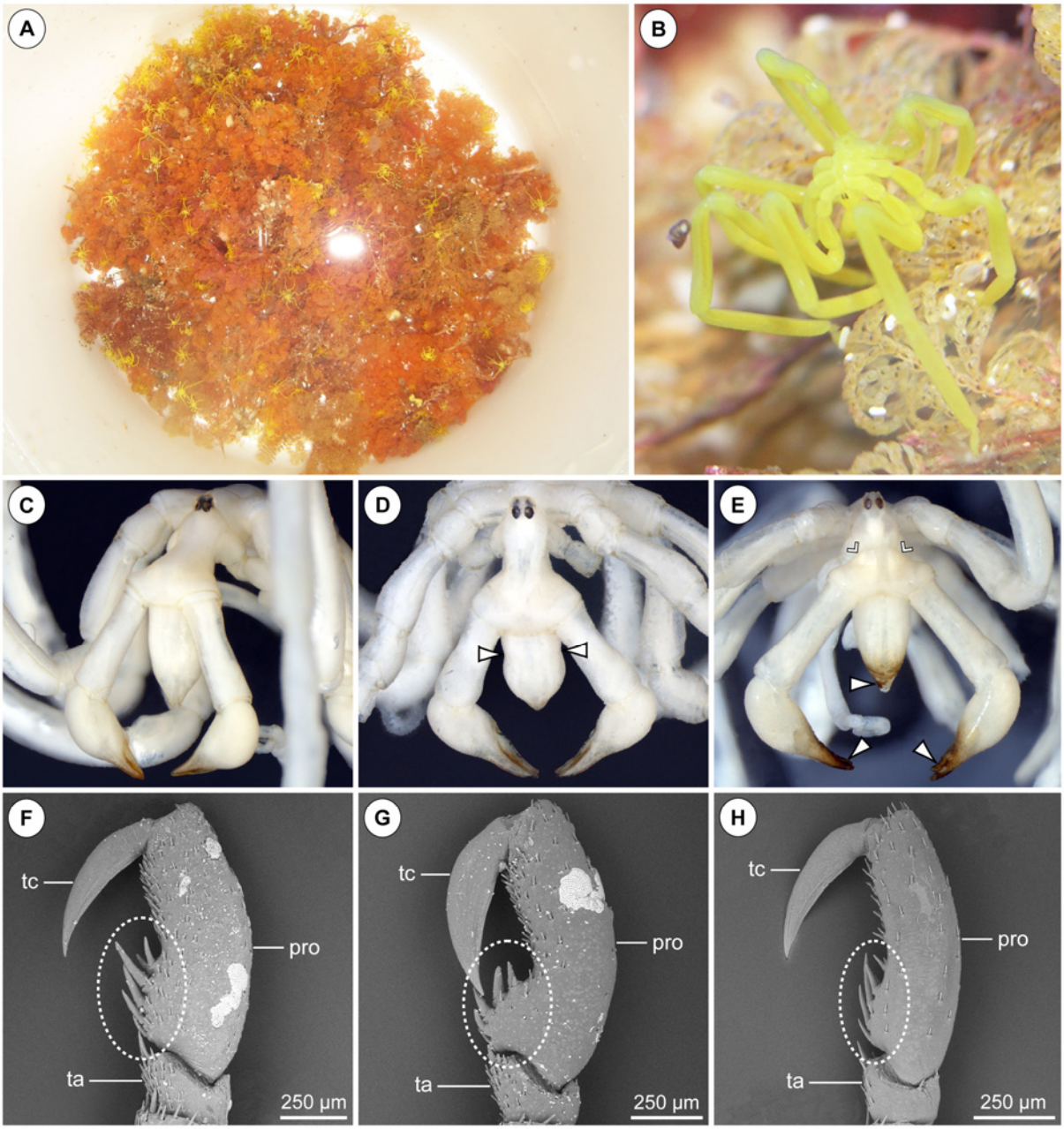
A
B
C
D
E
F
tc
pro
ta
250 µm
G
tc
pro
ta
250 µm
H
tc
pro
ta
250 µm

Fig. 4: Summary of embryonic morphogenesis of *Pseudopallene* sp.

Gray bars indicate the temporal onset and duration of developmental events in relation to the ten embryonic stages. A brief description of some morphological characteristics is provided for each event within the respective bar.

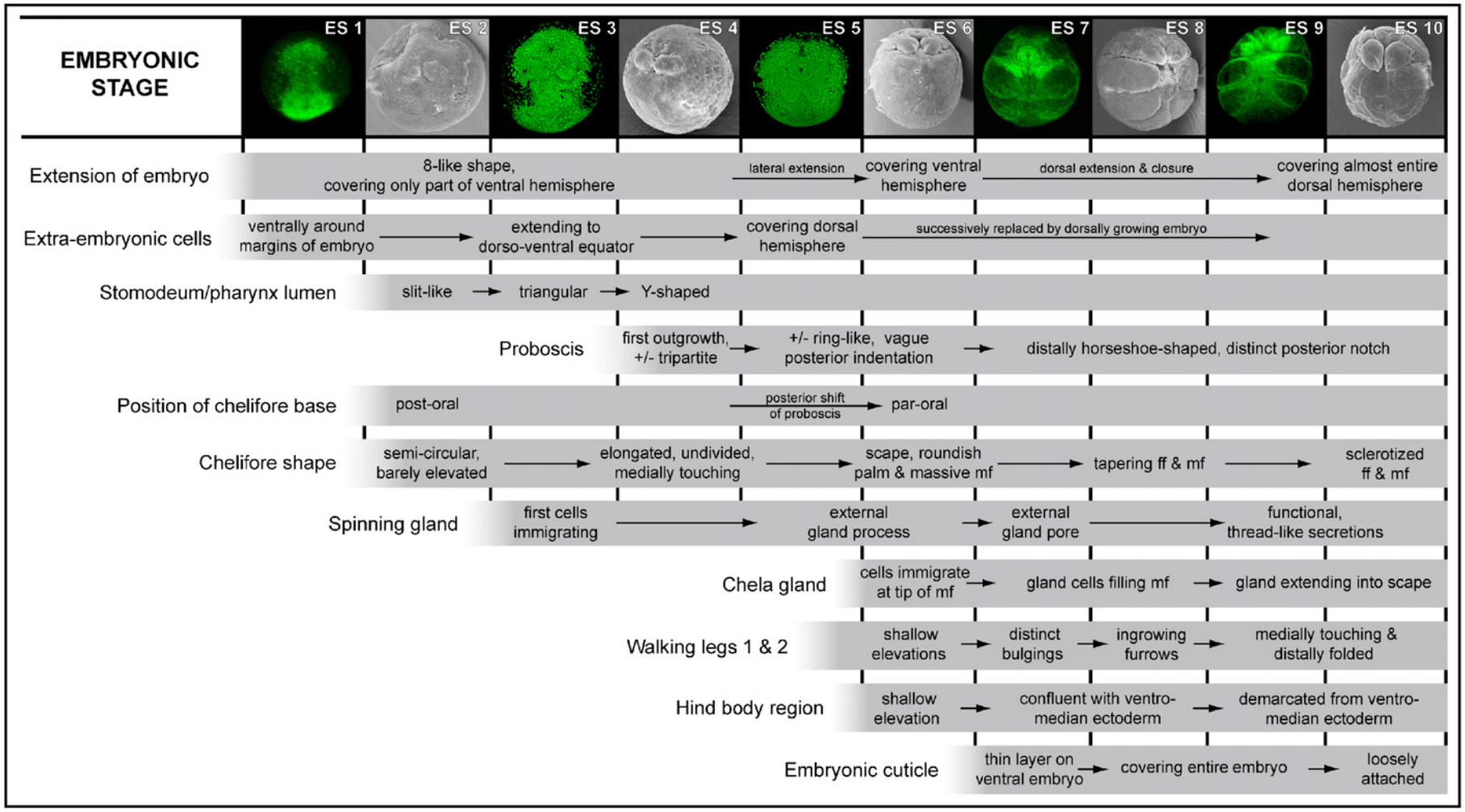
EMBRYONIC STAGE
ES 1
ES 2
ES 3
ES 4
ES 5
ES 6
ES 7
ES 8
ES 9
ES 10
Extension of embryo
8-like shape, covering only part of ventral hemisphere
lateral extension
covering ventral hemisphere
dorsal extension & closure
covering almost entire dorsal hemisphere
Extra-embryonic cells
ventrally around margins of embryo
extending to dorso-ventral equator
covering dorsal hemisphere
successively replaced by dorsally growing embryo
Stomodeum/pharynx lumen
slit-like
triangular
Y-shaped
Proboscis
first outgrowth, +/- tripartite
+/- ring-like, vague posterior indentation
distally horseshoe-shaped, distinct posterior notch
Position of chelifore base
post-oral
posterior shift of proboscis
par-oral
Chelifore shape
semi-circular, barely elevated
elongated, undivided, medially touching
scape, roundish palm & massive mf
tapering ff & mf
sclerotized ff & mf
Spinning gland
first cells immigrating
external gland process
external gland pore
functional, thread-like secretions
Chela gland
cells immigrate at tip of mf
gland cells filling mf
gland extending into scape
Walking legs 1 & 2
shallow elevations
distinct bulgings
ingrowing furrows
medially touching & distally folded
Hind body region
shallow elevation
confluent with ventro-median ectoderm
demarcated from ventro-median ectoderm
Embryonic cuticle
thin layer on ventral embryo
covering entire embryo
loosely attached

Fig. 5: Embryonic stages 1 – 3 of *Pseudopallene* sp.

SEM micrographs, nuclear stainings and tubulin labelings with nuclear counterstain. Asterisks indicate damaged regions. **A** ES 1. The germ band is 8-shaped and comprises hundreds of small, densely packed cells. Loosely arranged extra-embryonic cells surround the germ band's margins. **B-C** Early ES 2. **B** Anterior view. The slit-like stomodeum has formed at the anterior margin of the germ band. First signs of the chelifore anlagen appear as semi-circular furrows (dashed lines). Note lack of nuclei on the dorsal hemisphere, which is made up of few large macromeres. **C** Slightly earlier than **B**, antero-ventral view, Imaris volume (blend). A small tubulin-positive region is visible where cells immigrate to form the stomodeum. The semi-circular furrows of the developing chelifore anlagen are hardly visible (dashed lines). **D-F** Late ES 2. **D** Ventral view. The egg is locally deformed. Posterior to the stomodeum (arrow), the morphologically left chelifore anlage is more distinct and slightly elevated. **E** Postero-lateral view. Arrows indicate three large macromeres of the dorsal hemisphere. **F** Ventral view of anterior germ band region. The stomodeum has a slit-like shape. **G-J** ES 3. **G** Ventral view. The scattered extra-embryonic cells have expanded around the 8-shaped germ band and cover the complete ventral hemisphere. The semi-circular chelifore anlagen are more pronounced. **H** Anterior view, Imaris volume (blend). The stomodeum has deepened and assumed a triangular shape. The extra-embryonic cells have begun to extend across the anterior part of the dorsal hemisphere. **I** Optical transversal section at the level of the chelifore anlagen, Imaris section mode. Lateral within each chelifore anlage, cells of the future spinning gland start to immigrate. Cell processes remain apically attached (arrowheads), resulting in a flask-shape of cells. **J** Antero-ventral view, Imaris volume (blend). The stomodeal lumen is triangular and the surrounding tissue shows a faint sub-division in three sub-populations (arrowheads indicate borders).

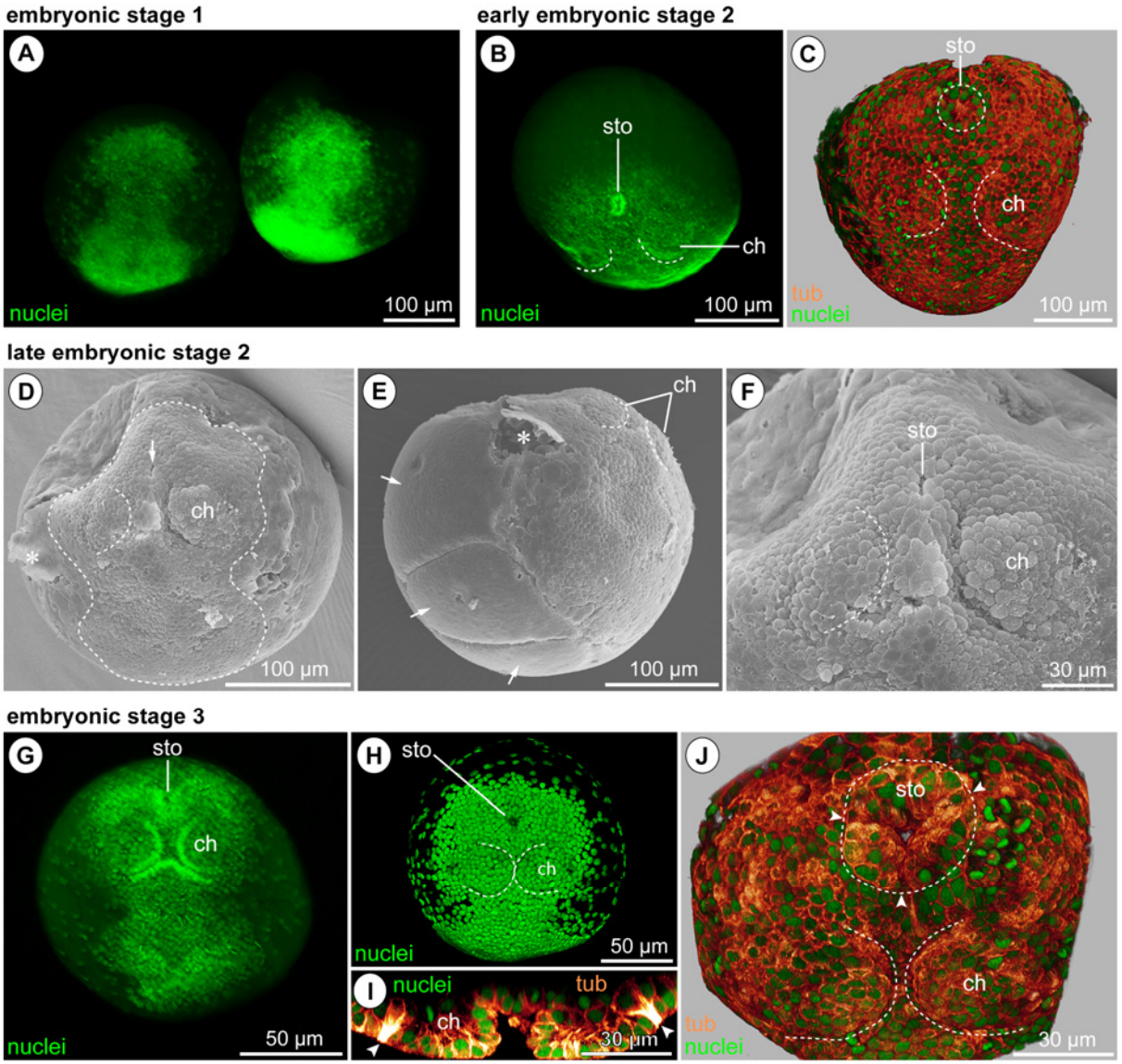
embryonic stage 1
early embryonic stage 2
A
B
C
sto
ch
nuclei
100 µm
tub
late embryonic stage 2
D
E
F
30 µm
embryonic stage 3
G
H
I
J
50 µm

Fig. 6: Embryonic stages 4 and 5 of *Pseudopallene* sp.

SEM micrographs, nuclear stainings and tubulin labelings with nuclear counterstain. Asterisks indicate damaged regions. **A-I** ES 4. **A** Ventro-lateral view. The embryo is still 8-shaped (dashed line). The proboscis has begun to protrude at the anterior pole, the chelifore anlagen being positioned posterior to it. **B** Ventral view. The chelifores meet medially. A constriction demarcates the future scape and palm (arrows). A nuclei-free area is visible where cells involved in spinning gland formation immigrate (arrowhead). **C** Antero-ventral view, Imaris volume (blend). The stomodeal lumen is Y-shaped (black arrowheads). The areas of immigrating spinning gland cells are clearly discernible (white arrowhead). **D** Lateral view. The extra-embryonic cells cover most of the dorsal hemisphere, macromeres remain only visible in the postero-dorsal region of the egg (arrowheads). **E-G** Development of the proboscis. **E** An unpaired antero-dorsal and two ventro-lateral cell populations start to protrude around the Y-shaped stomodeal lumen (arrowheads demarcate borders). **F** The cell masses protrude more distinctly, the division between the two ventro-lateral ones being more pronounced. The constriction (arrowheads) between the prospective scape and palm is visible in the chelifore anlage. **G** The three cell masses have been partially covered by a ring of surrounding ectodermal tissue (white arrowheads), becoming thus displaced internally. Posteriorly, a very shallow indentation remains externally visible (black arrowhead). **H-I** Spinning gland development. Imaris section mode. **H** Optical horizontal section. The regions of apically attaching processes of the immigrating cells are tubulin-positive (arrowheads). The anlage of the glandular duct is visible in the center. Several divisions are found around the morphologically right immigration region. **I** Optical transveral section at the level of the chelifores. The number of flask-shaped cells has increased, all of them remaining attached to the apical surface (arrowheads). **J-M** ES 5. **J** Ventral view. The embryo covers the entire ventral hemisphere. Apart from the chelifores, no distinct appendage anlagen are externally discernible. Anterior to the proboscis, a pair of tiny shallow depressions has developed (arrows). **K** Anterior view. The proboscis has begun to shift in a posterior direction. Antero-dorsal to the proboscis, the pre-cheliforal lobes that are medially still unfused are found (dashed lines). The proximal part of the chelifore has moved anteriorly, its distal end has widened. The spinning gland process starts to form (arrowhead). **L** Anterior view. At the distal tip of the chelifore, a tiny indentation (arrowhead) indicates the beginning outgrowth of the movable finger. **M** Detail of the proboscis. The former three cell populations are almost completely overgrown by surrounding ectodermal tissue (white arrowheads). A shallow posterior indentation remains discernible (black arrowhead). Arrows indicate the pair of pre-proboscideal depressions.

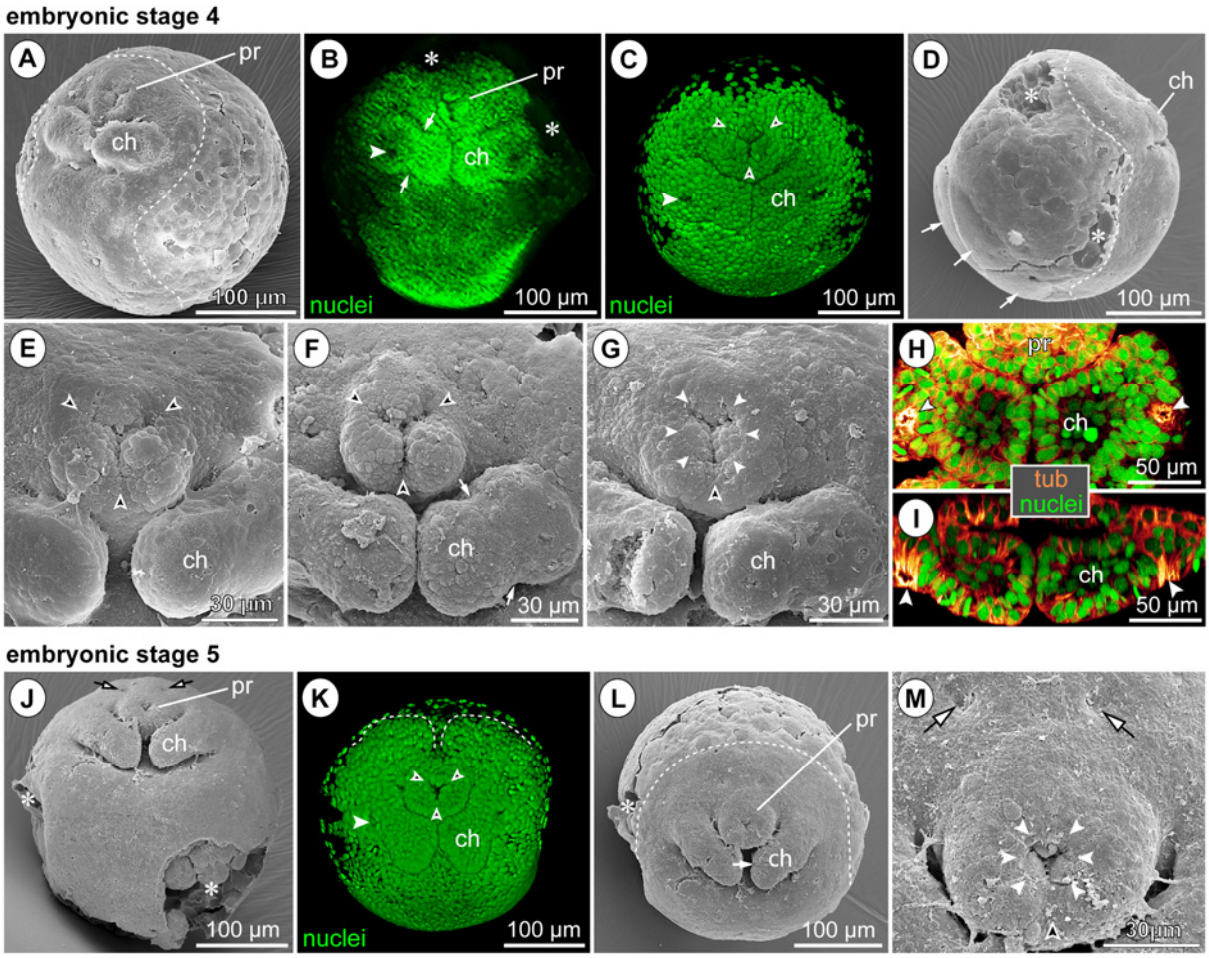
embryonic stage 4
A
pr
ch
100 µm
B
pr
ch
nuclei
100 µm
C
ch
nuclei
100 µm
D
ch
100 µm
E
ch
30 µm
F
ch
30 µm
G
ch
30 µm
H
pr
ch
tub
nuclei
50 µm
I
ch
50 µm
embryonic stage 5
J
pr
ch
100 µm
K
ch
nuclei
100 µm
L
pr
ch
100 µm
M
30µm

Fig. 7: Embryonic stages 6 and 7 of *Pseudopallene* sp.

SEM micrographs, nuclear stainings and tubulin or phalloidin labelings with nuclear counterstain. **A-H** ES 6. **A** Ventral view. An inconspicuous elevation demarcates the anlage of walking leg 1. Antero-lateral to the proboscis, a pair of shallow depressions related to nervous system development is visible (dashed circles). **B** Ventral view, Imaris volume (blend). Where the spinning gland process has formed, the scape of the chelifore shows a nuclei-free 'hole' (arrowhead). Movable and fixed finger of the chela are already discernible. A pair of shallow depressions (dashed oval) is found in walking leg segments 1 and 2, respectively. **C** Ventral view. The primordia of walking legs 1 and 2 represent shallow elevations. **D** Ventro-lateral view. The embryo starts to overgrow the dorsal hemisphere (dashed line). The spinning gland process is a small protrusion at the distal margin of the scape. **E** Anterior view, Imaris volume (blend). Anterior to the proboscis, the pre-cheliforal lobes have fused medially (compare to Fig. 6K). Pre-proboscideal pits (arrows) and antero-lateral depressions (dashed circles) are indicated. **F** Anterior view. The pre-proboscideal pits have deepened into distinct holes (arrows). At the posterior side of the proboscis, a shallow indentation remains visible (arrowhead). **G-H** Details of proboscis and chelifore. **G** Ventro-lateral view, Imaris volume (blend). An optical clipping plane has been used to reveal the interior of the scape. Cells of the spinning gland have migrated into the scape, a tubulin-positive tube connects the gland to its external process. Arrowhead marks the posterior indentation of the proboscis. **H** Optical horizontal section, Imaris section mode. A massive cluster of cells immigrates from the tip of the movable finger, cell processes remaining apically attached (arrows). The pharynx shows the typical Y-shaped lumen (arrowheads). **I-O** ES 7. **I** Ventral view. The anlagen of walking legs 1 and 2 are prominent elevations. The antero-lateral pair of depressions remains visible in nuclear stains (dashed circles). **J** Ventral view. The paired ventral depressions (dashed oval) are covered by the still delicate embryonic cuticle. **K** Detail of proboscis and chelifore. The chelifore shows a distinct external border between scape and palm. The spinning gland process bears a pore (arrowhead). At the inner margin of the fixed finger a small sub-terminal outgrowth has developed (arrow). **L** Lateral view. The post-cheliforal region of the embryo has expanded far dorsally. Arrowheads mark the dorsal extensions of the furrows that have started to form around the walking leg anlagen. **M** Anterior view. The antero-lateral depressions (dashed circles) are visible through the thin cuticular layer. No signs of the pre-proboscideal pits are detectable any longer. Arrowhead marks the posterior notch of the proboscis. **N** Ventro-lateral view of proboscis. The posterior notch has deepened (arrowhead), giving the distal proboscis portion a horseshoe-like shape. **O** Optical horizontal section through the chelifore, Imaris section mode. The chela gland reaches far into the palm. A slender duct connects it to the tip of the movable finger.

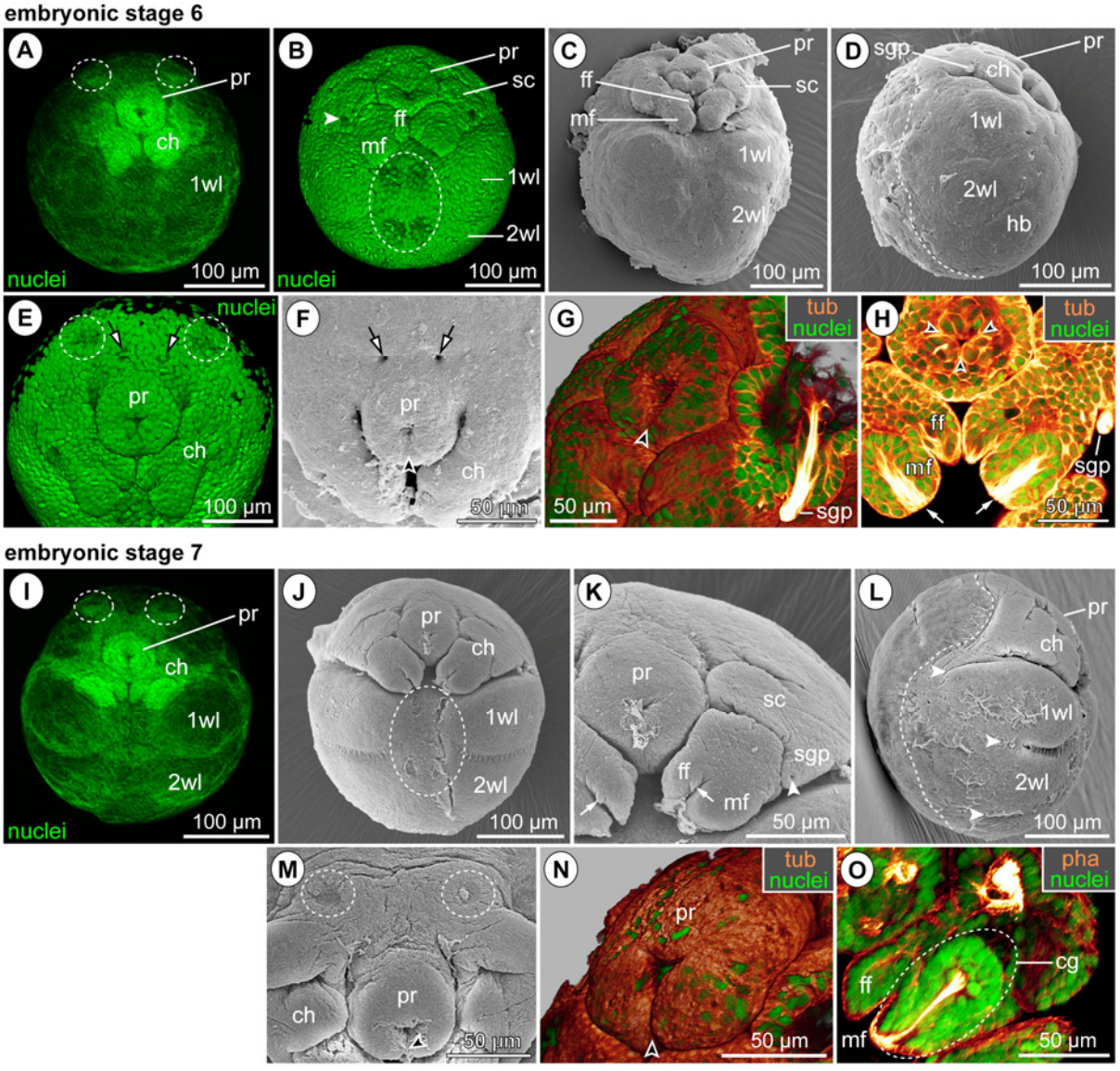
embryonic stage 6
A
pr
ch
1wl
nuclei
100 µm
B
pr
sc
ff
mf
1wl
2wl
nuclei
100 µm
C
pr
sc
ff
mf
1wl
2wl
100 µm
D
sgp
pr
ch
1wl
2wl
hb
100 µm
E
nuclei
pr
ch
100 µm
F
pr
ch
50 µm
G
tub
nuclei
50 µm
sgp
H
tub
nuclei
ff
mf
sgp
50 µm
embryonic stage 7
I
pr
ch
1wl
2wl
nuclei
100 µm
J
pr
ch
1wl
2wl
100 µm
K
pr
sc
sgp
ff
mf
50 µm
L
pr
ch
1wl
2wl
100 µm
M
ch
pr
50 µm
N
tub
nuclei
pr
50 µm
O
pha
nuclei
cg
ff
mf
50 µm

Fig. 8: Embryonic stages 8 – 10 of *Pseudopallene* sp.

SEM micrographs and nuclear stainings. **A-D** ES 8. **A** Ventral view. Proboscis not completely stained. The chela gland extends into the scape. Weak concentric rings at the walking legs tip (dashed circles) indicate telescope-like folded tissue of the elongating limbs. **B** Ventro-lateral view. The walking leg anlagen are distinctly separated from the surrounding regions. Paired ventral depressions remain discernible through the embryonic cuticle (dashed circle). The hind body region is still confluent with the more anterior ventral ectoderm. **C** Detail of proboscis and chelifore, showing the strongly developed embryonic cuticle in this region. **D** Lateral view. The embryonic cuticle covers the dorsal hemisphere. Arrowheads mark the dorsal extension of the proximal walking leg portions. **E-H** ES 9. **E** Ventral view. The posterior notch of the proboscis is visible in nuclear stains (black arrowhead). The walking legs touch their contra-lateral counterparts (white arrowheads). **F** Ventral view. The medially touching walking legs are visible through the embryonic cuticle. The hind body region is demarcated from the more anterior ventral ectoderm (arrow). **G** Detail of proboscis and chelifore. Thread-like secret (arrow) protrudes from the pore of the spinning gland process. **H** Lateral view. Arrowheads indicate dorsal extension of the proximal walking leg portions. **I-O** ES 10, pre-hatching stage. **I** Ventral view, morphologically right chelifore not completely stained. The posterior notch of the proboscis is visible (black arrowhead). The walking legs are pressed against their respective contra-lateral counterpart, forming a distinct median line in nuclear stains (white arrowheads). **J** Ventral view. The embryonic cuticle covers the pre-hatching embryo as a loose layer and conceals the walking leg anlagen. **K** Detail of proboscis and chelifore. Posterior notch of proboscis (arrowhead), thread-like secret of the spinning gland (framed white arrow) and sub-terminal outgrowth of the fixed finger (white arrow) are visible. **L** Lateral view. Ventrally, the embryonic cuticle of the post-cheliforal area is an undivided layer. The extensions of the walking legs are visible only at the dorso-lateral sides (arrowheads). **M-O** ES 10 with manually removed embryonic cuticle. **M** Ventral view. The walking legs are compressed underneath the embryonic cuticle. **N** Detail of proboscis and chelifore. The tips of fixed and movable finger are sclerotized, the sub-terminal outgrowth (white arrow) represents now an additional sclerotized spine. The posterior notch of the compressed proboscis is only weakly pronounced (arrowhead), thread-like secret (framed white arrow) protrudes from the spinning gland process. **O** Lateral view. The distal portions of the walking legs are folded in telescope-fashion (arrows), their proximal bases reach up far to the dorsal side (arrowheads).

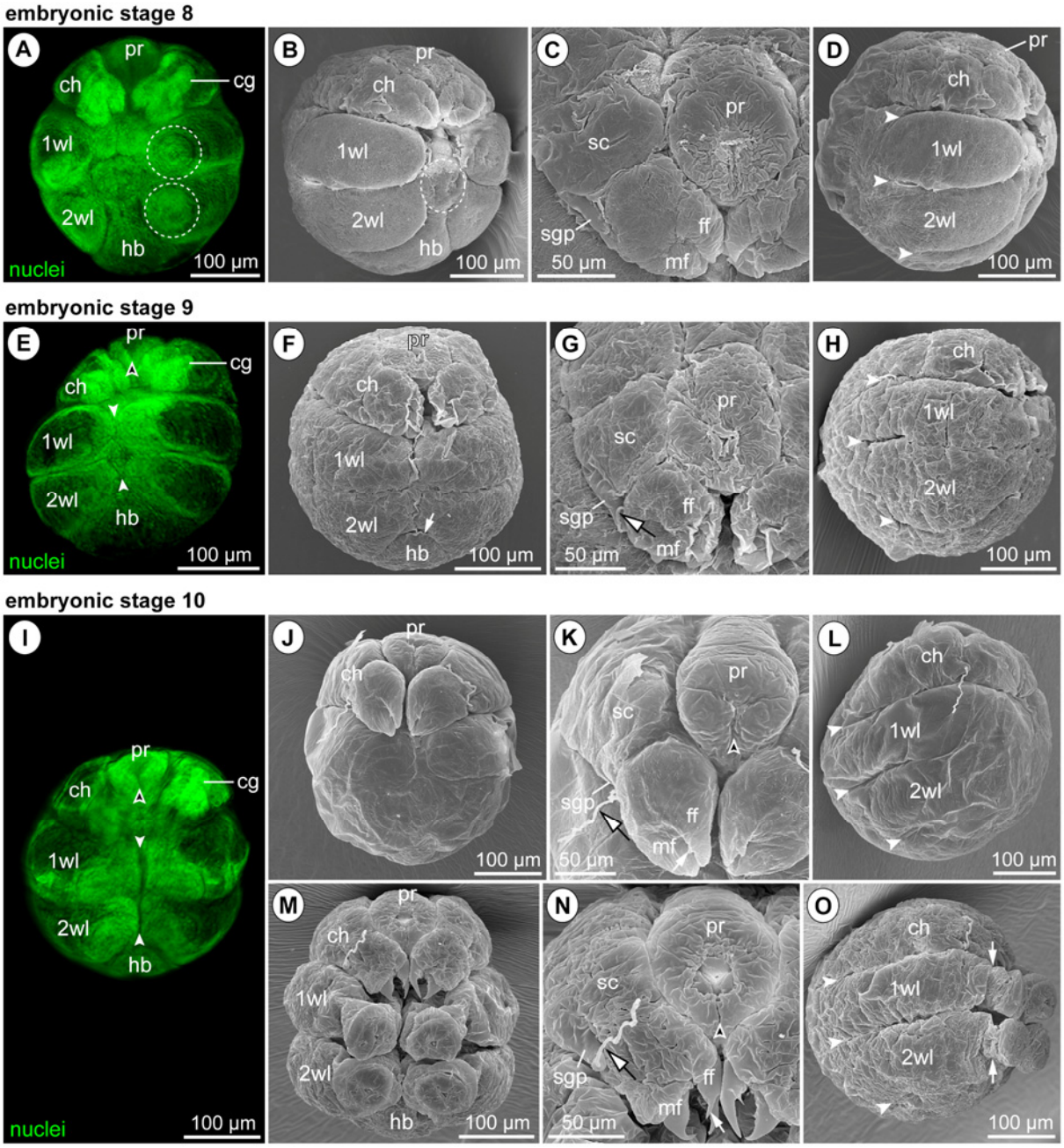
embryonic stage 8
A
pr
ch
cg
1wl
2wl
hb
nuclei
100 µm
B
pr
ch
1wl
2wl
hb
100 µm
C
pr
sc
sgp
ff
mf
50 µm
D
pr
ch
1wl
2wl
100 µm
embryonic stage 9
E
pr
cg
ch
1wl
2wl
hb
nuclei
100 µm
F
pr
ch
1wl
2wl
hb
100 µm
G
pr
sc
sgp
ff
mf
50 µm
H
ch
1wl
2wl
100 µm
embryonic stage 10
I
pr
ch
cg
1wl
2wl
hb
nuclei
100 µm
J
pr
ch
100 µm
K
pr
sc
sgp
ff
mf
50 µm
L
ch
1wl
2wl
100 µm
M
pr
ch
1wl
2wl
hb
100 µm
N
pr
sc
sgp
ff
mf
50 µm
O
ch
1wl
2wl
100 µm

Fig. 9: Summary of post-embryonic morphogenesis of *Pseudopallene* sp.
Horizontal gray bars indicate specific features in relation to the described post-embryonic stages. Brief descriptions of morphological characteristics are provided for each feature. Disruptions and switches of gray value along a horizontal bar indicate that observed changes in the feature in question are coupled to intermediate molts. Gradual changes of gray values symbolize processes with no direct relation to molting.

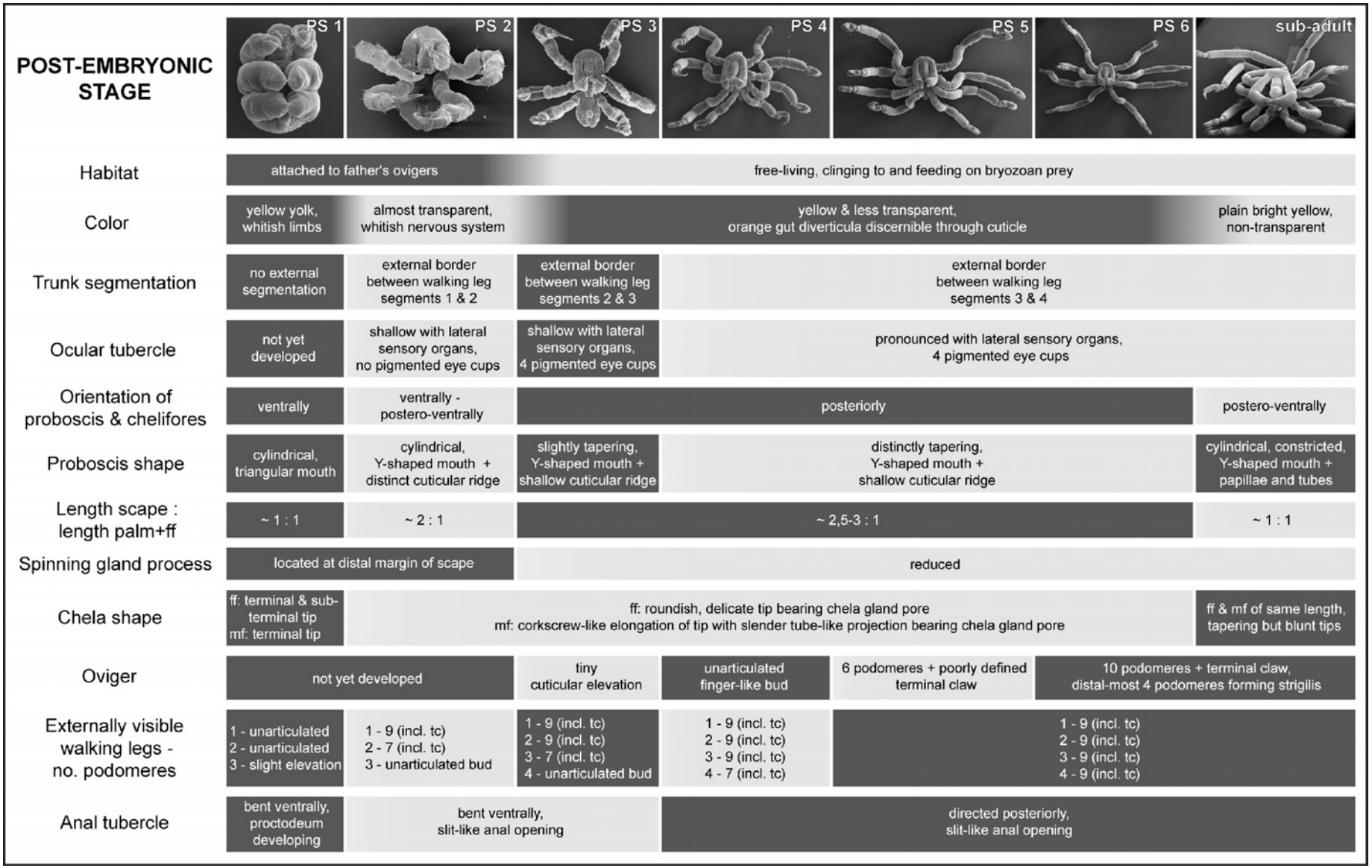
POST-EMBRYONIC STAGE
PS 1
PS 2
PS 3
PS 4
PS 5
PS 6
sub-adult
Habitat
attached to father's ovigers
free-living, clinging to and feeding on bryozoan prey
Color
yellow yolk, whitish limbs
almost transparent, whitish nervous system
yellow & less transparent, orange gut diverticula discernible through cuticle
plain bright yellow, non-transparent
Trunk segmentation
no external segmentation
external border between walking leg segments 1 & 2
external border between walking leg segments 2 & 3
external border between walking leg segments 3 & 4
Ocular tubercle
not yet developed
shallow with lateral sensory organs, no pigmented eye cups
shallow with lateral sensory organs, 4 pigmented eye cups
pronounced with lateral sensory organs, 4 pigmented eye cups
Orientation of proboscis & chelifores
ventrally
ventrally - postero-ventrally
posteriorly
postero-ventrally
Proboscis shape
cylindrical, triangular mouth
cylindrical, Y-shaped mouth + distinct cuticular ridge
slightly tapering, Y-shaped mouth + shallow cuticular ridge
distinctly tapering, Y-shaped mouth + shallow cuticular ridge
cylindrical, constricted, Y-shaped mouth + papillae and tubes
Length scape : length palm+ff
~ 1 : 1
~ 2 : 1
~ 2,5-3 : 1
~ 1 : 1
Spinning gland process
located at distal margin of scape
reduced
Chela shape
ff: terminal & sub-terminal tip
mf: terminal tip
ff: roundish, delicate tip bearing chela gland pore
mf: corkscrew-like elongation of tip with slender tube-like projection bearing chela gland pore
ff & mf of same length, tapering but blunt tips
Oviger
not yet developed
tiny cuticular elevation
unarticulated finger-like bud
6 podomeres + poorly defined terminal claw
10 podomeres + terminal claw, distal-most 4 podomeres forming strigilis
Externally visible walking legs - no. podomeres
1 - unarticulated
2 - unarticulated
3 - slight elevation
1 - 9 (incl. tc)
2 - 7 (incl. tc)
3 - unarticulated bud
1 - 9 (incl. tc)
2 - 9 (incl. tc)
3 - 7 (incl. tc)
4 - unarticulated bud
1 - 9 (incl. tc)
2 - 9 (incl. tc)
3 - 9 (incl. tc)
4 - 7 (incl. tc)
1 - 9 (incl. tc)
2 - 9 (incl. tc)
3 - 9 (incl. tc)
4 - 9 (incl. tc)
Anal tubercle
bent ventrally, proctodeum developing
bent ventrally, slit-like anal opening
directed posteriorly, slit-like anal opening

Fig. 10: Post-embryonic stage 1 of *Pseudopallene* sp. ('walking leg-bearing larva').
Stereo microscope images, SEM micrographs, nuclear stainings and histological sections. **A** Egg-bearing adult male of *Pseudopallene* sp., ventral view. The distal-most package (dashed outline) on the ovigers consists of hatched PS 1 that stay attached to it. **B** Removed package of hatched PS 1. The dorsal yellowish yolk is set off from the ventral whitish tissue of the proboscis and limbs. **C** Ventral overview. PS 1 bears proboscis, chelifores and the unarticulated anlagen of walking legs 1 and 2. **D** Dorsal overview. No external segmentation of the trunk is detectable. **E** Lateral overview, slightly older specimen. Note the bumpy appearance but not truly articulated condition of the walking leg anlagen. **F** Detail of the proboscis tip. The mouth opening is triangular. Posteriorly, a distinct notch marks the borders of the ventro-lateral proboscis antimeres (arrowhead). **G** Detail of the chela. The movable finger tapers into one terminal tip, the fixed finger exhibits an additional sub-terminal tip (arrow). **H** Detail of the spinning gland process. Hardened thread-like secretion (arrow) protrudes from the distal pore of the process. **I** Detail of the hind body region, dorsal towards the top. A shallow external groove (arrow) indicates the position of proctodeum formation. The primordia of walking leg pair 3 are only barely visible under the wrinkled cuticle. **J** Posterior view, Imaris volume (blend). Nuclei have immigrated interiorly where the proctodeum is formed. The primordia of walking leg pair 3 flank the anal tubercle laterally. Dorsally, a longitudinal region comprising only a single layer of loosely arranged nuclei is visible (arrowhead). **K** Histological transversal section through hind body region. A connection has been formed between the immigrating cells of the proctodeum and the yolk-containing midgut.

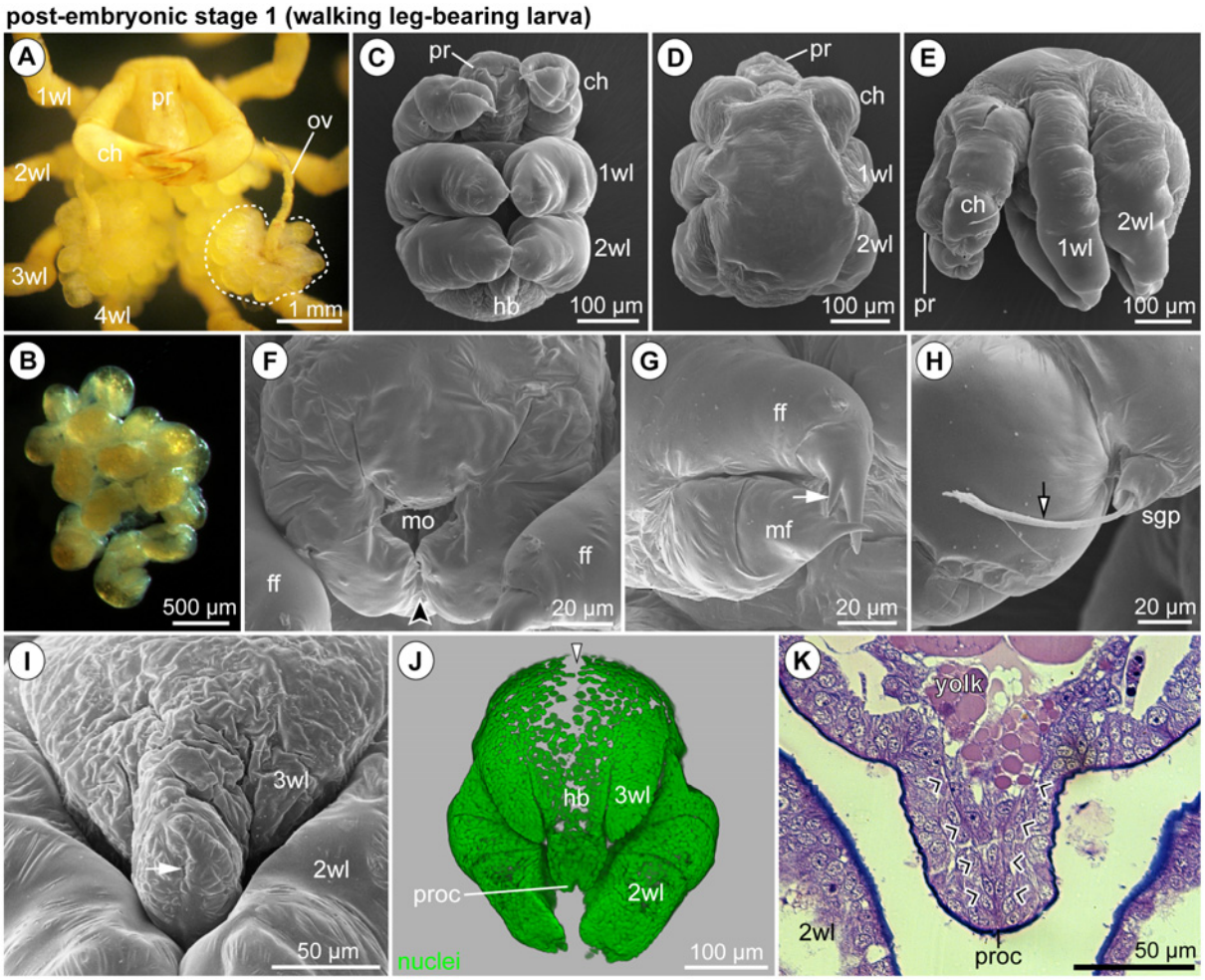
post-embryonic stage 1 (walking leg-bearing larva)
A
1wl
pr
ov
ch
2wl
3wl
4wl
1 mm
C
pr
ch
1wl
2wl
hb
100 µm
D
pr
ch
1wl
2wl
100 µm
E
ch
2wl
1wl
pr
100 µm
B
500 µm
F
mo
ff
ff
20 µm
G
ff
mf
20 µm
H
sgp
20 µm
I
3wl
2wl
50 µm
J
hb
3wl
proc
2wl
nuclei
100 µm
K
yolk
2wl
proc
50 µm

Fig. 11: Molting of post-embryonic stage 1 of *Pseudopallene* sp.

SEM micrographs and nuclear stainings. **A** Lateral overview of pre-molting PS 1. The cuticle is more tautened than in freshly hatched PS 1. The distal-most portion of the externally unarticulated walking leg 1 will give rise to the tarsus, propodus and terminal claw of PS 2. **B-D** Sequence of molting specimens, lateral view. The cuticle rips from anterior to posterior, along the bases of proboscis and the limbs (dashed lines). **E** Lateral view of emerging PS 2. PS 2 leaves the old cuticle antero-dorsally. **F&G** Detail of walking leg 1 of an old PS 1 specimen. Underneath the cuticle (arrowheads) the tissue of the growing walking leg is pressed into folds (arrows). The tissue folds extend in part far into the leg anlage. Proximally, correlation of folds to future leg articulation remains ambiguous. Distally, the region giving rise to the prospective tarsus, propodus and terminal claw can be identified. **F** Imaris volume (blend), anterior view. **G** Optical transversal section, Imaris section mode. **H** Detail of walking leg 1 of molting PS 1, cuticle manually removed. Terminal claw and heel spines of propodus and tarsus are still pressed into the tissue. The leg is covered with setae (mostly bifurcating). **I** Overview of molting PS 1, ventral view, cuticle manually removed. The chelifores remain stuck in the cuticle of PS 1 (white arrows). Note the curved, vaguely s-shaped appearance of the compressed walking legs (dashed white line).

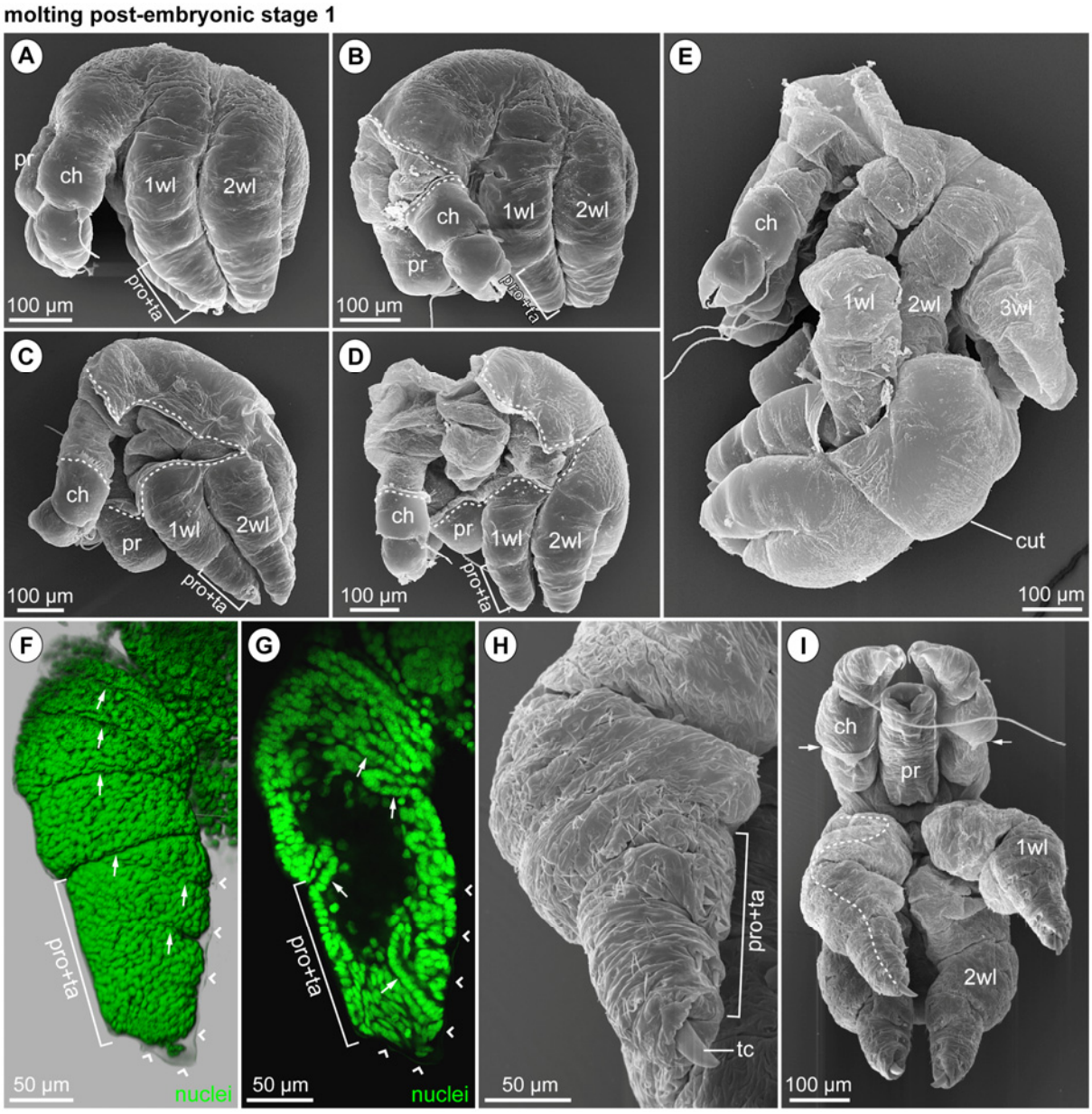
molting post-embryonic stage 1
A
pr
ch
1wl
2wl
pro+ta
100 µm
B
ch
1wl
2wl
pr
pro+ta
100 µm
E
ch
1wl
2wl
3wl
cut
100 µm
C
ch
pr
1wl
2wl
pro+ta
100 µm
D
ch
pr
1wl
2wl
pro+ta
100 µm
F
pro+ta
50 µm
nuclei
G
pro+ta
50 µm
nuclei
H
pro+ta
tc
50 µm
I
ch
pr
1wl
2wl
100 µm

Fig. 12: Post-embryonic stage 2 of *Pseudopallene* sp.

Stereo microscope images, SEM micrographs and nuclear stainings. **A** Egg-bearing adult male of *Pseudopallene* sp., ventral view. PS 2 specimens stay attached to the ovigers and cover more proximally attached egg packages. **B** Ventral overview. Note the transparency of the cuticle. Ganglia of the ventral nervous system are visible as whitish mass in the trunk. Midgut diverticula extend into the articulated walking legs 1 and 2. **D** Detail of the cephalosoma, anterior view. The shallow ocular tubercle lacks pigmented eye cups. The whitish brain shimmers through the cuticle (dashed outline). **D** Ventral overview. The unarticulated limb bud of walking leg 3 is directed posteriorly, the anal tubercle (arrow) points ventrally. **E** Dorsal overview. A distinct inter-segmental constriction (arrows) between walking leg segments 1 and 2 delimits the cephalosoma. **F** Detail of the proboscis tip and cheliforal scape. The mouth opening is Y-shaped and surrounded by a cuticular ridge that has distinct indentations (arrowheads) at the borders of the proboscis antimeres. The spinning gland process with its thread-like secretions is not yet reduced. **G** Detail of the chela tip. The delicate curved tip of the movable finger and the roundish tip of the fixed finger each bear a pore of the chela gland (arrow and arrowhead, respectively). **H** Optical transversal section through chelifores and proboscis, Imaris section mode. Autofluorescence of the cuticle gives the outlines of the structures. The chela gland extends through the entire chelifore into the cephalosoma. Its last third runs closely attached to the midgut diverticulum that reaches into the scape. Note the strong autofluorescent signal of the cuticularized pharynx with its oyster basket. **I** Detail of the completely articulated walking leg 1, posterior view, dorsal to the right. No auxiliary claws are formed. **J** Detail of walking leg 2, posterior view, dorsal to the bottom. Only seven podomeres (including terminal claw) are externally distinguishable. Note the ventrally pointing anal tubercle with the slit-like cuticular fold (arrow) of the anus at its tip.

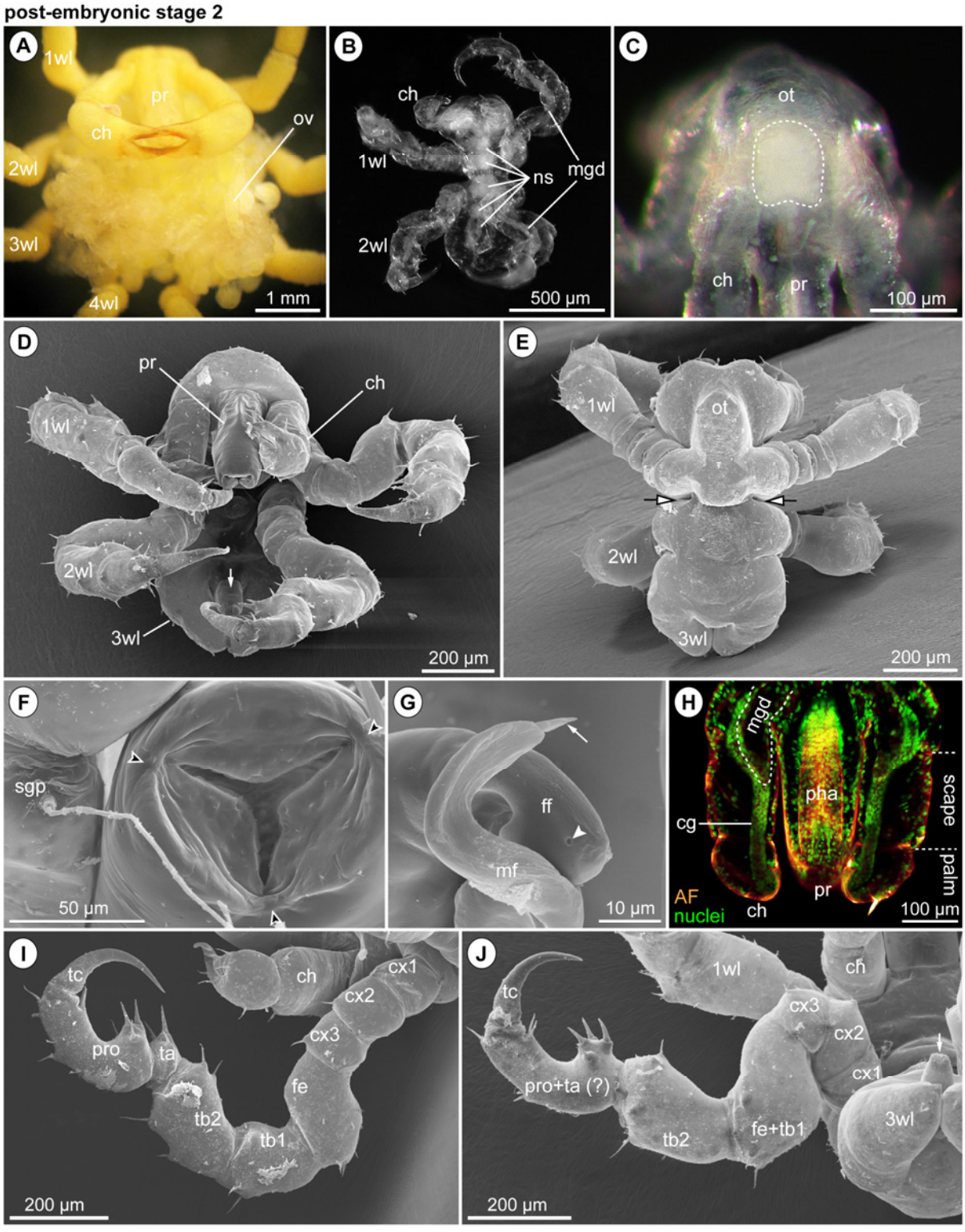
post-embryonic stage 2
A
1wl
pr
ch
ov
2wl
3wl
4wl
1 mm
B
ch
1wl
ns
mgd
2wl
500 µm
C
ot
ch
pr
100 µm
D
pr
ch
1wl
2wl
3wl
200 µm
E
1wl
ot
2wl
3wl
200 µm
F
sgp
50 µm
G
ff
mf
10 µm
H
mgd
pha
scape
cg
palm
AF
nuclei
ch
pr
100 µm
I
tc
ch
cx1
cx2
cx3
pro
ta
fe
tb2
tb1
200 µm
J
1wl
ch
tc
cx3
cx2
cx1
pro+ta (?)
3wl
tb2
fe+tb1
200 µm

Fig. 13: Walking leg articulation of PS 2 of *Pseudopallene* sp.
Autofluorescent signal, Imaris volume (MIP). **A** Walking leg 1, anterior view. The leg possesses the adult number of podomeres, the podomere borders being discernible as regions with higher signal intensity. **B** Walking leg 2, anterior view. The leg possesses only seven podomeres (including terminal claw), regions of future sub-divisions in precursor podomeres are not yet discernible. Note high signal intensity in the cuticular fold relating to the anal opening (arrowhead).

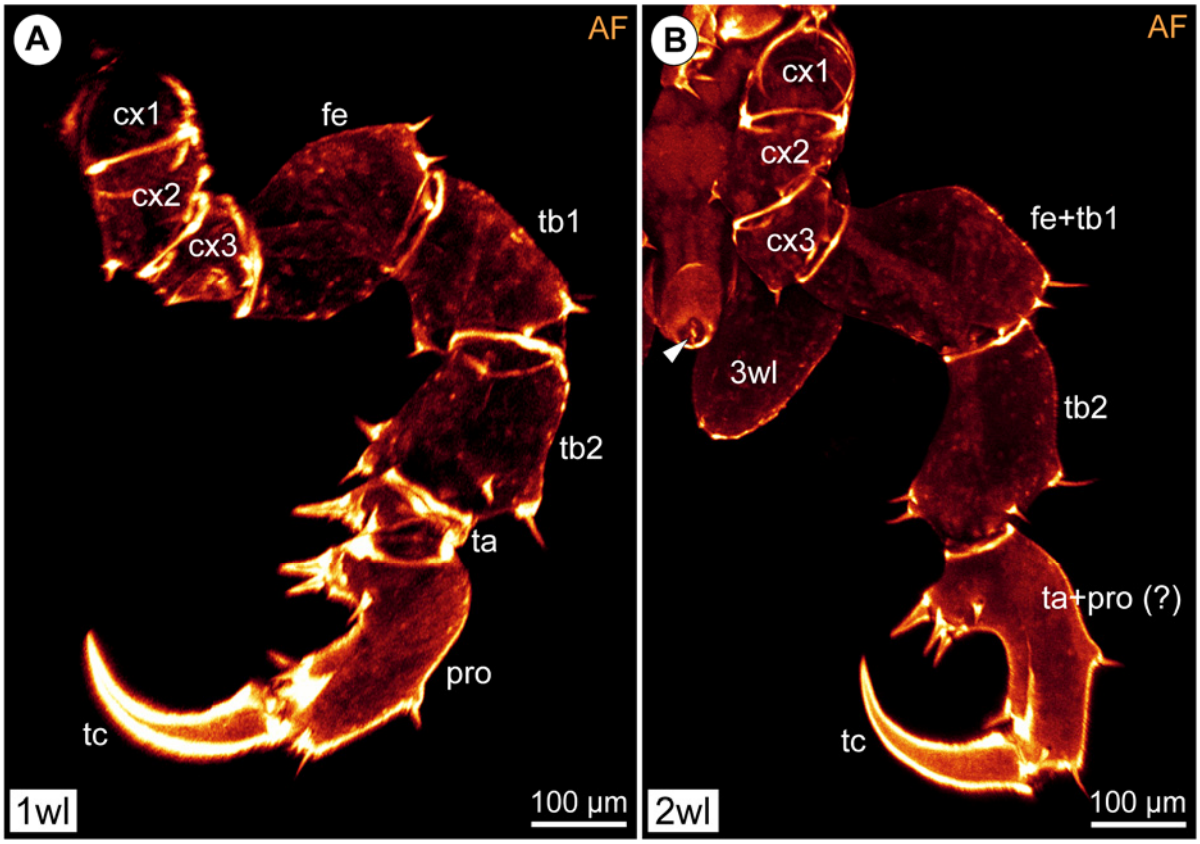
A
AF
cx1
fe
cx2
cx3
tb1
tb2
ta
pro
tc
1wl
100 µm
B
AF
cx1
cx2
cx3
fe+tb1
3wl
tb2
ta+pro (?)
tc
2wl
100 µm

Fig. 14: Post-embryonic stage 3 of *Pseudopallene* sp.

Stereo microscope images and SEM micrographs. Arrowheads mark epizoans attaching to the cuticle. **A** Ventral overview. Three pairs of articulated walking legs are formed. Note the non-transparency of this stage. **B** Ventral overview, same specimen as in **A**. The proboscis is directed posteriorly, running along the ventral side of the trunk. Note the ventrally pointing anal tubercle (arrow) and the flanking unarticulated limb buds of walking leg pair 4. Asterisk marks a damaged walking leg tip. **C** Detail of the cephalosoma, anterior view. The lateral sensory organs protrude from the ocular tubercle. **D** Detail of the cephalosoma, dorsal view. The ocular tubercle bears four pigmented eye cups. **E** Detail of proboscis and chelifores, postero-ventral view. At the slightly tapering tip of the proboscis, the Y-shaped mouth is surrounded by a cuticular ridge without distinct indentations. The movable finger of the chela possesses still the elongated curved tip (arrows). **F** Detail of the ventral side of the trunk, posterior view, dorsal to the bottom. The first elevation of the outgrowing oviger is detectable. **G** Detail of the completely articulated walking leg 2, anterior view, dorsal to the right. Femur and tibia 1 as well as tarsus and propodus are fully developed. **H** Detail of walking leg 3, posterior view, dorsal to the right. Only seven podomeres (including terminal claw) are externally distinguishable. The future sub-division of the *femur-tibia1* precursor podomere is indicated by framed arrows. Note the slit-like anal opening (white arrow).

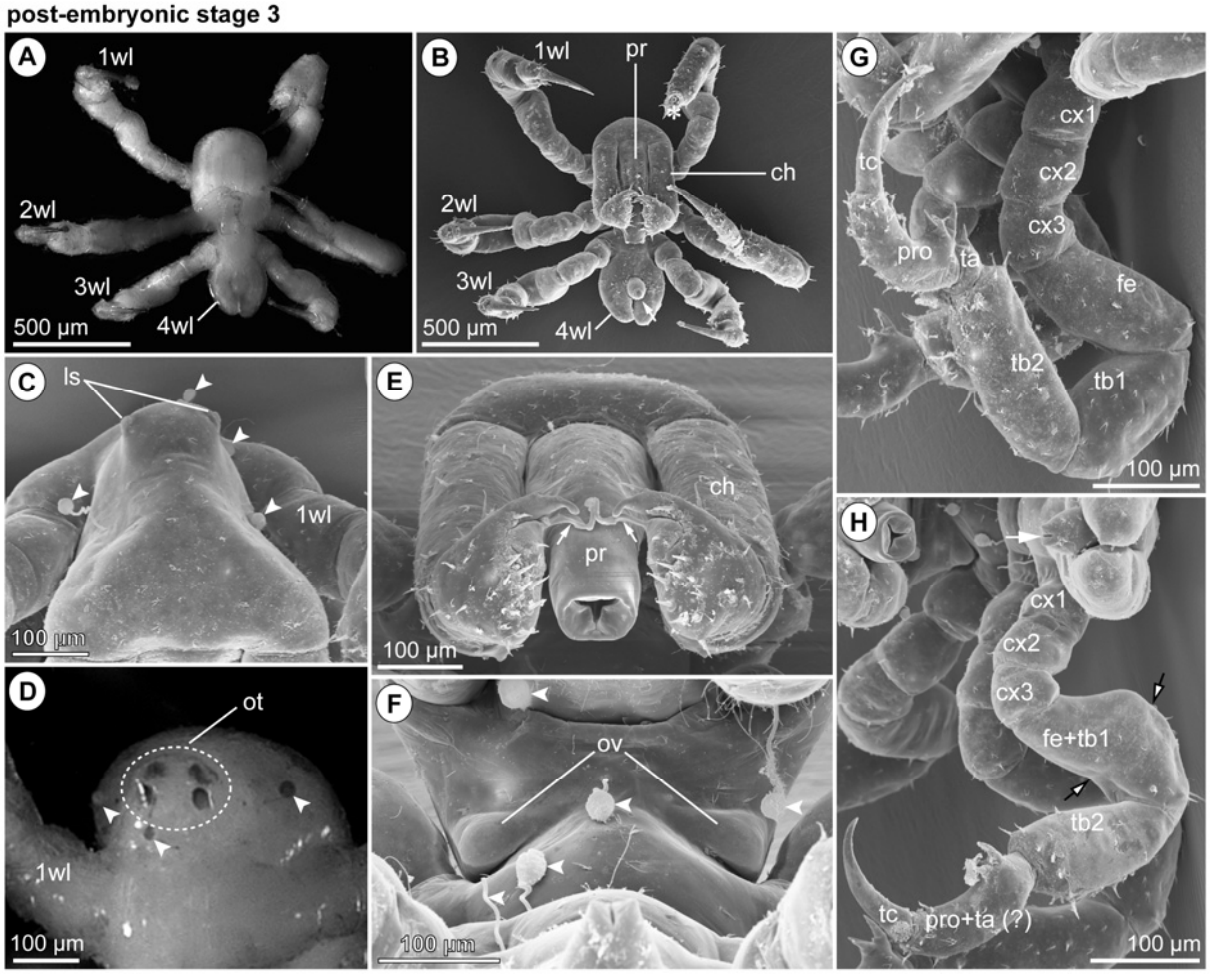
post-embryonic stage 3
A
1wl
2wl
3wl
4wl
500 µm
B
1wl
pr
ch
2wl
3wl
4wl
500 µm
G
cx1
tc
cx2
cx3
pro
ta
fe
tb2
tb1
100 µm
C
ls
1wl
100 µm
E
ch
pr
100 µm
H
cx1
cx2
cx3
fe+tb1
tb2
tc
pro+ta (?)
100 µm
D
ot
1wl
100 µm
F
ov
100 µm

Fig. 15: Post-embryonic stage 4 of *Pseudopallene* sp.

Stereo microscope images and SEM micrographs. **A** Ventral overview. Four pairs of articulated walking legs are formed. Buds of the ovigers are detectable on the ventral side of the trunk. **B** Ventral overview. The anal tubercle (arrow) is pointing posteriorly, in line with the trunk. **C** Dorsal overview. The trunk is fully segmented (white arrowheads). The arrow indicates the posteriorly directed anal tubercle. **D** Lateral overview. The ocular tubercle is a prominent elevation on the cephalosoma. Arrowheads mark the external segment borders. The future sub-division of the *femur-tibia1* precursor podomere in walking leg 4 is indicated by the framed arrows. **E** Detail of the chelae, antero-ventral view. Arrows mark the delicate elongated curved tip of the movable chela finger. Note the trapezoid shape of the palm. **F** Detail of proboscis and the oviger anlagen. The proboscis tapers distinctly along the p-d axis. The oviger anlage is an elongate but unarticulated limb bud. **G** Detail of walking leg 3, posterior view, dorsal to the right. Femur and tibia 1 as well as tarsus and propodus are fully developed. **H** Detail of walking leg pair 4, ventro-lateral view. Only seven podomeres (including terminal claw) are externally distinguishable. The future sub-division of the *femur-tibia1* precursor podomere is indicated by a framed arrow.

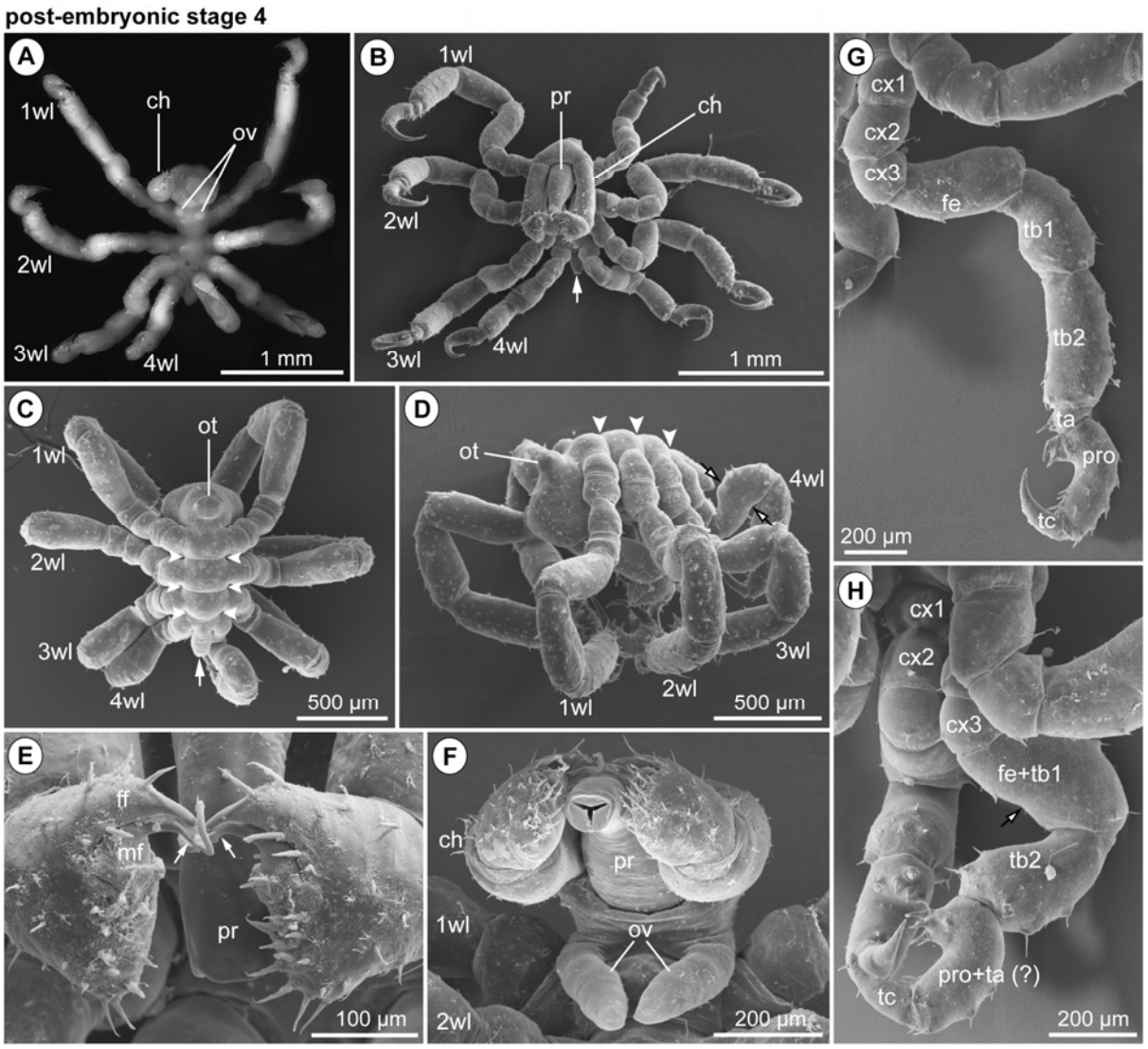
post-embryonic stage 4
A
1wl
ch
ov
2wl
3wl
4wl
1 mm
B
1wl
pr
ch
2wl
3wl
4wl
1 mm
G
cx1
cx2
cx3
fe
tb1
tb2
ta
pro
tc
200 µm
C
ot
1wl
2wl
3wl
4wl
500 µm
D
ot
4wl
3wl
2wl
1wl
500 µm
H
cx1
cx2
cx3
fe+tb1
tb2
pro+ta (?)
tc
200 µm
E
ff
mf
pr
100 µm
F
ch
pr
1wl
ov
2wl
200 µm

Fig. 16: Post-embryonic stages 5 and 6 of *Pseudopallene* sp.

SEM micrographs. **A-D** PS 5. **A** Ventral overview. **B** Posterior view, dorsal to the bottom. The still incompletely articulated ovigers are ventrally covered by the proboscis and chelifores. **C** Detail of oviger tip. The long distal-most podomere bears single cuticular spines (arrows), reminiscent of the future leaf-shaped denticulate spines of the strigilis. **D** Detail of walking leg 4, posterior view, dorsal to the right. Femur and tibia 1 as well as tarsus and propodus are fully developed. **E-H** PS 6. Asterisks mark damaged regions. **E** Ventral overview. **F** Detail of the cephalosoma, antero-ventral view. The base of the proboscis has 2,5 to 3 times the diameter of the tip. The delicate curved tip of the movable chela finger is still developed (arrows). The distal part of the completely articulated oviger protrudes from underneath the chelifores. **G** Detail of proboscis tip. The Y-shaped mouth opening is flanked on each side by three minute pores (arrowheads). **H** Detail of oviger tip. The distal-most four podomeres each bear a single row of leaf-shaped denticulate spines, forming together the strigilis. The terminal claw is equipped with two rows of denticulate outgrowths (arrowheads).

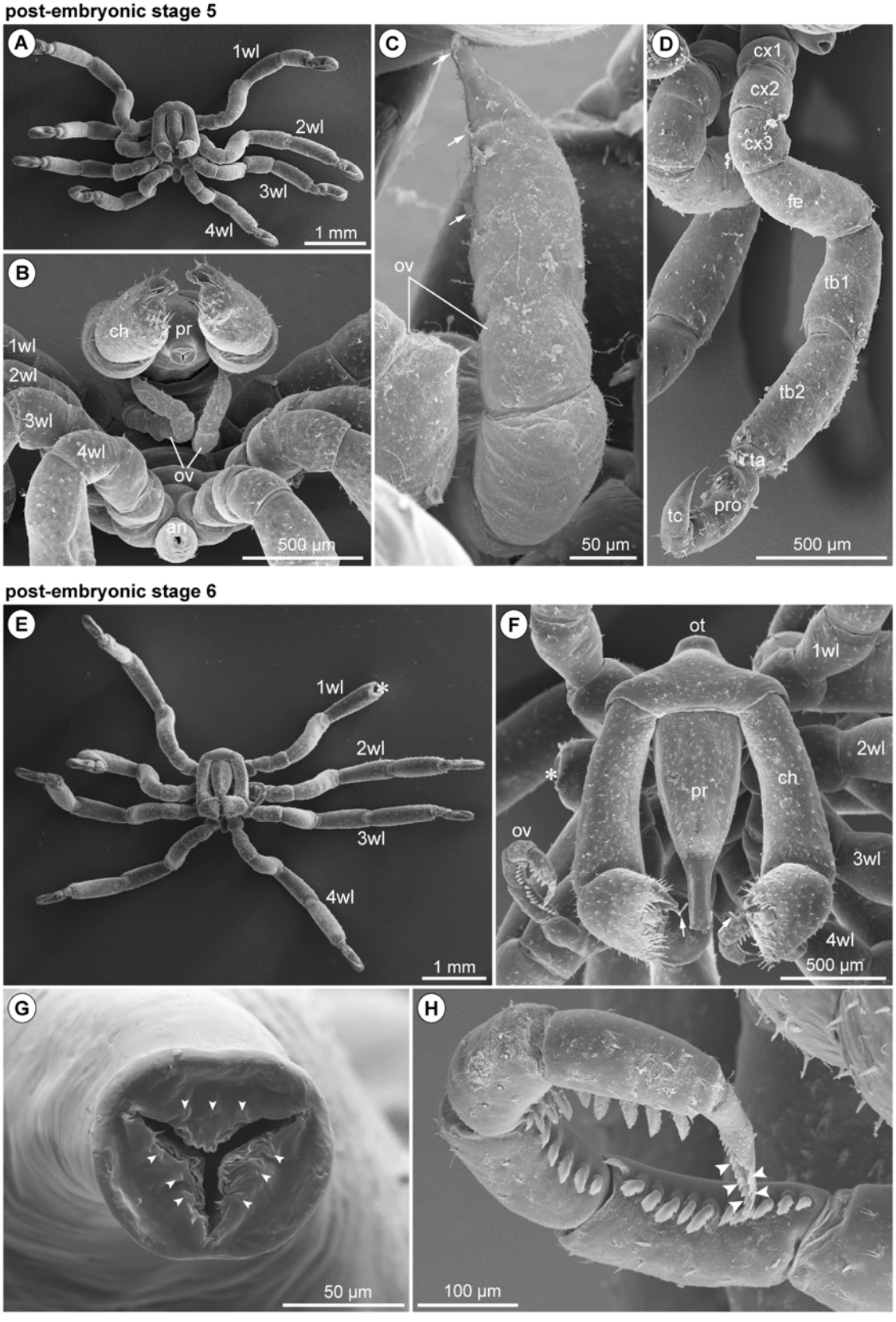
post-embryonic stage 5
A
1wl
2wl
3wl
4wl
1 mm
B
ch
pr
1wl
2wl
3wl
4wl
ov
an
500 µm
C
ov
50 µm
D
cx1
cx2
cx3
fe
tb1
tb2
ta
pro
tc
500 µm
post-embryonic stage 6
E
1wl
2wl
3wl
4wl
1 mm
F
ot
1wl
2wl
ch
pr
ov
3wl
4wl
500 µm
G
50 µm
H
100 µm

Fig. 17: Sub-adult of *Pseudopallene constricta* n. sp.

Stereo microscope images and SEM micrographs. **A** Detail of the cephalosoma, anterior view. The eye cups on the ocular tubercle are of orange-brown color (arrows). Arrowheads indicate the diagnostic constriction of the proboscis. **B** Same specimen and view as in **A**. Note again the distinct proboscis constriction (arrowheads). **C** Detail of proboscis tip. The Y-shaped mouth is on each side surrounded by three papillae in a field of small tube-like projections. **D** Magnification of three papillae. Each papilla bears a single pore, some of the surrounding small tubes are also equipped with distal pores (arrows). **E** Detail of ocular tubercle, anterior view. Note the protruding lateral sensory organs. **F** Coxa 2 of walking leg 4, ventral view. The elongated coxa 2 lacks the gonopore. **G** Posterior view. The movable chela finger lacks the corkscrew-shaped delicate tip of the preceding stages. The ovigers are held ventral to the trunk. **H** Detail of the distal oviger portion. The four distal-most podomeres of the strigilis are each equipped with one row of leaf-shaped cuticular spines. The terminal claw bears two rows of denticulate cuticular outgrowths on its distal half.

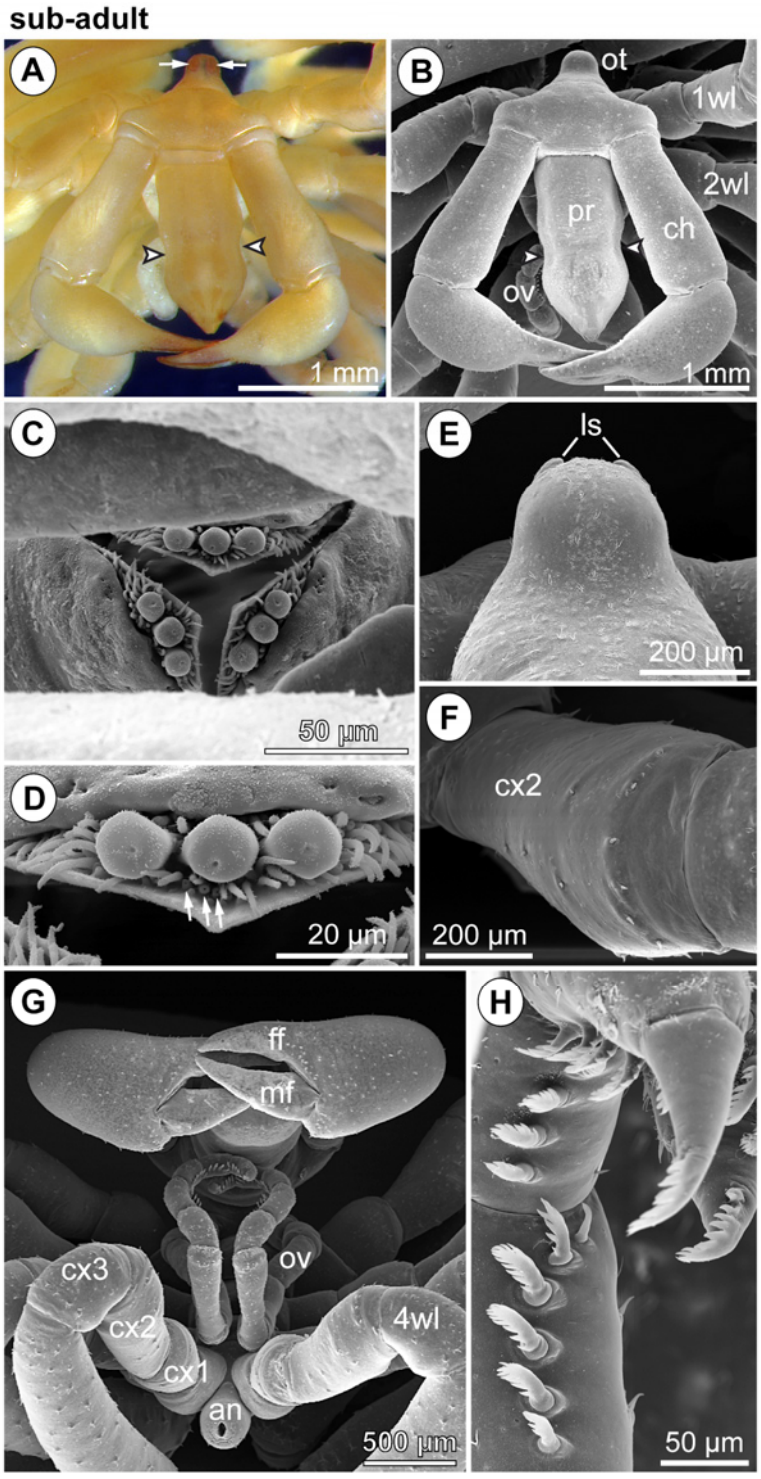
sub-adult
A
1 mm
B
ot
1wl
2wl
pr
ch
ov
1 mm
C
50 µm
D
20 µm
E
ls
200 µm
F
cx2
200 µm
G
ff
mf
ov
cx3
cx2
cx1
an
4wl
500 µm
H
50 µm

Fig. 18: Overview of tubulin-labeled embryos of *Pseudopallene* sp. in different stages.
Ventral view, flat preparations, Imaris volume (MIP). Stippled circles mark the stomodeum or pharynx. White arrows indicate apically converging processes of immigrating cells related to spinning gland development. Black arrows mark tubulin-positive duct of the spinning gland. Asterisks indicate regions that were damaged during dissection or in which one chelifore anlage has been removed mechanically or virtually to reveal the VNE of the palpal and ovigeral segments. Note first emergence of intensely tubulin-labeled spots in the pre-cheliforal lobe and VNE from ES 3 onwards (**B**,**C**). The spots are more clearly identifiable in the pre-cheliforal lobe (**C**,**D**,**E**) and remain in part distinguishable up to ES 6 (**F**). After formation of paired segmental depressions in the VNE of walking leg segments 1 and 2, unambiguous delimitation of single spots is not possible any longer (**E**,**F**). Scale bars = 100 µm.

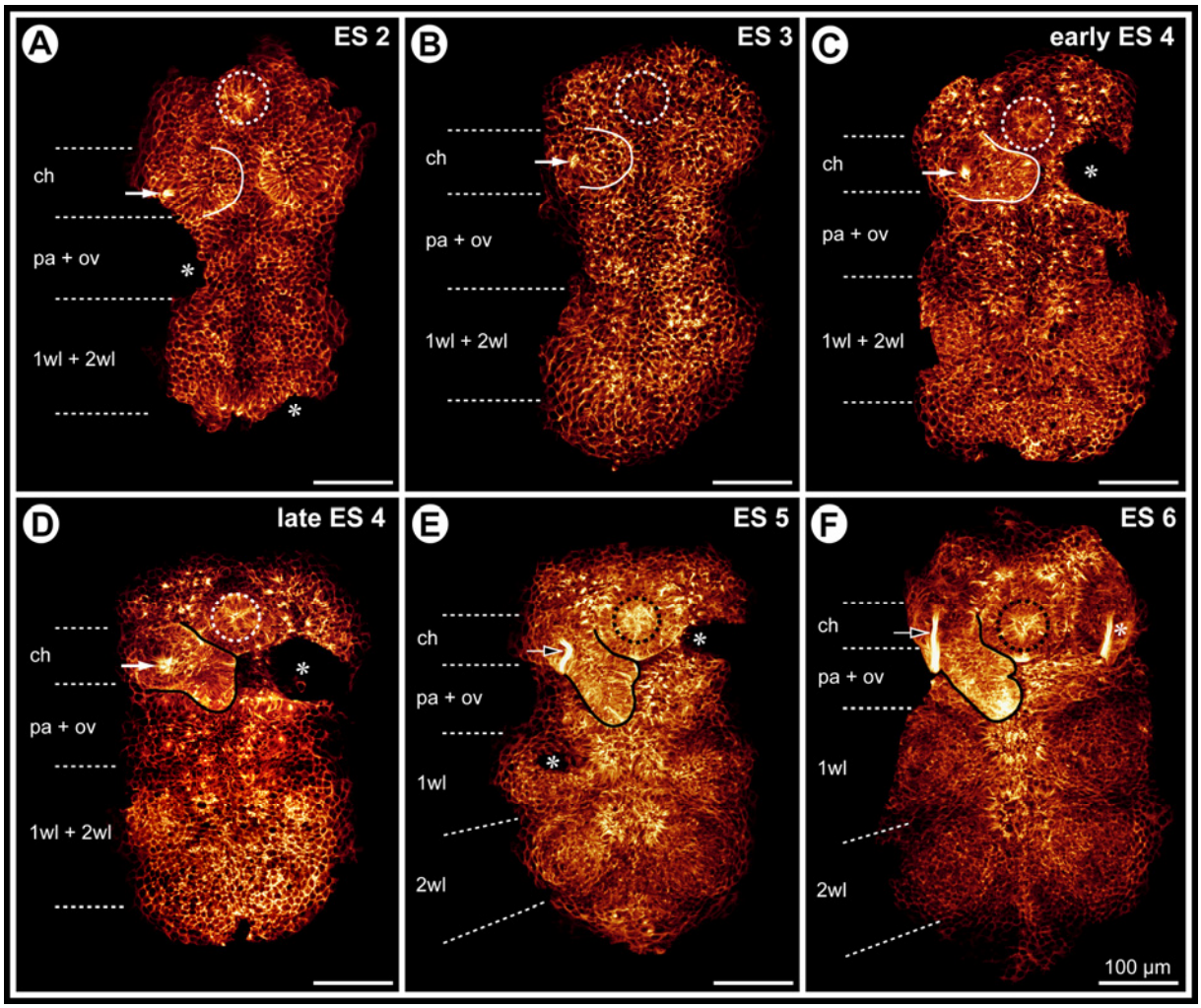
A
ES 2
ch
pa + ov
1wl + 2wl
B
ES 3
ch
pa + ov
1wl + 2wl
C
early ES 4
ch
pa + ov
1wl + 2wl
D
late ES 4
ch
pa + ov
1wl + 2wl
E
ES 5
ch
pa + ov
1wl
2wl
F
ES 6
ch
pa + ov
1wl
2wl
100 µm

Fig. 19: Early stratification and CIS formation in walking leg neuromere 1 of *Pseudopallene* sp. (ES 2-3 – late ES 4).

Optical sections of tubulin- and PH3-labeled embryos with nuclear counterstain. All horizontal sections represent 2D projections of curved composite sections. The level of the corresponding transversal sections are indicated to the right of **B**, **E**, and **H**, respectively. Morphologically left hemi-neuromeres are shown, dashed straight lines to the left indicate the midline region. Asterisks mark apically constricting cell cortices of columnar cells with basally displaced nucleus. White spots mark selected basally displaced nuclei. Stippled outlines in **D-I'** highlight extensions of the hemi-neuromere. Arrows mark selected pycnotic bodies (occurrence of cell death). Scale bars = 30 µm.

A-C' ES 2-3. **A,A'** Apical in the VNE, the more intensely tubulin-labeled areas relate to constricting cell cortices of cells with basally displaced nucleus, no fully formed CISs are recognizable as yet. **B** No spatial pattern is recognizable in the basally displaced nuclei, small clusters as well as linear arrangements being observable. **C,C'** The columnar cells of the single-layered VNE are underlain by scattered big entodermal cells (stars).

D-F' ES 3-4. **D,D'** Apical in the VNE, small nuclei-free regions have formed. Tiny spots with more intense tubulin labeling represent converging cell processes of flask-shaped immigrating cells (nascent CISs, selection marked by arrowheads). Note apical mitoses. **E** More nuclei are displaced basally. Some clusters of nuclei (selection marked by white spots) can be assigned to nascent CISs in optical section series. Several nuclei are even more basally displaced, the corresponding apically extending cell processes being seen in between the nuclei of this level (arrowhead, compare to **F'**). First pycnotic bodies are encountered in the midline region (arrows). **F,F'** The nuclei in the hemi-neuromere lie in 2-3 apico-basal levels. Nascent CISs comprising few flask-shaped cells (arrowheads) are closely adjoined by cells with basally displaced nuclei and only slightly constricted apical cell cortex (asterisks).

G-I' Late ES 4. **G,G'** CISs have become more defined in the apical VNE (selection marked by arrowheads). Note apical mitoses. **H** Basally, numerous pycnotic bodies line the margins of the hemi-neuromere (selection marked by arrows), in particular in the midline region. Especially in the posterior portion of the hemi-neuromere, immigrating cells in the CISs extend more basally (arrowhead marking apically extending cell processes, compare to **I'**). **I,I'** The nuclei in the hemi-neuromere lie in 3-4 apico-basal levels. Immigrating cells of anterior CISs (**I**) extend not as far basally as cells in posterior CISs (**I'**, compare also to **F'** for increase of immigrating cells within CIS over time).

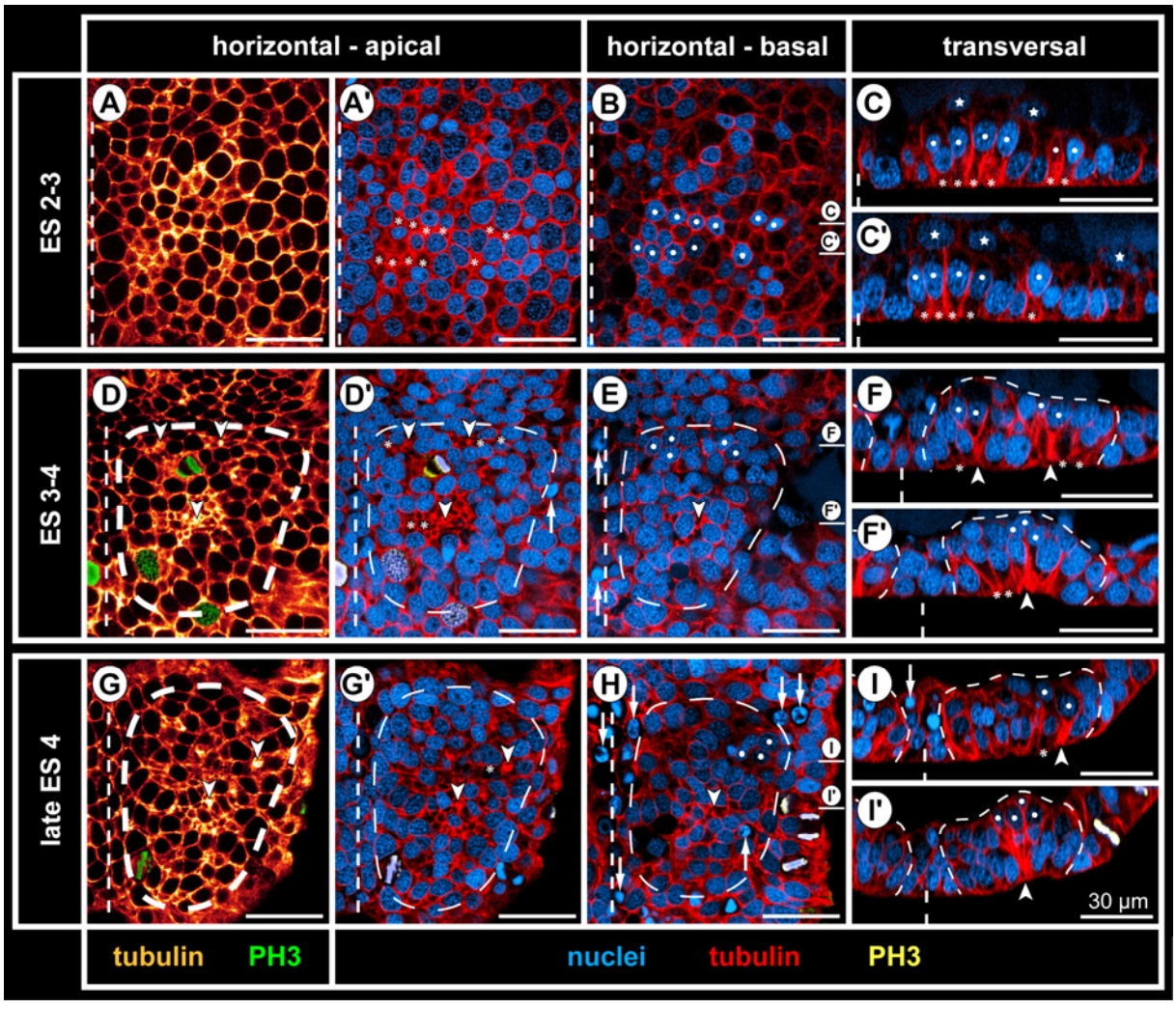
horizontal - apical
horizontal - basal
transversal
ES 2-3
ES 3-4
late ES 4
A
A'
B
C
C'
D
D'
E
F
F'
G
G'
H
I
I'
30 µm
tubulin
PH3
nuclei
tubulin
PH3

Fig. 20: Early stratification of the VNE and CIS formation in *Pseudopallene* sp.

Transversal histological sections through germ band of ES 3 in the region of the prospective walking leg segments 1 and 2. The midline region is indicated by the dashed line. Scale bars = 30 µm.

A Three hardly recognizable nascent CISs are marked in the VNE (arrows). Arrowhead indicates an apical tangential mitosis (anaphase).

B No CISs are discernible in this section. Arrowheads indicate two further apical and tangential mitoses (both metaphase).

Fig. 21: Bilaterally symmetric arrangement of CISs in the VNE of Pseudopallene sp. (ES 4).

Optical sections of tubulin- and PH3-labeled embryos, **A** shows 2D projection of curved composite section. Coarsely dashed line indicates the midline region. White spots mark basally displaced nuclei regions of flask-shaped cells in CISs. The levels of the transversal optical sections **B-E** are indicated by lines to the left in **A**. Scale bars = 30 µm.

A VNE of ovigeral and walking leg 1 segment, presumptive segment borders indicated by finely dashed lines. Several apical tubulin-labeled spots indicate the presence of CISs. Note differences in the distinctness of the spots, the apically converging cell processes of flask-shaped cells being in some cases placed less condensed. A largely bilaterally symmetric pattern of CISs is apparent (selected CISs marked by arrowheads). Note apical mitoses. White-framed black arrows indicate a conspicuous site of cell immigration lateral to each ovigeral hemi-neuromere. It is unclear whether this site of cell internalization relates to peripheral nervous system or gland development.

B Transversal section through anterior portion of ovigeral neuromere. The two contra-lateral CISs of a bilaterally symmetric pair do not always comprise a similar number of immigrating cells.

C Transversal section through posterior portion of ovigeral neuromere. The transversally arranged CISs are closely spaced with only one or maximally two apical cells in between.

D,E Transversal sections through anterior and posterior portion of walking leg neuromere 1, respectively. While the morphologically left CISs are well-defined, their contra-lateral counterparts are less distinct, being part of a wider region of cells with basally displaced nucleus (compare also to **A**). Presumably, the morphological right hemi-neuromere would have predated the left one in the formation of the apical depression characteristic of ES 5.

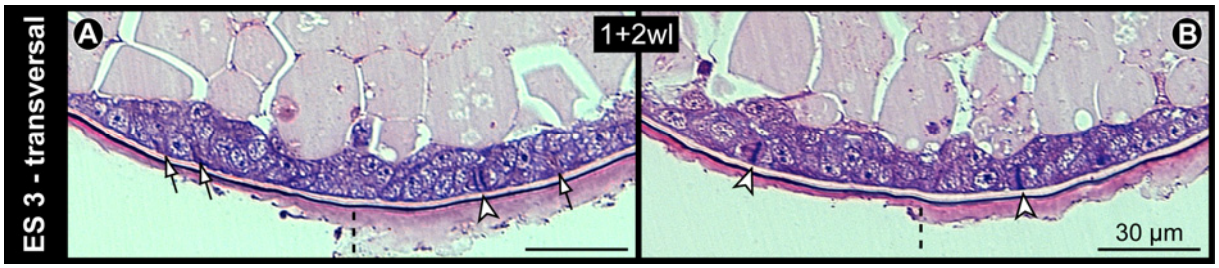
ES 3 - transversal
A
1+2wl
B
30 µm

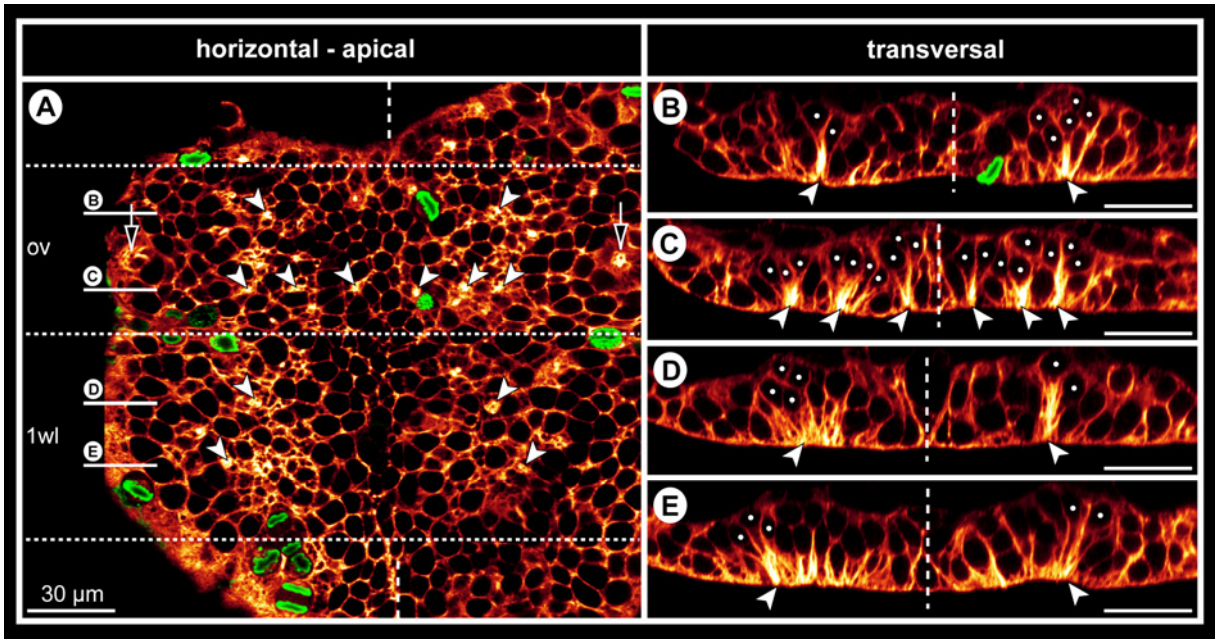
horizontal - apical
transversal
A
B
C
D
E
ov
1wl
30 µm

Fig. 22: Stereotypic CIS arrangement in walking leg neuromere 1 of *Pseudopallene* sp. (ES 4).
A-D Tubulin- and PH3 labeling of four different embryos (**A**,**A'** – **B**,**B'** – **C**,**C'** – **D**), in part shown with nuclear counterstain. Apical horizontal sections (2D projections of curved composite sections). The images lacking nuclear counterstain (**A**,**B**,**C**) correspond to the ones shown to their respective right (**A'**,**B'**,**C'**). Dashed outlines indicate the extensions of the two hemi-neuromeres. Filled arrowheads mark the six CISs that could be reliably identified in the great majority of specimens. Open arrowheads indicate less consistently encountered CISs in the postero-medial portion of the hemi-neuromeres. Ellipses highlight the region in which the apical depression begins to form. Arrows mark pycnotic bodies along the midline region. Note the apical, in part clearly tangentially oriented divisions. The question mark in **D** indicates a region in which a typical antero-lateral CIS could not be securely identified apically, presumably due to transient rearrangements resulting from the nearby apical mitoses. Scale bars = 30 µm. **E** Scheme of apical horizontal view of walking leg neuromere 1 in ES 4. Black spots indicate reliably identified CISs, gray spots the more irregularly recognizable CISs in the postero-medial region in which the apical depression (grayish area in the background) starts to form. Ectodermal cells (potentially with epidermal fate) surrounding the hemi-neuromeres are depicted in gray, the cells in the midline region are shown slightly smaller. Small dark gray dots in the latter represent pycnotic bodies.

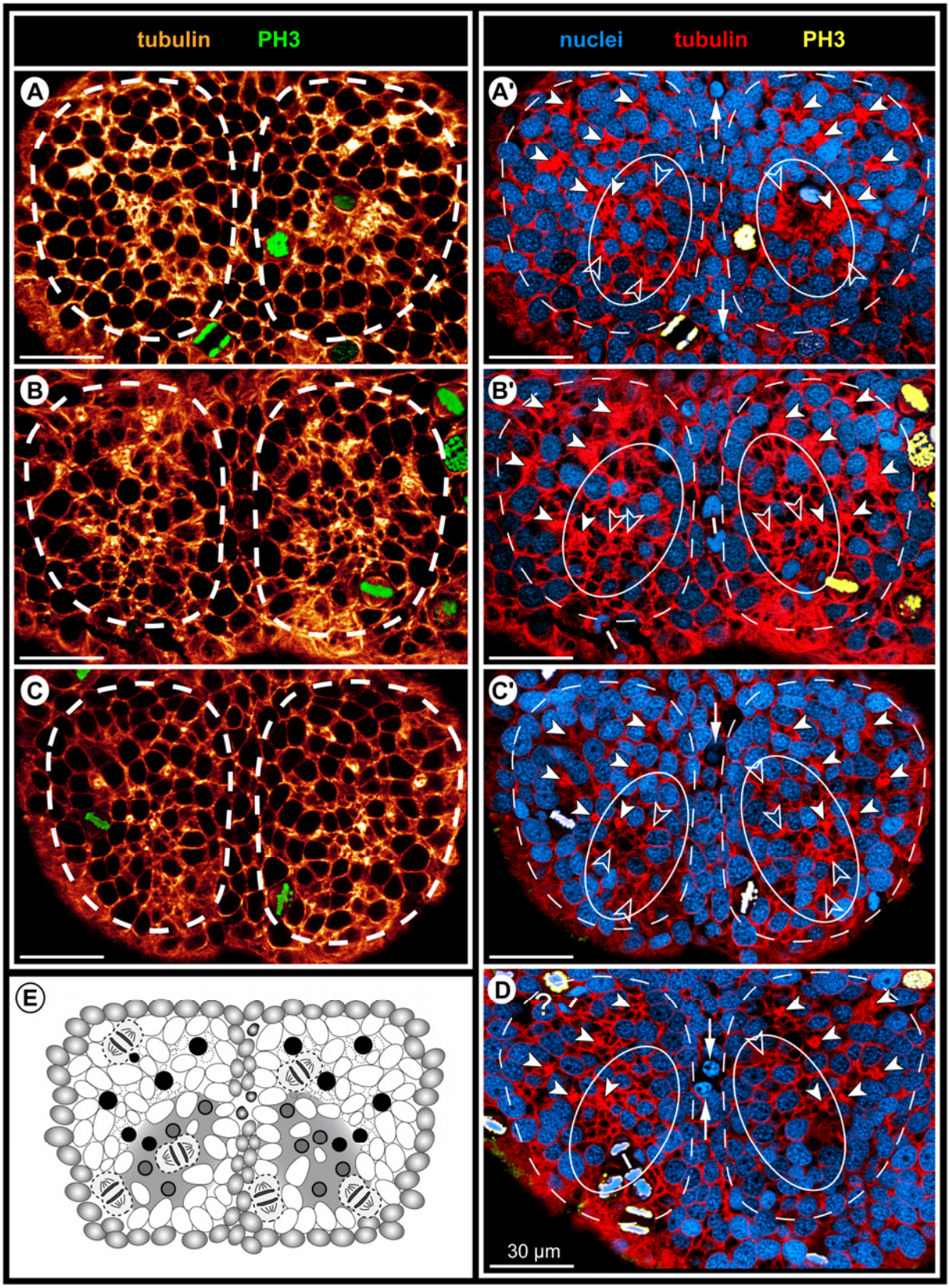
tubulin
PH3
nuclei
tubulin
PH3
A
A'
B
B'
C
C'
D
?
E
30 µm

Fig. 23: Mitotic activity and division orientation in the VNE of *Pseudopallene* sp. (ES 2 – ES 4).
Optical sections of tubulin- and PH3-labeled embryos with nuclear counterstain. Horizontal views (**A**,**C**,**E**) are 2D projections of curved composite sections. Coarsely dashed line indicates the midline region, finely dashed lines mark presumptive segment borders. In **A**, **C** and **E**, the level of the corresponding transversal sections of **B**, **D** and **F**, respectively, is indicated at the left side of the germ band. Stars mark scattered embryonic entodermal cells underlying the VNE. Scale bars = 30 µm.
In all three embryonic stages, mitoses are almost exclusively found in the apical layer of the VNE. Note the tangential orientation of cell divisions, being recognizable in meta-, ana- and telophase of mitosis. Small white lines connect the well-separated forming nuclei of two prospective sister cells during telophase. No preferred orientation of the divisions within the plane of the apical layer is assessable. In the late ES 4 specimen (**E**,**F**), the formation of the apical depression of walking leg neuromere 1 is already advanced. The white solid arrowhead marks a still recognizable CIS in the anterior portion of this neuromere. White spots in **F** highlight the flask-shaped cells of this CIS. Open arrowhead in **F** points at one of the exceptionally observed divisions of a cell with slightly basally displaced nucleus. White-framed black arrows in **E** indicate a conspicuous site of cell immigration lateral to each ovigeral hemi-neuromere (compare to Fig. 21A).

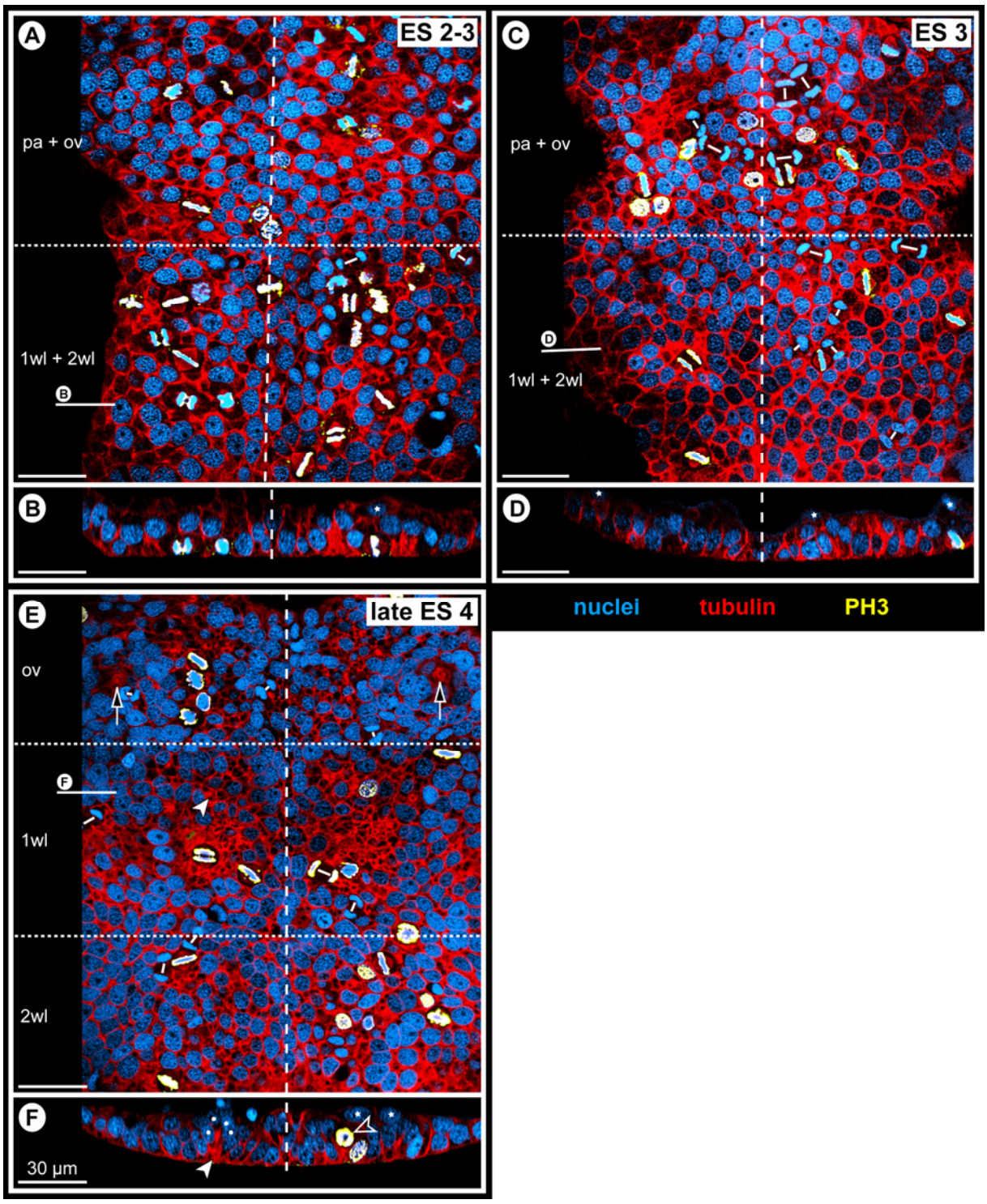
A
ES 2-3
pa + ov
1wl + 2wl
B
B
C
ES 3
pa + ov
D
1wl + 2wl
D
nuclei
tubulin
PH3
E
late ES 4
ov
F
1wl
2wl
F
30 µm

Fig. 24: Formation of central depression and compact hemi-ganglion anlagen in walking leg neuromere 1 of *Pseudopallene* sp. (ES 5 and ES 6).

Optical sections of tubulin- and PH3-labeled embryos with nuclear counterstain. All horizontal views (**A-B,D-E**) are 2D projections of curved composite sections. Morphologically left hemi-neuromeres are shown, dashed straight lines indicate the midline region. Stippled outlines highlight extensions of the hemi-neuromeres. Stars indicate damages in limb bud region. White spots mark small prospective epidermal cells that surround the central depression. Scale bars = 30 µm.

A-C ES 5. **A,A'** A central depression has formed apically, all cells in this region having basally displaced nuclei. Unequivocal identification of single CISs is not possible any longer. Only during division, the separating chromosomes and newly forming nuclei are encountered in apical positions within the depression. **B** Also basally the hemi-neuromere has become medio-laterally compressed, the GCs having compacted and forming a well-defined hemi-ganglion anlage. **C** First immigrating cells have detached basally (asterisks). Note decrease of the medio-lateral extensions of the midline region and its few remaining basal and often unpaired cells (open arrow) wedged between the hemi-ganglion anlagen.

D-F ES 6 **D,D'** Apically, no significant changes have occurred compared to ES 5. **E** Basally within the hemi-ganglion anlagen, single cells are found in division, representing NPs (open arrow). Scattered pycnotic bodies indicate occasional cell death (solid arrow). **F** Occasionally, cell arrangements reminiscent of CISs are recognizable within the hemi-ganglion anlage (white arrowhead and open spots). Asterisks mark detached basal GCs, open arrow points at unpaired median midline cell.

Fig. 25: Mitotic activity and division orientation in early hemi-ganglion anlagen of *Pseudopallene* sp. (ES 6).

Optical sections of tubulin- and PH3-labeled embryos with nuclear counterstain. Horizontal view in **A** represents 2D projections of curved composite sections. Dashed lines mark presumptive segment borders. Scale bars = 30 µm.

A Several mitoses occur in the center and at the margins of the paired apical depressions of walking leg neuromeres 1 and 2. Note tangential orientation of the cell divisions, being recognizable in meta-, ana- and telophase of mitosis. Small white lines connect the forming nuclei of two prospective sister cells during telophase. Star indicates damaged region in walking leg neuromere 1. **B** Sagittal section. Asterisks mark detached basal GCs. Note mitoses of two basal NPs (open arrowheads).

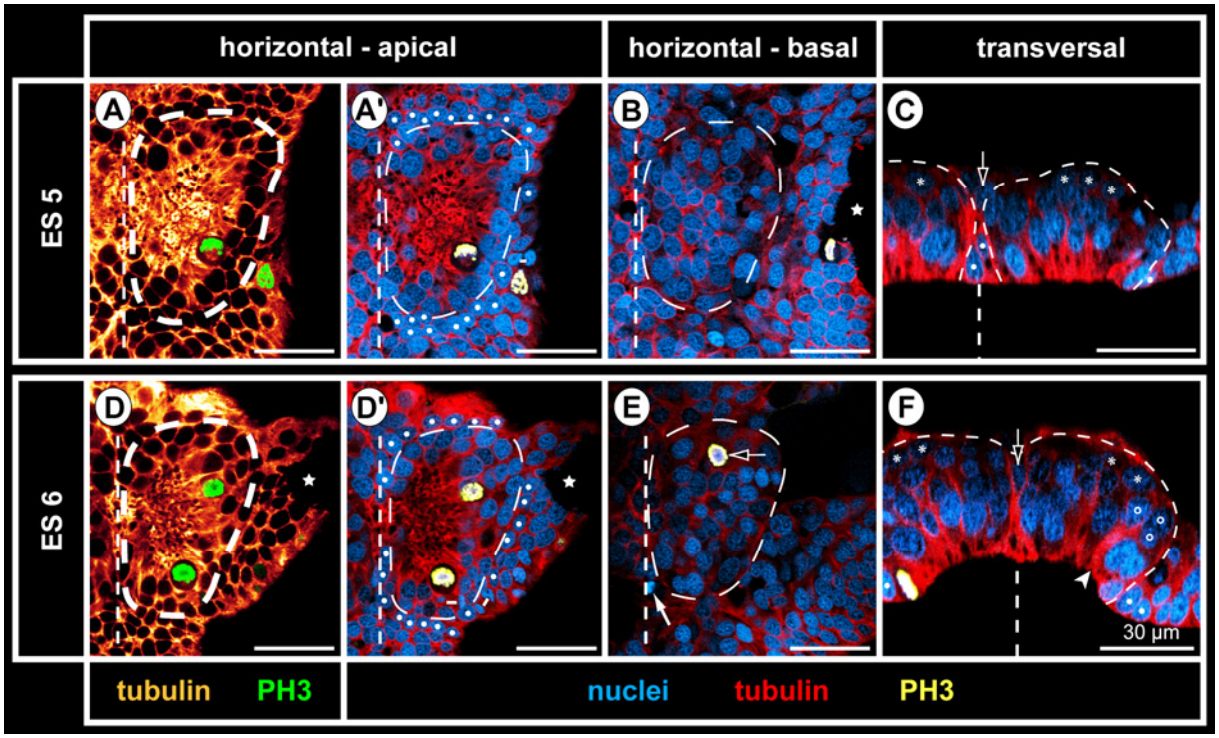
horizontal - apical
horizontal - basal
transversal
ES 5
ES 6
A
A'
B
C
D
D'
E
F
30 µm
tubulin
PH3
nuclei
tubulin
PH3

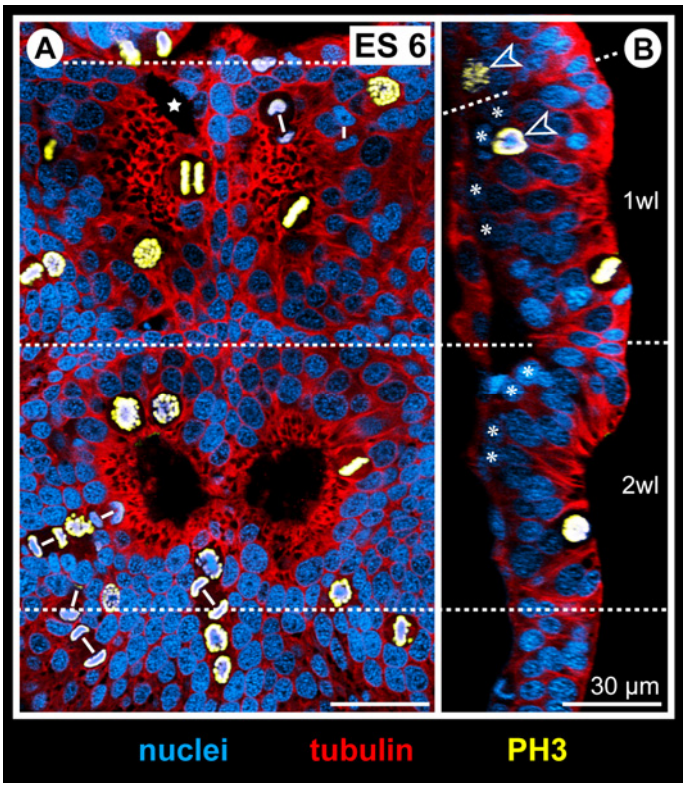
A
ES 6
B
1wl
2wl
30 µm
nuclei
tubulin
PH3

Fig. 26: Structure and cell proliferation in hemi-ganglion anlagen of walking leg neuromere 1 during advanced embryonic development of *Pseudopallene* sp. (ES 7 – ES 10).

Optical sections of tubulin- and PH3-labeled embryos with nuclear counterstain. Dashed line at the bottom of each image indicates the midline region. Small white lines connect the forming nuclei of two prospective sister cells during telophase. Asterisks mark big apical SCNPs that are not in division. Solid white arrowheads indicate sub-apical INPs. White spots mark small prospective epidermal cells that surround the central depression. Scale bars = 30 µm.

A,D,G Apical horizontal sections (2D projection of curved composite sections). Several big apical SCNPs surround the paired apical invaginations, some of them being in division. Prior to hatching (ES 9-10, **G**) compression of the apical hemi-ganglion portion by the outgrowing limb anlagen leads to a squeezed appearance of the invaginations and cells.

A',D',G' Sub-apical horizontal sections. Divisions of INPs are observable throughout the late phase of embryonic development, being predominantly located in the anterior and posterior regions of the hemi-ganglion anlagen. White-framed open arrows mark unpaired median cells of the midline region (putative glial cells).

A'',D'',G'' Basal horizontal sections. Segmental axonogenesis has started in early ES 7 (**A''**), a first transversal pathway (open arrowheads) being pioneered by neurons located in the antero-lateral basal region of the hemi-ganglion anlage (stippled ovals). Medially, the growth cones have not yet crossed to the contra-lateral side and are in close contact to some of the basal cells of the midline region (open spots). The arrow marks a pycnotic body. During later embryonic development intensely tubulin-labeled median cells remain distinguishable, directly adjacent to the undivided embryonic commissure (open spots, **D''**,**G''**). The commissure receives not only neurites from anteriorly positioned neurons (exemplarily shown by stippled ovals) but also input from the posteriorly located neurons within the hemi-ganglia (exemplarily shown in white-framed ovals).

B,C,E,F,H,I Transversal sections. Note the increasingly distinct structure of the ganglion anlagen from ES 7 to ES 10. The big apical SCNPs are underlain by a growing number of GCs (including INPs). Stars label smaller flask-shaped cells that appear to be in the process of immigration. White open arrowheads mark developing neuropil and axonal pathways at the basal side of the ganglion anlagen. White-framed open arrows indicate flattened median cells of the midline region (presumably glial cells). Upper white solid arrowhead in **H** marks one of the scattered basal precursor cells.

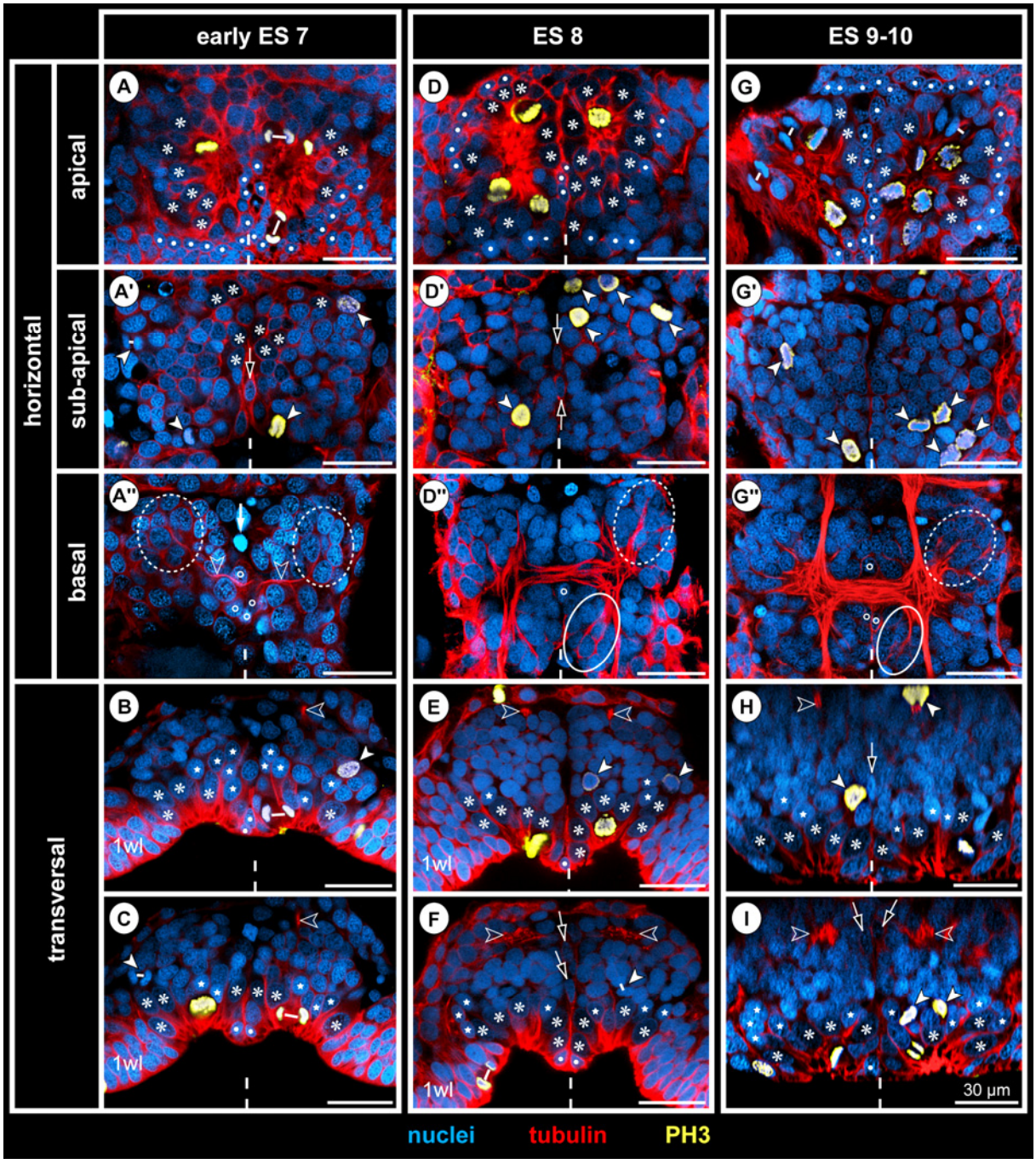
early ES 7
ES 8
ES 9-10
horizontal
apical
sub-apical
basal
transversal
A
A'
A''
B
C
D
D'
D''
E
F
G
G'
G''
H
I
1wl
30 µm
nuclei
tubulin
PH3

Fig. 27: SCNPs and INPs in the hemi-ganglion anlagen of walking leg neuromeres 1 and 2 of *Pseudopallene* sp. (ES 7).

Transversal histological sections. The midline region is indicated by the dashed straight line. Black-framed white arrowheads mark divisions of apical SCNPs. White-framed black arrowheads indicate divisions of sub-apical INPs. Scale bars = 30 µm.

A,**B** Ganglion anlage of walking leg neuromere 1. **A** more anterior than **B**. Note the spindle shape and less intensely stained nuclei of the SCNPs (especially in left hemi-ganglion anlage of **B**). Arrows point to basally differentiating neuropil.

C,**D** Ganglion anlage of walking leg neuromere 2, different specimen than in **A**,**B**. **C** more anterior than **D**. Some SCNPs that are not in division have been marked by asterisks. Note spindle shape of SCNPs (especially in right hemi-ganglion anlage of **D**). The apical division in **D** is clearly tangential, the nature of the sub-apical mitosis (white solid arrowhead) not unambiguously resolvable (sub-apical INP versus basally extending spindle-shaped SCNP).

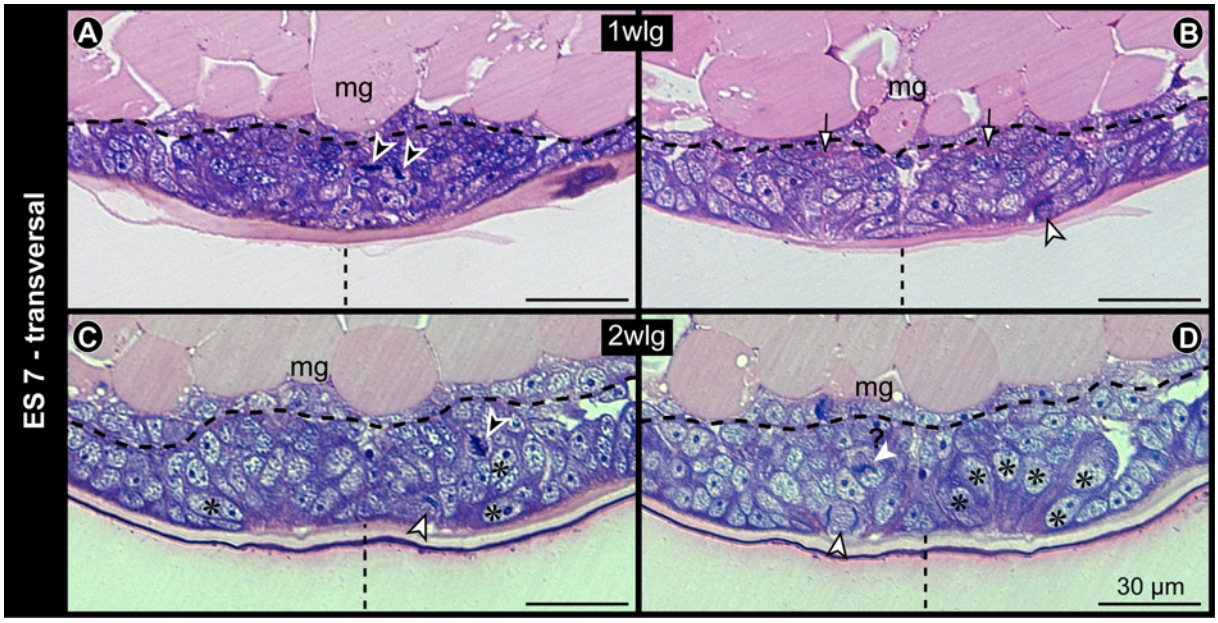
ES 7 - transversal
A
1wlg
mg
B
mg
C
2wlg
mg
D
mg
?
30 µm

Fig. 28: Asymmetric divisions of SCNPs during advanced neurogenesis of *Pseudopallene* sp. (ES 6 – ES 10).

Optical sections of tubulin- and PH3-labeled embryos with nuclear counterstain. Oblique slicers have been aligned to show asymmetries of forming sister cells as clearly as possible. As a consequence, sections are frequently oriented obliquely horizontal or transversal. Dashed lines indicate midline region. White spots mark prospective epidermal cells surrounding the central depression. White arrows mark bigger sister cells (= presumably self-renewing SCNPs). White solid arrowheads mark smaller sister cells. Note the asymmetric positioning and appearance of the forming nuclei in the differently sized sister cells. Frequently, signs of the weakly stained midbody of the degenerating spindle apparatus are still recognizable after the onset of cytokinesis (e.g. **A**,**D**,**I**). Scale bars = 20 µm.

A-C ES 6. **A** Apical 'horizontal' section through hemi-ganglion anlage of walking leg neuromere 1. **B** Apical 'horizontal' section through hemi-ganglion anlage of walking leg neuromere 2. Three asymmetric divisions are visible, the optical section having been aligned to clearly show the one with strongest PH3 signal. **C** Apical 'horizontal' section through hemi-ganglion anlage of walking leg neuromere 2.

D-F Early ES 7. **D** 'Transversal' section through hemi-ganglion anlage of walking leg neuromere 1. **E** Apical 'horizontal' section through hemi-ganglion anlage of walking leg neuromere 1. Two asymmetric SCNP divisions with onset of cytokinesis are visible amongst dividing cells in earlier stages of mitosis. **F** Apical 'horizontal' section through hemi-ganglion anlage of walking leg neuromere 2. The right arrow points at the cytoplasmatic compartment of a bigger sister cell (forming nucleus not included in section). Open arrowhead points to a symmetric division of an apical epidermis precursor.

G ES 8. 'Transversal' section through hemi-ganglion anlage of walking leg neuromere 1. Note the radial arrangement of the forming nuclei at the rim of the apical depression. It remains unresolved whether the marked cells to the left represent sister cells.

H ES 9. Apical 'horizontal' section through hemi-ganglion anlage of walking leg neuromere 1.

I ES 9-10. Apical 'horizontal' section through hemi-ganglion anlage of walking leg neuromere 2.

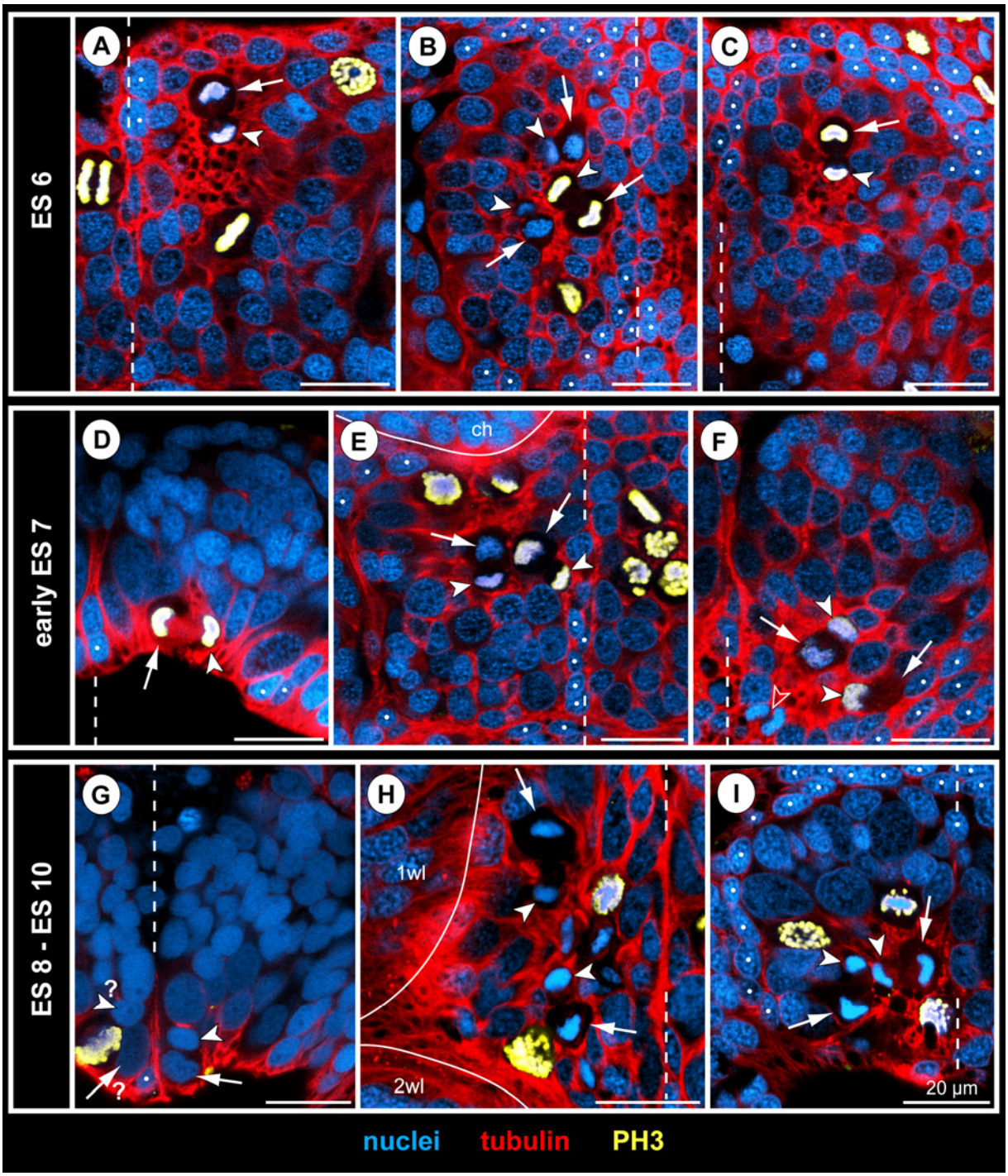
ES 6
A
B
C
early ES 7
D
E
ch
F
ES 8 - ES 10
G
?
?
H
1wl
2wl
I
20 µm
nuclei
tubulin
PH3

Fig. 29: Asymmetric divisions of SCNPs in late ES 7 of *Pseudopallene* sp.

F-actin labeling (TRITC-coupled phalloidin) with nuclear counterstain. Scale bars as indicated in each image.

A Ventral view of complete embryo, Imaris volume (MIP). Note F-actin-positive and largely nuclei-free paired apical depressions in walking leg neuromeres 1 and 2 (arrows). In proboscis and chelifore anlagen, intensely phalloidin-labeled structures represent differentiating muscles and parts of the spinning and chela glands.

B Composite horizontal optical section through ganglion anlage of walking leg neuromere 1. Section through morphologically right hemi-ganglion anlage is positioned slightly more apical than the one through the left. Divisions of big apical SCNPs are highlighted by arrowheads. Note absence of grid-like array of F-actin-positive spots within the invaginating depressions, indicating a lack of defined CISs in this developmental stage.

C,C' Details of single SCNP divisions (late telophase). Oblique slicers have been aligned to show asymmetries of forming sister cells as clearly as possible. As a consequence, the sections are oriented obliquely horizontal. **C** slightly more apical than **C'**. Arrow marks presumably self-renewing SCNP, arrowhead highlights smaller sister cell. Note the significant size differences of the resulting sister cells and the different morphology of the forming nuclei.

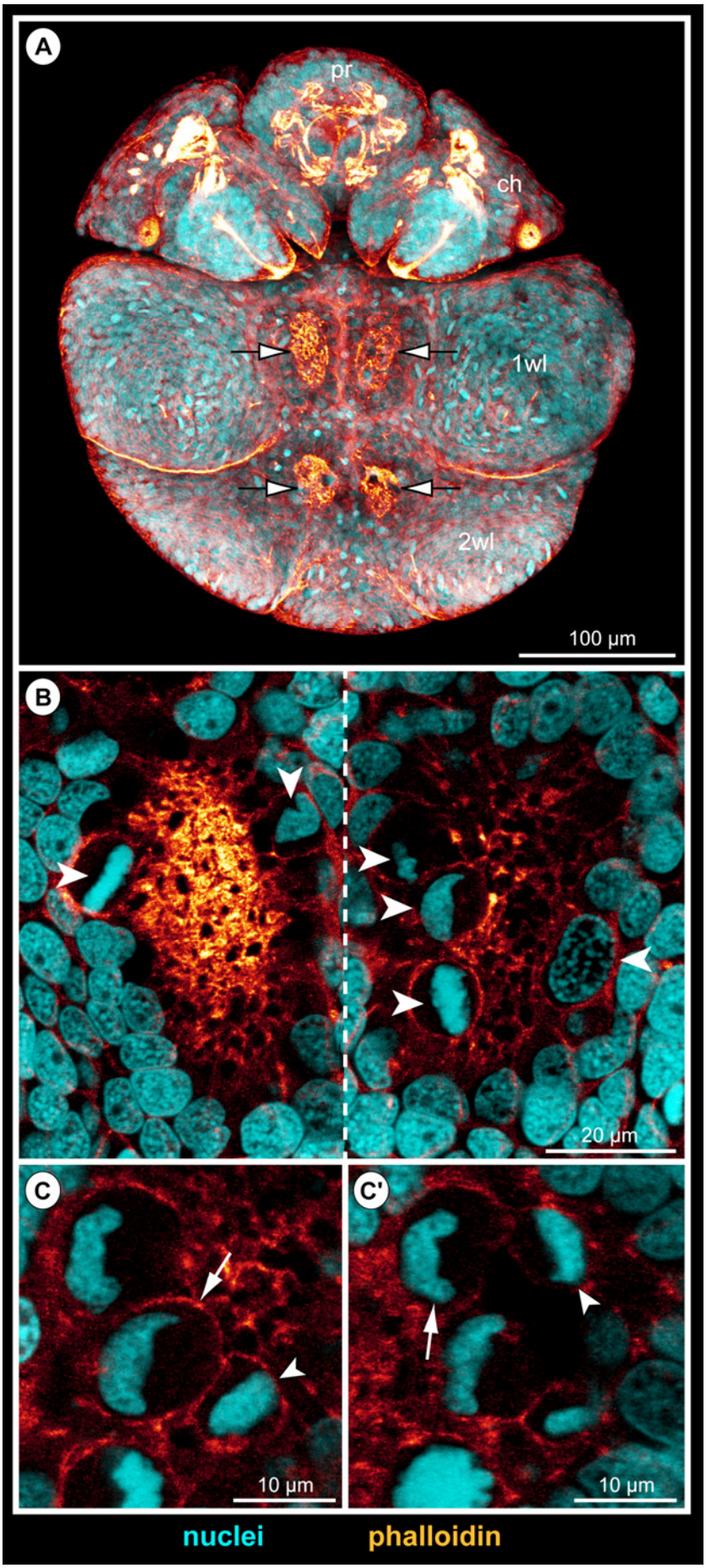
A
pr
ch
1wl
2wl
100 µm
B
20 µm
C
10 µm
C'
10 µm
nuclei
phalloidin

Fig. 30: Nucleus measurements of apical cells in developing walking leg neuromere 1 of *Pseudopallene* sp. (late ES 2 – ad).

The ellipsoid nuclei have been measured along their elongated axis. Arithmetic mean is shown, bars represent standard deviation. Small numbers below the values give the number of specimens analyzed (for further details see 2.8.3.2.).

Up to the formation of the central apical depression (indicated by dashed line A), flask-shaped immigrating cells with basally displaced nucleus (dark red squares) have been measured in comparison to cells with apical nucleus (yellow squares). From depression formation (dashed line A) to complete detachment of the apical cell clusters (dashed line B), the enlarging spindle- to flask-shaped cells lining the depression were measured (dark red circles). The values obtained for late embryonic stages (ES 9-10, stipples outlines) represent most likely an overestimation (for further explanation see 3.3.4.). After detachment of the apical cell clusters, nuclei within the latter have been measured (light red circles).

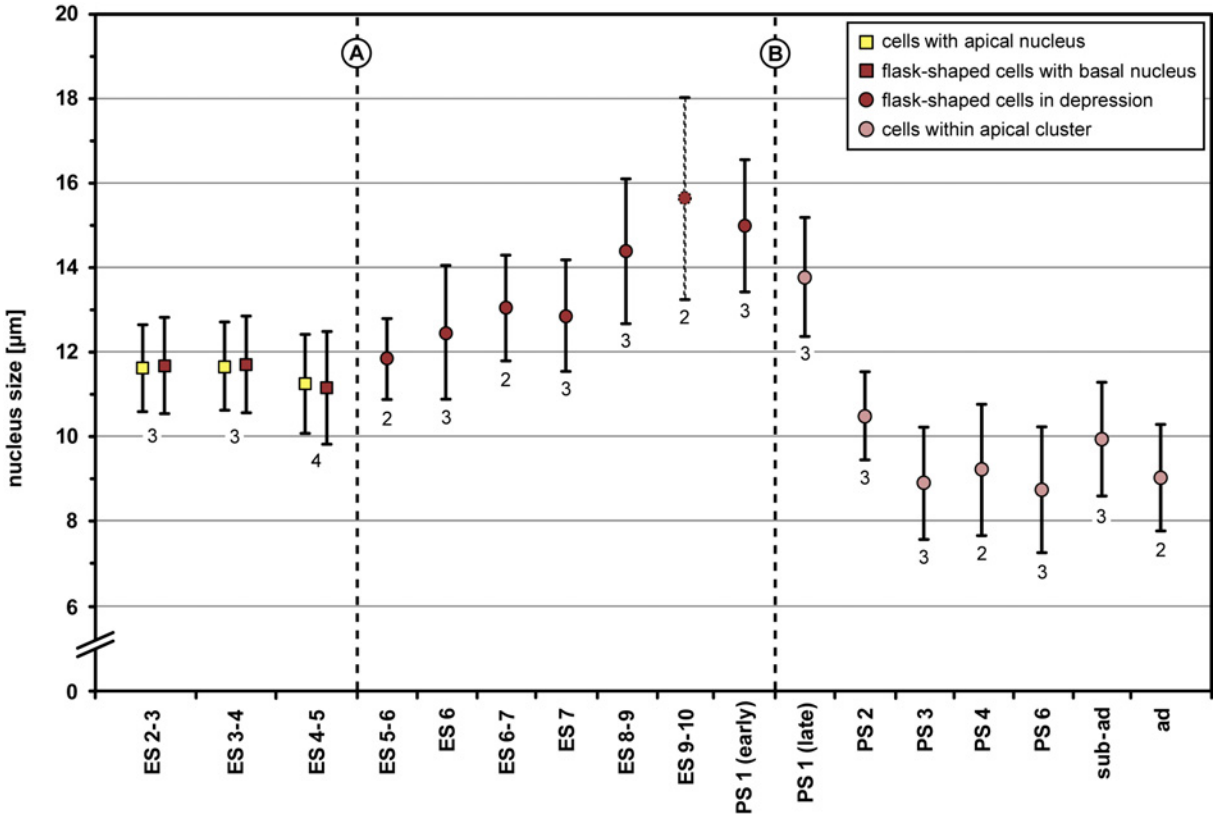
nucleus size [µm]
20
18
16
14
12
10
8
6
0
A
B
cells with apical nucleus
flask-shaped cells with basal nucleus
flask-shaped cells in depression
cells within apical cluster
3
3
4
2
3
2
3
2
3
3
3
2
3
3
2
3
3
2
ES 2-3
ES 3-4
ES 4-5
ES 5-6
ES 6
ES 6-7
ES 7
ES 8-9
ES 9-10
PS 1 (early)
PS 1 (late)
PS 2
PS 3
PS 4
PS 6
sub-ad
ad

Fig. 31: Cell count in the developing walking leg hemi-neuromere 1 of *Pseudopallene* sp. (late ES 2 – PS 6).

Each bar stands for an analyzed specimen. Dark red: immigrating cells with basally displaced nucleus / GCs (including all types of NPs). Yellow: cells with apical nucleus. Green: cells at the margins of apical central depression (ambiguous whether epidermal or neural fate). Light red: cells in apical cluster (in case of early PS 1 not yet fully detached and with deep invagination).

A Overview of counted cell numbers over the course of development. Note slow increase of immigrating/immigrated GCs up to ES 6 and their still considerable increase during the second phase of embryonic neurogenesis as well as in the post-embryonic phase.

B-**G** Spots-model of selected hemi-neuromere counts of different developmental stages. Ventral view to the left, medial view to the right. Note hemi-neuromere compaction along the medio-lateral axis during embryonic development (**B**-**D**). During the second phase of embryonic neurogenesis, the apico-basal extension of formed hemi-ganglion anlage increases dramatically (**D**-**F**). Only after hatching, the hemi-ganglion expands again along the medio-lateral axis (**F**,**G**). The images in **G** have been composed of two separate spot-models, having been obtained from a ventral and a dorsal scan of the same hemi-ganglion (stippled lines indicate borders between spot-models, for further details see 2.8.3.1.). Scale bars = 30 µm.

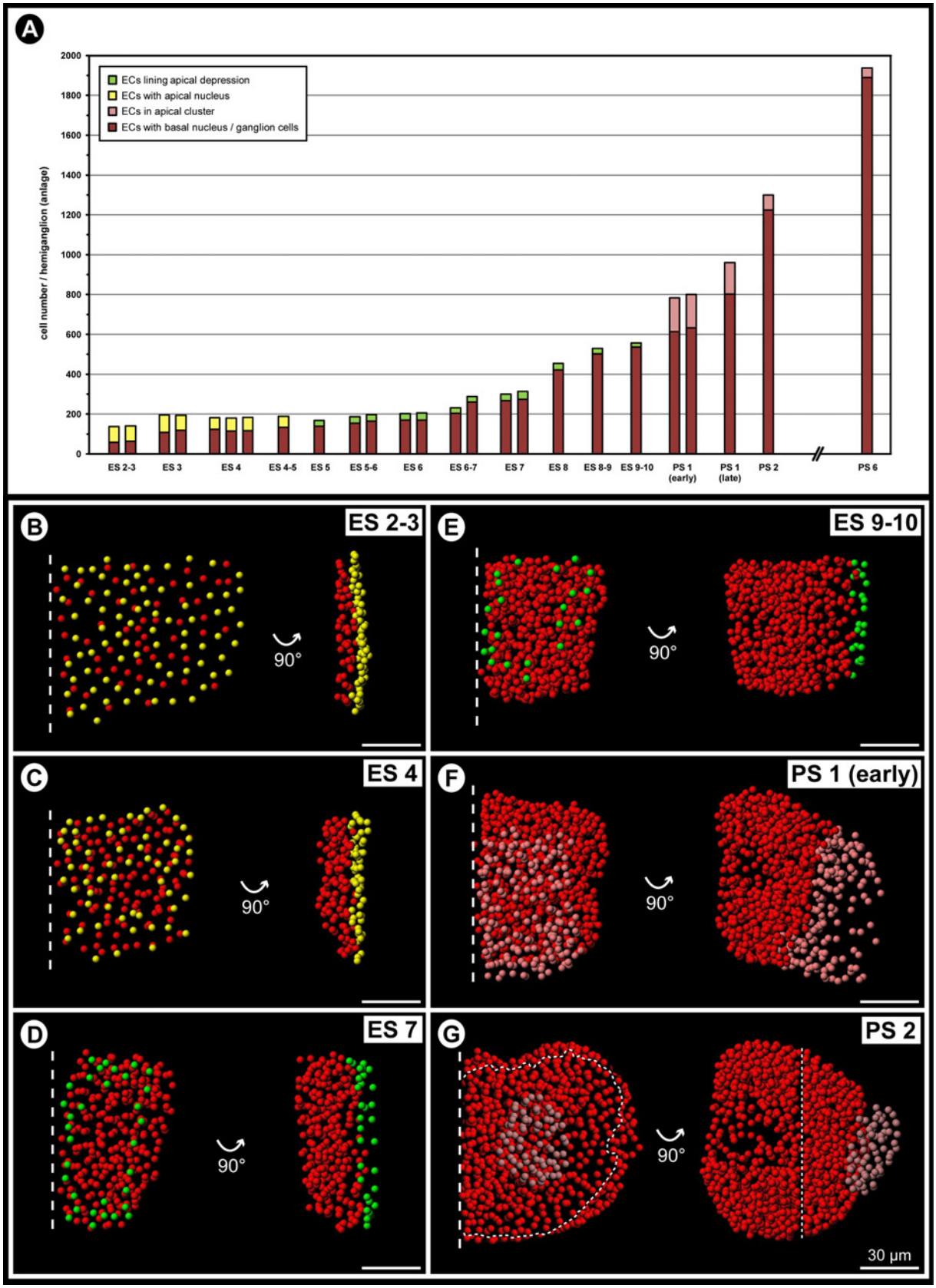
A
ECs lining apical depression
ECs with apical nucleus
ECs in apical cluster
ECs with basal nucleus / ganglion cells
cell number / hemiganglion (anlage)
0
200
400
600
800
1000
1200
1400
1600
1800
2000
ES 2-3
ES 3
ES 4
ES 4-5
ES 5
ES 5-6
ES 6
ES 6-7
ES 7
ES 8
ES 8-9
ES 9-10
PS 1 (early)
PS 1 (late)
PS 2
PS 6
B
ES 2-3
90°
C
ES 4
90°
D
ES 7
90°
E
ES 9-10
90°
F
PS 1 (early)
90°
G
PS 2
90°
30 µm

Fig. 32: Overview of different post-embryonic stages of *Pseudopallene* sp. and corresponding gross anatomy of the VNC (PS 1 – sub-ad).

A SEM micrographs, up to scale. A dramatic increase of overall body size is assessable during post-embryonic development. Scale bar = 1 mm.

B Tubulin labeling with nuclear counterstain. Imaris Surpass mode (volume, MIP). Images up to scale. New segmental ganglion anlagen are added during the first stages of post-embryonic development. A considerable increase of overall size is also assessable for the VNC, although not nearly as pronounced as for overall body size. White arrowheads mark some inter-segmental nerves that were not completely damaged during dissection of the nervous systems. Scale bar = 200 µm.

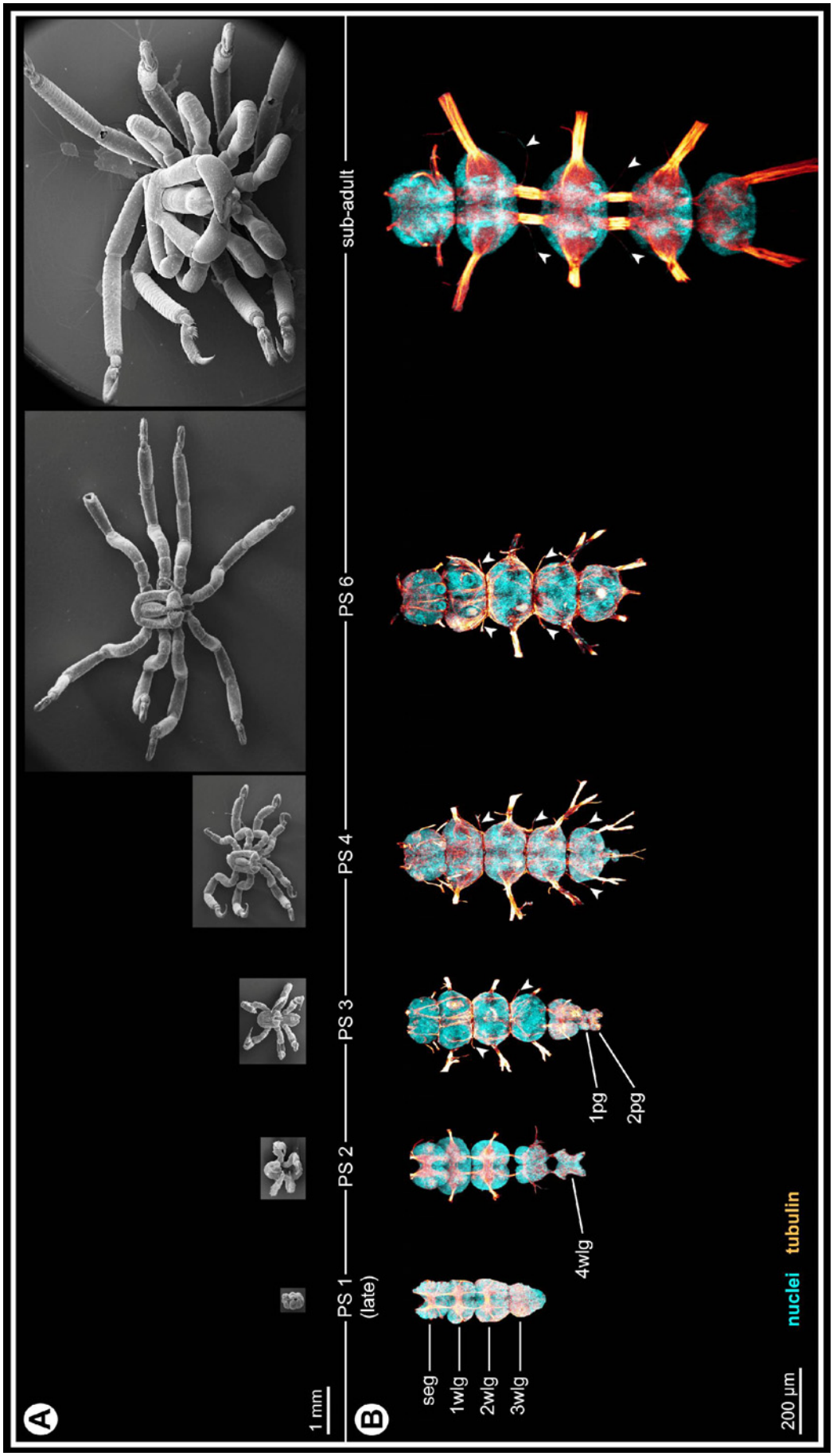
A
1 mm
PS 1
(late)
PS 2
PS 3
PS 4
PS 6
sub-adult
B
seg
1wlg
2wlg
3wlg
4wlg
1pg
2pg
200 µm
nuclei
tubulin

Fig. 33: Invaginated apical pits of the ventral neuromeres in early PS 1 of Pseudopallene sp. SEM micrographs. Scale bars as indicated in each image.

A Lateral view of specimen with removed distal portions of proboscis, chelifores and walking leg anlagen 1 and 2, anterior to the top, dorsal to the left. Arrowhead points to one of the deep apical pits of walking leg neuromere 1, being revealed under the detached ventral cuticle.

B Detail of cuticle region covering the apical pits of walking leg neuromere 1, ventral view. Note the paired depressions that correspond in position to the underlying invaginating pits of the neuromere.

C Ventral view of specimen with removed distal portions of proboscis, chelifores and walking leg anlagen 1 and 2. Asterisk marks pharynx with Y-shaped constricted lumen. The cuticle covering the ventral trunk has been removed to reveal the ventral side of walking leg segments 1 and 2.

D Ventral detail of the apical pits of the palpal and ovigeral neuromeres (paired arrowheads at the top and paired arrowheads at the bottom, respectively). At this stage, the ganglion anlagen of both neuromeres are already fused to form the sub-esophageal ganglion. The epidermis covers already the complete ventral side apart from the pits.

E Magnification of the area indicated in **C**. The deeply invaginated pits of walking leg neuromeres 1 and 2 are shown (arrowheads). As in the palpal and ovigeral segments, the epidermis covers the complete ventral side, except for the apical openings of the pits.

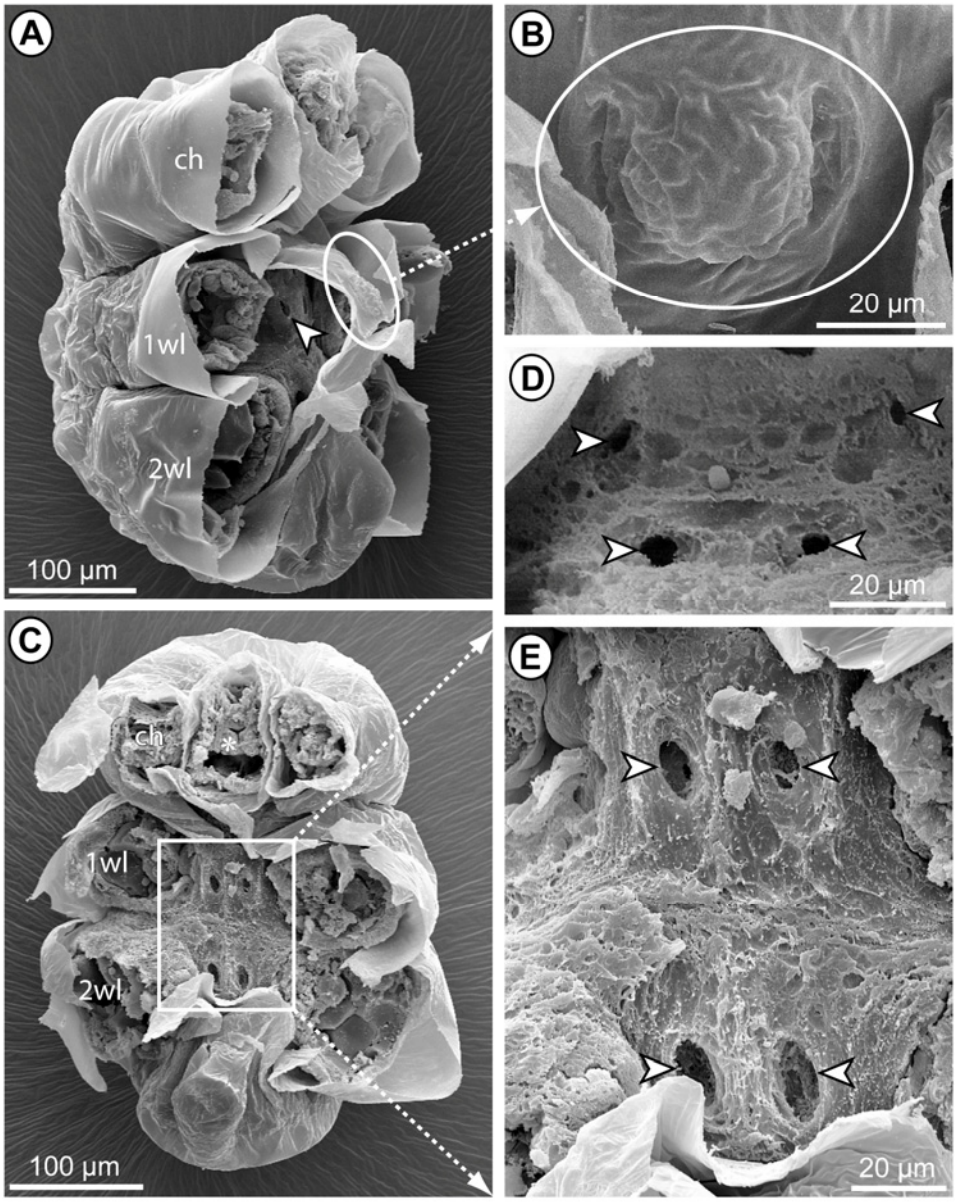
A
ch
1wl
2wl
100 µm
B
20 µm
D
20 µm
C
ch
*
1wl
2wl
100 µm
E
20 µm

Fig. 34: General structure of the developing CNS in early PS 1 of *Pseudopallene* sp.

Histological sections. Stars mark developing ganglionic neuropil. Arrows indicate lumen of the invaginated apical pits. Black-framed white arrowheads highlight divisions. White-framed black arrowheads indicate separation line between nascent apical cell cluster and underlying hemi-ganglion anlagen proper. White-framed gray arrowheads mark pycnotic bodies at the basal side of the nascent apical cell clusters. Note the lighter staining of the big spindle-shaped SCNPs lining the apical pits in comparison to the more basal GCs. Scale bars = 50 µm.

A Composite sagittal section of complete CNS (stippled line indicates border of two images). Sections lie lateral to the midline region. The apical pit of walking leg neuromere 2 is not in the plane of the section. The less differentiated walking leg neuromere 3 still lacks a distinct apical pit. Note the big lightly stained nuclei (stippled oval) in the brain anlage, representing NPs of the antero-medial cluster.

B Horizontal section through the nascent anterior cell cluster of the brain, anterior is to the bottom. In this section, the focus is set on the lumen of the apical pits. The clusters' continuity with the underlying brain anlage is apparent in more dorsal sections (not shown).

C-**F** Transversal sections through the ventral 'embryonic' ganglion anlagen. Note the distinct separation of the nascent apical cell clusters and the corresponding hemi-ganglion anlagen proper (**D**,**E**,**F**). Stippled black ovals (**C**,**E**) highlight median GC somata in close association with the larval commissure.

G Transversal section through anlage of 'post-embryonic' walking leg ganglion 3. White open arrowheads mark the longitudinally extending connective anlagen. Dark stippled outline marks the cells of the medio-laterally compressed midline region. Note the small apical area and low number of cells in the two hemi-ganglion anlagen.

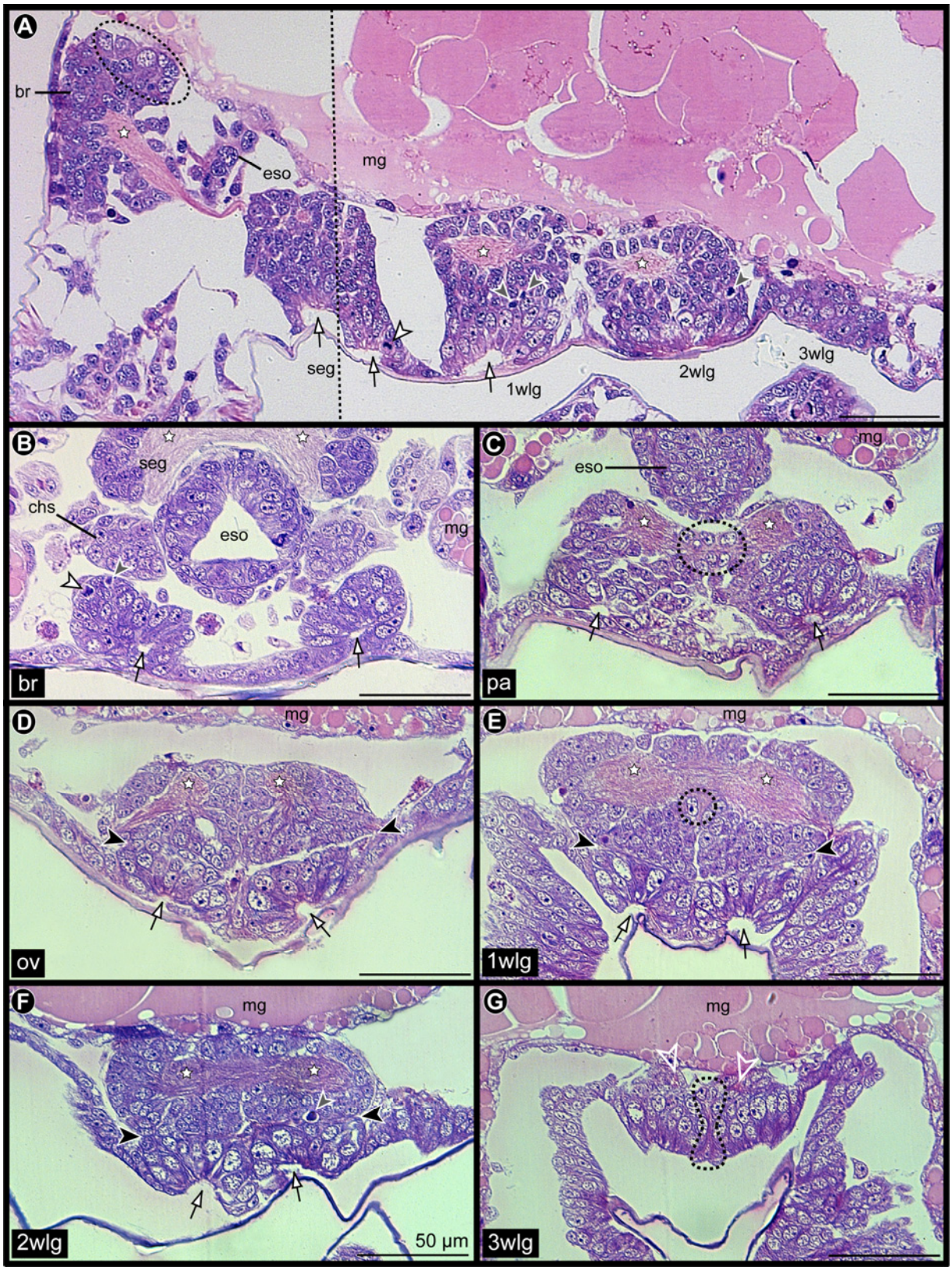
A
br
eso
mg
seg
1wlg
2wlg
3wlg
B
seg
chs
eso
mg
br
C
mg
eso
pa
D
mg
ov
E
mg
1wlg
F
mg
2wlg
50 µm
G
mg
3wlg

Fig. 35: Invaginated segmental pits, apical cluster detachment and mitotic activity in the CNS of *Pseudopallene* sp. (early and late PS 1).

A,B Ventral overview of the VNC in early and late PS 1. Imaris volumes (MIP) of tubulin and PH3-labeled specimens. White circles and ovals mark apical openings of the paired segmental pits. Stippled ovals indicate shallow apical depression of the anlage of walking leg ganglion 3. Asterisks indicate central cavity of completely detached apical cell clusters. Note decrease of overall mitotic activity from early to late PS 1. Scale bars = 50 µm.

C-H Deeply invaginated apical pits and detached apical clusters of the CNS. Optical transversal sections of tubulin- and PH3-labeled embryos with nuclear counterstain. Composite images in which the left side shows early PS 1 and the right one the corresponding region in late PS 1. Arrows point at the lumen of the apical pits or depressions. Solid white arrowheads indicate small flattened epidermis cells. Asterisks label selected big SCNPs (not in division). Open white arrowheads mark sub-apical divisions of INPs. Stars label basal neuropil or axonal pathways. Note decrease of mitotic activity from early to late PS 1 and the fully detached apical clusters with central cavity in three segments (ov-2wl). All images up to scale, scale bar = 30 µm.

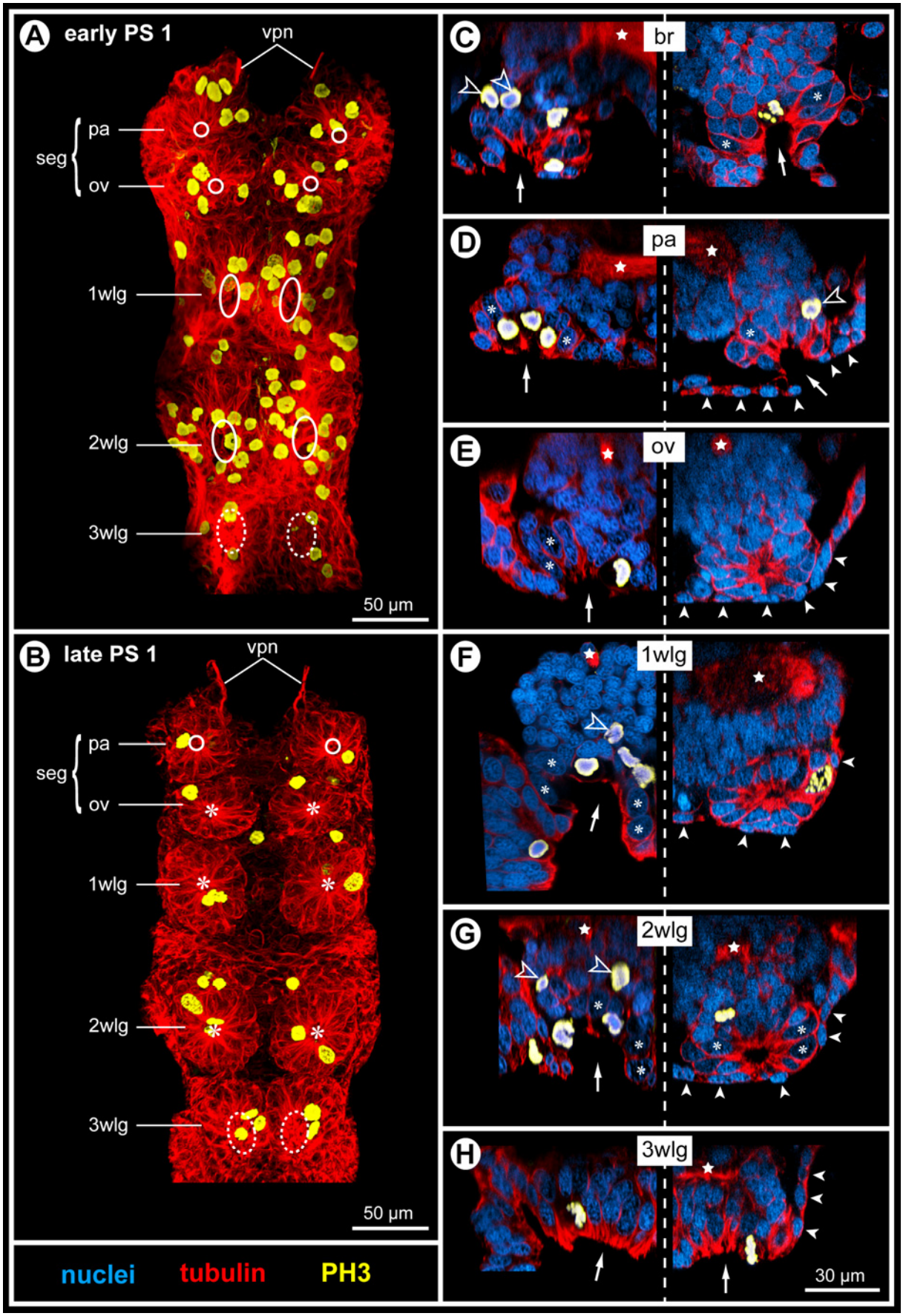
A early PS 1
vpn
seg
pa
ov
1wlg
2wlg
3wlg
50 µm
B late PS 1
vpn
seg
pa
ov
1wlg
2wlg
3wlg
50 µm
nuclei
tubulin
PH3
C
br
D
pa
E
ov
F
1wlg
G
2wlg
H
3wlg
30 µm

Fig. 36: Mitotic activity of NPs in apical pits and detached apical cell clusters of walking leg ganglia 1 and 2 of *Pseudopallene* sp. (early and late PS 1).

Optical sections of tubulin- and PH3-labeled specimens with nuclear counterstain. Horizontal views represent 2D projections of curved composite sections. Stippled outlines mark extensions of nascent apical clusters and ganglion anlagen proper (**A**,**A'**,**C**,**C'**) or anterior and posterior cell streams (**E'**,**G'**). Asterisks label SCNPs. White open arrowheads indicate sub-apical divisions of INPs. Stars mark basal neuropil or axonal pathways. Solid white spots label epidermis cells. Scale bars = 30 µm.

A-B Walking leg ganglion 1 of early PS 1. **A** Section led slightly basal to the small epidermal cells covering the rim of the pit in order to clearly reveal the SCNPs. White solid arrowhead indicates cell processes of three smaller flask-shaped cells intermingled between the SCNPs. **A'** Section shows the bottom of the pit, being characterized by massive proliferation activity of the lining SCNPs (bottom half of image). Anteriorly, two INP divisions are marked. At this stage, each nascent apical cluster extends across the postero-ventral side of the corresponding hemi-ganglion proper. **B** Transversal section through posterior portion of ganglion and nascent apical clusters (posterior to the apical pit). In this region, the connection between both structures is still continuous.

C-D Walking leg ganglion 2 of early PS 1. **C** and **C'** corresponding to **A** and **A'**, respectively. **D** Transversal section through anterior portion of ganglion and nascent apical clusters (anterior to the apical pit). The connection between both structures is still continuous. Note three distinctly tubulin-labeled median somata at the basal side of the commissure (open white spots).

E-F Walking leg ganglion 1 of late PS 1. **E** Section through detached apical cell clusters at the level of the central cavities. Note considerable size differences of SCNPs and the numerous smaller intermingled cells with more brightly stained nucleus. **E'** Section through the more defined anterior and posterior cell streams that extend basally to the apical clusters into the ganglion proper. Note divisions of INPs within the streams. **F** Transversal section showing one hemi-ganglion. The apical cluster is completely detached and covered by a thin layer of loosely spread epidermal cells.

G-H Walking leg ganglion 2 of late PS 1. **G**, **G'** and **H** corresponding to **E**, **E'** and **F**, respectively.

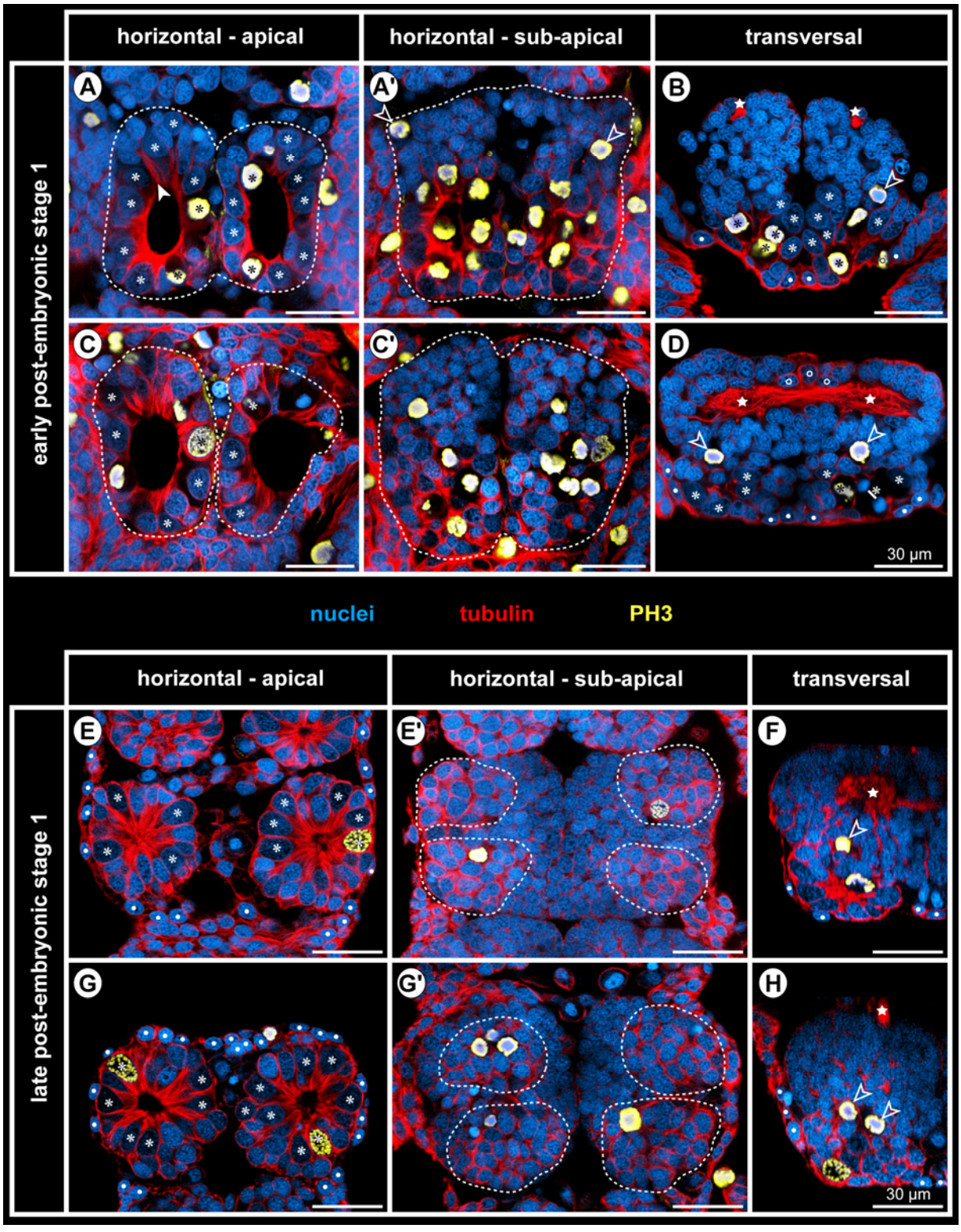
horizontal - apical
horizontal - sub-apical
transversal
early post-embryonic stage 1
A
A'
B
C
C'
D
30 µm
nuclei
tubulin
PH3
horizontal - apical
horizontal - sub-apical
transversal
late post-embryonic stage 1
E
E'
F
G
G'
H
30 µm

Fig. 37: Divisions of apical SCNPs and sub-apical INPs in walking leg ganglia 1 and 2 of *Pseudopallene* sp. (PS 1).

Histological sagittal sections at different levels in one specimen. Big black-framed arrows indicate bigger sister cell of asymmetric divisions (presumably self-renewing SCNPs). Black-framed white arrowheads marks smaller sister cell of asymmetric divisions or apical divisions in meta- or anaphase (asymmetry not assessable). White-framed black arrowheads mark smaller sub-apical divisions of INPs. White arrowheads in **A** mark divisions of epidermal precursors. Small arrows point at lumen of apical pits. Stars label basal ganglionic neuropil. Note the lighter staining of big apical SCNPs in comparison to the more basal smaller GCs. The orientation of the asymmetric division indicated in **A** appears radial, but lies in the lateral wall of the invaginated pit (lumen not in section plane). Asymmetry of the division labeled with question marks (**C)** could not be definitely assessed in the section series. Scale bars = 30 µm.

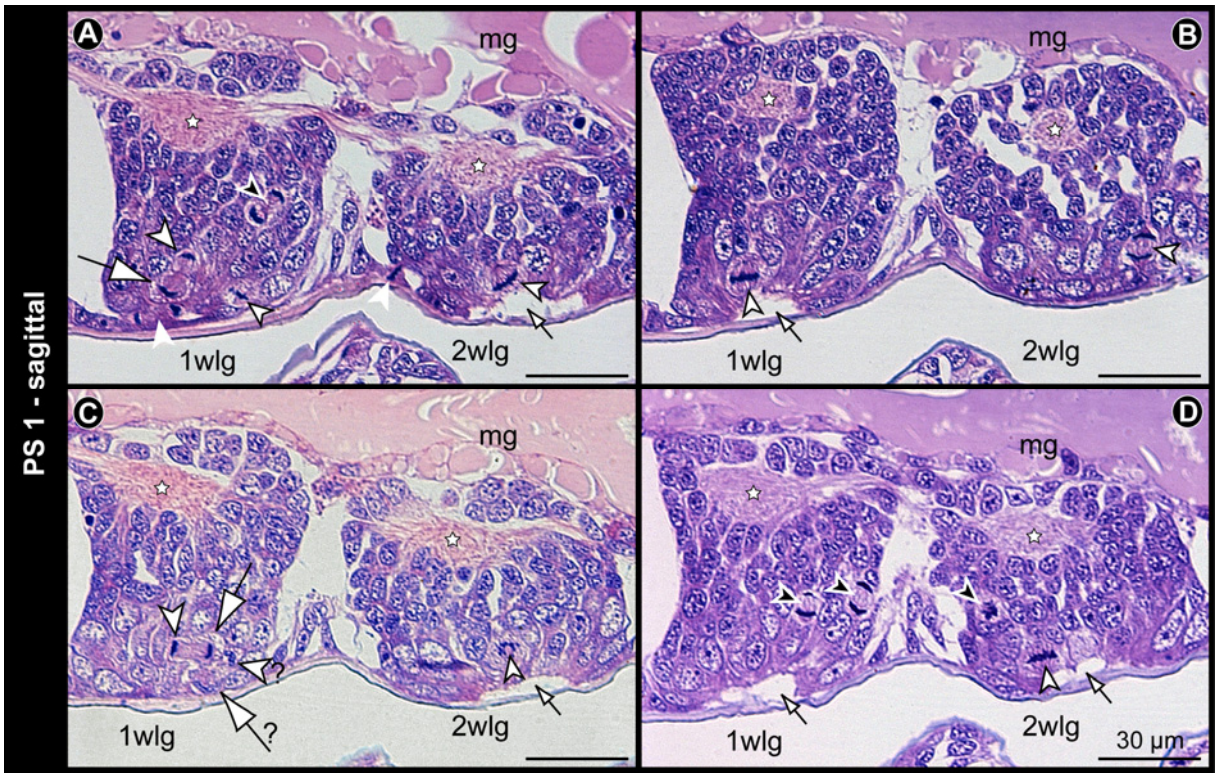
PS 1 - sagittal
A
mg
1wlg
2wlg
B
mg
1wlg
2wlg
C
mg
1wlg
?
?
2wlg
D
mg
1wlg
2wlg
30 µm

Fig. 38: General structure of the developing CNS in early PS 2 of *Pseudopallene* sp.

Histological sections. Stars mark developing ganglionic neuropil. Black-framed white arrows indicate regions where cell streams enter the underlying hemi-ganglion proper. White-framed black arrowheads indicate separation lines between (nascent) apical cell clusters and the underlying hemi-ganglia. Scale bars = 50 µm.

A Composite sagittal section of complete CNS (stippled straight line indicates border of two images). Sections are located lateral to the midline region. Stippled ovals highlight detached apical cell clusters. The apical cluster of the palpal neuromere lies not in the plane of the section. Note the apically attached ganglion anlagen of walking leg segments 3 and 4. White-framed black arrow points at the antero-lateral cell stream of the brain (prospective 'optic nerve').

B-**E** Transversal sections through different ventral ganglia/ganglion anlagen (as indicated in lower left corner). Note decreased cell size and darker nuclear staining in more anterior apical clusters (**B**,**C**) compared to more posterior ones (**D**,**E**). Black-framed white arrowhead in **E** marks apical SCNP division.

F Transversal section through primordium of walking leg ganglion 4. The primordium represents only a spatially restricted area of stratified ectoderm (~2 nuclei layers). Open white arrowheads mark barely recognizable longitudinal connective anlagen.

G Sagittal section through walking leg ganglion 2. The anterior cell stream is not properly visible in the section. Some cells of the apical cluster are still slightly bigger than the GCs.

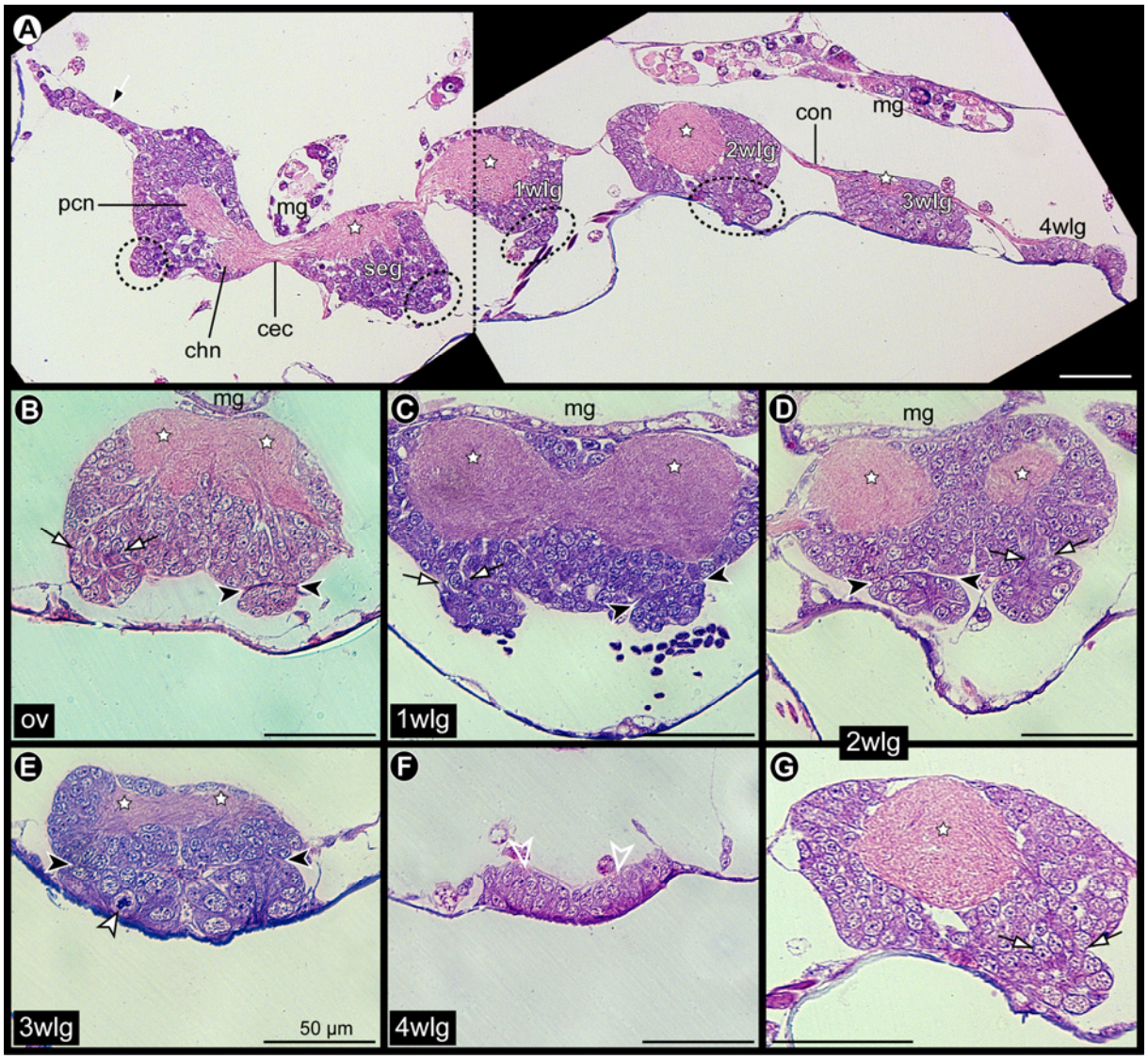
A
pcn
mg
seg
chn
cec
1wlg
2wlg
con
mg
3wlg
4wlg
B
mg
ov
C
mg
1wlg
D
mg
2wlg
E
3wlg
50 µm
F
4wlg
G

Fig. 39: Sensory setae, slit-like cuticular glands and apical clusters in PS 2 of *Pseudopallene* sp.
SEM micrographs (**A**,**B**,**D**) and tubulin labeling with nuclear counterstain (**C**). Scale bars as indicated in each image.

A Ventral view of trunk from walking leg segment 1 to anal tubercle. Note the single inter-segmental constriction between walking leg segments 1 and 2. In the externally still unsegmented posterior trunk region, local accumulations of tiny cuticular folds (open arrowheads) indicate the location of the underlying segmental ganglion anlagen.

B Detail of the ventral cuticle region highlighted in **A**. From PS 2 onwards, the cuticle of trunk (and appendages) bears bifurcate setae (open arrowhead; see also Fig. 11H) and tiny slit-like glands (arrows).

C Anterior *in-situ* view of walking leg ganglion 1. Imaris volume (blend), tubulin-labeling in orange, nuclear counterstain in blue. Clipping planes have been used to remove covering structures. The apical cell clusters (black-framed white arrowheads) are completely detached from the ventral epidermis and possess no direct connection to the cells of the slit-like epidermal glands (arrow) or the sensory setae (open arrowheads; visible due to cuticular autofluorescence). Note the lateral longitudinal muscles (bright orange-yellowish bands) that are located between apical cell clusters and ventral epidermis.

D Ventral view of dissected CNS. The primordium of walking leg ganglion 4 is missing. Arrowheads indicate the detached paired apical cell clusters. Note their slight size increase from anterior to posterior. Star marks the original position of the morphologically left apical cluster (posterior to star) of walking leg ganglion 2. Its anterior cell stream has been ripped during nervous system dissection. In the anlage of walking leg ganglion 3, the nascent apical clusters still cover the entire ventral side of the hemi-ganglia.

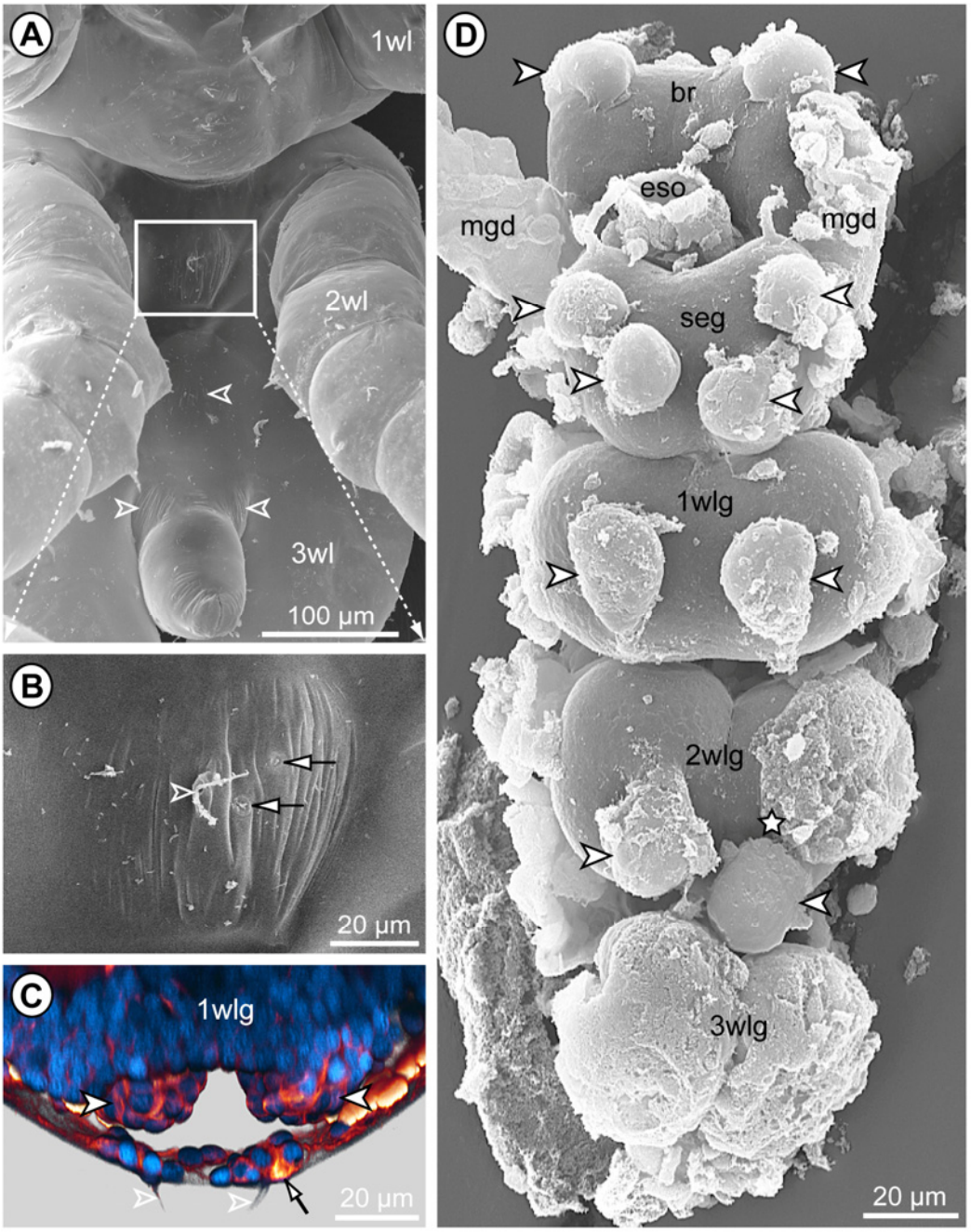
A
1wl
2wl
3wl
100 µm
B
20 µm
C
1wlg
20 µm
D
br
eso
mgd
mgd
seg
1wlg
2wlg
3wlg
20 µm

Fig. 40: Mitotic activity of NPs in detached and nascent apical cell clusters of the VNC of *Pseudopallene* sp. (PS 2).

Tubulin and PH3 labeling of CNSs with nuclear counterstain. Scale bars = 20 µm, except **A** = 50 µm.

A Composite ventral view of CNS. Imaris volume (MIP), nuclear counterstain not shown, stippled lines mark borders of separate images. Circle marks region through which the esophagus passes. Note restriction of mitoses to detached apical clusters in the anterior 'embryonic' ganglia (br–2wlg).

B-G Optical sections through detached and nascent apical clusters and underlying segmental ganglia/ganglion anlagen (as indicated in upper right corner). Transversal (**B**,**D**,**F**) or sagittal (**C**,**E**,**G**) sections above dashed lines, horizontal sections below dashed lines. White arrows mark anterior and posterior cell streams. Open arrowheads indicate sub-apical mitoses close to or within the cell streams. Asterisks (**F**,**G**) highlight apical SCNPs that are not in mitosis. Stars indicate basal neuropil or axonal pathways. Note the tiny central cavities in the detached clusters (br-2wlg) and the nuclei-free central depressions in the nascent apical clusters of the anlage of walking leg ganglion 3. The cell streams in more anterior ganglia are more clearly defined and encompass fewer cells (compare **B**,**D** vs. **F**). Note still recognizable different cell sizes and nuclear staining characteristics in anterior clusters, but lack of numerous closely spaced big SCNPs as characteristic of earlier stages.

H Optical section through primordium of walking leg ganglion 4. Transversal section above dashed line, horizontal section below dashed line. Open arrows indicate basal anlagen of the longitudinal connectives. Note in part recognizable tangential apical mitoses and lack of big SCNPs in this early neurogenic phase.

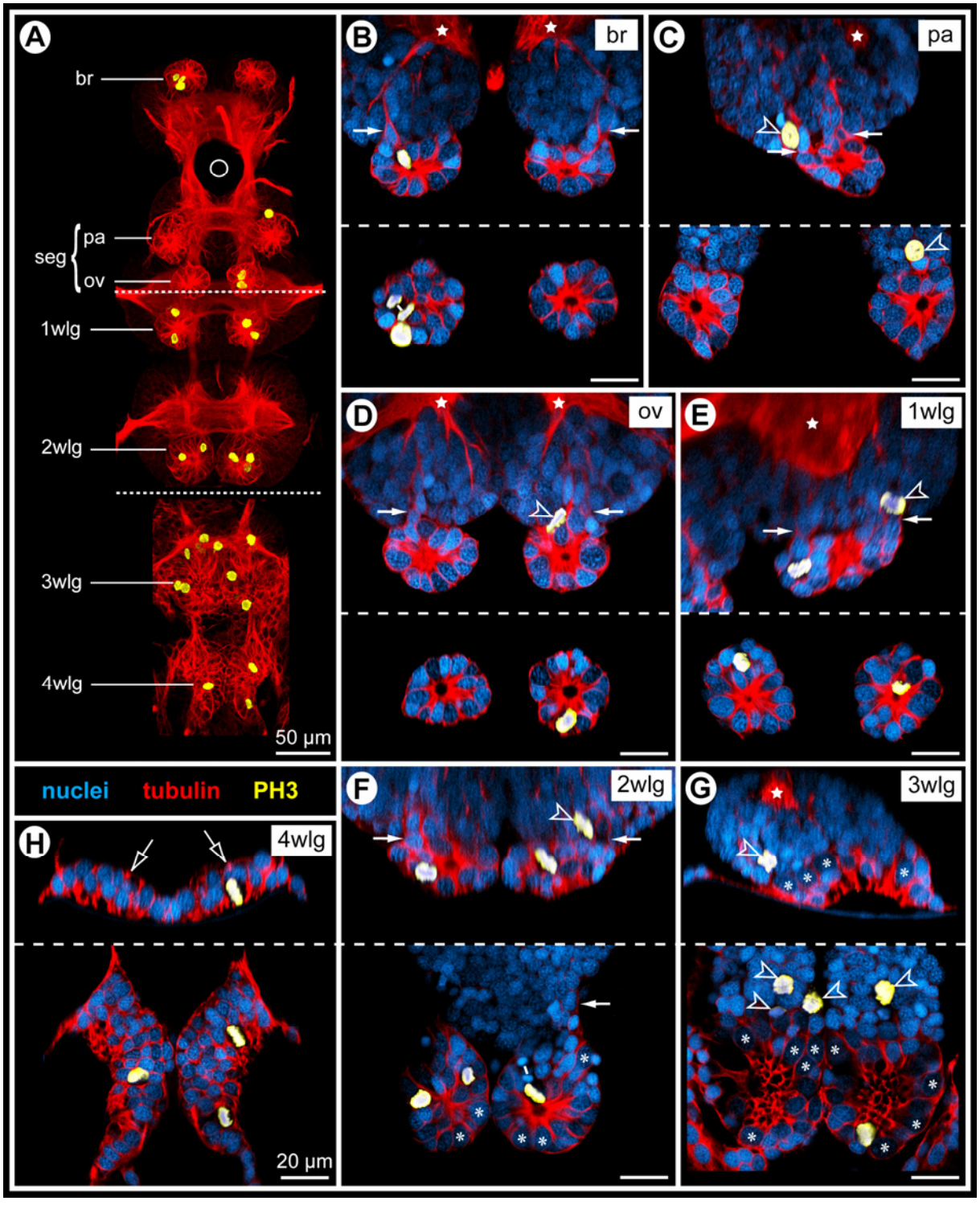
A
br
seg
pa
ov
1wlg
2wlg
3wlg
4wlg
50 µm
B
br
C
pa
D
ov
E
1wlg
nuclei
tubulin
PH3
F
2wlg
G
3wlg
H
4wlg
20 µm

Fig. 41: Mitotic activity of NPs in detached apical cell clusters and cell streams during advanced post-embryonic development of *Pseudopallene* sp. (PS 3 – PS 6).

Optical sections of tubulin- and PH3-labeled dissected CNSs with nuclear counterstain. White arrows label fibrous anterior and posterior cell streams. Big open arrowheads mark sub-apical mitoses close to or within cell streams. Small solid arrowheads indicate oblong nuclei of cells that migrate along the fibrous cell streams. Stars label basal ganglionic neuropil. In composite images (**B-D**,**H**,**J**,**K**), sagittal sections are shown above dashed horizontal lines, horizontal sections below dashed lines (except **D** with transversal section below dashed line). Note absence of distinctly bigger cells in the apical clusters, nuclei of the cluster cells being often slightly more intensely stained than neuronal nuclei. Scale bars = 20 µm.

A-C PS 3. **A** slightly oblique transversal section through sub-esophageal ganglion at the level of the ovigeral cell clusters. Note flattened nuclei (white-framed gray arrowheads) of glial cells in the neural sheath surrounding the functional ganglion. **B**,**C** Note well-defined fibrous cell streams in walking leg ganglion 1 (posterior cell stream ripped during dissection) as opposed to still diffuse cell streams in walking leg ganglion 4.

D-H PS 4. **D** Transversal section runs through antero-medial cell streams of apical brain clusters. Only peripheral regions of clusters themselves included in section. **E**,**F** Sagittal sections. **G** Horizontal section.

I-M PS 6. **I** Transversal section showing detail of ovigeral cell cluster and cell stream. Note the narrow neck of the nuclei (small solid arrowheads) of cluster cells that start to extend into the cell stream. **L** Sagittal section. **M** Horizontal section. The white line extends between two newly forming nuclei during telophase. The cell division is morphologically symmetric.

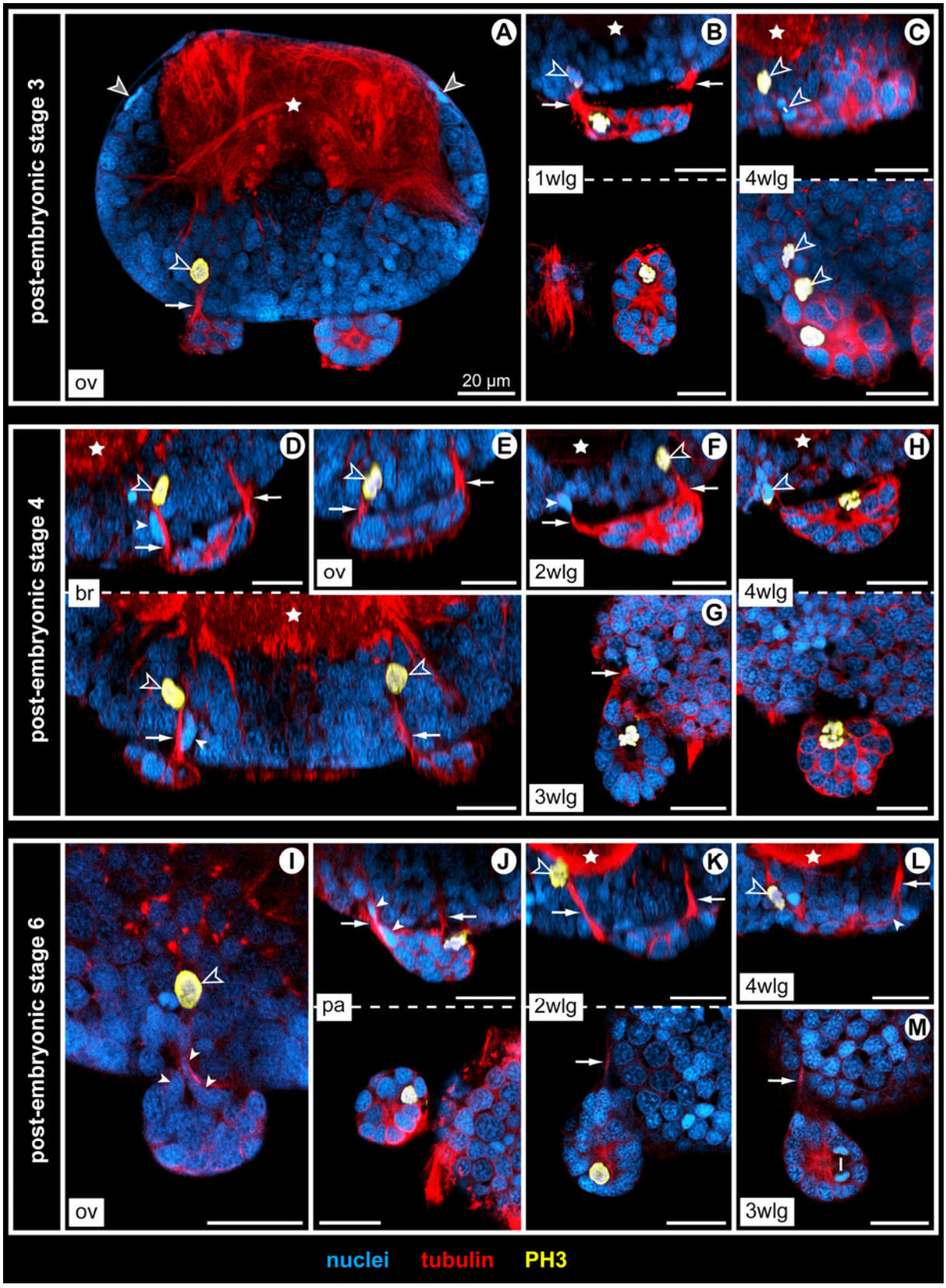
post-embryonic stage 3
A
B
C
ov
20 µm
1wlg
4wlg
post-embryonic stage 4
D
E
F
H
br
ov
2wlg
4wlg
G
3wlg
post-embryonic stage 6
I
J
K
L
M
ov
pa
2wlg
4wlg
3wlg
nuclei
tubulin
PH3

Fig. 42: Persistence of apical cluster-stream-systems into adult *Pseudopallene* sp. (PS 6 – ad).
Sagittal histological sections. Asterisks label apical optic neuropil. Arrows indicate fibrous cell streams. Arrowheads mark the few mitoses encountered in apical cell clusters. **A**,**F**,**K** represent composite overview images in which stippled lines indicate borders between separate images. Adjacent original images show sections at slightly different levels in order to depict more apical cell clusters. Stippled circles highlight apical clusters that are not shown in a separate detail. The palpal ovigeral cluster is not shown in any overview, owing to its far lateral position (see Fig. 39D). Note the similar or occasionally darker nuclear staining of the cluster cells compared to differentiated neuronal nuclei. The anterior brain cluster it located apical to the brain cortex at a level exactly between the protocerebral and the cheliforal neuropils. Scale bars as indicated in each image.
A-E PS 6. Note the tiny central cavity visible in **A**, **D** and **E** (stained in pink).
F-J Sub-adult female. From the sub-adult stage onwards, the ventral apical cell clusters typically assume a more elongated and flattened shape.
K-O Adult male.

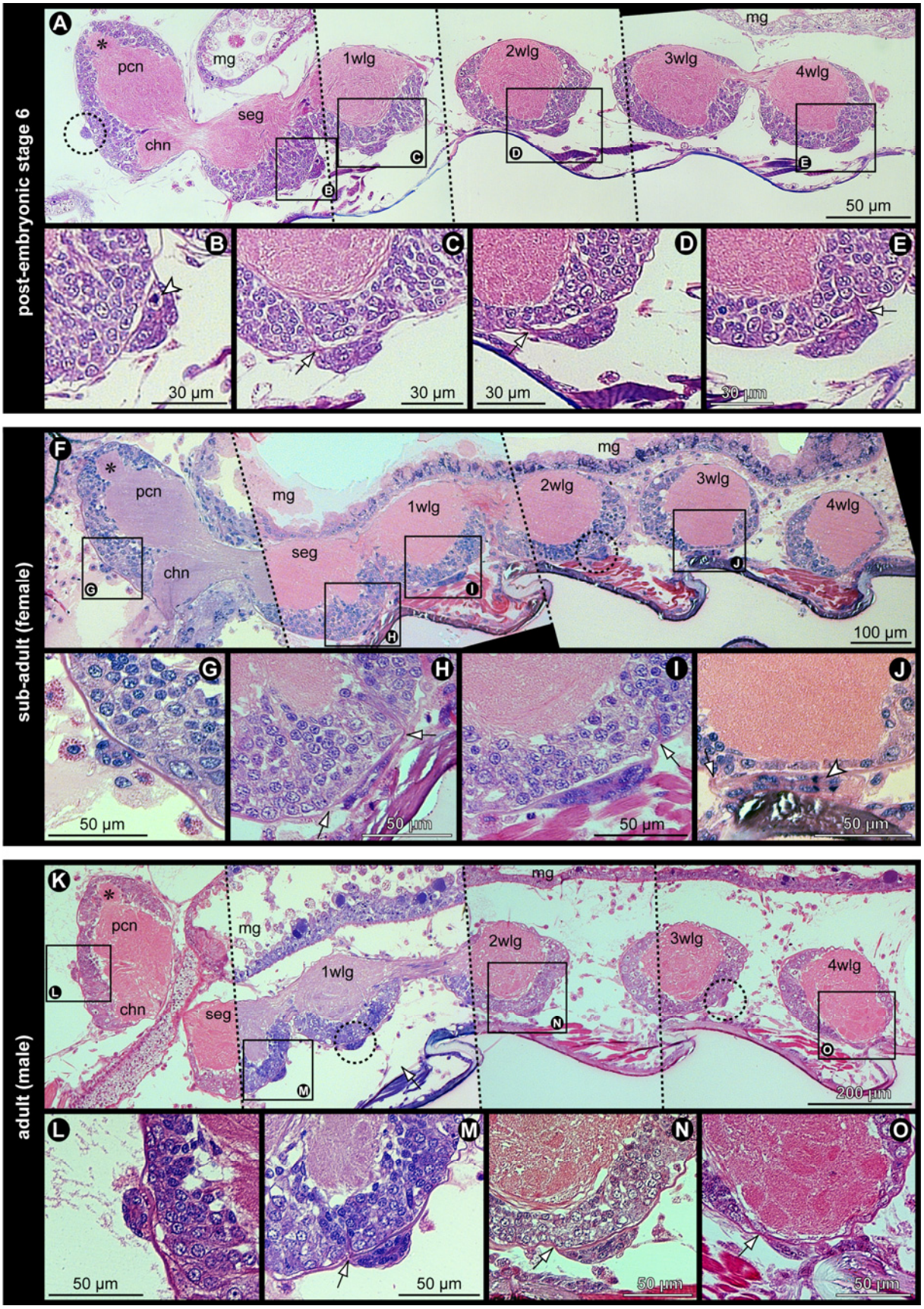
post-embryonic stage 6
A
pcn
mg
1wlg
2wlg
3wlg
4wlg
seg
chn
50 µm
B
C
D
E
30 µm
sub-adult (female)
F
G
H
I
J
100 µm
50 µm
adult (male)
K
L
M
N
O
200 µm

Fig. 43: Cell numbers in apical clusters during development of *Pseudopallene* sp. (PS 2 – ad).
Developmental stages are color-coded as shown in the legend in the upper left corner. Neuromere affiliation/segmental identity of the clusters is shown on x-axis. Each column represents the median of counted cell numbers per specific cluster and developmental stage. The sample size of counted clusters is shown at the bottom of each column. Sample size differences between different clusters of the same developmental stage relate to cluster damage or loss during dissection. 'Error' bars indicate maximum and minimum cell counts. Due to the comparably low sample size, results are not depicted in box-and-whisker plots with quartiles. Complete lack of values (PS 2 – 3wlg, 4wlg) is related to the early differentiation state of ganglion anlagen with no clearly delimitable clusters on the ventral side.

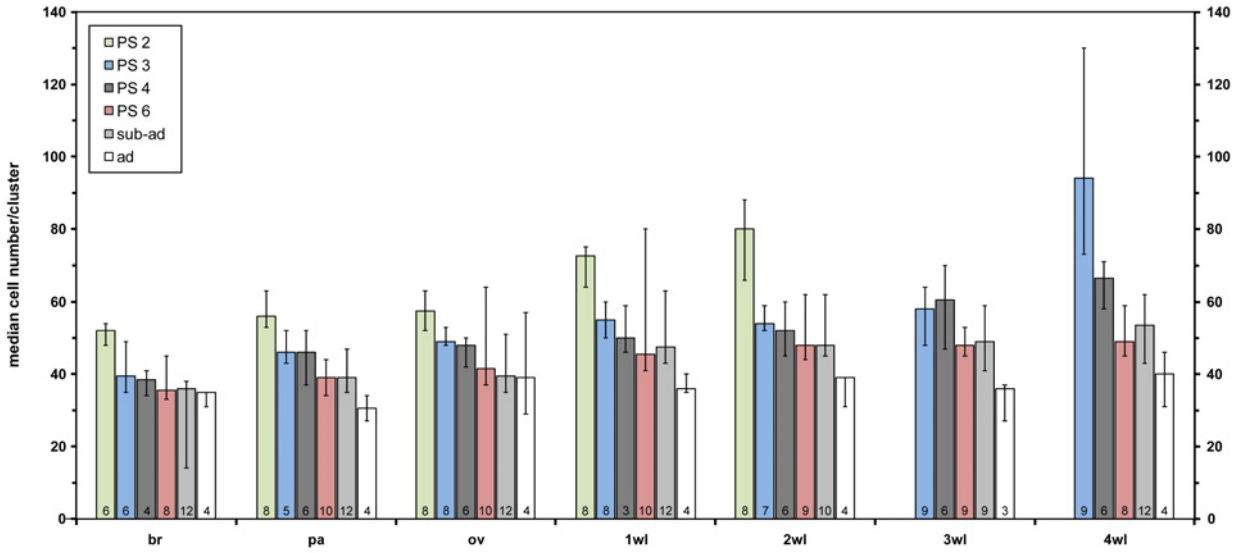
median cell number/cluster
PS 2
PS 3
PS 4
PS 6
sub-ad
ad
0
20
40
60
80
100
120
140
6 6 4 8 12 4
8 5 6 10 12 4
8 8 6 10 12 4
8 8 3 10 12 4
8 7 6 9 10 4
9 6 9 9 3
9 6 8 12 4
br
pa
ov
1wl
2wl
3wl
4wl

Fig. 44: Location of GNs in the CNS of Pycnogonida.

A Schematic drawings showing dorsal aspect (left) and CNS overview (right) of *Ammothea hilgendorfi* (modified from Strausfeld et al. 1998). Dark shading of the walking legs with setae indicates them as locations of chemoreceptors. Black dots within the four walking leg ganglia represent GNs. The U-shaped black structure in the brain represents the MBN.

B-L Histological sections through ventral ganglia of *Pseudopallene* sp. Black stippled ovals highlight regions containing GNs. Arrows point at selected GNs. Arrowheads indicate apical cell clusters. Ganglion identity as indicated in bottom left corner of each image. Scale bars = 100 µm.

B-D PS 6. **B** Sagittal section. **C** Transversal section. **D** Horizontal section. Note the two posterior ganglion anlagen.

E-L Adult. **E-G** Transversal sections. **H-L** Sagittal sections. Note medio-laterally elongate structure of some putative GNs in **E**.

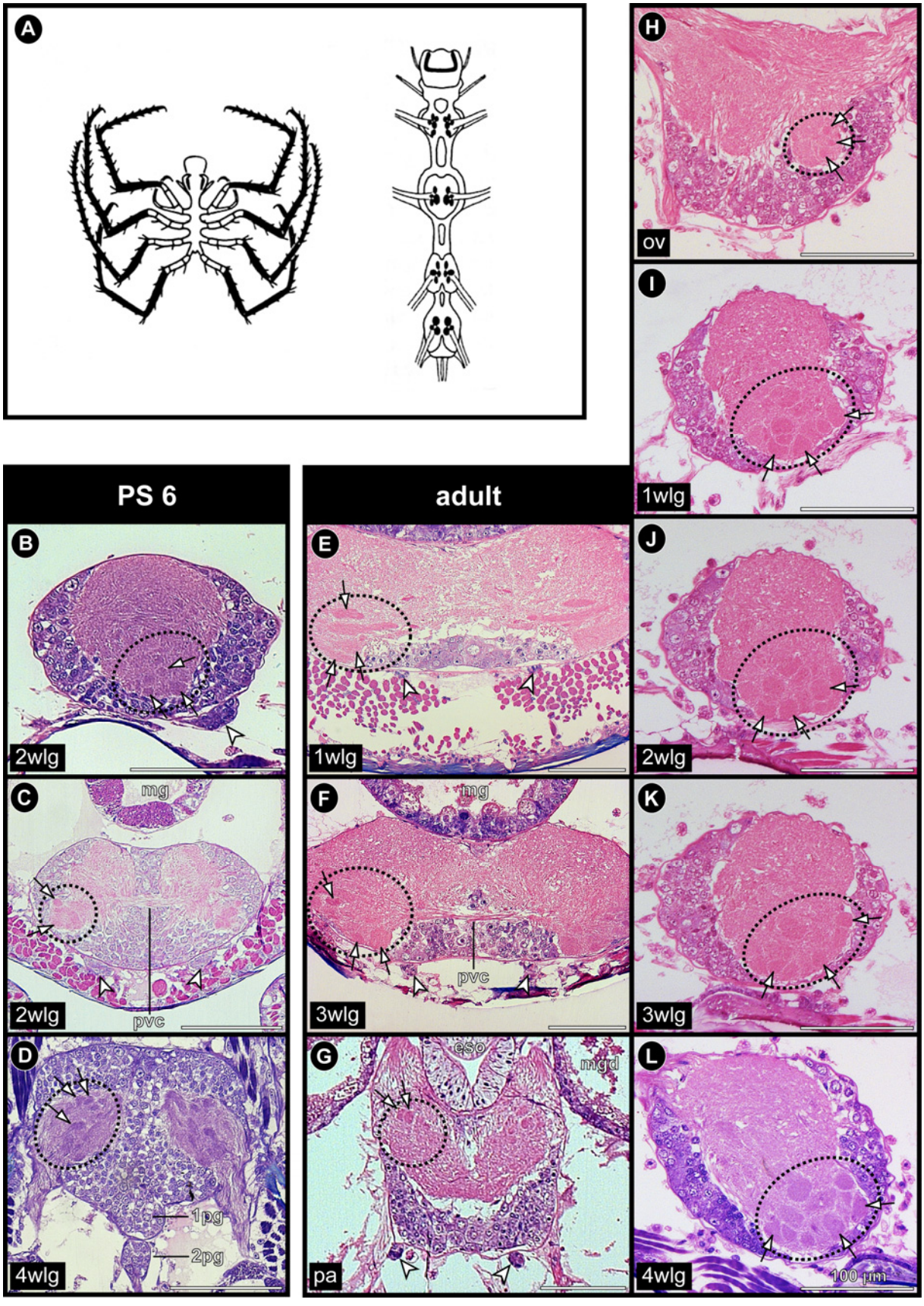
A
PS 6
adult
B
2wlg
C
mg
2wlg
pvc
D
1pg
2pg
4wlg
E
1wlg
F
mg
pvc
3wlg
G
eso
mgd
pa
H
ov
I
1wlg
J
2wlg
K
3wlg
L
4wlg
100 µm

Fig. 45: Early stratification and beginning CIS formation in the pre-cheliforal lobe of *Pseudopallene* sp. (ES 2- late ES 3).

Optical sections of tubulin- and PH3-labeled embryos with nuclear counterstain. All horizontal sections represent 2D projections of curved composite sections. The level of the corresponding transversal sections is indicated to the right of **A'**, **C'**, and **E'**, respectively. Morphologically left pre-cheliforal lobes shown, dashed straight lines to the left indicate the midline region. Circles mark the forming stomodeum/pharynx. Asterisks mark apical regions of selected columnar cells with basally displaced nucleus. Solid and open white arrowheads mark constricted apical processes of selected flask-shaped cells. Solid and open spots mark more basal regions of the same selected cells (compare horizontal and corresponding transversal sections). Note tangential orientation of cell divisions (where assessable). Scale bars = 30 µm.

A-B' Early ES 2. The cells of the stomodeal anlage are in the process of immigration (curved line in **B**). Note absence of distinct flask-shaped cells.

C-D' ES 2-3. Note increase of basally displaced nuclei (**C''**) resulting in a locally bi-layered structuring of the pre-cheliforal lobe (**D'**). The stomodeum has extended basally (outlines in **D,D'**). Arrow in **D'** points at two presumptive sister cells of an apical tangential division.

E-F' ES 3-4. First regions of more intense apical tubulin labeling (=nascent CISs) start to become discernible (open arrowheads in **A**). Note denser packing of basally displaced nuclei (**E''-F'**). Arrow in **E''** and **F'** points at one of the few basal mitoses (prophase). Star (**E-E''**) marks damaged region. Curved line (**F,F'**) highlights developing pharynx.

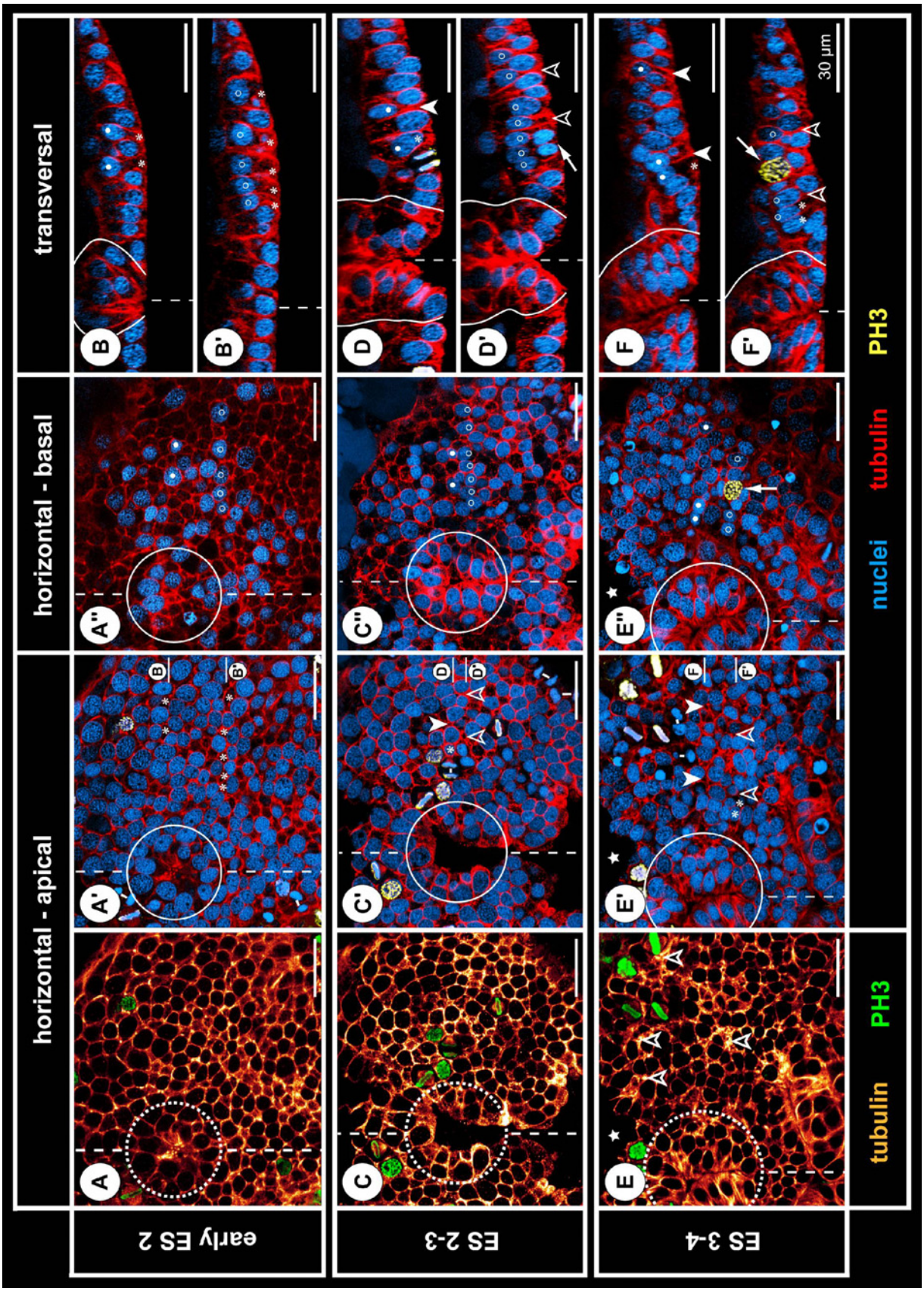
transversal
horizontal - basal
horizontal - apical
early ES 2
ES 2-3
ES 3-4
A
A'
A"
B
B'
C
C'
C"
D
D'
E
E'
E"
F
F'
30 µm
tubulin
PH3
nuclei
tubulin
PH3

Fig. 46: CIS pattern in the pre-cheliforal lobe of *Pseudopallene* sp. (ES 4 – ES 6).

Left column: Ventral overviews of pre-cheliforal lobe, proboscis and chelifore anlagen. Tubulin-labeled embryos, Imaris volume (MIP). Stippled circle marks developing pharynx. The chelifore anlagen are outlined. Stars in **G** and **I** indicate dissected chelifore. Note the bright spots in the pre-cheliforal lobe, relating to apically bundled cell processes of CISs. Scale bars = 50 µm.

Middle column: Apical optical sections through pre-cheliforal lobe of the same embryos as shown to the left, respectively. The apically bundled cell processes of selected CISs are highlighted by colored arrowheads. Color-coding serves to distinguish sub-groups: red = antero-medial CISs, green = lateral CISs, blue = medial CISs, yellow = central CISs, gray = posterior CISs, light blue = antero-median CIS, black = unidentified CISs. Stippled circle marks developing pharynx. Straight dashed line to the left indicates midline region. Small stippled oval (**E'-I'**) shows the position of the pre-proboscideal pit. Star in **C'** marks damaged region. Note apical cell divisions. Scale bars = 30 µm.

Right column: Schematic representation of the observed CIS pattern. Color-coding identical to middle column, the same CISs highlighted in the latter are indicated by arrowheads. Diameter of solid spots indicates distinctness of a CIS in the investigated specimens. Open colored spots with stippled outlines (**F**,**H**,**J**) indicate dissociation of CIS or insufficient resolution in the invaginating sub-regions of the pre-cheliforal lobe. Gray stippled outlines represent pre-proboscideal pit, antero-lateral depression and central depression. Note early appearance of the shallow central depression. Curved arrow at the antero-lateral side illustrates the morphogenetic rearrangement of the pre-cheliforal lobe in relation to the proboscis anlage.

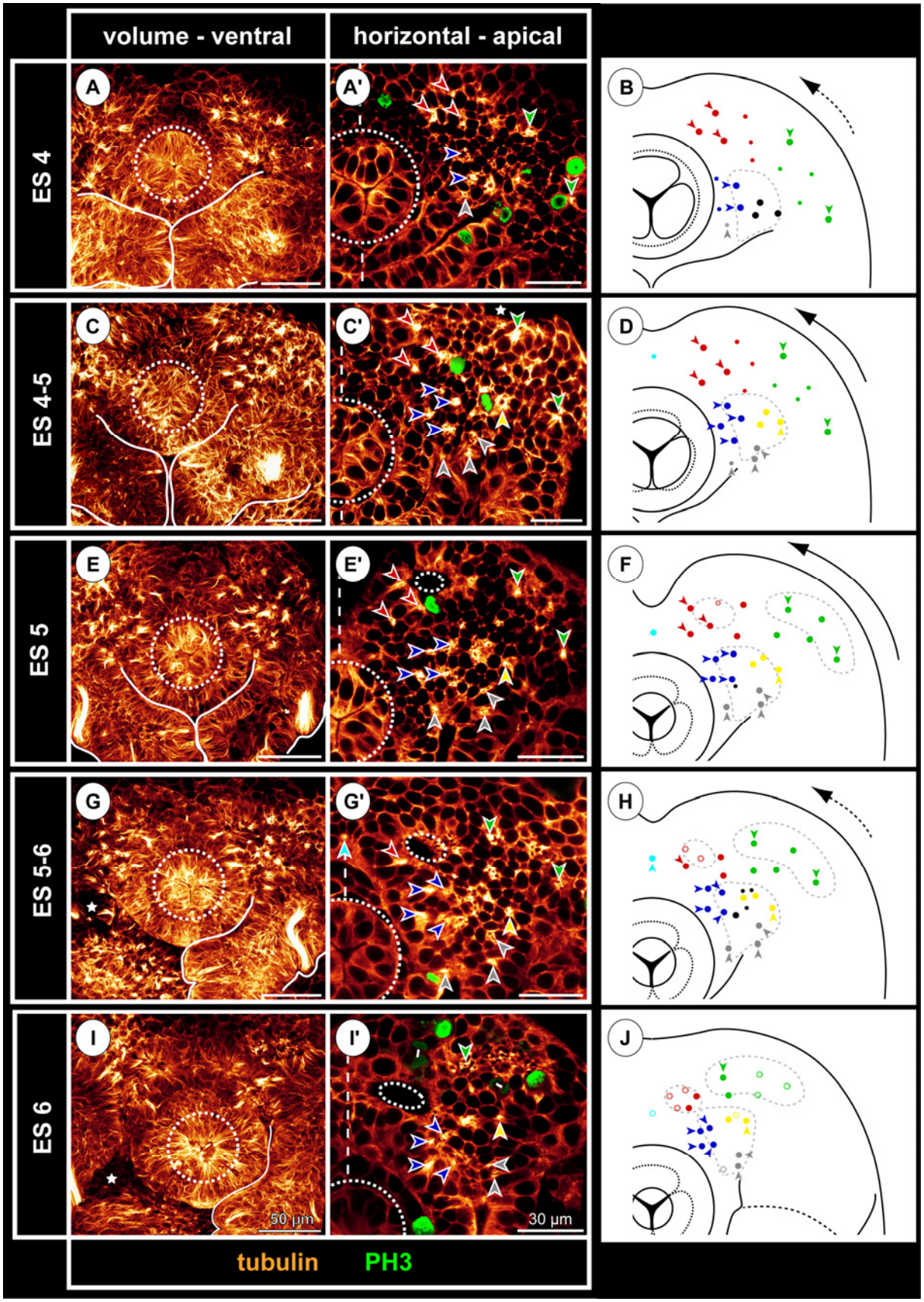
volume - ventral
horizontal - apical
ES 4
ES 4-5
ES 5
ES 5-6
ES 6
A
A'
B
C
C'
D
E
E'
F
G
G'
H
I
I'
J
50 µm
30 µm
tubulin
PH3

Fig. 47: Formation and development of pre-proboscideal pit, antero-lateral depression and central depression in the pre-cheliforal lobe of *Pseudopallene* sp. (ES 4 – ES 6).

Optical sections of tubulin- and PH3-labeled embryos with nuclear counterstain. All horizontal sections represent 2D projections of curved composite sections. The level of the corresponding transversal sections is indicated in the images of the right column. Morphologically left pre-cheliforal lobes shown, dashed straight lines indicate the midline region. Circles mark the developing pharynx.

Finely dashed outlines represent the sub-region from which the pre-proboscideal pit develops. Solid outlines indicate the sub-region from which the antero-lateral depression arises. Coarsely dashed outlines mark the sub-region of the central depression. Solid white arrowheads mark apically bundled cell processes of selected CISs (compare horizontal and corresponding transversal sections). Note several apical mitoses. Scale bars = 30 µm.

A-B' ES 4. White spots mark basally displaced nuclei of the flask-shaped cells constituting the CISs marked by white solid arrowheads.

C-D' ES 4-5. Open white arrowhead in **C'** and **D'** highlights one of the few mitoses (prophase) in flask-shaped cells. Note distinct central depression (**D'**), but no indications of pre-proboscideal pit or antero-lateral depression (**D**,**D'**). Star (**C**) marks damaged region.

E-F' ES 5. Paired white arrows in **E'** mark the presumptive border between protocerebral and cheliforal neuromeres. Note distinct invagination of pre-proboscideal pit (**E**,**F**). The CISs of the central depression have apico-basally elongated and comprise more cells (**F'**).

G-H' ES 5-6. Small arrow in **G** points at the unpaired antero-median CIS. Small arrow in **G'** indicates a persisting antero-medial CIS at the bottom of the invaginating pre-proboscideal pit. Postero-medial to the latter, a basal mitosis is visible (open white arrowhead). The paired bigger white arrows in **G'** mark the presumptive border between protocerebral and cheliforal neuromeres. Note persisting elongate appearance of the CISs in the central depression.

I-J' ES 6. The deepened pre-proboscideal pit starts to constrict basally (**J'**). White arrow in **I'** points at detached immature GCs/NPs posterior to the pre-proboscideal pit and medial to the central depression.

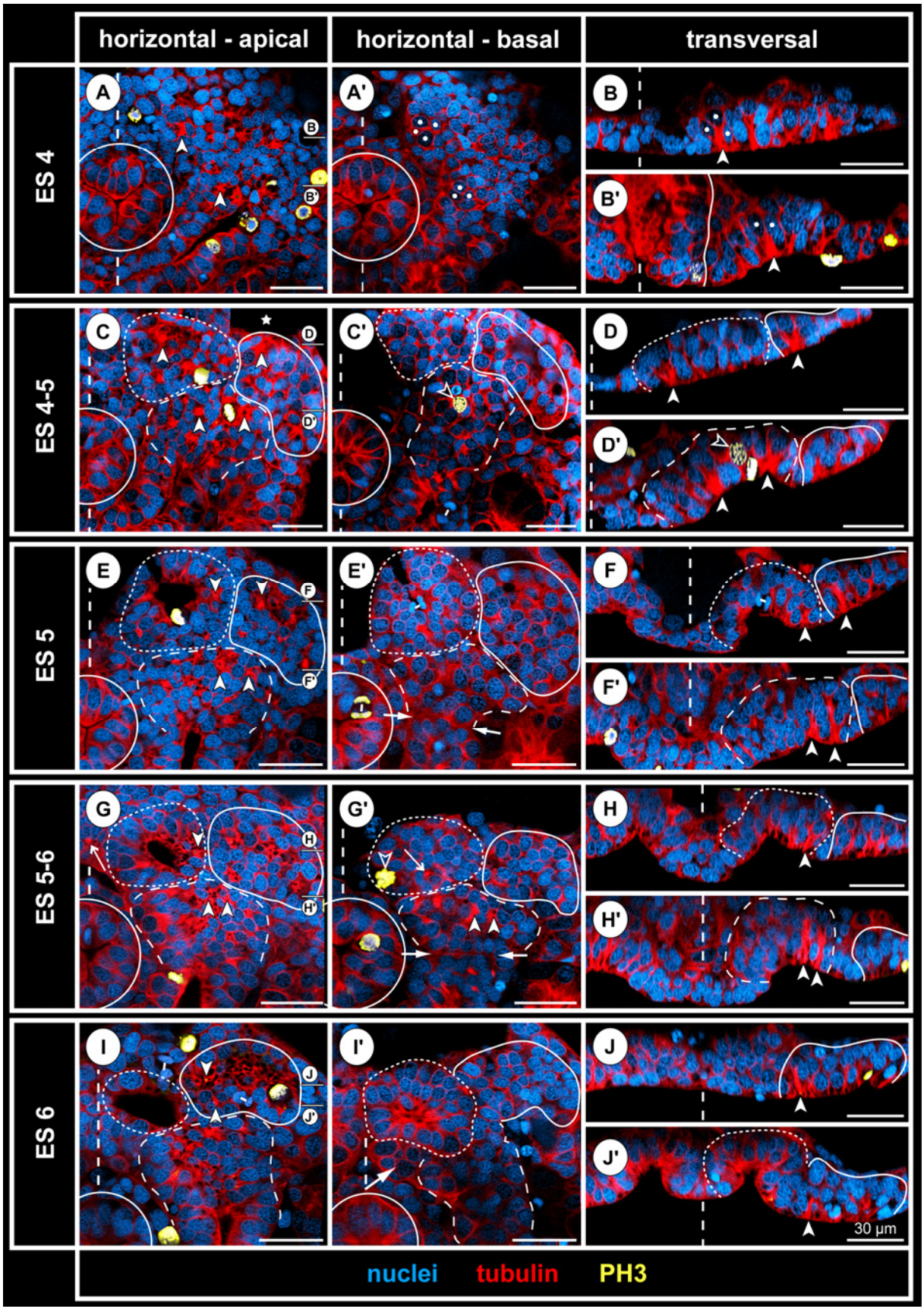
horizontal - apical
horizontal - basal
transversal
ES 4
ES 4-5
ES 5
ES 5-6
ES 6
A
A'
B
B'
C
C'
D
D'
E
E'
F
F'
G
G'
H
H'
I
I'
J
J'
30 µm
nuclei
tubulin
PH3

Fig. 48: Further development of pre-proboscideal pit, antero-lateral depression and central depression in the brain anlage of *Pseudopallene* sp. (ES 6-7 – ES 8-9).

Optical sections of tubulin- and PH3-labeled embryos with nuclear counterstain. Brain anlagen of left body half, dashed straight lines indicate the midline region. Finely dashed outlines frame the cells of the pre-proboscideal pit. Solid outlines mark the sub-region of the antero-lateral depression. Coarsely dashed outlines mark the sub-region of the central depression. Scale bars = 30 µm.

A-D' All horizontal sections represent 2D projections of curved composite sections. The level of the corresponding transversal sections is indicated in **A''** and **C''**, respectively. White spots mark selected epidermis cells adjoining the cell internalization regions of the brain.

A-B' ES 6. White solid arrowheads point at some few remaining recognizable CISs. White arrows (**A-A''**) mark the putative border between protocerebral and cheliforal neuromeres. White open arrowheads point at basal divisions (putative NPs). Note the tiny apical pore of the pre-proboscideal pit (**A'**,**B**) and the circular shaped of the antero-lateral depression (**A**,**A'**). Some portions of outgrowing axons (small arrow) are visible in the section of **A''**.

C-D' ES 7. The cells of the pre-proboscideal pit have completely detached from the apical surface. White arrowhead in **C'** marks apical mitosis close to the antero-lateral depression (specimen not PH3-labeled). Note almost perfect antero-posterior alignment of the spatially restricted antero-lateral and central depression. Basally, the cell stream between brain primordium and apical antero-lateral depression has become more defined (**C''**). Note differentiating protocerebral neuropil (stars in **C''-D'**) anterior to the pre-oral commissure (**C''**).

E-G ES 8-9. The compact three-dimensional anlage of the brain extends far basally into the embryo. Due to the simultaneous dorsal flexure of the protocerebral region, proper flat-preparation of the brain region is not possible any longer. Horizontal sections (**E-E''**) relate to the neuraxis and translate into approximate transversal body axis sections. Transversal sections (**F**,**G**) translate into oblique body axis horizontal sections. Asterisks label selected big SCNPs. Stars mark differentiating protocerebral neuropil.

E The brain anlage remains attached to the apical surface only via the antero-lateral depression (solid outlines) and the remainder of the central depression (coarsely dashed outline). The remaining small apical cells form the epidermis.

E',**E''** The bilaterally paired antero-medial cluster comprising NPs is attached to the basal side of the brain anlage (finely stippled outline). The antero-lateral cell stream (solid outlines) merges with the brain anlage antero-laterally (**E'**). The nascent brain cell cluster (coarsely dashed outline) as derivative of the central depression is wedged between proboscis and chelifore base and shows a deep invagination. Within the midline region, mitoses of NPs relating to the unpaired median proliferation cluster are visible (open white arrowheads in **E''**).

F,G Two different specimens. Note slight invagination of the antero-lateral depression (especially in **F**) and cell divisions in the latter (**G**). Open white arrowheads mark divisions close to or in the midline region. Arrows point at slender neurite bundle (= anlage of 'optic nerve') between protocerebral neuropil and the cells of the antero-lateral depression. The embryonic cuticle covers the antero-lateral depression (white arrowhead in **G**).

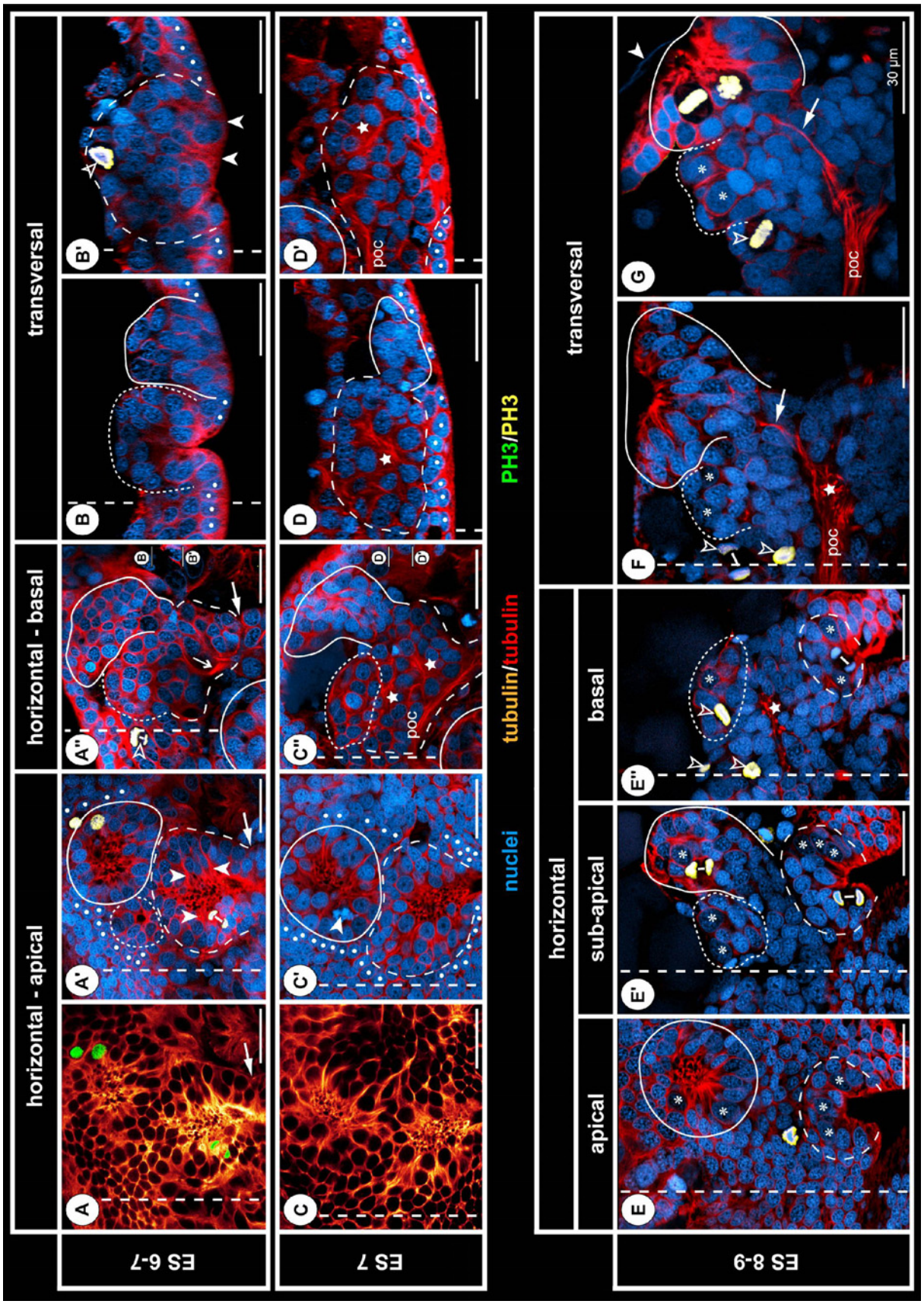
ES 6-7
ES 7
ES 8-9
horizontal - apical
horizontal - basal
transversal
horizontal
apical
sub-apical
basal
transversal
nuclei
tubulin/tubulin
PH3/PH3
poc
30 µm

Fig. 49: Cell proliferation regions in the brain of early PS 1 of *Pseudopallene* sp.

Histological sections through the larval brain. Arrows and big arrowheads mark sister cells of asymmetric divisions. Small arrowheads point at divisions of unspecified nature. Scale bars = 50 µm.

A,A' Horizontal sections, basal to the level of merging of antero-lateral cell streams with brain, anterior (body axis) to the top. Note the lightly stained bigger nuclei in the antero-medial clusters and the median proliferation cluster. Note also indications of column-like arrangements of the neuronal cells extending from the proliferation regions into the larval brain. The notable gap between brain and epidermis represents a fixation artifact.

B,B' Sagittal sections through lateral region of the larval brain. **B** Intensely stained region anterior to the antero-medial cell cluster represents proximal part of the antero-lateral cell stream. Note asymmetric division in nascent brain cell cluster. Small arrowhead marks mitosis in metaphase. **B'** Note asymmetric division in the antero-medial cell cluster.

C,C' Sagittal sections through medial region of the larval brain, different specimen than in **B**,**B'**. **C** Note smaller, sub-apical division in the antero-medial cell cluster. **C'** Note distinct size difference of cells in the median proliferation cluster and the underlying brain.

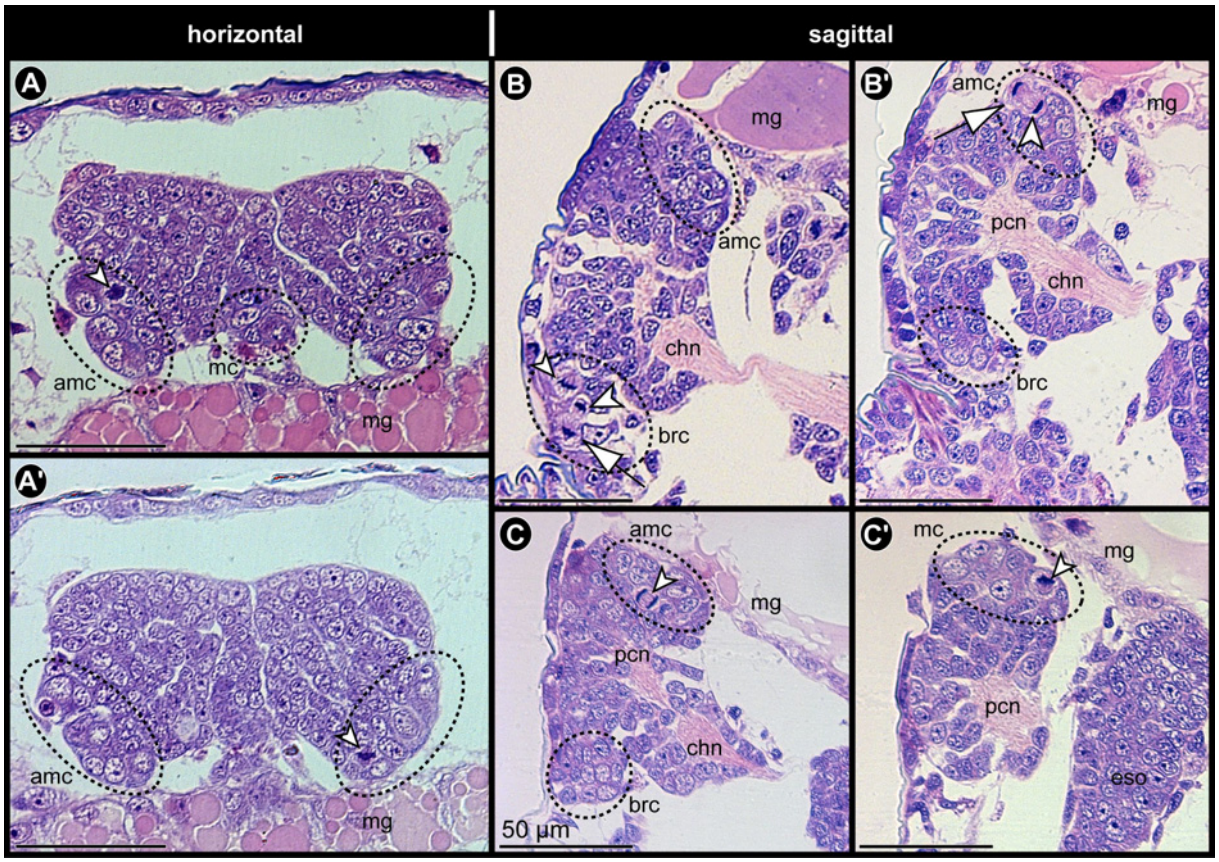
horizontal
sagittal
A
A'
B
B'
C
C'
amc
mc
mg
chn
brc
pcn
eso
50 µm

Fig. 50: Cell proliferation regions in the brain of the late walking leg-bearing larva of *Pseudopallene* sp. (late PS 1).

Tubulin- and PH3-labeled specimen with nuclear counterstain. Scale bars = 30 µm.

A Antero-lateral view of anterior body pole, Imaris volume (blend). Stippled outlines mark the derivatives of the antero-lateral depression. Note sub-division of this area into a lateral (1), medial (2) and anterior (3) region, corresponding to the anlagen of the lateral sensory organ, anterior and posterior eye, respectively. The arrow points at the protruding material of the lateral sensory organ anlage, being surrounded by a semi-circular furrow. Arrowheads indicate selected slit-like glands of the integument.

B-D Optical obliquely horizontal sections through the larval brain, anterior (body axis) to the bottom. Stippled ovals mark nascent apical brain cluster, unpaired median proliferation region and paired antero-medial cell clusters. **B** The eye anlagen (2 & 3) directly adjoin the region of apically concentrated cell processes (1) in which the lateral sensory organ is starting to develop. In the left body half, a protruding cell agglomeration of the latter already overlies the region of concentrated cell processes, leading to the appearance of a slight semi-circular furrow (solid curved line). Arrowheads mark the slender neurite bundle embedded in the antero-lateral cell stream. Arrow in the right body half points at the central invagination of the nascent brain cluster. **B'** Slightly sub-apical to **B**. Arrows mark the delicate neurite bundles between posterior eye anlagen and antero-lateral cell streams. Upper pair of arrowheads points at the proximal portion of the antero-lateral neurite bundle ('optic nerve' anlage) that connects to the protocerebral neuropil. Lower pair of arrowheads indicates a slender fibrous connection (anlage of postero-lateral cell stream) within the confluent region of nascent brain cell cluster and soma cortex. **B''** Even more basal than **B'**. The bilaterally paired antero-medial cell cluster has its maximal extensions basal to the level where the antero-lateral cell stream merges into the brain anlage. Arrows mark the antero-dorsally extending anterior branch of the chelifore nerve.

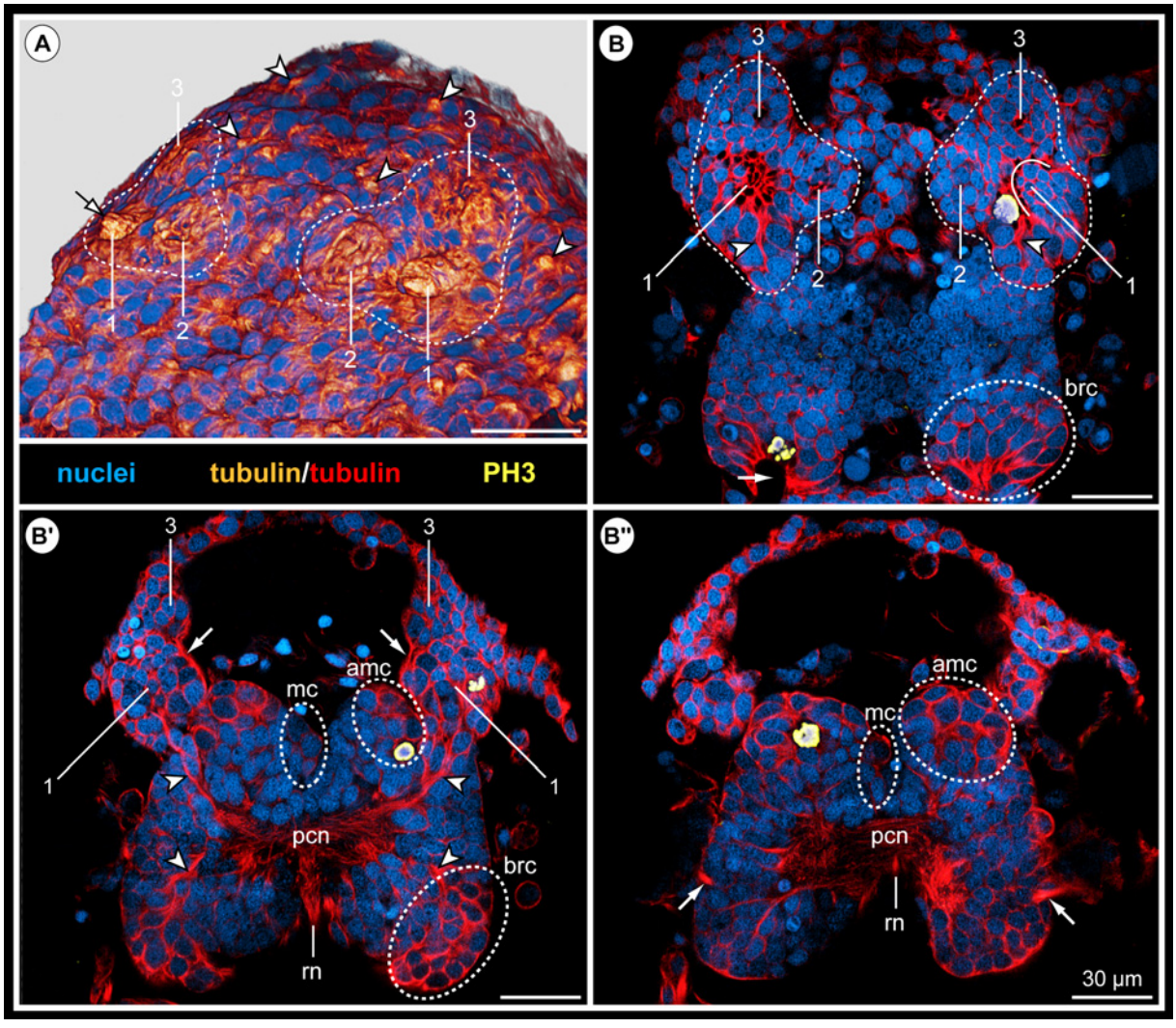
A
B
B'
B''
nuclei
tubulin/tubulin
PH3
brc
amc
mc
pcn
rn
30 µm

Fig. 51: Cell proliferation regions in the brain of PS 2 of *Pseudopallene* sp.

Tubulin- and PH3-labeled specimens with nuclear counterstain. Left, middle and right columns of images each correspond to one specimen. Positions and perspectives given in relation to the body axis. Scale bars = 30 µm.

A-A'' Posterior overview of dissected brains, Imaris volume (MIP). Circles mark the position of the esophagus. Note the bi-lobed overall appearance of the brains. Arrowheads indicate divisions within the antero-lateral cell stream/'optic nerve' anlage, within which several separate neurite bundles are embedded.

B-B'' Detail of apical-most portion of posterior brain hemispheres, Imaris volume (MIP), PH3 signal not shown. The more intensely tubulin labeled cells of the paired antero-medial clusters and the unpaired median cluster are distinctly discernible. Note the grape-like sub-structuring of the antero-medial clusters.

C-E'' Transversal optical sections. Mitoses are exclusively encountered apically, in relation to the paired antero-medial clusters, the unpaired median cluster or within the proximal portion of the antero-lateral cell stream. Unambiguous distinction of cell types based on size is not possible any longer, different staining intensity of nuclei is still encountered.

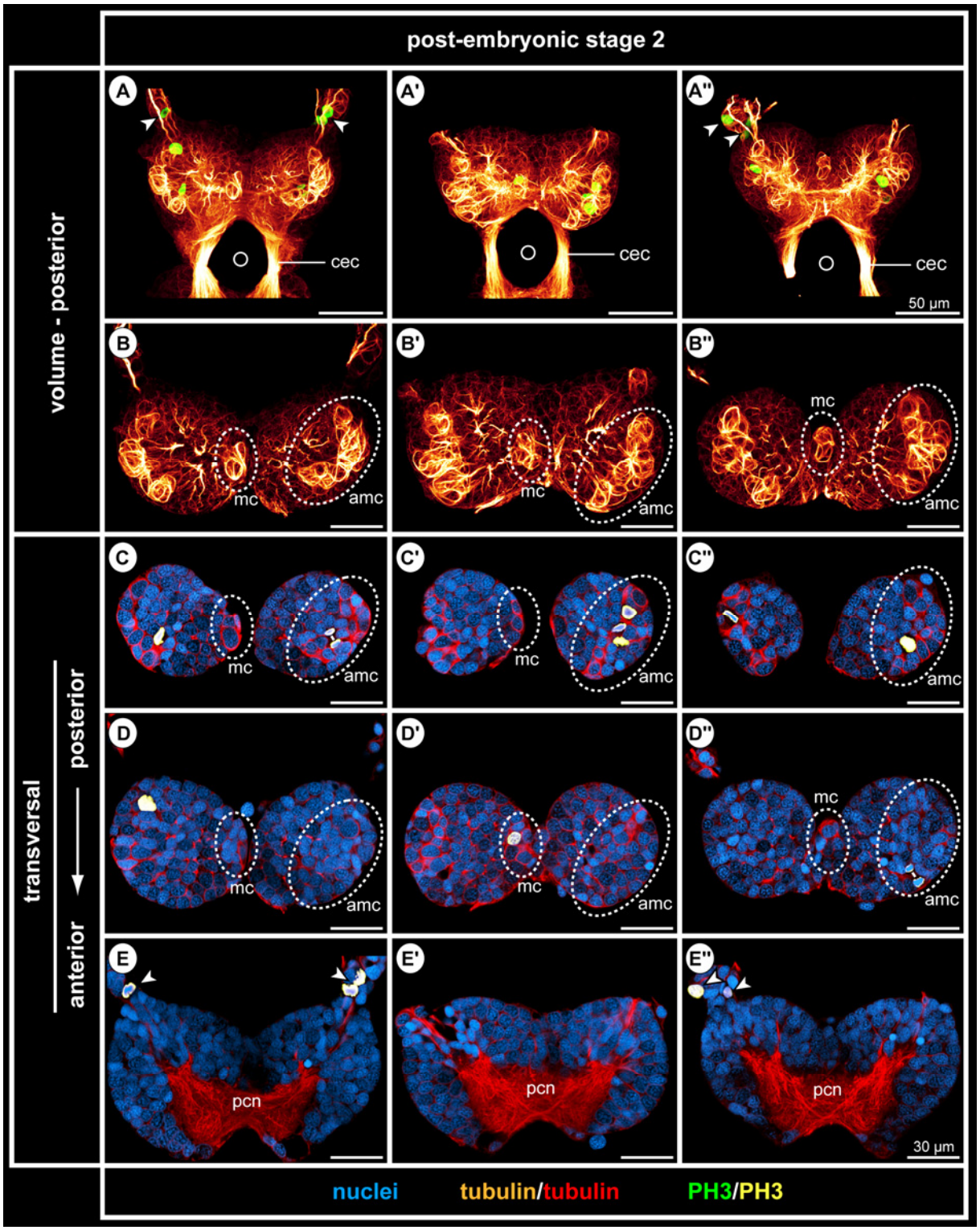
post-embryonic stage 2
volume - posterior
transversal
posterior
anterior
A
A'
A''
cec
50 µm
B
B'
B''
mc
amc
C
C'
C''
D
D'
D''
E
E'
E''
pcn
30 µm
nuclei
tubulin/tubulin
PH3/PH3

Fig. 52: Development of the protocerebral neuropil during post-embryonic development of *Pseudopallene* sp. (PS 1 – ad).

Optical sections of tubulin-labeled dissected brains with nuclear counterstain. Sections have been oriented to show the same differentiating sub-structures during development. Due to ongoing spatial shifts in the brain, the angle of the sections differs slightly between stages. The upper image of each stage is more ventral (according to neuraxis) than the lower image. Asterisks in **A** and **A'** indicate ripped circum-esophageal connectives. Corresponding sub-structures/regions are identically marked in all images.

Arrow: Merging region of antero-lateral cell stream/'optic nerve' with soma cortex. Beginning with PS 3, its neurites are tightly bundled while passing the neural sheath but already within the cortex split again partially (e.g. **C**,**D**,**E**).

Stippled oval: Basal optic neuropil, positioned directly below the soma cortex, at the periphery of the central protocerebral neuropil. Posteriorly, it is enclosed by some neurite bundles of the 'optic nerve' and local interneurons that extend dorso-medially, where they cross the midline (open arrowheads in **C-F'**).

Star: Apical optic neuropil, located within the antero-dorsal soma cortex, set off from central protocerebral neuropil. Receiving fibers from 'optic nerve' (e.g. **C'**,**D'**,**E'**).

Solid oval: Lobed lateral neuropil, bordered by a region of small globuli cells (not always distinctly set off from surrounding somata, see also Fig. 53A'), connected to contra-lateral counterpart via prominent transversal tract of the central protocerebral neuropil (small arrowheads in **A-F'**). The transversal tract originates most likely from the anterior-most protocerebral commissure bundle of PS 1 (**A**).

Stippled rectangle: Cross section through bundle of parallel axons of the ventral globuli cell region (see Fig. 53A'), representing part of the putative MBNs.

Solid white arrowhead: Root of the anterior and posterior cheliforal nerve branches (**B-C'**) or proximal portion of the anterior branch only (**E-F'**).

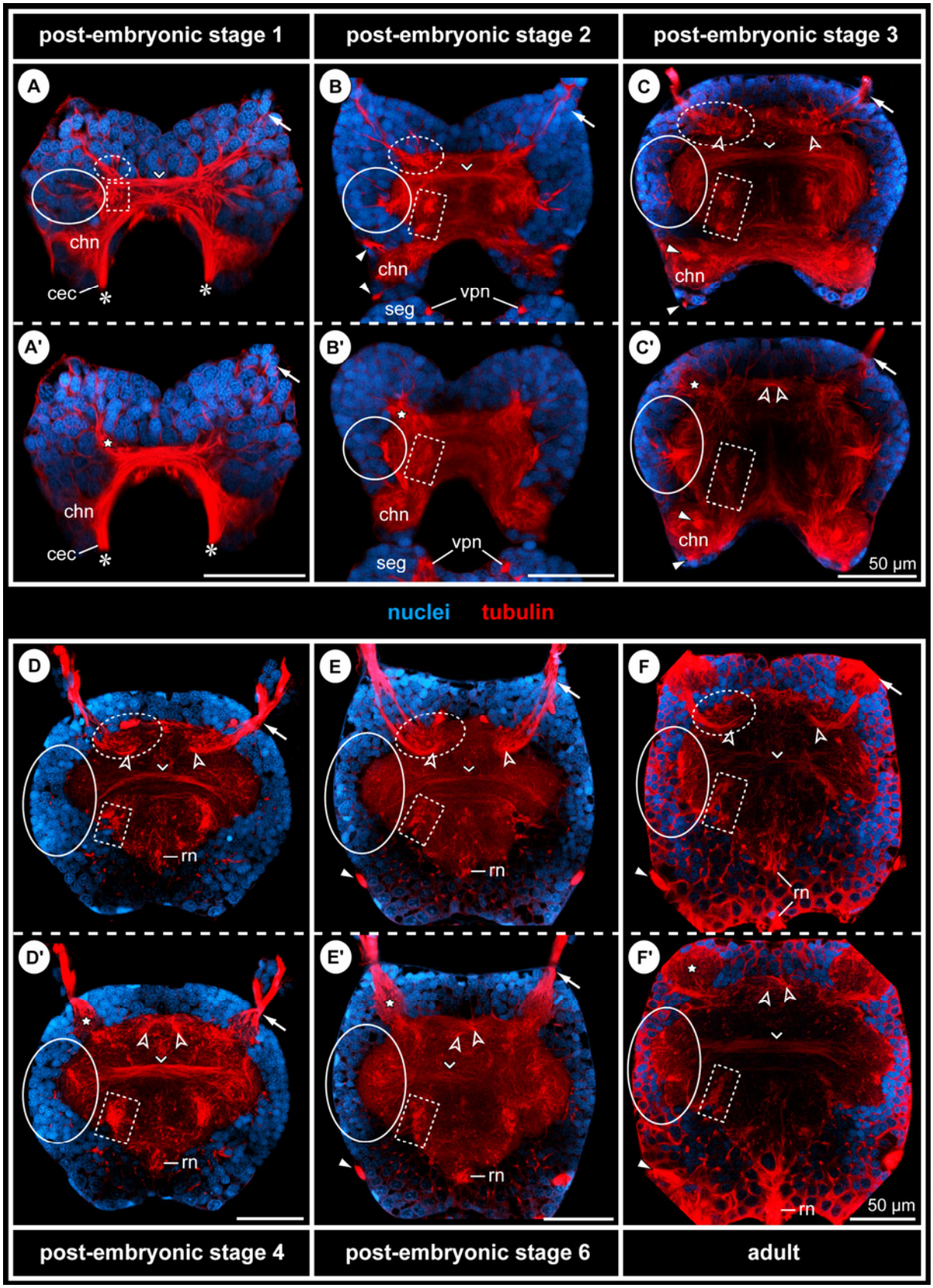
post-embryonic stage 1
post-embryonic stage 2
post-embryonic stage 3
A
B
C
chn
cec
chn
vpn
seg
chn
A'
B'
C'
chn
cec
chn
vpn
seg
chn
50 µm
nuclei tubulin
D
E
F
rn
rn
rn
D'
E'
F'
rn
rn
rn
50 µm
post-embryonic stage 4
post-embryonic stage 6
adult

Fig. 53: Selected aspects of adult brain architecture of *Pseudopallene* sp.

Tubulin-labeled dissected brains with nuclear counterstain. Scale bars = 50 µm.

A,A' Ventro-lateral view of adult brain (according to neuraxis, i.e., antero-lateral view according to body axis). Dashed line indicates the midline region. Black arrow points at antero-lateral thickening of the 'optic nerve'. White arrowhead marks anterior branch of the cheliforal nerve. **A** Imaris volume (blend). The brain cell cluster is discernible apically, external to the brain soma cortex. **A'** Imaris volume (MIP) of same brain in identical orientation as in **A**. Note the agglomeration of small globuli cell somata in the ventral brain cortex, directly anterior to the brain cell cluster. A second globuli cell soma region is located laterally in the contiguous cortex.

B,C Horizontal optical sections (2D projections of slightly curved composite sections) through the adult brain. **B** A curved transversal tract (open arrowheads) connects the apical optic neuropils (solid ovals) at the antero-dorsal side of the central protocerebral neuropil. Note a chiasm of tracts spanning between cheliforal neuropil/circum-esophageal connective and an as yet unidentified neuropil region in the protocerebrum. **C** White arrowhead points at the transversal tract spanning between the ventro-dorsally running parallel bundles of the putative MBNs. In the neuropilar region at its lateral side (stippled rectangle) intermingling with neurites from antero-dorsally located interneurons (potentially optic) and from more posterior locations are assessable (arrows).

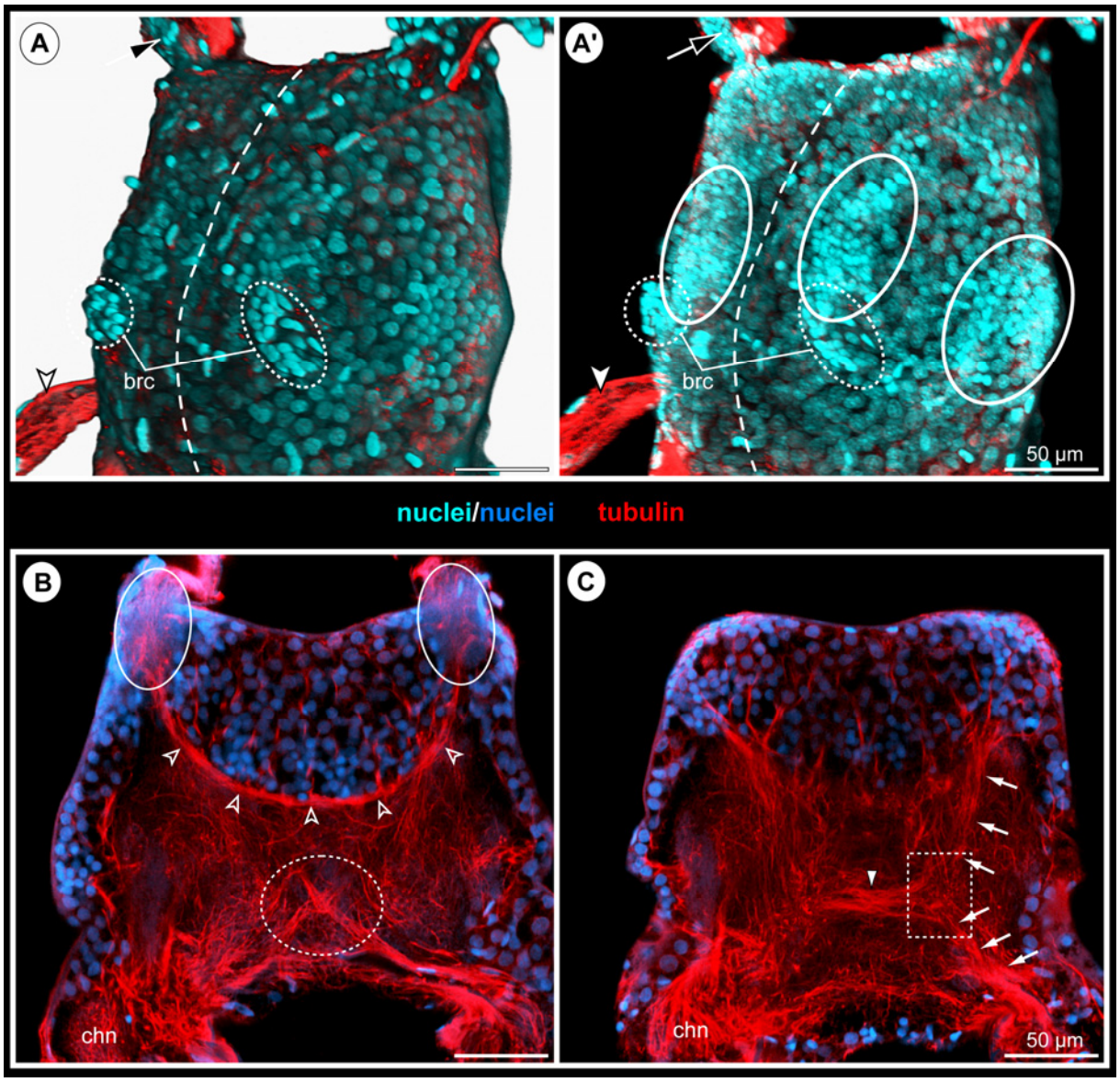
A
A'
brc
brc
50 µm
nuclei/nuclei
tubulin
B
C
chn
chn
50 µm

Fig. 54: Early anlagen of the major axonal pathways in the circum-esophageal region of *Pseudopallene* sp. (mid ES 6 – mid ES 7).

Ventral views of tubulin-labeled embryos, flat-preparations, Imaris volume (MIP). Clipping planes have been applied to remove non-target structures in more dorsal and ventral position. Double arrowheads mark antero-lateral neurite bundle that pioneers the pathway of the prospective 'optic nerve'. Stippled horizontal lines indicate border between cheliforal and palpal neuromeres. Asterisks label damaged regions. Scale bars = 30 µm.

A Mid ES 6. Small black arrowheads label neurites extending from neuronal somata underlying the central depression towards the primary pre-oral commissure.

B Late ES 6. Small white and black arrowheads indicate two different neurite bundles in the posterior part of the circum-esophageal commissure. Note delicate structure of the latter in the cheliforal region. Big black arrowheads label slender commissural bundle of the ovigeral commissure.

C Early ES 7. Small black arrowheads indicate centrally projecting neurites within the cheliforal and palpal neuromeres. Small white arrowheads mark locally recognizable bipartite structure of the connective anlagen. Big white arrowhead points at the well-established ovigeral commissure anlage. Note absence of palpal commissure anlage.

D Mid ES 7. Finely stippled oval indicates region of differentiating protocerebral neuropil. Coarsely dashed oval marks region of cheliforal neuropil formation. Triangular white arrowheads point at the two slender branches of the cheliforal segmental nerve anlage. Small white arrowheads highlight bipartite structure of the longitudinal connective anlagen between cheliforal and ovigeral neuromeres. Black arrowheads point at anlage of palpal commissure. Big white arrowhead at the bottom marks ovigeral commissure. White arrows point at palpal and ovigeral segmental nerve anlagen.

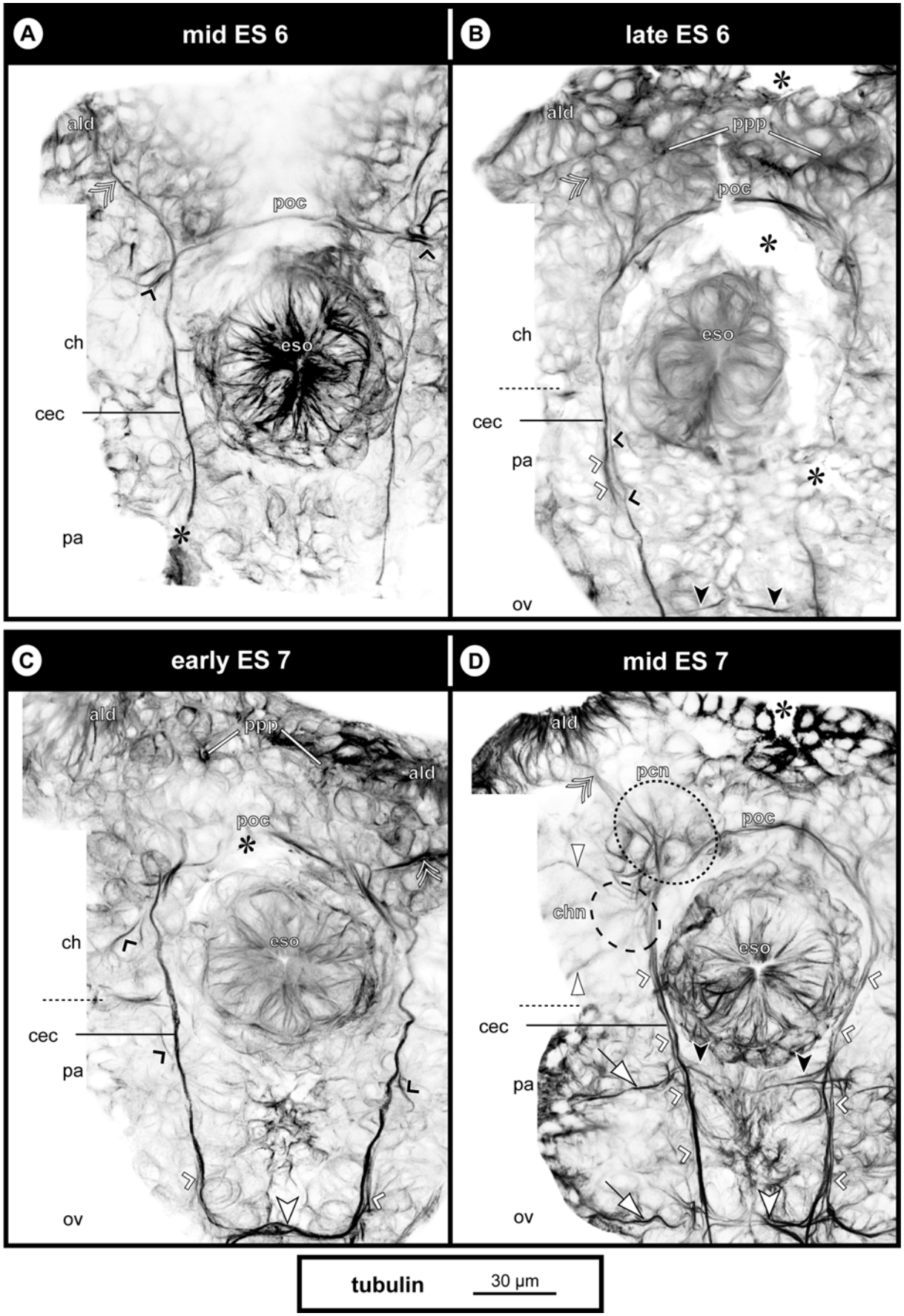
A
mid ES 6
ald
poc
ch
eso
cec
pa
B
late ES 6
ald
ppp
poc
ch
eso
cec
pa
ov
C
early ES 7
ald
ppp
ald
poc
ch
eso
cec
pa
ov
D
mid ES 7
ald
pcn
poc
chn
eso
cec
pa
ov
tubulin
30 µm

Fig. 55: Further differentiation of the major axonal pathways in the circum-esophageal region of *Pseudopallene* sp. (late ES 7 – early PS 1).

Ventral views of tubulin-labeled embryos, flat-preparations, Imaris volume (MIP). Clipping planes have been applied to remove non-target structures in more dorsal and ventral position. Double arrowheads mark antero-lateral neurite bundle that establishes the pathway of the prospective 'optic nerve'. Delicately stippled ovals indicate regions of differentiating protocerebral neuropil. Coarsely dashed ovals mark regions of cheliforal neuropil formation. Triangular white arrowheads point at the two branches of the cheliforal segmental nerve anlage. Stippled horizontal lines indicate border between cheliforal and palpal neuromeres. Big white arrowheads mark palpal and ovigeral commissures. White arrows point at palpal and ovigeral segmental nerve anlagen. Scale bars = 30 µm.

A Late ES 7. White arrowheads highlight persisting bipartite structure of the longitudinal connective anlagen between cheliforal and ovigeral neuromeres.

B Mid ES 8. Note considerable increase of the neurite bundles in the commissures and connectives (especially between palpal and ovigeral neuromeres).

C Late ES 9. Note more distinct differentiation of different pre-oral commissural bundles and approaching of the palpal and ovigeral commissures in the sub-esophageal ganglion anlage.

D Early PS 1. Note massive appearance and rectangular shape of the complete protocerebral neuropil region with its embedded commissural bundles. Palpal and ovigeral commissures are found in close vicinity, the connectives spanning between both neuromeres having thickened considerably.

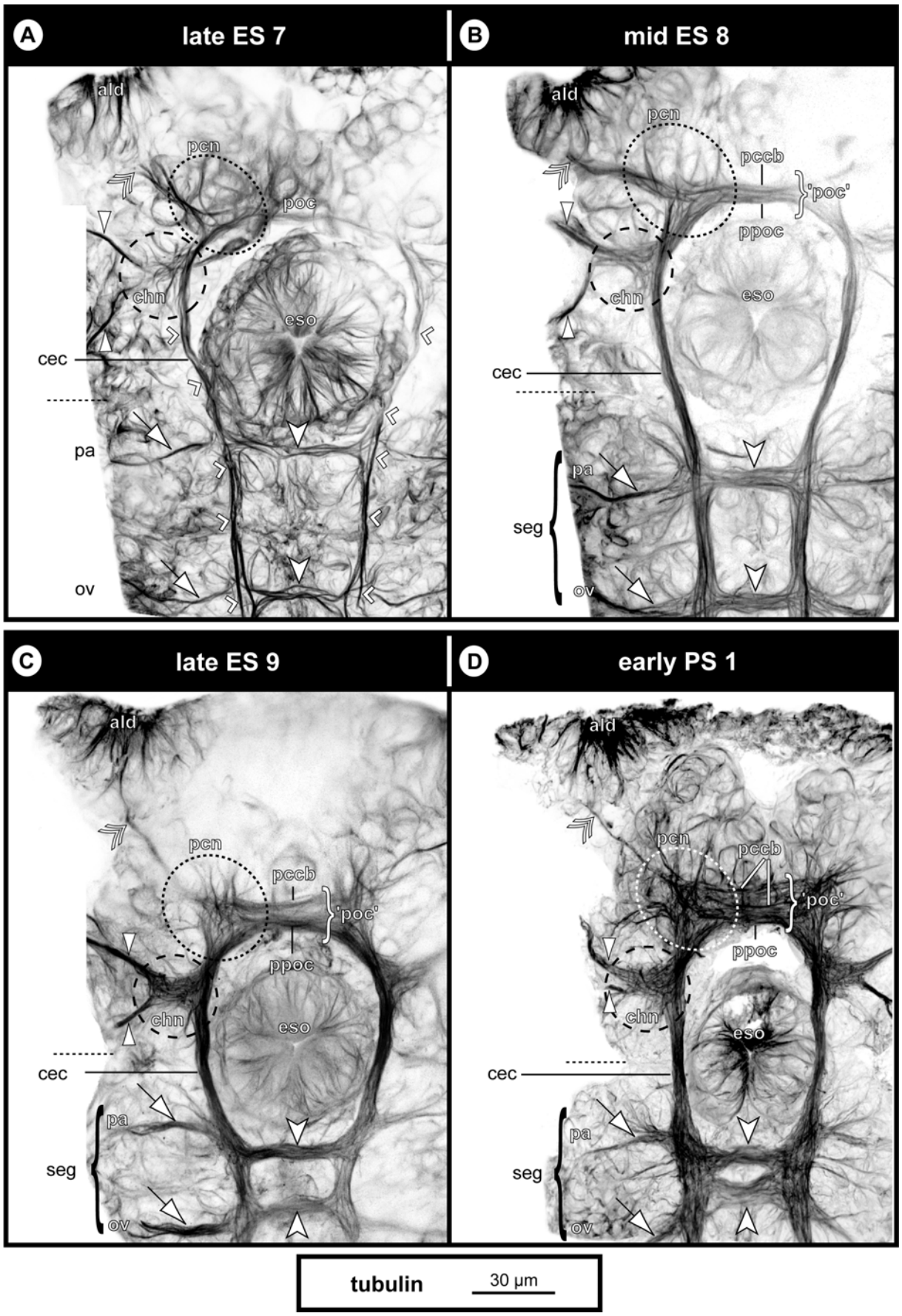
A
late ES 7
ald
pcn
poc
chn
eso
cec
pa
ov
B
mid ES 8
ald
pcn
pccb
'poc'
ppoc
chn
eso
cec
pa
seg
ov
C
late ES 9
ald
pcn
pccb
'poc'
ppoc
chn
eso
cec
pa
seg
ov
D
early PS 1
ald
pcn
pccb
'poc'
ppoc
chn
eso
cec
pa
seg
ov
tubulin
30 µm

Fig. 56: Early anlagen of the major axonal pathways in the VNC of *Pseudopallene* sp. (mid ES 6 – late ES 7).

Ventral views of tubulin-labeled embryos, flat-preparations, Imaris volume (MIP). Composite images, stippled horizontal lines indicate borders between two adjacent images. Clipping planes have been applied to remove non-target structures in more dorsal and ventral position. Small black arrowheads mark primary longitudinal neurite bundles. Asterisks label damaged regions. Scale bars = 30 µm.

A Mid ES 6. White arrows highlight early anlagen of palpal and ovigeral segmental nerves in morphological left body half.

B Early ES 7. Big white arrowhead points at well-established ovigeral commissure. Big black arrowheads indicate pioneering transversal neurites in walking leg neuromere 1. Triangular white arrowheads mark centrally projecting neurites within the palpal neuromere. White arrow points at early segmental nerve anlage of walking leg 1 in morphological left body half.

C Late ES 7. Small white arrowheads mark secondary longitudinal neurite bundle. Note differences in its posterior extension between both body halves. Big white arrowheads point at palpal and ovigeral commissures. Big black arrowheads indicate pioneering commissural bundles of walking leg neuromere 1. White arrows mark palpal and ovigeral segmental nerve anlagen.

Fig. 57: Further differentiation of the major axonal pathways in the VNC of *Pseudopallene* sp. (mid ES 8 – ES 10).

Ventral views of tubulin-labeled embryos, flat-preparations, Imaris volume (MIP). Composite images, stippled horizontal lines indicate borders between two adjacent images. Clipping planes have been applied to remove non-target structures in more dorsal and ventral position. Small black and white arrowheads mark primary and secondary longitudinal neurite bundles, respectively, in posterior trunk region. Big white arrowheads mark segmental commissures. White arrows point at segmental nerve anlagen. Asterisks label damaged regions. Note compaction of VNC along the a-p axis from ES 8 to ES 10. Scale bars = 30 µm.

A Mid ES 8. Triangular white arrowheads indicate proximally separate branches of the segmental nerve anlage of walking leg neuromere 1. Big black arrowheads mark separate transversally spanning neurite bundles anterior to the segmental commissure of walking leg neuromere 2.

B ES 9. Note compact architecture of the segmental commissure of walking leg neuromere 2.

C ES 10.

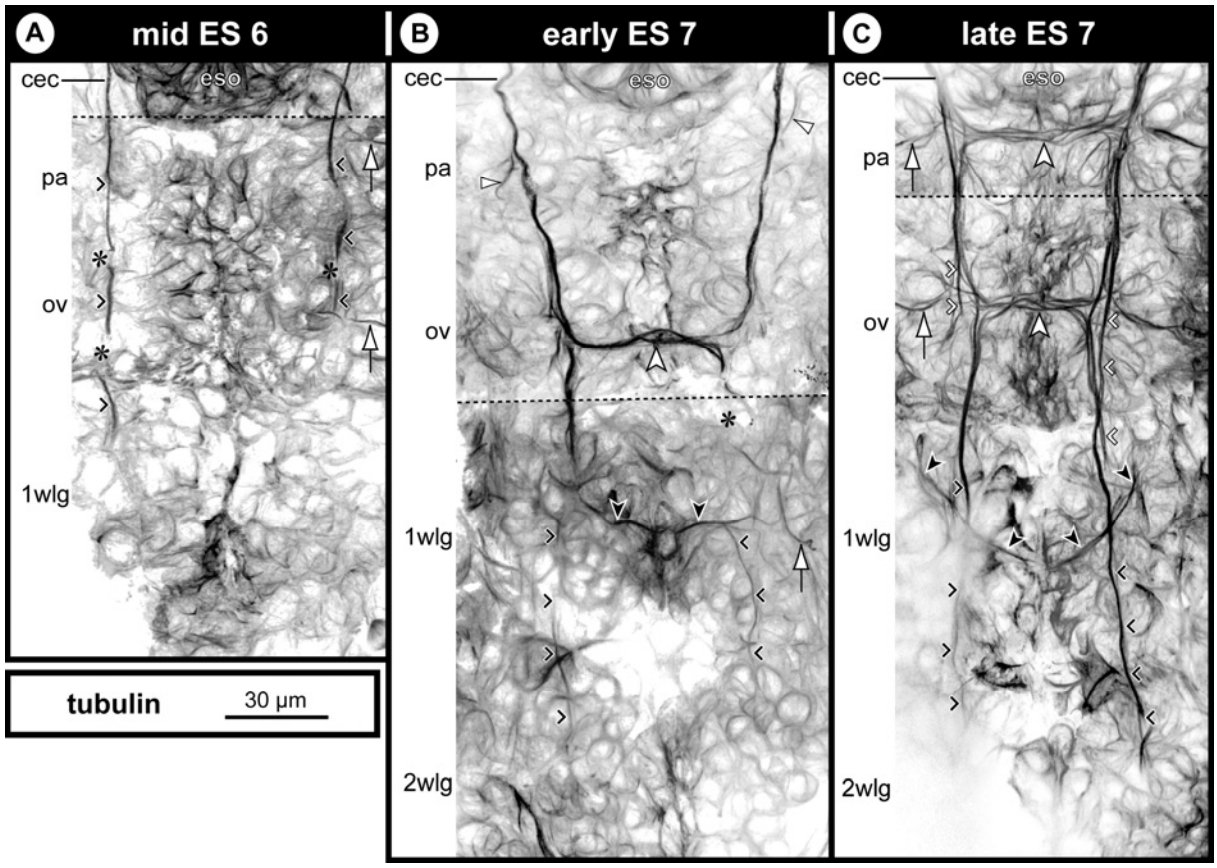
A
mid ES 6
B
early ES 7
C
late ES 7
cec
eso
pa
ov
1wlg
2wlg
tubulin
30 µm

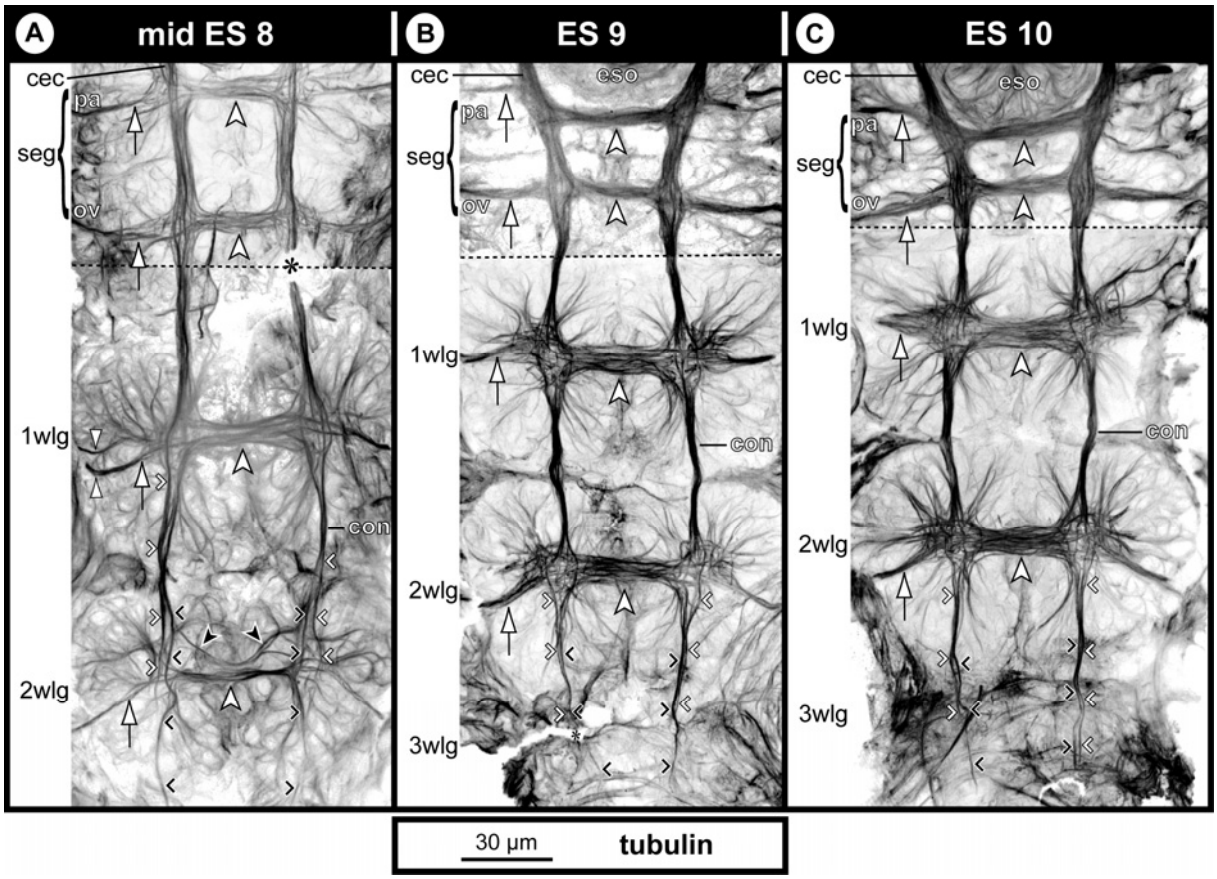
A
mid ES 8
B
ES 9
C
ES 10
cec
eso
pa
seg
ov
1wlg
2wlg
3wlg
con
30 µm
tubulin

Fig. 58: Differentiation of the major axonal pathways in the VNC of *Pseudopallene* sp. during early post-embryonic development (early PS 1 – PS 2).

Ventral views of tubulin-labeled dissected VNCs, Imaris volume (MIP). Composite images, stippled horizontal lines indicate borders between two adjacent images. Clipping planes have been applied to remove non-target structures in more dorsal and ventral position. Small black arrowheads mark longitudinal neurite bundles (connective anlagen) in posterior trunk region. White arrows point at segmental nerves. Triangular white arrowheads indicate separate branches of segmental nerves in walking leg segments. Scale bars = 50 µm.

A Early PS 1. Asterisk marks damaged connective region. Note beginning sub-division of the segmental commissures.

B Late PS 1. Double arrowhead indicates inter-segmental nerve between walking leg ganglia 1 and 2. Big black arrowheads mark first commissural neurite bundle of walking leg neuromere 3.

C PS 2. Double arrowhead indicates inter-segmental nerve between walking leg ganglia 1 and 2 (ripped off on morphologically left side during dissection). Big white arrowhead highlights well-developed compact commissure of walking leg ganglion anlage 3.

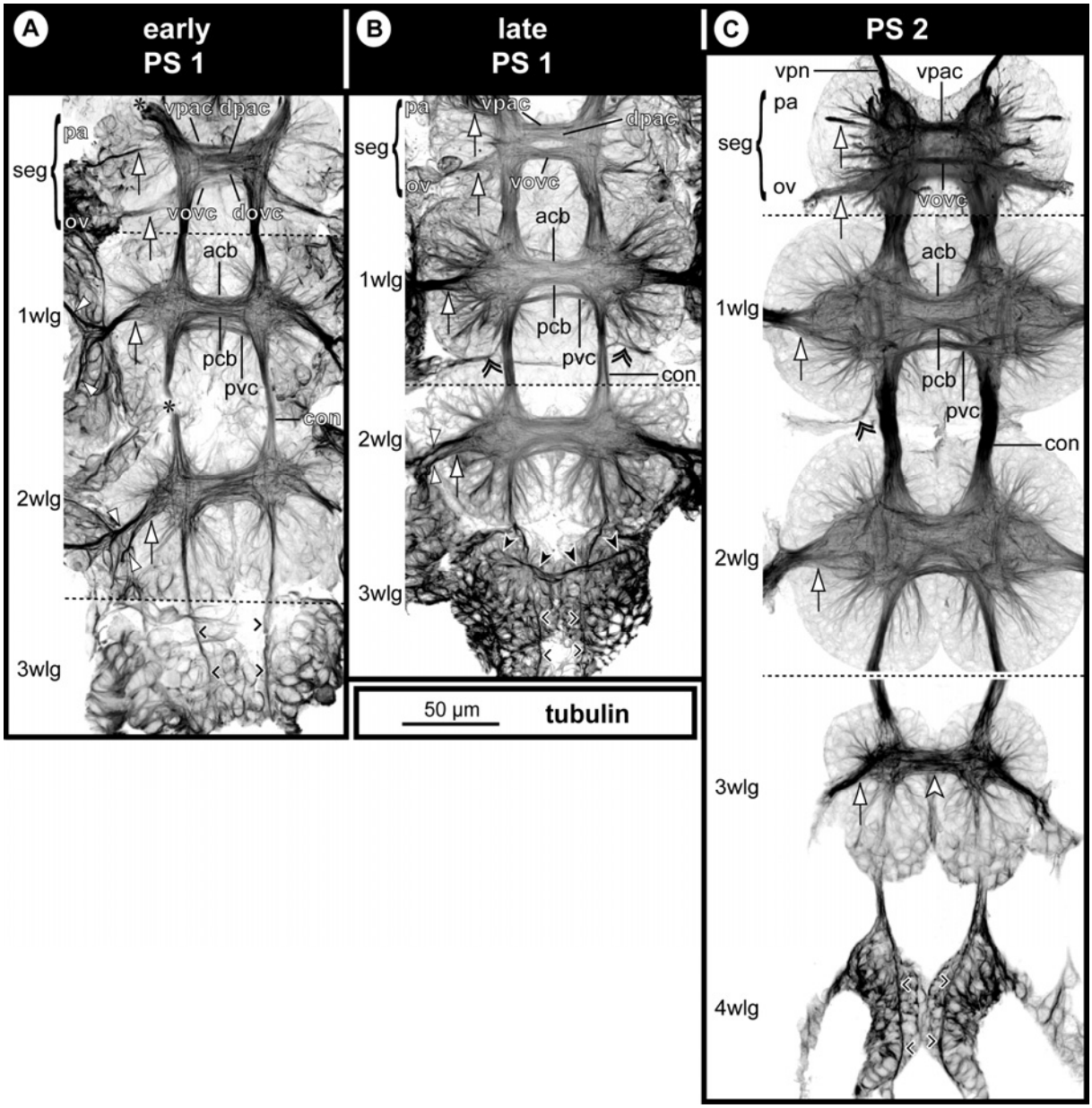
A
early
PS 1
B
late
PS 1
C
PS 2
vpac
dpac
pa
seg
ov
vovc
dovc
acb
1wlg
pcb
pvc
con
2wlg
3wlg
vpn
4wlg
50 µm
tubulin

Fig. 59: Development and fusion of the posterior ganglion anlagen of *Pseudopallene* sp. (PS 3 – ad).

Tubulin- and PH3-labeled dissected VNCs with nuclear counterstain (**A-D**) and histological sections of PS 6 and sub-adult specimens (**E-G**). Scale bars as indicated in each image.

A-C Ventral views of posterior ganglion anlagen, Imaris volume (MIP). Clipping planes have been applied to remove non-target structures in more dorsal and ventral position, only tubulin-labeling is shown. Developmental stages as indicated in left lower corner of each image. Triangular white arrowheads mark commissures of posterior ganglion anlagen. Note size decrease of posterior ganglion anlagen during the fusion process. The paired connectives and proctodeal nerves approach their contralateral counterpart medially.

D Sagittal optical section through walking leg ganglion 4 and posterior ganglion anlagen in PS 3. Dashed outlines highlight (nascent) apical clusters of walking leg ganglion 4 and posterior ganglion anlage 1. The cluster of the latter is already completely detached from the apical ectoderm. Note flask-shaped cells at the apical side of posterior ganglion anlage 2. Asterisks mark big SCNPs that are not in division.

E Sagittal section through walking leg ganglion 4 and posterior ganglion anlagen in PS 6. All ganglion anlagen are completely detached from the apical ectoderm. The posterior ganglion anlagen 1 and 2 have already decreased in size. Posterior ganglion anlage 1 has started to fuse with walking leg ganglion 4.

F,G Sagittal sections through walking leg ganglion 4 in a sub-adult. Posterior ganglion anlagen and walking leg ganglion 4 are completely fused. A dorsal neural sheath (triangular white arrowhead in **F**) still indicates the fusion line between them. Two closely spaced transversal neurite bundles (triangular white arrowheads in **G**) posterior to the dorsal neural sheath represent the commissures of the posterior ganglion anlagen. White arrows point at the posteriorly extending proctodeal nerve.

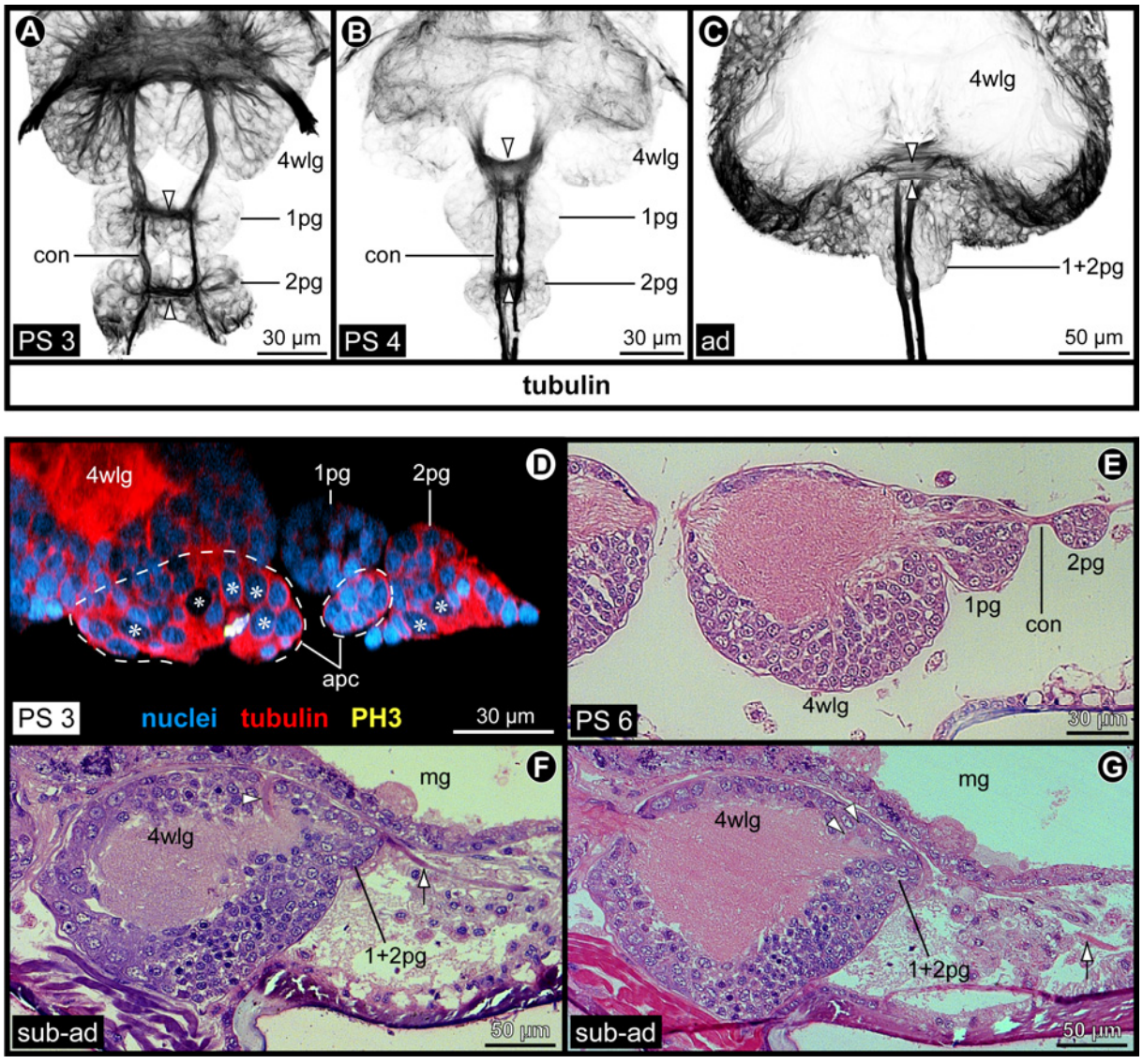
A
4wlg
1pg
con
2pg
PS 3
30 µm
B
4wlg
1pg
con
2pg
PS 4
30 µm
C
4wlg
1+2pg
ad
50 µm
tubulin
D
4wlg
1pg
2pg
apc
PS 3
nuclei
tubulin
PH3
30 µm
E
2pg
1pg
con
4wlg
PS 6
30 µm
F
mg
4wlg
1+2pg
sub-ad
50 µm
G
mg
4wlg
1+2pg
sub-ad
50 µm

Fig. 60: Expression of *Pseudopallene*-Delta during embryonic neurogenesis.

Ventral views of embryos (flat-preparations), WISH, in part with nuclear counterstain (**A**,**C**,**E**). Stars indicate manually removed chelifore. Asterisks mark unspecific labeling. Scale bars in overviews = 100 µm, in details = 50 µm.

A-B' ES 4. **A,A'** Ventral overviews of same specimen. Arrowhead indicates immigrating cells of the developing spinning gland. Arrows point at regions of slightly elevated expression levels in the VNE, potentially related to CIS formation. Note the low transcript concentration in the ventral midline region. **B,B'** Details of region in the pre-cheliforal lobe indicated in **A'**. Lateral part of pre-cheliforal lobe damaged during dissection. Arrows in **B** point at antero-medial CISs. Arrows in **B** point at central and lateral CISs.

C-D' ES 6. **C,C'** Ventral overviews of same specimen. Arrowhead indicates immigrating cells of the developing chela gland. **D,D'** Details of walking leg ganglion 1 anlage. **D** slightly more apical than **D'**. Black-framed arrows mark selected SCNPs with high expression level (in part in division). White arrows mark midline region.

E-F' Late ES 7. **E,E'** Ventral overviews of same specimen. Morphologically right chelifore has been only removed in **E'**. Arrowhead indicates differentiating duct of the chela gland. **F,F'** Details of walking leg ganglion 1 anlage. **F** slightly more apical than **F'**. Black-framed arrow marks apical SCNP in metaphase. White arrows mark midline region.

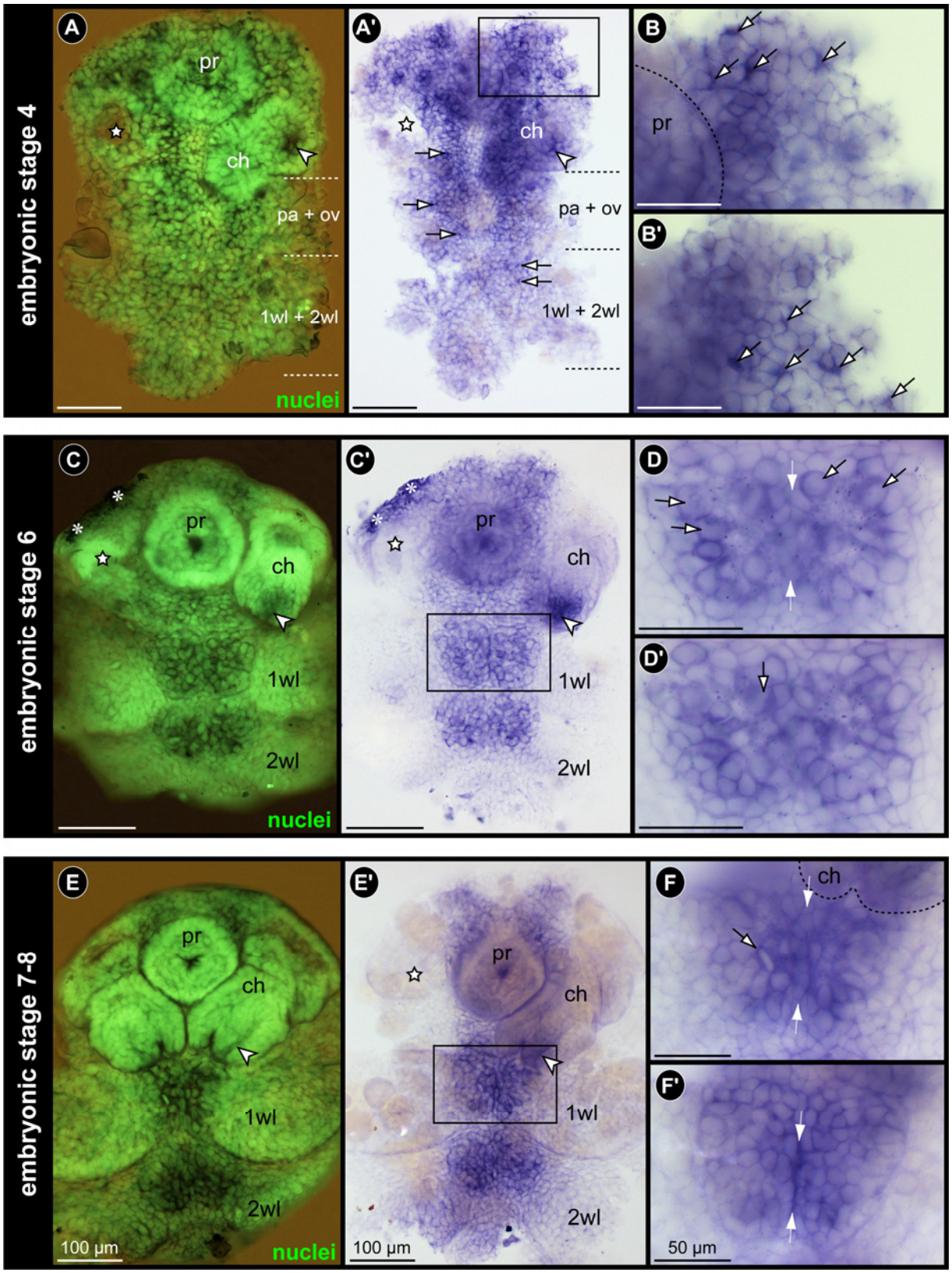
embryonic stage 4
A
pr
ch
pa + ov
1wl + 2wl
nuclei
A'
ch
pa + ov
1wl + 2wl
B
pr
B'
embryonic stage 6
C
pr
ch
1wl
2wl
nuclei
C'
pr
ch
1wl
2wl
D
D'
embryonic stage 7-8
E
pr
ch
1wl
2wl
100 µm
nuclei
E'
pr
ch
1wl
2wl
100 µm
F
ch
F'
50 µm

Fig. 61: Expression of *Pseudopallene*-Notch during embryonic neurogenesis.

Ventral overviews of embryos (flat-preparations), WISH, left image in each row shown with nuclear counterstain. Stars indicate manually removed chelifore. Asterisks mark unspecific labeling. Scale bars = 100 µm.

A,A' ES 4. Expression is found ubiquitously within the neuroectoderm.

B,B' ES 6. Note distinctly higher Notch expression in the walking leg ganglion anlagen. Arrowheads mark slightly higher transcript levels in walking leg anlagen.

C,C' Late ES 8. Note massive unspecific staining of the embryonic cuticle.

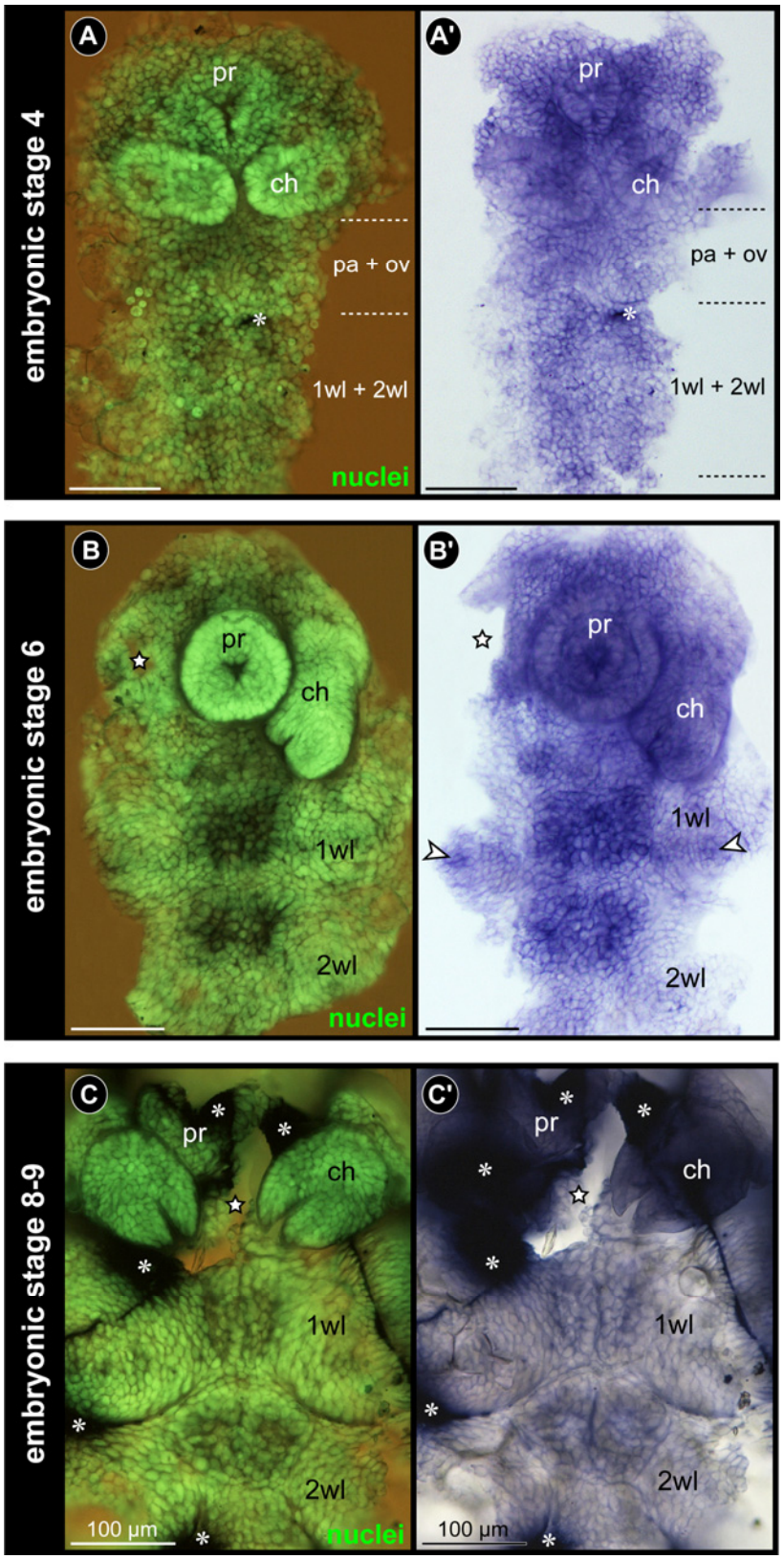
embryonic stage 4
A
pr
ch
pa + ov
1wl + 2wl
nuclei
A'
pr
ch
pa + ov
1wl + 2wl
embryonic stage 6
B
pr
ch
1wl
2wl
nuclei
B'
pr
ch
1wl
2wl
embryonic stage 8-9
C
pr
ch
1wl
2wl
100 µm
nuclei
C'
pr
ch
1wl
2wl
100 µm

Fig. 62: Comparison of callipallenid development (schematic).

The various callipallenid taxa show differing degrees of embryonization. At the time of hatching, the 'walking leg-bearing larvae' exhibit deviating levels of differentiation of the post-ovigeral trunk. Accordingly, there is no morphologically uniform hatching stage of callipallenids. Representatives possessing hatching larvae with a comparatively low degree of trunk differentiation (e.g. *Propallene*) tend to leave the father's oviger at an earlier stage than species with far advanced hatching larvae (e.g. *Callipallene*, *Neopallene*). Black arrows represent intermittent molts, the white arrow indicates further differentiation during embryonic development.

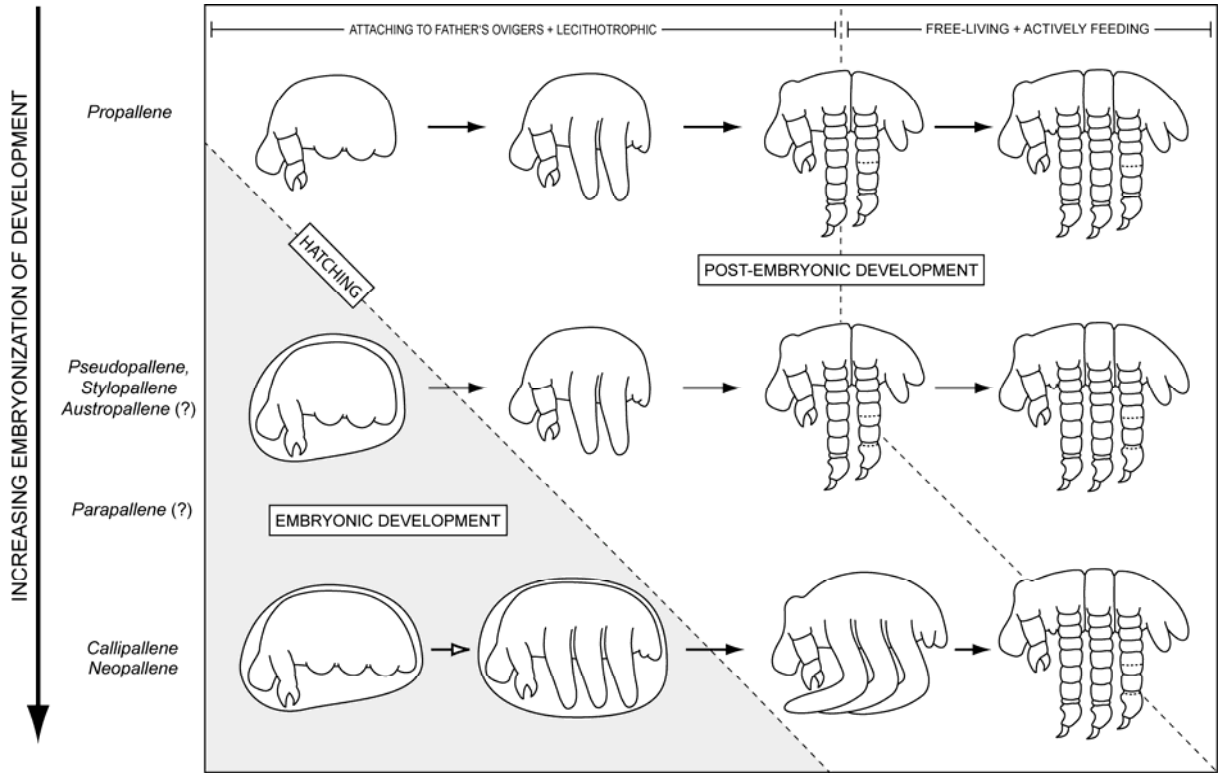
ATTACHING TO FATHER'S OVIGERS + LECITHOTROPHIC
FREE-LIVING + ACTIVELY FEEDING
INCREASING EMBRYONIZATION OF DEVELOPMENT
Propallene
HATCHING
POST-EMBRYONIC DEVELOPMENT
Pseudopallene,
Stylopallene
Austropallene (?)
Parapallene (?)
EMBRYONIC DEVELOPMENT
Callipallene
Neopallene

Fig. 63: Walking leg-bearing larvae of *Stylopallene cheilorhynchus* and *Callipallene* sp.
SEM micrographs and nuclear stainings. **A-C** *S. cheilorhynchus*. **A** Freshly hatched PS 1, antero-lateral view. Proboscis and chelifores of the specimen are still inserted in the ripped egg membrane (arrow) and probably an embryonic cuticle. The egg membrane is covered by a hardened sticky matrix via whose stalk-like projection (directed to the left) the egg remains attached to the father's oviger. The unarticulated limb buds of walking leg 1 and 2 protrude freely from the egg membrane. **B** PS 1, ventral view. Note the folds of the walking leg tissue beneath the cuticle. **C** PS 1, posterior view. A tiny interior primordium of walking leg 3 is detectable in the hind body region. The proctodeum/anus is forming beneath the cuticle. The distal-most portion of walking leg 2 will most likely give rise to tarsus, propodus and terminal claw. Proximal to this region, the differentiating tibia 2 may be discernible. **D-F** *Callipallene* sp. **D** Hatched and still attaching PS1, antero-lateral view. Note the elongate anlagen of walking leg pairs 1-3. The arrow indicates a piece of ripped egg membrane (plus part of embryonic cuticle?) that still covers the proboscis and is still attached to the spinning gland of the chelifore. Presumptive podomere regions are labeled along walking leg 1. **E** PS 1, lateral view, Imaris volume (blend). The spinning gland process is distinctly visible due to its autofluorescent signal. A shallow elevation of the developing ocular tubercle rises slightly anterior to walking leg 1. Note the primordium of walking leg 4 as well as the interior tissue folds of walking legs 1-3 that may partially directly relate to the borders of future leg podomeres. **F** PS 1, ventral view. Walking leg pair 3 is bent in an anterior direction, being wedged between walking leg pairs 1 and 2. The primordia of walking leg pair 4 are already externally detectable, flanking the hind body region that still lacks an anus.

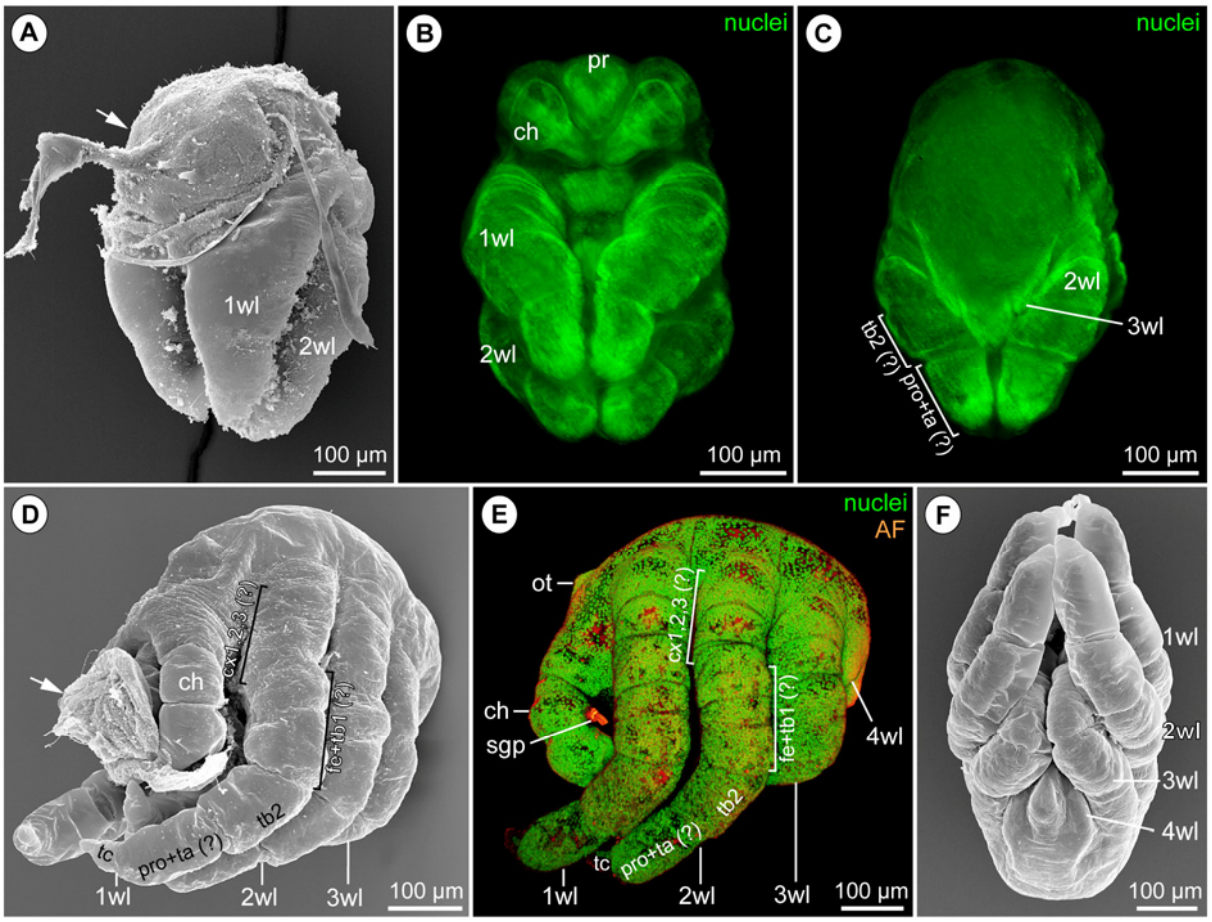
A
1wl
2wl
100 µm
B
nuclei
pr
ch
1wl
2wl
100 µm
C
nuclei
2wl
3wl
tb2 (?)
pro+ta (?)
100 µm
D
ch
cx1,2,3 (?)
fe+tb1 (?)
tb2
tc
pro+ta (?)
1wl
2wl
3wl
100 µm
E
nuclei
AF
ot
cx1,2,3 (?)
ch
sgp
fe+tb1 (?)
4wl
tb2
tc
pro+ta (?)
1wl
2wl
3wl
100 µm
F
1wl
2wl
3wl
4wl
100 µm

Fig. 64: Distribution of hatching stages mapped on two recent hypotheses of pycnogonid relationships.

Depicted phylograms have been simplified from Arango and Wheeler (2007) and Arabi et al. (2010). For simplicity, the terminal (*Nymphon floridanum*) that renders Nymphonidae polyphyletic in Arango and Wheeler (2007) has been omitted. Against the background of the study by Arabi et al. (2010), the reconstruction of the ancestral hatching stage of extant sea spiders remains ambiguous, due to the lack of developmental data on Austrodecidae and Colossendeidae. The protonymphon larva emerges as a ground pattern feature in the most parsimonious explanation for the observed distribution on the tree of Arango and Wheeler (2007). In both studies, 'Callipallenidae' resolve as paraphyletic grouping well nested within pycnogonids. Their mode of embryonized development represents a derived feature (black arrow). Nymphonidae are placed as terminal group that arises from within callipallenids. This position implies the reemergence of the free-living protonymphon stage in the nymphonid lineage. In this scenario, it remains unresolved, which hatching stage (free-living protonymphon, lecithotrophic attaching protonymphon, walking leg-bearing larva) represents the plesiomorphic condition of nymphonids (white arrow).

Fig. 65: Matrix notation of walking leg differentiation in *Pseudopallene* sp.

For further explanation of notation see text (4.1.7.4.). '+' stands for a first primordium of a walking leg, '0' codes externally unarticulated limb buds.

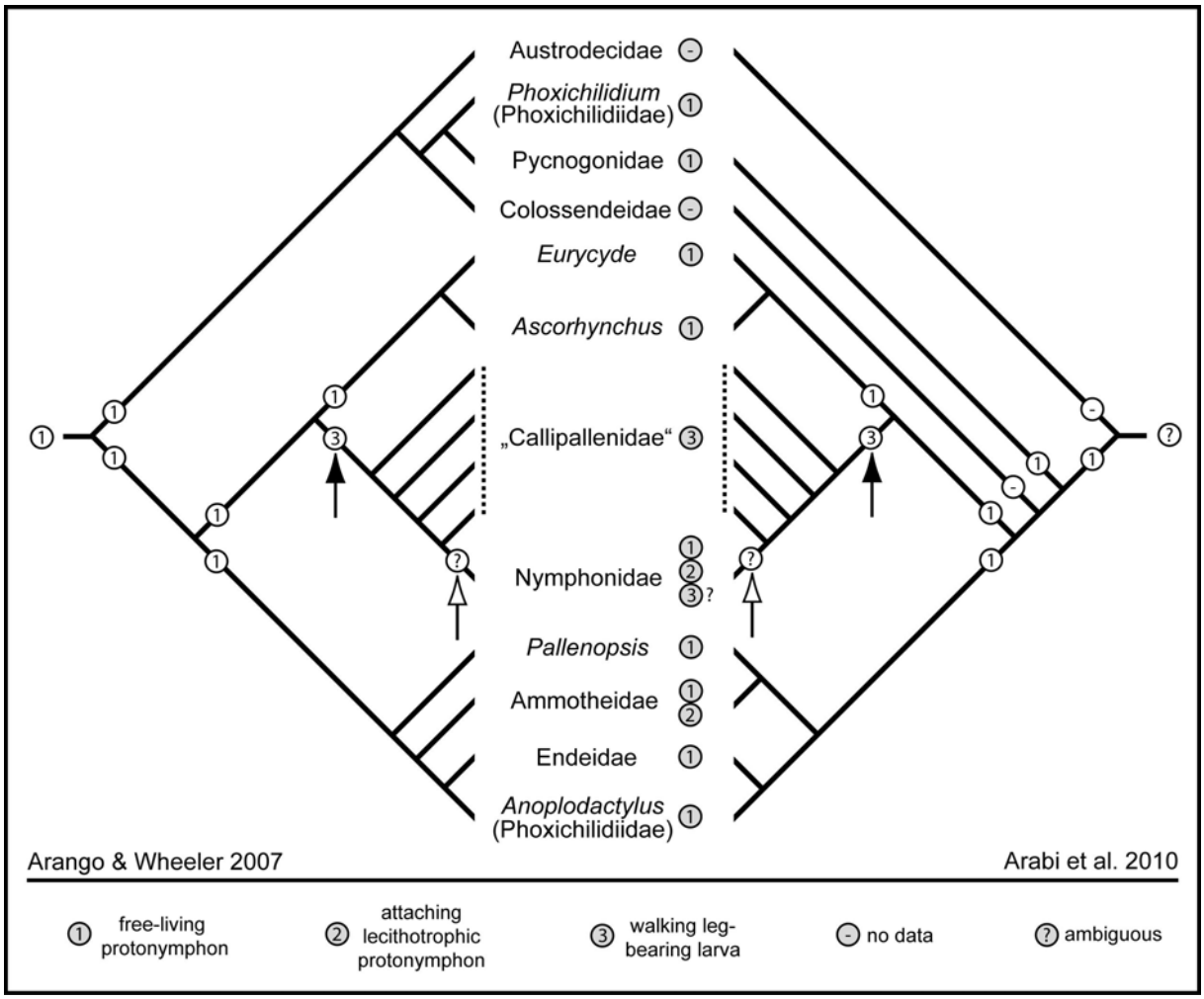
Austrodecidae -
Phoxichilidium (Phoxichilidiidae) 1
Pycnogonidae 1
Colossendeidae -
Eurycyde 1
Ascorhynchus 1
„Callipallenidae“ 3
Nymphonidae 1 2 3?
Pallenopsis 1
Ammotheidae 1 2
Endeidae 1
Anoplodactylus (Phoxichilidiidae) 1
Arango & Wheeler 2007
Arabi et al. 2010
1 free-living protonymphon
2 attaching lecithotrophic protonymphon
3 walking leg-bearing larva
- no data
? ambiguous

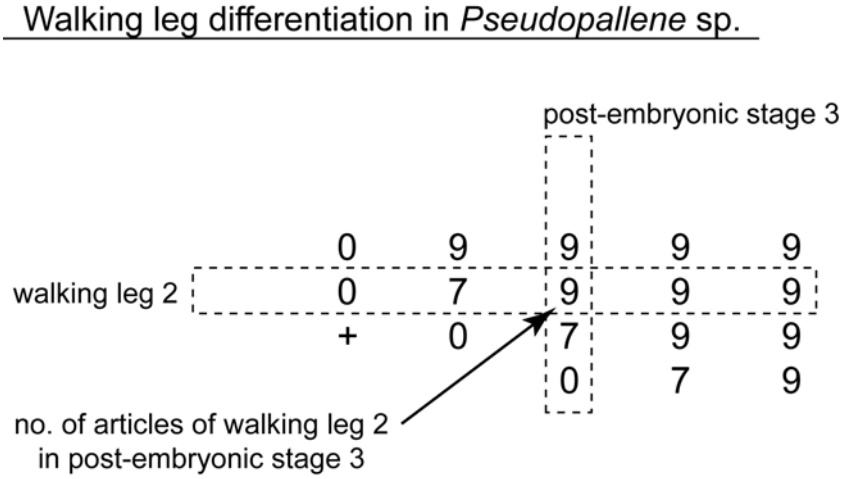
Walking leg differentiation in Pseudopallene sp.
post-embryonic stage 3
walking leg 2
0 9 9 9 9
0 7 9 9 9
+ 0 7 9 9
0 7 9
no. of articles of walking leg 2 in post-embryonic stage 3

Fig. 66: Walking leg differentiation patters within different pycnogonid taxa.
For explanation of notation see Fig. 65 and text. Criterion for the alignment of matrices is solely the number and composition of the walking legs, because the species-specific numbers of the respective post-embryonic stagings do often not refer to morphologically corresponding developmental stages. The entry value '8' indicates that tarsus and propodus are already separated, but femur and tibia 1 not yet. The value '3' relates to late limb bud stages for which an apparent underlying regionalization of the tissue is detectable. This is not considered as true articulation. Since transformation from 0 to '3' is most likely not separated by a molt, both states are summarized in one entry.

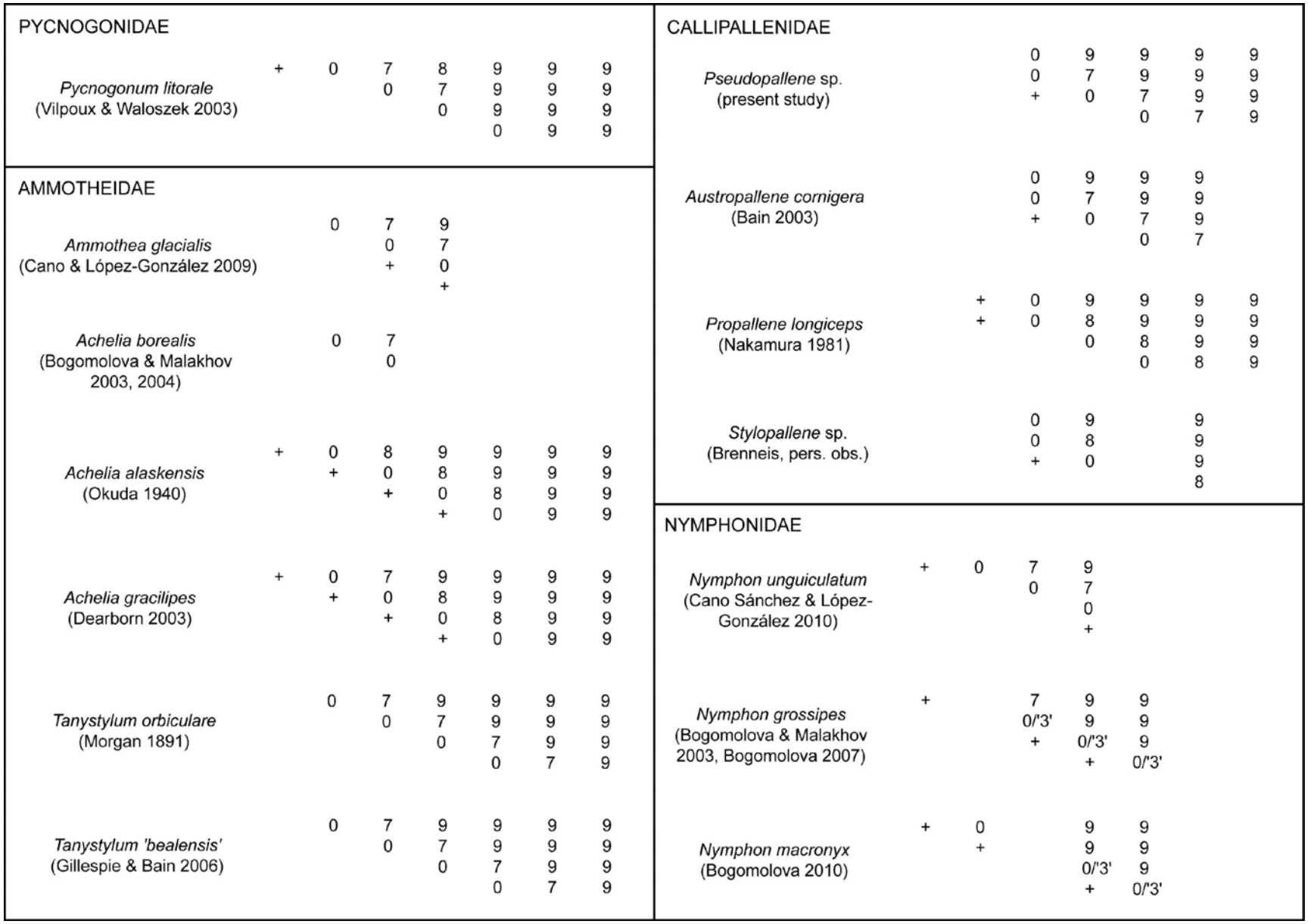
PYCNOGONIDAE
Pycnogonum litorale (Vilpoux & Waloszek 2003)
AMMOTHEIDAE
Ammothea glacialis (Cano & López-González 2009)
Achelia borealis (Bogomolova & Malakhov 2003, 2004)
Achelia alaskensis (Okuda 1940)
Achelia gracilipes (Dearborn 2003)
Tanystylum orbiculare (Morgan 1891)
Tanystylum 'bealensis' (Gillespie & Bain 2006)
CALLIPALLENIDAE
Pseudopallene sp. (present study)
Austropallene cornigera (Bain 2003)
Propallene longiceps (Nakamura 1981)
Stylopallene sp. (Brenneis, pers. obs.)
NYMPHONIDAE
Nymphon unguiculatum (Cano Sánchez & López-González 2010)
Nymphon grossipes (Bogomolova & Malakhov 2003, Bogomolova 2007)
Nymphon macronyx (Bogomolova 2010)

Fig. 67: Three phases of neurogenesis in a ventral hemi-neuromere of *Pseudopallene* sp.
Schematic drawings in sagittal view.
Initial phase (column on the left side): Gradual immigration of cells from the single-layered ectoderm. Apical tangential divisions provide additional cellular material. Only rarely flask-shaped immigrating cells are encountered in division. Gradually, CISs become identifiable (stippled and solid arrowheads), becoming again indistinct with ongoing basal displacement of the interspersed apical cell nuclei. Single flask-shape cells start to detach from the apical surface in the compacted primordial hemi-ganglion anlage, forming a loose basal layer of immature GCs.
Second phase (row at the bottom): Emergence of big spindle-shaped SCNPs within the apical depression of the multi-layered hemi-ganglion anlage. SCNPs divide in tangential or slightly oblique orientation. Smaller cells interspersed between them apparently immigrate independently. Sub-apical smaller INPs are found in the anterior and posterior portion of hemi-ganglion anlage. At the basal side of the latter, axonogenesis starts and proceeds rapidly. Main axonal pathways are established and a primordial ganglionic neuropil is formed. Occasionally, cells divide close to the basal neuropil, indicating that not all fully detached cells are post-mitotic. The shallow apical depression invaginates further into a deep pit, the prospective epidermis covering its apical rim.
Third phase (column on the right side): The cells lining the deep invagination detach from the ectoderm, forming an apical cluster with a small central cavity at the ventral side of the hemi-ganglion. After the detachment process, the epidermis is apically closed. The cluster remains in contact with the underlying hemi-ganglion via an anterior and a posterior cell stream. Along these streams, additional cell material migrates into the hemi-ganglion, being generated in the clusters as well as in the streams themselves. With ongoing development, the cell streams diminish to fibrous strands. Mitotic activity persists, but at a lower rate. The ganglionic neuropil increases considerably and therein glomerulus-like neuropils are formed (dark red spots in last image).

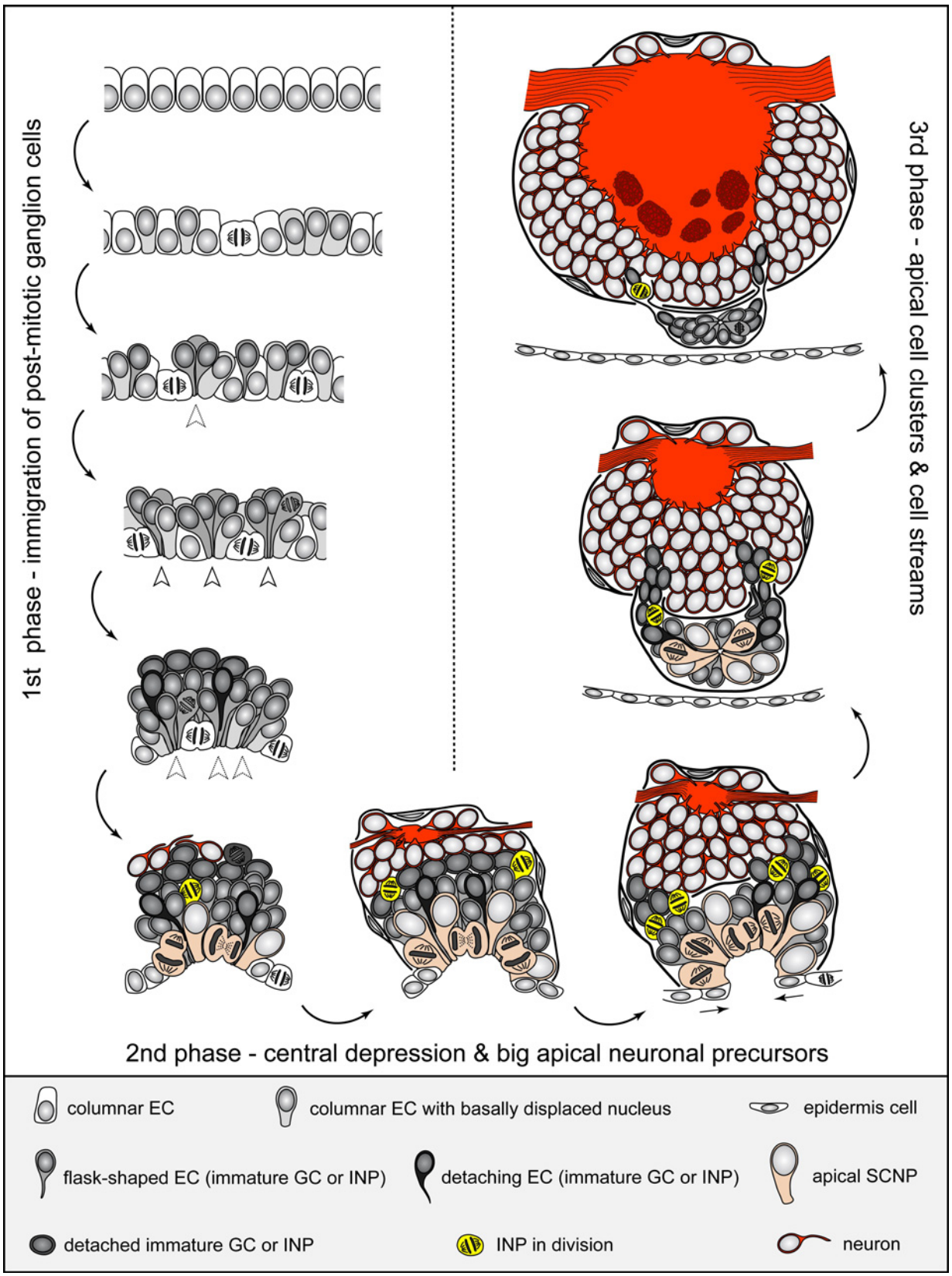
1st phase - immigration of post-mitotic ganglion cells
3rd phase - apical cell clusters & cell streams
2nd phase - central depression & big apical neuronal precursors
columnar EC
columnar EC with basally displaced nucleus
epidermis cell
flask-shaped EC (immature GC or INP)
detaching EC (immature GC or INP)
apical SCNP
detached immature GC or INP
INP in division
neuron

Fig. 68: Neurogenesis in *Callipallene* sp.

Tubulin labeling with nuclear counterstain and SEM micrographs. Scale bars as indicated in each image.

A-C Early stage of neurogenesis. **A** Ventral overview of germ band, flat-preparation, Imaris volume (MIP). Morphologically left half of the post-cheliforal region is missing (dissection damage). Note bright orange dots in pre-cheliforal lobes and in parts of the VNE relating to apically converging cell processes of CISs. Open white arrowhead indicates immigrating cells of the forming spinning gland. Solid white arrowheads mark conspicuous sites of cell immigration lateral to the palpal and ovigeral hemi-neuromeres. **B** Detail of pre-cheliforal lobe, horizontal 2D projection of curved composite optical sections. Dashed line marks midline region. Solid white arrowheads indicate apically converging cell processes of CISs. White arrows point at selected apical cell divisions. **C** Transversal optical section through pre-cheliforal lobe. Arrowheads mark CISs.

D-F Advanced stage of neurogenesis. **D** Ventral overview of embryo. The embryonic cuticle has been removed only partially. Anlagen of three walking legs are already discernible during embryonic development. Black-framed arrows mark segmental depressions of all four walking leg neuromeres. **E** Ventral overview of embryo, Imaris volume (blend). Solid white arrowheads indicate a depression within each pre-cheliforal lobe. Black-framed arrowheads mark segmental depressions of the four walking leg neuromeres, the nuclei of cells in these regions being displaced basally. Open white arrowheads indicate forming duct of the spinning glands. **F** Detail of VNE, walking leg segments 1-3, horizontal 2D projection of curved composite optical sections. Within the paired apical depressions, some more distinct spots of apically converging cell processes are still discernible.

G,H Comparison of CIS pattern in walking leg 1 hemi-neuromeres of *Callipallene* sp. (**G**, same stage as in **A-C**) and *Pseudopallene* sp. (**H**, ES 4). Note the similar number and arrangement of CISs and the beginning formation of an apical depression in the posterior region. Arrowhead with question mark in **G** marks CIS with no potential counterpart in **H**. The cells in the VNE of *Callipallene* sp. are smaller and more numerous. Dashed lines indicate midline region. Asterisk in **G** marks damaged region. Arrow in **G** points at apical tangential division.

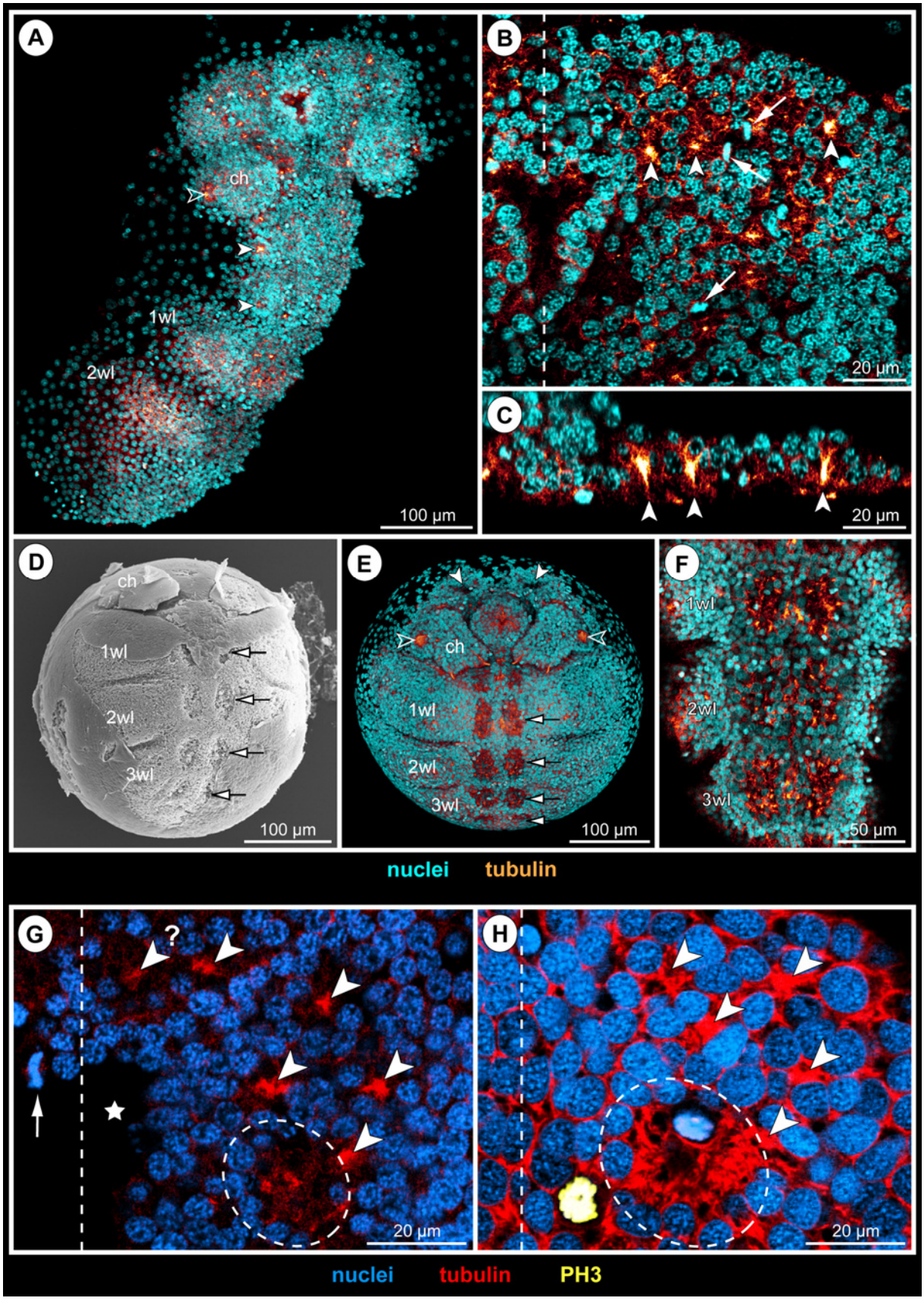
A
ch
1wl
2wl
100 µm
B
20 µm
C
20 µm
D
ch
1wl
2wl
3wl
100 µm
E
ch
1wl
2wl
3wl
100 µm
F
1wl
2wl
3wl
50 µm
nuclei tubulin
G
?
20 µm
H
20 µm
nuclei tubulin PH3

Fig. 69: Early neurogenesis in *Pycnogonum litorale*.

Tubulin labeling and nuclear staining, stage 4 according to Machner and Scholtz (2010). Dashed lines mark midline region. Scale bars as indicated in each image.

A Detail of pre-cheliforal lobe, horizontal 2D projection of curved composite optical sections. Dashed oval highlights forming pharynx. Note the scattered bright spots in the pre-cheliforal lobe.

B Overview of VNE, horizontal 2D projection of curved composite optical sections. Note the same bright apical spots as in the pre-cheliforal lobe. Their correspondence to cell processes of single cells or small clusters of cells with basally displaced nucleus remains to date unresolved.

C Overview of ventral VNE, horizontal 2D projection of curved composite optical sections. Note the low number of cells (as indicated by the nuclei) in the apical VNE of the developing protonymphon larva. Interspersed between the nuclei, less intensely stained lipid drops (embryonic yolk) are discernible.

Fig. 70: SCNPs during neurogenesis of *Stylopallene cheilorhynchus* and *Nymphon gracile*.

Optical sections of 'membrane'- and tubulin-labeled specimens (**A-C** and **D-F**, respectively) with nuclear counterstain. Oblique slicers have been aligned to show asymmetry/symmetry of forming sister cells as clearly as possible. As a consequence, sections are frequently oriented obliquely horizontal. Dashed lines mark midline region. Asterisks label big SCNPs that are not in division. White spots indicate epidermal cells. Scale bars = 10 µm.

A-C *Stylopallene cheilorhynchus*, 'horizontal' sections through anlagen of walking leg hemi-ganglia 1 of PS 1. **A** Apical section through morphologically left hemi-ganglion anlage. Note significant size differences between SCNPs and other GCs (e.g. in left lower corner). Arrow points at SCNP in metaphase. **B** Slightly sub-apical to **A**. Two asymmetric divisions are visible. Arrows mark the bigger, arrowheads the smaller of the future sister cells. Note the already formed membrane between the two cells of one division. **C** Apical section through morphologically right hemi-ganglion anlage. Arrow points at SCNP in prophase. Open arrowheads point at forming sister cells of a symmetric division of an INP amongst the more peripheral GCs

D-F *Nymphon gracile*, 'horizontal' sections through anlagen of walking leg hemi-ganglia 1 of PS 2. **D** Apical section through morphologically right hemi-ganglion anlage. Arrows indicate three SCNPs in metaphase (~tangential orientation). Open arrowhead marks smaller symmetric division (telophase) of an epidermal precursor bordering the hemi-ganglion anlage. **E** Apical section through morphologically left hemi-ganglion anlage. Arrow points at the bigger, arrowhead at the smaller future sister cell of an asymmetric division. Bluish halo on the right side represents autofluorescence of the larval cuticle. **F** Same hemi-ganglion anlage as in **E**, section slightly shifted to reveal differently sized sister cells of another asymmetric division (arrow and arrowhead).

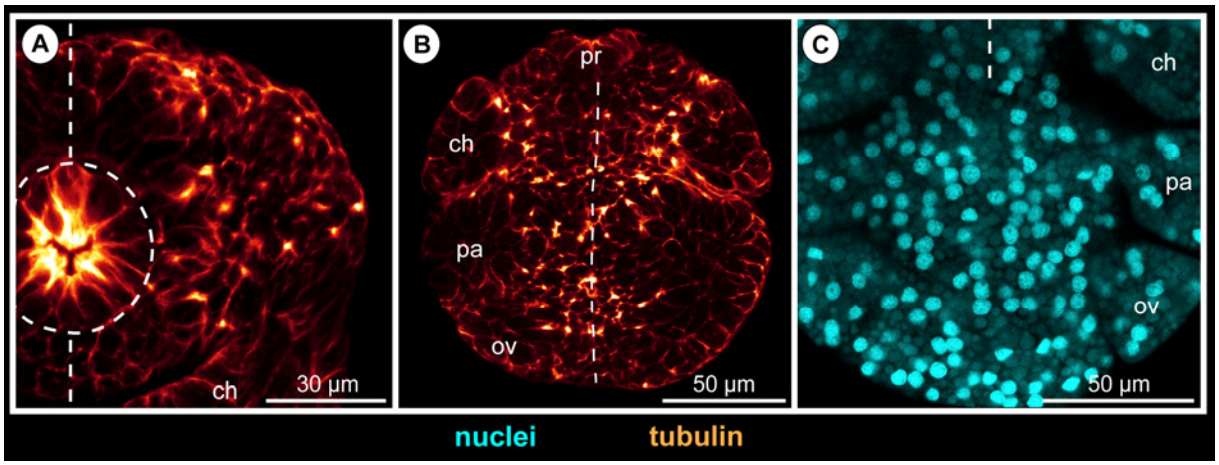
A
ch
30 µm
B
pr
ch
pa
ov
50 µm
C
ch
pa
ov
50 µm
nuclei
tubulin

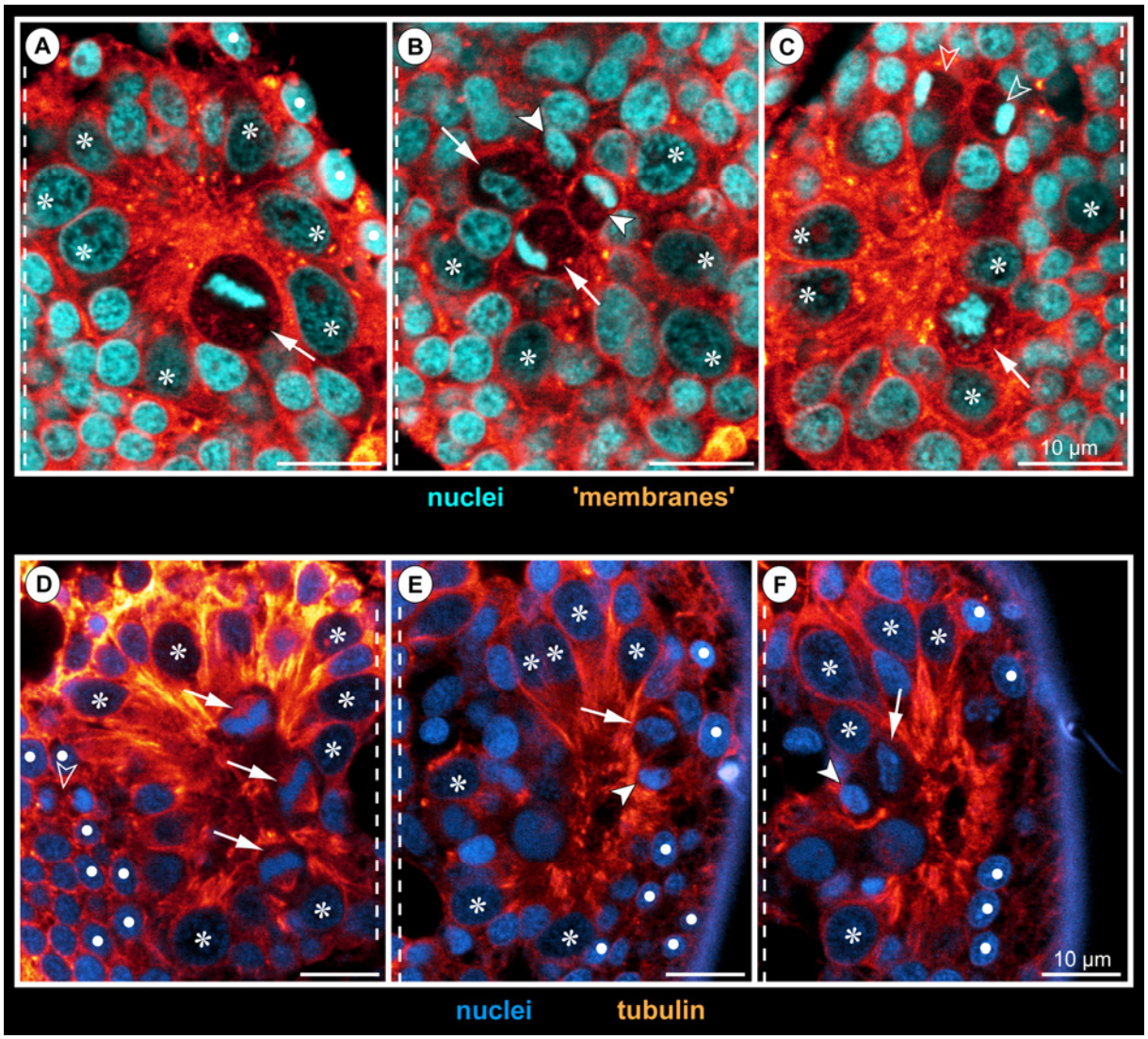
A
B
C
10 µm
nuclei
'membranes'
D
E
F
10 µm
nuclei
tubulin

Fig. 71: Segmentally paired apical cell clusters in other pycnogonid taxa.

A-C *Nymphon spinosum*. **A** Sagittal section through late post-embryonic stage (modified from Dogiel 1913). Arrowheads mark external apical clusters of the VNC. **B,C** Transversal sections through developing walking leg ganglion anlagen (modified from Dogiel 1911). **B** Early stage. The hemi-ganglion anlagen proper are formed by a compact GC mass. Ventral to the latter, nascent apical clusters with big spindle-shaped cells lining a shallow central depression are found. **C** Advanced stage. The hemi-ganglion anlage has considerable increased in size. Asterisk marks ganglionic neuropil. A separate apical cell cluster is connected to the hemi-ganglion anlage via a fibrous connection.

D Ventral view of post-embryonic stage 6 of *Nymphon grossipes* (modified from Bogomolova and Malakhov 2003). At the ventral side of the walking leg ganglia 1-3 small apical clusters are shown.

E Anlage of walking leg hemi-ganglion of *Achelia echinata* (modified from Sanchez 1959). The big spindle-shaped cells have detached from the apical epidermis, forming a cluster with central cavity. The detached cluster is not located external to the hemi-ganglion anlage but embedded within the latter's ventral soma cortex. Asterisk labels ganglionic neuropil.

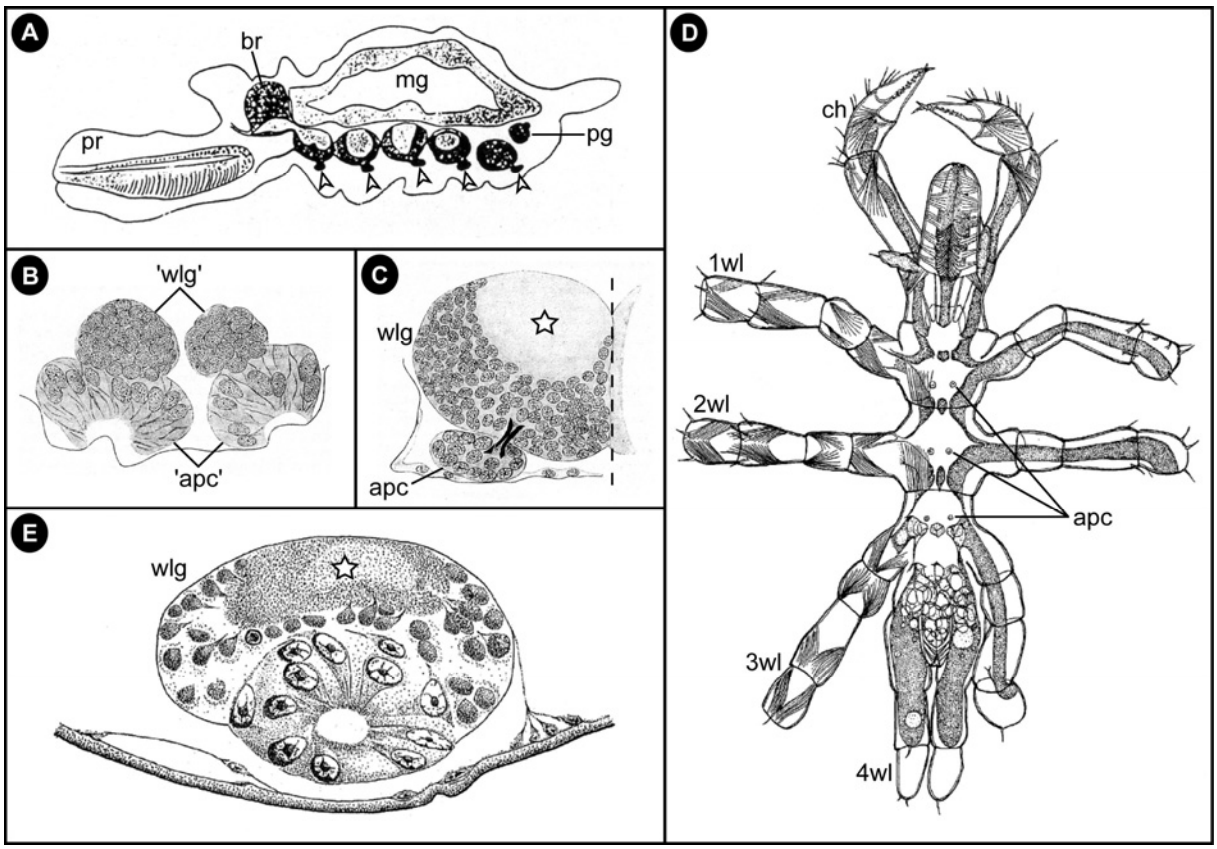
A
br
mg
pr
pg
B
'wlg'
'apc'
C
wlg
apc
D
ch
1wl
2wl
apc
3wl
4wl
E
wlg

Fig. 72: Neurogenesis in other arthropod lineages.

Schematic drawings of idealized sagittal sections of single ventral hemi-neuromeres. For the sake of simplicity, only three CISs/NBs are depicted per hemi-neuromere. See text sections 4.3.1. and 4.3.2. for references, which represent the basis for the schemes.

A Onychophora. NPs segregate individually from the apical VNE. Neither a spatio-temporally stereotypic segregation pattern, nor distinct proneural ASH expression domains/clusters are observable. Segregated NPs form a sub-apical layer and divide at least once in symmetric fashion, giving rise to immature neuronal cells (potentially also glial cells) and presumably some INPs. Basal-most, the first neuronal cells differentiate and extend growth cones anteriorly. In advanced stages, the segmental 'ventral organs' begin to form as transformations of the VNE, lying basal to the medullary cords.

B Euchelicerata (predominantly *Cupiennius salei*). CISs form sequentially in the single-layered VNE. ASH expression in proneural domains predates CIS formation. Mostly tangential cell divisions are found in the apical VNE. Occasionally, immigrating flask-shaped cells undergo mitosis (at least in *Limulus polyphemus*). Immature GCs detach and differentiate basally to persisting CISs. Several CISs become cell-rich units, being surrounded by glial-like sheath cells (division patterns not studied in detail). Symmetric divisions of INPs are encountered basally, close to the forming neuropil. Some CISs become internalized as epithelial vesicles during late embryogenesis. Sheath cell fate remains unresolved. The ventral epidermis overgrows the central hemi-segment region.

C Myriapoda (predominantly *Glomeris marginata*). Similar to euchelicerates. Yet, VNE cells are often more closely packed. Association of cell divisions with the CISs is observable, but existence of a specialized NP type remains ambiguous. At least in centipedes, a longitudinal primary tract with protocerebral origin predates segmental axonogenesis. Sheath cell existence remains unresolved. Detached INPs in sub-apical position are observable. The central hemi-neuromere invaginates and detaches, forming a transient ganglionic cavity and being overgrown by the ventral epidermis. Cell types and division patterns in advanced neurogenic stages await reinvestigation.

D 'Crustacea' (predominantly *Orchestia cavimana*). NBs form sequentially in a stereotypic ectodermal division sequence. They are maintained apically, giving rise to GMCs by repeated asymmetric radial divisions. Some NBs intermittently switch to symmetric tangential divisions to generate additional epidermal cells. GMCs divide once to produce immature GCs (neurons and/or glial cells). A distinct subset of segmental pioneer neurons is known for some malacostracans. NB fate remains currently unresolved. At least in *Daphnia magna*, no stereotypic proneural ASH expression in clusters is apparent.

E Hexapoda (predominantly *Drosophila melanogaster* and *Schistocerca* sp.). Similar to crustaceans. However, NBs are sequentially singled out (Notch signaling) from stereotypic clusters with proneural expression (members of achaete-scute complex) and immigrate into sub-apical position prior to proliferation. Most NBs undergo apoptosis after generation of their lineage. Association of NBs with specialized sheath and cap cells has so far only been reported in grasshoppers. The plesiomorphic character of these cells is accordingly questionable and they were omitted in the schemes.

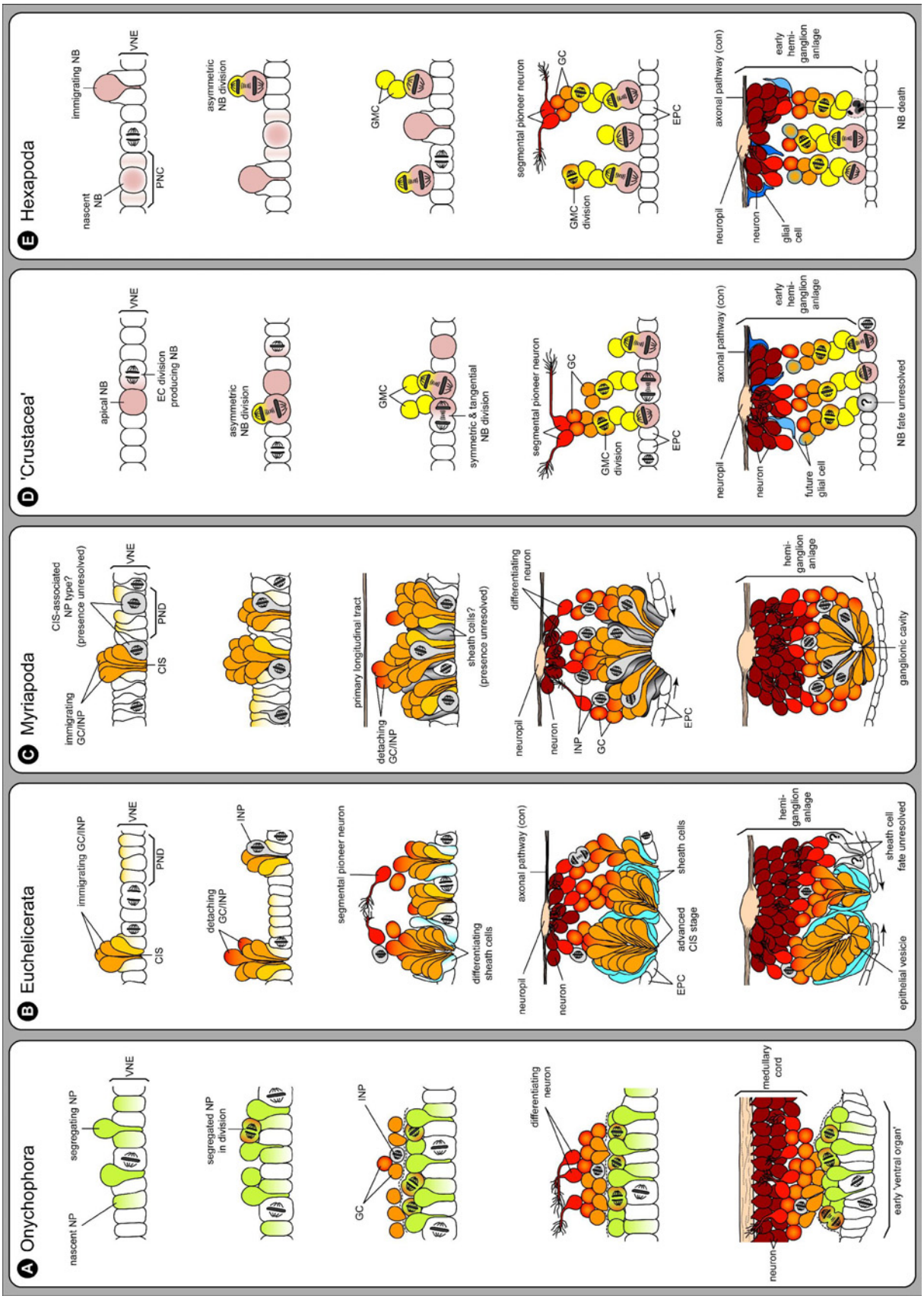
A Onychophora
nascent NP
segregating NP
VNE
segregated NP in division
GC
INP
differentiating neuron
neuron
medullary cord
early 'ventral organ'
B Euchelicerata
immigrating GC/INP
VNE
PND
CIS
detaching GC/INP
INP
segmental pioneer neuron
differentiating sheath cells
neuropil
axonal pathway (con)
neuron
sheath cells
advanced CIS stage
EPC
hemi-ganglion anlage
epithelial vesicle
sheath cell fate unresolved
C Myriapoda
CIS-associated NP type? (presence unresolved)
immigrating GC/INP
VNE
PND
CIS
primary longitudinal tract
detaching GC/INP
sheath cells? (presence unresolved)
differentiating neuron
neuropil
neuron
INP
GC
EPC
hemi-ganglion anlage
ganglionic cavity
D 'Crustacea'
apical NB
EC division producing NB
VNE
asymmetric NB division
GMC
symmetric & tangential NB division
segmental pioneer neuron
GC
GMC division
EPC
axonal pathway (con)
early hemi-ganglion anlage
neuropil
neuron
future glial cell
NB fate unresolved
E Hexapoda
immigrating NB
nascent NB
VNE
PNC
asymmetric NB division
GMC
segmental pioneer neuron
GC
GMC division
EPC
axonal pathway (con)
early hemi-ganglion anlage
neuropil
neuron
glial cell
NB death

Fig. 73: Cell strands between onychophoran VOs and developing medullary cords.
Transversal sections. Black arrowheads mark locally concentrated cellular connections between ventral neuroectoderm/VOs and underlying developing medullary cords. Asterisks indicate developing neuropil of the cords.

A Early stage of a VO in the trunk of *Paraperipatus amboinensis* (modified from Pflugfelder 1948).

B Early stage of the VO in the jaw segment of *Euperipatoides kanangrensis*, methylene blue-stained transversal section (Original: Joakim Eriksson).

C Early stage of a VO in the trunk of *Peripatus edwardsii* (modified from Kennel 1886).

D Advanced stage of a VO in the trunk of a newborn *Peripatus edwardsii* (modified from Kennel 1886). Note spatial separation of the medially approached VOs and the medullary cords.

E Advanced stage of a VO in the trunk of *Peripatus capensis* (modified from Sedgwick 1888). The depicted connections of VOs and medullary cords closely resemble the ones in **D**.

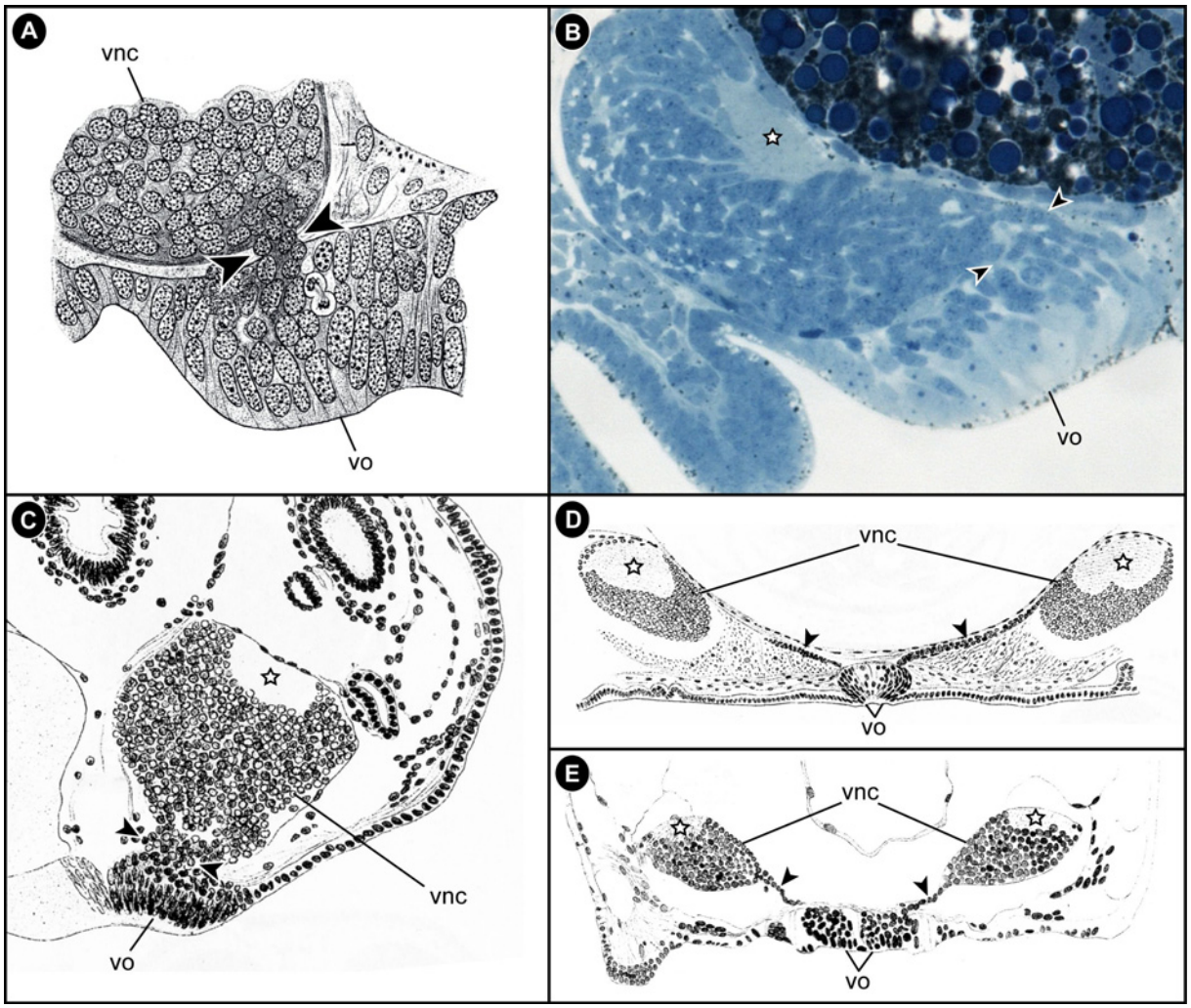
A
vnc
vo
B
vo
C
vnc
vo
D
vnc
vo
E
vnc
vo

Fig. 74: CIS arrangement and cellular composition in *Cupiennius salei*.

Tubulin labeling and nuclear counterstain of embryonic stage 12-13 (according to Wolff and Hilbrant 2011). Scale bars as indicated in each image.

A Ventral view of morphologically left hemi-neuromere of walking leg segment 1, Imaris volume (blend). Midline region is to the left. In tubulin-labeled specimens, CIS locations are already recognizable as dark spots and tiny local pits ('invaginations') in the surface of the hemi-neuromeres (exemplarily labeled by arrowheads).

B Identical hemi-neuromere as shown in **A**, horizontal 2D projection of curved composite optical sections. In horizontal section, CISs are characterized by a tiny central tubulin-negative spot from which the tubulin-positive processes of the flask-shaped cells radiate. Arrowheads mark selected CISs in correspondence to **A**.

C Map of CISs based on hemi-neuromere shown in **A** and **B**, Imaris Surpass (Spots). The spatial CIS array corresponds in detail to the map published by Döffinger and Stollewerk (2010) (see their fig. 1B,C). CIS designation follows the latter study. One additional small CIS was found in the tightly packed CIS array in the posterior hemi-neuromere region (marked by question mark), but needs confirmation in additional specimens.

D-G Optical 'transversal' sections through hemi-neuromere. Oblique slicers have been aligned to show as many of the flask-shaped cells as possible included within the selected CISs. Since the latter are often obliquely oriented in relation to the apical surface, the resulting sections are obliquely transversal. Note the differences in cell numbers within different CISs.

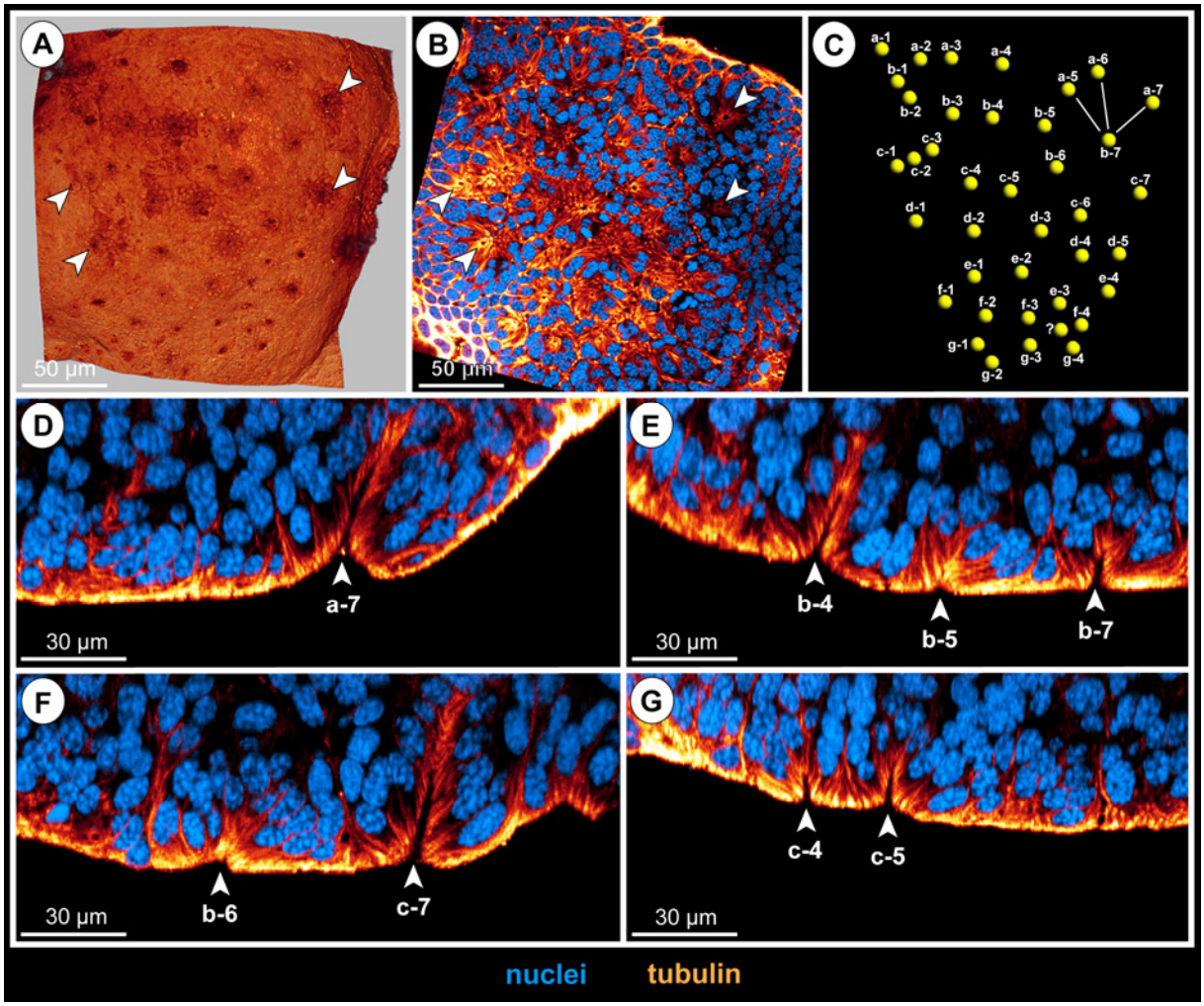
A
50 µm
B
50 µm
C
a-1
a-2
a-3
a-4
a-5
a-6
a-7
b-1
b-2
b-3
b-4
b-5
b-6
b-7
c-1
c-2
c-3
c-4
c-5
c-6
c-7
d-1
d-2
d-3
d-4
d-5
e-1
e-2
e-3
e-4
f-1
f-2
f-3
f-4
?
g-1
g-2
g-3
g-4
D
a-7
30 µm
E
b-4
b-5
b-7
30 µm
F
b-6
c-7
30 µm
G
c-4
c-5
30 µm
nuclei
tubulin

Fig. 75: Two scenarios on the evolution of euarthropod neurogenesis.

Both scenarios are set against the backbone of the Chelicerata (Pycnogonida + Euchelicerata) and Mandibulata (Myriapoda + Tetraconata) hypotheses. Onychophora are taken as outgroup but do not help significantly in the establishment of the euarthropod ground pattern. Color code of characteristic features: green = apomorphic, red = plesiomorphic, black = apomorphic vs. plesiomorphic unclear, gray = in need of verification. Gray box at the bottom shows the reconstructed features in the euarthropod stem lineage.

A Convergent evolution of pycnogonid SCNPs and tetraconate NBs.

B Common origin of pycnogonid SCNPs and tetraconate NBs from ancestral SCNP type with subsequent lineage-specific evolution of the latter. The critical assumption in this scenario is the occurrence of SCNPs in myriapods.

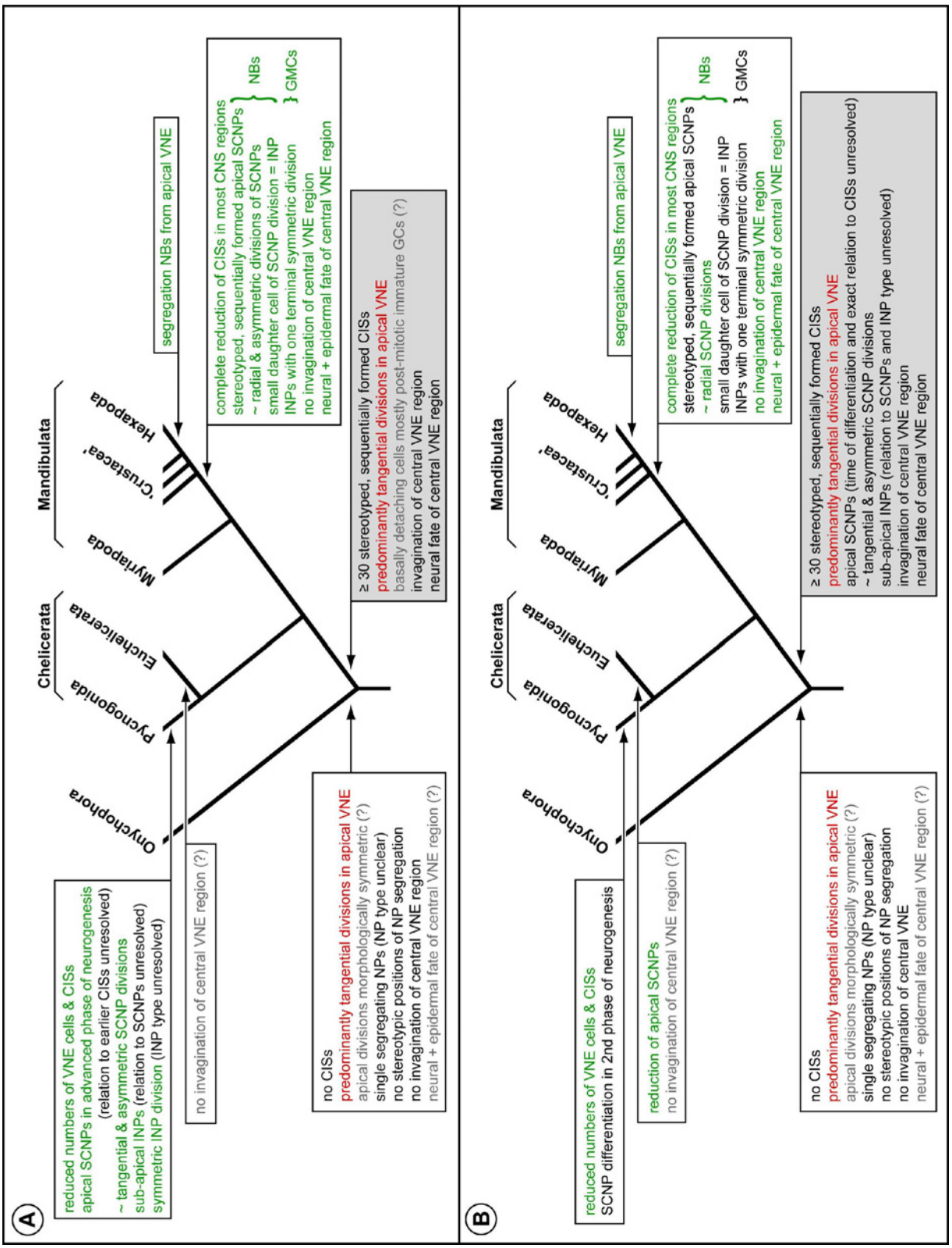
A
reduced numbers of VNE cells & CISs
apical SCNPs in advanced phase of neurogenesis
(relation to earlier CISs unresolved)
~ tangential & asymmetric SCNP divisions
sub-apical INPs (relation to SCNPs unresolved)
symmetric INP division (INP type unresolved)
no invagination of central VNE region (?)
no CISs
predominantly tangential divisions in apical VNE
apical divisions morphologically symmetric (?)
single segregating NPs (NP type unclear)
no stereotypic positions of NP segregation
no invagination of central VNE region
neural + epidermal fate of central VNE region (?)
Onychophora
Chelicerata
Pycnogonida
Euchelicerata
Mandibulata
Myriapoda
'Crustacea'
Hexapoda
segregation NBs from apical VNE
complete reduction of CISs in most CNS regions
stereotyped, sequentially formed apical SCNPs
~ radial & asymmetric divisions of SCNPs
small daughter cell of SCNP division = INP
INPs with one terminal symmetric division
no invagination of central VNE region
neural + epidermal fate of central VNE region
NBs
GMCs
≥ 30 stereotyped, sequentially formed CISs
predominantly tangential divisions in apical VNE
basally detaching cells mostly post-mitotic immature GCs (?)
invagination of central VNE region
neural fate of central VNE region
B
reduced numbers of VNE cells & CISs
SCNP differentiation in 2nd phase of neurogenesis
reduction of apical SCNPs
no invagination of central VNE region (?)
no CISs
predominantly tangential divisions in apical VNE
apical divisions morphologically symmetric (?)
single segregating NPs (NP type unclear)
no stereotypic positions of NP segregation
no invagination of central VNE
neural + epidermal fate of central VNE region (?)
Onychophora
Chelicerata
Pycnogonida
Euchelicerata
Mandibulata
Myriapoda
'Crustacea'
Hexapoda
segregation NBs from apical VNE
complete reduction of CISs in most CNS regions
stereotyped, sequentially formed apical SCNPs
~ radial SCNP divisions
small daughter cell of SCNP division = INP
INPs with one terminal symmetric division
no invagination of central VNE region
neural + epidermal fate of central VNE region
NBs
GMCs
≥ 30 stereotyped, sequentially formed CISs
predominantly tangential divisions in apical VNE
apical SCNPs (time of differentiation and exact relation to CISs unresolved)
~ tangential & asymmetric SCNP divisions
sub-apical INPs (relation to SCNPs and INP type unresolved)
invagination of central VNE region
neural fate of central VNE region

Fig. 76: Comparison of germ band size, cell number and cell sizes between callipallenids and spiders.

Tubulin-labeled embryos with nuclear counterstain, in part with additional PH3 labeling (**C**,**F**). Scale bars as indicated in each image.

A Ventral view of germ bands of *Cupiennius salei* (left, only left half of prosomal region shown), *Parasteatoda tepidariorum* (right) compared to *Callipallene* sp. (mid-top) and *Pseudopallene* sp. (mid-bottom), flat preparations, Imaris volume (MIP).

B Ventral detail of pre-cheliceral lobe of *C. salei* (left) and pre-cheliceral lobe up to palpal segment of *P. tepidariorum* (right) compared to anterior view of *Pseudopallene* sp. embryo (ES 4, middle), Imaris volume (blend), only nuclear stain shown. Note the small cell sizes and high cell number in both spiders in comparison to the callipallenid. Within the pre-cheliceral lobes of the spiders far more CISs than in *Pseudopallene* are discernible as tiny 'holes' in the nuclear stain.

C-F Comparison of cell size and cell numbers in the VNC of spiders and callipallenids. Horizontal 2D projections of curved composite optical sections. Dashed line marks midline region.

C *C. salei*, hemi-neuromere of walking leg segment 2. Note the apical mitoses scattered between the CISs.

D *Callipallene* sp., hemi-neuromere of walking leg segment 1. The apical area of the hemi-neuromere represents not even a quarter of the area in corresponding hemi-neuromeres of the two spider species (**C**,**F**). Neuroectodermal cell size appears similar to spiders. Asterisk marks damaged region.

E *Pseudopallene* sp., hemi-neuromere of walking leg segment 1. The apical area of the hemi-neuromere is significantly smaller and the neuroectodermal cells are slightly bigger than in the two spider species.

F *P. tepidariorum*, hemi-neuromere of walking leg segment 2. Note some scattered apical mitoses and the distinct tubulin labeling of CISs.

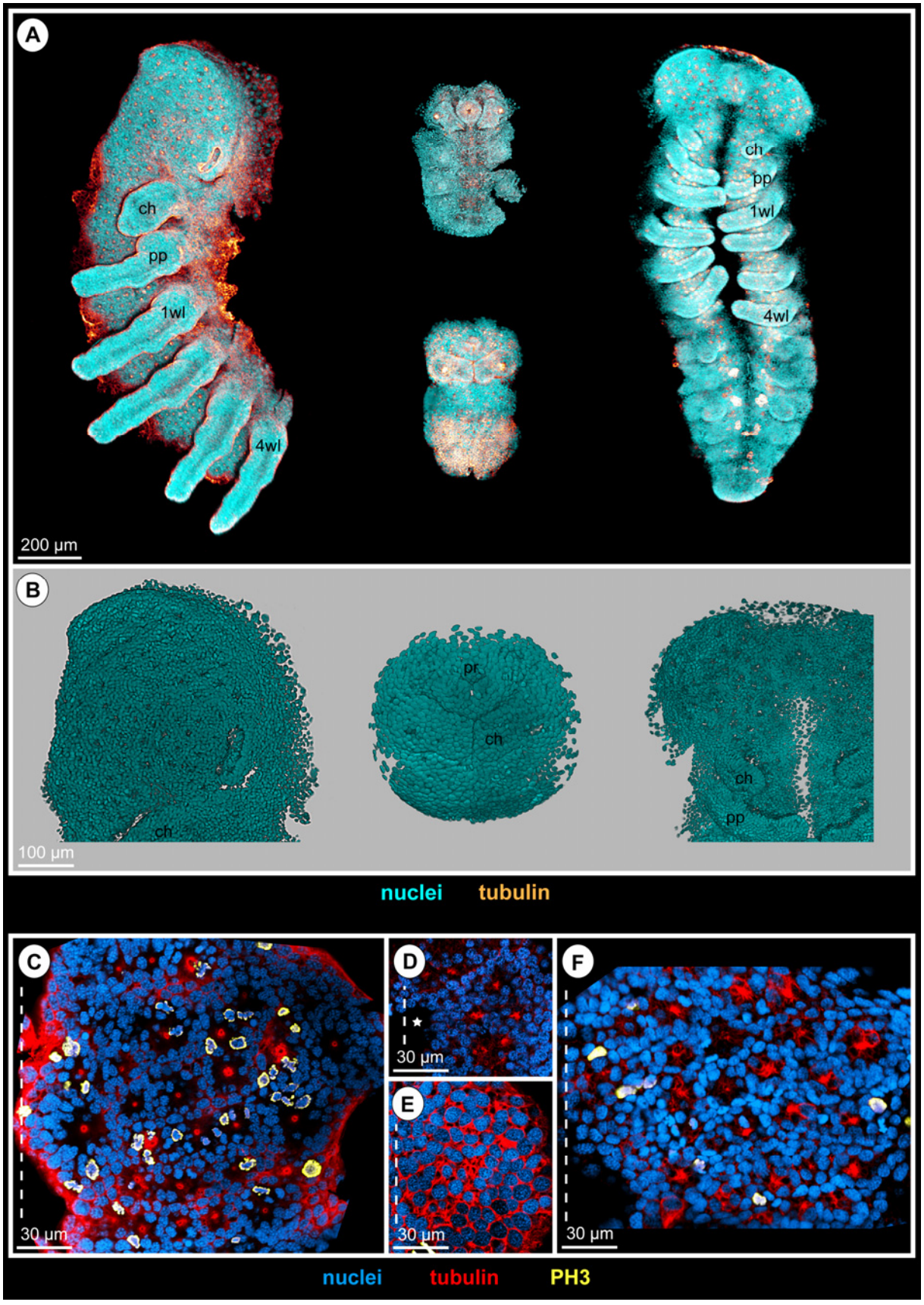
A
ch
pp
1wl
4wl
200 µm
B
ch
pr
ch
ch
pp
100 µm
nuclei tubulin
C
30 µm
D
30 µm
E
30 µm
F
30 µm
nuclei tubulin PH3

Fig. 77: Overview of CNS anatomy of different pycnogonid species.

A Lateral view of dissected CNS of *Cilunculus japonicus* (Ammotheidae), stereo microscope image. The midgut is still attached to the nervous system. The anteriorly directed midgut diverticulum of the chelifore is located directly lateral to the dorsal brain and the ventrally set off sub-esophageal ganglion. The esophagus (anteriorly extending pharynx is visible) runs between both ganglia. Note the bilobed appearance of the ganglionic neuropil in the sub-esophageal ganglion (arrowheads), indicating still its bipartite composition of palpal and ovigeral neuromere.

B Lateral view of dissected CNS of *Pseudopallene* sp. (Callipallenidae), stereo microscope image. Note the short circum-esophageal connective (arrowheads) spanning between cheliforal (i.e., deutocerebral) neuromere of the supra-esophageal brain and the palpal neuromere of the composite sub-esophageal ganglion.

C Dorsal view of dissected CNS of *Pycnogonum litorale* (Pycnogonidae), inverted fluorescence microscope image of serotonin-like immunoreactive sub-structures. Distinct long circum-esophageal connectives (arrowheads) extend between supra-esophageal brain and sub-esophageal ganglion. Note tripartite composition of the latter, the neuromere of walking leg segment 1 being posteriorly fused to the ovigeral neuromere. Star marks the course of the esophagus.

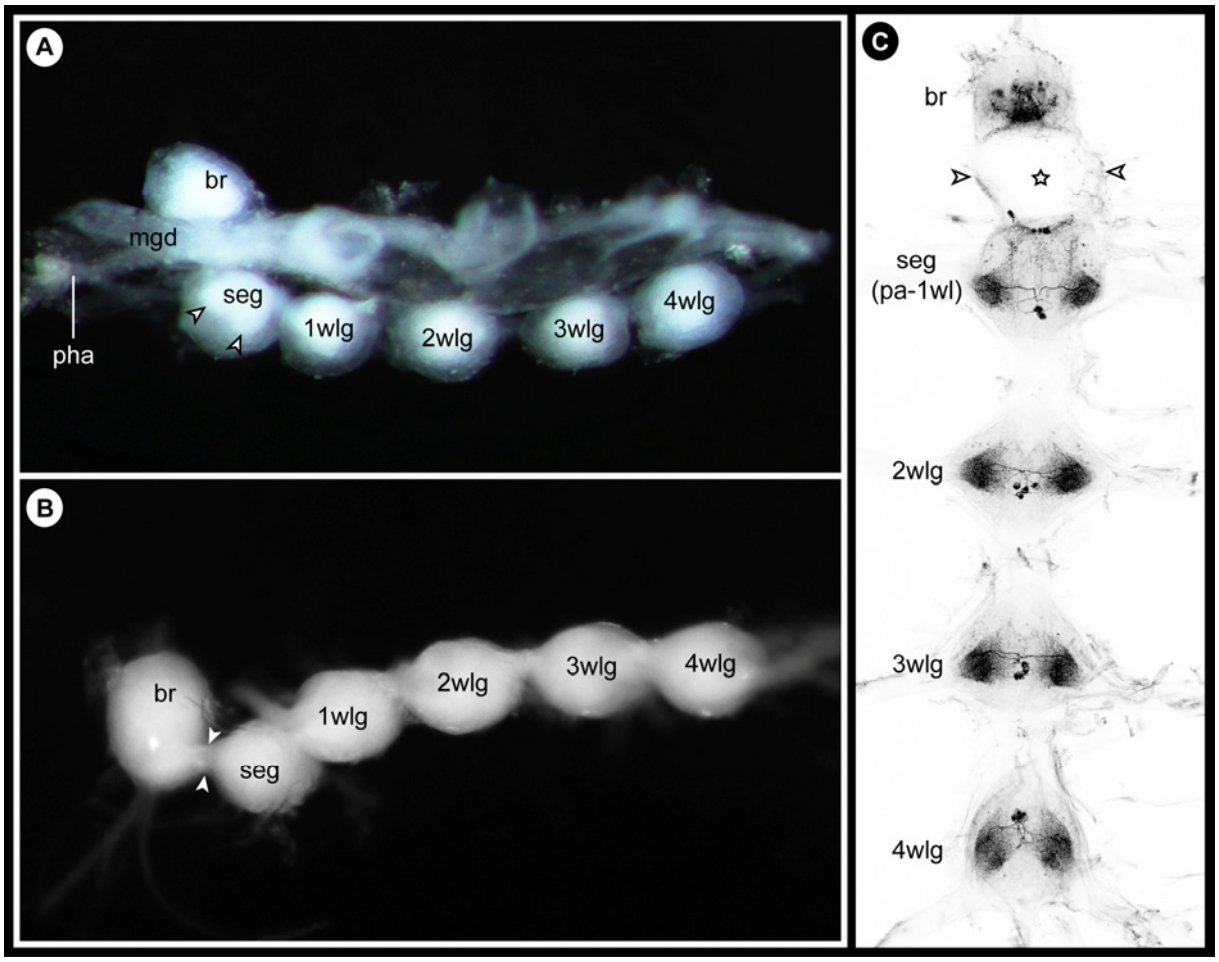
A
br
mgd
seg
1wlg
2wlg
3wlg
4wlg
pha
B
br
1wlg
2wlg
3wlg
4wlg
seg
C
br
seg
(pa-1wl)
2wlg
3wlg
4wlg

Fig. 78: Brain development in the pre-cheliforal lobe and morphogenesis of proboscis and chelifores in *Pseudopallene* sp. (ES 2-3 – late PS 1).

Schematic drawings.

In the pre-cheliforal lobe, the different invaginating sub-areas as well as the later on persisting proliferation regions of the detached brain anlage have been color-coded from ES 4-5 onwards. Dark gray outlines represent already detached GCs underlying the invaginating regions. Note that the neuromere affiliation of the central depression and its derivative, the apical brain cluster, remains ambiguous due to the posteriorly confluent deutocerebral groove between chelifore and proboscis. Simplified arrangements of neurite bundles and differentiating neuropil are depicted from ES 6-7 onwards in orange and yellow, respectively. Within the chelifore anlagen, the position and extension of the developing spinning gland (darker gray tones) and chela gland (light gray) can be followed. The overgrowing of the originally protruding pharyngeal cell sub-populations during proboscis development is shown from ES 4-5 to ES 5-6. Due to the postero-ventral shift of the proboscis anlage and the simultaneous antero-dorsally directed movement of pre-cheliforal lobe and chelifore base, the schemes of later stages (late ES 6-7 – PS 1) represent an increasingly more antero-dorsal view of the embryo/ hatched larva.

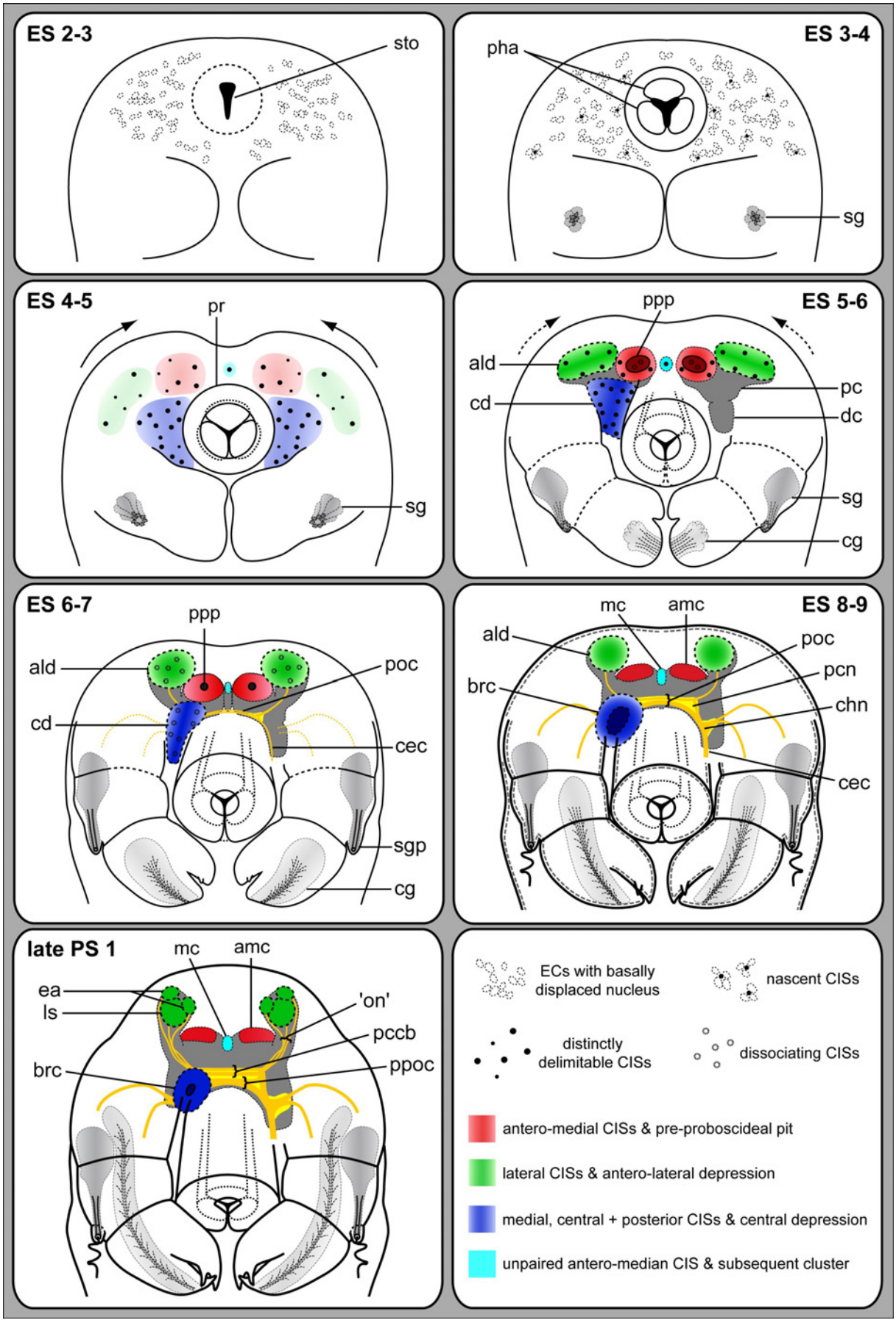
ES 2-3
sto
ES 3-4
pha
sg
ES 4-5
pr
sg
ES 5-6
ppp
ald
cd
pc
dc
sg
cg
ES 6-7
ppp
ald
poc
cd
cec
sgp
cg
ES 8-9
mc
amc
ald
poc
pcn
brc
chn
cec
late PS 1
mc
amc
ea
ls
'on'
pccb
brc
ppoc
ECs with basally displaced nucleus
nascent CISs
distinctly delimitable CISs
dissociating CISs
antero-medial CISs & pre-proboscideal pit
lateral CISs & antero-lateral depression
medial, central + posterior CISs & central depression
unpaired antero-median CIS & subsequent cluster

Explanations of Movies

Movie 1: Stomodeal cell immigration during ES 2 of *Pseudopallene* sp.

Tubulin labeling (orange) with nuclear counterstain (green), Imaris volume (blend), same embryo as shown in figure 5C.

The movie starts from antero-ventral view. The embryo turns first in ventral, then in lateral direction. Anteriorly in the germ band, a median tubulin-positive region is found where cells of the future stomodeum immigrate. The semi-circular furrows of the chelifore anlagen are only indistinctly recognizable. A virtual clipping plane along the sagittal axis of the embryo reveals the interiorly displaced nuclei of the immigrating stomodeal cells.

Movie 2: Detail of the outgrowing proboscis in ES 4 of *Pseudopallene* sp.

Tubulin labeling (orange) with nuclear counterstain (green), Imaris volume (blend).

The movie starts from ventral view. The embryo rotates first laterally, then dips backwards. The arrangement of the three cell populations creates the characteristic Y-shaped pharynx lumen. A distinct ring-like ridge of surrounding ectodermal cells starts to cover these cell populations (compare to Fig. 6G). At this stage, the medially touching chelifore anlagen are still positioned fully posterior to the proboscis.

Movie 3: Detail of proboscis in ES 7 of *Pseudopallene* sp.

Tubulin labeling (orange) with nuclear counterstain (green), Imaris volume (blend).

The movie starts from ventral view. The embryo rotates first laterally, then dips backwards. The developing mouth opening has a triangular shape. A distinct notch is found at the posterior margin of the proboscis, giving its distal-most portion a horseshoe-like appearance. The chelifore scapes that flank the proboscis laterally are damaged in this specimen.

Movie 4: Chela gland extensions, cuticular slit-like glands and sensory setae of PS 2 of *Pseudopallene* sp.

Nuclear staining (green) and autofluorescence (glow), Imaris volume (MIP) and oblique slicer, same specimen as in figure 12H.

The movie starts with a volume of chelifores and proboscis in antero-ventral view (in relation to body axis), zooms in and shows an virtual section series through both structures. In addition to the big sensory setae on the chela, the cuticle bears scattered tiny slit-like glands and bifurcate setae on chelifores and proboscis. The chela gland extends beyond the scape, being attached to the primordial midgut diverticulum of the chelifore. Note strong autofluorescent signal of the cuticular oyster basket in the pharynx.

Movies 5 and 6: VNE of ES 2-3 of *Pseudopallene* sp.

Virtual horizontal section series, Imaris oblique slicer passing from apical to basal through the VNE of walking leg neuromere 1.

Movie 5: Specimen 1.

Tubulin labeling (glow) with nuclear counterstain (blue), same embryo as in figure 19A-C'.

Note the beginning constriction of the apical cortices of cells with basally displaced nucleus. Some apical tangential cell divisions are visible. The VNE is underlain by scattered embryonic entodermal cells with big, apico-basally flattened nuclei. The VMR is characterized by lower density and basal extension of cells. Basally located yolk fragments show weak blue labeling, smaller (putatively degenerating) nuclei are scattered medially between them.

Movie 6: Specimen 2.

Tubulin (glow) and PH3 labeling (green) with nuclear counterstain (blue), same embryo as in figure 23A (mirror image).

See specimen 1 (Movie 5) for further details. In specimen 2, the VNE cells are already more densely packed than in specimen 1, but no distinct CISs are formed yet. Numerous apical tangential divisions are PH3-labeled.

Movie 7: CISs in the neuroectoderm of early ES 4 of *Pseudopallene* sp.

Tubulin (glow) and PH3 labeling (green) of a germ band, flat preparation, Imaris volume (MIP), same embryo as in figure 18C. The morphologically left chelifore anlage has been masked (Imaris contour surface).

Note tubulin-positive spots representing apically bundled processes of flask-shaped cells in CISs of the pre-cheliforal lobes and VNE. Numerous apical mitoses are PH3-labeled, in some cases with clearly tangential orientation of the division.

Movie 8: CISs in the VNE of ES 4 of *Pseudopallene* sp.

Tubulin (glow) and PH3 labeling (green) of a complete embryo, Imaris volume (MIP).

The post-cheliforal region of the germ band is shown in ventral view, swings slightly from side to side before zooming into the VNE region of walking leg neuromere 1. Note the largely bilaterally symmetric array of the bright CIS-spots in this region and their lack in the VMR. Several tangential mitoses in metaphase and later stages are discernible.

Movies 9-11: CIS pattern in walking leg neuromere 1 of ES 4 of *Pseudopallene* sp.

Tubulin (glow) and PH3 labeling (green) with nuclear counterstain, virtual horizontal section series, Imaris oblique slicer passing from apical to basal through the neuromere.

Movie 9: Specimen 1.

Same embryo as in figure 22A,A' (mirror image). The positions of the six consistently identified CISs are indicated by green spots before the slicer starts to move basally. Note higher concentration of apical cell processes in the posterior portion of the neuromere, indicating the beginning formation of the apical depression. The VMR has a lower apico-basal extension than the more lateral hemi-neuromeres. Note presence of small, heterogeneously labeled degenerating nuclei in VMR and at the margins of the hemi-neuromeres.

Movie 10: Specimen 2:

Same embryo as in figure 22B,B', see specimen 1 (Movie 9) for further explanation. Note that the apically bundled processes of the CISs are better defined than in specimen 1.

Movie 11: Specimen 3:

Same embryo as in figure 22D, see specimen 1 (Movie 9) for further explanation. CISs have not been marked by spots. Note high number of degenerating nuclei within and underneath the VMR and at the margins of the hemi-neuromeres. Far basally, a single cell in mitosis is PH3-labeled. Its nature (immigrated NP versus entodermal cell) is not unequivocally resolved.

Movie 12: Asymmetric SCNP divisions in the developing walking leg hemi-ganglion 2 of ES 6 of *Pseudopallene* sp.

Tubulin (red) and PH3 labeling (yellow) with nuclear counterstain (blue), virtual horizontal section series, Imaris oblique slicer passing from apical to basal through apical hemi-ganglion portion, midline region to the right, same embryo as in figure 28B.

The SCNPs have only started to enlarge. Apically in the section series, a PH3-positive asymmetric SCNP telophase is passed close to the rim of the depression (left-bottom). Three additional asymmetric SCNP divisions are located in the center of the depression, the most obvious one being strongly PH3-labeled.

Movie 13: Asymmetric SCNP divisions in the developing walking leg hemi-ganglion 1 of late ES 7 of *Pseudopallene* sp.

Phalloidin labeling (glow) with nuclear counterstain (cyan), virtual horizontal section series, Imaris oblique slicer passing from apical to basal through apical hemi-ganglion portion, midline region to the right, same embryo as in figure 29 (mirror image).

The SCNPs have considerably enlarged. Four SCNP divisions are visible including a prophase (bottom-left), a metaphase (bottom-right) and two late stages (after cytokinesis) with morphologically asymmetric sister cells (mid-right, top-right). The smaller cell of each division lies more basally. A slight shift in the two channels is due to movement of the embryo during the recording process.

Movie 14: SCNP and INP divisions in the developing walking leg ganglion 1 of early ES 7 of *Pseudopallene* sp.

Tubulin (red) and PH3 labeling (yellow) with nuclear counterstain (blue), virtual transversal section series, Imaris oblique slicer passing from posterior to anterior through ganglion anlage, same embryo as in figures 26A-C and 28D.

The apical SCNPs are significantly bigger than the more lateral ectodermal cells of the protruding walking leg anlagen and the apical cells of the VMR (prospective epidermal cells). Amongst others, two PH3-labeled tangential asymmetric divisions are passed in the right hemi-ganglion anlage. Note several sub-apical INP divisions and the medio-laterally compacted cells of the VMR that are wedged between the hemi-ganglion anlagen. Basal-most, delicate transversally extending neurite bundles are discernible.

Movie 15: SCNP and INP divisions in the developing walking leg ganglion 1 of ES 8 of *Pseudopallene* sp.

Tubulin (red) and PH3 labeling (yellow) with nuclear counterstain (blue), virtual transversal section series, Imaris oblique slicer passing from posterior to anterior through ganglion anlage, same embryo as in figures 26C-E and 28G (mirror image).

The apical SCNPs have enlarged further. Note increased GC number compared to early ES 7 (Movie 14) and distinctly protruding walking leg anlagen lateral to the hemi-ganglia. In the first section of the series, the sister cells of a tangential asymmetric division are visible in the right hemi-ganglion anlage. Especially medially, the SCNPs show a largely bilaterally symmetric arrangement. In the left hemi-ganglion anlage, the arrangement and shape of two nuclei in this medial region indicate a prior asymmetric division (compare to Fig. 28G). Note several sub-apical INP divisions and the further developed basal embryonic commissure The apical VMR cells (epidermal cells) are clearly distinguishable from the SCNPs. Several unpaired medio-laterally flattened nuclei are wedged between the hemi-ganglion anlagen (putative glial cells with VMR origin). First signs of the beginning separation of apical and basal ganglion portion are already detectable in the middle of the series.

Movie 16: Nascent apical cell clusters and cell divisions in the developing walking leg ganglion 1 of early PS 1 of *Pseudopallene* sp.

Tubulin (red) and PH3 labeling (yellow) with nuclear counterstain (blue), virtual transversal section series, Imaris oblique slicer passing from posterior to anterior through ganglion anlage, same specimen as in figure 36A-C'.

Note the deepening of the apical invaginations as well as numerous divisions of SCNPs and several sub-apical INPs. While the nascent apical cell clusters remain connected to the underlying ganglion proper via diffuse anterior and posterior cell streams, a distinct separation of both regions is apparent in the middle of the section series. Note a marked increase of the ganglionic neuropil, which is dorsally covered by up to two soma layers. The postero-ventral commissure bundle (passed first in proceeding series) is already separated from the remaining commissural bundles. Note several medial somata with intensely tubulin-labeled cytoskeleton closely associated with the commissural bundles. Dorsally, flattened nuclei of glial cells are scattered in the ganglionic neural sheath.

Movie 17: Detaching apical cell clusters and cell divisions in the developing walking leg ganglion 1 of late PS 1 of *Pseudopallene* sp.

Tubulin (red) and PH3 labeling (yellow) with nuclear counterstain (blue), virtual transversal section series, Imaris oblique slicer passing from posterior to anterior through ganglion anlage.

The apical pits have completely closed and a small central cavity is formed in the resulting apical cell cluster. The foremost apical poles of the cluster cells (including SCNPs) are directed towards the cavity. A thin layer formed by epidermal cells with small apico-basally flattened nucleus covers the cell clusters. Note persisting size differences between the cluster cells, SCNP divisions within clusters as well as some smaller INP divisions in the anterior and posterior cell streams. Several intensely labeled pycnotic bodies

point to the occurrence of cell death between apical clusters and ganglion proper and in part also within the cell streams.

Movie 18: Completely detached apical cell clusters and connecting cell streams in walking leg ganglion 1 of early PS 2 of *Pseudopallene* sp.

Tubulin (red) and PH3 labeling (yellow) with nuclear counterstain (blue), virtual transversal section series, Imaris oblique slicer passing from posterior to anterior through ganglion.

The apical cell clusters are separated from the ventral epidermis by longitudinal muscles. The cell streams are more defined, having lost in diameter. Size differences between cluster cells are not as prominent anymore, but in part still discernible. Morphological identification of SCNPs has become ambiguous. Only a single mitosis is PH3-labeled in the left cluster-stream-system. Note some pycnotic bodies in the cell streams and within the soma cortex. The ganglionic neuropil has significantly gained in volume. Anterior to the distinct postero-ventral commissure, a more elaborate commissural system has developed from the originally compact embryonic commissural bundle. It comprises several separate transversal tracts, which are embedded in midline-spanning neuropil.

Movie 19: Ovigeral cluster-stream-system in the composite sub-esophageal ganglion of PS 3 of *Pseudopallene* sp.

Tubulin (red) and PH3 labeling (yellow) with nuclear counterstain (blue), virtual transversal section series, Imaris oblique slicer passing from posterior to anterior through the ganglion, same specimen as in figure 41A.

Distinct size differences between cluster cells are no longer assessable. The connecting cell streams have further diminished to fibrous strands along which only few cells with elongated nucleus appear to immigrate into the soma cortex. One PH3-labeled cell in the left anterior cell stream is in prophase. On the right side, the slicer proceeds into the more antero-lateral palpal cluster stream system. Note several flattened nuclei of glial cells in the neural sheath. Antero-dorsally, the ganglion is slightly damaged.

Movie 20: Cell count in walking leg ganglion 1 and affiliated apical cluster of PS 6 of *Pseudopallene* sp.

Tubulin labeling (red) with nuclear counterstain (blue), Imaris volume (blend) and oblique slicer.

The movie shows the ventral two thirds of the walking leg ganglion and starts in ventral view. The ganglion rotates 360 degrees around the z-axis (counter-clockwise). Each nucleus of the morphological left hemi-ganglion and apical cell cluster has been marked with a spot (red and light red, respectively). To illustrate the principle of the cell count, an oblique slicer passes from ventral to dorsal to show the single virtual section planes in which nuclei were manually marked. Note the distinct inter-segmental nerve between walking leg ganglia 1 and 2.

Movie 21: Brain and sub-esophageal ganglion and affiliated cluster-stream-systems of PS 2 of *Pseudopallene* sp.

Tubulin (glow) and PH3 labeling (green) with nuclear counterstain (blue), Imaris volume (blend) and oblique slicers, same specimen as in figure 40. The anterior-most regions of the brain (neuraxis) are not included in the scan.

(1) The movie starts in ventral view. The volume turns laterally to reveal the anatomical separation of supra-esophageal brain and sub-esophageal ganglion. Note the unpaired median rostral nerve that extends from the posterior side of the brain and targets the dorsal proboscis antimere as well as the bilaterally paired ventral proboscis nerve leaving the sub-esophageal ganglion anteriorly. Apart from its two main segmental nerve branches, a third posterior nerve leaves the cheliforal neuromere, representing nerve no. 5 *sensu* Wirén (1918).

(2) The volume focuses on the sub-esophageal ganglion and an oblique slicer passes from ventral to dorsal, revealing the apical cell clusters with central cavities and some mitoses at the clusters' transitions into the cell streams. Further dorsally, the ventral palpal and ovigeral commissures are distinctly discernible, lying apical to the midline-spanning ganglionic neuropil in which a system of additional commissural bundles has started to differentiate (compare to movie 20).

(3) The volume focuses on the brain and an oblique slicer passes from posterior to anterior (neuraxis). The apical brain cluster with its distinct cell streams and two mitoses in the morphological right half are visible. The section series ends with a focus on the U-shaped, midline-spanning arrangement of neurite bundles that are a characteristic part of the putative mushroom body-like neuropil (compare to figure 44A). Note close association of the antero-medial cell streams with the somata lying apical to this structure, but as yet the absence of morphologically conspicuous globuli cells.

Movies 22-27: CISs and development of invaginating sub-regions in the pre-cheliforal lobe of *Pseudopallene* sp. (ES 4 – ES 6-7).

Tubulin labeling (glow) with nuclear counterstain (blue), Imaris volume (MIP and blend), same embryos as in figures 46; 47; 48A-B'.

The movies start in ventral view. Initially, they show MIP volumes of the tubulin signal only to reveal the intensely labeled spots of CISs, focus subsequently on the left pre-cheliforal lobe and then switch to the blend mode with included nuclear counterstain. Blend volumes are shifted in different directions to give an impression of the apically invaginating pre-proboscideal pit, antero-lateral depression and central depression. Note as well the gradual overgrowing and internalization of the three pharyngeal cell masses by surrounding proboscideal tissue.

Movie 22: ES 4.

Several CISs are already formed. Apart from the posterior portion of the central depression, no invaginating sub-regions are as yet detectable in the pre-cheliforal lobe.

Movie 23: ES 4-5.

Note higher number and better definition of CISs. The antero-median region between the pre-cheliforal lobes is damaged in this specimen. In addition to the slight posterior invagination of the central depression, first weak signs of the forming depression of the pre-proboscideal pit are detectable in the blend volume.

Movie 24: ES 5.

Within the forming the pre-proboscideal pit (slightly damaged), some CISs are still identifiable. In the blend volume, the beginning medio-lateral compression of the central depression can be noticed and tiny pits are discernible where some of its advanced CISs are positioned (similar to spiders). Laterally, an oblong nucleus-free region represents the primordial antero-lateral depression.

Movie 25: ES 5-6.

Initially, the MIP volume rotates 360 degrees around the z-axis (counter-clockwise) to reveal the far basally extending cell process bundles of the CISs in the pre-cheliforal lobe and in the palpal and ovigeral neuromeres (right chelifore dissected to reveal the VNE of this region). Note the distinct unpaired antero-median CIS in this specimen. In the blend volume, pre-proboscideal pit, medio-laterally compressed central depression and shallow oblong antero-lateral depression are discernible.

Movie 26: ES 6.

Note reduced number of delimitable CISs in the pre-cheliforal lobes and the palpal and ovigeral neuromeres (right chelifore dissected to reveal the VNE of this region). Already in the MIP volume, the pre-proboscideal pit is recognizable as a conspicuous structure. Note more anterior position of the antero-lateral depression and persistence of some central and medial CISs at the margins of the groove-shaped central depression.

Movie 27: ES 6-7.

Initially, the MIP volume dips slightly backwards to show the apical nuclei-free regions in the palpal and ovigeral neuromeres (right chelifore dissected to reveal the VNE of this region), being indicative of the delayed formation of segmental invaginations. In the pre-cheliforal lobe, some more intensely labeled bundles represent persisting CISs amongst the massed apical cell processes of the central depression. In the blend volume, a tiny pore is detectable as only external remainder of the pre-proboscideal pit. The antero-lateral depression has shifted further anteriorly and assumed a circular shape.

Movie 28: Circum-esophageal region and nascent cell clusters in early PS1 of *Pseudopallene* sp.
Tubulin (glow) and PH3 labeling (green) of a dissected circum-esophageal nervous system, Imaris volume (MIP), anterior-most portion of the brain (neuraxis) not included in the scan. A clipping plane has been applied to remove more ventrally extending pharynx portions.

The movie starts in ventral view. The embryo rotates 180 degrees around the z-axis (counter-clockwise). Note multiple mitoses in the nascent cell clusters of the brain (antero-lateral to pharynx) and of the palpal and ovigeral neuromeres (posterior to pharynx). Especially in lateral view the different apico-basal levels of the mitoses are clearly visible. Note also mitoses within the pharyngeal cells. The circum-esophageal connective of the left body half has been damaged during dissection.

Movie 29: Eye primordia, lateral sensory organ anlagen and larval brain of late PS 1 of *Pseudopallene* sp.

Tubulin (glow) and PH3 labeling (green) with nuclear counterstain (blue), virtual horizontal section series, Imaris oblique slicer passing from dorsal to ventral, anterior (body axis) to the bottom, same specimen as in figure 50.

The section series starts in the antero-dorsal larval epidermis, the cell clusters representing the eye primordia and the lateral sensory organ anlagen are passed first (compare to labeling in figure 50). Note several bigger cells surrounding the smaller cells of the lateral sensory organ anlage. Delicate neurite bundles extend basally into the 'optic nerve'/antero-lateral cell stream from the eye primordia and the lateral sensory organ anlage. The antero-medial cluster comprising proliferating big and smaller cells with distinct tubulin labeling of the cytoskeleton extends medio-basally to the region where the 'optic nerve' anlage merges with the ipsi-lateral brain hemisphere. Anteriorly, the apical brain cell cluster with deep apical pit is visible. Note mitoses in one big cell close to the lateral sensory organ anlage, amongst the cells of the 'optic nerve' anlage as well as within the antero-medial cluster and the apical brain cluster.

Movie 30: Brain soma cortex with globuli cell agglomerations in the adult of *Pseudopallene* sp.

Tubulin labeling (red) with nuclear counterstain (cyan) of a dissected brain, Imaris volume (MIP), same object as in figure 53A,A'.

The movie starts in ventro-lateral view (neuraxis). The brain rotates around the z-axis (counter-clockwise) to show the ventral and lateral globuli cell agglomerations in the brain soma cortex (compare to labeling in Fig. 53A'). Posteriorly, the unpaired median rostral nerve and the massive cheliforal nerve branches are intensely tubulin-labeled. Anteriorly, the antero-lateral thickenings of the proximal 'optic nerve' portion are discernible. Note cells with small and intensely labeled nuclei also in this anterior-most soma cortex region, which is underlain by the apical optic neuropil.

APPENDICES

Appendix A: List of used chemical solutions and recipes

Solution	Chemical composition		Preparation	
10x PBS (pH 7,4)	18,6mM	NaH_2PO_4	2,46 g	NaH_2PO_4
	84,1 mM	Na_2HPO_4	11,94 g	Na_2HPO_4
	175mM	NaCl	102,2 g	NaCl
			dissolve	in 800 ml ddH_2O
			add	ddH_2O to 1000 ml
			adjust	pH to 7,4
			→ prepare 1x PBS by 1:10 dilution in ddH_2O, then readjust pH to 7,4	
20x SSC (pH 7.0)	3 M	NaCl	175,3 g	NaCl
	300 mM	$Na_3C_6H_5O_7$	88,2 g	$Na_3C_6H_5O_7$ x $2H_2O$
			dissolve	in 800 ml ddH_2O
			adjust	pH to 7.0
			add	ddH_2O to 1000 ml
			sterilize	by autoclaving
			→ prepare 2x SSC and 0,2x SSC by dilution of 20x SSC and addition of Tween-20 to 0.1% in final solution	
50x TAE buffer	2M	Tris-acetate	242 g	Tris base
	50 mM	EDTA	dissolve	in 600 ml ddH_2O
			100 ml	0,5 M EDTA (pH 8,0)
			57,1 ml	glacial acetic acid
			add	ddH_2O to 1000 ml
			→ prepare 1x TAE buffer by 1:50 dilution in ddH_2O	
AP buffer (pH 9.5)	100 mM	NaCl	200 µl	NaCl stock (5 M)
	50 mM	$MgCl_2$	500 µl	$MgCl_2$ stock (1 M)
	100 mM	Tris-HCl	1 ml	Tris-HCl stock (1 M, pH 9.5)
	0.1%	Tween-20	10 µl	Tween-20
			add	ddH_2O to 10 ml
			adjust	pH to 9.5
			→ prepare AP buffer directly prior to staining reactions	

Solution	Chemical composition		Preparation	
Basic fuchsin	1%	basic fuchsin in ddH_2O	1g	basic fuchsin
			dissolve	in 90 ml ddH_2O
			add	ddH_2O to 100 ml
Bouin's fixative			15 ml	saturated aqueous picric acid
			5 ml	37% formaldehyde (methanol-stabilized)
			1 ml	glacial acetic acid
Collagenase-hyaluronidase mix	1 mg/ml	collagenase	30 mg	collagenase (SIGMA, #C0130)
	1 mg/ml	hyaluronidase	30 mg	hyaluronidase (SIGMA, #H3884)
		in 1xPBS	30 ml	1xPBS
			mix	by stirring at RT until completely dissolved
			aliquot	and store at -20°C
DABCO-Glycerol	~2,5%	DABCO	2,5 g	DABCO (1,4 – Diazabicyclo – [2,2,2] – octan)
	90%	glycerol	dissolve	in 10 ml 1xPBS
			add	90 ml glycerol and mix well
			aliquot	and store at -20°C
EDTA (0,5M, pH 8.0)	0,5 M	Na_2EDTA in ddH_2O	93,05 g	Na_2EDTA x $2H_2O$
			480 ml	ddH_2O
			add	10 M NaOH until pH 8,0 (EDTA dissolves)
			add	ddH_2O to 500 ml
FA/PBTw	3,7%	formaldehyde in PBTw	5 ml	37% formaldehyde (methanol-stabilized)
			45 ml	PBTw
			mix	thoroughly
Hyb buffer (~pH 8.25)	50%	formamide	50 ml	formamide
	2x	SSC	10 ml	20x SSC
	0.1%	Tween-20	100 µl	Tween-20
	50 µg/ml	yeast tRNA	250 µl	yeast tRNA stock (20 mg/ml)
	50 µg/ml	heparin	250 µl	heparin stock (20 mg/ml)
			add	ddH_2O to 100 ml
Hyb wash buffer	50%	formamide	25 ml	formamide
	1x	SSC	25 ml	2x SSC

Solution	Chemical composition		Preparation	
LB medium			10 g	tryptone
			5 g	yeast extract
			5 g	NaCl
			dissolve	in 1000 ml ddH_2O
			adjust	pH to 7,0
			sterilize	by autoclaving
Methylene blue-azure II	0,5%	methylene blue	1 g	methylene blue
	0,5%	borax	1 g	borax
	0,5%	azure II	dissolve	in 90 ml ddH_2O
			add	ddH_2O to 100 ml
			1g	azure II
			dissolve	in 90 ml ddH_2O
			add	ddH_2O to 100 ml
			mix	both solutions 1:1
NBT/BCIP staining buffer	55 µM	NBT (= oxidant)	4,5 µl	NBT ($C_{40}H_{30}Cl_2N_{10}O_6$, SIGMA) stock solution (10 mg/ml)
	189 µM	BCIP (= substrate)	3,5 µl	BCIP ($C_8H_6BrClNO_4P$, SIGMA) stock solution (20 mg/ml)
			1 ml	AP buffer (pH 9,5)
PBTw	1x	PBS	10 ml	10x PBS
	0,1%	Tween-20	100 µl	Tween-20
			add	ddH_2O to 100 ml and mix well
PBTx	1x	PBS	10 ml	10x PBS
	0,5%	BSA	0,5 g	BSA (bovine serum albumine)
	0,3%	Triton X-100	300 µl	Triton X-100
	1,5%	DMSO	1,5 ml	DMSO (dimethylsulfoxide)
			add	ddH_2O to 100 ml and mix well
PBTx+N	5%	NGS in PBTx	50 µl	NGS (Normal Goat Serum, DAKO, #X0907)
			add	950 µl PBTx and mix thoroughly
PFA/SW	4%	formaldehyde in natural sea water	16 %	formaldehyde in ddH_2O (from paraformaldehyde, methanol-free, ELECTRON MICROSCOPY SCIENCES, #15710)
			dilute	1:4 in filtered natural sea water

Solution	Chemical composition		Preparation	
PFA/PBS	4%	formaldehyde in 1xPBS	10 g	paraformaldehyde (PFA, methanol-free)
			26 ml	10xPBS
			224 ml	ddH_2O
			heat	mixture under constant stirring in water bath to 70°-80°C
			add	single drops of 1N NaOH until PFA dissolves
			cool	down, aliquot and store at -20°C
Proteinase K solution	10 µg/ml	Proteinase K in 1xPBS or PBTw	1 µl	Proteinase K (ROTH, #7528) stock solution (20 mg/ml in ddH_2O)
			2 ml	1xPBS or PBTw
TBS (pH 7,5)	0,9%	NaCl	9 g	NaCl
	10 mM	Tris-HCl	1,58 g	Tris-HCl
			dissolve	in 800 ml ddH_2O
			add	ddH_2O to 1000 ml
			adjust	pH to 7,5

Preparation of agar plates:

LB/ampicillin plates

- dissolve 15 g agar in 1000 ml LB medium
- sterilize by autoclaving
- cool down to 50°C
- add 0,1 g ampicillin
- pour into petri dishes & let agar harden
- store at 4°C

LB/ampicillin/IPTG/X-Gal plates (blue-white screening of colonies)

- spread 100 µl of 100mM IPTG (isopropyl-β-D-thiogalactopyranoside, PROMEGA, # V3955) and 20 µl of 50 mg/ml X-Gal (5-bromo-4-chloro-3-indolyl-β-D-galactopyranoside dissolved in dimethylformamide, PROMEGA, # V3941) over surface of LB/ampicillin plate
- allow to absorb for 30 min prior to use

Appendix B: Overview of histological sections on *Pseudopallene* sp.

Fixation: Bouin's fixative with subsequent washing and storage in 70% ethanol at room temperature

Embedding: Technovit 7100 (KULZER Histo-Technik), 1,5 – 2 µm sections

Staining: Methylene blue-azure II (6-7 min) / basic fuchsin counterstain (30-40 sec)

Developmental stage	# specimens	Orientation sectioning plane	Quality of section series
ES 3	2	2x oblique	interpretation difficult due to orientation, staining inhomogeneous between sections
ES 4	6	1x sagittal	many sections lost, some sections only weakly stained
		1x horizontal	slightly oblique, staining inhomogeneous between sections
		1x transversal	slightly oblique, most sections with good staining
		3x oblique	interpretation difficult due to orientation, staining consistently good
ES 5-6	4	3x horizontal	2x slightly oblique, staining of neuroectoderm too strong for clear cell distinction 1x many sections lost & inhomogeneous staining between sections
		1x transversal	apparently misdeveloped with many rounded cells and cell death (→ pycnotic bodies)
ES 7-8	7	1x sagittal	some rows of sections only weakly stained
		2x horizontal	1x staining consistently good 1x slightly oblique, anteriorly damaged, staining inhomogeneous between sections
		2x transversal	1x staining consistently good 1x slightly oblique, one chelifore damaged, brain region incomplete and distorted
		2x oblique	interpretation difficult due to orientation, staining consistently good

Developmental stage	# specimens	Orientation sectioning plane	Quality of section series
ES 9	3	1x sagittal	staining of VNC very/too strong
		1x horizontal	staining consistently good
		1x transversal	slightly oblique, staining consistently good, sub-esophageal ganglion damaged
PS 1	10	5x sagittal	1x staining consistently good 1x staining consistently good, brain region folded, fixation artifacts 1x staining consistently good, many sections with folds 2x significant fixation artifacts
		2x horizontal	1x staining consistently good 1x staining often only weak, many sections with folds
		2x transversal	1x brain region weakly stained, VNC staining good 1x slightly oblique, staining predominantly good, sub-esophageal ganglion and 1wlg damaged
		1x oblique	interpretation difficult due to orientation, nervous system damaged
PS 2	3	1x sagittal	staining predominantly good, sub-esophageal ganglion slightly damaged
		1x horizontal	staining predominantly good
		1x transversal	staining consistently good
PS 6	3	1x sagittal	staining predominantly good
		1x horizontal	staining inhomogeneous between sections
		1x transversal	staining inhomogeneous between sections
Sub-adult	1	1x sagittal	staining weak & inhomogeneous between sections
Adult	2	1x sagittal (♂)	staining predominantly good
		1x transveral (♀)	staining predominantly good, ventral side of trunk (with VNC) often folded

Appendix C: Laboratory procedures prior to *in-situ* hybridization

RNA extraction

Total RNA was extracted from embryonic tissue (preserved in RNAlater RNA stabilization reagent, QIAGEN, # 76104) using a RNeasy® Mini Kit (QIAGEN, #74104). Between 20-30 mg material consisting of a mixture of different embryonic stages was used per extraction. In the final step of the manufacturer's protocol, the extracted total RNA was eluted in 40 µl RNase-free water. After concentration measurement with a spectrophotometer (NanoVue™, Version 4282 V1.7.3, GE HEALTHCARE), the obtained total RNA was stored at -80°C until further use.

cDNA synthesis

Total RNA was reverse-transcribed into single-stranded cDNA using the SuperScript III First-Strand Synthesis System for RT-PCR (INVITROGEN, #18080-051). Random hexamers were chosen as primers for the reaction. The volume of total RNA solution added to the reaction was adjusted to contain approximately 1 µg of RNA. Obtained cDNA was aliquoted and stored at -20°C.

Construction of degenerate primers

Degenerate primers were used in order to obtain fragments of the chosen target genes from the cDNA. For this purpose, sequences of the respective gene's homologues in other arthropod taxa were downloaded from the databases of the National Center for Biotechnology Information (NCBI) and aligned with the BIOEDIT Sequence Alignment Editor software (Version 7.0.5.3, Hall 1999). Degenerate primers were designed in sequence regions exhibiting a high degree of conservation across the different arthropod lineages. The primers' melting temperatures were checked with the SIGMA oligo design tool and with the web-based program OLIGOCALC. Using the same tools, possible self-complementarity of primers as well as their potential for internal hairpin formation was assessed and attempted to hold at a minimum. For each target gene, at least two forward and two reverse primers were designed (Table 6).

PCR reactions with degenerate primers

For each gene, at least two separate primary PCR reactions were run, using the synthesized cDNA as template. In reaction 1, the respective outer-most primer pair (for_01 & rev_02) was added. In reaction 2, the nested primer pair (for_02 & rev_01) was used (in case of more primers, additional combinations were tested). A low annealing temperature of 50°C was chosen as default setting. At least in theory, this leads to a lower specificity in the primers' binding

behavior. However, it has proven to give in most cases equivalent and sometimes even better results in comparison to an annealing temperature adjusted to the individual primer pairs (personal communication Joakim Eriksson; personal observation).

Subsequently, secondary PCRs were run, using the primary PCR products as templates. All possible primer combinations were tried on the PCR product of reaction 1, whereas only the nested primer pair was used on the product of reaction 2 for a second time.

Five microliters of all primary and secondary PCR products were checked via gel electrophoresis on a gel (1% agarose in 1xTAE-buffer).

Tab. 6: Sequences of degenerate primers used in the study to obtain fragments of the five genes/gene families from cDNA of *Pseudopallene* sp. Primers in bold letters represent the final pairings with which obtained target gene fragments were amplified (see 3.7., Tab. 5).

Gene / Gene family	**Degenerate primer sequences (5' – 3')**
Notch	for_01: GATGYCAGAAYGGBGGCACMTG **for_02: TGYGCHTCMARACCTTGYCGTAATGG** **rev_01: GCRTCATCYAARTGGCAAARAARACC** rev_02: CAATBGAAAGAVCCDGGGGTRTTGA
Delta	for_01: TTMRABTTMWCRTGGSYRGG **for_02: TCBCTHATMGTBGARGCVTGGCA** rev_01: AADARWCCDCCCCADCCTTC **rev_02: GCAMGGYYKGTGATTKGTRCA**
Prospero	for_01: ACMYTSACRCCVATRCACCTRMG **for_02: AAGGCSAAGYTSATGTTCYTYT** rev_01: GTAKATRGMCTTCTTCCAMGACTG **rev_02: TTBGGMGAYTTGAAGTAYT**
Snail	for_01: CBARGCAYMRDCWGWTBCAYTG for_02: GGRGCMYTSAARATGCAYATHMGSAC rev_01: TKGCADSYRTAYTTYTTSACDTC **rev_02: SARVGACATCCTKGARAAAGWYTT** (same primer binding on both strands)
ASH	for_01: GTNGCHCGSMGVAAYGARMGBGA for_02: GBGARCGNAAYMGVGTMAARC **for_03: CWVGTCAACHWVGGNTTYGC** **rev_01: TCVACYTTGCTCAWYTTYTTGTT** rev_02: GATGTAYTCGACBGCHGATYTCA rev_03: AADTCNAKVAGHTCNTSDYCWT

(1) PCR product showed a single distinct band with the expected length

→ direct purification of product, using a High Pure PCR Product Purification Kit (ROCHE, #11732668001).

(2) PCR product showed multiple bands, including one with the expected length

→ repetition of reaction with increased reaction volume of 100 µl (see below) → gel electrophoresis on 0,7% agarose gel → cutting out of target band → gel purification according to protocol specified in the purification kit.

(3) None of the PCR products showed any bands of correct length

→ repetition of reactions either with a range of different annealing temperatures (Gradient-PCR) or with changes in the primer concentrations. If these approaches did still not yield positive results, new degenerated primers were designed (e.g. *Pseudopallene*-ASH).

Cloning of gene fragments

A pGEM®-T Easy Vector System II (PROMEGA, #A1380) was used for cloning of purified gene fragments. The applied protocol for the ligation of gene fragments into the vector and the following transformation of competent cells deviated from the procedure specified in the kit's manual: Only 0,5 µl of the T4 DNA Ligase and of the pGEM®-T Easy vector were added to 5 µl of 2X Rapid Ligation Buffer, whereupon the mixture was divided into two equal portions à 3 µl. To each of these, 2 µl of a purified gene fragment were added. The ligation reaction was conducted at 4°C and lasted at least overnight, often even several nights. For the transformation step, 50 µl of JM109 High Efficiency Competent Cells (provided in the kit, aliquoted into 1,5 µl Eppendorf tubes and stored at -80°C) were thawed on ice, the 5 µl of the ligation reaction being added subsequently. Following incubation on ice for 30 minutes, the cells were heat-shocked for 35-40 seconds at 42°C in a heat block or water bath and immediately back-transferred to ice for two minutes. After addition of 200 µl LB medium to the cells, the resulting transformation culture was incubated for one hour at 37°C on a horizontal shaker (~200 rpm). The complete volume was plated onto LB/ampicillin/IPTG/X-Gal culture plates and incubated overnight (at least 12 h) at 37°C.

Picking of colonies, purification of the vector DNA and sequencing

The incubated culture plates were checked for colonies the next day. Depending on the number of grown colonies, up to 25 different clones were picked per plate, using sterile toothpicks. Preferably, white colonies were chosen. However, in case of less than twenty white colonies on a plate, also blue colonies were included. Picked clones were (1) used as template for a colony PCR as well as (2) introduced on a numbered replica plate (LB/ampicillin) that was subsequently incubated at 37°C for several hours. For colony PCR, M13 forward and M13 reverse primers

(PROMEGA, # Q5601) were used. The binding sites of these primers in the vector enclose its insert region. Based on a comparison of the obtained PCR product lengths to the expected length of the respective target gene fragments, clones were chosen for sequencing, picked from the replica plate and inoculated overnight at 37°C on a horizontal shaker (~200 rpm) in 50 ml Falcon tubes containing 3 ml LB medium and 3 µl ampicillin solution (50 mg/ml). For vector purification a QIAprep Spin Miniprep Kit (QIAGEN, # 27106) was used, adhering to the therein specified standard protocol. The concentration of the purified vector DNA was measured with a spectrophotometer. Of each clone, a sample of 15 µl (diluted in double-distilled water to a concentration between 50–100 ng/µl) was sent for sequencing to EUROFINS MWG OPERON.

Sequence analysis

Identification of the flanking vector regions in the obtained sequences was accomplished with the VECSCREEN tool on the NCBI website. Following manual removal of the identified vector regions in BIOEDIT, the sequences were blasted as translated nucleotide queries against the NCBI protein database, using the BLASTX tool.

(1) The query was identified as target gene fragment and fragment length exceeded 300 bp.

→ All correct clones were aligned in BIOEDIT and checked for sequence differences at nucleotide and amino acid level, which might be due to amplification or sequencing errors, the occurrence of different alleles or the possible existence of different gene copies (paralogues). One clone was chosen for the synthesis of a DIG-labeled antisense RNA probe (see below).

(2) The query was identified as target gene fragment, but fragment length was too short for probe synthesis (<300 bp).

→ Specific primers directed against the sequenced fragment were designed in order to elongate the gene fragment via rapid amplification of 5' and/or 3' cDNA ends (see below).

(3) No target gene hits were recovered for any of the sequenced clones.

→ Either additional clones from the culture plates were sent for sequencing, or new degenerate primers were designed against (other) conserved regions of the target gene.

Rapid amplification of 5' and 3' cDNA ends (RACE)

For 5' RACE, three gene-specific reverse primers (SP1, SP2, SP3) directed against the sequenced short fragment of the target gene were constructed. For 3' RACE, only two gene-specific forward primers (SP5, SP5.2) were designed. Picking of a range of possible specific primers was accomplished in the web-based program PRIMER3PLUS. A ROCHE 5'/3' RACE Kit, 2nd Generation (#03353621001) and the therein provided protocol was used. Products of the initial and the nested RACE PCRs (see below) were checked via gel electrophoresis. Obtained fragments were purified, ligated, cloned, sequenced and analysed as described above.

Synthesis of digoxigenin (DIG)-labeled antisense RNA probes

Chosen gene fragments were amplified from the respective vectors via PCR (Colony PCR program, see below), using the M13 forward and M13 reverse primers. Concentrations of the linear PCR products were measured with a spectrophotometer. For reverse *in-vitro* transcription into DIG-labeled antisense RNA probes ROCHE reagents were used (DIG RNA Labeling Mix, 10x conc., #11277073910 / SP6 RNA Polymerase, #11487671001 / T7 RNA Polymerase, #10881775001 / Transcription Buffer, 10x conc., #11465384001) and the protocol specified in the DIG RNA Labeling Mix was followed. Depending on the orientation of the inserted gene fragment in the vector, either SP6 or T7 RNA polymerase was used to synthesize antisense RNA probes. In the final step of the protocol, DEPC-treated RNase-free water was used to dissolve the precipitated RNA probes and 1 µl of RNase Inhibitor was added. The probes were aliquoted and stored at -80°C until further use.

Websites and used web-based tools

EUROFINS MWG OPERON: http://www.eurofinsdna.com/de/home.html

NATIONAL CENTER FOR BIOTECHNOLOGY INFORMATION (NCBI):

Homepage: http://www.ncbi.nlm.nih.gov/

VECSCREEN: http://www.ncbi.nlm.nih.gov/VecScreen/VecScreen.html

BLASTX: http://blast.ncbi.nlm.nih.gov/Blast.cgi?PROGRAM=blastx&BLAST_PROGRAMS=blastx&PAGE_TYPE=BlastSearch&SHOW_DEFAULTS=on&LINK_LOC=blasthome

CDD (Conserved Domain Database): http://www.ncbi.nlm.nih.gov/Structure/cdd/wrpsb.cgi

OLIGOCALC: Oligonucleotide Properties Calculator: http://www.basic. northwestern.edu/biotools/oligocalc.html

PRIMER3PLUS: http://www.primer3plus.com/cgi-bin/dev/primer3plus.cgi

SIGMA-ALDRICH®:

Homepage: http://www.sigmaaldrich.com/united-kingdom.html

Oligo design: http://www.sigmaaldrich.com/configurator/servlet/DesignCenter

PCR programs

Primary PCR

25,00 µl	**total reaction volume**	**Program:**		
2,00 µl	cDNA			
2,50 µl	PCR buffer		2' 00'':	94°C
2,50 µl	dNTPs		30'':	94°C
0,50 µl	forward primer	35-40x	30'':	50°C
0,50 µl	reverse primer		1' 00'':	72°C
0,25 µl	TAQ polymerase		3' 00'':	72°C
16,75 µl	ddH_20		∞:	4°C

Secondary PCR

30,00 µl	**total reaction volume**	**Program:**		
1,00 µl	primary PCR product			
3,00 µl	PCR buffer		2' 00'':	94°C
3,00 µl	dNTPs		30'':	94°C
2,00 µl	forward primer	35-40x	30'':	50°C
2,00 µl	reverse primer		1' 00'':	72°C
0,30 µl	TAQ polymerase		3' 00'':	72°C
18,70 µl	ddH_20		∞:	4°C

Secondary PCR for subsequent gel purification

100,00 µl	**total reaction volume**	**Program:**		
1,00 µl	PCR product			
10,00 µl	PCR buffer		2' 00'':	94°C
10,00 µl	dNTPs		30'':	94°C
5,00 µl	forward primer	35-40x	30'':	50°C
5,00 µl	reverse primer		1' 00'':	72°C
1,00 µl	TAQ polymerase		3' 00'':	72°C
68,00 µl	ddH_20		∞:	4°C

Colony PCR

10,5 µl	**total reaction volume**
1,0 µl	PCR buffer
1,0 µl	dNTPs
0,5 µl	M13 forward primer
0,5 µl	M13 reverse primer
0,5 µl	TAQ polymerase
7,0 µl	ddH_20

Program:

	2’ 00’’:	94°C
40x	30’’:	94°C
	30’’:	50°C
	1’ 00’’:	72°C
	3’ 00’’:	72°C
	∞:	4°C

Initial 5’ RACE PCR

50,0 µl	**total reaction volume**
5,0 µl	dA-tailed cDNA product
5,0 µl	PCR buffer
1,0 µl	dNTPs
1,0 µl	Oligo dT-anchor primer
1,0 µl	gene-specific reverse primer SP2
0,5 µl	TAQ polymerase
36,5 µl	ddH_20

Program (all RACE PCRs):

	2’ 00’’:	94°C
	30’’:	94°C
10x	30’’:	60°C
	1’ 00’’:	72°C
	30’’:	94°C
25x	30’’:	60°C
	1’ 00’’-9’ 00’’:	72°C
	7’ 00’’:	72°C
	∞:	4°C

Nested 5’ RACE PCR

50,0 µl	**total reaction volume**
1,0 µl	first PCR product
5,0 µl	PCR buffer
1,0 µl	dNTPs
1,0 µl	PCR anchor primer
1,0 µl	gene-specific reverse primer SP3
0,5 µl	TAQ polymerase
40,5 µl	ddH_20

Initial / nested 3’ RACE PCR

50,0 µl	**total reaction volume**
1,0 µl	cDNA product / first PCR product
5,0 µl	PCR buffer
1,0 µl	dNTPs
1,0 µl	gene-specific forward primer SP5 / SP5.2
1,0 µl	PCR anchor primer
0,5 µl	TAQ polymerase
40,5 µl	ddH_20

Appendix D: Cell counts of hemi-neuromeres in walking leg segment 1

List of cell numbers counted in hemi-neuromeres of walking leg segment 1 during development of *Pseudopallene* sp. (ES 2-3 – PS 6). Cells are sorted in different categories, depending on the developmental stage (see 3.3.6. for details).

Stage	# specimens	# apical ECs	# ECs basal nucleus/basally detached	# ECs rim of invagination	# ECs apical cell cluster	# cells total
ES 2-3	2	78	59	-	-	137
		76	64	-	-	140
ES 3	2	88	108	-	-	196
		76	118	-	-	194
ES 4	3	59	123	-	-	182
		65	115	-	-	180
		66	117	-	-	183
ES 4-5	1	55	133	-	-	188
ES 5	1	-	138	30	-	168
ES 5-6	2	-	150	32	-	182
		-	165	33	-	198
ES 6	2	-	169	34	-	203
		-	169	36	-	205
ES 6-7	2	-	204	27	-	231
		-	260	28	-	288
ES 7	2	-	267	33	-	300
		-	274	39	-	313
ES 8	1	-	422	32	-	454
ES 8-9	1	-	502	27	-	529
ES 9-10	1	-	536	22	-	558
PS 1 (early)	2	-	613	-	171	784
		-	632	-	160	792
PS 1 (late)	1	-	803	-	157	960
PS 2	1	-	1225	-	75	1300
PS 6	1	-	1889	-	48	1937

Appendix E: Selected descriptive statistics of apical cell cluster analysis

Overview of all cell counts performed of the apical cell clusters post-embryonic stages (PS 2 – ad) of *Pseudopallene* sp. A total of 299 cell clusters were counted across all stages and ganglia. Minimum and maximum as well as median and arithmetic mean cell numbers per cluster and ganglion are given. Remarkably low or high minimum and maximum numbers are indicated by exclamation mark. Secure identification of outliers was hampered by low sample size, all counted clusters having been included in the average values.

Brain

Stage	# specimens	# analyzable clusters	minimum #cells/cl.	maximum #cells/cl.	median #cells/cl.	mean #cells/cl.
PS 2	3	6	48	54	52	51,5
PS 3	3	6	35	49	39,5	40,7
PS 4	2	4	34	41	38,5	38,0
PS 6	4	8	33	45	35,5	36,1
Sub-adult	6	12	14 !	38	36	32,7
Adult	2	4	31	35	35	34,0

Palp (anterior clusters of sub-esophageal ganglion)

Stage	# specimens	# analyzable clusters	minimum #cells/cl.	maximum #cells/cl.	median #cells/cl.	mean #cells/cl.
PS 2	4	8	53	63	56	57,1
PS 3	3	5	43	52	46	47,4
PS 4	3	6	37	52	46	44,8
PS 6	5	10	34	44	39	38,8
Sub-adult	6	12	35	47	39	39,3
Adult	2	4	27	34	30,5	30,5

Oviger (posterior clusters of sub-esophageal ganglion)

Stage	# specimens	# analyzable clusters	minimum #cells/cl.	maximum #cells/cl.	median #cells/cl.	mean #cells/cl.
PS 2	4	8	52	63	57,5	56,8
PS 3	4	8	48	53	49	49,8
PS 4	3	6	42	50	48	47,5
PS 6	5	10	37	64 !	41,5	44,4
Sub-adult	6	12	35	51	39,5	40,6
Adult	2	4	29	57 !	39	41,0

Walking leg 1

Stage	# specimens	# analyzable clusters	minimum #cells/cl.	maximum #cells/cl.	median #cells/cl.	mean #cells/cl.
PS 2	4	8	64	75	72,5	70,6
PS 3	4	8	50	60	55	55,3
PS 4	2	3	46	59	50	51,7
PS 6	5	10	41	80 !	45,5	49,0
Sub-adult	6	12	43	63	47,5	49,4
Adult	2	4	35	40	36	36,8

Walking leg 2

Stage	# specimens	# analyzable clusters	minimum #cells/cl.	maximum #cells/cl.	median #cells/cl.	mean #cells/cl.
PS 2	4	8	66	88	80	79,1
PS 3	4	7	52	59	54	54,6
PS 4	3	6	45	60	52	52,2
PS 6	5	9	44	62	48	49,3
Sub-adult	5	10	45	62	48	49,7
Adult	2	4	31	39	39	37,0

Walking leg 3

Stage	# specimens	# analyzable clusters	minimum #cells/cl.	maximum #cells/cl.	median #cells/cl.	mean #cells/cl.
PS 2	ganglion proper and ventral clusters not yet morphologically distinguishable					
PS 3	5	9	48	64	58	57,1
PS 4	3	6	47	70	60,5	58,8
PS 6	5	9	45	53	48	48,3
Sub-adult	5	9	41	59 !	49	49,4
Adult	2	3	27	37	36	33,3

Walking leg 4

Stage	# specimens	# analyzable clusters	minimum #cells/cl.	maximum #cells/cl.	median #cells/cl.	mean #cells/cl.
PS 2	ganglion proper and ventral clusters not yet morphologically distinguishable					
PS 3	5	9	73	130 !	94	93,4
PS 4	3	6	58	71	66,5	65,3
PS 6	5	8	45	59	49	51,1
Sub-adult	6	12	43	62	53,5	53,0
Adult	2	4	31	46	40	39,3